AFRL-SR-AR-TR-06-0032

REPORT DOCUMENTATION PAGE

1. REPORT DATE (DD-MM-YYYY)	2. REPORT TYPE	3. DATES COVERED (From - To)
1-23-2006	Final Technical Report	4-1-2002 - 8-31-2005

4. TITLE AND SUBTITLE
Study of triggering of electromagnetic pulses from isomeric materials - II

5a. CONTRACT NUMBER

5b. GRANT NUMBER
F49620-02-1-0187

5c. PROGRAM ELEMENT NUMBER

6. AUTHOR(S)
James J. Carroll

5d. PROJECT NUMBER

5e. TASK NUMBER

5f. WORK UNIT NUMBER

7. PERFORMING ORGANIZATION NAME(S) AND ADDRESS(ES)
Youngstown State University
One University Plaza
Youngstown, OH 44555

8. PERFORMING ORGANIZATION REPORT NUMBER
GC69-02-Final

9. SPONSORING / MONITORING AGENCY NAME(S) AND ADDRESS(ES)
USAF, AFRL
AF Office of Scientific Research
4015 Wilson Boulevard, Room 713
Arlington, VA 22203-1954

10. SPONSOR/MONITOR'S ACRONYM(S)

11. SPONSOR/MONITOR'S REPORT NUMBER(S)

12. DISTRIBUTION / AVAILABILITY STATEMENT
Unlimited

DISTRIBUTION STATEMENT A
Approved for Public Release
Distribution Unlimited

13. SUPPLEMENTARY NOTES

14. ABSTRACT
Metastable excited nuclear states, isomers, have been of strong interest for decades, with studies motivated by their physical properties and the promise of high-energy-density applications. Much research has concentrated on so-called triggered gamma emission as a means of controlling the release of energy stored in these isomers. This research comprises a very specialized sub-field of nuclear physics and, as such, has often suffered from a lack of connection with the larger body of more traditional studies. The YSU isomer Physics Project has taken a broad view of triggering studies with the aim of providing a firm foundation to this maturing field. This report reviews work conducted by this project related to triggered gamma emission, isomer production reactions and the development of new trigger approaches.

15. SUBJECT TERMS

16. SECURITY CLASSIFICATION OF:			17. LIMITATION OF ABSTRACT	18. NUMBER OF PAGES	19a. NAME OF RESPONSIBLE PERSON
a. REPORT	b. ABSTRACT	c. THIS PAGE			Peter J. Kasvinsky
Unclassified	Unclassified	Unclassified	Unlimited	261	19b. TELEPHONE NUMBER (include area code) 330-941-3091

TECHNICAL REPORT

INTRODUCTION

Metastable excited nuclear states, isomers, have been a major subject of inquiry since their discovery in 1921, with studies motivated in different ways by their physical properties. Isomer halflives run the gamut from rather modest (like the $T_{1/2} \sim 14$ ms shape isomer of ^{242}Am) to extremely long (like the essentially stable spin isomer ^{180m}Ta, with $T_{1/2} > 10^{15}$ years). Quite short-lived isomers also exist. In all cases, the existence of an isomer reflects specific nuclear structure that creates some type of potential barrier against electromagnetic decay of the metastable level to lower-lying states. For so-called spin isomers, it is the angular momentum arising from a particular single-particle configuration that provides such a barrier, forcing electromagnetic decays to be restricted to high multipolarities. A further inhibition for K isomers of deformed nuclei comes from a need to significantly re-orient the angular momentum vector, whose projection on the body axis of nuclear symmetry is K. A full discussion of the underlying mechanisms of isomer formation is beyond this present paper, but an excellent review may be found in Ref. [1]. The population and decay of isomers can give considerable insight into nuclear structure [2].

Isomers have also been of great interest for potential applications, primarily due to the ability of some isomers to store tremendous amounts of energy, e. g. the K isomer ^{178m2}Hf stores 2.46 MeV per nucleus, or about 1.2 GigaJoules/gram, with a halflife of 31 years. Its natural decay follows a complex cascade of transitions that has recently been clarified [3] under this grant, terminating at the stable ground state. Harnessing this stored energy could give a source of "clean" nuclear energy for various applications [4]. Some other isomers do not have stable ground states, but might still be valuable in providing a sequence of energy-releasing beta or alpha decays [5].

Whatever the motivation, much effort has been expended to investigate the triggering of an energy release from long-lived isomers, mainly as a burst of gamma rays. A number of issues come to the fore when considering this topic: what isomers would be best to examine, what mechanism(s) would allow external control or bypass of the natural decay, and how would one experimentally measure a triggered release from small amounts of isomers. Of course, the experimental goal would be to measure the energy required for the triggering entity (photons, neutrons, etc.) and the cross section for the reaction. The production of isomers in quantities sufficient for precision experiments is also an important goal.

In 2001, an extensive review [5] discussed the general topic with a focus on triggering initiated by photons and a view of the systematics of isomer triggering as deduced from the closely-related "activation" of isomers. Just one isomer exists in nature (^{180m}Ta) and its triggered energy release has been conclusively demonstrated (see Refs. [6-8] and references therein). Up to now the main method of predicting possible trigger energies for other isomers was to consider their relationship to the systematics of isomer activation for neighboring isotopes and to trigger levels found to depopulate ^{180m}Ta. This approach was most notably used in the case of the 31-year isomer of ^{178}Hf. It was

suggested in 1995 that on this basis a trigger level might be found "near 2.8 MeV" [9] from the "speculation that [trigger] levels are prevalent and lie between 2.5 - 2.8 MeV" [10]. First trigger experiments were attempted in 1996 by inelastic scattering of alpha particles at Orsay, with a repeat in 1997, but as yet no firm results are known. The first photon triggering experiments began in late 1998 and the positive indications reported therefrom [11, 12] began the present intense, and controversial [13], period of research.

The field of study of triggered gamma emission from isomers is now moving into a new era, defined by less reliance on systematics predictions and utilizing the greatly improved spectroscopic level data from more traditional experiments. With the ability to identify and target specific potential trigger transitions, one can anticipate a greatly increased pace of research. Within this context, the work conducted by the YSU Isomer Physics Project under AFOSR support has provided a considerable base of fundamental knowledge and has significantly advanced the field. Such basic information as cross sections for different reaction mechanisms is central to any evaluation of the feasibility of isomers for applications.

A total of twenty manuscripts have been published during the period of performance of this grant period. One manuscript is in press for 2006 while two others have been submitted and are under review. Also, twenty invited and three contributed presentations by the PI resulted from grant sponsorship and six contributed presentations/posters were made by undergraduate students supported hereby. In addition, the PI served as Co-Program Chairman of three international scientific conferences in this field and as Co-Chairman of a session on these topics at another meeting. The PI served as well as a reviewer for the Science and Technology Center in Ukraine during 2005.

The essential technical details of the papers may be found in Appendix A while Appendices B and C list Invited and Contributed Presentations, respectively, under this grant period. A few highlights are listed below to indicate the degree to which the YSU Isomer Physics Project has contributed to a firm foundation for possible applications of long-lived isomers.

HIGHLIGHTS OF PUBLISHED RESULTS

Experimental tests of triggered gamma emission occupy a rather narrow field within nuclear physics. As such, this work is somewhat removed from the mainstream of nuclear physics and has suffered from a perceived lack of firm founding in traditional, experimentally-verified concepts of the larger field. The extremely large integral cross sections from initial reports of triggering of ^{180m}Ta perpetuated this perception until later work showed that improved measurements were indeed in agreement with established nuclear systematics [14]. Finally, for ^{180m}Ta it was possible to make first identifications of specific nuclear states in level schemes with the energies that provided absorption of incident photons to cause triggered gamma emission [8]. Work conducted under this grant has contributed significantly to the foundations of triggered gamma emission and explored several new concepts. A few recent highlights will be given to indicate the breadth and depth of these efforts.

"Design and characterization of a compact multi-detector array for studies of induced gamma emission: Spontaneous decay of ^{178m2}Hf as a test case," P. Ugorowski, R. Propri, S. A. Karamian, D. Gohlke, J. Lazich, N. Caldwell, R. S. Chakrawarthy, M. Helba, H. Roberts and J. J. Carroll, Nuclear Instruments and Methods A (submitted 2006).

Summary:

Some published reports (see the survey in Ref. [13]) have claimed evidence that triggered gamma emission could be induced from ^{178m2}Hf using incident real photons near 10 keV. To investigate these claims with improved sensitivity, a final implementation of the YSU miniball array was utilized at the BL12B2 beamline at SPring-8. Results obtained during irradiations will be presented in a later manuscript, but prior to that a fully-detailed characterization of the miniball system was performed using natural decay of ^{178m2}Hf. This provided a baseline of natural events from which to compare measurements that could, in principle, have produced induced events.

"$K^{\pi} = 0^{+}$ 2.29 s isomer in neutron-rich ^{174}Tm," R. S. Chakrawarthy, P. M. Walker, J. J. Ressler, E. F. Zganjar, G. C. Ball, M. B. Smith, A. N. Andreyev, S. F.Ashley, R. A. E.Austin, D. Bandyopadhyay, J. A. Becker, J. J. Carroll, D. S. Cross, D. Gohlke, J. J. Daoud, P. E. Garrett, G. F. Grinyer, G. Hackman, G. A. Jones, R. Kanungo, W. D. Kulp, Y. Litvinov, A. C. Morton, W. J. Mills, C. J. Pearson, R. Propri, C. E. Svensson, R. Wheeler and S. J. Williams, Physical Review C (accepted 2006).

Summary:

This paper describes the characterization of a newly-discovered isomer based on measurements performed using the so-called 8π detector array and spallation ion source (ISAC) at TRIUMF. The array consists of twenty Compton-suppressed Ge detectors and was coupled with a new internal array of conversion-electron detectors.

"Production of long-lived hafnium isomers in reactor irradiations," S. A. Karamian, J. J. Carroll, J. Adam, E. N. Kulagin and E. P. Sabalin, High Energy Density Physics (submitted 2005); "Production of the ^{178m2}Hf isomer using a 4.5-GeV electron accelerator," S. A. Karamian, J. J. Carroll, J. Adam and N. A. Demekhina, Nuclear Instruments and Methods A 530, 463 (2004).

Summary:

The first of these papers describes a new, more accurate measurement of the cross section for production of this long-lived isomer using reactor neutrons, including an improved measurement for so-called burnup, or depletion, of the isomer itself in that environment. The second paper describes a first measurement of the cross section for production of this isomer using high-energy bremsstrahlung.

"Nuclear excitation and de-excitation in resonant electronic transitions," M. R. Harston and J. J. Carroll, Laser Phys. 14, 1452 (2004); "Limits on nuclear excitation and deexcitation of $^{178}Hf^{m2}$ by electron-nucleus coupling," M. R. Harston and J. J. Carroll, Laser Phys. 15, 487 (2005).

Summary:

The first paper describes the general calculation of probabilities for NEET (nuclear excitation by electron transitions) which occurs as a result of coupling between the nucleus and atomic transitions under certain conditions. The second paper describes a detailed calculation of the NEET probabilities for the $^{178m2}Hf$ nucleus. These probabilities are small and do not agree with the suggestion that NEET is the mechanism responsible for claims of low-energy triggering.

"Studies of high-K isomers at TRIUMF-ISAC," M. B. Smith, P. M. Walker, R. S. Chakrawarthy, R. A. E.Austin, G. C. Ball, J. J. Carroll, E. Cunningham, P. Finlay, P. E. Garrett, G. F. Grinyer, G. Hackman, B. Hyland, K. Koopmans, W. D. Kulp, J. R. Leslie, A. A. Phillips, R. Propri, P. H. Regan, F. Sarazin, M. A. Schumaker, H. C. Scraggs, T. Shizuma, C. E. Svensson, J. von Schwarzenberg, J. C. Waddington, D. Ward, J. L. Wood, B. Washbrook and E. F. Zganjar, Nucl. Phys. A 746, 617 (2004).

Summary:

This paper describes the scope of and some results from the program of studies of high-K isomers conducted at TRIUMF using ISAC and the 8π array. The class of high-K isomer includes $^{178m2}Hf$ and ^{180m}Ta, for example.

"Gamma rays emitted in the decay of 31-year $^{178m2}Hf$," M. B. Smith, P. M. Walker, G. C. Ball, J. J. Carroll, P. E. Garrett, G. Hackman, R. Propri, F. Sarazin and H. C. Scraggs, Phys. Rev. C 68, 031302(R) (2003).

Summary:

1. Some reports claiming evidence in support of low-energy triggering of $^{178m2}Hf$ have reported the appearance of "new" gamma lines that appear only during irradiation of an isomeric target. The term "new" indicates that the gamma transitions reported do not appear in the natural decay cascades from the 31-year m2 isomer. The statistical nature of the reported data for these "new" lines is poor, but if one assumes that the lines do appear, then it is important to insure that they are now weakly-populated transitions in the natural decay, hitherto unobserved. This paper describes the detailed measurement of the natural decay of $^{178m2}Hf$, from which a number of newly observed gamma decays from the 31-year isomer and between the two 8^- bands were detected. Other unplaced "new" gamma lines were discussed which may have influenced claims of nearby lines appearing due to triggering.

"'Forced-gamma emission' studies involving nuclear isomers using fast neutrons and bremsstrahlung x rays," N. A. Guardala, J. L. Price, J. H. Barkyoumb, R. J. Abbundi, G. Merkel and J. J. Carroll, in *Applications of Accelerators in Research and Industry* (American Institute of Physics, Melville, New York, 2003).

Summary:

This paper describes and proposes a series of experiments to study fast-neutron- and photon-induced triggering of selected nuclear isomers. These isomers have halflives in the range of 42.6 minutes to 57.4 days. Although not sufficiently long-lived to provide reasonable storage for applications, they may be suitable for experiments with equipment available at the Naval Surface Warfare Center, Carderock Division (NSWCCD).

"Possible Ways for Triggering the ^{179m2}Hf isomer," S. A. Karamian, J. J. Carroll, L. A. Rivlin, A. A. Zadernovsky and F .J. Agee, Laser Phys. 14, 1 (2004).

Summary:

The 25.1-day isomer of ^{179}Hf may prove useful in trigger experiments and can be produced, in principle, in sufficient amounts for testing. Modern nuclear level data supports the identification of at least three different potential trigger methods based on specific candidates for intermediate states as discussed in this paper.

"An Experimental Perspective On Triggered Gamma Emission From Nuclear Isomers," J. J. Carroll, Laser Physics Letters (in press for 2004).

Summary:

This paper surveyed the status of the field of study into induced gamma emission, and in particular detailed the conflicting results into low-energy triggered gamma emission from ^{178m2}Hf.

"Ups and downs of nuclear isomers," P. J. Walker and J. J. Carroll, Physics Today June 2005, p. 39.

Summary:

This paper surveys the aspects of nuclear isomers that allows them to provide unique tests of nuclear structure and to suggest possible applications.

MANUSCRIPT IN PROGRESS

Preparation of a manuscript describing the searches for "slow" and "prompt" low-energy triggered gamma emission from ^{178m2}Hf has begun and submission to Physical Review C is anticipated during the first third of 2006. This manuscript will therefore describe work performed under this grant. The working title is "Tests of low-energy

triggered gamma emission from ^{178m2}Hf using monochromatic synchrotron radiation at SPring-8."

Experiments performed during the grant period at Germany's Gesellschaft für Schwerionenforschung (Darmstadt) and the University of Stuttgart are still being analyzed and manuscript may be expected at some time during 2006. These were a search for new long-lived isomers and a study of population of ^{176m}Lu by (γ, γ') reactions (with complimentary nuclear resonance fluorescence measurements), respectively.

REFERENCES

1. P. M. Walker and G. Dracoulis, Nature 399, 35 (1999).
2. P. M. Walker and J. J. Carroll, Physics Today, 39 (June 2005).
3. M. B. Smith, P. M. Walker, G. C. Ball, et al., Phys Rev. C 68, 031302(R) (2003).
4. H. Roberts, Hyperfine Int. 107, 91 (1997).
5. J. J. Carroll, S. A. Karamian, L. A. Rivlin, et al., Hyperfine Int. 135, 3 (2001).
6. D. Belic, C. Arlandini, J. Besserer, et al., Phys. Rev. Lett. 83, 5242 (1999).
7. D. Belic, C. Arlandini, J. Besserer, et al., Phys. Rev. C 65, 035801 (2002).
8. P. M. Walker, G. D. Dracoulis, and J. J. Carroll, Phys. Rev C 64, 061302 (2001).
9. C. B. Collins and J. J. Carroll, Laser Phys. 5, 209 (1995).
10. C. B. Collins, J. J. Carroll, Y. T. Oganessian, et al., Laser Phys. 5, 280 (1995).
11. C. B. Collins, F. Davanloo, M. C. Iosif, et al., Phys. Rev. Lett. 82, 695 (1999).
12. C. B. Collins, F. Davanloo, M. C. Iosif, et al., Laser Phys. 9, 8 (1999).
13. J. J. Carroll, Laser Phys. Lett. 1, 275 (2004).
14. S. A. Karamian and J. J. Carroll, Laser Phys. 11, 23 (2001).

APPENDIX A

PUBLICATIONS FROM WORK CONDUCTED UNDER GRANT

"Design and characterization of a compact multi-detector array for studies of triggered gamma emission: spontaneous decay of ^{178m2}Hf as a test case," P. Ugorowski, R. Propri, S. A. Karamian, J. Lazich, D. Gohlke, N. Caldwell, S. C. Ravuri, M. Helba and J. J. Carroll, Nucl. Instrum. Meth. A (submitted 2006). **PREPRINT**

"$K^{\pi} = 0^{+}$ 2.29 s isomer in neutron-rich ^{174}Tm," R. S. Chakrawarthy, P. M. Walker, J. J. Ressler, C. J. Pearson, G. C. Ball, D. Bandyopadhyay, E. F. Zganjar, M. B. Smith, A. N. Andreyev, S. Ashley, R. A. E. Austin, J. A. Becker, J. J. Carroll, D. S. Cross, D. Gohlke, J. J. Daoud, P. E. Garrett, G. F. Grinyer, G. Hackman, G. A. Jones, R. Kanungo, Y. Litvinov, A. C. Morton, W. J. Mills, R. Propri, C. E. Svensson, R. Wheeler and S. J. Williams, Phys. Rev. C (accepted for 2006). **PREPRINT**

"Production of long-lived hafnium isomers in reactor irradiations," S. A. Karamian, J. J. Carroll, J. Adam, E. N. Kulagin, and E. P. Shabalin, High Energy Density Phys. (submitted 2005). **PREPRINT**

"Ups and downs of nuclear isomers," P. M. Walker and J. J. Carroll, Physics Today June 2005, p. 39. **REPRINT**

"Limits on nuclear excitation and de-excitation of ^{178m2}Hf by electron-nucleus coupling," M. R. Harston and J. J. Carroll, Laser Physics 15, 487 (2005). **REPRINT**

"Nuclear excitation and de-excitation in resonant electronic transitions," M. R. Harston and J. J. Carroll, Laser Physics 14, 1452 (2004). **REPRINT**

"Production of the ^{178m2}Hf isomer using a 4.5-GeV electron accelerator," S. A. Karamian, J. J. Carroll, J. Adam and N. A. Demekhina, Nuclear Instruments and Methods A 530, 463 (2004). **REPRINT**

"Studies of high-K isomers at TRIUMF-ISAC," M. B. Smith, P. M. Walker, R. S. Chakrawarthy, R. A. E. Austin, G. C. Ball, J. J. Carroll, E. Cunningham, P. Finlay, P. E. Garrett, G. Grinyer, G. Hackman, B. Hyland, K. Koopmans, W. D. Kulp, J. R. Leslie, A. A. Phillips, R. Propri, P. H. Regan, F. Sarazin, M. A. Schumaker, H. C. Scraggs, T. Shizuma, C. E. Svensson, J. von Schwarzenberg, J. C. Waddington, D. Ward, J. L. Wood, B. Washbrook and E. F. Zganjar, Nuclear Physics A 746, 617 (2004). **REPRINT**

"An Experimental Perspective On Triggered Gamma Emission From Nuclear Isomers," J. J. Carroll, Laser Physics Letters 1, 275 (2004). **REPRINT**

"Possible Ways for Triggering the ^{179m2}Hf isomer," S. A. Karamian, J. J. Carroll, L. A. Rivlin, A. A. Zadernovsky and F .J. Agee, Laser Physics 14, 166 (2004). **REPRINT**

"Formation of the high-spin ^{179m2}Hf isomer in reactor irradiations," S. A. Karamian, J. J. Carroll, J. Adam, E. N. Kulagin and E. P. Shabalin, Laser Physics 14, 438 (2004). **REPRINT**

"Driven energy release of nuclear isomers," L.A. Rivlin, J.J. Carroll and F. J. Agee, Laser Physics 14, 435 (2004). **REPRINT**

"'Forced-gamma emission' studies involving nuclear isomers using fast neutrons and bremsstrahlung x rays," N. A. Guardala, J. L. Price, J. H. Barkyoumb, R. J. Abbundi, G. Merkel and J. J. Carroll, in *Applications of Accelerators in Research and Industry* (American Institute of Physics, Melville, New York, 2003). **REPRINT**

"Gamma rays emitted in the decay of 31-year ^{178m2}Hf," M. B. Smith, P. M. Walker, G. C. Ball, J. J. Carroll, P. E. Garrett, G. Hackman, R. Propri, F. Sarazin and H. C. Scraggs, Phys. Rev. C 68, 031302(R) (2003). **REPRINT**

"Hybridization of atomic-nuclear excitations and pumping of nuclear levels," S. A. Karamian and J. J. Carroll, Laser Phys. 13, 1182 (2003). **REPRINT**

"Photon scattering experiments on ^{176}Hf and the systematics of low-lying dipole modes in the stable even-even Hf isotopes $^{172, 178, 180}$Hf," M. Scheck, D. Belic, P. von Brentano, J. J. Carroll, A. Gade, H. von Garrel, U. Kneissl, C. Kohstall, A. Linnemann, N. Pietralla, H. H. Pitz, F. Stedile, R. Toman and V. Werner, Phys. Rev. C 67, 064313-1-7 (2003). **REPRINT**

"Initial search for triggered gamma emission from ^{178}Hf^{m2} using the YSU miniball array," J. J. Carroll, J. Burnett, T. Drummond, J. Lepak, R. Propri, D. Smith, S. A. Karamian, J. Adam, F. Stedile and F. J. Agee, Hyperfine Int. 143, 37 (2003). **REPRINT**

"Proposal for Observation of a Hidden Nuclear Population Inversion," F. J. Agee, J. J. Carroll, L. A. Rivlin and V. Vuletic, Hyperfine Int. 143, 7 (2003). **REPRINT**

"Beam-based production of ^{178m2}Hf," J. Paul Farrell, V. Dudnikov, J. J. Carroll and G. Merkel, Hyperfine Int. 143, 55 (2003). **REPRINT**

"Possibility of combining nuclear level pumping in a plasma with lasing in a solid," S. A. Karamian and J. J. Carroll, Hyperfine Int. 143, 69 (2003). **REPRINT**

"Gamma spectroscopy of Hf-178m2 using synchrotron x-rays," H. E. Roberts, M. Helba, J. J. Carroll, J. Burnett, T. Drummond, J. Lepak, R. Propri, Z. Zhong and F. J. Agee, Hyperfine Int. 143, 111 (2003). **REPRINT**

"Non-radiative triggering of long-lived nuclear isomers," A. A. Zadernovsky and J. J. Carroll, Hyperfine Int. 143, 153 (2003). **REPRINT**

"Photo-induced depopulation of the $^{180}Ta^{m}$ isomer via low-lying intermediate states: Structure and astrophysical implications," D. Belic, C. Arlandini, J. Besserer, J. de Boer, J. J. Carroll, J. Enders, T. Hartmann, F. Käppeler, H. Kaiser, U. Kneissl, E. Kolbe, K. Langanke, M. Loewe, H. J. Maier, H. Maser, P. Mohr, P. von Neumann-Cosel, A. Nord, H. H. Pitz, A. Richter, M. Schumann, F.-K. Thielemann, S. Volz, and A. Zilges, Phys. Rev. C 65, 035801-1-13 (2002). **REPRINT**

DESIGN AND CHARACTERIZATION OF A COMPACT MULTI-DETECTOR ARRAY FOR STUDIES OF INDUCED GAMMA EMISSION: SPONTANEOUS DECAY OF ^{178m2}Hf AS A TEST CASE

P. Ugorowski,[a] R. Propri,[a] S. A. Karamian,[b] D. Gohlke,[a] J. Lazich,[a] N. Caldwell,[a] R. S. Chakrawarthy,[c,d] M. Helba,[e] H. Roberts[e] and J. J. Carroll[a*]

[a] Department of Physics and Astronomy, Youngstown State University, One University Plaza, Youngstown, OH 44555
[b] Flerov Laboratory of Nuclear Reactions, Joint Institute for Nuclear Research, 141980 Dubna, Russia
[c] Department of Chemistry, Simon Fraser University, Burnaby, British Columbia V5A 1S6 Canada
[d] TRIUMF, Vancouver, British Columbia V6T 2A3, Canada
[e] SRS Technologies, Inc., Systems Technology Group, Huntsville, AL 35806

Abstract

Reports that incident photons near 10 keV can induce the emission of gamma rays with concomitant energy release from the 31-year isomer of ^{178}Hf challenge established models of nuclear and atomic physics. In order to provide a direct and independent assessment of these claims, a multi-detector system was designed as a specialized research tool. The so-called YSU miniball is unique in its combination of performance characteristics, compact size and portability, enabling it to be easily transported to and placed within the confines of beamline hutches at synchrotron radiation sources. Monochromatic synchrotron radiation was used in the most recent studies from which evidence of prompt triggering was claimed, suggesting similar sites for independent tests of these results. The miniball array consists of six high-efficiency BGO scintillators coupled with a single 65% Ge detector and provides time-resolved gamma-ray calorimetry rather than purely spectroscopic data. The need to record high detected folds from the array (up to seven-fold gamma coincidences) makes this system different in practice from standard spectroscopic arrays for which data is typically restricted to triples or lower folds. Here the system requirements and design are discussed, as well as its performance as characterized using the well-known natural decay cascades of ^{178m2}Hf. This serves as the foundation for subsequent high-sensitivity searches for low-energy triggering of gamma emission from this isomer.

PACS: 23.20.Lv; 27.70.+q, 29.30.-h, 29.30.Kv

Keywords: Multi-detector array, gamma-ray calorimetry, induced gamma emission, isomer, ^{178m2}Hf

* Corresponding author: jjcarroll@cc.ysu.edu
Tel: 330-941-3617 FAX: 330-941-3121

1. Introduction

The possibility that nuclear energy could be released in a relatively clean fashion from long-lived nuclear isomers has been under consideration for decades [1]. Such metastable states are capable of storing considerable energy for rather long durations. The archetype is ^{180m}Ta, being an excited state with a halflife greater than 10^{15} years and located 75 keV above the unstable ground state [2]. An induced depopulation of this isomer due to irradiation of samples with real photons (bremsstrahlung) was first observed in 1987 [3] with detailed confirmation and characterization of the process coming later (see Ref. [4] and references therein). The induced depopulation was accompanied by a release of the stored 75 keV, but was initiated by incident photons of at least 1 MeV, proving to be a sink rather than a source of energy. Nevertheless, the existence of transitions connecting the isomer to levels that decay to the ground state provided intriguing insight into weak components in the wavefunctions [5].

Other isomers have been suggested as being potentially of greater practical value [1]. Principal among these is the 31-year-lived isomer ^{178m2}Hf, storing 2.446 MeV per nucleus, or about 1.3 GigaJoules/gram at natural density. Studies which attempted to replicate the induced depopulation of ^{180m}Ta for ^{178m2}Hf have concentrated so far on rather low energies, using real photons below 100 keV from bremsstrahlung and synchrotrons. Experiments using virtual photons via Coulomb excitation have been conducted on ground-state ^{178}Hf targets, providing results that support the possibility of induced depopulation of ^{178m2}Hf by transitions with energies greater than 300 keV [6, 7]. Reference [8] surveys the experimental landscape as of early 2004, and later results or additional details of previous results are described in Refs. [9-11]. The controversial nature of the positive results, in light of several carefully-conducted null measurements, perhaps reached its zenith with the recent report [9] that induced depopulation of the ^{178m2}Hf isomer, with $J^{\pi} = K^{\pi} = 16^{+}$, proceeded through an intermediate, higher-lying state that subsequently decayed to the ground state in a single transition. Since only a modest-multipolarity transition from isomer to intermediate state could be expected, this would seem to require a $\Delta J > 10$ transition for the purported decay transition.

While the latter claim of induced depopulation of ^{178m2}Hf would appear to require little further consideration, other previous claims are not unphysical *a priori*, although theoretical analyses have cast doubt on the purported mechanism [12, 13]. As in the case of ^{180}Ta and other nuclei (see, for example, Ref. [14]), the presence of K-forbidden transitions in ^{178}Hf, likely required for an induced depopulation, would provide important nuclear structure information. Depletion caused by incident photons of low energies, reported to be near 10 keV, would also have important implications to the understanding of nuclear-electron couplings and potential applications. Also, despite continued positive claims the magnitude of the effect remains rather small. Thus, improved experimental methods by which to better examine these claims will be valuable.

All of the most recent positive results (see the survey of Ref. [8] and Refs. [9, 11]) were obtained using monochromatic synchrotron radiation (either from bending magnets or undulators) as the source of incident photons. Most null experiments were, in contrast,

obtained using continuum radiation sources, including bremsstrahlung [15] or "white" synchrotron radiation [10, 16, 17] and thus presented unique experimental challenges that differed from the positive measurements. Also, in the null results of Refs. [9, 11] no special timing instruments were used by which any relationship between pulses of synchrotron radiation and gamma rays emitted from the ^{178m2}Hf sample could have been recorded. It has been claimed that excess gamma-ray emission triggered by incident photons near 10 keV was prompt, coming within a few nanoseconds of the pulses of synchrotron radiation [11, 18], and thus that the duty cycle of the synchrotron would lead to a washing out of the signal without timing information. Reference [18] suggests (see page 164) that this explains the null measurements. An independent examination of the positive reports of prompt triggered gamma emission, induced by monochromatic synchrotron radiation near 10 keV, requires a different approach than was taken in the works of Refs. [10, 16, 17]. For this purpose, a multi-detector gamma spectroscopic system was developed in a compact configuration that permitted its emplacement within the confines of the radiation hutch at the BL12B2 beamline of the SPring-8 synchrotron. This beamline was chosen as providing similar radiation characteristics to those utilized to obtain some positive results at SPring-8. These independent tests will be described in a future work [19].

This paper will first discuss the design requirements and implementation for the miniball system (Section 2) as needed to search for prompt triggered gamma emission from ^{178m2}Hf. Then the sensitivity of the array for detection of gamma-ray cascades will be covered, as measured from the well-known natural decay of this isomer. This will include determination of the system efficiency and detection limits for gamma-ray calorimetry (Section 3).

2. Detection system

2.1 Design requirements and configuration

Many multi-detector arrays have been constructed for high-resolution gamma-ray spectroscopy [20], such as the well-known Gammasphere system. The large value and physical size of these systems and their associated instrumentation make it infeasible to consider transporting them to sites such as SPring-8 and emplacing them within the confines of beamline hutches for experiments of short duration. Thus, it was necessary to develop a unique system of modest size that combined some spectroscopic capabilities with the essential ability to perform gamma-ray calorimetry. The present system was designated as the *YSU miniball*, stressing its similarities with much larger arrays, although its design is predicated on a very specific type of experiment. Initial design of the system occurred in 2001 [21] and an implementation was used in works described in Refs. [8, 15].

Figure 1 is a schematic energy-level diagram of the ^{178}Hf nucleus, which possesses several isomers. The long-lived (metastable) levels are those at 1,147.4 keV, with a halflife of 4 s (*m1*), and at 2,446.1 keV, with a halflife of 31 years (*m2*). The figure shows the main transitions resulting from the natural decay of the 31-year

isomer [22]. Also depicted is a sketch of a general process of induced energy release that begins with excitation of a nucleus initially in the *m2* state to a higher-lying intermediate state. Back-decay (E) of the intermediate state to the isomer provides only elastic scattering of the incident entity, assumed to be real photons. Other decay branches of the intermediate state may bypass the *m2* level and initiate cascades that eventually reach the stable ground state. These branches would provide a means by which the 2,446.1 keV stored by the 31-year isomer could be released via gamma rays and conversion electrons. These branches may be generally characterized as *prompt* (P), in which the cascade from the intermediate state reaches the ground-state band immediately, *slow* (S), in which the cascade reaches the *m1* band, and *other* (O). The latter type of cascade bypasses the 4-s isomer, but may pass through some states that have significant halflives on the time scale of a detection system. Reports of induced energy release, so-called triggered gamma emission, have so far been restricted to incident photons energies near 10 keV. Below an energy of (2,446.1 + 10) keV, known levels have halflives less than 1.5 ns with the exception of the *m1* metastable state and a shorter-lived isomer at 1,554.0 keV ($T_{1/2}$ = 77.5 ns) [2].

Figure 1 placement

As mentioned above, recent reports of positive evidence of triggering indicated that the gamma emission was prompt, coming within 1 ns of the pulse of incident synchrotron radiation [11]. In that work, a small-volume Ge detector was used to measure gamma rays emitted from a sample containing ^{178m2}Hf as it was being irradiated with monochromatic synchrotron radiation near 10 keV. Spectroscopic information was recorded as well as the time between gamma detection and individual pulses of incident radiation. Those pulses were of 20 - 50 ps duration and were separated by several nanoseconds – the time of the pulses was determined by placing an avalanche photodiode in the beam (behind the sample) [11]. Although "1 GHz electronics" were employed for the photodiode [11], the true time resolution between pulses and gamma-ray detection was no doubt more on the order of 10 ns as is typical for Ge detectors. In any event, that report precludes cascades that are delayed by passage through the 77.5-ns isomer.

The ^{178}Hf nucleus provides a natural way of testing this claim of prompt gamma emission without the need to record the times for pulses of incident synchrotron radiation. As discussed in Refs. [15, 21] and seen in Fig. 1, spontaneous decay of the *m2* isomer occurs via two bursts of gamma rays, each of which consists of a cascade with inter-transition delays less than 1.5 ns. The first burst occurs from transitions within the *m1* band, after decay of the *m2* state, and is stopped briefly by the 4-s isomer. The total energy released in the first cascade from the 16^+ *m2* isomer to the 8^- *m1* isomer is 1,298.7 keV, while the energy released in the second cascade from the *m1* isomer to the ground state is 1,147.4 keV. Within each cascade the gamma rays are simultaneous on the scale of the resolving time of Ge spectrometers. If the gamma rays were detected with sufficiently high efficiency by a large-solid angle array, a summation of their energies would coincide with the total energies of the bursts, minus any energy lost into conversion electrons and therefore invisible to the Ge detectors. Conversely, prompt gamma emission due to the claimed induced energy release would produce a single burst

of gamma rays with total energy of (2,446.1 + 10) keV. Gamma-ray calorimetry would therefore distinguish clearly between prompt triggered events and those from natural decay. Such high-summed-energy cascades could only be due to triggering, so they would be of necessity correlated with incident pulses of synchrotron radiation without any need to explicitly record the time of those pulses.

The YSU miniball is designed to perform this function of time-resolved gamma-ray calorimetry using a compact array. A photograph of the miniball located with the BL12B2 hutch at SPring-8 is shown in Fig. 2. A balance between performance and portability was achieved by using six 3.0" diameter × 2.5" long BGO crystals to provide high solid angle (about 83% of 4π) and high intrinsic efficiency. NaI(Tl) crystals were employed in previous implementations [15, 21], but the lower peak-to-Compton ratio of that scintillator material compared with BGO made interpretation of spectra more difficult, thus the change to BGO. Many reports of induced energy release indicated evidence of the emission of gamma rays at energies not part of the natural decay cascades (see the survey of Ref. [8]). High-resolution spectroscopy would be advantageous in identifying any such unusual gamma rays, but this would be precluded by the use of BGO scintillators. In order to insure that every gamma-emission event observed by the array contained one gamma ray having a precisely determined energy, a 65% relative efficiency p-type Ge detector was coupled instrumentally to the BGO crystals. The large-volume Ge detector observed the sample through a gap between BGO detectors along one of the diagonals of a cubic support structure.

Figure 2 placement

Use of a p-type crystal, with its associated thin Al-end window, was beneficial for spectra taken under irradiation in that the window would provide filtering of any incident radiation near 10 keV that was scattered toward the detector. Aluminum windows on the BGO crystal housings provided similar shielding, minimizing the chance of pile up between scattered synchrotron radiation and gamma rays.

Figure 2 also shows the placement of a second Ge detector (10% efficiency n-type) and an x-ray detector, both of which observed the sample through other diagonals of the cube. These were used as parts of independent systems to obtain a separate singles spectrum (no coincidence) and a calibration of the scattered synchrotron radiation during exposures. They have no impact on the characterization of the miniball system and are not discussed further.

2.2 Instrumentation

A schematic of the pulse-processing instrumentation for the miniball is given in Fig. 3. Once data acquisition was enabled, recording of a gamma-emission event was initiated only when the Ge detector observed a gamma ray. One preamplifier output from the Ge detector was sent to an Ortec 579 Fast Filter Amplifier and then to an Ortec 583 constant-fraction (CF) discriminator to provide a master gate channel. The ARC method [23] was employed with this discriminator and its threshold set a minimum energy for

recorded gamma rays into the Ge detector. The discriminator's NIM output was stretched and converted to TTL by a Stanford DG535 pulse generator. The output from the pulse generator served as the system gate and its width and delay could be adjusted over a wide range.

Figure 3 placement

High voltage to the Ge detector was provided using a standard Ortec module that utilized manual front-panel controls. High voltage to each BGO's PMT was provided by a single octal NIM module from Radiation Technologies, Inc. that was computer controlled and allowed remote changes on the order of a few volts.

A FERA/CAMAC system was employed to record spectroscopic and time information from the detectors, chosen for its flexible programmability using Sparrow's KMaxNT software and for buffering and fast transfer of data. A customized toolsheet was built in this platform to control data acquisition, including operating parameters like ADC thresholds, data word sizes, use of zero-suppression, buffer size, etc., and to monitor individual detector energy and time spectra in real-time. The FERA hardware was managed by a CMC 203 driver that received the system gate and distributed it to two Ortec AD413A quad 8k peak-sensing ADC's and a Silena 4418/T octal TDC. Spectroscopic pulses from the Ge detector were input to an Ortec 672 linear amplifier with a shaping time of 2 μs and its unipolar output was digitized with one channel of an AD413A. Output from the BGO PMT's was routed first to an Ortec CF8000 octal CF discriminator. A buffered spectroscopic signal was available from each CF8000 channel whereby spectroscopic signals from the BGO detectors were fed to separate Ortec 672 amplifiers with shaping times of 2 μs. The bipolar signals from these amplifiers were digitized by other channels of the AD413A's after inversion, which provided the best linearity and resolution.

Negative NIM signals were output by each channel of the CF8000 as timing signals when the incoming PMT pulses exceeded adjustable thresholds. These timing signals were stretched by separate channels of an Ortec GG8010 and then converted to ECL standard signals by separate channels of a Phillips 7126 level translator prior to being input to the TDC. The leading edge of the gate distributed by the driver via the FERA bus served as a START pulse to the TDC and the pulses originating from BGO PMT's served as STOP markers. This allowed recording of the relative time interval between a master Ge signal and those from each individual BGO detector. The TDC provided an active time window of 2.8-μs duration, during which START-STOP times were logged as distributed over 3840 channels – the module used an additional 256 channels for sliding-scale non-linearity compensation. The resolution of the TDC was 0.73 ns/channel, considerably shorter than the inherent time resolution obtainable from the Ge and BGO detectors after pulse processing, being both on the order of tens of ns. The temporal relationships between the gate, spectroscopic and timing pulses are shown in Figs. 4 and 5.

Figure 4 placement

Figure 5 placement

Although not suitable for extended discussion herein, it is worth noting that while CAMAC is an international standard this is not the case for the FERA system. The Fast Encoding and Readout ADC approach was developed by Lecroy to provide data transfers between CAMAC modules at rates in excess of that supported by the CAMAC backplane. FERA utilizes ECL signals on a front-panel bus distributed and managed by the driver module. Via handshakes the driver receives data from ADC's and TDC's and assembles these separate parameters (data pieces) into an event, then buffers many events either internally or in a separate memory module. In this system, when the internal buffer was ¾ full, a Look At Me (LAM) was sent to the controlling computer to cause an upload of data. FERA handshake protocols are not fully standardized, therefore the amount of effort required to regularize communications between the driver and the Ortec and Silena modules should not go unrecognized. It is also worth noting that direct observation of signals on the FERA bus destabilized the communications between driver and other modules, an impediment to this regularization.

An absolute time for each event was assigned with 20-ns resolution by the CMC 203 CAMAC driver based on when it received a gate relative to the start of acquisition. Each parameter was a 32-bit word, two of which were used to record the absolute event time. This instrumental resolution was far better than that supported by the detectors themselves. A one-parameter header of constant digital value was inserted at the beginning of each event, so that events in which incomplete handshakes caused some parameters to be lost by the driver could be excluded as having too few parameters. A total of nineteen 32-bit parameters was recorded in each good event – off-line sorting of the data sets indicated that only 1 out of every 300 events was incomplete and such bad events were discarded off-line prior to data analysis.

Zero-suppression mode was not employed in the ADC's so as to avoid having events of varying lengths. Each ADC module possessed four inputs with a processing time of 6 μs per active input and 1.8 μs per inactive input. Readout of the ADC's to the driver was found experimentally to require 7.4 μs following the end of digitization. The total processing time for the ADC's could, therefore, vary in duration, but the TDC introduced a fixed deadtime of 33 μs that included digitization of the START-STOP delay and readout of the module. Output of additional gates from the DG535 was inhibited for a period chosen at 50 μs to avoid the possibility of interference with processing of the current event.

Proper digitization of spectroscopic and TDC STOP signals required use of the GG8010 and DG535 units to introduce appropriate delays at various points in the different channels. These modules also allowed matching of pulse widths to the demands of subsequent units in the data streams. For example, the Ge spectroscopic pulse was input into a linear amplifier set for triangular shaping with a 2-μs time constant. This shaping time had the added effect of introducing a delay of 5 μs between the peak of the initial pulse from the Ge preamplifier and the amplified pulse. The output of the DG535,

serving as the system gate, was delayed and its width set to insure full digitization of the spectroscopic pulse by the ADC.

The use of preamplifiers for the BGO signals was considered, but rejected due to the inability to maintain a sufficiently fast risetime with available units. The PMT outputs were input directly into the CF8000, which produced both time marks and buffered spectroscopic signals. Tests showed that the best resolution for a BGO crystal was obtained by using the bipolar amplifier outputs and triangular shaping. The resulting resolution was found to be 8% for the ^{60}Co 1332 keV peak, as shown in Fig. 6. Proper digitization of peak heights by the ADC's required those peaks to not occur within 1 μs of the start or end of the gate. A gate duration of 5 μs was utilized to meet this condition based on the delays and widths of the spectroscopic pulses for the Ge and BGO channels.

Figure 6 placement

As mentioned previously, timing pulses from the CF8000 were stretched, delayed and converted to ECL as needed for proper digitization by the TDC. Valid STOP signals had to reach the TDC during its 2.8-μs active period that began with the leading edge of the gate. Lack of a valid STOP pulse to the TDC during the active period was recorded as an increment of one count within the sliding-scale region. Invalid STOPs occurred for several reasons, as discussed later. The delays were selected so that true coincidence STOPS appeared at roughly channel 1500 for each TDC input by obtaining coincidence curves using the histogramming feature of the Tektronix TDS-5104 1-GHz digital oscilloscope. Figure 5 shows a scope trace displaying the gate and STOP pulses from a single BGO, generated with a ^{60}Co source. Also shown in the figure is a histogram of the numbers of STOP pulses occurring as a function of time. The delay for this STOP stream was set so that coincidence between gamma rays entering the Ge (START) and this BGO produced a time marker within the gate.

Off-line sorting of data sets to extract singles or higher-fold spectra for any detector or combination of detectors was accomplished using an in-house software suite that was custom designed [24] for the miniball system. The software allowed sorting based on energy and timing parameters for each detector and determination of summed energy and detected fold from the BGO crystals.

Standard calibration sources were used to assess the basic performance of the miniball system as was done in earlier stages of its development [15]. Because the spontaneous decay of ^{178m2}Hf has been extensively characterized [22] and because the eventual aim was to perform trigger studies in subsequent experiments [19], it was decided to perform efficiency calibrations using a mixed ^{178m2}Hf/^{172}Hf sample. This approach benefited from the number and distribution of gamma lines, and the available coincidence.

One particular test with a standard calibration source was particularly valuable. A ^{137}Cs source was employed to investigate the possibility of Compton scattering in one detector causing coincident events in other detectors. Discriminator thresholds in the

miniball instrumentation eliminated x rays from recorded events, so that only random coincidences should have been in evidence from this single-line source. Figure 7a shows a time spectrum obtained for one BGO crystal. A small coincidence peak was seen and interpreted as being due to Compton cross-talk between the Ge and that BGO. Such cross-talk could occur between any detectors. A 1-mm Pb wrap was applied around the BGO crystals as they extended within the cubic support structure, resulting in the time spectrum shown in Fig. 7b in which this cross-talk was eliminated. It should be noted that no filters were applied to the faces of any of the detectors, other than the thin Al detector housings.

Figure 7 placement

3. Characterization using ^{178m2}Hf decay

3.1 Sample composition and configuration

The miniball performance was principally characterized by gamma rays emitted in spontaneous decays within a mixed ^{178m2}Hf/^{172}Hf source. This characterization was chosen, as mentioned above, to serve as the foundation for experiments conducted specifically to search for evidence of prompt induced energy release during subsequent irradiations with synchrotron radiation.

Figure 8 shows a photograph of the sample employed in this work, attached to a positioning arm. The mechanical construction of the sample consisted of an Al frame that held together two 1-mm thick Be disks. The hafnium material was deposited by evaporation on one Be disk and occupied a roughly circular spot near the center of that disk.[†] The details of the distribution are not important for the present discussion, other than the fact that the radioactive Hf did not constitute a point source. The active content included 0.37 μCi of ^{178m2}Hf (2.0×10^{13} nuclei or 5.79 ng) and 0.29 μCi of ^{172}Hf (9.3×10^{11} nuclei or 0.26 ng) at the time of the tests in June 2004. It has been estimated [25] that the total hafnium content was approximately 2,500× that of the active ^{178m2}Hf material, which was produced by proton spallation [26]. The isomer-to-ground-state ratio for ^{178}Hf in the sample was also estimated [25] to be about 1:500. The sample was held within the miniball in the central cavity formed by the faces of the BGO crystals using the aluminum positioning arm that extended through one of the half diagonals of the cubic support structure. One full diagonal of the cube was reserved as the entrance and exit channels for synchrotron radiation. The large Ge detector coupled to the BGOs, an independent small Ge and an x-ray detector utilized separate half diagonals as viewing ports. The positioning arm was affixed outside the miniball structure to a translation table so that the sample could be moved remotely in a vertical plane. The orientation of

---

[†] The distribution of hafnium material within the deposit was determined by passing a narrow (0.5 mm × 0.5 mm) beam of monochromatized synchrotron radiation set to the L_3 edge of Hf through the opening in the Al sample frame. Transmission of the radiation was recorded by pre- and post-sample ionization chambers as a function of sample position as it was raster-scanned across the fixed beam axis. (This procedure is discussed in detail in a forthcoming manuscript on searches for prompt triggered gamma emission.)

the sample was determined by the eventual need to irradiate the largest possible area of the hafnium deposit with a beam spot of smaller dimensions.

Figure 8 placement

3.2 Singles spectra, timing and detector efficiencies

Gamma radiation emitted due to natural decay of ^{178m2}Hf and ^{172}Hf within the mixed sample was recorded by the miniball system for a period of about 74 hours. At regular intervals of about 12 hours, the small dewar on the Ge detector was filled and data acquisition was halted for this period. The BGO PMT's were gain matched after each fill by minor adjustments to their operating voltages via software control. The Ge detector evidenced no gain drift and its voltage was maintained throughout the measurement. The data set consisted of 6,831 3.5-MB files, each containing about 48,000 recorded events, from which a singles Ge spectrum was extracted as shown in Fig. 9. This was accomplished by first removing events of incorrect length, i.e. wrong number of parameters, which comprised about 0.3% of the data. Then the data was sorted without imposition of any conditions on coincidence between the Ge and BGO detectors or on detector pulse heights. The inset in the figure shows an expanded section of the spectrum that contains the doublet of lines at 213 keV and 217 keV that occur in the spontaneous decay of ^{178m2}Hf. The latter of these lines comes from the $9^- \rightarrow 8^-$ transition just above the *m1* isomer while the former originates with the $4^+ \rightarrow 2^+$ transition in the ground-state band (see Fig. 1). The doublet is well-separated, indicating excellent performance for spectroscopy with this detector and confirming no measurable gain shift. All peaks in the spectrum were positively identified as corresponding to gamma rays from spontaneous decay of ^{178m2}Hf, ^{172}Hf and its daughters, and natural background. The total event rate in the Ge was 1.2 kHz and deadtime resulting from this rate was on the order of 6%.

Figure 9 placement

An initial question was the degree to which the efficiency of the large-volume Ge detector was influenced by the small gap through which it viewed the central cavity of the miniball. The restricted view was due to the BGO crystals and their Pb wraps and would partially shield the sample from view by the Ge detector. It was not possible to test this in the beamline hutch, so data were taken at Youngstown State University. Ge singles spectra were extracted from miniball data obtained using the hafnium source in two different geometric configurations: first, with the BGOs and Pb wraps in place and, second, with those BGOs and wraps removed which would otherwise have restricted the view of the Ge detector. Figure 10a shows the "direct" efficiencies obtained from these measurements using the standard form

$$N_i = ATf_i\varepsilon_i \quad , \tag{1}$$

where N_i is the number of counts contained within a given full-energy Ge peak, A is the sample activity, T is the acquisition live time, f_i is the fraction of decay events that emit γ_i

and ε_i is the full-energy peak efficiency for detection of the specific gamma ray. The f_i values used in Eq. (1) were obtained from the ENSDF [2] as listed in Appendix A and peak fits were obtained using the commercial FitzPeaks program [27]. The effect of the gap between BGO crystals was to suppress the overall efficiency, but less so at higher gamma-ray energies where the cross section for photoelectric interactions decreases. Gamma rays entered only the central section of the Ge crystal and Compton-scattered photons therefrom had other opportunities to interact in the outer part of the detector. This produced the flattened efficiency curve shown in Fig. 10a when all BGO and wraps were in-place. Figure 10b shows the actual Ge efficiency curve from data obtained at SPring-8, being about 0.35% near 1 MeV.

Figure 10 placement

It was possible to provide an additional verification of the magnitude of the direct efficiency values. The method described in Appendix B was employed to obtain efficiencies based on the relationship between the number of counts in individual full-energy peaks and corresponding sum peaks appearing in the singles spectrum. Efficiencies determined in this way for specific pairs of gamma-ray energies are also plotted in Fig. 10b. It was not necessary for full-energy peaks in the Ge singles spectrum to be corrected for summing losses due to the small relative magnitude of this effect. The situation was different for the scintillators, as discussed below, which were closer to the sample and therefore had higher detection efficiencies.

Singles spectra were also extracted for each BGO detector and one example is shown in Fig. 11. Again, no sorting conditions were imposed on the data, but the instrumentation required coincidence with a count from the Ge detector. The largest peaks in the spectrum were identified with intense gamma rays from ^{178m2}Hf and ^{172}Hf decays. The spectrum excludes the low-energy part of the 89/93-keV doublet due to the minimum thresholds in the CF discriminator. Clearly, spectroscopy with the BGO was severely inhibited due to the wide peaks, particularly for the many overlapping lines from the hafnium source. This same difficulty was found when attempting to determine the BGO efficiency using multi-line calibration sources such as ^{152}Eu. In no case could FitzPeaks provide meaningful fits for BGO spectra, but the well-known TV program [28] was able to provide accurate fits for singlets, with systematic errors on the order of 5% or less for sources such as ^{109}Cd or ^{137}Cs. It was also possible to obtain reasonable fits for the lines from ^{60}Co which were sufficiently resolved (see Fig. 6) and the efficiency for gamma-ray detection at 1,332 keV in a single BGO crystal was about 1%. The paucity of points from single-line sources did not provide a suitable efficiency calibration over a wide range of energies, so a different procedure was employed.

Figure 11 placement

A time spectrum obtained from a single BGO detector is shown in Figure 12, extracted from the full data set. A START signal opened an active interval for the TDC such that STOP pulses occurring during this interval were distributed throughout the spectrum, as discussed above. Events in which a) no gamma ray entered the BGO

crystal, b) no STOP pulse was generated because its energy was below the discriminator threshold, or c) a STOP pulse was generated too late for the active window, were recorded in the sliding-scale section. Delays in the timing channels placed coincidence between Ge and BGO detectors at roughly the center of the active range. The shape of the coincidence curve in the figure indicated walk from low-energy pulses in the Ge channel as the origin of the shoulder to the left of the main coincidence peak. The smaller shoulder to the right was due to walk in the BGO channel. The full width of the narrow coincidence peak was 70 channels, corresponding to a resolving time of 51 ns. Based on the constant level of background far from the narrow peak, 0.72% of the counts within the 70-channel width corresponded to random coincidences with respect to the Ge START. Taking a larger width of 700 channels ensured inclusion of true coincidences with walk of either START or STOP signals and of those counts only 2.7% were due to random coincidences. Herein, a full sorting width of 700 channels was employed, but the effective resolving time for true coincidences was still on the order of 50 ns.

Figure 12 placement

Figure 13 shows a part of the γ-γ ("doubles") spectrum for the Ge and one specific BGO, extracted from the data set under the condition of coincidence as discussed above. While singles spectra (like that of Fig. 11) were too complex for fitting, projections of specific ranges in the γ-γ data allowed analysis using TV. Software gates (called cuts in TV) were made using this software,[‡] such as the one shown in Fig. 13 around the 495-keV peak in the Ge projection. The BGO projection for this cut therefore contained coincident photopeaks and Compton events originating in the *m1* band of Fig. 1, and random coincidences. BGO spectra obtained from different cuts were quite sparse compared with a full projection and fits to the broad peaks were performed using the known energies of gamma rays emitted in ^{178m2}Hf and ^{172}Hf decays. Figure 14 shows two BGO spectra corresponding to cuts on 495-keV and 325-keV lines in the Ge projection.

Figure 13 placement

Figure 14 placement

Efficiency values for gamma rays detected by a BGO and in coincidence with the Ge detector were obtained using the peak fits from cut spectra and are plotted in Fig. 15a. Considering a BGO spectrum that resulted from a specific Ge cut around γ_i, the number of counts N_{ji} in a full-energy peak therein was given by

$$N_{ji} = N_i f_{j|i} \varepsilon_j \quad , \qquad (2)$$

[‡] Many other spectrum analysis programs were available, including the powerful Radware suite. The miniball system produces asymmetric data from the different detector types and so TV was chosen as being best suited to this application.

where N_i corresponds to the value in Eq. (1) provided that the cut process included standard background subtraction using channels in the continuum to the right and left of the Ge peak for γ_i. The ε_j denotes the efficiency for detection of a specific γ_j in the BGO in coincidence with the given γ_i on which the cut was made in the Ge projection. The factor $f_{j|i}$ is the fraction of decay events that emit the particular γ_j provided that γ_i was also emitted (see Appendix A). A cut taken on the Ge 213-keV line provided BGO efficiencies for the coincident 325-keV and 426-keV lines. Likewise, a cut on the Ge 426-keV line provided BGO efficiencies for 213 keV and 325 keV. Thus, cross-checking was performed between efficiency values at each specific energy obtained using different cuts. It is worth noting that cut spectra corresponding to the ground state band did not include full-energy gamma-ray peaks at 89 keV and 93 keV from the $8^- \rightarrow 8^+$ and $2^+ \rightarrow 0^+$ transitions, respectively, or from X rays following electron conversion. This was due to the small size of the corresponding unamplified BGO signals which were below the minimum discriminator thresholds. Nevertheless, the spectra evidenced summations between these gamma rays and the main features at 213 keV, 325 keV and 426 keV. Also, summations appeared between X rays emitted following conversion of the 89- and 93-keV transitions and the main gamma lines. These sum events result from triple coincidences in which γ_i enters the Ge detector and both γ_j and γ_k enter a single BGO crystal. To determine the direct efficiencies from Eq. (2), counts in identifiable sum peaks within the BGO singles spectrum were added to the full-energy counts of individual gamma rays. The resulting efficiencies reflected values for hypothetical single-lines sources.

Figure 15 placement

Efficiency values were also determined based on the relationship between individual and sum peaks using the method of Appendix B. Despite their larger statistical errors, their magnitudes confirm the direct efficiencies as shown in Fig. 15a. Systematic errors in fitting of the broad BGO peaks are not shown, but were estimated to be on the order of 10%.

Each scintillator evidenced a unique efficiency curve, as expected. The principal causes were that each detector lay at a slightly different spacing from the sample and that self-absorption was different for each specific sample orientation relative to a given detector. In one case, the CF8000 threshold was obviously lower, enhancing the efficiency for low-energy gamma rays recorded from that BGO. For the following analysis, an averaged efficiency was determined as shown in Fig. 15b to represent the canonical single BGO response.

3.3 Physical multiplicity and detected fold

The miniball system was designed to perform time-resolved calorimetry for gamma-ray cascades resulting from natural decay of ^{178m2}Hf and from possible prompt induced energy release. Figure 16 shows bi-dimensional plots of the Ge energy vs. the summed energy from the scintillators for different values of detected coincidence fold. Every event records at least one gamma ray, from the Ge crystal, so the total detected

fold is designated as 1 + F, where F is the detected fold from the six BGO detectors. Sorting was performed as described above with F being the number of BGO's that produced a valid STOP pulse within the respective coincidence period of the individual detector. The summed gamma-ray energy registered from the BGO detectors was then obtained by adding the individual spectroscopic data from the separate scintillators.

Each natural decay of ^{178m2}Hf produces (see Fig. 1) two gamma-ray bursts from cascades separated by the 4-s *m1* isomer. Only a single cascade occurs below that isomer, releasing a total energy of 1,147 keV and possessing a physical multiplicity of five. However, the 93-keV transition is strongly converted ($\alpha_{93} = 4.74$) and it and the 89-keV transition are suppressed in the BGO spectra due to the discriminator levels. This means that the effective physical multiplicity is reduced to three unless the 89-keV or 93-keV gamma rays register in the Ge detector. The effective triplet cascade then contains the 213-, 325- and 426-keV transitions for a total energy of 964 keV. The cascade above the 4-s isomer releases 1,298.7 keV and contains a number of branches, so that the physical multiplicity ranges from 4 – 6. The first step of the decay, the $16^+ \rightarrow 13^-$ transition at 12.7 keV, is completely converted with $\alpha_{12.7} = 1.39\times10^7$ so the effective physical multiplicity ranges from 3 – 5. The most intense branch (70.7%) occurs through the 574-, 495- and 217-keV transitions with a physical multiplicity of three (53.1% for the gamma-ray triplet). All gamma-ray triplets contribute a total of 72.2%.

Figure 16 placement (full page for a-i)

Decay of ^{172}Hf nuclei in the sample produces gamma rays emitted in many different branched cascades from transitions in ^{172}Lu and ^{172}Yb. From the established nuclear data [2], on the order of 30 cascades correspond to a physical multiplicity of two, on the order of 140 cascades correspond to a physical multiplicity of three and on the order of 360 cascades correspond to a physical multiplicity of four. Higher multiplicity cascades are also possible. Decays of ^{172}Hf and ^{172}Lu can lead to different daughter levels, so cascades of identical physical multiplicity may represent various total energies released by the gamma-ray transitions. Despite the complexity of cascades following ^{172}Hf decay, a physical multiplicity of three represents a major component.

For a given physical multiplicity, the frequency with which a given detected fold F would occur could be modeled using a simple Monte Carlo code. Figure 17a shows a histogram of the calculated detected fold F assuming an energy of 250 keV (thus a BGO photopeak efficiency of 5.4%) for all gammas in the cascade and a physical multiplicity of three. In this idealized case, the detected folds appear in the absolute intensities listed in Table 1 and plotted in Fig. 17a. Also given are measured total counts within bi-dimensional Ge vs. summed BGO spectra for different coincident folds. The general agreement between measured and calculated intensities for different folds is surprisingly good, considering that the spectra contained contributions from different physical multiplicities. Another factor that reduced the accuracy of the calculation was that some coincidence counts in a BGO in coincidence were due to Compton rather than photopeak interactions. Some gamma rays reaching a BGO in coincidence did not provide a valid STOP pulse due to their pulse height so that those events were recorded as having a

detected fold of F - 1 rather than F. This was also the case when coincident summing occurred within a single BGO. For prompt triggered gamma emission, the physical multiplicity will be on the order of eight so that the anticipated distribution of detected folds will be that of Fig. 17b.

Figure 17 placement

Table 1 placement

3.4 Calorimetry

The spectrum of Fig. 16a, with expanded section in Fig. 16b, shows data for a detected fold of 1 + 1 (Ge + any one BGO[§]) and contains numerous paired gamma-ray peaks. In the case of ^{178m2}Hf decay in the cascade below the *m1* isomer, detection of 213 keV in the Ge coincident with detection of 325 keV in one BGO provides a peak while the converse (325 keV in the Ge, 213 keV in the BGO) provides its partner. A line drawn in Fig. 16a connecting these two peaks represents a locus of constant total deposited energy at 538 keV. This is significantly less than the total cascade energy since the physical multiplicity is five and the detected fold is only 1 + 1. Examination of the 1 + 2 spectrum of Fig. 16c, with expanded section in Fig. 16d, shows two loci of γ-γ-γ peaks corresponding to deposited energies of 964 keV and 1,286 keV, representing nearly the full ^{178m1}Hf → ^{178g}Hf and ^{178m2}Hf → ^{178m1}Hf cascades, respectively.

The 1 + 3 spectrum of Figs. 16d and 16e also evidences a locus of 1,286 keV from several cascade branches with physical multiplicity of four above ^{178m1}Hf, while one peak is seen that corresponds to decay of ^{178m1}Hf to the ground state with summed energy of 1,057 keV. The latter peak is actually a doublet of 89-keV and 93-keV lines in the Ge detector from events of physical multiplicity of four in the ground-state band. The peak corresponding to 93 keV in the Ge detector is smaller since the transition is heavily converted. No other peaks from the ground state band can appear with such high detected fold since the 89-keV and 93-keV peaks were suppressed from the BGO detectors due to discriminator thresholds.

In addition to features identified with ^{178m2}Hf, loci of constant summed energy appear in the spectra from cascades following ^{172}Hf decay. For a detected fold of 1 + 1 in Figs. 16a and 16b, paired peaks appear from 900-keV and 1,093-keV transitions, giving a summed energy of 1,993 keV. Many other peaks from ^{172}Hf decay contribute to the 1 + 1 spectrum, although in some instances both partners do not appear. This occurs when the energy of one of the gamma rays is too low to register in the BGO spectrum. For any detected fold, different summed energy loci exist from the numerous decay branches. Gamma-ray cascades in ^{172}Lu have summed energies less than 240 keV. Summed energies of ^{172}Yb cascades reach as high as 2,343 keV (2.57%) after decay of ^{172}Lu, with a total of 9.59% exceeding 2,200 keV.

---

§ This differs from Fig 13 which shows doubles data between the Ge and one specific BGO, but without restrictions on what is recorded by the other BGO scintillators. Figure 16a contains doubles between the Ge and any BGO for the case that exactly one of the BGO registers a coincident gamma ray.

suggested in 1995 that on this basis a trigger level might be found "near 2.8 MeV" [9] from the "speculation that [trigger] levels are prevalent and lie between 2.5 - 2.8 MeV" [10]. First trigger experiments were attempted in 1996 by inelastic scattering of alpha particles at Orsay, with a repeat in 1997, but as yet no firm results are known. The first photon triggering experiments began in late 1998 and the positive indications reported therefrom [11, 12] began the present intense, and controversial [13], period of research.

The field of study of triggered gamma emission from isomers is now moving into a new era, defined by less reliance on systematics predictions and utilizing the greatly improved spectroscopic level data from more traditional experiments. With the ability to identify and target specific potential trigger transitions, one can anticipate a greatly increased pace of research. Within this context, the work conducted by the YSU Isomer Physics Project under AFOSR support has provided a considerable base of fundamental knowledge and has significantly advanced the field. Such basic information as cross sections for different reaction mechanisms is central to any evaluation of the feasibility of isomers for applications.

A total of twenty manuscripts have been published during the period of performance of this grant period. One manuscript is in press for 2006 while two others have been submitted and are under review. Also, twenty invited and three contributed presentations by the PI resulted from grant sponsorship and six contributed presentations/posters were made by undergraduate students supported hereby. In addition, the PI served as Co-Program Chairman of three international scientific conferences in this field and as Co-Chairman of a session on these topics at another meeting. The PI served as well as a reviewer for the Science and Technology Center in Ukraine during 2005.

The essential technical details of the papers may be found in Appendix A while Appendices B and C list Invited and Contributed Presentations, respectively, under this grant period. A few highlights are listed below to indicate the degree to which the YSU Isomer Physics Project has contributed to a firm foundation for possible applications of long-lived isomers.

HIGHLIGHTS OF PUBLISHED RESULTS

Experimental tests of triggered gamma emission occupy a rather narrow field within nuclear physics. As such, this work is somewhat removed from the mainstream of nuclear physics and has suffered from a perceived lack of firm founding in traditional, experimentally-verified concepts of the larger field. The extremely large integral cross sections from initial reports of triggering of ^{180m}Ta perpetuated this perception until later work showed that improved measurements were indeed in agreement with established nuclear systematics [14]. Finally, for ^{180m}Ta it was possible to make first identifications of specific nuclear states in level schemes with the energies that provided absorption of incident photons to cause triggered gamma emission [8]. Work conducted under this grant has contributed significantly to the foundations of triggered gamma emission and explored several new concepts. A few recent highlights will be given to indicate the breadth and depth of these efforts.

"Design and characterization of a compact multi-detector array for studies of induced gamma emission: Spontaneous decay of ^{178m2}Hf as a test case," P. Ugorowski, R. Propri, S. A. Karamian, D. Gohlke, J. Lazich, N. Caldwell, R. S. Chakrawarthy, M. Helba, H. Roberts and J. J. Carroll, Nuclear Instruments and Methods A (submitted 2006).

Summary:

Some published reports (see the survey in Ref. [13]) have claimed evidence that triggered gamma emission could be induced from ^{178m2}Hf using incident real photons near 10 keV. To investigate these claims with improved sensitivity, a final implementation of the YSU miniball array was utilized at the BL12B2 beamline at SPring-8. Results obtained during irradiations will be presented in a later manuscript, but prior to that a fully-detailed characterization of the miniball system was performed using natural decay of ^{178m2}Hf. This provided a baseline of natural events from which to compare measurements that could, in principle, have produced induced events.

"$K^{\pi} = 0^{+}$ 2.29 s isomer in neutron-rich ^{174}Tm," R. S. Chakrawarthy, P. M. Walker, J. J. Ressler, E. F. Zganjar, G. C. Ball, M. B. Smith, A. N. Andreyev, S. F.Ashley, R. A. E.Austin, D. Bandyopadhyay, J. A. Becker, J. J. Carroll, D. S. Cross, D. Gohlke, J. J. Daoud, P. E. Garrett, G. F. Grinyer, G. Hackman, G. A. Jones, R. Kanungo, W. D. Kulp, Y. Litvinov, A. C. Morton, W. J. Mills, C. J. Pearson, R. Propri, C. E. Svensson, R. Wheeler and S. J. Williams, Physical Review C (accepted 2006).

Summary:

This paper describes the characterization of a newly-discovered isomer based on measurements performed using the so-called 8π detector array and spallation ion source (ISAC) at TRIUMF. The array consists of twenty Compton-suppressed Ge detectors and was coupled with a new internal array of conversion-electron detectors.

"Production of long-lived hafnium isomers in reactor irradiations," S. A. Karamian, J. J. Carroll, J. Adam, E. N. Kulagin and E. P. Sabalin, High Energy Density Physics (submitted 2005); "Production of the ^{178m2}Hf isomer using a 4.5-GeV electron accelerator," S. A. Karamian, J. J. Carroll, J. Adam and N. A. Demekhina, Nuclear Instruments and Methods A 530, 463 (2004).

Summary:

The first of these papers describes a new, more accurate measurement of the cross section for production of this long-lived isomer using reactor neutrons, including an improved measurement for so-called burnup, or depletion, of the isomer itself in that environment. The second paper describes a first measurement of the cross section for production of this isomer using high-energy bremsstrahlung.

"Nuclear excitation and de-excitation in resonant electronic transitions," M. R. Harston and J. J. Carroll, Laser Phys. 14, 1452 (2004); "Limits on nuclear excitation and deexcitation of $^{178}Hf^{m2}$ by electron-nucleus coupling," M. R. Harston and J. J. Carroll, Laser Phys. 15, 487 (2005).

Summary:

The first paper describes the general calculation of probabilities for NEET (nuclear excitation by electron transitions) which occurs as a result of coupling between the nucleus and atomic transitions under certain conditions. The second paper describes a detailed calculation of the NEET probabilities for the $^{178m2}Hf$ nucleus. These probabilities are small and do not agree with the suggestion that NEET is the mechanism responsible for claims of low-energy triggering.

"Studies of high-K isomers at TRIUMF-ISAC," M. B. Smith, P. M. Walker, R. S. Chakrawarthy, R. A. E.Austin, G. C. Ball, J. J. Carroll, E. Cunningham, P. Finlay, P. E. Garrett, G. F. Grinyer, G. Hackman, B. Hyland, K. Koopmans, W. D. Kulp, J. R. Leslie, A. A. Phillips, R. Propri, P. H. Regan, F. Sarazin, M. A. Schumaker, H. C. Scraggs, T. Shizuma, C. E. Svensson, J. von Schwarzenberg, J. C. Waddington, D. Ward, J. L. Wood, B. Washbrook and E. F. Zganjar, Nucl. Phys. A 746, 617 (2004).

Summary:

This paper describes the scope of and some results from the program of studies of high-K isomers conducted at TRIUMF using ISAC and the 8π array. The class of high-K isomer includes $^{178m2}Hf$ and ^{180m}Ta, for example.

"Gamma rays emitted in the decay of 31-year $^{178m2}Hf$," M. B. Smith, P. M. Walker, G. C. Ball, J. J. Carroll, P. E. Garrett, G. Hackman, R. Propri, F. Sarazin and H. C. Scraggs, Phys. Rev. C 68, 031302(R) (2003).

Summary:

1. Some reports claiming evidence in support of low-energy triggering of $^{178m2}Hf$ have reported the appearance of "new" gamma lines that appear only during irradiation of an isomeric target. The term "new" indicates that the gamma transitions reported do not appear in the natural decay cascades from the 31-year m2 isomer. The statistical nature of the reported data for these "new" lines is poor, but if one assumes that the lines do appear, then it is important to insure that they are now weakly-populated transitions in the natural decay, hitherto unobserved. This paper describes the detailed measurement of the natural decay of $^{178m2}Hf$, from which a number of newly observed gamma decays from the 31-year isomer and between the two 8^- bands were detected. Other unplaced "new" gamma lines were discussed which may have influenced claims of nearby lines appearing due to triggering.

"'Forced-gamma emission' studies involving nuclear isomers using fast neutrons and bremsstrahlung x rays," N. A. Guardala, J. L. Price, J. H. Barkyoumb, R. J. Abbundi, G. Merkel and J. J. Carroll, in *Applications of Accelerators in Research and Industry* (American Institute of Physics, Melville, New York, 2003).

Summary:

This paper describes and proposes a series of experiments to study fast-neutron- and photon-induced triggering of selected nuclear isomers. These isomers have halflives in the range of 42.6 minutes to 57.4 days. Although not sufficiently long-lived to provide reasonable storage for applications, they may be suitable for experiments with equipment available at the Naval Surface Warfare Center, Carderock Division (NSWCCD).

"Possible Ways for Triggering the ^{179m2}Hf isomer," S. A. Karamian, J. J. Carroll, L. A. Rivlin, A. A. Zadernovsky and F .J. Agee, Laser Phys. 14, 1 (2004).

Summary:

The 25.1-day isomer of ^{179}Hf may prove useful in trigger experiments and can be produced, in principle, in sufficient amounts for testing. Modern nuclear level data supports the identification of at least three different potential trigger methods based on specific candidates for intermediate states as discussed in this paper.

"An Experimental Perspective On Triggered Gamma Emission From Nuclear Isomers," J. J. Carroll, Laser Physics Letters (in press for 2004).

Summary:

This paper surveyed the status of the field of study into induced gamma emission, and in particular detailed the conflicting results into low-energy triggered gamma emission from ^{178m2}Hf.

"Ups and downs of nuclear isomers," P. J. Walker and J. J. Carroll, Physics Today June 2005, p. 39.

Summary:

This paper surveys the aspects of nuclear isomers that allows them to provide unique tests of nuclear structure and to suggest possible applications.

MANUSCRIPT IN PROGRESS

Preparation of a manuscript describing the searches for "slow" and "prompt" low-energy triggered gamma emission from ^{178m2}Hf has begun and submission to Physical Review C is anticipated during the first third of 2006. This manuscript will therefore describe work performed under this grant. The working title is "Tests of low-energy

triggered gamma emission from ^{178m2}Hf using monochromatic synchrotron radiation at SPring-8."

Experiments performed during the grant period at Germany's Gesellschaft für Schwerionenforschung (Darmstadt) and the University of Stuttgart are still being analyzed and manuscript may be expected at some time during 2006. These were a search for new long-lived isomers and a study of population of ^{176m}Lu by (γ, γ') reactions (with complimentary nuclear resonance fluorescence measurements), respectively.

REFERENCES

1. P. M. Walker and G. Dracoulis, Nature 399, 35 (1999).
2. P. M. Walker and J. J. Carroll, Physics Today, 39 (June 2005).
3. M. B. Smith, P. M. Walker, G. C. Ball, et al., Phys Rev. C 68, 031302(R) (2003).
4. H. Roberts, Hyperfine Int. 107, 91 (1997).
5. J. J. Carroll, S. A. Karamian, L. A. Rivlin, et al., Hyperfine Int. 135, 3 (2001).
6. D. Belic, C. Arlandini, J. Besserer, et al., Phys. Rev. Lett. 83, 5242 (1999).
7. D. Belic, C. Arlandini, J. Besserer, et al., Phys. Rev. C 65, 035801 (2002).
8. P. M. Walker, G. D. Dracoulis, and J. J. Carroll, Phys. Rev C 64, 061302 (2001).
9. C. B. Collins and J. J. Carroll, Laser Phys. 5, 209 (1995).
10. C. B. Collins, J. J. Carroll, Y. T. Oganessian, et al., Laser Phys. 5, 280 (1995).
11. C. B. Collins, F. Davanloo, M. C. Iosif, et al., Phys. Rev. Lett. 82, 695 (1999).
12. C. B. Collins, F. Davanloo, M. C. Iosif, et al., Laser Phys. 9, 8 (1999).
13. J. J. Carroll, Laser Phys. Lett. 1, 275 (2004).
14. S. A. Karamian and J. J. Carroll, Laser Phys. 11, 23 (2001).

APPENDIX A

PUBLICATIONS FROM WORK CONDUCTED UNDER GRANT

"Design and characterization of a compact multi-detector array for studies of triggered gamma emission: spontaneous decay of ^{178m2}Hf as a test case," P. Ugorowski, R. Propri, S. A. Karamian, J. Lazich, D. Gohlke, N. Caldwell, S. C. Ravuri, M. Helba and J. J. Carroll, Nucl. Instrum. Meth. A (submitted 2006). **PREPRINT**

"$K^{\pi} = 0^{+}$ 2.29 s isomer in neutron-rich ^{174}Tm," R. S. Chakrawarthy, P. M. Walker, J. J. Ressler, C. J. Pearson, G. C. Ball, D. Bandyopadhyay, E. F. Zganjar, M. B. Smith, A. N. Andreyev, S. Ashley, R. A. E. Austin, J. A. Becker, J. J. Carroll, D. S. Cross, D. Gohlke, J. J. Daoud, P. E. Garrett, G. F. Grinyer, G. Hackman, G. A. Jones, R. Kanungo, Y. Litvinov, A. C. Morton, W. J. Mills, R. Propri, C. E. Svensson, R. Wheeler and S. J. Williams, Phys. Rev. C (accepted for 2006). **PREPRINT**

"Production of long-lived hafnium isomers in reactor irradiations," S. A. Karamian, J. J. Carroll, J. Adam, E. N. Kulagin, and E. P. Shabalin, High Energy Density Phys. (submitted 2005). **PREPRINT**

"Ups and downs of nuclear isomers," P. M. Walker and J. J. Carroll, Physics Today June 2005, p. 39. **REPRINT**

"Limits on nuclear excitation and de-excitation of ^{178m2}Hf by electron-nucleus coupling," M. R. Harston and J. J. Carroll, Laser Physics 15, 487 (2005). **REPRINT**

"Nuclear excitation and de-excitation in resonant electronic transitions," M. R. Harston and J. J. Carroll, Laser Physics 14, 1452 (2004). **REPRINT**

"Production of the ^{178m2}Hf isomer using a 4.5-GeV electron accelerator," S. A. Karamian, J. J. Carroll, J. Adam and N. A. Demekhina, Nuclear Instruments and Methods A 530, 463 (2004). **REPRINT**

"Studies of high-K isomers at TRIUMF-ISAC," M. B. Smith, P. M. Walker, R. S. Chakrawarthy, R. A. E. Austin, G. C. Ball, J. J. Carroll, E. Cunningham, P. Finlay, P. E. Garrett, G. Grinyer, G. Hackman, B. Hyland, K. Koopmans, W. D. Kulp, J. R. Leslie, A. A. Phillips, R. Propri, P. H. Regan, F. Sarazin, M. A. Schumaker, H. C. Scraggs, T. Shizuma, C. E. Svensson, J. von Schwarzenberg, J. C. Waddington, D. Ward, J. L. Wood, B. Washbrook and E. F. Zganjar, Nuclear Physics A 746, 617 (2004). **REPRINT**

"An Experimental Perspective On Triggered Gamma Emission From Nuclear Isomers," J. J. Carroll, Laser Physics Letters 1, 275 (2004). **REPRINT**

"Possible Ways for Triggering the ^{179m2}Hf isomer," S. A. Karamian, J. J. Carroll, L. A. Rivlin, A. A. Zadernovsky and F .J. Agee, Laser Physics 14, 166 (2004). **REPRINT**

"Formation of the high-spin ^{179m2}Hf isomer in reactor irradiations," S. A. Karamian, J. J. Carroll, J. Adam, E. N. Kulagin and E. P. Shabalin, Laser Physics 14, 438 (2004). **REPRINT**

"Driven energy release of nuclear isomers," L.A. Rivlin, J.J. Carroll and F. J. Agee, Laser Physics 14, 435 (2004). **REPRINT**

"'Forced-gamma emission' studies involving nuclear isomers using fast neutrons and bremsstrahlung x rays," N. A. Guardala, J. L. Price, J. H. Barkyoumb, R. J. Abbundi, G. Merkel and J. J. Carroll, in *Applications of Accelerators in Research and Industry* (American Institute of Physics, Melville, New York, 2003). **REPRINT**

"Gamma rays emitted in the decay of 31-year ^{178m2}Hf," M. B. Smith, P. M. Walker, G. C. Ball, J. J. Carroll, P. E. Garrett, G. Hackman, R. Propri, F. Sarazin and H. C. Scraggs, Phys. Rev. C 68, 031302(R) (2003). **REPRINT**

"Hybridization of atomic-nuclear excitations and pumping of nuclear levels," S. A. Karamian and J. J. Carroll, Laser Phys. 13, 1182 (2003). **REPRINT**

"Photon scattering experiments on ^{176}Hf and the systematics of low-lying dipole modes in the stable even-even Hf isotopes $^{172, 178, 180}$Hf," M. Scheck, D. Belic, P. von Brentano, J. J. Carroll, A. Gade, H. von Garrel, U. Kneissl, C. Kohstall, A. Linnemann, N. Pietralla, H. H. Pitz, F. Stedile, R. Toman and V. Werner, Phys. Rev. C 67, 064313-1-7 (2003). **REPRINT**

"Initial search for triggered gamma emission from ^{178}Hf^{m2} using the YSU miniball array," J. J. Carroll, J. Burnett, T. Drummond, J. Lepak, R. Propri, D. Smith, S. A. Karamian, J. Adam, F. Stedile and F. J. Agee, Hyperfine Int. 143, 37 (2003). **REPRINT**

"Proposal for Observation of a Hidden Nuclear Population Inversion," F. J. Agee, J. J. Carroll, L. A. Rivlin and V. Vuletic, Hyperfine Int. 143, 7 (2003). **REPRINT**

"Beam-based production of ^{178m2}Hf," J. Paul Farrell, V. Dudnikov, J. J. Carroll and G. Merkel, Hyperfine Int. 143, 55 (2003). **REPRINT**

"Possibility of combining nuclear level pumping in a plasma with lasing in a solid," S. A. Karamian and J. J. Carroll, Hyperfine Int. 143, 69 (2003). **REPRINT**

"Gamma spectroscopy of Hf-178m2 using synchrotron x-rays," H. E. Roberts, M. Helba, J. J. Carroll, J. Burnett, T. Drummond, J. Lepak, R. Propri, Z. Zhong and F. J. Agee, Hyperfine Int. 143, 111 (2003). **REPRINT**

"Non-radiative triggering of long-lived nuclear isomers," A. A. Zadernovsky and J. J. Carroll, Hyperfine Int. 143, 153 (2003). **REPRINT**

"Photo-induced depopulation of the $^{180}Ta^{m}$ isomer via low-lying intermediate states: Structure and astrophysical implications," D. Belic, C. Arlandini, J. Besserer, J. de Boer, J. J. Carroll, J. Enders, T. Hartmann, F. Käppeler, H. Kaiser, U. Kneissl, E. Kolbe, K. Langanke, M. Loewe, H. J. Maier, H. Maser, P. Mohr, P. von Neumann-Cosel, A. Nord, H. H. Pitz, A. Richter, M. Schumann, F.-K. Thielemann, S. Volz, and A. Zilges, Phys. Rev. C 65, 035801-1-13 (2002). **REPRINT**

DESIGN AND CHARACTERIZATION OF A COMPACT MULTI-DETECTOR ARRAY FOR STUDIES OF INDUCED GAMMA EMISSION: SPONTANEOUS DECAY OF ^{178m2}Hf AS A TEST CASE

P. Ugorowski,[a] R. Propri,[a] S. A. Karamian,[b] D. Gohlke,[a] J. Lazich,[a] N. Caldwell,[a] R. S. Chakrawarthy,[c,d] M. Helba,[e] H. Roberts[e] and J. J. Carroll[a*]

[a] Department of Physics and Astronomy, Youngstown State University, One University Plaza, Youngstown, OH 44555
[b] Flerov Laboratory of Nuclear Reactions, Joint Institute for Nuclear Research, 141980 Dubna, Russia
[c] Department of Chemistry, Simon Fraser University, Burnaby, British Columbia V5A 1S6 Canada
[d] TRIUMF, Vancouver, British Columbia V6T 2A3, Canada
[e] SRS Technologies, Inc., Systems Technology Group, Huntsville, AL 35806

Abstract

Reports that incident photons near 10 keV can induce the emission of gamma rays with concomitant energy release from the 31-year isomer of ^{178}Hf challenge established models of nuclear and atomic physics. In order to provide a direct and independent assessment of these claims, a multi-detector system was designed as a specialized research tool. The so-called YSU miniball is unique in its combination of performance characteristics, compact size and portability, enabling it to be easily transported to and placed within the confines of beamline hutches at synchrotron radiation sources. Monochromatic synchrotron radiation was used in the most recent studies from which evidence of prompt triggering was claimed, suggesting similar sites for independent tests of these results. The miniball array consists of six high-efficiency BGO scintillators coupled with a single 65% Ge detector and provides time-resolved gamma-ray calorimetry rather than purely spectroscopic data. The need to record high detected folds from the array (up to seven-fold gamma coincidences) makes this system different in practice from standard spectroscopic arrays for which data is typically restricted to triples or lower folds. Here the system requirements and design are discussed, as well as its performance as characterized using the well-known natural decay cascades of ^{178m2}Hf. This serves as the foundation for subsequent high-sensitivity searches for low-energy triggering of gamma emission from this isomer.

PACS: 23.20.Lv; 27.70.+q, 29.30.-h, 29.30.Kv

Keywords: Multi-detector array, gamma-ray calorimetry, induced gamma emission, isomer, ^{178m2}Hf

* Corresponding author: jjcarroll@cc.ysu.edu
Tel: 330-941-3617 FAX: 330-941-3121

1. Introduction

The possibility that nuclear energy could be released in a relatively clean fashion from long-lived nuclear isomers has been under consideration for decades [1]. Such metastable states are capable of storing considerable energy for rather long durations. The archetype is ^{180m}Ta, being an excited state with a halflife greater than 10^{15} years and located 75 keV above the unstable ground state [2]. An induced depopulation of this isomer due to irradiation of samples with real photons (bremsstrahlung) was first observed in 1987 [3] with detailed confirmation and characterization of the process coming later (see Ref. [4] and references therein). The induced depopulation was accompanied by a release of the stored 75 keV, but was initiated by incident photons of at least 1 MeV, proving to be a sink rather than a source of energy. Nevertheless, the existence of transitions connecting the isomer to levels that decay to the ground state provided intriguing insight into weak components in the wavefunctions [5].

Other isomers have been suggested as being potentially of greater practical value [1]. Principal among these is the 31-year-lived isomer ^{178m2}Hf, storing 2.446 MeV per nucleus, or about 1.3 GigaJoules/gram at natural density. Studies which attempted to replicate the induced depopulation of ^{180m}Ta for ^{178m2}Hf have concentrated so far on rather low energies, using real photons below 100 keV from bremsstrahlung and synchrotrons. Experiments using virtual photons via Coulomb excitation have been conducted on ground-state ^{178}Hf targets, providing results that support the possibility of induced depopulation of ^{178m2}Hf by transitions with energies greater than 300 keV [6, 7]. Reference [8] surveys the experimental landscape as of early 2004, and later results or additional details of previous results are described in Refs. [9-11]. The controversial nature of the positive results, in light of several carefully-conducted null measurements, perhaps reached its zenith with the recent report [9] that induced depopulation of the ^{178m2}Hf isomer, with $J^{\pi} = K^{\pi} = 16^{+}$, proceeded through an intermediate, higher-lying state that subsequently decayed to the ground state in a single transition. Since only a modest-multipolarity transition from isomer to intermediate state could be expected, this would seem to require a $\Delta J > 10$ transition for the purported decay transition.

While the latter claim of induced depopulation of ^{178m2}Hf would appear to require little further consideration, other previous claims are not unphysical *a priori*, although theoretical analyses have cast doubt on the purported mechanism [12, 13]. As in the case of ^{180}Ta and other nuclei (see, for example, Ref. [14]), the presence of *K*-forbidden transitions in ^{178}Hf, likely required for an induced depopulation, would provide important nuclear structure information. Depletion caused by incident photons of low energies, reported to be near 10 keV, would also have important implications to the understanding of nuclear-electron couplings and potential applications. Also, despite continued positive claims the magnitude of the effect remains rather small. Thus, improved experimental methods by which to better examine these claims will be valuable.

All of the most recent positive results (see the survey of Ref. [8] and Refs. [9, 11]) were obtained using monochromatic synchrotron radiation (either from bending magnets or undulators) as the source of incident photons. Most null experiments were, in contrast,

obtained using continuum radiation sources, including bremsstrahlung [15] or "white" synchrotron radiation [10, 16, 17] and thus presented unique experimental challenges that differed from the positive measurements. Also, in the null results of Refs. [9, 11] no special timing instruments were used by which any relationship between pulses of synchrotron radiation and gamma rays emitted from the ^{178m2}Hf sample could have been recorded. It has been claimed that excess gamma-ray emission triggered by incident photons near 10 keV was prompt, coming within a few nanoseconds of the pulses of synchrotron radiation [11, 18], and thus that the duty cycle of the synchrotron would lead to a washing out of the signal without timing information. Reference [18] suggests (see page 164) that this explains the null measurements. An independent examination of the positive reports of prompt triggered gamma emission, induced by monochromatic synchrotron radiation near 10 keV, requires a different approach than was taken in the works of Refs. [10, 16, 17]. For this purpose, a multi-detector gamma spectroscopic system was developed in a compact configuration that permitted its emplacement within the confines of the radiation hutch at the BL12B2 beamline of the SPring-8 synchrotron. This beamline was chosen as providing similar radiation characteristics to those utilized to obtain some positive results at SPring-8. These independent tests will be described in a future work [19].

This paper will first discuss the design requirements and implementation for the miniball system (Section 2) as needed to search for prompt triggered gamma emission from ^{178m2}Hf. Then the sensitivity of the array for detection of gamma-ray cascades will be covered, as measured from the well-known natural decay of this isomer. This will include determination of the system efficiency and detection limits for gamma-ray calorimetry (Section 3).

2. Detection system

2.1 Design requirements and configuration

Many multi-detector arrays have been constructed for high-resolution gamma-ray spectroscopy [20], such as the well-known Gammasphere system. The large value and physical size of these systems and their associated instrumentation make it infeasible to consider transporting them to sites such as SPring-8 and emplacing them within the confines of beamline hutches for experiments of short duration. Thus, it was necessary to develop a unique system of modest size that combined some spectroscopic capabilities with the essential ability to perform gamma-ray calorimetry. The present system was designated as the *YSU miniball*, stressing its similarities with much larger arrays, although its design is predicated on a very specific type of experiment. Initial design of the system occurred in 2001 [21] and an implementation was used in works described in Refs. [8, 15].

Figure 1 is a schematic energy-level diagram of the ^{178}Hf nucleus, which possesses several isomers. The long-lived (metastable) levels are those at 1,147.4 keV, with a halflife of 4 s (*m1*), and at 2,446.1 keV, with a halflife of 31 years (*m2*). The figure shows the main transitions resulting from the natural decay of the 31-year

isomer [22]. Also depicted is a sketch of a general process of induced energy release that begins with excitation of a nucleus initially in the *m2* state to a higher-lying intermediate state. Back-decay (E) of the intermediate state to the isomer provides only elastic scattering of the incident entity, assumed to be real photons. Other decay branches of the intermediate state may bypass the *m2* level and initiate cascades that eventually reach the stable ground state. These branches would provide a means by which the 2,446.1 keV stored by the 31-year isomer could be released via gamma rays and conversion electrons. These branches may be generally characterized as *prompt* (P), in which the cascade from the intermediate state reaches the ground-state band immediately, *slow* (S), in which the cascade reaches the *m1* band, and *other* (O). The latter type of cascade bypasses the 4-s isomer, but may pass through some states that have significant halflives on the time scale of a detection system. Reports of induced energy release, so-called triggered gamma emission, have so far been restricted to incident photons energies near 10 keV. Below an energy of (2,446.1 + 10) keV, known levels have halflives less than 1.5 ns with the exception of the *m1* metastable state and a shorter-lived isomer at 1,554.0 keV ($T_{1/2}$ = 77.5 ns) [2].

Figure 1 placement

As mentioned above, recent reports of positive evidence of triggering indicated that the gamma emission was prompt, coming within 1 ns of the pulse of incident synchrotron radiation [11]. In that work, a small-volume Ge detector was used to measure gamma rays emitted from a sample containing ^{178m2}Hf as it was being irradiated with monochromatic synchrotron radiation near 10 keV. Spectroscopic information was recorded as well as the time between gamma detection and individual pulses of incident radiation. Those pulses were of 20 - 50 ps duration and were separated by several nanoseconds – the time of the pulses was determined by placing an avalanche photodiode in the beam (behind the sample) [11]. Although "1 GHz electronics" were employed for the photodiode [11], the true time resolution between pulses and gamma-ray detection was no doubt more on the order of 10 ns as is typical for Ge detectors. In any event, that report precludes cascades that are delayed by passage through the 77.5-ns isomer.

The ^{178}Hf nucleus provides a natural way of testing this claim of prompt gamma emission without the need to record the times for pulses of incident synchrotron radiation. As discussed in Refs. [15, 21] and seen in Fig. 1, spontaneous decay of the *m2* isomer occurs via two bursts of gamma rays, each of which consists of a cascade with inter-transition delays less than 1.5 ns. The first burst occurs from transitions within the *m1* band, after decay of the *m2* state, and is stopped briefly by the 4-s isomer. The total energy released in the first cascade from the 16^+ *m2* isomer to the 8^- *m1* isomer is 1,298.7 keV, while the energy released in the second cascade from the *m1* isomer to the ground state is 1,147.4 keV. Within each cascade the gamma rays are simultaneous on the scale of the resolving time of Ge spectrometers. If the gamma rays were detected with sufficiently high efficiency by a large-solid angle array, a summation of their energies would coincide with the total energies of the bursts, minus any energy lost into conversion electrons and therefore invisible to the Ge detectors. Conversely, prompt gamma emission due to the claimed induced energy release would produce a single burst

of gamma rays with total energy of (2,446.1 + 10) keV. Gamma-ray calorimetry would therefore distinguish clearly between prompt triggered events and those from natural decay. Such high-summed-energy cascades could only be due to triggering, so they would be of necessity correlated with incident pulses of synchrotron radiation without any need to explicitly record the time of those pulses.

The YSU miniball is designed to perform this function of time-resolved gamma-ray calorimetry using a compact array. A photograph of the miniball located with the BL12B2 hutch at SPring-8 is shown in Fig. 2. A balance between performance and portability was achieved by using six 3.0" diameter × 2.5" long BGO crystals to provide high solid angle (about 83% of 4π) and high intrinsic efficiency. NaI(Tl) crystals were employed in previous implementations [15, 21], but the lower peak-to-Compton ratio of that scintillator material compared with BGO made interpretation of spectra more difficult, thus the change to BGO. Many reports of induced energy release indicated evidence of the emission of gamma rays at energies not part of the natural decay cascades (see the survey of Ref. [8]). High-resolution spectroscopy would be advantageous in identifying any such unusual gamma rays, but this would be precluded by the use of BGO scintillators. In order to insure that every gamma-emission event observed by the array contained one gamma ray having a precisely determined energy, a 65% relative efficiency p-type Ge detector was coupled instrumentally to the BGO crystals. The large-volume Ge detector observed the sample through a gap between BGO detectors along one of the diagonals of a cubic support structure.

Figure 2 placement

Use of a p-type crystal, with its associated thin Al-end window, was beneficial for spectra taken under irradiation in that the window would provide filtering of any incident radiation near 10 keV that was scattered toward the detector. Aluminum windows on the BGO crystal housings provided similar shielding, minimizing the chance of pile up between scattered synchrotron radiation and gamma rays.

Figure 2 also shows the placement of a second Ge detector (10% efficiency n-type) and an x-ray detector, both of which observed the sample through other diagonals of the cube. These were used as parts of independent systems to obtain a separate singles spectrum (no coincidence) and a calibration of the scattered synchrotron radiation during exposures. They have no impact on the characterization of the miniball system and are not discussed further.

2.2 Instrumentation

A schematic of the pulse-processing instrumentation for the miniball is given in Fig. 3. Once data acquisition was enabled, recording of a gamma-emission event was initiated only when the Ge detector observed a gamma ray. One preamplifier output from the Ge detector was sent to an Ortec 579 Fast Filter Amplifier and then to an Ortec 583 constant-fraction (CF) discriminator to provide a master gate channel. The ARC method [23] was employed with this discriminator and its threshold set a minimum energy for

recorded gamma rays into the Ge detector. The discriminator's NIM output was stretched and converted to TTL by a Stanford DG535 pulse generator. The output from the pulse generator served as the system gate and its width and delay could be adjusted over a wide range.

Figure 3 placement

High voltage to the Ge detector was provided using a standard Ortec module that utilized manual front-panel controls. High voltage to each BGO's PMT was provided by a single octal NIM module from Radiation Technologies, Inc. that was computer controlled and allowed remote changes on the order of a few volts.

A FERA/CAMAC system was employed to record spectroscopic and time information from the detectors, chosen for its flexible programmability using Sparrow's KMaxNT software and for buffering and fast transfer of data. A customized toolsheet was built in this platform to control data acquisition, including operating parameters like ADC thresholds, data word sizes, use of zero-suppression, buffer size, etc., and to monitor individual detector energy and time spectra in real-time. The FERA hardware was managed by a CMC 203 driver that received the system gate and distributed it to two Ortec AD413A quad 8k peak-sensing ADC's and a Silena 4418/T octal TDC. Spectroscopic pulses from the Ge detector were input to an Ortec 672 linear amplifier with a shaping time of 2 μs and its unipolar output was digitized with one channel of an AD413A. Output from the BGO PMT's was routed first to an Ortec CF8000 octal CF discriminator. A buffered spectroscopic signal was available from each CF8000 channel whereby spectroscopic signals from the BGO detectors were fed to separate Ortec 672 amplifiers with shaping times of 2 μs. The bipolar signals from these amplifiers were digitized by other channels of the AD413A's after inversion, which provided the best linearity and resolution.

Negative NIM signals were output by each channel of the CF8000 as timing signals when the incoming PMT pulses exceeded adjustable thresholds. These timing signals were stretched by separate channels of an Ortec GG8010 and then converted to ECL standard signals by separate channels of a Phillips 7126 level translator prior to being input to the TDC. The leading edge of the gate distributed by the driver via the FERA bus served as a START pulse to the TDC and the pulses originating from BGO PMT's served as STOP markers. This allowed recording of the relative time interval between a master Ge signal and those from each individual BGO detector. The TDC provided an active time window of 2.8-μs duration, during which START-STOP times were logged as distributed over 3840 channels – the module used an additional 256 channels for sliding-scale non-linearity compensation. The resolution of the TDC was 0.73 ns/channel, considerably shorter than the inherent time resolution obtainable from the Ge and BGO detectors after pulse processing, being both on the order of tens of ns. The temporal relationships between the gate, spectroscopic and timing pulses are shown in Figs. 4 and 5.

Figure 4 placement

Figure 5 placement

Although not suitable for extended discussion herein, it is worth noting that while CAMAC is an international standard this is not the case for the FERA system. The Fast Encoding and Readout ADC approach was developed by Lecroy to provide data transfers between CAMAC modules at rates in excess of that supported by the CAMAC backplane. FERA utilizes ECL signals on a front-panel bus distributed and managed by the driver module. Via handshakes the driver receives data from ADC's and TDC's and assembles these separate parameters (data pieces) into an event, then buffers many events either internally or in a separate memory module. In this system, when the internal buffer was ¾ full, a Look At Me (LAM) was sent to the controlling computer to cause an upload of data. FERA handshake protocols are not fully standardized, therefore the amount of effort required to regularize communications between the driver and the Ortec and Silena modules should not go unrecognized. It is also worth noting that direct observation of signals on the FERA bus destabilized the communications between driver and other modules, an impediment to this regularization.

An absolute time for each event was assigned with 20-ns resolution by the CMC 203 CAMAC driver based on when it received a gate relative to the start of acquisition. Each parameter was a 32-bit word, two of which were used to record the absolute event time. This instrumental resolution was far better than that supported by the detectors themselves. A one-parameter header of constant digital value was inserted at the beginning of each event, so that events in which incomplete handshakes caused some parameters to be lost by the driver could be excluded as having too few parameters. A total of nineteen 32-bit parameters was recorded in each good event – off-line sorting of the data sets indicated that only 1 out of every 300 events was incomplete and such bad events were discarded off-line prior to data analysis.

Zero-suppression mode was not employed in the ADC's so as to avoid having events of varying lengths. Each ADC module possessed four inputs with a processing time of 6 μs per active input and 1.8 μs per inactive input. Readout of the ADC's to the driver was found experimentally to require 7.4 μs following the end of digitization. The total processing time for the ADC's could, therefore, vary in duration, but the TDC introduced a fixed deadtime of 33 μs that included digitization of the START-STOP delay and readout of the module. Output of additional gates from the DG535 was inhibited for a period chosen at 50 μs to avoid the possibility of interference with processing of the current event.

Proper digitization of spectroscopic and TDC STOP signals required use of the GG8010 and DG535 units to introduce appropriate delays at various points in the different channels. These modules also allowed matching of pulse widths to the demands of subsequent units in the data streams. For example, the Ge spectroscopic pulse was input into a linear amplifier set for triangular shaping with a 2-μs time constant. This shaping time had the added effect of introducing a delay of 5 μs between the peak of the initial pulse from the Ge preamplifier and the amplified pulse. The output of the DG535,

serving as the system gate, was delayed and its width set to insure full digitization of the spectroscopic pulse by the ADC.

The use of preamplifiers for the BGO signals was considered, but rejected due to the inability to maintain a sufficiently fast risetime with available units. The PMT outputs were input directly into the CF8000, which produced both time marks and buffered spectroscopic signals. Tests showed that the best resolution for a BGO crystal was obtained by using the bipolar amplifier outputs and triangular shaping. The resulting resolution was found to be 8% for the ^{60}Co 1332 keV peak, as shown in Fig. 6. Proper digitization of peak heights by the ADC's required those peaks to not occur within 1 μs of the start or end of the gate. A gate duration of 5 μs was utilized to meet this condition based on the delays and widths of the spectroscopic pulses for the Ge and BGO channels.

Figure 6 placement

As mentioned previously, timing pulses from the CF8000 were stretched, delayed and converted to ECL as needed for proper digitization by the TDC. Valid STOP signals had to reach the TDC during its 2.8-μs active period that began with the leading edge of the gate. Lack of a valid STOP pulse to the TDC during the active period was recorded as an increment of one count within the sliding-scale region. Invalid STOPs occurred for several reasons, as discussed later. The delays were selected so that true coincidence STOPS appeared at roughly channel 1500 for each TDC input by obtaining coincidence curves using the histogramming feature of the Tektronix TDS-5104 1-GHz digital oscilloscope. Figure 5 shows a scope trace displaying the gate and STOP pulses from a single BGO, generated with a ^{60}Co source. Also shown in the figure is a histogram of the numbers of STOP pulses occurring as a function of time. The delay for this STOP stream was set so that coincidence between gamma rays entering the Ge (START) and this BGO produced a time marker within the gate.

Off-line sorting of data sets to extract singles or higher-fold spectra for any detector or combination of detectors was accomplished using an in-house software suite that was custom designed [24] for the miniball system. The software allowed sorting based on energy and timing parameters for each detector and determination of summed energy and detected fold from the BGO crystals.

Standard calibration sources were used to assess the basic performance of the miniball system as was done in earlier stages of its development [15]. Because the spontaneous decay of ^{178m2}Hf has been extensively characterized [22] and because the eventual aim was to perform trigger studies in subsequent experiments [19], it was decided to perform efficiency calibrations using a mixed ^{178m2}Hf/^{172}Hf sample. This approach benefited from the number and distribution of gamma lines, and the available coincidence.

One particular test with a standard calibration source was particularly valuable. A ^{137}Cs source was employed to investigate the possibility of Compton scattering in one detector causing coincident events in other detectors. Discriminator thresholds in the

miniball instrumentation eliminated x rays from recorded events, so that only random coincidences should have been in evidence from this single-line source. Figure 7a shows a time spectrum obtained for one BGO crystal. A small coincidence peak was seen and interpreted as being due to Compton cross-talk between the Ge and that BGO. Such cross-talk could occur between any detectors. A 1-mm Pb wrap was applied around the BGO crystals as they extended within the cubic support structure, resulting in the time spectrum shown in Fig. 7b in which this cross-talk was eliminated. It should be noted that no filters were applied to the faces of any of the detectors, other than the thin Al detector housings.

Figure 7 placement

3. Characterization using ^{178m2}Hf decay

3.1 Sample composition and configuration

The miniball performance was principally characterized by gamma rays emitted in spontaneous decays within a mixed ^{178m2}Hf/^{172}Hf source. This characterization was chosen, as mentioned above, to serve as the foundation for experiments conducted specifically to search for evidence of prompt induced energy release during subsequent irradiations with synchrotron radiation.

Figure 8 shows a photograph of the sample employed in this work, attached to a positioning arm. The mechanical construction of the sample consisted of an Al frame that held together two 1-mm thick Be disks. The hafnium material was deposited by evaporation on one Be disk and occupied a roughly circular spot near the center of that disk.[†] The details of the distribution are not important for the present discussion, other than the fact that the radioactive Hf did not constitute a point source. The active content included 0.37 μCi of ^{178m2}Hf (2.0×10^{13} nuclei or 5.79 ng) and 0.29 μCi of ^{172}Hf (9.3×10^{11} nuclei or 0.26 ng) at the time of the tests in June 2004. It has been estimated [25] that the total hafnium content was approximately 2,500× that of the active ^{178m2}Hf material, which was produced by proton spallation [26]. The isomer-to-ground-state ratio for ^{178}Hf in the sample was also estimated [25] to be about 1:500. The sample was held within the miniball in the central cavity formed by the faces of the BGO crystals using the aluminum positioning arm that extended through one of the half diagonals of the cubic support structure. One full diagonal of the cube was reserved as the entrance and exit channels for synchrotron radiation. The large Ge detector coupled to the BGOs, an independent small Ge and an x-ray detector utilized separate half diagonals as viewing ports. The positioning arm was affixed outside the miniball structure to a translation table so that the sample could be moved remotely in a vertical plane. The orientation of

[†] The distribution of hafnium material within the deposit was determined by passing a narrow (0.5 mm × 0.5 mm) beam of monochromatized synchrotron radiation set to the L_3 edge of Hf through the opening in the Al sample frame. Transmission of the radiation was recorded by pre- and post-sample ionization chambers as a function of sample position as it was raster-scanned across the fixed beam axis. (This procedure is discussed in detail in a forthcoming manuscript on searches for prompt triggered gamma emission.)

the sample was determined by the eventual need to irradiate the largest possible area of the hafnium deposit with a beam spot of smaller dimensions.

Figure 8 placement

3.2 Singles spectra, timing and detector efficiencies

Gamma radiation emitted due to natural decay of ^{178m2}Hf and ^{172}Hf within the mixed sample was recorded by the miniball system for a period of about 74 hours. At regular intervals of about 12 hours, the small dewar on the Ge detector was filled and data acquisition was halted for this period. The BGO PMT's were gain matched after each fill by minor adjustments to their operating voltages via software control. The Ge detector evidenced no gain drift and its voltage was maintained throughout the measurement. The data set consisted of 6,831 3.5-MB files, each containing about 48,000 recorded events, from which a singles Ge spectrum was extracted as shown in Fig. 9. This was accomplished by first removing events of incorrect length, i.e. wrong number of parameters, which comprised about 0.3% of the data. Then the data was sorted without imposition of any conditions on coincidence between the Ge and BGO detectors or on detector pulse heights. The inset in the figure shows an expanded section of the spectrum that contains the doublet of lines at 213 keV and 217 keV that occur in the spontaneous decay of ^{178m2}Hf. The latter of these lines comes from the $9^- \rightarrow 8^-$ transition just above the *m1* isomer while the former originates with the $4^+ \rightarrow 2^+$ transition in the ground-state band (see Fig. 1). The doublet is well-separated, indicating excellent performance for spectroscopy with this detector and confirming no measurable gain shift. All peaks in the spectrum were positively identified as corresponding to gamma rays from spontaneous decay of ^{178m2}Hf, ^{172}Hf and its daughters, and natural background. The total event rate in the Ge was 1.2 kHz and deadtime resulting from this rate was on the order of 6%.

Figure 9 placement

An initial question was the degree to which the efficiency of the large-volume Ge detector was influenced by the small gap through which it viewed the central cavity of the miniball. The restricted view was due to the BGO crystals and their Pb wraps and would partially shield the sample from view by the Ge detector. It was not possible to test this in the beamline hutch, so data were taken at Youngstown State University. Ge singles spectra were extracted from miniball data obtained using the hafnium source in two different geometric configurations: first, with the BGOs and Pb wraps in place and, second, with those BGOs and wraps removed which would otherwise have restricted the view of the Ge detector. Figure 10a shows the "direct" efficiencies obtained from these measurements using the standard form

$$N_i = ATf_i\varepsilon_i \quad , \tag{1}$$

where N_i is the number of counts contained within a given full-energy Ge peak, A is the sample activity, T is the acquisition live time, f_i is the fraction of decay events that emit γ_i

and ε_i is the full-energy peak efficiency for detection of the specific gamma ray. The f_i values used in Eq. (1) were obtained from the ENSDF [2] as listed in Appendix A and peak fits were obtained using the commercial FitzPeaks program [27]. The effect of the gap between BGO crystals was to suppress the overall efficiency, but less so at higher gamma-ray energies where the cross section for photoelectric interactions decreases. Gamma rays entered only the central section of the Ge crystal and Compton-scattered photons therefrom had other opportunities to interact in the outer part of the detector. This produced the flattened efficiency curve shown in Fig. 10a when all BGO and wraps were in-place. Figure 10b shows the actual Ge efficiency curve from data obtained at SPring-8, being about 0.35% near 1 MeV.

Figure 10 placement

It was possible to provide an additional verification of the magnitude of the direct efficiency values. The method described in Appendix B was employed to obtain efficiencies based on the relationship between the number of counts in individual full-energy peaks and corresponding sum peaks appearing in the singles spectrum. Efficiencies determined in this way for specific pairs of gamma-ray energies are also plotted in Fig. 10b. It was not necessary for full-energy peaks in the Ge singles spectrum to be corrected for summing losses due to the small relative magnitude of this effect. The situation was different for the scintillators, as discussed below, which were closer to the sample and therefore had higher detection efficiencies.

Singles spectra were also extracted for each BGO detector and one example is shown in Fig. 11. Again, no sorting conditions were imposed on the data, but the instrumentation required coincidence with a count from the Ge detector. The largest peaks in the spectrum were identified with intense gamma rays from ^{178m2}Hf and ^{172}Hf decays. The spectrum excludes the low-energy part of the 89/93-keV doublet due to the minimum thresholds in the CF discriminator. Clearly, spectroscopy with the BGO was severely inhibited due to the wide peaks, particularly for the many overlapping lines from the hafnium source. This same difficulty was found when attempting to determine the BGO efficiency using multi-line calibration sources such as ^{152}Eu. In no case could FitzPeaks provide meaningful fits for BGO spectra, but the well-known TV program [28] was able to provide accurate fits for singlets, with systematic errors on the order of 5% or less for sources such as ^{109}Cd or ^{137}Cs. It was also possible to obtain reasonable fits for the lines from ^{60}Co which were sufficiently resolved (see Fig. 6) and the efficiency for gamma-ray detection at 1,332 keV in a single BGO crystal was about 1%. The paucity of points from single-line sources did not provide a suitable efficiency calibration over a wide range of energies, so a different procedure was employed.

Figure 11 placement

A time spectrum obtained from a single BGO detector is shown in Figure 12, extracted from the full data set. A START signal opened an active interval for the TDC such that STOP pulses occurring during this interval were distributed throughout the spectrum, as discussed above. Events in which a) no gamma ray entered the BGO

crystal, b) no STOP pulse was generated because its energy was below the discriminator threshold, or c) a STOP pulse was generated too late for the active window, were recorded in the sliding-scale section. Delays in the timing channels placed coincidence between Ge and BGO detectors at roughly the center of the active range. The shape of the coincidence curve in the figure indicated walk from low-energy pulses in the Ge channel as the origin of the shoulder to the left of the main coincidence peak. The smaller shoulder to the right was due to walk in the BGO channel. The full width of the narrow coincidence peak was 70 channels, corresponding to a resolving time of 51 ns. Based on the constant level of background far from the narrow peak, 0.72% of the counts within the 70-channel width corresponded to random coincidences with respect to the Ge START. Taking a larger width of 700 channels ensured inclusion of true coincidences with walk of either START or STOP signals and of those counts only 2.7% were due to random coincidences. Herein, a full sorting width of 700 channels was employed, but the effective resolving time for true coincidences was still on the order of 50 ns.

Figure 12 placement

Figure 13 shows a part of the γ-γ ("doubles") spectrum for the Ge and one specific BGO, extracted from the data set under the condition of coincidence as discussed above. While singles spectra (like that of Fig. 11) were too complex for fitting, projections of specific ranges in the γ-γ data allowed analysis using TV. Software gates (called cuts in TV) were made using this software,[‡] such as the one shown in Fig. 13 around the 495-keV peak in the Ge projection. The BGO projection for this cut therefore contained coincident photopeaks and Compton events originating in the *m1* band of Fig. 1, and random coincidences. BGO spectra obtained from different cuts were quite sparse compared with a full projection and fits to the broad peaks were performed using the known energies of gamma rays emitted in ^{178m2}Hf and ^{172}Hf decays. Figure 14 shows two BGO spectra corresponding to cuts on 495-keV and 325-keV lines in the Ge projection.

Figure 13 placement

Figure 14 placement

Efficiency values for gamma rays detected by a BGO and in coincidence with the Ge detector were obtained using the peak fits from cut spectra and are plotted in Fig. 15a. Considering a BGO spectrum that resulted from a specific Ge cut around γ_i, the number of counts N_{ji} in a full-energy peak therein was given by

$$N_{ji} = N_t f_{j|t} \varepsilon_j \quad , \tag{2}$$

‡ Many other spectrum analysis programs were available, including the powerful Radware suite. The miniball system produces asymmetric data from the different detector types and so TV was chosen as being best suited to this application.

where N_i corresponds to the value in Eq. (1) provided that the cut process included standard background subtraction using channels in the continuum to the right and left of the Ge peak for γ_i. The ε_j denotes the efficiency for detection of a specific γ_j in the BGO in coincidence with the given γ_i on which the cut was made in the Ge projection. The factor $f_{j|i}$ is the fraction of decay events that emit the particular γ_j provided that γ_i was also emitted (see Appendix A). A cut taken on the Ge 213-keV line provided BGO efficiencies for the coincident 325-keV and 426-keV lines. Likewise, a cut on the Ge 426-keV line provided BGO efficiencies for 213 keV and 325 keV. Thus, cross-checking was performed between efficiency values at each specific energy obtained using different cuts. It is worth noting that cut spectra corresponding to the ground state band did not include full-energy gamma-ray peaks at 89 keV and 93 keV from the $8^- \rightarrow 8^+$ and $2^+ \rightarrow 0^+$ transitions, respectively, or from X rays following electron conversion. This was due to the small size of the corresponding unamplified BGO signals which were below the minimum discriminator thresholds. Nevertheless, the spectra evidenced summations between these gamma rays and the main features at 213 keV, 325 keV and 426 keV. Also, summations appeared between X rays emitted following conversion of the 89- and 93-keV transitions and the main gamma lines. These sum events result from triple coincidences in which γ_i enters the Ge detector and both γ_j and γ_k enter a single BGO crystal. To determine the direct efficiencies from Eq. (2), counts in identifiable sum peaks within the BGO singles spectrum were added to the full-energy counts of individual gamma rays. The resulting efficiencies reflected values for hypothetical single-lines sources.

Figure 15 placement

Efficiency values were also determined based on the relationship between individual and sum peaks using the method of Appendix B. Despite their larger statistical errors, their magnitudes confirm the direct efficiencies as shown in Fig. 15a. Systematic errors in fitting of the broad BGO peaks are not shown, but were estimated to be on the order of 10%.

Each scintillator evidenced a unique efficiency curve, as expected. The principal causes were that each detector lay at a slightly different spacing from the sample and that self-absorption was different for each specific sample orientation relative to a given detector. In one case, the CF8000 threshold was obviously lower, enhancing the efficiency for low-energy gamma rays recorded from that BGO. For the following analysis, an averaged efficiency was determined as shown in Fig. 15b to represent the canonical single BGO response.

3.3 Physical multiplicity and detected fold

The miniball system was designed to perform time-resolved calorimetry for gamma-ray cascades resulting from natural decay of ^{178m2}Hf and from possible prompt induced energy release. Figure 16 shows bi-dimensional plots of the Ge energy vs. the summed energy from the scintillators for different values of detected coincidence fold. Every event records at least one gamma ray, from the Ge crystal, so the total detected

fold is designated as 1 + F, where F is the detected fold from the six BGO detectors. Sorting was performed as described above with F being the number of BGO's that produced a valid STOP pulse within the respective coincidence period of the individual detector. The summed gamma-ray energy registered from the BGO detectors was then obtained by adding the individual spectroscopic data from the separate scintillators.

Each natural decay of ^{178m2}Hf produces (see Fig. 1) two gamma-ray bursts from cascades separated by the 4-s *m1* isomer. Only a single cascade occurs below that isomer, releasing a total energy of 1,147 keV and possessing a physical multiplicity of five. However, the 93-keV transition is strongly converted ($\alpha_{93} = 4.74$) and it and the 89-keV transition are suppressed in the BGO spectra due to the discriminator levels. This means that the effective physical multiplicity is reduced to three unless the 89-keV or 93-keV gamma rays register in the Ge detector. The effective triplet cascade then contains the 213-, 325- and 426-keV transitions for a total energy of 964 keV. The cascade above the 4-s isomer releases 1,298.7 keV and contains a number of branches, so that the physical multiplicity ranges from 4 – 6. The first step of the decay, the $16^+ \rightarrow 13^-$ transition at 12.7 keV, is completely converted with $\alpha_{12.7} = 1.39\times10^7$ so the effective physical multiplicity ranges from 3 – 5. The most intense branch (70.7%) occurs through the 574-, 495- and 217-keV transitions with a physical multiplicity of three (53.1% for the gamma-ray triplet). All gamma-ray triplets contribute a total of 72.2%.

Figure 16 placement (full page for a-i)

Decay of ^{172}Hf nuclei in the sample produces gamma rays emitted in many different branched cascades from transitions in ^{172}Lu and ^{172}Yb. From the established nuclear data [2], on the order of 30 cascades correspond to a physical multiplicity of two, on the order of 140 cascades correspond to a physical multiplicity of three and on the order of 360 cascades correspond to a physical multiplicity of four. Higher multiplicity cascades are also possible. Decays of ^{172}Hf and ^{172}Lu can lead to different daughter levels, so cascades of identical physical multiplicity may represent various total energies released by the gamma-ray transitions. Despite the complexity of cascades following ^{172}Hf decay, a physical multiplicity of three represents a major component.

For a given physical multiplicity, the frequency with which a given detected fold F would occur could be modeled using a simple Monte Carlo code. Figure 17a shows a histogram of the calculated detected fold F assuming an energy of 250 keV (thus a BGO photopeak efficiency of 5.4%) for all gammas in the cascade and a physical multiplicity of three. In this idealized case, the detected folds appear in the absolute intensities listed in Table 1 and plotted in Fig. 17a. Also given are measured total counts within bi-dimensional Ge vs. summed BGO spectra for different coincident folds. The general agreement between measured and calculated intensities for different folds is surprisingly good, considering that the spectra contained contributions from different physical multiplicities. Another factor that reduced the accuracy of the calculation was that some coincidence counts in a BGO in coincidence were due to Compton rather than photopeak interactions. Some gamma rays reaching a BGO in coincidence did not provide a valid STOP pulse due to their pulse height so that those events were recorded as having a

detected fold of F - 1 rather than F. This was also the case when coincident summing occurred within a single BGO. For prompt triggered gamma emission, the physical multiplicity will be on the order of eight so that the anticipated distribution of detected folds will be that of Fig. 17b.

Figure 17 placement

Table 1 placement

3.4 Calorimetry

The spectrum of Fig. 16a, with expanded section in Fig. 16b, shows data for a detected fold of 1 + 1 (Ge + any one BGO[§]) and contains numerous paired gamma-ray peaks. In the case of ^{178m2}Hf decay in the cascade below the *m1* isomer, detection of 213 keV in the Ge coincident with detection of 325 keV in one BGO provides a peak while the converse (325 keV in the Ge, 213 keV in the BGO) provides its partner. A line drawn in Fig. 16a connecting these two peaks represents a locus of constant total deposited energy at 538 keV. This is significantly less than the total cascade energy since the physical multiplicity is five and the detected fold is only 1 + 1. Examination of the 1 + 2 spectrum of Fig. 16c, with expanded section in Fig. 16d, shows two loci of γ-γ-γ peaks corresponding to deposited energies of 964 keV and 1,286 keV, representing nearly the full ^{178m1}Hf → ^{178g}Hf and ^{178m2}Hf → ^{178m1}Hf cascades, respectively.

The 1 + 3 spectrum of Figs. 16d and 16e also evidences a locus of 1,286 keV from several cascade branches with physical multiplicity of four above ^{178m1}Hf, while one peak is seen that corresponds to decay of ^{178m1}Hf to the ground state with summed energy of 1,057 keV. The latter peak is actually a doublet of 89-keV and 93-keV lines in the Ge detector from events of physical multiplicity of four in the ground-state band. The peak corresponding to 93 keV in the Ge detector is smaller since the transition is heavily converted. No other peaks from the ground state band can appear with such high detected fold since the 89-keV and 93-keV peaks were suppressed from the BGO detectors due to discriminator thresholds.

In addition to features identified with ^{178m2}Hf, loci of constant summed energy appear in the spectra from cascades following ^{172}Hf decay. For a detected fold of 1 + 1 in Figs. 16a and 16b, paired peaks appear from 900-keV and 1,093-keV transitions, giving a summed energy of 1,993 keV. Many other peaks from ^{172}Hf decay contribute to the 1 + 1 spectrum, although in some instances both partners do not appear. This occurs when the energy of one of the gamma rays is too low to register in the BGO spectrum. For any detected fold, different summed energy loci exist from the numerous decay branches. Gamma-ray cascades in ^{172}Lu have summed energies less than 240 keV. Summed energies of ^{172}Yb cascades reach as high as 2,343 keV (2.57%) after decay of ^{172}Lu, with a total of 9.59% exceeding 2,200 keV.

---

§ This differs from Fig 13 which shows doubles data between the Ge and one specific BGO, but without restrictions on what is recorded by the other BGO scintillators. Figure 16a contains doubles between the Ge and any BGO for the case that exactly one of the BGO registers a coincident gamma ray.

If claims of prompt triggered gamma emission from ^{178m2}Hf are correct, then the summed energy in an induced cascade would be about (2,446 + 10) keV. The data shown in Fig. 16 evidenced no locus of coincident peaks at this summed energy and indeed none should occur for natural decays of the hafnium species in the sample. Figure 16g shows a 1 + 4 spectrum with coincidence again determined by the wide (700-channel) time sort. The counts are quite low and distributed over a range of energies in the BGO dimension, suggesting a number of unresolved gamma-ray peaks. This is consistent with the numerous cascades of physical multiplicity five that occur in ^{172}Hf decay. The largest summed energy from these distributed counts would be about 2,300 keV. It is interesting in Fig. 16g that the energies of coincident gamma rays from the Ge detector are those resulting from ^{178m2}Hf decay. Thus, these counts appear to be due to random coincidences between decays from the different hafnium species. Figure 16h shows a 1 + 4 spectrum, but sorted on the narrow coincidence peak of Fig. 12 that contains a smaller fraction of random events. The number of counts is greatly reduced, as expected if random coincidences were the source of events in Fig. 16g. Random coincidences at a quite low level continue to appear for higher detected folds, such as $F = 5$ in Fig. 16i (wide time sort). A narrow time sort on $F = 5$ and wide and narrow sorts for $F = 6$ exhibit widely-scattered single events with total spectral counts of 53, 38 and 0, respectively.

In the subsequent experiment to examine gamma emission during irradiation with synchrotron radiation [19], it would be desired to determine the cross section for any prompt triggered events. It is possible to foresee two possible outcomes from this experiment:

1. Sufficient prompt induced gamma emission will occur so that identifiable peaks will appear in bi-dimensional Ge vs. summed-BGO spectra, or
2. Insufficient prompt induced gamma emission will occur to produce identifiable peaks in bi-dimensional spectra and only scattered background counts appear.

In the first case, cuts in the $1 + F$ spectra could be taken and the resulting peaks fitted in the summed-energy BGO projections. This would determine the measured rates for detection of specific γ^{1+F} events and the placement of peaks along a locus of constant total deposited energy would allow the individual gamma-ray energies to be deduced. The reaction rate for induced events could then be determined from the detection rate of each peak by using the measured efficiencies for the different detectors at the appropriate energies and by assuming some value for f of the specific γ^{1+F} cascade. An assumption of $f \approx 1$ would be reasonable for any prompt cascade through the ground-state band since there would be no branching and only a few transitions would be significantly converted. The cross section for prompt induced gamma emission would finally be deduced from the reaction rate, the number of target ^{178m2}Hf nuclei and the incident photon flux.

To validate this approach, it was applied to various $1 + F$ bi-dimensional spectra to find the ^{178m2}Hf activity. The fitted counts within a peak resulting from a coincidence of $1 + F$ gamma rays was obtained using the TV program as $N_{(1+F)}$ where γ_i enters the Ge detector and γ_j, γ_k, etc. enter the BGO scintillators. The peak counts are given approximately by

$$N_{(1+F)} \approx RTf_{(1+F)}\varepsilon_i \left(\frac{6!}{(6-F)!} \right) \prod_{\alpha=j}^{F} \varepsilon_\alpha \prod_{\beta=M-(1+F)}^{M} (1 - f_{\beta|(1+F)} 6\varepsilon_\beta) \quad , \qquad (3)$$

where the probabilities for photopeak detection of the gamma rays are ε_i (Ge) and ε_j, etc. (BGO). The rate at which emission-causing events occur is R and the measurement live time is T. Equation (3) represents the detection of $(1 + F)$ gamma rays for which the joint emission probability is $f_{(1+F)}$ (see Appendix A). The combinatorial factor gives the chance of detection of F distinct gamma rays in the six BGO scintillators. Should the physical multiplicity M be larger than $(1 + F)$, Eq. (3) must exclude the possibility that additional gamma rays enter any detector, in which case either the detected fold would have been different or a different total deposited energy would have arisen in the bi-dimensional spectrum. The latter case reflects coincidence summing (see Appendix B) and can occur in the Ge as well as the scintillators. The Ge efficiency is, however, much smaller at a given energy than the BGO values and their uncertainties, and is therefore neglected in the final product within Eq. (3). In that term, $f_{\beta|(1+F)}$ is the joint probability that a specific additional gamma ray is emitted given that the $(1 + F)$ photopeak gamma rays were emitted.

When applied to peaks corresponding to natural decays of ^{178m2}Hf, the rate R represents the sample activity. Using Eq. (3), the ^{178m1}Hf → ^{178g}Hf cascade in 1 + 1 (Fig. 16a and 16b), 1 + 2 (Fig. 16c and 16d) and 1 + 3 (Fig. 16e and 16f) bi-dimensional spectra reproduce the known value of 0.37 μCi within ± 15%. Application of the same procedure to peaks from the more complex ^{178m2}Hf → ^{178m1}Hf cascades reproduces the known activity to within ± 30%.

An alternate means of determining the rate of prompt triggering would be required in the second case, where no identifiable peaks occurred in the bi-dimensional spectra. The detected rate for emitted gamma rays could only be determined from the total count within a region of the spectra that corresponds to a specific summed BGO energy. For example, considering the width of peaks in the BGO dimension, events from a prompt triggered cascade would reside between total energy lines of about 2,380 keV and 2,530 keV. Using effective efficiencies for Ge and BGO detectors averaged over this section of the bi-dimensional spectrum and an estimated f value, the reaction rate could be estimated. To determine if this procedure was feasible in practice, it was tested for regions in which natural decay of ^{178m2}Hf appears.

Sum-energy ranges of 1,200 - 1,370 keV and 885 - 1,040 keV were used in the 1 + 2 spectrum of Fig. 16b to count the total events from cascades above and below the 4-s isomer of ^{178}Hf, respectively. These were found to be 4,271,050 and 7,029,212 while in

those same regions the counts within the full-energy peaks from ^{178m2}Hf cascades were 2,706,250 and 3,174,291. Thus, 63% and 45% of the total counts in the sum-energy ranges reside in full-energy peaks from this nuclide while the remaining counts are due to Compton events for ^{178m2}Hf gamma rays, photopeak and Compton events from ^{172}Hf decays, and other background. This background should include some contribution from cosmic rays, which will appear even with the shortest possible coincidence times. In order to estimate the activity based on the total counts within the ranges, and without basing this estimate on knowledge of specific peaks, it was necessary to employ some effective values for the joint emission probability and for the Ge and BGO efficiencies.

The estimated rate $R^{est}_{(1+F)}$ of emission-causing events based on the total counts N_{tot} within a sum-energy range from the 1 + 2 spectrum was determined using

$$R^{est}_{(1+2)} = \frac{N_{tot}}{T(3f)\left(30\left\langle \varepsilon_{Ge}\varepsilon^2_{BGO}\right\rangle\right)} \quad . \tag{4}$$

Even without knowledge of specific peaks in the 1 + 2 spectrum, it is clear that triplet gamma-ray cascades will provide the dominant contribution to the total counts. Counts due to a triplet will appear spread over three peaks having the same sum-energy range due to the permutations of detection in the Ge and the scintillators. Taking the total counts in the sum-energy range means adding the contributions from all three peaks resulting from permutations for triplet detection. The Ge efficiency, however, was determined from Eq. (1) separately for each individual peak based on the full joint emission probability. Simply adding the numbers of events within all three permutations of the full-energy peaks overcounts the joint emission probability, thus the appearance of $3f$ in Eq. (4). For heavily-branched cascades or when strong conversion occurs, the joint probability will differ significantly from unity. However, without knowledge of the specific cascades, a value of $f \approx 1$ is the only justifiable choice.

The Ge and BGO efficiencies for a 1 + 2 spectrum enter as a product of the form $\varepsilon_{Ge}\varepsilon^2_{BGO}$ (see Eq. (3)). When employing the total counts within a sum-energy range, an average value over that range must be utilized. Using the total counts corresponding to ^{178m1}Hf → ^{178g}Hf decay, an estimated rate of $R^{est}_{(1+F)}$ = 33,670 s^{-1} was found, equivalent to an activity of 0.91 μCi. The sum-energy range corresponding to ^{178m2}Hf → ^{178m1}Hf cascades provided $R^{est}_{(1+F)}$ = 18,500 s^{-1}, equivalent to 0.50 μCi.

Application of the same procedure to the 1 + 3 spectrum (Fig. 16d and 16e) gives rate estimates that are about a factor of 3 – 4 lower than the known ^{178m2}Hf activity of 0.37 μCi. For the ^{178m2}Hf → ^{178m1}Hf sum-energy range, this was attributed to the use of $f \approx 1$ when the actual joint probability is about 0.1. The low value for the ^{178m1}Hf → ^{178g}Hf sum-energy range was attributed to the fact that the low-energy gamma rays in the cascade (89 keV and 93 keV) do not register if they enter the scintillators, so that the total number of counts in the range is too low for the given multiplicity. Application of the procedure to the 1 + 4 spectrum (Fig. 16g and 16h) gives no estimate

from the ground-state band (both 89- and 93-keV gamma rays must register for a total detected fold of five) and an estimate equivalent to 0.02 μCi for the ^{178m2}Hf → ^{178m1}Hf cascades.

Prompt induced gamma emission could be expected to exhibit little branching and few gamma rays out of the total multiplicity near 8 would have such low energies as to not be registered by the BGO detectors. Thus, the approach should provide a reasonable upper limit to the rate of such events should no peaks be in evidence in the bi-dimensional spectra.

The small number of counts within the summed-energy range of 2,380 keV - 2,530 keV, centered around (2,446 + 10) keV, will serve as the background in the subsequent experiment [19]. Table 2 lists measured total counts due to natural decay in this region for bi-dimensional Ge vs. summed BGO spectra of different detected folds. The minimum detectable rates for gamma rays due to prompt triggering are also given, corresponding to three standard deviations of the background counts in the range for the specified fold.

Table 2 placement

4. Summary

Claims of prompt gamma emission from ^{178m2}Hf induced by incident photons near 10 keV require confirmation by independent tests designed specifically for this type of event. The YSU miniball system is uniquely suited to such studies based on its capability for time-resolved gamma-ray calorimetry and is sufficiently compact and portable to be transported to and placed within synchrotron radiation hutches. The system has been characterized by the natural decay of ^{178m2}Hf as a prelude to a search for low-energy prompt energy release from this 31-year isomer. The sensitivity and detection limits for data obtained using the miniball were established.

5. Acknowledgments

The authors wish to thank Phil Walker (University of Surrey), Greg Lane (Australian National University) and Jo Ressler (Simon Fraser University) for valuable discussions. Special thanks go to M.-T. Tang, J.-J. Lee and K. Liang of the Taiwan National Synchrotron Radiation Research Center (NSRRC) and H. Suematsu of JASRI/SPring-8 for the gracious use of the BL12B2 contract beamline at SPring-8, and to SRS Technologies, Inc. for supplying the ^{178m2}Hf/^{172}Hf sample. Thanks also to Richard Sumner of CheeseCote Mountain CAMAC and Richard Laughlin of YSU Electronics Maintenance. Support for this work was provided by the DCI Postdoctoral Research Fellowship Program under contract 2002-H061400-000 and the US Air Force Office of Scientific Research under contract F49620-02-1-0187.

Appendix A – Probabilities for individual and coincident gamma rays

The probability that an individual gamma is emitted following decay of ^{178m2}Hf is tabulated in the ENSDF [2] and adopted values are listed in Table A.1. Weak transitions found in Ref. [22] are not included as they could not be observed in this work.

Table A.1 placement

The above literature values were used in the determination of the efficiency for the Ge detector, from peak counts in the singles spectrum extracted without sort conditions from the miniball data and using Eq. (1) in the main text. Determination of efficiencies for gamma rays detected by single BGO scintillators requires the probabilities for double coincidences, since the instrumentation requires coincidence with the Ge detector. These probabilities may be calculated as follows based on the literature data in the following way.

Thirteen unique cascades from ^{178m2}Hf → ^{178m1}Hf were identified as shown in Table A.2, again excluding the weak transitions found in Ref. [22]. The branching ratios for each transition were found from the f and α values according to

$$b_i = f_i(1+\alpha_i) \quad , \tag{A.1}$$

where b_i is the probability for a given branch from a given level, and f_i and α_i are the corresponding gamma probability and conversion coefficient. From these values it is possible to determine the total likelihood that any given cascade will occur. Based on Table A.2, the 574-keV transition is described by $b_{574} = (0.707 + 0.111 + 0.0741) = 0.892$, and from Eq. (A.1), $f_{574} = 0.880$. This agrees, as it should, with the literature value in Table A.1.

Table A.2 placement

The joint probability that 574-keV and 495-keV gamma rays are emitted in coincidence is then found by

$$f_{574,495} = f_{574} f_{495|574} = f_{495} f_{574|495} \quad . \tag{A.2}$$

It is straightforward from Table A.2 and Eq. (A.1) to find the conditional probability

$$f_{495|574} = \left(\frac{0.707}{0.707+0.111+0.0741}\right)\left(\frac{1}{1+0.0199}\right) = 0.777 \quad , \tag{A.3}$$

so that the joint probability $f_{574,495} = 0.684$. In a similar manner the joint probability for a triple coincidence may be found from Table A.2, as occurs when a single BGO exhibits sum peaks (γ_i detected by the Ge and both γ_j and γ_k detected by the BGO) or when two BGO detectors receive separate gamma rays. Only one cascade occurs in

^{178m1}Hf → ^{178g}Hf decay and the joint probabilities then reduce to the product of the *f* values for the specific transitions.

While a tabular approach for enumerating possible cascades was simple for ^{178m2}Hf, it is not well suited for gamma rays resulting from decay of ^{172}Hf and its daughters. Among ^{172}Yb transitions there are forty energy levels and about 2,000 possible cascades following ^{172}Hf decay. The more general approach of Ref. [29] was used to determine *f* values needed to evaluate selected gamma rays following ^{172}Hf decay.

Appendix B - Determination of detector efficiencies via sum peaks of cascade gamma rays

Placement of the hafnium sample within the central cavity of the miniball represents a close geometry between source and detectors. The ^{178m2}Hf and ^{172}Hf radioisotopes emit cascades of gamma rays, so *true coincidence summing* (TCS) could be expected to impact the values of detector efficiencies determined from the counts within full-energy peaks. If the goal of the miniball system was to be able to compare the rates of emission at specific gamma energies from the natural decay, during and without irradiation by external photons, then efficiencies would not be required and TCS could be ignored. However, the possibility of emission of new gamma-ray lines from a prompt triggered cascade required determination of the detector efficiencies and the role of TCS.

The general topic is discussed in Ref. [30] and numerous analytical, empirical and computational methods have been developed (see, for example, Refs. [29, 31]). The methods all seek to correct the efficiencies determined directly from counts in full-energy peaks for events lost to summations. Herein it was desired to not only obtain such corrections, but also to determine the detector efficiencies based on comparison of the counts in sum peaks to the counts in the individual full-energy peaks. The latter would provide a verification of the direct efficiency values, and the radionuclide activities which enter the calculations in different order. No method has been applied previously to the hafnium nuclides of interest in this work, nor does the literature discuss the determination of efficiencies from the sum-to-individual-peak counts.

The present approach considers two gamma rays designated as γ_1 and γ_2, emitted in coincidence within a prompt cascade that may include other transitions. Entrance of both gamma rays into a single BGO detector causes a summation and a loss of counts from the respective photopeaks according to

$$N_j = N_i f_j \varepsilon_j (1 - S_j) \quad , \tag{B.1}$$

where N_i is taken from Eq. (1) and N_j, f_j, and ε_j are the number of photopeak counts, the emission probability per decay, and the photopeak efficiency, respectively, corresponding to γ_j. (recall that γ_i was already detected in coincidence in the Ge detector). A is the sample activity and T the acquisition live time. Self-absorption may occur as gamma rays emitted from the hafnium nuclei exit the sample through the Al frame (see Fig. 8), but this simply contributes to the real efficiency of a detector and does not appear explicitly in Eq. (B.1). All counts removed from the photopeak due to summations of any type are accounted for in the coefficient S_j. This includes, but is not limited to, summations with both full-energy and Compton events from γ_k and with both full-energy and Compton events from gamma rays other than γ_i, γ_j and γ_k in the same cascade. The number of counts appearing in a BGO sum peak, N_Σ, due to γ_j and γ_k is

$$N_\Sigma = (N_i f_j \varepsilon_j)(f_{k|ji} \varepsilon_k) = (N_i f_k \varepsilon_k)(f_{j|ki} \varepsilon_j) \quad , \tag{B.2}$$

reflecting the symmetry between peak-to-peak summations in the BGO crystal. The $f_{j|ki}$ is the conditional probability per decay that γ_j is emitted given that γ_k was emitted (to the same BGO) and γ_i was emitted for the Ge. These may be found as discussed in Appendix A.

In many instances, the parameter S_j will be approximately constant for a specific γ_j and γ_k pair. Then Eqs. (B.1) and (B.2) may be solved to obtain

$$\varepsilon_j = \sqrt{\frac{N_j N_\Sigma}{ATN_k f_j f_{j|ki}}} \tag{B.3}$$

and

$$1 - S_j = 1 - S_k = \sqrt{\frac{N_j N_k f_{j|ki}}{N_i N_\Sigma f_j}} \tag{B.4}$$

The correction to an efficiency value determined directly from the photopeak areas is

$$\varepsilon_j^{corr} = \frac{\varepsilon_j}{1 - S_j} \quad . \tag{B.5}$$

In this approximation, the photopeak efficiencies for multi-line sources, such as ^{178m2}Hf and ^{172}Hf, may be determined through Eq. (B.3) or Eq. (B.5). Cascades emitted from ^{178m2}Hf satisfy the above approximation for a number of paired gamma rays which corresponded to sum peaks that did not exhibit contamination from actual transitions at that energy or from nearby ^{172}Hf lines. The values are plotted in Fig. 10b for the Ge detector and in Fig. 15 for a BGO detector. Direct efficiencies in Fig. 10 are uncorrected as S differs little from unity. The above method is similar to the more involved approach developed in Ref. [32] and efficiency values obtained by the two calculations typically agree to within less than 1%. Thus, the ^{178m2}Hf/^{172}Hf source may be valuable for efficiency calibrations of detectors even when TCS is significant.

REFERENCES

1. J. J. Carroll, S. A. Karamian, L. A. Rivlin, et al., Hyperfine Int. **135** (2001) 3.
2. National Nuclear Data Center Online Evaluated Nuclear Structure Data File (ENSDF), www.nndc.bnl.gov, Brookhaven National Laboratory, (2005)
3. C. B. Collins, C. D. Eberhard, J. W. Glesener, et al., Phys. Rev. C **37** (1988) 2267.
4. I. Bikit, L. Lakosi, J. Sáfár, et al., Phys. Rev. C **59** (1999) 2272.
5. P. M. Walker, G. D. Dracoulis, and J. J. Carroll, Phys. Rev C **64** (2001) 061302.
6. D. Cline, J. Modern Opt. (Proc. 35th Winter Colloquium on the Physics of Quantum Electronics) (in press for 2005).
7. A. B. Hayes, D. Cline, C. Y. Wu, et al., Phys. Rev. Lett. **89** (2002) 242501.
8. J. J. Carroll, Laser Phys. Lett. **1** (2004) 275.
9. C. B. Collins, N. C. Zoita, F. Davanloo, et al., Laser Phys. Lett. **2** (2005) 162.
10. I. Ahmad, J. C. Banar, J. A. Becker, et al., Phys Rev. C **71** (2005) 024311.
11. C. B. Collins, N. C. Zoita, F. Davanloo, et al., Radiat. Phys. Chem. **71** (2004) 619.
12. M. R. Harston and J. J. Carroll, Laser Phys. **15** (2005) 487.
13. E. V. Tkalya, Phys Rev. C **71** (2005) 024606.
14. G. D. Dracoulis, G. J. Lane, F. G. Kondev, et al., Phys Rev. C **71** (2005) 044326.
15. J. J. Carroll, J. Burnett, T. Drummond, et al., Hyperfine Int. **143** (2002) 37.
16. I. Ahmad, J. C. Banar, J. A. Becker, et al., Phys Rev. C **67** (2003) 041305(R).
17. I. Ahmad, J. C. Banar, J. A. Becker, et al., Phys. Rev. Lett. **87** (2001) 0725031.
18. C. B. Collins, N. C. Zoita, F. Davanloo, et al., Laser Phys. **14** (2004) 154.
19. J. J. Carroll and others, Phys Rev. C (in preparation for 2006).
20. I. Y. Lee, M. A. Deleplanque, and K. Vetter, Rep. Prog. Phys. **66** (2003) 1095.
21. J. J. Carroll, S. A. Karamian, M. K. Boyle, et al., Laser Phys. **11** (2001) 6.
22. M. B. Smith, P. M. Walker, G. C. Ball, et al., Phys Rev. C **68** (2003) 031302(R).
23. EG&G Ortec Modular Pulse-Processing Electronics and Semiconductor Radiation Detectors, 1997/1998, p 2.139.
24. R. Propri and others, in *Proceedings of the 7th AFOSR Workshop on Isomers and Quantum Nucleonics*, Dubna, Russia, 2005.
25. H. Roberts, G. Terry, M. Helba, et al., Analysis of Hf made at the LANL Nuclear Accelerator, Report prepared for the Army Research Laboratory (2003).
26. H. A. O'Brien, Nuclear Instruments and Methods **B40/41** (1989) 1126.
27. FitzPeaks, JF Computing Services (http://www.jimfitz.demon.co.uk/fitzpeak.htm), (2005)
28. TV, Institute of Nuclear Physics, University of Cologne, Germany, http://www.ikp.uni-koeln.de/~fitz/, (2003)
29. K. Sinkko and H. Aaltonen, Calculation of the true coincidence summing correction for different sample geometries in gamma-ray spectroscopy, Finnish Centre for Radiation and Nuclear Safety Report STUK-B-VALO 40 (1985).
30. G. Gilmore and J. D. Hemingway, *Practical Gamma-Ray Spectrometry*, (John Wiley & Sons, New York, 1995) Chapter 7.
31. S. H. Byun, W. V. Prestwich, K. Chin, et al., Nucl. Inst. Meth. A **535** (2004) 674.
32. T. Vidmar, M. Korun, and A. Likar, Nucl. Inst. Meth. **A 508** (2003) 404.

TABLES

Table 1: Absolute intensities for different folds calculated for an idealized cascade of effective physical multiplicity three and determined from the total counts in measured bi-dimensional Ge vs. summed BGO spectra.

F	Ideal intensity	Measured intensity
0	0.46	0.48
1	0.46	0.43
2	0.084	0.085
3	0	0.0038
4	0	0.00026
5	0	0.000011
6	0	0.00000014

Table 2: Measured total background counts (natural decay) and minimum detectable emission rates for sum-energy range corresponding to prompt induced emission, if any, from ^{178m2}Hf.

F	Total counts	Minimum gamma-ray detection rate [s^{-1}]
1 (wide sort)	32,180	2.56×10^{-3}
(narrow sort)	14,352	1.71×10^{-3}
2 (wide sort)	57,097	3.41×10^{-3}
(narrow sort)	7,986	1.27×10^{-3}
3 (wide sort)	24,853	2.25×10^{-3}
(narrow sort)	1,283	5.10×10^{-4}
4 (wide sort)	4,342	9.39×10^{-4}
(narrow sort)	106	1.47×10^{-4}
5 (wide sort)	253	2.27×10^{-4}
(narrow sort)	2	2.02×10^{-5}
6 (wide sort)	3	2.47×10^{-5}
(narrow sort)	0	$< 1.01 \times 10^{-5}$

Table A.1: Literature values [2] for emission probabilities and conversion coefficients for gamma rays resulting from decay of ^{178m2}Hf. Errors on the adopted f values are given in the ENSDF format. Also given are calculated emission probabilities using the method described below.

E_i [keV]	f_i	α_i	f_i^{calc}
12.7	7.178×10^{-8} (2)	1.39×10^{7}	7.181×10^{-8}
88.862	0.644 (10)	0.492	0.670
93.185	0.172 (3)	4.73	0.174
213.434	0.814 (11)	0.234	0.810
216.668	0.646 (10)	0.289	0.645
237.431	0.093 (2)	0.222	0.092
257.646	0.167 (4)	0.136	0.166
277.403	0.0138 (7)	0.13	0.0133
296.812	0.0969 (2)	0.090	0.0968
309.50	0.00019 (20)	8.66	0.00019
325.557	0.941 (11)	0.0626	0.941
426.360	0.970 (13)	0.0294	0.971
454.05	0.167 (3)	0.0249	0.164
495.013	0.713 (22)	0.0199	0.705
535.036	0.0941 (4)	0.0165	0.0908
574.215	0.879 (29)	0.0139	0.880

Table A.2: Unique cascades in decay of ^{178m2}Hf → ^{178m1}Hf and their likelihood based on literature values.

Cascade, E [keV]	Probability
12.7 → 574.2 → 495 → 216.7	0.707
12.7 → 574.2 → 257.6 → 454.1 →	0.111
12.7 → 574.2 → 257.6 → 237.4 → 216.7	0.0741
12.7 → 296.8 → 535 → 454.1 →	0.0544
12.7 → 296.8 → 535 → 237.4 → 216.7	0.0363
12.7 → 296.8 → 277.4 → 495 → 216.7	0.0118
12.7 → 296.8 → 277.4 → 257.6 → 454.1 →	0.00184
12.7 → 296.8 → 277.4 → 257.6 → 237.4 → 216.7	0.00123
309.5 → 535 → 454.1 →	0.000938
309.5 → 535 → 237.4 → 216.7	0.000626
309.5 → 277.4 → 495 → 216.7	0.000202
309.5 → 277.4 → 257.6 → 454.1 →	3.18×10^{-5}
309.5 → 277.4 → 257.6 → 237.4 → 216.7	2.12×10^{-5}

FIGURE CAPTIONS

Figure 1: Partial level diagram of ^{178}Hf, showing the dominant electromagnetic transitions occurring during spontaneous decay of the 31-year isomer [2]. The weak transitions found in the experiment of Ref. [22] are not shown. The total widths of cascade arrows represent the relative transition intensities, while their darkened widths indicate the gamma intensities. Transition energies in keV. The primary initial step in the *m2* decay occurs by a heavily-converted 12.7-keV E3 transition and the corresponding arrow does not attempt to represent its intensity. Also shown is a depiction of a hypothesized triggering process by excitation of nuclei already in the 31-year isomeric state to a higher-lying intermediate level, as described in the text.

Figure 2: YSU miniball array within the experimental hutch of the BL12B2 beamline at SPring-8. Labeled items are (a) a 65% Ge detector (part of miniball system), (b) a cubic support structure holding six BGO crystal/PMT assemblies, (c) a sample positioning arm, attached to a translation stage, (d) exit port from the support structure for synchrotron radiation. The additional small-volume Ge and x-ray detectors are independent from the miniball instrumentation.

Figure 3: Schematic of the pulse-processing instrumentation for the miniball array. The Ge detector provided the master gate for the system as described in the text.

Figure 4: Oscilloscope trace showing (a) the Ge detector preamp signal, (b) the Ge CFD timing pulse, (c) the system gate and (d) the output of the spectroscopy amplifier from the Ge signal. The time scale is 2 μs per division.

Figure 5: Oscilloscope trace showing (a) the system gate, (b) a BGO timing STOP signal, (c) a histogramming box that determines the magnitude of negative-going STOP pulses that will be recorded and (d) a histogram showing the frequency of STOP pulses as a function of time. The histogram provides the coincidence curve used to set delays on the time channels. The time scale is 1 μs per division.

Figure 6: Comparison of Ge and BGO energy resolutions for a ^{60}Co calibration source (obtained at Youngstown State University during preliminary testing).

Figure 7: (a) A TDC spectrum showing the distribution of STOP pulses from one BGO obtained from a ^{137}Cs source. Compton scattering between detectors results in a small coincidence curve, while in (b) this cross-talk between detectors has been eliminated by wrapping the detectors with 1 mm Pb.

Figure 8: Sample containing ^{178m2}Hf and ^{172}Hf, attached to the positioning arm and held in the central cavity of the miniball. Pb wraps around the BGO's were added after this picture. The diagonal of the cube containing the positioning arm is not perpendicular to the diagonal through which the synchrotron radiation was intended to pass in later experiments, necessitating a 15° orientation of the sample face with respect to the beam axis.

Figure 9: Ge singles spectrum extracted from the miniball data without sort conditions and acquired for a total of about 74 hours without irradiation. Major peaks from natural decay of ^{178m2}Hf (bare) and ^{172}Hf (ovals) are labeled.

Figure 10: (a) Plot showing measured efficiencies for the Ge detector using well-known gamma rays from ^{178m2}Hf and ^{172}Hf decays. Filled symbols indicate values obtained when the full miniball is assembled, including Pb wraps on the BGO crystals. The open symbols indicate values obtained when the BGO and their wraps are removed that would otherwise restrict the Ge detector's view of the central cavity. These measurements were made at Youngstown State University to determine the flattening of the efficiency curve due to the miniball configuration. (b) Plot showing measured efficiencies for the Ge detector using the hafnium source, taken at SPring-8 in the BL12B2 beamline hutch over a period of about 74 hours. Efficiencies were determined directly from the counts within full-energy peaks (filled symbols) and also from selected sum peaks by the method of Appendix B (open symbols).

Figure 11: Singles spectrum from a specific BGO detector and extracted without sort conditions from the full data set. Major peaks are labeled as in Fig. 9. Peak widths were too large to permit effective peak fitting, resolution of doublets or identification of smaller-intensity peaks.

Figure 12: Time spectrum for a specific BGO detector showing the distribution of STOP pulses. The "true" coincidence width is 51 ns, although a wider channel range was used in some time sorts to include the effects of walk of the Ge time mark (START) and BGO time mark (STOP).

Figure 13: Section of a bi-dimensional "doubles" spectrum displaying coincident events between the Ge detector and a specific BGO crystal. While full BGO singles spectra like that in Fig. 11 do not permit effective peak fitting, projections of slices ("cuts") of the doubles spectrum simplify the BGO spectra and do allow peak fitting. One cut is shown, made for events in which the full energy of the 495-keV gamma ray in ^{178m2}Hf $\rightarrow$ ^{178m1}Hf decay is deposited in the Ge detector.

Figure 14: (a) BGO projection (larger pane) obtained by a cut on the 495-keV photopeak in the Ge projection (short, top pane). The simplified structure in the BGO projection allowed identification and effective fitting of full-energy and sum peaks. (b) BGO projection obtained by a cut on the 325-keV Ge photopeak. Two coincident transitions are of too low energy to be recorded in the BGO due to discriminator levels. However, they appear as summations to the larger gamma-ray peaks at 213 keV and 426 keV, as do X rays resulting from electron conversion.

Figure 15: (a) Plot showing measured efficiencies for a specific BGO detector using well-known gamma rays from ^{178m2}Hf and ^{172}Hf decays. Data were taken at SPring-8. Filled symbols indicate values obtained using the photopeak counts after inclusion of counts lost to summation. When possible, multiple values for the efficiency of each gamma ray were extracted from different cuts, providing an internal cross-check. Open

symbols show values obtained by comparison of sum peaks from major gamma rays to the corresponding photopeak areas. (b) Effective single-BGO efficiency, obtained as the average of values from the six separate BGO detectors. Errors shown are systematic as statistical errors are comparable in magnitude to the size of the symbols. The curve is drawn to guide the eye.

Figure 16: Bi-dimensional spectra showing events corresponding to different detected folds and displayed by the energy deposited in the Ge and the total energy deposited in all six BGO detectors: (a) corresponds to $F = 1$ with (b) being an expanded view; (c) corresponds to $F = 2$ with (d) being an expanded view; and (e) corresponds to $F = 3$ with (f) being an expanded view. Plots (a) – (f) were obtained by sorting the data on the wide time range. Plots (g) and (i) show data extracted using the wide time range for $F = 4$ and 5, respectively. Plot (h) shows a detected fold of $F = 4$ extracted using the narrow time range. Plots of $F = 5$ for the narrow time range and of $F = 6$ using either time range exhibit a small number of widely-scattered events that are not easily visible in print. The total counts in the $F = 5$ narrow-time sort spectrum is 53. The total counts in the $F = 6$ wide and narrow-time sort spectra are 38 and 0, respectively. Selected sum-energy loci are indicated as discussed in the text.

Figure 17: Simulated distribution of BGO detected folds, F, for different physical multiplicities M for a cascade of gamma rays having an energy of 250 keV and a corresponding efficiency. The histogram of (a), with M = 3, represents the dominant cases for natural decay of ^{178m2}Hf and measured total counts in the spectra of Fig. 16. The histogram of (b), with M = 8, represents the expected distribution of detected BGO folds for prompt triggered events, if any, from ^{178m2}Hf.

Fig 1

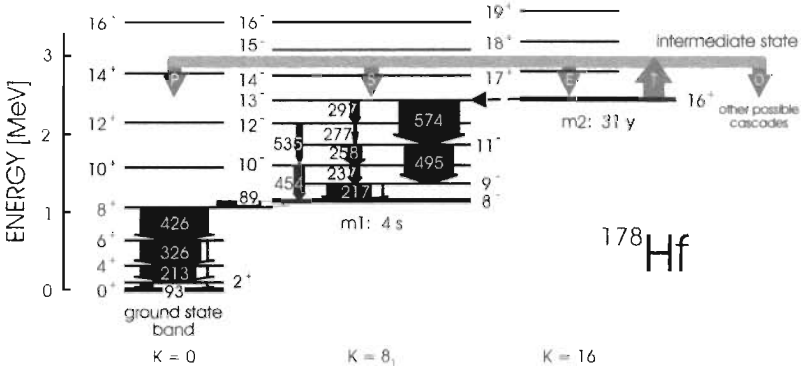
ENERGY [MeV]
0
1
2
3
16+
14+
12+
10+
8+
6+
4+
0+
426
326
213
93
2+
ground state band
K = 0
16-
15-
14-
13-
12-
10-
8+
297
277
258
237
217
574
495
535
454
89
m1: 4 s
K = 8
19+
18+
17+
16+
intermediate state
other possible cascades
m2: 31 y
11-
9-
8-
K = 16
178Hf

Fig. 1

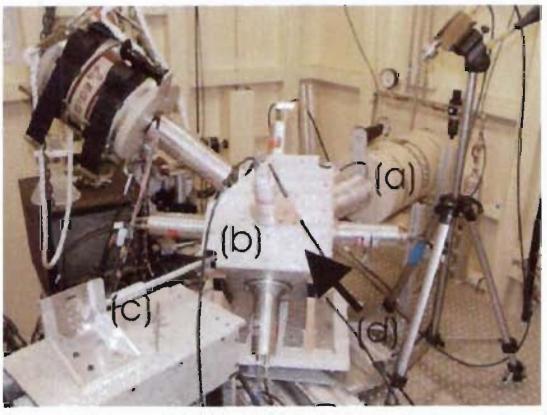

Fig. 2

Fig 3

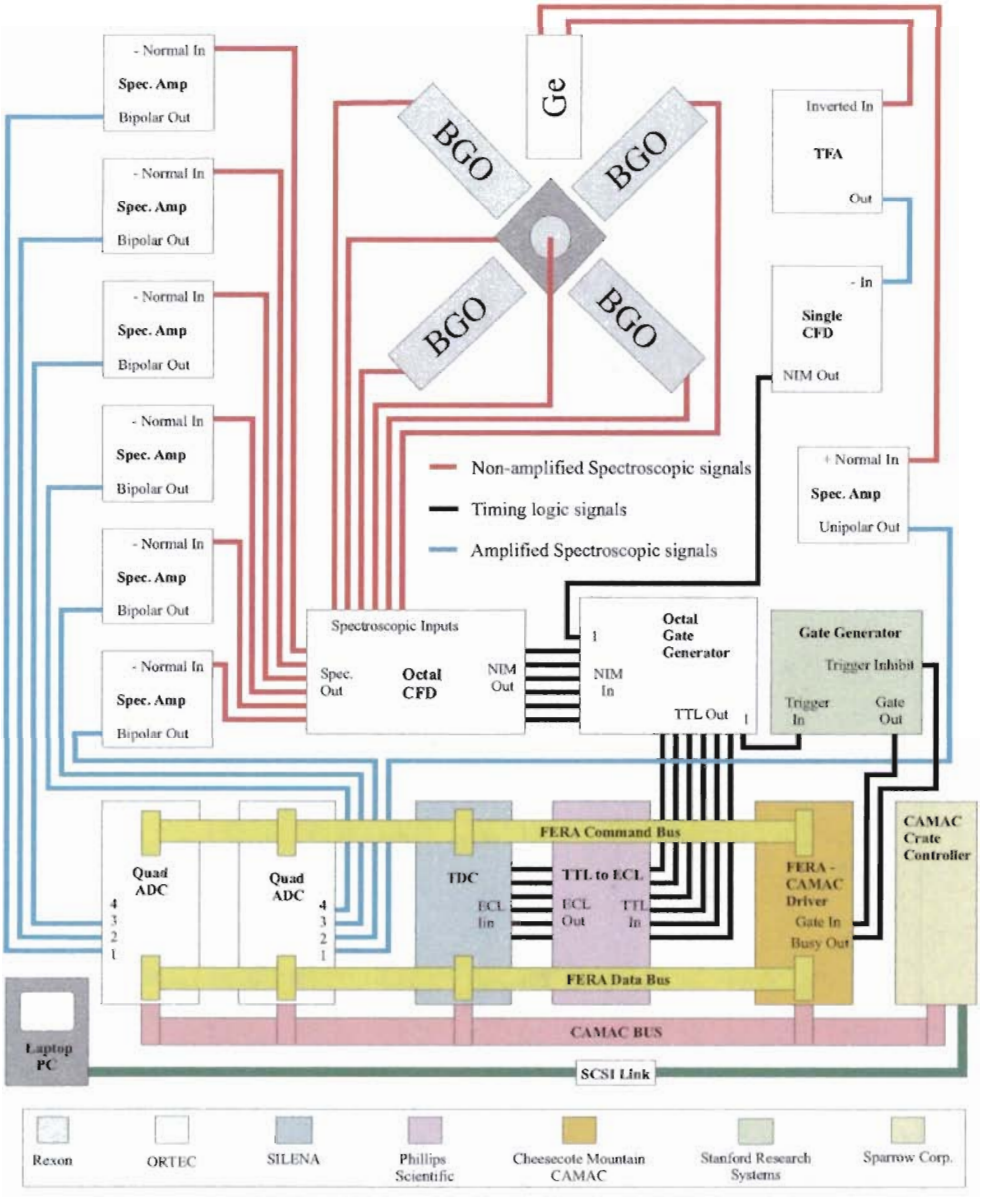
- Normal In
Spec. Amp
Bipolar Out
Ge
BGO
BGO
BGO
BGO
Inverted In
TFA
Out
- In
Single CFD
NIM Out
+ Normal In
Spec. Amp
Unipolar Out
Non-amplified Spectroscopic signals
Timing logic signals
Amplified Spectroscopic signals
Spectroscopic Inputs
Spec. Out
Octal CFD
NIM Out
Octal Gate Generator
NIM In
TTL Out
Gate Generator
Trigger Inhibit
Trigger In
Gate Out
Quad ADC
FERA Command Bus
TDC
TTL to ECL
ECL In
ECL Out
TTL In
FERA - CAMAC Driver
Gate In
Busy Out
CAMAC Crate Controller
FERA Data Bus
CAMAC BUS
Laptop PC
SCSI Link
Rexon
ORTEC
SILENA
Phillips Scientific
Cheesecote Mountain CAMAC
Stanford Research Systems
Sparrow Corp.

Fig. 3

Fig 4

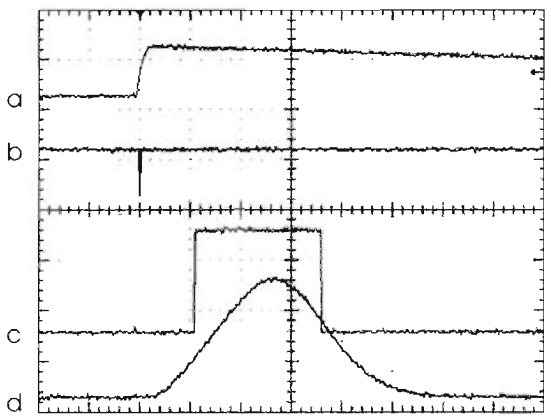

Fig. 4

Fig 5

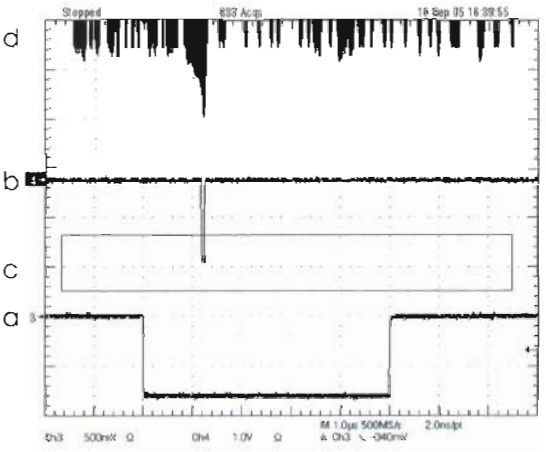
Stopped
833 Acqs
16 Sep 05 16:39:55
d
b
c
a
Ch3 500mV Ω
Ch4 1.0V Ω
M 1.0µs 500MS/s
A Ch3 ∖ -940mV
2.0ns/pt

Fig. 5

Fig 6

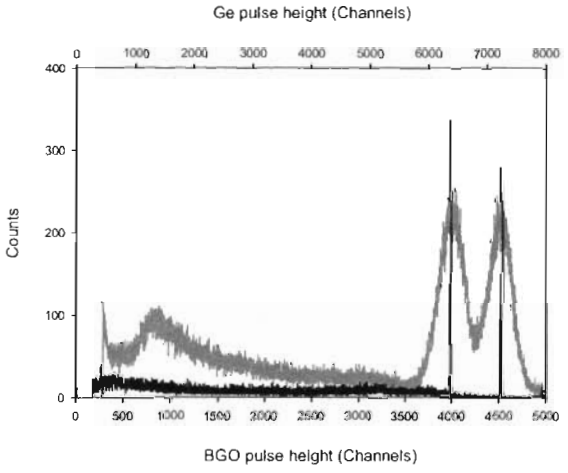
Ge pulse height (Channels)
0
1000
2000
3000
4000
5000
6000
7000
8000
400
300
200
100
0
Counts
0
500
1000
1500
2000
2500
3000
3500
4000
4500
5000
BGO pulse height (Channels)

Fig. 6

Fig 7

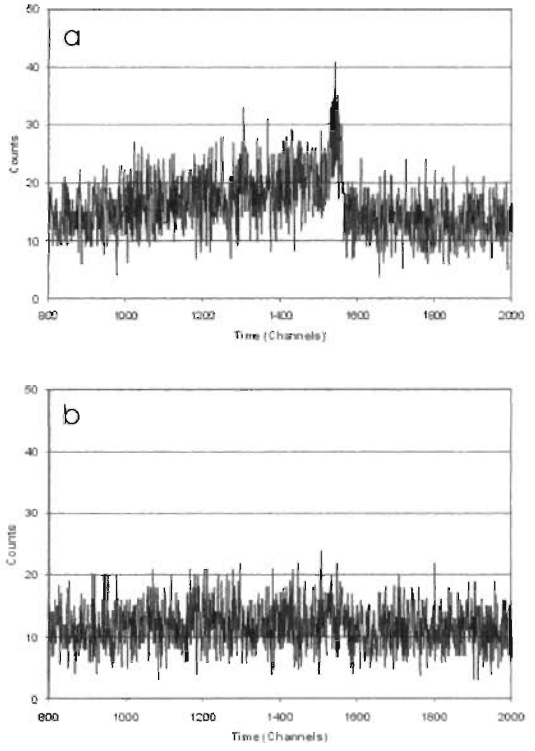
a
b
Counts
Time (Channels)
0
10
20
30
40
50
800
1000
1200
1400
1600
1800
2000

Fig. 7

Fig. 8

Fig 9

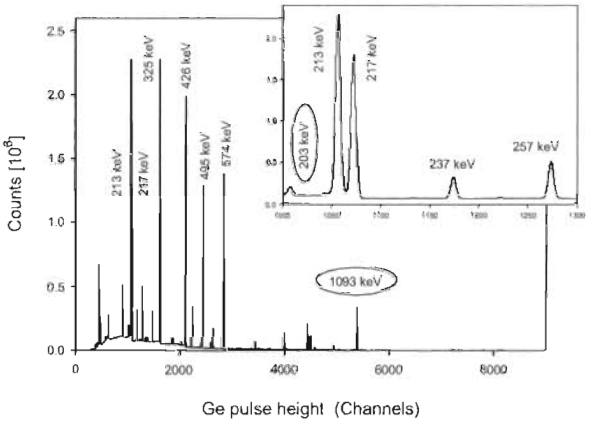
Counts [10^6]
2.5
2.0
1.5
1.0
0.5
0.0
0
2000
4000
6000
8000
Ge pulse height (Channels)
213 keV
217 keV
325 keV
426 keV
495 keV
574 keV
1093 keV
203 keV
213 keV
217 keV
237 keV
257 keV

Fig. 9

Fig 10

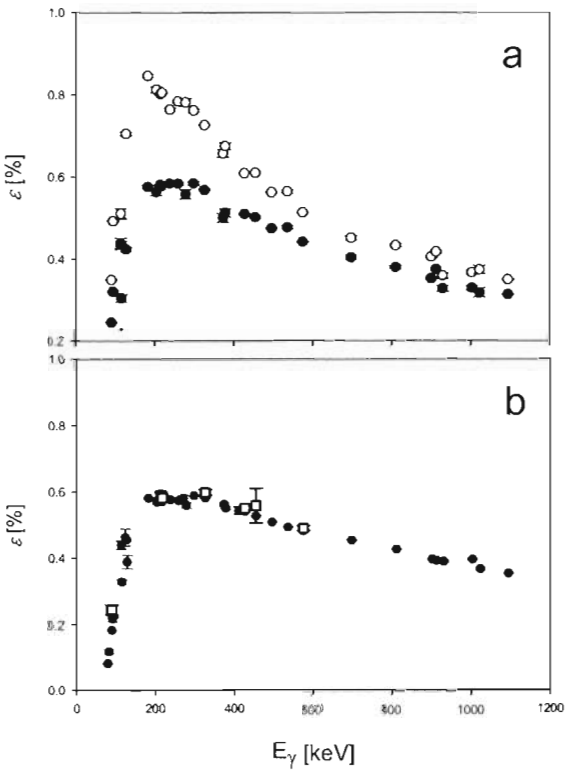

Fig. 10

Fig 11

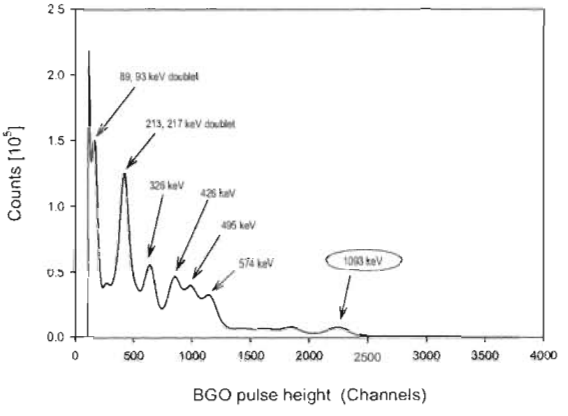
89, 93 keV doublet
213, 217 keV doublet
326 keV
426 keV
496 keV
574 keV
1093 keV
Counts [10^5]
BGO pulse height (Channels)
0.0
0.5
1.0
1.5
2.0
2.5
0
500
1000
1500
2000
2500
3000
3500
4000

Fig. 11

Fig 12

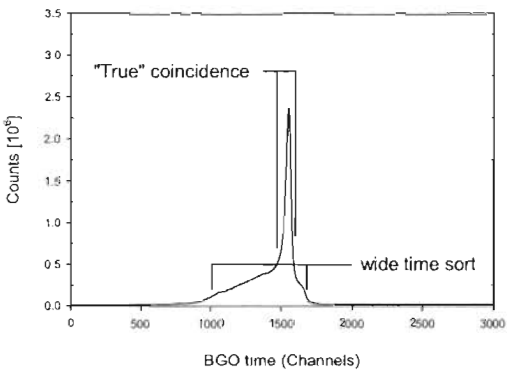
"True" coincidence
wide time sort
Counts [10^5]
BGO time (Channels)
0.0
0.5
1.0
1.5
2.0
2.5
3.0
3.5
0
500
1000
1500
2000
2500
3000

Fig. 12

Fig 13

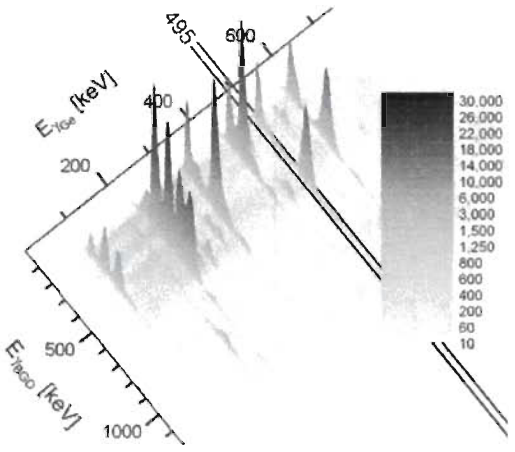
495
600
400
200
E_{ICE} [keV]
500
1000
E_{TACO} [keV]
30,000
26,000
22,000
18,000
14,000
10,000
6,000
3,000
1,500
1,250
800
600
400
200
60
10

Fig. 13

Fig 14

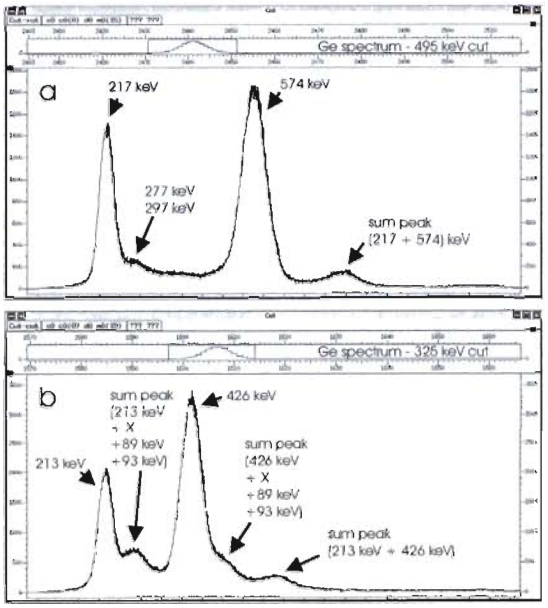
Ge spectrum - 495 keV cut
a
217 keV
574 keV
277 keV
297 keV
sum peak
(217 + 574) keV
Ge spectrum - 325 keV cut
b
sum peak
(213 keV
+ X
+ 89 keV
+ 93 keV)
426 keV
213 keV
sum peak
(426 keV
+ X
+ 89 keV
+ 93 keV)
sum peak
(213 keV + 426 keV)

Fig. 14

Fig 15

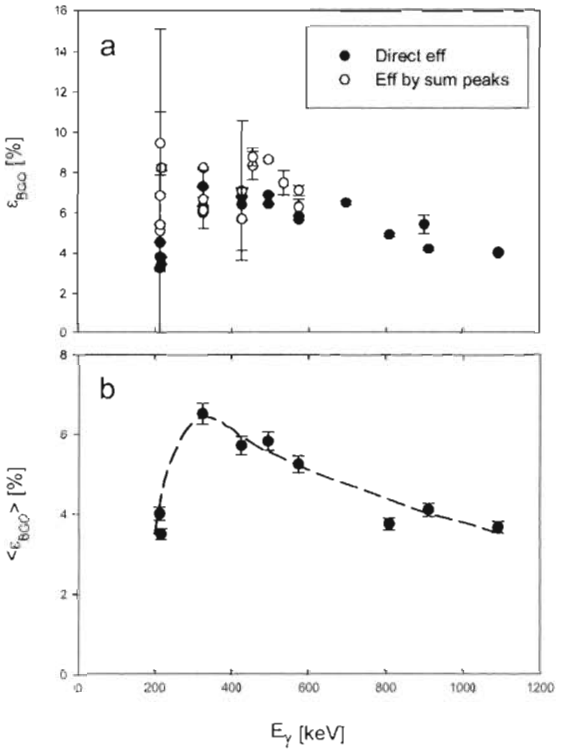
a
Direct eff
Eff by sum peaks
ε_{BGO} [%]
b
$<\varepsilon_{BGO}>$ [%]
E_γ [keV]

Fig. 15

Fig 16a-f

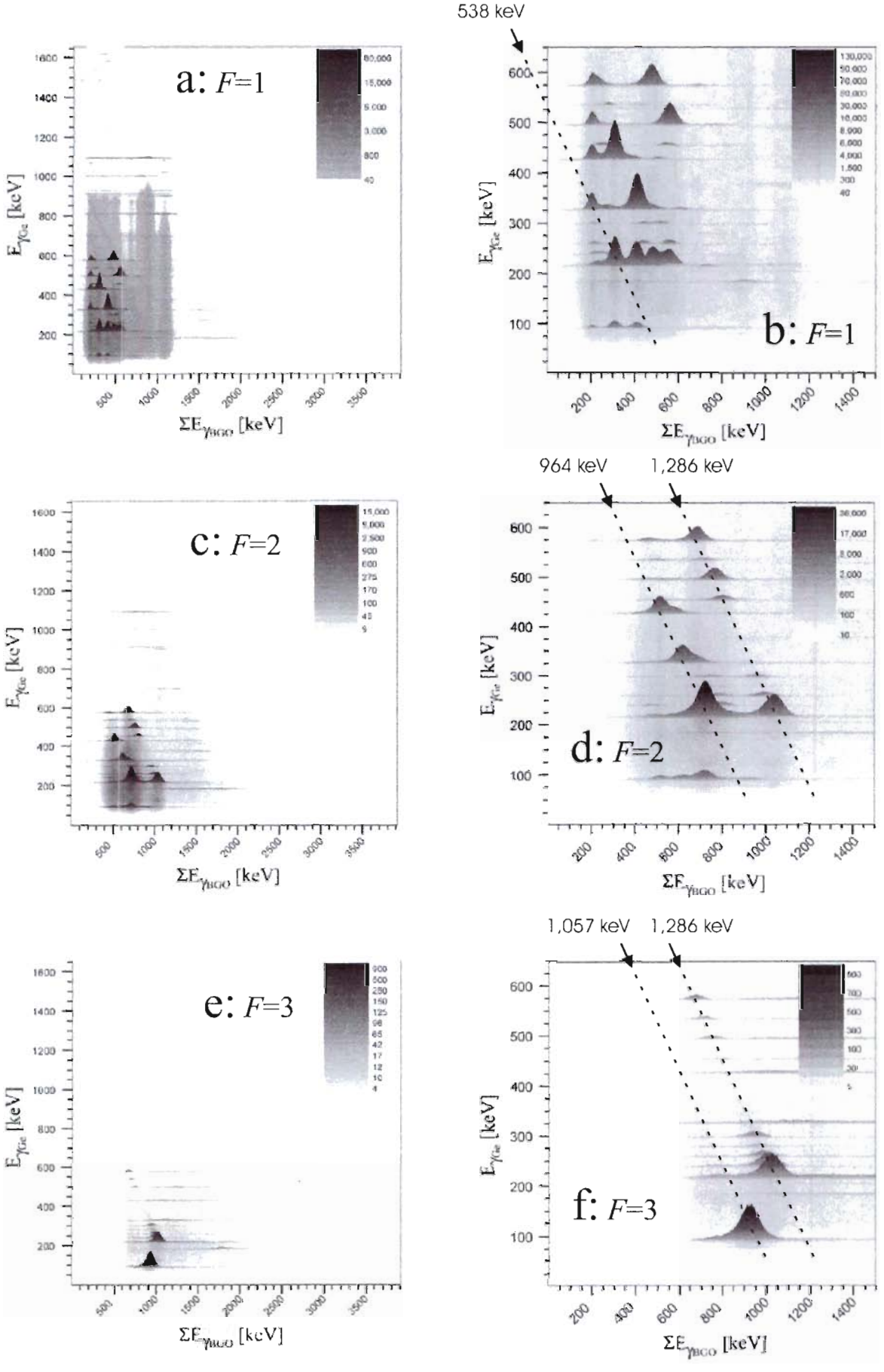

Fig. 16a-f

Fig 16g-i

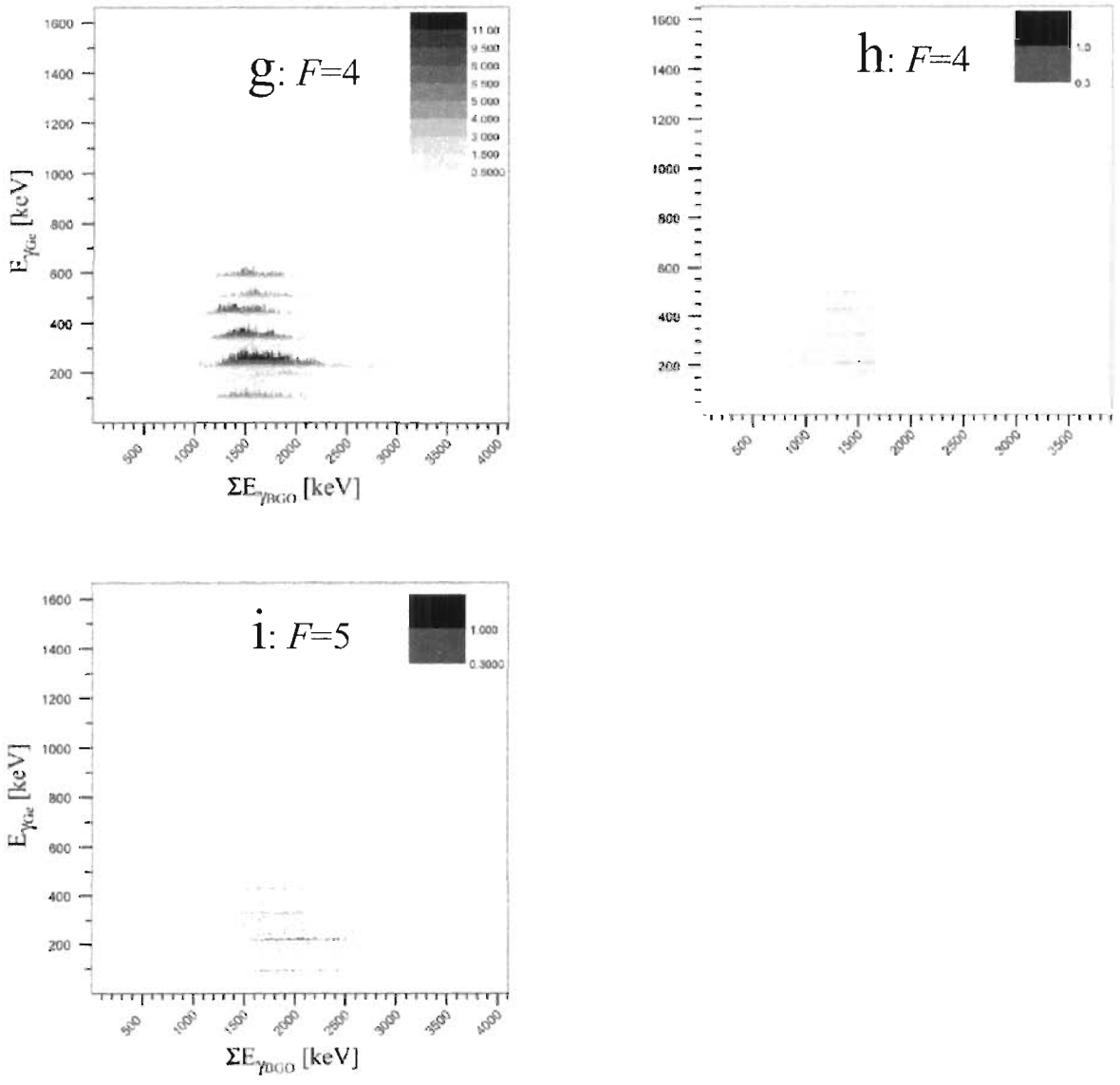

Fig. 16g-i

Fig 17

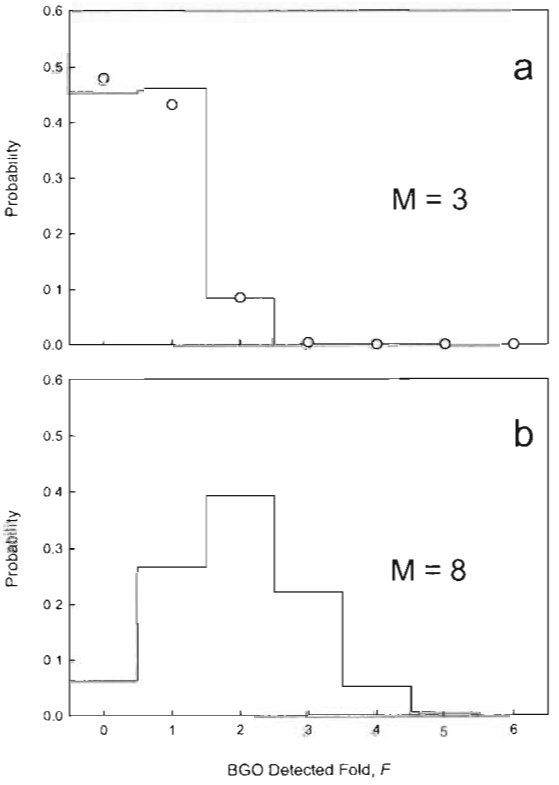
a
M = 3
b
M = 8
Probability
Probability
0.0
0.1
0.2
0.3
0.4
0.5
0.6
0
1
2
3
4
5
6
BGO Detected Fold, F

Fig. 17

$K^\pi = 0^+$ 2.29 s isomer in neutron-rich ^{174}Tm

R.S. Chakrawarthy,[1,2,*] P.M. Walker,[3] J.J. Ressler,[2] E.F. Zganjar,[4] G.C. Ball,[1] M.B. Smith,[1] A.N. Andreyev,[1] S.F Ashley,[3] R.A.E. Austin,[5] D. Bandyopadhyay,[6] J.A. Becker,[7] J.J. Carroll,[8] D.S. Cross,[2] D. Gohlke,[8] J.J. Daoud,[1,3] P.E. Garrett,[1,6] G.F. Grinyer,[6] G. Hackman,[1] G.A. Jones,[3] R. Kanungo,[1] W.D. Kulp,[9] Y. Litvinov,[10] A.C. Morton,[1] W.J. Mills,[11] C.J. Pearson,[1] R. Propri,[8] C.E. Svensson,[6] R. Wheeler,[8,3] and S.J. Williams[3]

[1] *TRIUMF, 4004 Wesbrook Mall, Vancouver, British Columbia V6T 2A3, Canada.*
[2] *Dept. of Chemistry, Simon Fraser University, Burnaby, British Columbia V5A 1S6, Canada.*
[3] *Dept. of Physics, University of Surrey, Guildford, Surrey GU2 7XH, United Kingdom.*
[4] *Dept. of Physics and Astronomy, Baton Rouge, Louisiana 70803, USA.*
[5] *Dept. of Astronomy and Physics, St. Mary's University, Halifax, Nova Scotia B3H 3C3, Canada.*
[6] *Dept. of Physics, University of Guelph, Guelph, Ontario N1G 2W1, Canada.*
[7] *Lawrence Livermore National Laboratory, Livermore, California, USA.*
[8] *Dept. of Physics and Astronomy, Youngstown State University, Youngstown, Ohio 44555, USA*
[9] *School of Physics, Georgia Institute of Technology, Atlanta, Georgia 30332-0430, USA*
[10] *GSI, Planckstrasse 1, Darmstadt 64291, Germany.*
[11] *Dept. of Physics, Simon Fraser University, Burnaby, BC V5A 1S6, Canada.*

(Dated: December 21, 2005)

Gamma-ray and conversion-electron spectroscopy have established the existence of a 2.29(1) s, $K^\pi = 0^+$, isomeric state in neutron-rich ^{174}Tm. The isomer de-excites via 100- and 152-keV electromagnetic transitions. First results from a newly commissioned Si(Li) detector array have established their $M1$ and $E3$ multipolarities, respectively. The single-particle configurations of the excited states suggest that the $E3$ transition originates from a $\pi h_{11/2}^{-1} \rightarrow \pi d_{3/2}$ configuration change, while the $M1$ transition occurs between members of a Gallaghar-Moszkowski doublet. From the measured half-life, the deduced $B(E3)$ value of 0.024(2) W.u. is highly hindered. The reported measurements resolve ambiguities in the previously proposed β decay scheme of ^{174}Er to ^{174}Tm.

PACS numbers: 21.10Tg, 23.20.Lv, 23.20.Nx, 27.70.+q

Models of exotic neutron-rich nuclei predict interesting, as yet unexplored, new physics [1]. However, these nuclei are largely difficult to access in experiments. Isomeric states are proving to be a convenient tool to access and explore excited states in neutron-rich nuclei [2]. In well-deformed nuclei, isomerism can usually be ascribed to K-forbidden and/or high-multipolarity transitions [3]. After accounting for these aspects, the reduced hindrance then depends primarily on 'local' nuclear-structure K-mixing effects, such as density of states, deviations from axial symmetry, and Coriolis mixing [3]. Taken together, these many influences severely complicate the prediction of isomer decay rates. Nevertheless, the experimental identification of isomeric states has a pivotal role in studies of nuclei approaching the drip-lines [2, 4], and even of some of the heaviest nuclei synthesized to-date [5]. While there is evidence for exotic proton and two-proton decay modes of isomers near the proton drip-line [6], analogous questions regarding the neutron decay mode of isomers in the neutron-rich region are still open [7]. Additionally, one of the goals of a future study of neutron-rich nuclei in the Dy-Hf region is to search for the possible existence of an 'island' of β-decaying high-K isomers [3, 8]. Furthermore, isomer production, especially with high-energy proton-induced reactions, is still poorly understood, and will be important for future radioactive-beam projects. There are open questions on the reaction mechanism and production cross sections of isomers in even-even, odd-even, and odd-odd nuclei [9]. Additional complications arise due to the unknown release times of isomers and exotic nuclei from, for example, surface-ionization ion sources. Thus, experiments form a crucial component to address these issues.

A new program of research in the deformed, isomer-rich, 170-190 mass region [3, 8, 10] has been launched at the Isotope Separator and Accelerator (ISAC) facility sited at TRIUMF, Vancouver, Canada. In the present work we report on the characterization of a new 2.29 s isomer in neutron-rich ^{174}Tm ($Z = 69$). The motivation to study such deformed odd-odd nuclei is based on their level structures, whose excitation spectra are among the most intricate and poorly characterized in nuclear structure physics [11]. This is associated with partially blocked pairing, high level density (resulting in a multitude of low-lying configurations), and complex decay patterns. The high probability of isomeric states is a key feature in the spectra of these nuclei, and their identification can lead to unambiguous temporal ordering of excited states. Such is the case with ^{174}Tm, as presented here.

In the present series of experiments, nuclei far from the line of β-stability are produced at the ISAC facility using 30μA 500 MeV proton-induced reactions on a Ta target. The reaction products de-excite during transit while long

*Electronic address: rsc1@triumf.ca

lived isomers ($T_{1/2} \geq$ few milli-seconds) allow a fraction of the isotopes to be delivered in an excited state. The reaction products are extracted using a surface ionization source, and accelerated to an energy of 30 keV. A high-resolution mass analyzer separates species with different mass number, which are then transported to experimental stations such as the 8π spectrometer. This spectrometer has been reconfigured in a close-packed configuration [12], and is comprised of 20 Compton-suppressed high-purity germanium detectors. The low-energy beams from ISAC are focused at the center of the 8π array and stopped in a 12.7 mm wide continuous-loop collector tape that is fed from a large aluminum storage chamber. The movable tape transport facility removes long-lived activity from the focus of the 8π array and minimizes the contaminating activity present in an isobaric beam. Within the 8π array, an aluminum hemispherical mounting houses five Si(Li) detectors in a pentagonal geometry, cooled to liquid-nitrogen temperatures. Typically, the off-line intrinsic resolution of the (cooled) Si(Li) detectors is 2.9-keV at 975-keV (K-shell converted electron of the 1063-keV transition in ^{207}Bi); while the in-beam resolution is 1.85-keV at 302-keV (K-shell converted electron of the 364-keV transition in ^{174}Tm β-decay). Each of the five Si(Li) detectors, 5 mm thick, circular in shape, and with an area of 200 mm^2, was mounted at a distance of 2.2 cm from the beam focus. The Pentagonal Array for Conversion Electron Spectroscopy (PACES) covers 8% of the solid angle [13].

In two sets of experiments several of the known high-K isomers in the Dy-Hf region, with half-lives ranging from a few milli-seconds to several minutes, have been accessed [14]. We report here the spectroscopy of a new 2.29(1) s isomer in the neutron-rich nucleus ^{174}Tm. An initial study measuring only the γ-transitions was presented at ENAM04 [15]. The A=174 isobaric beam was implanted into the movable tape transport facility, with beam-off/beam-on/beam-off cycling times of 2s/2s/2s, 2s/3s/3s, 5s/10s/10s, and 10s/100s/50s. Any remnant radioactive decay from the beam-particles missing the tape were monitored in the initial beam-off period after moving the tape.

Singles and coincidence $\gamma-\gamma$, γ-electron, and electron-electron data were acquired and sorted offline into several matrices; these include γ-time, electron-time, $\gamma-\gamma$, γ-electron, and electron-electron coincidence matrices. Standard radioactive sources of ^{152}Eu, ^{133}Ba, ^{207}Bi, as well as the known γ-ray and electron peaks from ^{174}Tm ground-state β decay, were utilized to calibrate the spectra. The accumulated γ-ray data were dominated by the ground-state β-decay of ^{174}Tm ($T_{1/2}$= 5.4 min). The detection of new-isomers is compounded by the presence of multiple decay-sources of varying intensities in the form of (here, A=174) isobaric contaminants as well as ionized fluoride/oxide molecular-beams (leading to decays from the A=158 and A=155 mass chains). Despite contamination, a judicious choice of cycling-times enabled rather clean separation of, especially, short-lived isomers. The yields of the A=174 oxide-beam, mainly emanating from the decay of ^{158}Er and ^{158}Tm, were measured to be 13% and 1% of the ^{174}Tm$_{g.s.}$ yield, respectively; while the decays from the A=174 fluoride-beam, primarily from ^{155}Tm, was measured to be at a 0.03% level. Fig. 1 shows the singles γ-ray spectrum, after subtracting the dominant ^{174}Tm$_{g.s.}$ activity. The inset shows the growth and decay curve of the 2.29(1) s isomer in the 2s/3s/3s tape cycle [15]; the prominent peaks are the 100.3- and 152.1-keV γ-ray transitions, and the Tm K X-rays. The ground-state to isomer ratio, (later on, corrected for electron conversion), is 200:1, and demonstrates the device sensitivity. The two coincident γ-ray transitions were, in addition, also known to be present in the ground-state β decay of ^{174}Er, which has a half life of 3.3 min [16, 17]. From the $\gamma-\gamma$ coincidence data, K-conversion coefficients of 3.1(1) and 1.13(6) were extracted, respectively, for these two transitions, and were the basis for $M1$-assignments in the previous works [15, 17].

The ground-state spin and parity of ^{174}Tm are known to be $I^\pi = 4^-$, as deduced from the ground-state systematics of the odd-proton Tm isotopes and the $N = 105$ isotones, and the allowed-unhindered β-decay proceeding to the lowest two excited 5^- states in ^{174}Yb [18]. However, the excited states in ^{174}Tm populated in the $I^\pi = 0^+$ ground-state β decay of ^{174}Er must be of low spin. Hence an unobserved low-energy, high-multipolarity transition was postulated, between the low-spin states observed following β decay and the high-spin ground state [17]. However, several issues could not be resolved from γ-ray spectroscopy alone. These relate to the large intensity difference between the two, seemingly $M1$, γ-ray transitions at 100- and 152-keV; the absence of a 252-keV cross-over $E2$ transition; and speculation that the isomeric state could be a new excited state, the decay of which could not itself be established, requiring population from a hypothesised high-K β-decaying isomer in ^{174}Er [15].

A closer examination of the K-electron conversion coefficient for the 152-keV transition, extracted from X-ray and γ-ray intensities [15, 17], reveals that it agrees, within error, with the values expected [19] for a $M1$ multipolarity (α_K= 0.81) and an $E3$ multipolarity (α_K= 1.18). Furthermore, a $E3$ multipolarity for the 152-keV transition would explain the large intensity imbalance with the 100-keV transition, that arises from the earlier deduction of $M1$ multipolarity for both transitions. However, the L-conversion coefficients would differ greatly (α_L= 0.12 and 4.1 for $M1$ and $E3$ multipolarity, respectively), motivating a measurement involving a conversion-electron spectrometer. Therefore, in a follow-up experiment, a new conversion-electron spectrometer, PACES, was brought on-line at the 8π-spectrometer station. The singles conversion-electron spectrum obtained by subtracting (with appropriate time restrictions) the transitions from the 5.4 m ^{174}Tm ground state β-decay is depicted in Fig. 2. This clearly illustrates electrons from K-, L-, and M-converted transitions that are involved in the isomer-decay, in addition to the Tm K_α

and K_β X-rays. The conversion-electron spectrum, gated by the 100-keV γ-ray transition, is shown in Fig. 3. The key feature is the prominent peak at 142-keV due to L-conversion, with the K- and M-conversion peaks being of relatively low intensity in this spectrum. The deduced conversion coefficients, as well as the K/L and L/M intensity ratios, compare very well with an $E3$ multipolarity assignment for the 152-keV transition, and rule out the $M1$ alternative. Similarly, the conversion electron data unambiguously assign $M1$ multipolarity to the 100-keV transition. The K-, L- and M-conversion coefficients from the present and the previous data are shown in Table 1. The deduced isomer decay scheme is depicted in the inset of Fig. 3. Analysis of the electron-electron coincidence matrix shows the expected coincidence relationships between the K- and L-conversions emanating from the two coincident transitions.

As discussed, the ground-state spin-parity of ^{174}Tm was deduced to be 4^-. In view of the lack of a cross-over γ-ray transition (I_γ 252-keV $\leq$ 0.34 % I_γ 100-keV) or a highly-converted $M4$ transition, in the 'singles' conversion-electron spectrum (Fig. 1), it is reasonable to infer that the 100- and 152-keV transitions are of stretched $M1$ and $E3$ character, respectively. A 100-keV $M1$ transition would not give rise to such a long half-life, so the 152-100 keV transition ordering is well-defined. Accordingly, the spin-parity sequence is (in increasing energy order) either $4^- - 5^- - 8^+$ or $4^- - 3^- - 0^+$. Only the 0^+ assignment for the 252-keV isomer is consistent with the known indirect feeding from the β decay of ^{174}Er [16, 17].

Since this is one of the most deformed regions of the nuclear chart, the levels can be classified by the 'K quantum number, equal to the value of the spin of each intrinsic state. Thus, the isomer acquires a $K^\pi = 0^+$ assignment. The identification of the isomer contradicts the previous claim of observing the 100- and 152-keV γ-ray transitions in coincidence with β particles from the ^{174}Er ground-state decay [16, 17]. Transitions with energies 637-, 643-, 708-, 714-, 766-, and 773-keV were observed in both the LBNL and GSI ^{174}Er β decay data [16, 17], though not in the present work, as an erbium beam is not produced efficiently by the ion source. These γ-ray transitions likely feed the $K^\pi = 0^+$ isomer, and originate from low-spin levels, consistent with a scenario of allowed Gamow-Teller β decay. Indeed, the summed singles-intensities of all these transitions [17] is 94(4)% of the total ($\gamma + e^-$) intensity of each of the 100- and 152-keV transitions (from the deduced $M1$ and $E3$ assignments, respectively). Furthermore, a direct ^{174}Er ($I^\pi = 0^+_{g.s}$)$\rightarrow$ ^{174}Tm($I^\pi = 0^+_{isomer}$) Fermi-transition will be strongly suppressed due to the non-analogue nature of the orbitals involved, consistent with the observed intensity flow.

The same selection rule also forbids β decay of the ^{174}Tm isomer to ^{174}Yb $K^\pi = 0^+$ levels. An upper limit of 1.0(5)% β decay branch could be deduced for such a forbidden decay. This limit was determined from the peak-free region of the electron spectrum from the 2s/3s/3s tape cycle after background subtraction from the e$^-$-time data. (A significant branch would indicate the importance of the so-called correction terms [20].)

A simple structural description of the observed states can be obtained purely by considering the available single-particle orbitals near the Fermi surface. For ^{174}Tm, the relevant proton single-particle Nilsson orbitals have quantum numbers $1/2^+[411]$ and $7/2^-[523]$, at a calculated quadrupole deformation of $\beta_2 \sim 0.28$ [21]. These orbitals couple with the neutron Nilsson orbitals, namely, $7/2^-[514]$, $5/2^-[512]$, and $1/2^-[521]$, to produce a set of low-lying intrinsic states in ^{174}Tm. By comparison to the odd-A neighbours, the odd proton of ^{174}Tm is likely to be in the $1/2^+[411]$ Nilsson orbital (^{173,175}Tm $I^\pi_{g.s.} = 1/2^+$), and the odd neutron in the $7/2^-[514]$ Nilsson orbital (^{173}Er,^{175}Yb $I^\pi_{g.s.} = 7/2^+$). Following the empirical Gallagher-Moszkowski (GM) rules [22], a coupling of the orbitals $\pi 1/2^+[411] \otimes \nu 7/2^-[514]$, a spin-parallel triplet state, is especially energetically favored, and gives rise to the ground-state spin-parity of $K^\pi = 4^-$. The observation of allowed-unhindered β decay to the $K^\pi = 5^-$ states in ^{174}Yb lends further support to this assignment [18].

The $K^\pi = 3^-$ state at 100-keV is suggested to be the singlet coupling of the GM-doublet arising out of the same orbitals, $\pi 1/2^+[411] \otimes \nu 7/2^-[514]$. The 100-keV $M1$ transition is then a K-allowed transition between the GM-doublet members. Indeed, calculations based on the Quasi-Particle Phonon Model (QPM) predict the two lowest-lying intrinsic states in ^{174}Tm as a result of such a coupling, and the calculated splitting of 94-keV is very close to the observed splitting of 100-keV (neglecting zero-point rotational motion) [11]. The contribution of this quasiparticle configuration is about 66% and 63% in the triplet and singlet states, respectively; a small contribution of 12% is calculated to arise from a Q_{22} collective vibration.

The $K^\pi = 0^+$ state at 252-keV is seen to result from a favored coupling of the $\pi 7/2^-[523] \otimes \nu 7/2^-[514]$ Nilsson orbitals. The 152-keV $E3$ transition is then a K-allowed proton-hole transition from the intruder $h_{11/2}(\otimes h_{9/2})$ orbital to the normal-parity $d_{3/2}$ orbital. Incidentally, for this configuration the protons and neutrons occupy the spin-orbit partners of the 1h orbital; such states are, supposedly, highly favored due to an attractive proton-neutron interaction. The 152-keV transition occurs between two intrinsic states differing only in the proton orbital, while the neutron orbital is a spectator. Likewise, the 100-keV transition involves a proton spin-flip. Thus, the two observed transitions in the decay scheme of the 2.29 s isomer can be explained as being K-allowed transitions that occur between three deformed intrinsic states involving only proton excitations. In well-deformed odd-odd nuclei, in addition to the usual K-selection rule, there is a two-particle transition selection rule involving the so called "non-overlap" forbiddenness, such that a simultaneous change of proton and neutron intrinsic configurations is severely hindered [23]. The proposed exci-

tation scheme is consistent with the requirements of these two selection rules. From the measured half-life of 2.29 s, a $B(E3)$ value of 0.021(1) W.u. (using theoretical value of $\alpha(theo)_{(total)} = 6.61$) or, using the measured conversion electron coefficient $\alpha(expt.)_{(K+L+M)} = 5.5(5)$, a $B(E3)$ value of 0.024(2) W.u. could be deduced for the 152 keV, $K^\pi = 0^+ \rightarrow K^\pi = 3^-$, transition. In terms of the hindrance factor, defined as [24]

$$F_W = \frac{T_{1/2\gamma}(experiment)}{T_{1/2\gamma}(Weisskopf)}, \qquad (1)$$

the $E3$ transition is calculated to have $F_W = 42(4)$ ($\alpha(expt.)_{(K+L+M)}$=5.5(4)) or 48.7(2) ($\alpha(theo)_{(total)} = 6.61$) , which is well within the prescribed range for a K-allowed ΔK=3, $E3$ decay [24].

In summary, through γ-ray and conversion electron spectroscopy the excitation energy and decay properties of the 2.29 s isomeric level in ^{174}Tm have been firmly established. The results of three different experiments [15–17] can be combined to explain all the data consistently with a minimum number of states. The isomeric level is characterized by a $K^\pi = 0^+$ assignment and the two coincident γ-ray transitions involve mainly proton excitations. The deduced transition rate is hindered but well within the prescribed limits of K-allowed $E3$ decays. It is important for future experiments on heavy neutron-rich nuclei that there should be simultaneous measurements of both γ-rays and conversion electrons, in order to derive unambiguous level schemes.

Acknowledgments: We are grateful to the hard work put in by the TRIUMF accelerator personnel for a smooth operation of the Cyclotron-ISAC facility during the experiments. This work was supported in part by NRC/NSERC Canada, U. K. EPSRC, U.S. Dept. of Energy, and DARPA Microsystems Technology Office through U.S. AFOSR contract F49620-03-C-0024 with Brookhaven Technology Group, Inc. USA. Few of us (JJC, DG, and RW) acknowledge support by the U.S. AFOSR under contract F49620-02-1-0817, and RP was supported by the Army Research Laboratory via contract W911CX-05-C-0081 to Ecopulse, Inc. USA.

[1] J. Dobaczewski, I. Hamamoto, W. Nazarewicz, and J.A. Sheikh, Phys. Rev. Lett. **72**, 981 (1994).
[2] M. Caamano, *et al.*, Eur. Phys. J. **A23**, 201 (2005).
[3] P.M. Walker and G.D. Dracoulis, Nature (London), **399**, 35 (2001).
[4] H. Grawe, A. Blazhev, M. Górska, I. Mukha, C. Plettner, E. Roeckl, F. Nowacki, R. Grzywacz, and M. Sawicka, EPJA **25**, s01, 357 (2005).
[5] F.R. Xu, E.G. Zhao, R. Wyss and P.M. Walker, Phys. Rev. Lett. **92**, 252501, (2004).
[6] I. Mukha, *et al.*, Phys. Rev. Lett. **95**, 022501 (2005); I. Mukha *et al.*, Nature (London) (in press).
[7] P.M. Walker and J.J. Carroll, Phys. Today **58**, 39 (2005).
[8] P.M. Walker and G.D. Dracoulis, Hyperfine Interact. **135**, 83 (2001).
[9] B.L. Zhukov, M.V. Mebel, V.M. Kokhanyuk, A.S. Iljinov, A.Yu. Zyuzin, and J.S. Vincent, Phys. Rev. C **68**, 054611 (2003).
[10] K. Jain, *et al.* Nuc. Phys. **A591**, 61(1995).
[11] A.K. Jain, R.K. Sheline, D.M. Headly, P.C. Sood, D.G. Burke, I. Hrivnacova, J. Kvasil, D. Nosek, and R.W. Hoff, Rev. Mod. Phys. **70**, 843 (1998).
[12] G.C. Ball *et al.*, J. Phys. G **31**, S1491 (2005).
[13] E. Zganjar *et al.*, (*to be published*).
[14] M.B. Smith *et al.*, Nuc. Phys. **A746**, 617 (2004).
[15] R.S. Chakrawarthy *et al.*, EPJA **25**, s01, 125 (2005).
[16] R.M. Chasteler *et al.*, Z. Phys. A **332**, 239 (1989).
[17] K. Becker *et al.*, Nucl. Phys. **A522**, 557 (1991).
[18] N. Kaffrell and W. Kurcewicz, Nuc. Phys. **A255**, 339 (1975).
[19] F. Rösel, H.M. Fries, K. Alder, and H.C. Pauli, At. Data Nucl. Tables **21**, 91 (1978); http://ie.lbl.gov/programs/icc/icc.html.
[20] S. Raman, T.A. Walkiewicz, and H. Behrens, At. Data Nucl. Tables **16**, 451 (1975).
[21] W. Nazarewicz, M.A. Riley, and J.D. Garrett, Nuc. Phys. **A512**, 61 (1990).
[22] C.J. Gallagher and S.A. Moszkowski, Phys. Rev. **111**, 1282 (1958).
[23] C.J. Gallagher, Nuc. Phys. **16**, 215 (1960).
[24] K.E.G. Löbner, Phys. Lett. B **26** 369 (1968).

TABLE I: Relative γ-ray intensities, experimental and theoretical internal conversion coefficients (ICC)

E_γ keV	I_γ	ICC (present expt.)	ICC (Ref. [17])	ICC (theo., Ref.[19])	Multipolarity
152.1	66.5(6)	α_K 1.13 $\pm$ 0.06	α_K 0.54 $\pm$ 0.06	$\alpha_K(E3)$ 1.18	*E3*
		α_L 3.31 $\pm$ 0.48	-	$\alpha_L(E3)$ 4.10	
		α_M 1.10 $\pm$ 0.12	-	$\alpha_M(E3)$ 0.99	
100.3	100.0(6)	α_K 3.1 $\pm$ 0.01	α_K 1.7 $\pm$ 0.3	α_K $(M1)$ 2.66	*M1*
		α_L 0.45 $\pm$ 0.10	-	$\alpha_L(M1)$ 0.40	
		α_M 0.14 $\pm$ 0.03	-	$\alpha_M(M1)$ 0.09	

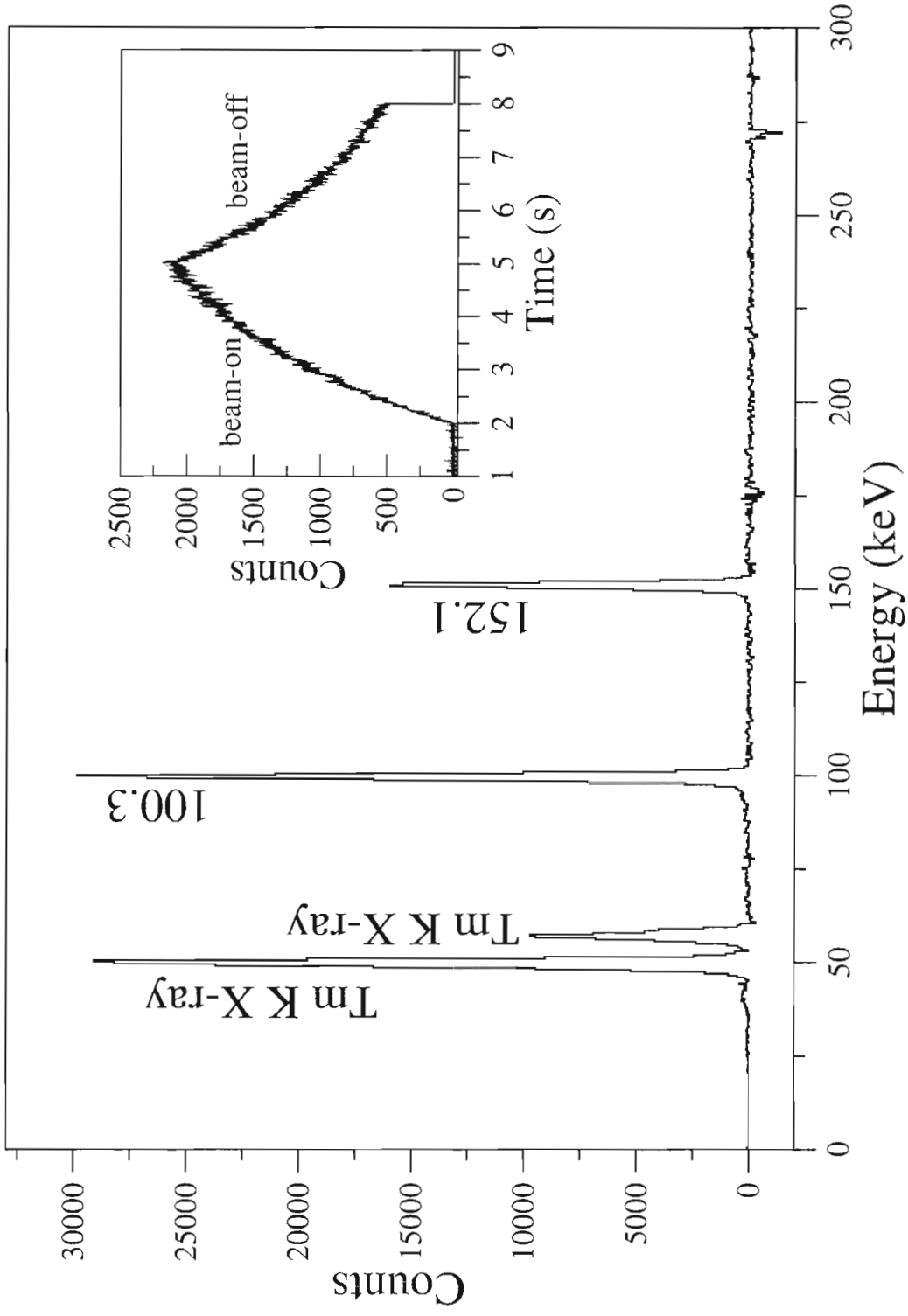

FIG. 1: The short-lived singles γ-ray spectrum showing prominently the Tm K X-rays and the 100- and 152-keV γ-ray transitions. The 5.4 m ^{174}Tm ground-state β-decay component has been subtracted. The inset shows the growth and decay of the isomer gated by the 100-keV γ-ray transition.

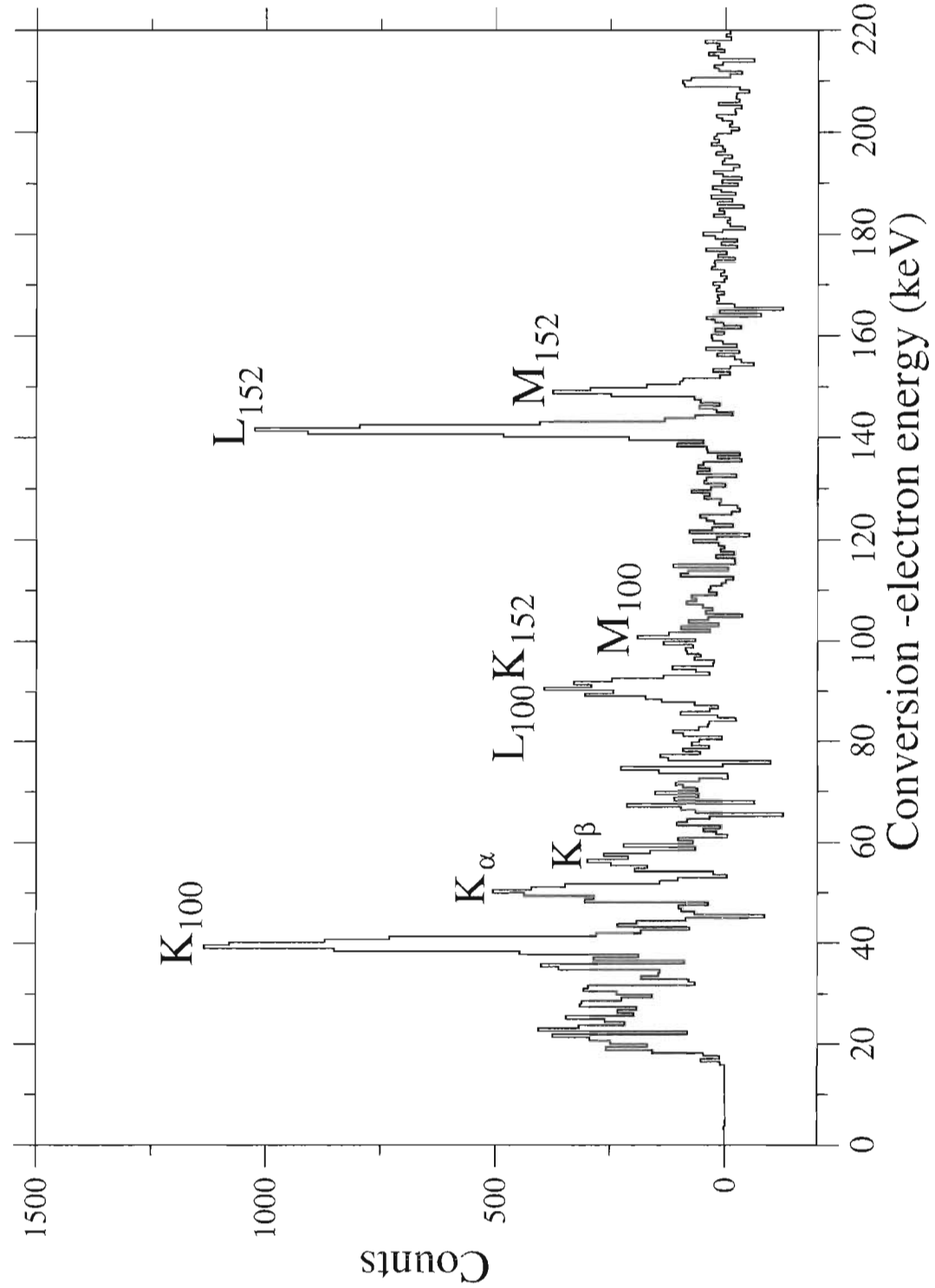

FIG. 2: The singles conversion-electron spectrum obtained by subtracting the 5.4 m ^{174}Tm ground-state β-decay component. K_γ denotes the conversion-electron corresponding to the γ-ray transition, while the Tm X-rays are labelled as K_α/K_β.

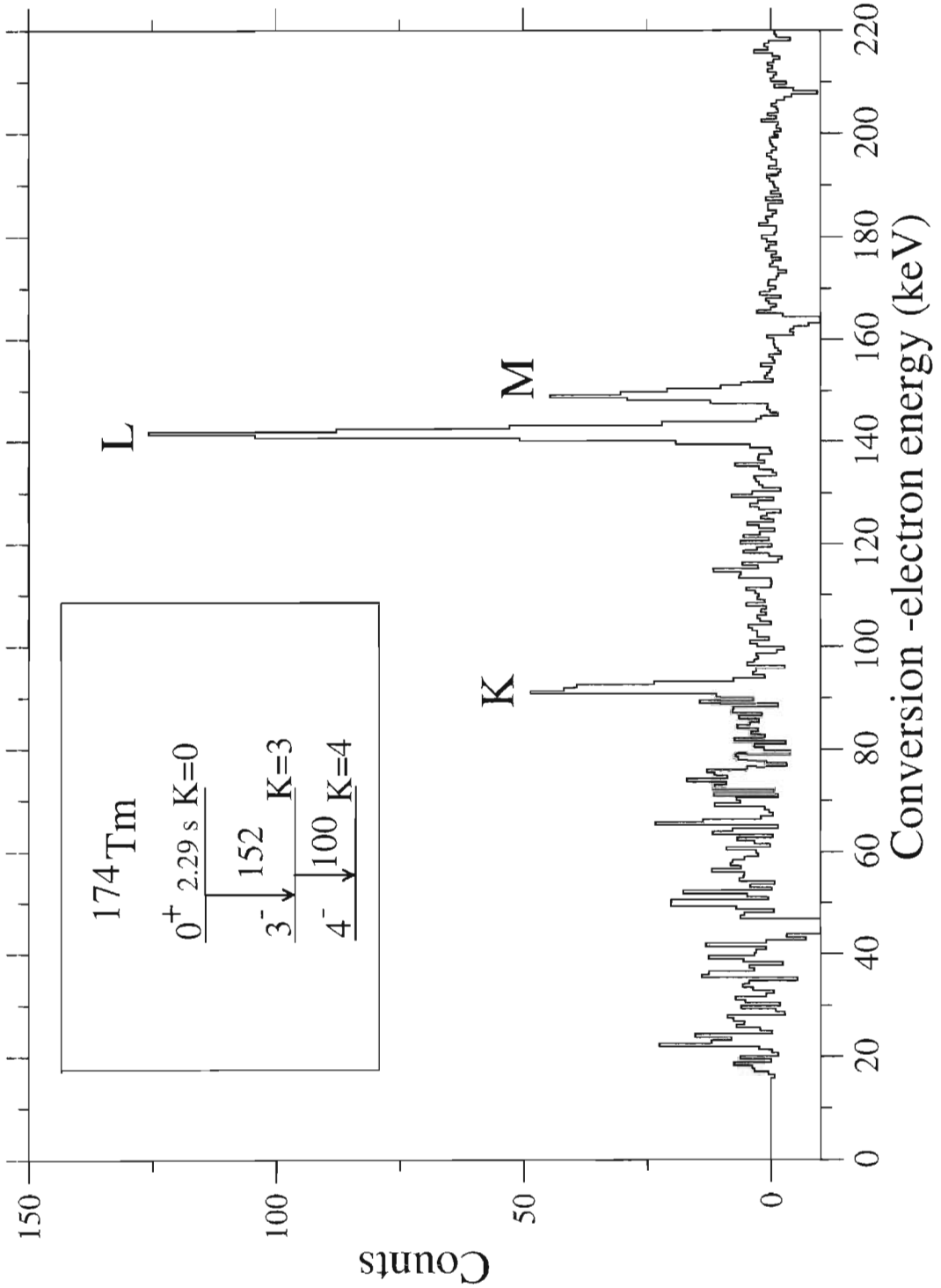

FIG. 3: The conversion-electron spectrum gated by the 100-keV γ-ray transition. The earlier [15, 17], incorrect, $M1$-multipole assignment for the 152-keV transition would have given rise to strong K-conversion and very little L- and M-conversion. The inset depicts the isomer decay-scheme as a result of the present work.

PRODUCTION OF LONG-LIVED HAFNIUM ISOMERS IN REACTOR IRRADIATIONS

S. A. Karamian,[a *] J. J. Carroll,[b] J. Adam,[a †] E. N. Kulagin,[a] and E. P. Shabalin [a]

[a]Joint Institute for Nuclear Research, Dubna 141980, Russia

[b]Youngstown State University, Youngstown, Ohio 44555, USA

ABSTRACT

Experiments on production of the long-lived ^{178m2}Hf isomer in reactor irradiations are described. Properties of this nuclide are promising for its potential application as a relatively safe power source characterized by high density of accumulated energy. Metal ^{nat}Hf samples were activated in the Dubna IBR-2 reactor at positions corresponding to different neutron fluxes. Samples were bare or shielded by Cd and CB_4 layers. The gamma activity of the samples was analyzed with Ge gamma spectrometers during a two-year period following their irradiation. In the presence of the dominant activation products ^{175}Hf and ^{181}Hf, the high-spin isomers ^{178m2}Hf and ^{179m2}Hf were also detected despite relatively low levels. The isomer-to-ground-state ratios and cross-sections were determined from the measured yields. For ^{178m2}Hf, the cross section for burnup (destruction) by neutron capture after its production was also estimated, clarifying the results from earlier experiments. In the context of suggestions for use of ^{178m2}Hf for applications, the results confirm that large-scale production of this isomer by reactor irradiations is not feasible. In contrast, the efficiency of production for ^{179m2}Hf is much higher and an amount of about 10^{16} atoms may be produced in standard reactor irradiations. For ^{178m2}Hf, more productive methods are known, in particular fast neutron irradiations at $E_n \geq 14$ MeV and spallation reactions at intermediate energies. Neutron cross-sections for isomers may also be significant in astrophysics.

---

* Corresponding author. *E-mail address:* karamian@nrmail.jinr.ru (S.A. Karamian)
Postal address: FLNR, JINR, Joliot-Curie Str., 6, Dubna, 141980, Russia
Tel.: +7-496-216-4668; Fax: +7-496-216-5083

† *Permanent address:* Inst. Nuc. Phys., Řez., CZ-25068, Prague, Czech.Rep.

PACS: 28.20-v; 29.25.Rm; 84.60.Ve

Keywords: Energy storage; Isomer nuclide; Production; Reactor neutrons; Cross-sections

I. INTRODUCTION

High energy-density sources are needed for modern aero-space devices and for other applications. A compact, portable and safe source can attract an attention of engineers of different specializations. The isotopes, like ^{238}Pu and ^{210}Po were used since many years, but their disadvantage was entirely clear because such a source being destructed should create a biologically dangerous α-radioactive pollution. Other nuclear power sources are ecologically dirty as well. During recent years, an interest has appeared to the energy stored by nuclear isomers. The ^{178m2}Hf isomer is recognized in literature as most promising because it does not create daughter radioactive products longer-lived than 4 s, emits only photons and soft electrons and is characterized by high energy density of 1.3 GJ/g. This would be a source of relatively clean nuclear energy, which is not very dangerous even in a view of accidental destructions. Possible ways for energy release due to a triggering of ^{178m2}Hf by some external stimulus (like X-rays) were discussed in special literature, but were not clarified until now. However, even without stimulation this long-lived ($T_{1/2}$ = 31 y) source can find an application as a power supply unit for microelectronics devices in systems restricted in the size and weight. Therefore, it would be important to find relatively simple and inexpensive method for massive production of ^{178m2}Hf. Reactor irradiations are known to be most productive for accumulation of radioactive isotopes, and the reactor yield of the ^{178m2}Hf isomer has been measured in the present work.

Total and activation cross-sections as well as resonance parameters for slow neutron radiative capture may be found for stable Hf isotopes in the tabulations of Refs. [1, 2]. It is well-known that the main activity induced in natural hafnium targets is due to the production of ^{175}Hf (70-day halflife) and ^{181}Hf (42-day halflife) after (n,γ) reactions. In addition, the short-lived first metastable (m_1) isomers of ^{178}Hf, ^{179}Hf and ^{180}Hf are also formed with cross-

sections that are sufficient for successful detection. However, the production of high-spin second metastable (m_2) isomer via (n,γ) reactions in isotopes like ^{178}Hf and ^{179}Hf are more problematic. Only recently has a measurement appeared in the literature for the production of $J^{\pi} = (25/2^-)$ ^{179m2}Hf [3]. The production of the famous $J^{\pi} = 16^+$ isomer ^{178m2}Hf was reliably detected from its activity in 1973 [4], but the cross section was deduced using some assumptions that deserve additional investigation.

The population of high-spin states following neutron capture may be expected to have a rather low probability due to the need for their population by stretched cascades of many γ rays. This type of cascade is characterized statistically by a relatively low yield. High-fluence irradiations are normally required in order to produce an observable activity for such low-yield products, but this introduces another complication in that a significant "burnup," or depletion, of the produced nuclei may occur. For some products the destruction cross-section can be higher than 1,000 barns. Therefore, fluences above 0.5×10^{21} n/cm^2 should be avoided to produce negligible burnup, or the remaining activity after irradiation would suggest a production cross-section that was significantly underestimated.

Fast neutrons within a reactor spectrum are sometimes useful for isomers production via ($n, n'\gamma$) reactions. These reactions may complicate the analysis of experiment and must be kept in mind when designing experiments for the measurement of low-yield exotic radionuclides by reactor irradiations. In the present work, the production of the high-spin isomers ^{178m2}Hf and ^{179m2}Hf isomers was observed and quantitatively characterized, taking into account such factors. These measurements therefore serve to augment the existing data obtained in high-flux irradiations for the former isomer [4] and to provide new information for the latter [3]. The burnup of ^{178m2}Hf by (n, γ) reactions was also investigated, expanding the results of Ref. [5].

II. EXPERIMENTAL DETAIL

In a first series of experiments, metal Hf samples of about 20 mg were irradiated in an outer channel of the IBR-2 Dubna reactor of the Frank Laboratory of Neutron Physics, Joint Institute for Nuclear Research. Metal Hf targets of natural isotopic composition are advantageous as compared to an enriched target in their chemical purity and lower resonance-absorption factors. The standard method of Cd difference was applied for the isolation of the separate effects of thermal and epi-Cd neutrons. The neutron spectrum at the location of the targets was well-known from previous experiments, but NiCr-alloy samples were nevertheless irradiated as spectators. The activity of ^{51}Cr served to calibrate the slow neutron flux while ^{58}Co was produced in a reaction with fast neutrons at $E_n > 0.8$ MeV and was used for calibration of the fast neutron flux.

Following their irradiation, the activity of the samples was studied using a 20% efficiency HPGe gamma detector. The spectroscopic system allowed a count rate up to 15 kHz while preserving a reasonable dead time less than 25% and a spectral resolution on a level of 1.8 keV for the ^{60}Co lines. Standard test sources (^{152}Eu and others) were used for energy and efficiency calibrations of the γ spectrometer.

In measured spectra from the activated Hf samples, γ lines were observed and their peak areas quantitatively determined for the following radionuclides: ^{175}Hf, ^{179m2}Hf, ^{180m}Hf and ^{181}Hf. The bulk of the activity was due to ^{175}Hf (70 d) and ^{181}Hf (42.4 d) formed in (n, γ) reactions. Negligible activity was contributed from admixtures of other elements in the Hf material. Only Zr was present in a quantity of about 3%, while the concentration of other elements was estimated to be on the level of less than 1 ppm. The detected yields of ^{175}Hf and ^{181}Hf were used as additional, intrinsic calibrators of the neutron fluxes and then the thermal cross-section σ_{th}=(0.44±0.02) b and resonance integral I_γ =(5.8±0.7) b were deduced for

^{180m}Hf production in the ^{179}Hf(n, γ) reaction. The resulting values were in good agreement with the tabulated data [1], confirming the accurate calibration of the neutron flux in these irradiations.

A yield of the high-spin ^{179m2}Hf isomer was detected and clearly originated from reactions with fast neutrons, since the effect of thermal neutrons was found to be insignificant for its production. This conclusion was definite because bare and Cd-shielded samples showed the same activity of ^{179m2}Hf within the standard error. No γ lines from ^{178m2}Hf were observed in this first series of irradiations, reflecting its low production yield and the presence of much higher activities of other nuclides.

A second series of experiments was performed in order to significantly improve the sensitivity of the measurements for detection of the low-yield isomers. At the same position in the outer channel, a larger Hf sample was placed for a longer duration. The sensitivity was improved by three orders-of-magnitude, but this was still insufficient for observation of ^{178m2}Hf. A strong increase in the neutron flux was then sought to increase the production of this isomer. In the reactor, an inner channel was available that allowed an irradiation near, but outside, the active core within a cylindrical region shielded by a 3-mm layer of CB_4. A Hf sample was exposed there for eighteen days, after which decay of the resulting activity was followed for two years. Finally, activity of ^{178m2}Hf was successfully observed and its yield determined after the third series of irradiations.

At the inner location, the thermal flux was determined in earlier experiments to be about 0.5×10^{12} neutrons/(cm^2 s), thus during the eighteen-day irradiation a fluence near 10^{18} n/cm^2 could be accumulated. In the present experiments, the value of flux was not used explicitly since all measurements were carried out in a relative mode by comparing the activities of ^{178m2}Hf, ^{179m2}Hf and ^{180m}Hf nuclei to those of spectators and intrinsic calibrators ^{175}Hf, ^{181}Hf and ^{95}Zr which were present within the targets. Such a method is reliable and

accurate in the presence of shields. Data processing requires special care for high-sensitivity measurements of neutron-production cross sections. The burnup of isomeric nuclei produced during the irradiation must be taken into account when the neutron fluence exceeds 10^{20} n/cm^2. In the present irradiations, however, even in the inner channel the fluence was 100 times lower. This is due to the fact that IBR-2 is a pulsed reactor constructed specially for time-of-flight spectroscopy, not to achieve a high mean power. With this fluence, burnup of high-spin hafnium isomers or other double neutron-capture reactions may be expected to have a probability below 10^{-3} compared to the probability for single neutron capture. Nevertheless, some excess activity of ^{182}Ta was detected beyond that which could be attributed to single neutron capture on a small admixture of ^{181}Ta in the target. This excess production of ^{182}Ta was likely due to the double neutron capture process: ^{180}Hf$(n, \gamma)^{181}$Hf$\rightarrow$ ^{181}Ta$(n, \gamma)^{182}$Ta.

Also, in order to achieve a higher absolute yield of ^{178m2}Hf in the second and third experimental series, relatively thick metal samples were used. Self-absorption of thermal and resonance neutrons could not be neglected for these thicker samples, which were rods of 1-mm cross-sectional dimension.

The well-known equation describing the reaction rate per target nucleus when exposed to comparable fluxes of thermal and resonance neutrons is

$$r = (\sigma_{th} + \frac{I_\gamma}{k})F_{th} \quad , \tag{1}$$

where F_{th} is the thermal neutron flux. The coefficient k reflects the particular characteristics of the spectrum of irradiating neutrons, being a fixed constant for a definite location of each irradiation station in a specific reactor. It may be defined approximately as

$$k = \frac{F_{th}}{F_{res}} \ln(E_2 / E_1) \quad , \tag{2}$$

where E_1 and E_2 define the "resonance" range of neutron energies and F_{res} is the flux of resonance neutrons. For simplicity, one can introduce the notation:

$$\sigma_{eff} = (\sigma_{th} + \frac{I_\gamma}{k}) \quad . \tag{3}$$

In the first series of experiments, the numerical value $k = 5$ was determined and this was in agreement with extensive previous measurements carried out in the outer channel of the IBR-2 reactor. The outer and inner channels used in this work are separated by only air and a shutter which is opened when the outer channel is used. Thus, the same value of k was used for irradiations at the inner location, while the effect of CB_4 and self-shielding was considered separately as described below.

The production rate of some nuclide in a target of definite composition and mass can be expressed as follows:

$$\frac{dN}{dt} = \frac{N_A \cdot c \cdot a \cdot m}{\mathcal{M}} (\sigma_{th} \cdot \tau_{th} + \frac{I_\gamma}{k} \tau_{res}) F_{th} \quad , \tag{4}$$

where N_A is Avogadro's Number, c is the mass concentration of the element of interest in g/g, a is the abundance of a particular isotope of that element, m is the total mass of the irradiated target and $\mathcal{M}$ is the atomic mass of the element. The τ_{th} and τ_{res} factors are dimensionless attenuation coefficients reflecting self-absorption in the target layer for thermal and resonance neutrons, respectively. Each may reach a maximum value of unity for targets of negligible thickness or be significantly smaller for thick targets.

Equation (4) describes the (n,γ) capture reaction with slow neutrons. The F_{th} and k parameters represent characteristics of the reactor, while all but one of the other parameters must be specified for a definite nuclide in the target, i. e. the capturing isotope. The lone exception is the factor τ_{th}, which is a unique parameter characteristic of all reactions with thermal neutrons in a target of specific composition and thickness and is independent of the particular capturing isotope. Unlike τ_{th}, τ_{res} is individualized because the resonance energies

and peak cross-sections are extremely specific to each isotope and vary irregularly from one nuclide to another. Strong absorption near the resonance peak for one isotope may produce absolutely no influence on the resonances of other nuclides. The partial thickness of the target corresponding to the individual isotopes will also depend on c, a and M, and this is important for resonance neutron absorption.

In the outer channel, neither the first nor the second series of irradiations were sufficiently intense to produce a detectable yield of ^{178m2}Hf. However, the dominant activities of ^{175}Hf, ^{181}Hf and ^{95}Zr were measured with high accuracy. Using Eq. (4), the concentration of Zr was evaluated numerically, as well as the τ_{th} coefficient specific to the target and the resonance absorption coefficient τ_{res} specific to ^{181}Hf production via the ^{180}Hf(n,γ) reaction. For ^{175}Hf and ^{95}Zr, resonance absorption was insignificant due to the low concentration of ^{174}Hf and ^{94}Zr nuclides within the target. These evaluated parameters were then employed in the analysis of the measurements carried out following the irradiation near the active core that had much higher flux.

In this inner location, the thermal neutron flux was strongly attenuated (almost absorbed entirely) by the 3-mm thick CB_4 shield, while the transmission of neutrons was also influenced at other energies below 20 eV. No sharp cut-off occurs since the total cross-section of boron varies smoothly with neutron energy. Therefore, activation by thermal neutrons could be excluded and the effect of resonance neutrons was characterized by a corrected resonance integral $I_\gamma(corr)$ as follows:

$$I_\gamma(corr) = I_\gamma \frac{\int_0^{E_{max}} E_n^{-1} \chi(E_n) g\Gamma_n dE_n}{\int_0^{E_{max}} E_n^{-1} g\Gamma_n dE_n} \quad , \tag{5}$$

where I_γ is the tabulated resonance integral, $\chi(E_n)$ is the calculated transmission function through the CB_4 filter, and $g\Gamma_n$ is the resonance strength obtained from the data of Ref. [1]. Using so-calculated $I_\gamma(corr)$ values, one can calibrate the resonance neutron flux inside the CB_4 shield, again determined from the measured activities of high-yield ^{175}Hf and ^{181}Hf. For both isotopes the self-absorption coefficients τ_{res} are known from the outer-channel experiment described above, but the τ_{res} value corresponding to production of ^{178m2}Hf in the ^{177}Hf(n,γ) reaction was not calibrated. Although one may assume stronger absorption for ^{177}Hf than for ^{180}Hf, taking into account the resonance strengths for both nuclides. A more precise estimate for the τ_{res} of ^{177}Hf was obtained on the basis of the resonance excitation function given in Ref. [2], as compared to ^{180}Hf.

Finally, the total number of resonance neutron capture events by ^{177}Hf nuclei in the target was deduced. From this value the isomer-to-ground state ratio σ_m/σ_g may be determined for ^{178}Hf whenever activity of ^{178m2}Hf is measured.

III. RESULTS

In gamma spectra measured after two-years cooling of the Hf sample exposed to a fluence of about 10^{18} n/cm^2 (in the inner channel), characteristic lines from ^{178m2}Hf decay were found as shown in Fig. 1. Their intensities were still much lower than the lines resulting from the dominant ^{175}Hf and ^{181}Hf activities. This could be expected for the 31-year-lived isomer, which should be produced with a low yield that is suppressed by its high angular momentum and resulted in an isomer-to-ground state ratio on the level of about 10^{-8} or less. The spectrum contains many lines of different origin, including those from activated admixtures within the sample, from natural background and from summations of the gamma rays with characteristic X- rays of the emitting atoms within the sample and the Pb within the detector shield. The panels in Fig. 1 show gamma lines from ^{178m2}Hf decay as well as some other lines that are not related to this analysis.

Fig.1

Table 1 gives the number of counts detected for gamma transitions from ^{178m2}Hf decay at 426.4, 495.0 and 574.2 keV, in comparison with the major lines of ^{175}Hf and ^{181}Hf. Lines from ^{178m2}Hf at lower energies were completely obscured by the large Compton background despite the cooling period. The statistical error in the peak area of the line at 574.2 keV is poor because this lies near the strongly-manifested Compton ridge due to γ lines from ^{95}Zr and ^{95}Nb detected at energies of about 750 keV. Better accuracy was reached for the other two lines and the observed intensities were sufficient to define the number of ^{178m2}Hf nuclei within the activated target, taking into account all necessary factors of efficiency and decay. By comparing this number to the calculated total number of ^{177}Hf(n, γ) events, as described above, this gave the experimentally measured σ_{m2}/σ_g ratio for ^{178}Hf. The latter value was determined for resonance neutrons transmitted through the CB_4 filter. However, a similar σ_{m2}/σ_g ratio should be valid for slow neutrons in general, including thermal neutrons. Such regularity has been experimentally confirmed in many cases when the σ_m/σ_g ratio was determined both from measured σ_{th} and I_γ values, e. g. the case of the ^{180m}Hf isomer [1].

Taking the σ_{m2}/σ_g ratio so-obtained and then using the known [1] σ_{th} and I_γ parameters for the ^{177}Hf(n, γ) reaction, the partial σ_{th} and I_γ for population of ^{178m2}Hf were deduced. The accuracy of this result cannot be expected to be very high due to the modest statistics (see Table 1). In principle, however, the present data were taken under more clean conditions than in previous measurements reported in the literature and should be reliable.

Neutron capture cross-sections for Hf nuclides are summarized in Table 2 with literature data taken from Ref. [1]. The present results are given for the reactions of particular interest, ^{177}Hf(n, γ)^{178m2}Hf, ^{178}Hf(n, γ)^{179m2}Hf and ^{178m2}Hf(n, γ)^{179g,m2}Hf. The latter reaction which is responsible for ^{178m2}Hf destruction (burnup) may be especially exotic and is discussed in more detail below.

More than thirty years ago, activity of the ^{178m2}Hf isomer was observed [4] from isotopically-enriched hafnium targets irradiated within a high-power reactor. Gamma spectra of this isomer were carefully studied using state-of-the-art techniques available at that time. However, the production cross section given in Ref. [4] may not be very accurate because it was determined by only considering the effect of thermal neutrons, neglecting the resonance neutron flux, and assuming that the "burnup" (destruction) cross section was at a rather low level of less than 20 b. It is well-known that a purely thermal flux does not exist in any reactor near its active core and the presence of resonance neutrons changes the yields of reaction products. Also the ^{178m2}Hf yield could be strongly reduced due to the burnup process at the fluences applied in the work of Ref. [4], $\geq 10^{21}$ n/cm^2. The degree of burnup definitely depends on the values of σ_{th} and I_γ for the isomeric nucleus, but the relatively low σ_{th} given in Ref. [4] was unexpected.

Values of σ_{th} and I_γ for neutron capture show for many nuclei a correlation with the level density of neutron resonances. Standard estimations using the Gilbert-Cameron formula [6], verified by known neutron resonance densities for various nuclides, predict a much higher resonance density for ^{178m2}Hf than that known for the ^{178g}Hf nucleus. The former nucleus may be characterized by a level density comparable with the measured resonance density for ^{177}Hf, or perhaps even larger. Thus, similar values of σ_{th} and I_γ can be expected for ^{178m2}Hf and ^{177}Hf nuclei and these are much larger than the 20 b used in Ref. [4]. Recently, the burnup cross-section due to thermal neutrons was measured in Ref. [7] for the ^{177m}Lu isomer and a value of σ_{th} = 590 b was obtained, including both neutron capture and superelastic scattering components. Noting that ^{177m}Lu also possesses high spin and excitation energy similar to ^{178m2}Hf, one may expect them to have comparable burnup cross-sections. Such arguments motivated the present independent measurements of the ^{178m2}Hf production cross section in reactor irradiations and an evaluation of the role of burnup which depends on neutron flux.

There is no doubt that the number of produced ^{178m2}Hf nuclei was determined correctly in the earlier experiment [4], although the cross-section was underestimated by a factor of 10 using an incorrect approximation. Now that yield [4] may be taken and combined with appropriate corrections so that it can be compared with the present cross-sections. To make this recalculation of the cross section corresponding to the earlier experiment, the following assumptions are made:

1. The effective cross-section of Eq. (3) is, in general, appropriate to account for the contribution of resonance neutrons.
2. An effective, or net, production cross-section, σ_{pro}, calculated with the σ_{th} and I_γ from the current experiment, should be valid for the conditions of Ref. [4] when an appropriate value of $k = 20$ (suitable for a well-thermalized spectrum as would be expected for that experiment) is taken.
3. The yield of ^{178m2}Hf measured in Ref. [4] in a high-fluence irradiation may then be reproduced with the calculated σ_{pro} by taking into account a much larger burnup effect than was assumed in the earlier work.

Following this approach, the effective cross-section for burnup in the ^{178m2}Hf(n, γ) reaction was deduced. The accumulation of a given product nucleus in the presence of burnup is given by

$$N_{net}(\Phi) = \frac{N_t \sigma_{pro}}{(\sigma_t - \sigma_{burn})}\left[e^{-\sigma_{burn}\Phi} - e^{-\sigma_t \Phi}\right] \quad , \tag{6}$$

where N_{net} and N_t are the net number of product nuclei and the number of target nuclei at the start of the irradiation, respectively, Φ is the neutron fluence, σ_{burn} and σ_t are the capture cross-sections that take into account the burnup of the product and target nuclei, respectively. The σ_{pro} value is the physical production cross-section without burnup. All σ values are defined to be effective, as in Eq. (3).

Combining the present production cross-section results with the yield measurements of Ref. [4] as described above, the effective burnup cross-section, σ_{burn}, was deduced for the ^{178m2}Hf isomer using Eq. (6). This effective cross-section is a linear combination of σ_{th} and I_γ values summed for two exit channels of the capture reaction, together corresponding to the formation of ^{179}Hf product nuclei in either its ground state (g) or its 25-day-lived m_2 state.

Fortunately, decomposition of σ_{burn} was possible because σ_{th} and I_γ parameters have already been directly measured for production of ^{179m2}Hf after irradiation of ^{178m2}Hf in Ref. [5]. The ground-state yield may also be determined by subtraction of the ^{179m2}Hf contribution from the total burnup yield of ^{178m2}Hf. It was assumed that the ratio σ_{m2}/σ_g for production of ^{179m2}Hf and ^{179g}Hf nuclei in neutron capture by ^{178m2}Hf should be approximately the same for both thermal and resonance neutrons. The partial σ_{th} and I_γ for the ^{178m2}Hf(n, γ)^{179g}Hf branch are therefore deduced and should be added to the previously known values for the branch of the reaction that populates ^{179m2}Hf. Thus, the burnup of ^{178m2}Hf due to neutron capture reactions is now characterized by the total σ_{th} and I_γ values, although with only modest accuracy. Nevertheless, the general behavior of production and burnup processes has been clarified by the present experiment.

Table 3 compares the cross-sections for ^{178m2}Hf production in reactions with slow and fast neutrons. The upper limit therein for the ^{178}Hf(n, $n'\gamma$) reaction was determined based on the present measurements. Fast neutrons with $E_n \geq 3$ MeV could, in principle, activate the ^{178m2}Hf state located at a 2.446-MeV excitation energy. Fast neutrons can certainly penetrate through the CB_4 shield without significant absorption and their flux was measured by activation of a Ni spectator. Thus, a cross-section can be deduced for fast neutron production of ^{178m2}Hf if its production is attributed to the (n, $n'\gamma$) reaction. However, the values of σ_{m2} and σ_{m2}/σ_g obtained in such a manner are unphysically large when the reaction's the spin deficit of $\Delta J = 31/2$ is considered for a hypothetical ^{178}Hf(n, $n'\gamma$)^{178m2}Hf reaction. Recall that

$\Delta J = J_m - J_t - 1/2$. Finally, it was assumed that the deduced cross-section for fast-neutron production of ^{178m2}Hf is just an upper limit, while the dominant means of producing this isomer is due to slow neutron capture. The ^{179}Hf(n, $2n$) reaction with 14.5-MeV neutrons was characterized in Refs. [8, 9]. The efficient production of ^{178m2}Hf in that reaction makes it one of the best methods for accumulation of this isomer, but the achievable flux of 14-MeV neutrons restricts the real use of this reaction for large-scale manufacture. In the case of reactor irradiations, neutrons with energies greater than 10 MeV appear with very low probability.

Table 4 summarizes cross-sections for ^{179m2}Hf production which are described in more detail in Ref. [3]. In that work it was explained that the main production mechanism was the (n, $n'\gamma$) reaction, unlike the situation found now for ^{178m2}Hf production. The difference may be attributed primarily to the spin deficit (ΔJ) values, which causes a preference in the (n, γ) reaction for ^{178m2}Hf, but in the (n, $n'\gamma$) reaction for ^{179m2}Hf. The absolute cross-section for ^{179m2}Hf production is not particularly low and in standard reactor irradiations quantities as large as μg ^{179m2}Hf could be accumulated. Nanogram amounts are achievable for ^{178m2}Hf, but this would appear to be insufficient for applications or for using the isomer as target or beam nuclei in experiments.

IV. DISCUSSION

The results summarized in Tables 2 - 4 permit the plot of Fig. 2, showing the systematics of the isomer-to-ground ratio versus spin-deficit for production of hafnium isomers. This plot leads to some interesting points and, perhaps, a general conclusion. It can be seen in Fig. 2 that the σ_m/σ_g ratio follows a regular exponential decrease with increasing ΔJ. The (n, γ), (n, $n'\gamma$) and (n, $2n$) reactions demonstrate separate curves with individual slopes in the log plot. A natural explanation for the appearance of different curves is that the

projectile angular momentum increases with the neutron kinetic energy. In general, the systematics does not demonstrate any unexpected behavior, but the plot allows a quantitative definition of real values for specific reactions. It can, therefore, be used to make estimates of σ_m/σ_g values for other cases. It is important to note is that the systematics cover a wide range in angular momentum, as high as $J = 16$ for isomers populated in the (n, γ) reaction and corresponding to a σ_m/σ_g ratio lower than 10^{-8}. Such values are not typical in comparison with other measurements known in the literature for neutron-induced reactions.

Fig.2

The conclusion that ^{179m2}Hf is produced in via $(n, n'\gamma)$ reactions while, conversely, ^{178m2}Hf is produced via (n,γ) reactions is supported by Fig. 2 in addition to the arguments given above. In this plot the upper limits determined for ^{178m2}Hf production via the $(n, n'\gamma)$ reaction and for ^{179m2}Hf production in the (n, γ) reaction deviate from the systematic pattern, both lying far above the curves corresponding to the respective reactions. Following the systematic trends, it appears that the real cross-section for production of ^{179m2}Hf via (n, γ) reactions is negligible in reactor irradiations as compared with the much larger cross section for $(n, n'\gamma)$ reactions, and vise versa for ^{178m2}Hf.

The present result that there are significant cross sections for burnup of ^{178m2}Hf in the ^{178m2}Hf$(n, \gamma)^{179m2,g}$Hf reaction equal in total σ_{th}=235 b and I_γ=5600 b is worth further discussion. Such large values are known for many other nuclei, e. g. the ^{177}Hf nucleus with odd neutron number is characterized by even higher values, as is known from Ref. [1]. In the even-even ^{178}Hf nucleus, a pair of neutrons is decoupled in the m2 state, so that the isomeric nucleus can manifest itself for as equivalent in behavior to an odd-neutron nucleus. Thus, the observed large burnup cross-section is not out of scale [1], unlike the extremely large (n, γ) cross-section for burnup of ^{178m2}Hf reported in Ref. [10]. That value was not reproduced by the present measurements.

Table 2 shows that the population of the ground state appears with 4× higher probability than the m2 state, but stronger selectivity was not manifested. This can be understood in the following way. Figure 3 shows a partial level scheme for ^{179}Hf, the daughter of the burnup reaction on ^{178m2}Hf. Compound-nucleus states of ^{179}Hf are excited after neutron capture by ^{178m2}Hf and possess $J^{\pi} = 31/2^{+}$ or $33/2^{+}$ and a fixed excitation energy near 8,546 keV. For the lower-lying structure, the important features are the m_2 isomer in ^{179}Hf with $J^{\pi} = 25/2^{-}$ at 1,106 keV and the two rotational bands built on the ground and isomeric states. Many other bands exist [11] and the population of m_2 and g states may initially proceed via such bands near the top of the cascade that follows neutron capture. However, these decay paths will eventually reach the bands shown in Fig. 3. Direct transitions can also take place from the compound-nucleus state to the ground or *m2* bands, but, of course, many different cascade paths contribute to the population of a given final state because the level density above $E^{*} = (4 - 5)$ MeV is high in hafnium nuclei.

There is no spin deficit for the burnup reaction on ^{178m2}Hf leading to the high-spin ^{179m2}Hf state and it should be strongly populated. It is possible that some preference for this final state may arise due to its high K value and the fact that there is a similar structure of the target and product *m2* isomers. However, this experiment demonstrated a preference for population of the ground state. A first conclusion is that the K quantum number and structure tagging do not survive past neutron capture at E^{*} above 8 MeV. This may explain the nearly equal population of the m_2 and ground states.

Fig.3

A similar lack of selectivity to structure details at $E^{*} > B_n$ was concluded from the measurements of Ref. [12] on depopulation of the ^{180m}Ta isomer by fast neutron inelastic

scattering, in accordance with the basic ideas of the statistical model. In that work, no preferential population of the ground state was observed, unlike the present case of capture on ^{178m2}Hf. The question remains why there exists even a modest preference for ground-state population following the (n, γ) reaction on ^{178m2}Hf. One must take into account the presence of many levels of appropriate spin near and below the compound-nucleus state and these will be populated after neutron capture with equal probability without any influence of structure effects. Thus, selectivity for reaching either the ground or m2 states cannot appear near the top of the cascades. One must speculate that the modest preference for the ground state arises due to the position of the m2 level at 1.1 MeV. Some cascades proceeding to the ground state may obtain a higher probability simply because they possess a larger reserve of energy above the ground state than those reaching the isomer, thus providing more possibilities for branching. This idea has not yet been developed in detail.

The above interpretation can be modified if superelastic scattering (SES) [13] contributes a significant part of the observed total burnup cross-section. Until now, SES for ^{178m2}Hf was not measured and theoretical estimates allow a wide range for this cross-section. This process was not accounted for in the present analysis. There is a lack of sufficiently-developed simulation procedures for reactions with high-spin isomers, despite interesting experimental data may be found in the literature [7,12, 14-16].

V. SUMMARY

Production of the high-spin ^{178m2}Hf isomer in ^{nat}Hf targets was successfully observed after their activation with the reactor neutrons at fluences lower than 10^{18} n/cm^2. It was established that ^{178m2}Hf is mainly produced due to the capture of slow neutrons in (n, γ) reaction, while ^{179m2}Hf is produced in the $(n, n'\gamma)$ reaction with fast neutrons. The production cross-sections are very different, so that it is possible to accumulate ^{179m2}Hf in a microgram amount after standard irradiations, but only nanograms of ^{178m2}Hf. Comparing the present measurements

with the published data, the destruction (burnup) cross-section was deduced for ^{178m2}Hf due to a second neutron capture from the reactor flux. The partial σ_{th} and I_γ values were specified for the burnup process leading to both m_2 and g states in ^{179}Hf. Also, the isomer-to-ground state ratios for hafnium isomers in neutron-induced reactions were systematized. The potential application of the ^{178m2}Hf isomer as a reservoir for energy storage and pulsed release has already been discussed extensively in the literature. However, the present results, as well as those in the literature, do not support an optimistic view of reactors as a source of large-scale manufacture of ^{178m2}Hf . Other reactions may prove more efficient for production of this long-lived isomer. Spallation reactions with protons of intermediate energy, or neutron irradiations at an energy of 14 MeV and higher must be the most productive as is discussed recently in Ref. [17]. Isomeric nuclei may play some role in cosmogenic nucleosynthesis. Their production and destruction cross-sections should be in account at respecting simulations that are well-developed in modern astrophysics.

ACKNOWLEDGEMENTS

The authors gratefully acknowledge support from the United States Air Force Office of Scientific Research under contract F49620-02-01-0187.

REFERENCES

1. S. F. Mughabghab, *Neutron Cross Sections, Volume 1. Neutron Resonance Parameters and Thermal Cross Sections, Part B, Z= 61-100* (Academic Press, 1984).
2. V. McLane, C. L. Dunford, and P. F. Rose, *Neutron Cross Sections, Volume 2. Curves* (Academic Press, 1988).
3. S. A. Karamian, J. J. Carroll, J. Adam, et al., Laser Phys. **14**, 438 (2004).
4. R. G. Helmer and C. W. Reich, Nuclear Physics **A211**, 1 (1973).

5. S. A. Karamian, Y. T. Oganessian, J. Adam, et al., in *VI International School-Seminar "Heavy-Ion Physics"*, Dubna, Russia, (World Scientific, Singapore, 1998), p. 565.

6. A. Gilbert and A.G.W. Cameron, Canadian J. Phys. **43**, 1446 (1965).

7. O. Roig, G. Bélier, J.-M. Daugas, et al., Nucl. Inst. Meth. A **521**, 5 (2004).

8. M. B. Chadwick and P. G. Young, Nucl. Sci. Eng. **108**, 117 (1991).

9. Y. Weixiang, L. Hanlin, and Z. Wenrong, Chinese J. Nucl. Phys. **14**, 326 (1992).

10. G. V. Muradian, O. Y. Shatrov, M. A. Voskanian, et al., Phys. Atomic Nucl. **66**, 6 (2003).

11. S. M. Mullins, G. D. Dracoulis, A. P. Byrne, et al., Phys Rev. C **61**, 044315 (2000).

12. S. A. Karamian, C. B. Collins, J. J. Carroll, et al., Phys. Rev. C **59**, 755 (1999).

13. G. Reffo and M. H. MacGregor, Nucl. Sci. Eng. **114**, 124 (1993).

14. I. A. Kondurov, Y. V. Petrov, E. M. Korotkikh, et al., Phys. Lett. B **106**, 383 (1981).

15. Y. T. Oganessian and S. A. Karamian, Hyperfine Int. **107**, 43 (1997).

16. D. Belic, C. Arlandini, J. Besserer, et al., Phys. Rev. C **65**, 035801 (2002).

17. S.A. Karamian, Phys. Atomic Nucl. (Moscow), **68**, 1827 (2005).

TABLES

Table 1. Number of peak counts in the γ lines from ^{178m2}Hf compared to the lines of ^{175}Hf and ^{181}Hf (see Fig. 1). The gamma spectrum was taken after two-years "cooling" of a metal ^{nat}Hf sample activated with reactor neutrons.

Nucleus	E_γ [keV]	Counts	Statistical error
^{178m2}Hf	426.4	19,321	6.3 %
	495.0	12,461	7.6 %
	574.2	16,627	10. 4%
^{175}Hf	343.4	1.086×10^9	0.2 %
	432.8	1.599×10^7	0.3 %
^{181}Hf	482.0	1.487×10^8	0.3 %

Table 2. Neutron capture cross-sections for hafnium isotopes.

Target	J^π_t	Product	J^π_p	σ_{th} [barn]	I_γ [barn]	σ_m/σ_g	Reference
^{174}Hf	0^+	^{175}Hf	$5/2^-$	561	436	—	[1]
^{176}Hf	0^+	^{177}Hf	$7/2^-$	23.5	880	—	[1]
^{177}Hf	$7/2^-$	^{178g}Hf	0^+	373	7,173	—	[1]
		^{178m1}Hf	8^-	0.96	—	1.6×10^{-3}	[1]
		^{178m2}Hf	16^+	2.6×10^{-6}	5×10^{-5}	$(7\pm2) \times 10^{-9}$	Present
^{178}Hf	0^+	^{179g}Hf	$9/2^+$	84	1,950	—	[1]
		^{179m1}Hf	$1/2^-$	53	—	0.63	[1]
		^{179m2}Hf	$25/2^-$	$\leq 2 \times 10^{-4}$	$\leq 1.3 \times 10^{-3}$	$\leq 2.4 \times 10^{-6}$	Present
^{178m2}Hf	16^+	^{179g}Hf	$9/2^+$	190	4,500	(0.24±0.07)	Present*
		^{179m2}Hf	$25/2^-$	45±5	1,060±60	—	[5]
^{179}Hf	$9/2^+$	^{180g}Hf	0^+	41	630	—	[1]
		^{180m}Hf	8^-	0.45	6.9	1.1×10^{-2}	[1]
^{180}Hf	0^+	^{181}Hf	$1/2^-$	13.04	35.0	—	[1]

* Obtained by comparison of present results with those of Ref. [4].

Table 3. Summary of the production of ^{178m2}Hf via different neutron-induced reactions.

Reaction	Energy	ΔJ	Cross-section [mb]	σ_m/σ_g	Reference
^{177}Hf(n,γ)	Thermal	12	2.6×10^{-3}	—	Present
	Resonance	12	$I_\gamma = 5 \times 10^{-2}$	$(7\pm2) \times 10^{-9}$	Present
^{178}Hf($n,n'\gamma$)	$E_n \geq 3$ MeV	31/2	$\leq 7 \times 10^{-3}$	$\leq 2.5 \times 10^{-6}$	Present
^{179}Hf($n,2n$)	$E_n = 14.5$ MeV	11	7.3	3.5×10^{-3}	[8]

Table 4. Summary of the production of ^{179m2}Hf via different neutron-induced reactions.

Reaction	Energy	ΔJ	Cross-section [mb]	σ_m/σ_g	Reference
^{178}Hf(n,γ)	Thermal	12	≤ 0.2	$\leq 2.4 \times 10^{-6}$	Present
	Resonance	12	$I_\gamma \leq 13$	$\leq 7 \times 10^{-6}$	Present
^{179}Hf($n,n'\gamma$)	$E_n \geq 1.5$ MeV	15/2	4.5±0.5	$(1.6\pm0.2) \times 10^{-3}$	Present
^{180}Hf($n,2n$)	$E_n = 14.8$ MeV	12	25	7×10^{-3}	[8]

FIGURES

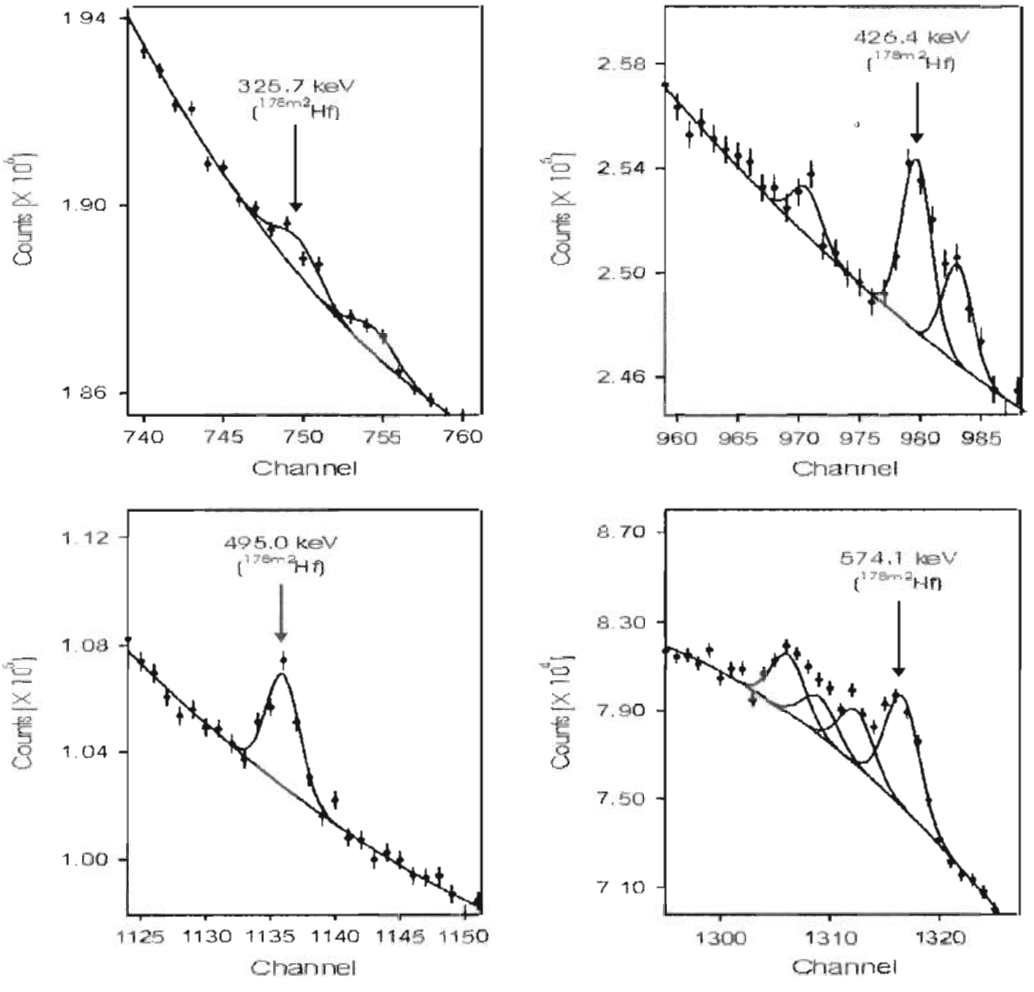

Fig. 1

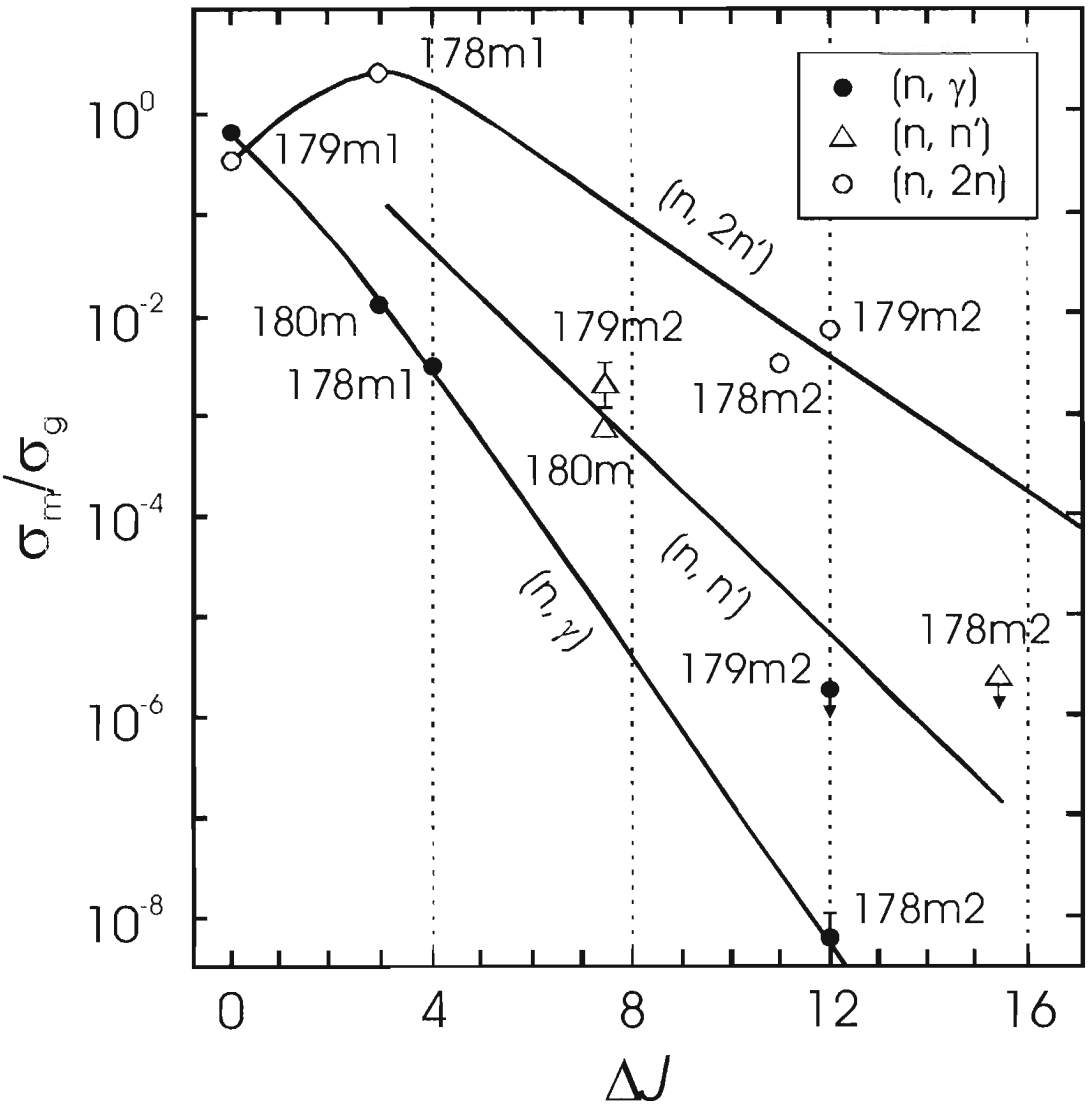
178m1
179m1
(n, γ)
(n, n')
(n, 2n)
(n, 2n')
180m
179m2
178m1
179m2
178m2
180m
(n, n')
(n, γ)
178m2
179m2
178m2
10^0
10^{-2}
10^{-4}
10^{-6}
10^{-8}
σ_m/σ_g
0
4
8
12
16
ΔJ

Fig. 2

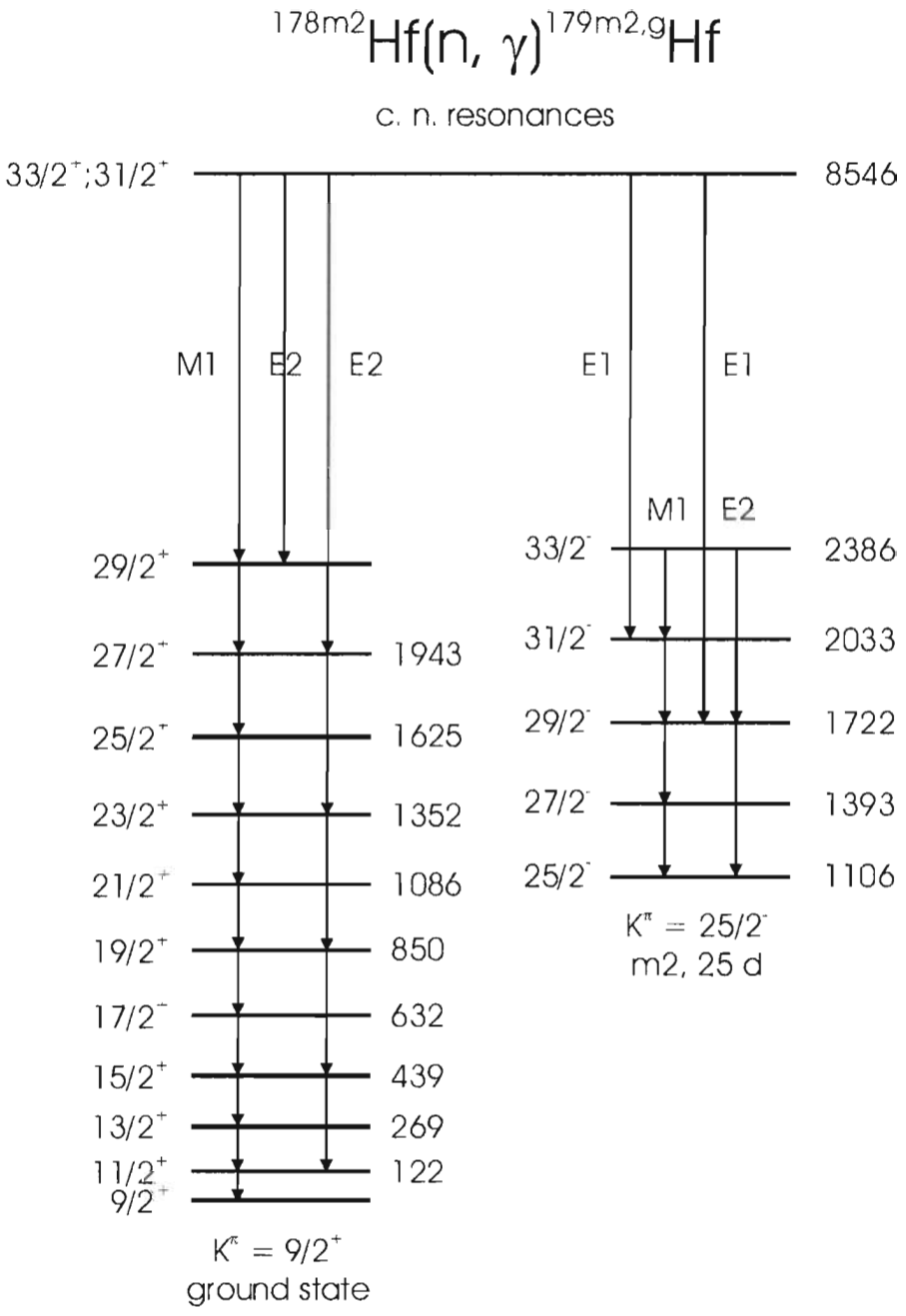
178m2Hf(n, γ)179m2,gHf
c. n. resonances
33/2+;31/2+
8546
M1
E2
E2
E1
E1
M1
E2
29/2+
33/2-
2386
27/2+
1943
31/2-
2033
25/2+
1625
29/2-
1722
23/2+
1352
27/2-
1393
21/2+
1086
25/2-
1106
19/2+
850
Kπ = 25/2-
m2, 25 d
17/2-
632
15/2+
439
13/2+
269
11/2+
122
9/2+
Kπ = 9/2+
ground state

Fig. 3

FIGURE CAPTIONS

Figure 1: Panels show sections of the gamma spectrum collected from the metal ^{nat}Hf sample after neutron irradiation in the inner channel of the IBR-2 reactor, and after two-years cooling time. Lines corresponding to decay of the ^{178m2}Hf isomer are identified and peak fits are shown from which the counts of Table 1 were determined.

Figure 2: Measured values of the isomer-to-ground-state ratio versus spin deficit (ΔJ) parameter for hafnium isomers produced in neutron-induced reactions. Numerical data and references are given in Tables 2 – 4. For simplicity, points according to the literature are given without error bars.

Figure 3: Partial level scheme depicting population of the m_2 and ground states in ^{179}Hf after the ^{178m2}Hf(n, γ) reaction with slow neutrons. The cascades shown illustrate the discussion in the text.

Ups and Downs of Nuclear Isomers

Isomers are set apart from other nuclear excitations by their long half-lives. That longevity facilitates the study of nuclear structure and astrophysics, and it suggests a variety of practical applications.

Philip M. Walker and James J. Carroll

What could one do with a clean source of nuclear energy? That tantalizing question reflects a dream that some have hoped to realize by exploiting the energy-storage capabilities of nuclear isomers. But the hope hinges on facets of nuclear behavior that remain unknown despite decades of study. Electromagnetic transitions and β decay, the basic mechanisms that largely determine isomer half-lives, are well understood. In many cases, however, it is still not possible to predict half-lives even to within an order of magnitude.

Today's isomer research seeks a better understanding of the degrees of freedom that will reveal new aspects of nuclear structure and lead the way to new applications. In this article, we lay out the essential ingredients of nuclear isomerism and take a look at future possibilities.

Metastable excited states

The term "isomer" is borrowed from chemistry, where it refers to molecules that have different geometrical configurations of the same collection of atoms. Isomeric nuclei, as distinguished from isotopes, are different states of the same numbers of protons *and* neutrons. Whereas chemical isomers have energy states that are similar, sometimes identical, to each other, nuclear isomers always have different energies. Excitation energies can be as high as several MeV.

An interesting example of a nuclear isomer is ^{99m}Tc, an excited state of technetium-99. The "m" after the mass number denotes a metastable state—that is, a long-lived isomer. The half-life of ^{99m}Tc is six hours and its excitation energy above the nuclear ground state of ^{99}Tc is 143 keV. By contrast, typical half-lives of excited nuclear states are about a picosecond. Isomers live at least a thousand times longer. The appellation is usually reserved for excited nuclear states that live longer than a nanosecond. The superscript "m" is even more restrictive; it's reserved for isomers with half-lives of more than a millisecond. If a nuclear species has more than one metastable isomer, an ordinal number after the "m" distinguishes between them in ascending order of excitation energy.

Perhaps the most widely known nuclear isomer is the long-lived hafnium excitation ^{178m2}Hf. With a half-life of 31 years, it sits 2.4 MeV above the stable ^{178}Hf ground state. The exceptional combination of high excitation energy and conveniently long half-life has led to claims for practical applications that have lent the hafnium isomer unusual visibility (see PHYSICS TODAY, May 2004, page 21).

Nature's sole example of an isomer long-lived enough to be called stable is ^{180m}Ta. This tantalum isomer's half-life exceeds 10^{15} years. One can only quote a lower lifetime limit, because the isomer's spontaneous decay has never been observed. But the isomer sits 77 keV above a ground state that is itself unstable, with a β-decay half-life of only eight hours.

Isomers can lose their excess energy by the usual radioactive decay modes: α, β, or γ. The favored mode in any particular case depends on the energies and quantum numbers of the states involved. Decay by neutron or proton emission, or even by fission, is possible for some isomers.

What can isomers reveal about nuclei and about the environments—for example, sites of astrophysical nucleosynthesis—in which they are formed? How can nuclear isomers be put to practical uses here on Earth?

Isomers in the clinic

The nuclear isomer that is most often ingested for clinical purposes is ^{99m}Tc. It has excellent properties for medical imaging: a convenient half-life of six hours and an equally convenient soft-gamma-ray decay energy of 141 keV. Another useful feature is technetium's ability to bind chemically with many biomolecules. Furthermore, the isomer is easy to produce. One can, for example, bombard molybdenum-98 with neutrons from a reactor to make ^{99}Mo, which then β-decays with a half-life of 66 hours to ^{99m}Tc. The technetium isomer is probably the most widely used of all radioactive isotopes for medical diagnostics. It is used to image the brain, bones, heart, lungs, and other organs (see figure 1).

It's not, in fact, the emission of the 141-keV gamma that gives ^{99m}Tc its desirably long half-life. The six hours are taken almost entirely by the first step in the isomer's descent to the ground state. That preliminary step is a 2-keV decay by electron conversion, in which nuclear excitation energy is carried away by the ejection of an orbital electron from the atom. The subsequent emission of the 141-keV gamma from the nucleus takes less than a nanosecond.

The long half-life of the first step of ^{99m}Tc decay is attributable to the isomer's angular momentum. Its spin J and parity π are $J^\pi = 9/2^+$. But the state 2 keV below the isomer has $J^\pi = 7/2^+$. Therefore the initial 2-keV electromagnetic step between those two states is governed by an electric-octupole (E3) transition-matrix element. A direct 143-keV transition from the isomer straight to the $J^\pi = 9/2^+$ ground state would have magnetic-hexadecapole (M4) character. Such high-multipole electromagnetic transitions are very slow.

Philip Walker *is a professor of physics at the University of Surrey in England.* **James J. Carroll** *is a professor of physics at Youngstown State University in Ohio.*

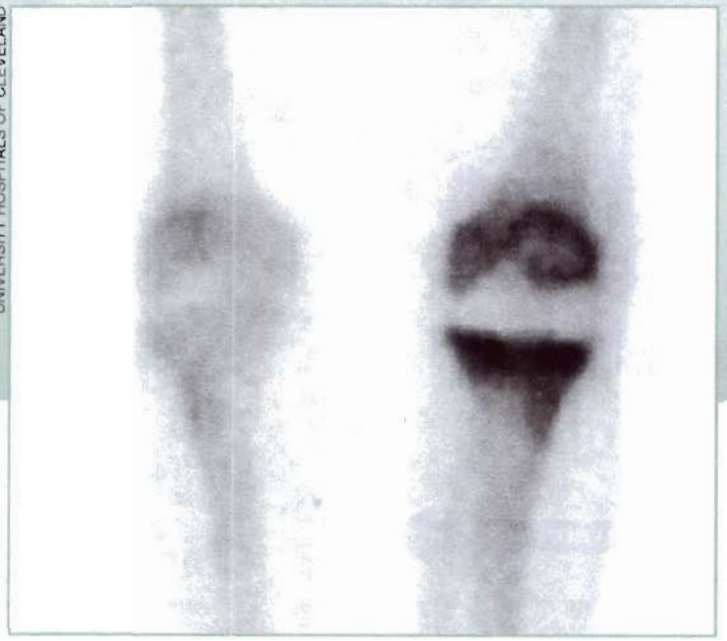

Figure 1. Medical imaging with the technetium isomer ^{99m}Tc shows a front view of a patient with septic arthritis in the left knee. The widely used isomer decays with a half-life of six hours by emitting a 141-keV photon. The isomeric material, bound to a ligand compound, was injected intravenously. The ligand preferentially seeks out metabolically active sites such as the inflamed knee in this case. The radioactive emission was mapped by a gamma camera whose crystalline sodium iodide scintillator elements scan around the patient.

Another unusual aspect of ^{99m}Tc is that technetium ($Z = 43$) has no stable nuclei. Its longest-lived isotope, ^{98}Tc, has a half-life of 4 million years. Therefore it's not found in natural deposits on Earth. It was the first new element to be produced artificially (in 1937). Hence its name, from the Greek *technetos*, meaning artificial. Promethium ($Z = 61$), the only other element lighter than lead that has no stable isotopes, was first made in the laboratory in 1945.

Isomers in the stars

Because Tc has no stable isotopes, it is especially interesting for astrophysics. From observations of its lines in atomic spectra of red-giant stars, one finds that Tc is being made in such stars by nuclear reactions between other elements. Visible light from Tc atoms far away brings to us the most compelling evidence of nature's ongoing cosmic alchemy.

The study of naturally occurring radionuclides surviving from Earth's formation has provided the most accurate information about the age of our planet—about 4.6 billion years. Nuclides with half-lives of much less than a billion years are now at low or vanishing abundance. For example, uranium-238, with a half-life of 4.47×10^9 years, is now the most abundant uranium isotope by far. But ^{235}U, on which most fission power depends, has a half-life of only 7.04×10^8 years and an abundance of 0.7% relative to ^{238}U. If Earth had formed with equal abundances of each, the ^{235}U/^{238}U abundance ratio would now be 2.4%. Therefore, there must have been several times more ^{238}U to start with. But that starting point depends on the details of stellar nucleosynthesis.

Nuclear isomers probe this astrophysical alchemy and the stellar environments in which it takes place. With its half-life much longer than the 10^{10}-year age of the cosmos, ^{180m}Ta is the only naturally occurring isomer that's stable on the scale of stellar lifetimes. But many isomers that β-decay on much shorter time scales can serve as useful stellar probes.

The exceptional half-life of ^{180m}Ta, like that of ^{99m}Tc, hinges on angular momentum. This time, though, the isomer's own high spin is the impediment. Its spin–parity state is 9^-. A short-lived excited state 37 keV below the isomer has $J^\pi = 2^+$, and the nuclear ground state is 1^+. Therefore, electromagnetic transitions from the isomer, if they exist, would have E7 and M8 character. But such high-multipole transitions have never been seen.

For tantalum in stars, the issue is the β-decaying ground state of ^{180}Ta. If the star is hot enough (above 10^9 K), excitation and de-excitation of nuclei by thermal photons will yield an equilibrium mixture of the ground and isomeric states. That's the kind of environment required for slow-neutron-capture (s-process) nucleosynthesis (see the article by John Cowan and Friedrich-Karl Thielemann in PHYSICS TODAY, October 2004, page 47).

If one of the nuclear states in such an equilibrium β-decays with a short half-life, then the longer-lived state will be depleted—that is, its effective half-life is reduced. The case of ^{180}Ta is of particular interest because the transition probabilities for γ-excitation to higher-lying states from which it *can* decay have recently been measured.[1] From those measurements, and the fact that ^{180m}Ta exists on Earth (albeit with the lowest abundance of any stable nuclide), one can infer that s-process production of the isomer takes place in stars at modest temperatures less than 3×10^8 K.

However, the actual mechanism by which ^{180m}Ta is synthesized remains a mystery. Proton capture and neutrino reactions are two possibilities. The name tantalum is particularly appropriate to the ongoing challenge of puzzling out the isomer's origins. The mythological Tantalus, miscreant son of Zeus, is perpetually punished by being kept just out of reach of food and water.

A central role

Isomers were first foreseen by Fredrick Soddy, long before the discovery of the neutron. In 1917 he wrote, "We can have isotopes with identity of atomic weight, as well as of chemical character, which are different in their stability and mode of breaking up." Otto Hahn is usually credited with the first experimental observation of isomers, in uranium salts in 1921. But the key observations came in 1935, when nuclear physicists in the Soviet Union and Britain found isomers in bromine and indium.[2] These discoveries were soon followed by Carl von Weizsacker's theoretical explanation in terms of angular-momentum quantum numbers.[3] He was describing "spin traps," which turn out to be the principal class of isomers. Spin traps relax very slowly because high-multipole electromagnetic transition amplitudes are intrinsically weak.

The explanation for the existence of high-spin states came from the formulation of the nuclear shell model in

1949. Indeed, the existence of isomers demanded the shell model. Individual nucleon orbits must be able to carry high angular momentum, and the existence of isomers depends on the quantum numbers of those individual orbits. Notwithstanding this strong tie to the single-particle emphasis of the shell model, isomers also provided essential information for the collective aspects of nucleons in the nucleus. In 1953, Aage Bohr and Ben Mottelson[4] interpreted the energies of the ^{180}Hf states one sees following the decay of ^{180m}Hf as being characteristic of a quantum rotor, with energies proportional to $J(J + 1)$. Thus did isomers take their place at the center of nuclear-structure investigations.

In the 1960s, nuclear isomers provided the first examples of superdeformed nuclei; they were twice as long as they were wide. The superdeformed americium isomer ^{242m}Am, discovered in 1962, decays by fission.[5] At the end of the decade, the cobalt isomer ^{53m}Co yielded the first observation of decay by direct proton emission.[6] Those discoveries have paved the way to extensive investigations of the associated decay phenomena.[7] No one has yet found an isomer that decays by neutron emission.

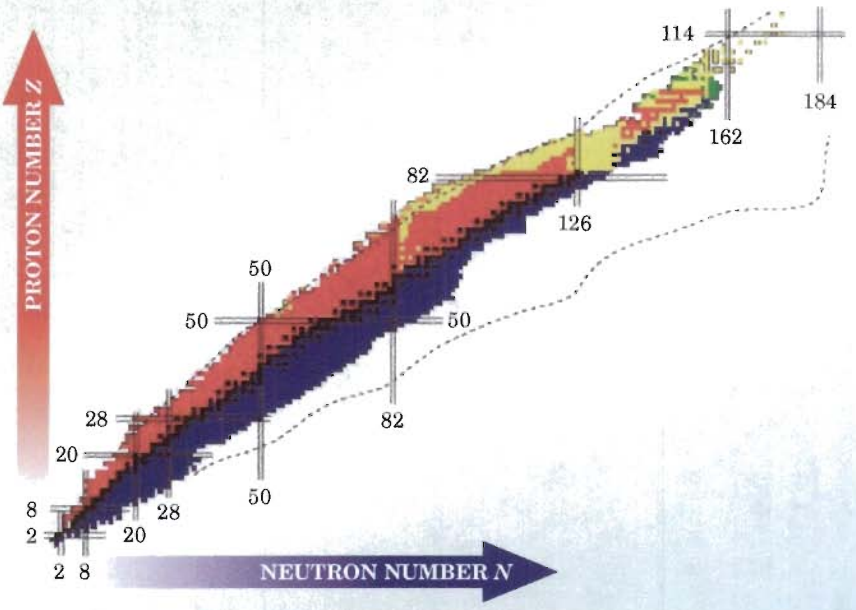

Figure 2. The chart of nuclides shows naturally occurring stable nuclides (black squares) clustered along the valley of nuclear stability. Unstable nuclear species known from the laboratory are shown in color. Double lines indicate magic (closed-shell) neutron and proton numbers. The dashed outer contour, indicating the limits of nuclear binding, shows that many neutron-rich nuclides are yet to be discovered. Microsecond isomers promise especially sensitive access to presently unknown nuclides.

Neutron-rich nuclides

Let us focus on some recent developments and unsolved problems. Access to heavy nuclides on the neutron-rich side of the valley of stability is experimentally difficult, but highly desirable. Figure 2 shows this wide-open region of unknown nuclides. The physics objectives include the understanding of neutron skins of such nuclei—the outer volume into which the neutron distribution extends significantly beyond the proton distribution. One also wants to determine the structure of nuclides along the path of rapid-neutron-capture (r-process) nucleosynthesis. Understanding the r process could yield deep insight into supernova explosions. Because nuclear binding becomes very weak

Box 1. Broken Pairs and Isomer Half-Lives

All even–even nuclides (that is, those having even proton and neutron numbers) have ground states of zero total-angular-momentum quantum number J and positive parity π. That's because all the single-particle nucleon orbits are paired, giving the state of lowest total energy. Here we neglect the contribution of collective rotation of the entire nucleus, which can in general add energy and angular momentum to that arising from the individual nucleon orbits (see box 2). Excitation of the nucleus may break up a pair of nucleons, with one or both being promoted to higher orbits. This excitation is called a two-quasiparticle state to emphasize the importance of the pairing interaction, which modifies the energy and wavefunction of the nuclear level.

The remaining even–even core of nucleons contributes no excitation energy or angular momentum. That role belongs to the quasiparticles. Suppose two quasiparticles (that is, two broken-pair nucleons) in different orbits each had $J^\pi = 11/2^+$. The total angular momentum of the nucleus would come from their vector sum. In that case, J^π could range from 0^+ to 11^+, depending on the relative orientation of the quasiparticle spins. Thus, high nuclear spin can result from as few as two unpaired nucleons.

"Spin-trap" isomers occur in even–even nuclei in just this way, when excited states require large-multipole electromagnetic transitions for their decay. In ^{178}Hf, for example, the 31-year 16^+ isomer has four-quasiparticle character—that is, one broken neutron pair and one broken proton pair. But spin-trap isomers can also occur in odd–even or odd–odd nuclei. The nuclide ^{180}Ta is odd–odd. Its two-quasiparticle 1^+ ground state already has one unpaired proton and one unpaired neutron. The ultralong-lived 9^- isomer ^{180m}Ta also has two-quasiparticle character, but with very different relative orientations of the neutron and proton orbits. High angular momentum explains these isomers qualitatively. But quantitatively, the situation is less satisfactory.

Both the spherical nuclear shell model of orbiting nucleons and the deformed-shell (Nilsson) model, which allows for nonspherical shapes, predict the existence of isomers. But beyond these shell models of independently orbiting nucleons, there are additional interactions between the unpaired nucleons and the core, and between quasiparticles, that are hard to quantify. They lead to uncertainties on the order of 100 keV in the predicted excitation energies of isomers. There is also significant uncertainty in the calculation of isomer decay rates to collective rotational or vibrational states of the core.

Although the bulk behavior of the wavefunctions of isomers and other excited states are relatively well understood, the full details are still missing. Because electromagnetic decay rates depend sensitively on the overlap between wavefunctions for initial and final states, small discrepancies on the wings of the wavefunctions can lead to very different results. Additional data will be required for sorting out the relative importance of the different mechanisms that contribute to isomer decay.

with increasing neutron excess, mean-field theoretical models may turn out to be completely inadequate in the neutron-rich domain.

A promising way of producing and studying neutron-rich nuclides and their excited states was pioneered at the GANIL laboratory in Caen, France, and the GSI laboratory in Darmstadt, Germany. At these heavy-ion accelerator facilities, projectile nuclei fragment in high-energy collisions with target nuclei, and one finds isomers amid the debris.

In a recent experiment at GSI, Monica Caamaño and coworkers bombarded a beryllium-9 target with stripped lead-208 nuclei accelerated to an energy of 1 GeV per nucleon.[8] The fragments of the Pb nucleus, after being tracked through a magnetic separator, were stopped and their γ-decay photons were measured in germanium detectors (see figure 3). The experimenters were able to associate the emitted gammas, ion by ion, with specific fragments over decay-sequence correlation times as long as 100 μs. In this way, Caamaño and company identified 11 new isomeric states of neutron-rich nuclides with mass numbers from 188 to 203. The isomeric half-lives ranged from 10 ns to 1 ms.

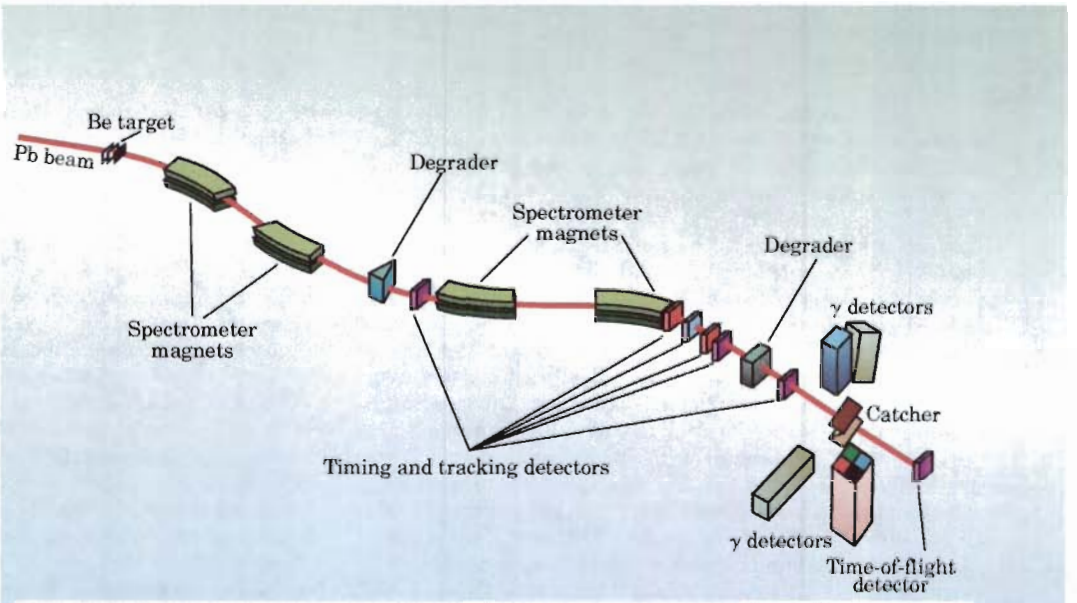

Figure 3. The fragment separator at GSI, the heavy-ion accelerator facility in Darmstadt, Germany, is a prolific source of newly discovered isomers. In a recent experiment,[8] lead-208 nuclei, accelerated to 1 GeV per nucleon, fragment on a beryllium target. Fragments are separated and steered by magnets, and tracked and timed by wire-chamber and scintillation detectors. They are finally stopped by a "catcher" in the middle of an array of segmented germanium detectors that record gamma-ray photons from the de-excitation of isomers.

These neutron-rich nuclides are still some way from the neutron-skin regime and the r-process pathway. Nevertheless, such studies are paving the way to those longer-term objectives. At the same time, the experiments have already uncovered unexpected nuclear-structure effects. An important feature of isomers with half-lives in the microsecond region is the experimenter's ability to correlate fragments of the projectile nucleus with their decay products. A few microseconds is long enough to track and identify the fragments, yet short enough to distinguish time-correlated decay events from accidental background correlations.

For longer-lived fragments, one can observe isomer and ground-state properties by injecting the fragments into a storage ring.[9] In recent measurements of heavy, neutron-rich nuclei by the storage-ring technique, experimenters were seeking, among other things, a predicted $J^\pi = 18^+$ isomer of ^{188}Hf that might have intriguing similarities to the much-touted isomer ^{178m2}Hf, whose spin–parity is 16^+. The data are still under analysis.

The development of new, high-intensity projectile-fragmentation facilities is now a key part of planning for the future of nuclear physics worldwide, with projects such as RIA (Rare Isotope Accelerator) in the US and FAIR (Facility for Antiproton and Ion Research) in Germany. While addressing a wide range of nuclear and applied-science issues, these new facilities will provide important new opportunities for the study of isomers, especially in heavy, neutron-rich nuclides.

Superheavy nuclides

The search for the heaviest possible elements is a quest of long standing. For the so-called superheavy elements—those with more than 100 protons—the strong nuclear force between adjacent nucleons is insufficient to overcome the longer-range Coulomb repulsion between the protons. Their existence relies on subtle shell-model effects on the orbits of protons and neutrons inside the nucleus. Such small effects can, in fact, yield long half-lives—but just how long remains uncertain. We don't know, for example, the true nature of the predicted "island of stability" at nuclear masses beyond the present experimental limits.

Superheavy nuclei can have isomer states. Indeed, such isomers can live longer than their ground states.[10] Fission is often described by the liquid-drop model. A key feature of the superheavy isomers is that the nucleon-pair breaking which makes their formation possible also breaks down the superfluidity of the nucleon fluid inside the nucleus. It becomes viscous, and that slows down the fission process. The probability for α-particle decay is also reduced by the pair breaking. For example, an isomer of darmstadtium-270 (the name was officially given to element 110 two years ago) has been found to have a half-life some 60 times longer than its ground state. Thus the predicted abundance of isomers in superheavy nuclei could be of great help in the exploration of that extreme frontier of the nuclear landscape.

Vibration and rotation

The total angular momentum of a nucleus has contributions from individual nucleon orbits and from collective rotation of the nucleus as a whole. Bonded pairs of orbits and, especially, closed shells of such pairs contribute no net angular momentum. In strongly deformed nuclei, nucleon numbers are far from shell closure, and collective rotation usually dominates the low-energy, high-angular-momentum structure. This happens when the orbits of unpaired nucleons cannot generate much angular momentum on their own. In that case, high total angular momentum results most easily (at low energies) from high collective rotation plus a lesser contribution from any unpaired orbits.

There is, however, a small region of nuclides around ^{178}Hf ($Z = 72$ and $N = 106$, see figure 4) where isomers are

"yrast." The term, from the Swedish word for dizziest, refers to the lowest-energy nuclear state for a given angular momentum. For an yrast isomer, the contribution of collective rotation to the angular momentum is minimal. The isomers near ^{178}Hf are yrast as a result of high-spin nucleon orbitals close to the Fermi surface. That effect is well described by the deformed-shell model[11] (see box 1).

Vibrational excitations of deformed nuclei are known to be energetically disfavored. They are far from the yrast states. Recent findings, however, have given evidence for a new type of energetically favored vibrational behavior based on isomers. This effect arises because the maximum-angular-momentum vibrational states have energies proportional to J, whereas rotational energies depend quadratically on J. Thus, as angular momentum increases, rotational excitations become increasingly expensive relative to vibrational excitations. Lee Pattison (University of Manchester, UK) and coworkers have reported a dramatic consequence of this competition.[12] On top of the $J^{\pi} = 25^{+}$ isomer of osmium-182, they found a sequence of vibrational excitations that are, in fact, yrast. Their theoretical understanding of this structure is, thus far, based on a model of "tidal waves" that offers a new perspective on nuclear excitation modes.

Isomer decay in deformed nuclei

So far the discussion has concentrated on the utility of isomers for illuminating other nuclear phenomena. Now we take a closer look at isomer decay rates, focusing on so-called K isomers in deformed nuclei. The quantum number K is (in units of $\hbar$) the projection of the nuclear angular momentum on the symmetry axis of the nucleus (see box 2). The decay of isomers by electromagnetic transitions of multipole order lower than ΔK, the difference in K between initial and final states, requires a mixing of K values in either state. This K mixing need only have a small influence on the wave function to produce a dominant effect on the rates of otherwise forbidden de-excitation transitions.

Three distinct mechanisms have been proposed for the requisite K mixing. First, there is Coriolis-force mixing in the noninertial rest frame of the rotating nucleus. One can view the Coriolis effect as causing fluctuations in the orientation of the nucleus without any fluctuation in its shape. Second, because K conservation depends on axial symmetry, asymmetric wavefunction components can instigate K mixing. That effect is equivalent to nuclear shape fluctuations with orientation fixed. Finally, there is statistical mixing: Quantum states of the same spin and parity, but different K, can mix significantly by virtue of fortuitous near-degeneracies between their energies. Such accidental degeneracies become more common with increasing density of energy levels. And the level density, in turn, grows with excitation energy.

Each of the three K-mixing mechanisms, on its own, has had some success in fitting the isomer data.[7] But a unified approach has yet to be developed, and the relative importance of the different mechanisms remains to be determined. The situation leaves the prediction of some isomer half-lives uncertain by many orders of magnitude.

Inducing premature decay

Let's return to our opening question about clean energy sources. A special feature of nuclear isomers is that they carry excess energy. And that energy can be released through the electromagnetic interaction. Indeed, the energy release can be induced by photon bombardment. In other words, one can shorten the isomer's decay time and thus release the excitation energy in a controlled manner.

That much is well established. For example, the 10^{15}-year isomer ^{180m}Ta can be converted to the 8-hour β-decaying ^{180}Ta ground state by photon bombardment, a process that has been studied in detail.[1,13] But

Box 2. *K* Isomers

The orientation of a deformed isomer's spin relative to the symmetry axis can strongly affect its half-life. Nuclei with magic (closed-shell) neutron or proton numbers of 2, 8, 20, 28, 50, 82, or 126 (see figure 2) are more or less spherical in their ground states and low-energy excitations. But far away from closed shells, the shape is typically prolate, with well-defined symmetry about the long axis (see the illustration at right). A prolate nucleus can rotate collectively, but quantum mechanics forbids collective rotation about an axis of cylindrical symmetry. The total angular momentum of the nucleus is a vector sum of contributions from collective rotation and orbits of unpaired nucleons. Whatever their relative contributions, the total angular momentum's component $K\hbar$ along the symmetry axis is a constant of the motion.

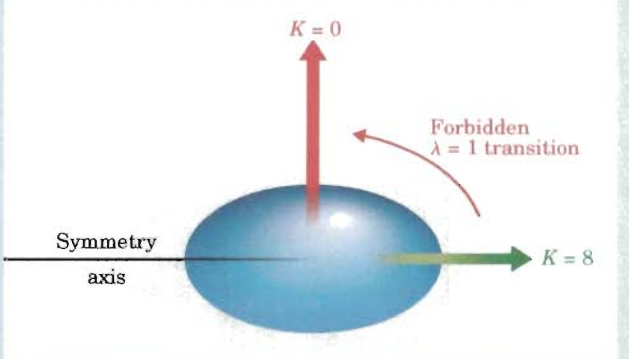

In the noninertial rotating reference frame, however, K is not strictly conserved, primarily because of the Coriolis effect. Just as cyclones—another Coriolis manifestation—have their angular momenta aligned with Earth's axis, nucleon orbits tend to become aligned with the nuclear rotation. The result is a mixing of different K states.

The K quantum number introduces a nuclear-transition selection rule based on the direction as well as the magnitude of the angular momentum: In an electromagnetic de-excitation transition, the change in K should not exceed λ, the transition multipole order. Transitions that violate this condition are called K-forbidden. The drawing above illustrates a K-forbidden dipole ($\lambda = 1$) transition between prolate $J = 8$ nuclear states. In the initial $K = 8$ orientation, the angular momentum can be aligned with the symmetry axis because it arises completely from unpaired nucleon orbits rather than collective rotation. But in the lower-energy $K = 0$ orientation, the $J = 8$ angular momentum is entirely from collective rotation.

Rather than being strictly forbidden, such transitions are severely hindered. The result is long-lived excitation states—that is, nuclear isomers. These "K isomers" form a distinct class of isomers in axially symmetric deformed nuclei. Their distribution in the N-Z plane of neutron and proton numbers (see figure 4), clustered around the 31-year isomer of hafnium-178, is quite distinct from the two clusters of closed-shell (spin-trap) isomers near $N = 82$ and $Z = 82$.

unfortunately, the energy of the incident photon that liberates the isomer's 77-keV excitation energy has to exceed an MeV! Although this γ-induced de-excitation has interesting astrophysical implications, it hardly seems like the basis for a practical energy-storage device.

The scientific interest in such matters entered a new and controversial phase following claims made in 1999 that ^{178m2}Hf could release its 2.4 MeV of stored energy when bombarded by x-ray photons with energies of less than 100 keV. If such triggering were indeed possible at a reasonable rate, the practical implications could have been major.

The ensuing complex story of claims and counterclaims has been told in an article by one of us[14] and in the May 2004 PHYSICS TODAY news story cited above. We don't wish to repeat those arguments here. Suffice it to say that the original claims have not been confirmed to the satisfaction of the nuclear physics community. There are ongoing efforts to quantify the photon de-excitation of ^{178m2}Hf. The physics of isomer interaction with the radiation field implies that the de-excitation will almost certainly be possible at some photon energy. But that threshold energy, while of scientific interest, will very likely be too high to be of practical use. Of course, other isomers may prove themselves useful.

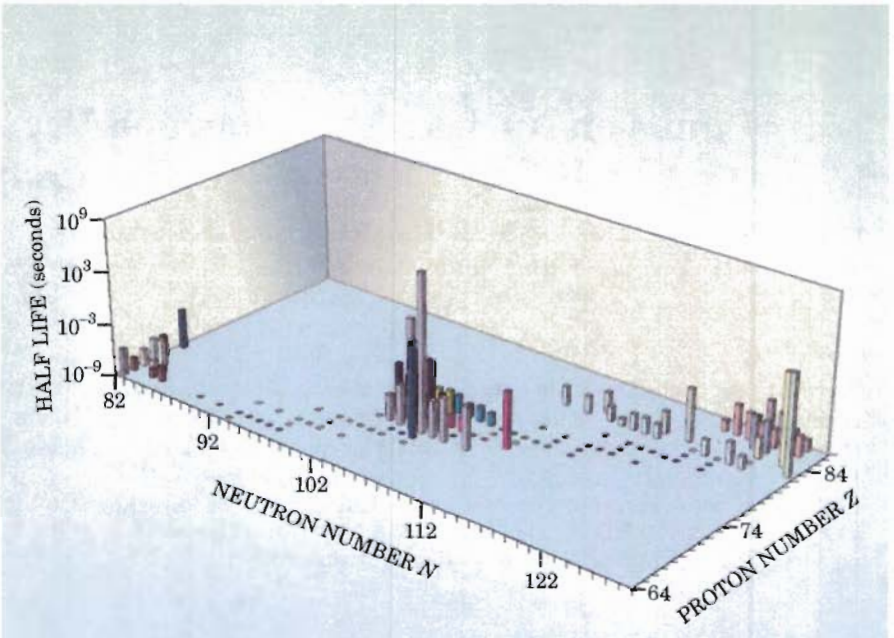

Figure 4. Clustering of heavy isomers on the N-Z plane. Half-lives for high-spin isomers are indicated logarithmically by column height (squares in the plane are stable nuclides). There are three distinct isomer clusters. At left and right are the spin-trap isomers (see box 1) near the magic number 82 of neutrons and protons, respectively. In the center, clustered around the 31-year (10^{9}-second) hafnium-178 isomer (N = 106 and Z = 72) are the K isomers (see box 2).

One can consider, for example, the possibility of stimulated emission from isomers, and even the construction of a γ-ray laser based on isomer decay. Line broadening, the most critical impediment to isomer lasing, might perhaps be overcome by exploiting the Mössbauer effect. But many other difficulties remain.[15] Nevertheless, the potential applications of isomers are widespread, and a better understanding of the processes that control their decay may lead to key advances.

The atomic environment can have a large effect on nuclear decay rates—for example, through the electron-conversion process. To take an extreme case: If all the electrons were stripped from a ^{179}Hf atom while its nucleus was in the $J^{\pi} = 16^{+}$ isomeric state, its half-life would increase from the usual 31 years to 10^{6} years. More promising for applications, of course, are techniques for hastening isomer decay. For example, a 20% half-life reduction has been demonstrated[16] for highly stripped ions of an isomer of iron-57. Less dramatic is the recently discovered 1% shortening of the ground-state half-life of ^{7}Be when the atoms are caged within C_{60} buckeyballs.[17] The sensitivity of nuclear decay to the atomic environment gives hope that mixed atomic–nuclear effects may eventually provide a way to induce energy release from isomers.

Exploiting the practical promise of isomers will require a much improved understanding of their basic properties. Theorists Wojciech Satula (University of Warsaw) and Ramon Wyss (Royal Institute of Technology, Stockholm) have reviewed the considerable recent progress in the understanding of high-spin nuclear excitations.[18] For the experimental progress of nuclear physics, isomers are excellent tools for accessing species far from the valley of stability, particularly for the study of neutron-rich heavy nuclides, and even superheavy nuclides.

References

1. D. Belic et al., *Phys. Rev. C* **65**, 035801 (2002).
2. B. Kurtchatov, I. Kurtchatov, L. Moussovski, L. Roussinov, *Comptes Rendus Acad. Sci.* **200**, 1201 (1935); L. Szilard, T. A. Chalmers, *Nature* **135**, 98 (1935).
3. C. F. von Weizsacker, *Naturwissenschaften* **24**, 813 (1936).
4. A. Bohr, B. R. Mottelson, *Phys. Rev.* **90**, 717 (1953).
5. S. M. Polikanov et al., *Sov. Phys. JETP* **15**, 1016 (1962).
6. K. P. Jackson et al., *Phys. Lett. B* **33**, 281 (1970).
7. P. M. Walker, G. D. Dracoulis, *Nature* **399**, 35 (1999); *Hyperfine Int.* **135**, 83 (2001).
8. M. Caamaño et al., *Eur. Phys. J. A* **23**, 201 (2005).
9. Y. A. Litvinov et al., *Phys. Lett. B* **573**, 80 (2003).
10. F. R. Xu, E. G. Zhao, R. Wyss, P. M. Walker, *Phys. Rev. Lett.* **92**, 252501 (2004); S. Hofmann et al., *Eur. Phys. J. A* **10**, 5 (2001).
11. K. Jain et al., *Nucl. Phys. A* **591**, 61 (1995).
12. L. K. Pattison et al., *Phys. Rev. Lett.* **91**, 182501 (2003).
13. P. M. Walker, G. D. Dracoulis, J. J. Carroll, *Phys. Rev. C* **64**, 061302(R) (2001).
14. J. J. Carroll, *Laser Phys. Lett.* **1**, 275 (2004).
15. G. C. Baldwin, J. C. Solem, *Rev. Mod. Phys.* **69**, 1085 (1997); J. J. Carroll, S. Karamian, L. Rivlin, A. Zadernovsky, *Hyperfine Int.* **135**, 3 (2001).
16. W. R. Phillips et al., *Phys. Rev. Lett.* **62**, 1025 (1989).
17. T. Ohtsuki et al., *Phys. Rev. Lett.* **93** 112501 (2004).
18. W. Satula, R. A. Wyss, *Rep. Prog. Phys.* **68**, 131 (2005). ■

Laser Physics, Vol. 15, No. 4, 2005, pp. 487–491.

Limits on Nuclear Excitation and Deexcitation of $^{178}Hf^{m2}$ by Electron–Nucleus Coupling

M. R. Harston* and J. J. Carroll

Department of Physics, Youngstown State University, Youngstown, Ohio 44455, USA

*e-mail: mharston@cc.ysu.edu

Received October 7, 2004

Abstract—Nuclear excitation in transitions that are resonant with electronic deexcitations are discussed in the context of recent claims of the triggering of the decay of $^{178}Hf^{m2}$ by irradiation with low-energy photons (C. Collins *et al.*, Laser Phys. **14**, 154 (2004)). The upper limits for the NEET cross sections are $\sigma < 10^{-31}$ cm^2 for transitions filling L-shell holes. These results are significantly below the values of 10^{-22} cm^2 reported by Collins *et al.* and confirm the recent results by Tkalya (E. Tkalya, Phys. Rev. C. **68**, 064611 (2003)). These calculations suggest that NEET is unlikely to be the mechanism responsible for the reported apparent enhancements of ^{178}Hf nuclear line intensities by X-ray irradiation.

1. INTRODUCTION

There has been considerable interest in recent years in the investigation of low-energy triggering of the decay of the 2.45-MeV isomeric state $^{178}Hf^{m2}$ [1]. Null results have been obtained by several groups (see the summary in Ref. [1]). Collins and coworkers [2, 3] have, however, reported enhancements in the decay rate corresponding to a cross section for triggering by photons with energies close to the L-shell edge, that is, 2×10^{-3} of the photoionization cross section. The suggested mechanism for triggering was the NEET process, i.e., the excitation of the nucleus by resonant deexcitation of an initially excited electronic state. This process has been detected in the excitation of ^{197}Au following irradiation by photons with energies just above the K-shell edge. The probability for NEET excitation after creation of a K-shell hole was found to be $(5.0 \pm 0.6) \times 10^{-8}$ [4]. Initial theoretical estimates [5] indicated a significantly larger theoretical NEET probability, but a more recent calculation [6] gives a NEET probability of 3.6×10^{-8}, in reasonable agreement with experiment.

The principal object of this article is to obtain estimates of NEET probabilities and cross sections for various possible NEET transitions in $^{178}Hf^{m2}$ in order to examine the claims of low-energy triggering in this nuclide.

2. THEORY

Let us consider the deexcitation of an initially excited electronic state i in an atom with the nucleus in level I. In most cases, this state deexcites to a lower lying state by a radiative or Auger transition. In the case of a NEET transition, the electronic state deexcites by the exchange of a virtual photon with the nucleus, which is excited to the level E. Symmetry requires that the electronic transition have the same multipolarity as that of the nuclear transition. The probability for the decay of the electronic state by NEET as opposed to purely electronic decay is known as the NEET probability. This probability is given by

$$P_{\mathrm{NEET}}(i \longrightarrow f) = \left(1 + \frac{\Gamma_f}{\Gamma_i}\right) \frac{|V_{if}(\pi L)|^2}{(\omega_e - \omega_N)^2 + (\Gamma_i + \Gamma_f)^2/4}, \quad (1)$$

where Γ_i and Γ_f are the total widths of the initial and final (f) hole states; ω_e and ω_N are the energies of the electronic and nuclear transitions, respectively; and $V_{if}(\pi L)$ is the NEET matrix element. Here and below, we use relativistic units ($c = m = \hbar = 1$) unless otherwise stated. The matrix element is given by

$$|V_{if}(\pi L)|^2 = 4\pi\alpha\omega_N^{2L+2} \frac{(C_{j_i 1/2 L 0}^{j_f 1/2})^2}{L^2[(2L+1)!!]^2} |M_e(\pi L)|^2 B_{I \to E}(\pi L), \quad (2)$$

where α is the fine structure constant, j_i and j_f are the total angular momenta of the initial and final electronic subshells, $B_{I \to E}(\pi L)$ is the reduced nuclear transition probability for a transition from the initial nuclear state to the excited nuclear state, $M_e(\pi L)$ is the electronic matrix element for the transition, and $C_{j_i 1/2 L 0}^{j_f 1/2}$ is a Clebsch–Gordan coefficient. The nuclear electromagnetic moment is here related to the reduced nuclear matrix element by

$$B_{I \to E}(\pi L) = \frac{|\langle j_E \| M(\pi L) \| j_I \rangle|^2}{(2j_I + 1)}, \quad (3)$$

Table 1. Level properties for low-lying electronic levels of hafnium

Subshell	Energy, keV	Width, eV	Photoexcitation cross section, $\times 10^{-20}$ cm^2
$1s$	65.351	42	0.28
$2s$	11.271	5.6	1.1
$2p_{1/2}$	10.739	5.0	2.1
$2p_{3/2}$	9.561	4.9	4.6
$3s$	2.600	12.7	3.0
$3p_{1/2}$	2.365	4.5	5.1
$3p_{3/2}$	2.108	6.5	14.8
$3d_{3/2}$	1.716	1.5	12.5
$3d_{5/2}$	1.662	3.0	8.5

where $M(\pi L)$ is the electromagnetic transition operator [7] and j_I and j_E are the spins of the initial and excited nuclear states, respectively.

The cross section for production of a given initial atomic state followed by a NEET process can be calculated by summing over NEET transitions that fill the given hole state:

$$\sigma_{\mathrm{NEET}}(i) = \sigma_{PE}(i)\Sigma_f P_{\mathrm{NEET}}(i \longrightarrow f), \qquad (4)$$

where $\sigma_{PE}(i)$ is the cross section for photoexcitation of the hafnium atom, yielding the initial electronic hole state i.

Once an excited level E is populated by NEET, it may either decay back to the initial nuclear state I or to another nuclear level. The experimentally observable cross section for the population of a nuclear level F by excitation from the level I via the level E, $\sigma_{I\to E\to F}$, is given by

$$\sigma_{I\to E\to F}(i) = \sigma_{\mathrm{NEET}}(i)R_{I\to E\to F}, \qquad (5)$$

where $R_{I\to E\to F}$ is the branching ratio for decay to the state F:

$$R_{I\to E\to F} = \frac{\lambda_{E\to F}}{\lambda_{E\to F}+\lambda_{E\to I}}, \qquad (6)$$

where $\lambda_{E\to F}$ is the total (IC + γ) decay rate from level E to level F and $\lambda_{E\to I}$ is the total decay rate from level E to level I. Equation (6) assumes that the nuclear level E possesses only two decay branches.

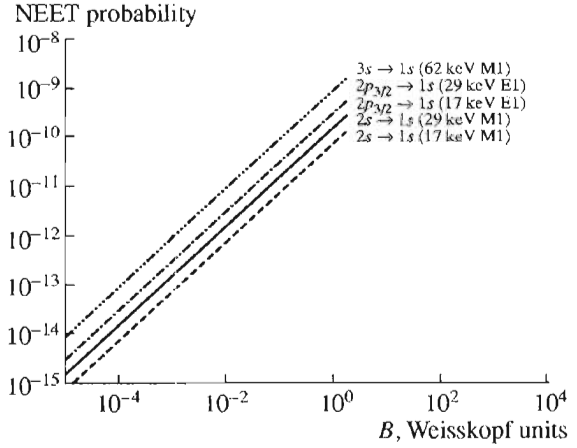

Fig. 1. Probabilities for $L = 1$ NEET transitions to nuclear levels at 17, 29, and 62 keV filling a K-shell hole. The curves for the $2p_{3/2} \longrightarrow 1s$ (17 keV E1) and $2s \longrightarrow 1s$ (29 keV M1) coincide.

3. RESULTS

According to the nuclear-level scheme in [8], only two levels lying within 80 keV of the m2 isomer (2446.1 keV above the ground level) have been fully characterized. One of these is the level lying at 2433.3 keV, which corresponds to the 13^- level of the $K = 8_1$ band. This level is populated in the 12.7-keV E3 deexcitation of the m2 isomer, its dominant decay branch. The other level lies at 2485 keV above the ground state and corresponds to the 12^- level of the $K = 8_2$ band. Such a level could be excited from the m2 level by a 39-keV M4 transition. There is some tentative data for levels lying 17, 28.6, and 62 keV above the m2 level, but none of these has a spin/parity assignment. Nevertheless, we can derive upper limits on the NEET probabilities and NEET cross sections for excitation of these levels by considering the lowest multipolarity transitions possible, namely, M1, E1, and E2 transitions. In the following, we have calculated the transition-matrix elements in Eq. (2) using Dirac–Fock electron wave functions [9]. Electronic transitions appropriate to the multipolarities considered here are $n'\kappa' \longrightarrow n\kappa$ with $n = 1, 2$, $n' = 2$–5, and $|\kappa| \le 3$, with κ being the relativistic quantum number. Table 1 contains a summary of the energies, widths, and photoexcitation cross sections for the orbitals of hafnium with $n \le 3$ based on data in [10–12].

There have been no claims of triggering near the K edge [1], but only $1s$ vacancies can support NEET for the known nuclear levels discussed above, due to energy conservation. In Fig. 1, we show the NEET probabilities as a function of B for several transitions filling $1s$ holes. The results for $B = 1$ Weisskopf unit (W.u.) can be considered as effective upper limits for $L = 1$ transitions, which are likely to be significantly hindered. NEET transitions with $L > 1$ have significantly smaller probabilities than those with $L = 1$, even for intraband E2 transitions, for which B can attain values near 100 W.u.

For both E1 and M1 transitions, the total NEET probability for filling a $1s$ hole for $B = 1$ W.u. is of the order of 10^{-9} or less. The $3s \longrightarrow 1s$ transition probabil-

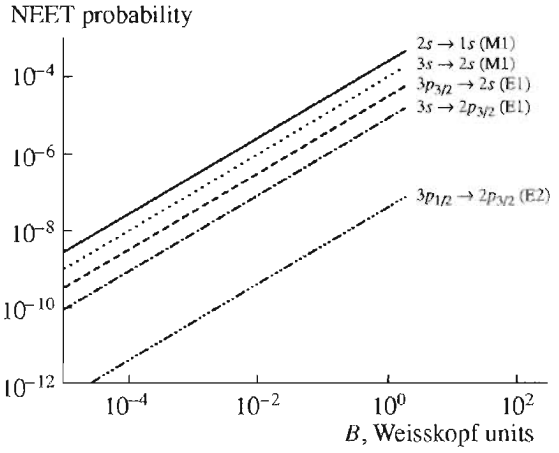

Fig. 2. Probabilities for NEET transitions filling K- and L-shell holes assuming perfect energy matching between the nuclear and electronic transitions.

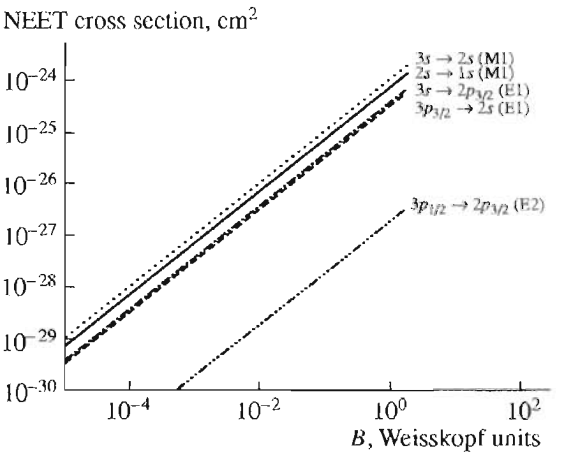

Fig. 3. Cross sections for NEET transitions filling K- and L-shell holes assuming perfect energy matching between the nuclear and electronic transitions.

ity, for the level lying 62 keV above the m2 isomer, is largest because energy matching is the closest in this case, with a detuning $\delta = \omega_e - \omega_N$ value less than 1 keV. The other transitions are far from resonance and have energy mismatches of the order of tens of keV. Excitation of the level lying 39 keV above the m2 isomer by an M4 NEET transition has a probability of less than 10^{-25} even for $B = 1$ W.u., due to the high multipole order and the large detuning. We emphasize that the NEET probability is zero for L-shell excitations of the known nuclear levels.

We now consider NEET transitions filling L-shell holes. Since there are no known nuclear levels lying within 16 keV above the m2 isomer, such NEET transitions require hypothesizing the existence of an unknown nuclear level. We can derive upper limits on the NEET probabilities by assuming that the hypothetical nuclear level exists with an energy that would give perfect resonance with the electronic transition ($\delta = 0$). NEET probabilities calculated on this basis are shown in Fig. 2. Using Eq. (4) gives the cross sections shown in Fig. 3. If we assume $B < 1$ W.u., then we obtain an upper limit on the NEET probabilities of $P_{\mathrm{NEET}} < 2 \times 10^{-4}$ for transitions filling L shells. The corresponding result for transitions filling the K shell is $P_{\mathrm{NEET}} < 2 \times 10^{-3}$, in agreement with previous results on the $Z = 70$ atom [13]. These correspond to excitation cross sections of the order of 10^{-23} cm^2, using Eq. (4) and values from Table 1. Such cross sections are relatively large, but it must be remembered that these are extreme upper limits, since the probability of a nuclear level lying within a few keV above the isomeric level is remote. Furthermore, as discussed below, these cross sections are purely for nuclear excitation and do not take into account the process of nuclear deexcitation to lower lying nuclear levels. We can compare these cross sections with the cross sections for direct nuclear photoexcitation. The integrated cross sections for nuclear photoexcitation for transitions at 10 keV with $B = 1$ W.u. are 4×10^{-23} cm^2 eV for E1 transitions, 1×10^{-31} cm^2 eV for E2 transitions, and 4×10^{-25} cm^2 eV for M1 transitions. The recent experiments by Collins used narrow-bandwidth radiation with a bandwidth of the order of 0.1–1 eV. Such bandwidths are much larger than the widths for nuclear photoexcitation but much smaller than the energy scale (≈keV) of the gross features in the above-threshold electronic photoexcitation cross section. Thus, to obtain estimates of integrated cross sections for nuclear photoexcitation by NEET, we can simply multiply the above-mentioned NEET cross sections by the beam width. For a 1-eV wide beam, the integrated cross section for NEET is 10^{-23} cm^2 eV for the E1 $3d_{3/2} \longrightarrow 2p_{3/2}$ transition, 10^{-24} cm^2 eV for the M1 $3s \longrightarrow 2s$ transition, and 10^{-27} cm^2 eV for the E2 $3p_{3/2} \longrightarrow 2p_{1/2}$ transition. Hence, for equal B values, the cross section for direct E1 photonuclear excitation is one order of magnitude larger than that for the E1 NEET transition at $\delta = 0$, while for the M1 and E2 transitions, the cross sections for direct photonuclear excitation are, respectively, one and four orders of magnitude smaller than those for the NEET transitions at $\delta = 0$.

A recent theoretical calculation on NEET excitation in $^{178}\mathrm{Hf}^{m2}$ by the filling of L-shell holes was reported by Tkalya [14], who also assumed perfect energy matching between the electronic and nuclear transitions. The NEET matrix elements and probabilities obtained here are in good agreement with those reported by Tkalya: the values agree within 20% except in the case of the $3s \longrightarrow 2p_{3/2}$ transition, where the squared matrix element in the present calculation is 1.6×10^{-4} eV^2, which is somewhat smaller than the value of 2.7×10^{-3} eV^2 reported in [14].

Table 2. Summary of branching ratios for the dominant nuclear excitation and deexcitation pathways

Excited level E	Final level F	$(\pi L)_{IE}$	$(\pi L)_{EF}$	R ($f = 100$)	R ($f = 66$)
15^-	13^-	E1	E2	6×10^{-15}	4×10^{-14}
14^+	13^-	E2	E1	4×10^{-5}	3×10^{-4}
15^+	13^-	M1	M2	9×10^{-16}	7×10^{-15}

In order to calculate the branching ratio for deexcitation of level E to a nuclear level other than the m2 isomer, some assumptions have to be made about the type of nuclear state E produced in the NEET process. The most favorable cases for an excitation from the $J\pi = 16^+$, $K = 16$ m2 isomer to any higher lying state would be E1, M1, or E2. We will consider the likelihood of various angular-momenta assignments for the hypothetical level based on these multipolarities. In the case of an E2 excitation due to NEET, it would be possible to reach a level having $J = 14$, 15, 16, 17, or 18. This level is required by the assumption of perfect matching with L-shell transitions to be about 11 keV or less above the isomer and, therefore, lies no higher than about 2457 keV. Note that triggered energy release has been claimed near both the L1 and L3 edges, namely, at 11.27 and 9.56 keV, respectively [2, 3]. Members of the $K = 0$ ground-state band attain angular momenta through collective rotation and reach only $J = 14$ by an excitation of 2777 keV. The highest angular momentum achieved by rotational band members built on other intrinsic states by 2457 keV arises in the $J\pi = 13^-$, $K = 8$ level in the m1-isomer band, and this is below the m2 isomer. It is clear that any hypothetical level with $J > 13$ postulated at or below 2457 keV would be vast, with its large angular momentum coming from a single-particle structure rather than collective rotation. It would, therefore, be an isomer as well, though none has been detected thus far.

Assuming the existence of a previously undiscovered level of high intrinsic angular momentum near 2457 keV that can be excited from the m2 isomer, the question remains as to how its decay could branch to other levels. Again, a comparison of the minimum angular momentum of the hypothetical state E, $J\pi = 14^+$, shows that only the $J\pi = 13^-$, $K = 8$ level is available for a reasonable decay path by modest multipolarity. Reaching this proposed level E would require an E2 transition, since the nuclear excitation and decay of E to the 13^- level would be E1. M1 or E2 transitions from m2 to E could produce $J\pi = 15^+$ or 15^-. Again, the paucity of lower lying levels of significant angular momentum suggests that an energy-releasing branch is only likely to the same 13^- state. Supposing angular momenta $J > 15$ for level E would only increase the difficulty involved in finding a suitable level to which it could decay in order to release the nuclear excitation. We reject the temptation to introduce yet another hypothetical state as a destination for such a decay branch. Thus, the most likely among improbable designations for the trigger level E would be $J\pi = 14^+$, 15^+, or 15^-. On this basis, characteristics for the deexcitation of E are shown in Table 2. Branching ratios have been estimated by the same procedure as in [14], using the relation $\lambda_{EF} = \lambda^W_{EF} H_{EF}$ with λ^W_{EF} as the Weisskopf B value, and the hindrance H_{EF} was derived from

$$H_{EF} = f^{(|K_E - K_F| - L_{EF})}, \quad (7)$$

where f is the reduced hindrance and L_{EF} is the multipolarity of the $E \longrightarrow F$ transition. In [14], a value of $f = 100$ was assumed, which yielded branching ratios of approximately 10^{-14} for M1 and E1 transitions and 10^{-5} for E2 transitions. For ^{178}Hf, the B value of the dominant decay branch by the 12.7-keV E3 transition of the m2 isomer is reproduced with a value of $f = 66$ [15]. This gives the values for R shown in Table 3. Using the above results together with Eq. (5), the results for the total deexcitation cross sections are shown in Table 3. The upper limit on the total deexcitation cross section for NEET transitions filling L-shell holes then becomes $\sigma_{I \to E \to F}(L) < 10^{-31}$ cm^2. This result is in agreement with the results of [14], where an upper limit of $\sigma_{I \to E \to F}(L) < 10^{-32}$ cm^2 was deduced.

4. CONCLUSIONS

NEET transitions filling the L shell of hafnium require the existence of an unknown nuclear level lying within 11 keV of the isomeric level. Upper limits on the NEET probability can be derived assuming a B value of 1 Weisskopf unit (W.u.) for the nuclear transition and perfect energy matching between the nuclear and electronic transitions. The extreme upper limit on the triggering cross section is $\sigma < 10^{-31}$ cm^2, supporting the recent results presented in [14]. This is significantly

Table 3. Summary of NEET probabilities and cross sections for the dominant transitions

Transition	πL	P_{NEET}	σ_{NEET} (cm^2)	R	$\sigma_{I \to E \to F}$ (cm^2)
$3s \longrightarrow 2s$	M1	1.1×10^{-4}	1×10^{-24}	10^{-14}	10^{-38}
$3p_{3/2} \longrightarrow 2s$	E1	2.8×10^{-5}	2×10^{-25}	10^{-14}	10^{-39}
$3s \longrightarrow 2p_{3/2}$	E1	8.0×10^{-6}	4×10^{-25}	10^{-14}	10^{-39}
$3p_{3/2} \longrightarrow 2p_{3/2}$	E2	4.0×10^{-8}	3×10^{-27}	10^{-4}	10^{-31}

Table 4. Subshell internal conversion coefficients, $\alpha_{n\kappa}$, for the 12.7 keV E3 decay of $^{178}Hf^{m2}$

Subshell $n\kappa$	$\alpha_{n\kappa}$
$2p_{1/2}$	4.0×10^6
$2p_{3/2}$	5.7×10^6
$3s$	9.7×10^3
$3p_{1/2}$	1.5×10^6
$3p_{3/2}$	1.9×10^6
$3d_{3/2}$	2.9×10^5
$3d_{5/2}$	4.6×10^5
$4s$	2.8×10^3
$4p_{1/2}$	3.8×10^5
$4p_{3/2}$	4.8×10^5
$4d_{3/2}$	7.0×10^4
$4d_{5/2}$	1.1×10^5
$5s$	5.0×10^2
$5p_{1/2}$	5.5×10^4
$5p_{3/2}$	6.6×10^5
$5d_{3/2}$	3.9×10^3
Total	1.5×10^7

less than the cross section deduced from the experimental data in [2, 3]. Hence, it would seem that the reported γ-ray enhancements are far too large to be explained by NEET.

In [2, 3], the electron bridge was also mentioned as a potential mechanism for photon-induced decay of the isomer. The electron bridge is a third-order or higher contribution to the γ-decay rate of the nucleus and occurs when an initially excited nuclear state decays by excitation of an electron to a virtual state that deexcites to a lower lying final electronic state. Experimental data on the electron bridge is scarce. In [16], the 80.7-keV M4 decay of $^{193}Ir^m$ was examined experimentally, and it was suggested that the electron bridge constitutes approximately 20% of the γ-decay rate. Since the internal conversion coefficient in this case is approximately 1.5×10^5, this would correspond to an electron-bridge contribution to the total rate on the order of 10^{-5}–10^{-6} of the total rate. The energy (12.7 keV) and multipolarity (E3) for $^{1782}Hf^m$ decay are not the same as those for $^{193}Ir^m$ decay. Hence, the electron-bridge contributions could be different also. However, both decays share the characteristic that the dominant internal conversion occurs in the L shell (see Table 4). Additionally, the radial operators of the matrix elements for internal conversion by E3 and M4 transitions are such that the region of space that gives the dominant contribution to the matrix elements is approximately the same in both cases. Hence, the electron-bridge contribution in ^{178}Hf might not be too far from that in ^{193}Ir. We are currently evaluating the electron-bridge contribution to $^{178}Hf^{m2}$ with an eye to determining the extent to which this contribution could be changed by the presence of electron holes due to photon irradiation with low-energy X rays. At the present time, the most plausible explanation of the results in [2, 3] would appear to be an anomaly in the subtraction of the background γ-decay spectrum from the spectrum collected during the synchrotron pulse.

ACKNOWLEDGMENTS

The authors acknowledge financial support from the US Air Force Office of Scientific Research (contract no. F49620-02-1-0187).

REFERENCES

1. J. J. Carroll, Laser Phys. Lett. **1**, 275 (2004).
2. C. B. Collins, N. C. Zoita, A. C. Rusu, *et al.*, Europhys. Lett. **57**, 677 (2002).
3. C. B. Collins, N. C. Zoita, F. Davanloo, *et al.*, Laser Phys. **14**, 154 (2004).
4. S. Kishimoto, Y. Yoda, M. Setoi, *et al.*, Phys. Rev. Lett. **85**, 1831 (2000).
5. E. V. Tkalya, Nucl. Phys. A **539**, 209 (1992).
6. M. R. Harston, Nucl. Phys. A **690**, 446 (2001).
7. A. Bohr and B. R. Mottelson, in *Nuclear Structure* (Benjamin, New York, 1969; Mir, Moscow, 1971), Vol. 1, p. 382.
8. Evaluated Nuclear Structure Data File, www.nndc.bnl.gov.
9. I. P. Grant, B. J. McKenzie, P. H. Norrington, *et al.*, Comput. Phys. Commun. **21**, 207 (1980).
10. R. B. Firestone, *Table of Isotopes*, 8th ed. (Wiley, New York, 1998).
11. E. Storm and H. I. Israel, Nucl. Data Tables **A7**, 565 (1970).
12. J. L. Campbell and T. Papp, At. Data Nucl. Data Tables **77**, 1 (2001).
13. M. R. Harston and J. J. Carroll, Laser Phys. **14**, 1452 (2004).
14. E. V. Tkalya, Phys. Rev. C **68**, 064611 (2003).
15. P. M. Walker and G. D. Dracoulis, Hyperfine Interact. **135**, 83 (2001).
16. V. A. Zheltonozhskii, P. N. Muzalev, A. F. Novogorodov, and M. A. Ukhin, Sov. Phys. JETP **67**, 16 (1988).
17. F. Rosel, H. M. Fries, K. Alder, and H. C. Pauli, At. Data Nucl. Data Tables **21**, 291 (1978).

Laser Physics, Vol. 14, No. 11, 2004, pp. 1452–1456.

Nuclear Excitation and De-excitation in Resonant Electronic Transitions

M. R. Harston and J. J. Carroll

Department of Physics and Astronomy, Youngstown State University, University Plaza 1, Youngstown, Ohio, USA

e-mail: mharston@cc.ysu.edu

Received March 31, 2004

Abstract—Two nuclear processes involving a nuclear transition that is resonant with an electronic transition are discussed. In one, known as BIC, the nucleus de-excites by excitation of an electron to a bound orbital, and thus this process constitutes a subthreshold contribution to the nuclear decay rate. In the second process, known as NEET, nuclear excitation occurs by de-excitation of an initially excited electronic state. The current status of experiment and theory for these two processes is reviewed. Theoretical results for NEET for different electronic transitions in several nuclei are presented in order to consider upper limits on the NEET probability.

1. INTRODUCTION

In this article, we discuss two processes (Fig. 1) that can populate or depopulate nuclear levels by coupling of the nucleus to the atomic electrons. The first process is a nuclear decay process known as bound (or subthreshold) internal conversion (BIC). In BIC decay, the de-excitation of the nucleus is accompanied by excitation of a bound electron to an excited bound orbital. The second process, the reverse of BIC, is a nuclear excitation process known as NEET (nuclear excitation by electronic transitions), where an initially excited electronic state de-excites by transfer of energy to the nucleus. NEET was first proposed theoretically by Morita [1] in 1973, but convincing evidence for the process was only seen in 2000 [2]. Evidence for BIC decay also appeared at the same time [3]. In Section 2, we summarize the theoretical basis common to both the NEET and BIC processes. In Sections 3 and 4, we review the current status of experiment and theory for BIC and NEET. Finally, in Section 5, we present theoretical results on NEET transitions in order to discuss upper limits on NEET probabilities.

2. THEORY COMMON FOR BIC AND NEET

Let us consider a pair of initial and final electronic states with energies $\varepsilon_{i,f}$ and a pair of initial and final nuclear states with energies $\omega_{i,f}$. The time-independent wave functions for these states satisfy the equations

$$H^e\varphi_{i,f} = \varepsilon_{i,f}\varphi_{i,f}, \quad (1)$$

and

$$H^N\chi_{i,f} = \omega_{i,f}\chi_{i,f}, \quad (2)$$

where H^e and H^N are the electronic and nuclear Hamiltonians, respectively. We will further suppose that the energy $E_i = \varepsilon_i + \omega_i$ lies close to the energy $E_f = \varepsilon_f + \omega_f$, so that two pairs of combined electron–nuclear levels are nearly degenerate. We can couple the pair of states i and f to give a total time-dependent wave function:

$$\Psi(t) = c_i(t)\varphi_i\chi_i + c_f(t)\varphi_f\chi_f. \quad (3)$$

Substituting this wave function into the time-dependent Schrödinger equation yields the following coupled equations for the time-dependent coefficients $c_{i,f}(t)$ in relativistic units:

$$i\frac{dc_i}{dt} = (E_i - i\Gamma_i/2)c_i + V_{if}c_f, \quad (4)$$

$$i\frac{dc_f}{dt} = V_{if}c_i + (E_f - i\Gamma_f/2)c_f, \quad (5)$$

where $\Gamma_{i,f}$ are the total widths

$$\Gamma_i = \Gamma_i^e + \Gamma_i^N \quad (6)$$

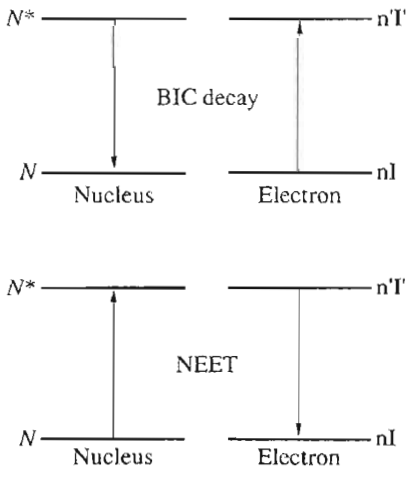

Fig. 1. The BIC and NEET processes.

and V_{if} is the coupling matrix element. The probability for a nuclear transition giving rise to the nuclear state f is given by

$$P_f = \Gamma_f \int |c_f|^2 dt. \quad (7)$$

Solving the coupled equations and integrating then yields the following result for the nuclear transition rate to the state f in the weak coupling limit:

$$\lambda_f = \frac{(\Gamma_i + \Gamma_f)|V_{if}|^2}{(E_i - E_f)^2 + (\Gamma_i + \Gamma_f)^2/4}. \quad (8)$$

In cases involving excitation or decay of isomeric states, the nuclear level widths are less than 10^{-6} eV, corresponding to half-lives longer than nanoseconds. The electronic level widths arise from the usual processes associated with filling of a hole state: radiative or Auger decay. If the hole is in the inner electronic shells, a typical value for the electronic width for a medium to high Z atom is of the order of one electronvolt or tens of electronvolts. Thus, for excitation or de-excitation of isomeric states from long-lived ground or isomeric states, the total level widths appearing in the above equation will be dominated by the electronic widths.

In the case of NEET excitation, it is convenient to define the nuclear excitation probability for an initially excited electronic state. This is just the nuclear transition rate divided by the total rate for de-excitation of the hole, so that $P_{\mathrm{NEET}} = \lambda_f/\Gamma_i$. Using Eq. (8) gives a result for P_{NEET} that is precisely the same as that obtained by an S-matrix method [4]. We can also see from Eq. (8) that, in order to maximize the nuclear transition rate, we should minimize the energy mismatch $\delta = E_i - E_f$. One technique that can be used to reduce the energy mismatch is to use the charge-state dependence of the electronic binding energies.

The coupling matrix element can be calculated by a standard multipole expansion of the electron–nucleus interaction and is essentially the same as that appearing in normal internal conversion decay except that the final-state continuum electron wave function is replaced by the appropriate bound electron wave function. The result is

$$|V_{if}|^2 = 4\pi\alpha\omega^{2L+2}\frac{(C^{j_i 1/2}_{j_f 1/2 L 0})^2}{L^2[(2L+1)!!]^2}|M_e(\pi L)|^2 B(\pi L), \quad (9)$$

where ω is the nuclear transition energy, $B(\pi L)$ is the nuclear electromagnetic transition moment, and $M_e(\pi L)$ is the electronic matrix element. For a magnetic multipole transition, the latter is given by

$$M_e(ML) = (\kappa_i + \kappa_f)\int [g_i f_f + g_f f_i] h_L(\omega r) dr, \quad (10)$$

where $g_{i,f}$ and $f_{i,f}$ are the large and small components of the Dirac radial wave functions for the initial or final electronic states having relativistic quantum numbers $\kappa_{i,f}$. In order for the matrix element V_{if} to be nonzero, it is clear that the nuclear and electronic transitions must have the same spin and parity changes.

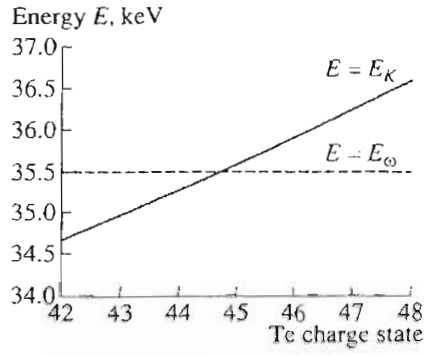

Fig. 2. The charge state dependence of the K-shell binding energy in highly charged ions of Te.

3. STATUS OF EXPERIMENT AND THEORY FOR BIC DECAY

BIC decay is an extra contribution to the decay rate that adds to the usual γ decay and above-threshold internal conversion decay contributions:

$$\lambda_t = \lambda_\gamma + \lambda_{\mathrm{IC}} + \lambda_{\mathrm{BIC}}. \quad (11)$$

One can define a subthreshold conversion coefficient in precisely the same way as the above-threshold conversion coefficient, by dividing the BIC rate by the rate for nuclear γ decay:

$$\alpha_{\mathrm{BIC}} = \frac{\lambda_{\mathrm{BIC}}}{\lambda_\gamma}. \quad (12)$$

Evidence for BIC decay has come from experiments on highly charged ions of ^{125}Te. This nucleus has a first excited state at 35.5 keV that decays by an M1 transition, which, in the neutral atom, is converted predominantly in the K shell. The K-shell conversion coefficient in the neutral atom is 12.0, whilst the total conversion coefficient is 13.9. The binding energy in the neutral atom is 31.8 keV. When the atom is ionized, the binding energy increases with charge state (Fig. 2) and a charge state is eventually reached when the binding energy becomes greater than the nuclear transition energy. This occurs at charge state $q = 45+$. Hence, K-shell conversion by the normal above-threshold process should be energetically forbidden in the ions with $q > 44$. Experiments at GANIL by the Bordeaux group [3, 5] have nevertheless indicated a significant contribution from K-shell decay in the ions 45+ and 46+. The most recent experiment [3] employed a detection system that enabled both K-shell X rays following IC decay and nuclear γ rays to be detected in coincidence with a sig-

Table 1. Summary of experiment and theory for recent results on bound internal conversion in highly charged ions of ^{125}Te. The quantity χ is the ratio of K-shell X rays to nuclear γ rays

Charge state	χ^{Exp}	χ^{Theory}
45+	12.5 ± 6.2	7.1
46+	2.86 ± 0.99	2.4

nal associated with a particular ion. The deduced ratios of K-shell X rays to nuclear γ rays are shown in Table 1. Since a nonzero ratio can only occur by conversion in the K shell, and since the above-threshold process should be energetically forbidden in these charge states, these results, particularly that for the 46+ ion, indicate a significant contribution from a subthreshold internal conversion (BIC) process.

This can be understood in the following way. If excitation of a K-shell electron occurs to a bound level, then we expect such an excitation to occur to a Rydberg level of s symmetry, since this will maximize the electronic matrix elements. Calculation of the electronic energy level spectrum with Dirac–Fock electron wave functions [6, 7] indicates that electronic transitions $1s \longrightarrow ns$ can lie within a few electronvolts of resonance for different values of n depending on the charge state. Thus, $n = 17$ lies close to resonance in Te^{45+}, $n = 8$ in Te^{46+}, and $n = 7$ in Te^{47+}. Furthermore, excitation of the $1s$ electron leaves a K-shell hole that can be filled by a $2p$ electron in a fast $2p \longrightarrow 1s$ transition, which has a typical width of the order of several electronvolts and is therefore of the same order of magnitude as the energy mismatches for the aforementioned electronic transitions. In the case of BIC, the total widths are thus dominated by the width of the electronic hole state resulting from the NEET transition.

In the experiment of [3], the first nuclear excited state is produced in collisions of Te ions with a thorium target. This produces initially excited electronic states that will decay rapidly to one of the five electronic states with the configuration $1s^2 2s^2 2p_{1/2}^{x} 2p^{y}$. However, the lifetimes of electronic states having $2p$ shell occupancies ($x < 2$) that differ from that in the ground state ($x = 2$) can be sufficiently long for such excited states to survive on a timescale that is comparable with the time (several nanoseconds) for the Te ions to enter the region seen by the photon detection system. Thus, one has to consider BIC decay in these excited states. The different $2p$ shell occupancy in these initial electronic states modulates the energy of the $1s \longrightarrow ns$ transition at the electronvolt level. This considerably enhances the possibility of very close energy matching between the electronic and nuclear transitions. In the 45+ ion, the closest energy matching occurs for the $1s \longrightarrow 17s$ transition from the $1s^2 2s^2 2p_{1/2}^{1} 2p_{3/2}^{2}$ $J = 3/2$ initial state, which has a δ value of approximately 1 eV. Interestingly, this yields a BIC coefficient that is approximately equal to the IC coefficient in the neutral atom. Furthermore, in the 45+ ion, the separation between Rydberg s states around $n = 17$ is approximately 10 eV. This means that electronic transitions that are several electronvolts off-resonance in $n = 17$ can be closer to resonance in $n = 18$ and $n = 16$ states, so that several n states contribute to the BIC decay rate of this ion. Summing over the final states for each initial electronic state and averaging over the initial electronic states yields theoretical results for the ratios of K-shell X rays to γ rays shown in Table 1. These are in reasonable agreement with the experimental results given above.

It is noteworthy that, in the 48+ ion (configuration $1s^2 2s^2$), the absence of $2p$ electrons has the result that the width for filling of a $1s$ hole is much smaller than in ions with $q < 48$ (where the widths are dominated by the fast $2p \longrightarrow 1s$ radiative transition). This means that the theoretical BIC rates go practically to zero, in agreement with the experimental result of no K-shell X rays in this ion.

4. STATUS OF EXPERIMENT AND THEORY FOR NEET

There have been many experimental attempts to observe NEET transitions in several nuclei (see [8] and references therein), including ^{189}Os (69.537 keV level, M1 transition), ^{197}Au (77.351 keV, M1 transition), and ^{237}Np (102.96 keV, E1 transition). These three nuclei have a low-lying nuclear excited state with an excitation energy close to that of an electronic transition filling a K-shell hole. In the experiments, the K-shell hole was produced either by photoexcitation (by narrow and broadband sources) or by electron bombardment. Early experiments appear to have given false positive results for a variety of reasons, including spurious backgrounds from photoexcitation or inelastic electron scattering. In only one case has there been a clear unambiguous signal of NEET: in the experiment of Kishimoto *et al.* [2] using a very narrowband source at Spring-8 with a bandwidth of 19 eV. In this case, the photon energy could be tuned to lie just above the K-shell ionization threshold and production of the first excited state of ^{197}Au was detected by measurement of delayed radiation associated with the internal conversion decay of this state. Subtraction of a below-threshold background spectrum allowed a decay curve to be obtained with a half-life equal to the known half-life of this state. The NEET transition responsible for the signal is expected to be the $3s \longrightarrow 1s$ transition for which $\delta = -51$ eV. The experiment yielded a result for the NEET probability of $(5.0 \pm 0.6) \times 10^{-8}$ that was significantly smaller than the previous theoretical results ($P_{NEET} = 1.3 \times 10^{-7}$). In fact, the latter contained a spurious factor of $(2L + 1)$ in the matrix elements, which led to an overestimate by a factor of 3. When this is corrected and the matrix elements are calculated with Dirac–Fock elec-

tron wave functions, the theoretical result becomes 3.6×10^{-8} [8], in very good agreement with experiment. Thus, the theoretical description of NEET embodied in Eq. (8) now gives an adequate description of the nuclear excitation rate by NEET.

Two recent and very careful experiments have been carried out on excitation of the first excited state of ^{189}Os, where there is a possible NEET transition involving filling of a K-shell hole, again by a $3s$ electron. One experiment by Ahmad *et al.* [9] gave the limit $P_{NEET} < 9 \times 10^{-10}$. Another by Aoki *et al.* [10] gave the limit $P_{NEET} < 4.1 \times 10^{-10}$. Both these are consistent with the theoretical result of $P_{NEET} = 1.1 \times 10^{-10}$ [7]. The small NEET probability in ^{189}Os compared to ^{197}Au is due to the much larger energy mismatch in the ^{189}Os case ($\delta = 1.28$ keV against $\delta = -0.051$ keV in the case of ^{197}Au). These experimental and theoretical results are summarized in Table 2.

Several experiments have investigated nuclear excitation in a laser-produced plasma of ^{235}U ions (see [11] and references therein). In this case, the transition to the very low-lying first excited state at 76.8 eV lies close to the energy of a $6p \longrightarrow 5d$ ($q \sim 10+$) or $6d \longrightarrow 6p$ ($q \sim 23+$) electronic transition. The population of a particular charge state can in principle be optimized by choosing appropriate laser conditions. The experiments are based on detection of the very low energy (~1 eV) IC electrons from the 27-min decay of the excited nuclear state. Problems associated with the detection of such low-energy electrons, particularly in the presence of significant backgrounds from exoelectrons (electrons associated with the relaxation of defects created by ions in the laser plasma) and α decay, are probably responsible for an early likely erroneous claim of a positive nuclear excitation signal from a plasma of ^{235}U heated to a temperature of approximately 100 eV by a CO_2 laser at an intensity of 10^{10} W/cm^2 [12]. More recent attempts to repeat this experiment using Nd:YAG lasers at laser intensities of 10^{11} W/cm^2 or greater have given null results [13, 14].

Table 2. Summary of experiment and theory for recent results on NEET probabilities

Nuclide	Experiment	Theory
^{189}Os	$<4 \times 10^{-10}$	1.1×10^{-10}
^{197}Au	$(5.0 \pm 0.5) \times 10^{-8}$	3.6×10^{-8}

5. UPPER LIMITS ON NEET PROBABILITIES

It is of interest to address the following question: How large can NEET probabilities be in other systems? It is clear that, since P_{NEET} is proportional to the nuclear electromagnetic moment, $B(\pi L)$, one expects NEET probabilities to be largest for transitions of low multipole order. We will thus focus on M1 transitions and consider NEET probabilities for different electronic transitions in several different nuclei.

Figures 3–5 show the NEET probability as a function of the energy mismatch for $Z = 54$, 70, and 80 nuclei for a hypothetical transition with $B(M1) = 1$ Weisskopf unit (W.u.). It is clear that, for each Z, the $2s \longrightarrow 1s$ transition gives the largest value of P_{NEET} due to the electron wave functions being largest in the near-field region. At very small values of the energy mismatch, the NEET probability can attain values of 10^{-4} in the $Z = 70$ atom. It is to be stressed that such a value for P_{NEET} could only be reached for M1 transitions with $B(M1) \approx 1$ W.u. In practice, many M1 transitions are significantly hindered, which would lead to correspondingly smaller values for P_{NEET}. Thus, for example, the $B(M1)$ factors for the above-mentioned transitions in ^{197}Au and ^{189}Os are 4.1×10^{-3} W.u. and 2.5×10^{-3} W.u., respectively. In addition, if the transition multipolarity were to be larger than 1, the NEET probability would also decrease significantly. Any K hindrance of the transition would also further reduce the B

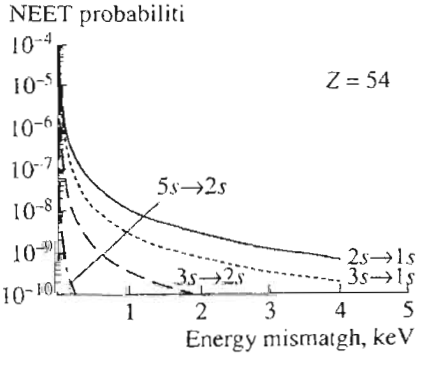

Fig. 3. NEET probabilities for M1 NEET transitions in the $Z = 54$ nucleus for $B = 1$ W.u.

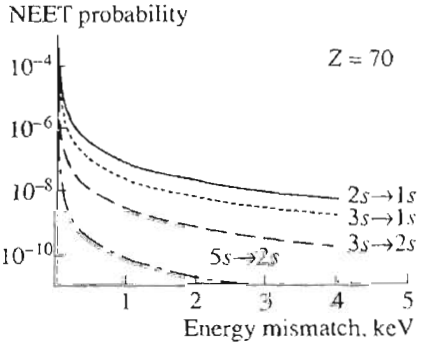

Fig. 4. NEET probabilities for M1 NEET transitions in the $Z = 70$ nucleus for $B = 1$ W.u.

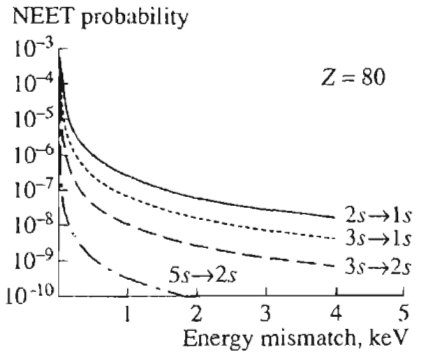

Fig. 5. NEET probabilities for M1 NEET transitions in the $Z = 80$ nucleus for $B = 1$ W.u.

value. Hence, the NEET probabilities in the figures are likely to be upper estimates of achievable probabilities [15].

It has been noted above, in the context of BIC decay, that very close energy matching between the nuclear and electronic transitions can be achieved by using the charge-state dependence of the electronic binding energies. This has not been used successfully so far in the case of NEET. However, laser plasmas and EBIT devices may be able to create sufficient populations of appropriate ions to enable new systems to be investigated.

ACKNOWLEDGMENTS

This research was supported by the US Air Force Office of Scientific Research under AFOSR contract no. F49620-02-1-0187.

REFERENCES

1. M. Morita, Prog. Theor. Phys. **49**, 1574 (1973).
2. S. Kishimoto, Y. Yoda, M. Seto, *et al.*, Phys. Rev. Lett. **85**, 1831 (2000).
3. T. Carreyre, M. R. Harston, M. Aiche, *et al.*, Phys. Rev. C **62**, 23411 (2000).
4. E. V. Tkalya, Nucl. Phys. A **539**, 209 (1992).
5. F. Attallah, M. Aiche, J.-F. Chemin, *et al.*, Phys. Rev. C **55**, 1665 (1997).
6. M. R. Harston, T. Carreyre, J.-F. Chemin, *et al.*, Nucl. Phys. A **676**, 143 (2000).
7. F. Karpeshin, M. R. Harston, F. Attallah, *et al.*, Phys. Rev. C **53**, 1640 (1996).
8. M. R. Harston, Nucl. Phys. A **690**, 447 (2001).
9. I. Ahmad, J. C. Banar, J. A. Becker, *et al.*, Phys. Rev. Lett. **87**, 072503 (2001).
10. K. Aoki, K. Hosono, K. Tanimoto, *et al.*, Phys. Rev. C **64**, 044609 (2001).
11. M. R. Harston and J.-F. Chemin, Phys. Rev. C **59**, 2462 (1999).
12. Y. Izawa and C. Yamanaka, Phys. Lett. B **88**, 59 (1979).
13. G. Claverie, J.-F. Chemin, M. M. Aleonard, F. Gobet, *et al.*, Phys. Rev. C (in press), private communication.
14. V. Meot, private communication.
15. Note added in proof: a recent calculation of the probability of NEET in the m2 isomer of ^{178}Hf assuming perfect energy-matching found $P_{NEET} \leq 2 \times 10^{-4}$ for filling of L-shell holes by E1 and M1 transitions. (E. Tkalya, Phys. Rev. C **68**, 064611 (2003)). Those results are approximately one order of magnitude smaller than the current results for K-shell filling in the $Z = 70$ atom, consistent with the lower value of the L-shell wave-function in the near-field region compared to that for the K-shell.

Available online at www.sciencedirect.com
SCIENCE DIRECT®
ELSEVIER Nuclear Instruments and Methods in Physics Research A 530 (2004) 463–472
NUCLEAR INSTRUMENTS & METHODS IN PHYSICS RESEARCH Section A
www.elsevier.com/locate/nima

Production of the ^{178m2}Hf isomer using a 4.5-GeV electron accelerator

S.A. Karamian[a,*], J.J. Carroll[b], J. Adam[a,c], N.A. Demekhina[d]

[a] *Joint Institute for Nuclear Research, Dubna, Moscow region 141980, Russia*
[b] *Youngstown State University, Youngstown, OH 44555, USA*
[c] *Nuclear Physics Institute, Rez, CZ-25068, Prague, Czech Republic*
[d] *Institute of Physics, Yerevan 375036, Armenia*

Received 22 March 2004; accepted 21 April 2004

Available online 15 June 2004

Abstract

High-productivity methods are required for the accumulation of long-lived isomers in amounts that are sufficient for the creation of experimental targets. A tantalum sample was activated with the Yerevan synchrotron using 4.5-GeV bremsstrahlung and the presence of ^{178m2}Hf was detected with good statistical accuracy by γ-activity measurements. The integrated and mean cross-section values were deduced from the experiment. The isomer-to-ground-state ratio was then estimated and compared with that known for the $p+$ Ta reaction studied at 660 MeV. In the present experiment, both converter and target were relatively thin for better definition of the experimental conditions. However, an assembly designed for high-productivity irradiations should be thick and then the converter can also serve as the target sample when irradiated with a high-energy electron beam. The optimization of the isomer production was solved analytically and the largest estimated yield was determined as calibrated to the experimental yield. The maximum yield of ^{178m2}Hf was found to be of about 3×10^9 nuclei/s using an electron beam current of 100 μA. This is lower than the yield achieved with proton beams, although for a practical comparison the total cost and radiation safety conditions should be considered. The present results provide a basis for numerical estimations.

PACS: 23.20.Lv; 25.20.Lj; 25.30.Rw

Keywords: Electron beam; Bremsstrahlung; 4.5 GeV; Ta target; Activation; Isomer; Cross-section; Yield; Productivity optimization

1. Introduction

Studies of high-spin nuclear isomers can provide important information regarding both nuclear structure [1,2] and innovative applications [3]. A triggered release of the energy stored in nuclear isomers may permit the creation of pulsed sources of gamma radiation, perhaps even a gamma-ray laser. The specific energy stored by some isomers for long periods of time is much greater than that of standard sources of energy. For instance, the high-spin $K^{\pi} = 16^+$ isomeric state ^{178m2}Hf stores a

*Corresponding author. Tel.: +7-096-216-4668; fax: +7-096-216-5083.
E-mail address: karamian@nrmail.jinr.ru (S.A. Karamian).

0168-9002/$ - see front matter © 2004 Elsevier B.V. All rights reserved.
doi:10.1016/j.nima.2004.04.224

specific energy of about 1.3 MJ/mg with a half-life of 31 years. To study mechanisms by which a release of this energy might be triggered, a critical requirement is that samples of isomeric atoms must be available in mg or even larger amounts. It is established that the largest quantity of ^{178m2}Hf was produced at Los Alamos with 800 MeV protons from a high-current accelerator (formerly LAMPF). The advantage of this method was the ability to accumulate the isomer as a by-product within a massive tantalum beam dump during the operation of the accelerator for other experiments [4]. However, the isomeric material produced in this way contains a very high activity of other radionuclides and the corresponding gamma background remains high even after chemical isolation of the hafnium fraction. The 1.87-year-lived isotope ^{172}Hf is the most problematic contaminant. The productivity of ^{178m2}Hf in spallation reactions with protons at intermediate energies was systematically studied for Ta, W and Re targets at Dubna using the 660 MeV synchrocyclotron [5–7]. From those works, some recommendations were deduced as to methods by which to optimize spallation production of the isomer. However, no scheme was proposed by which to overcome the basic disadvantage presented by the accompanying production of high contaminant activities.

Better quality sources of ^{178m2}Hf were successfully produced by the ^{176}Yb(^{4}He,2n) reaction using a 36 MeV ^{4}He-ion beam and subsequent chemical processing of the irradiated Yb target [8]. Mass separation was finally performed on the remaining material. The problem of isomer separation from the stable ^{178}Hf ground state has not yet been solved. The production of the long-lived isomer by the (^{4}He,2n) reaction is disadvantaged by a much lower absolute yield as compared to the spallation reaction. It is known [9] that the production reaction ^{179}Hf(n, 2n)^{178m2}Hf has a reasonably good cross-section for 14-MeV incident neutrons. The absolute yield is, however, restricted by practical limitations of neutron generators exploiting the d + T reaction.

Recently, an attempt was made to observe the production of ^{178m2}Hf in reactor irradiations of a ^{nat}Hf target. It was assumed that some reasonable yield could be obtained due to the ^{178}Hf(n,n′) reaction with the neutrons in the fission spectrum. So far, only an upper limit for the cross-section has been deduced because of the high remaining activity from other products—more sensitive measurements are expected after a longer cooling time. Nevertheless, the production of ^{179m2}Hf by (n,n′) reactions was observed [10].

Here the possibility of producing the ^{178m2}Hf isomer was investigated using 4.5-GeV bremsstrahlung from an electron synchrotron. The productivity with photons cannot be expected to be higher than in the previous reactions due to the generally lower cross-section characteristic of photonuclear interactions as compared to hadronic interactions. Still experimental results on photon production of this important isomer have not been reported and the present measurements should be valuable in assessing the feasibility of different production approaches. Above 1.5 GeV, the photon interaction is characterized by a cross-section of about 0.12 mb/nucleon. Below this energy, meson-generating resonances are known in the 200–800 MeV range and giant multipole resonances for photoabsorption appear for $E_\gamma \leqslant 100$ MeV. The quasi-deuteron mechanism of photoabsorption also makes a significant contribution at $E_\gamma \leqslant 400$ MeV. Overall, the cross-section of photon interactions with the nucleus systematically decreases with increasing E_γ. The bremsstrahlung spectrum produced by high-energy electrons falls as E_γ^{-1}, so the major contribution to the nuclear reaction yield is created by photons with $E_\gamma \leqslant 1000$ MeV. The energy transferred to a heavy nucleus by photon reactions in this range should be comparable to that released in the proton interactions at 800 MeV [4] and at 660 MeV [5–7]. As a result, the production of a variety of radionuclides can be expected as occurs with proton-induced spallation. Among the radioactive products, high-spin isomers must be represented and the experimental observation of the long-lived ^{178m2}Hf isomer was indeed possible. The present work provides an important test of the isomer-to-ground-state ratio for high-spin isomers formed in high-energy electromagnetic interactions with complex nuclei and an estimation of the efficiency for accumulation of significant amounts of ^{178m2}Hf using an electron accelerator.

2. Measurements

Fig. 1 shows a schematic of the experimental arrangement at the Yerevan 4.5-GeV electron synchrotron. The electron beam was extracted from the storage ring and struck a tungsten converter having a 0.3-mm thickness. Transmitted beam electrons and electron–positron pairs generated at the converter were deflected by a magnetic field while the bremsstrahlung photons continued forward within a very narrow cone. Collimators installed far from the converter shielded a target from background scattered radiation. The target was made of twenty 0.1-mm thick layers of natural tantalum. The initial electron energy of 4.5 GeV was reduced by about 8% in the converter and the bremsstrahlung flux was attenuated to a mean value by a factor of about 0.85 due to the absorption within the 2-mm Ta target. These factors were taken into account in the data processing, but were not very pronounced. So the approximation of thin converter and thin target could be made to simplify the analysis. The tantalum target was irradiated in 1986 for other purposes and fortunately it was saved up to now, providing the best possible condition for the detection of the 31-year-lived ^{178m2}Hf isomer. Many other radionuclides were produced during the irradiation with higher yields than ^{178m2}Hf, but they have almost decayed completely and did not interfere with the detection of a relatively low activity of ^{178m2}Hf.

The tantalum target activity was measured using a HPGe spectrometer of 20% efficiency (relatively

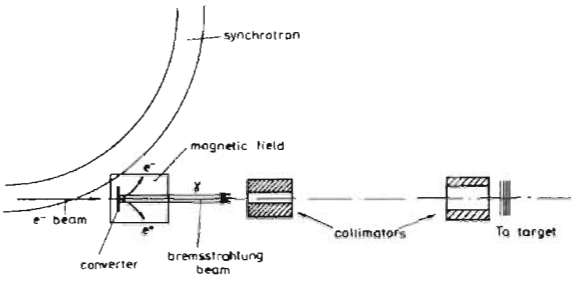

Fig. 1. Schematic showing the experimental arrangement used for the irradiation of the Ta target with 4.5-GeV bremsstrahlung at the Yerevan synchrotron.

to the standard NaI scintillator), combined with compatible electronics to provide an energy resolution of about 1.8 keV for the ^{60}Co γ lines. The tantalum foils were distributed to form a two-foil folded layer of 0.2-mm thickness in order to reduce self-absorption of the emitted gamma rays. Even with this arrangement, self-absorption was still not negligible, especially for $E_\gamma \leqslant 250$ keV, and a correction factor was used to take into account the emission efficiency from a sample of finite thickness, t:

$$\varepsilon = (\mu t)^{-1}(1 - e^{-\mu t}) \quad (1)$$

where $\mu(E_\gamma)$ is the linear attenuation coefficient for gammas in tantalum.

Another correction factor to the detector efficiency should account for the finite size (area) of the active source. An efficiency calibration of the Ge detector was done using the normal procedure with standard radioisotope sources of known activity. Such sources are typically small and so can be approximated as point sources. In contrast, the tantalum sample covered an area of about $45 \times 45\,\mathrm{mm}^2$ and was installed close to the detector since the low activity from the 31-year isomer required the maximum detection efficiency. The approximation of a point source was not applicable in this case and the solid angle was calculated in order to correct the efficiency. The following equation was used to approximate the mean detection solid angle when activity is uniformly distributed within a circle of radius R_s:

$$\bar{\Omega} = 2\pi\left(\frac{L}{R_s}\right)^2\left(1 - \frac{L}{\sqrt{L^2 + R_d^2}}\right) \times \ln\left[1 + \left(\frac{R_s}{L}\right)^2\right] \text{(sr)}. \quad (2)$$

Here L is the distance between the centers of the source and detector. It was assumed that the sensitive volume of the detector was restricted to the circular entrance window of radius R_d and the planes of the source and detector circles were parallel.

A third correction was needed since the efficiency could be influenced by simultaneous detection of two or more γ quanta emitted promptly

from a single decay event. In the natural decay cascade of ^{178m2}Hf, 4 to 5 quanta are emitted and using a close geometry they can generate a sum-signal response in the detector that reduces the intensity of photoabsorption peaks in the γ-ray spectrum. This is not a random pile-up effect that is dependent on the count rate. Sum signals arise even with weak activity sources whenever the cascade multiplicity $M_\gamma > 1$ and the solid angle of detection provides sufficient efficiency. Additional measurements were arranged to test the magnitude of this effect for this experiment. The detector efficiency was calibrated at close and far distances using specific point sources that were selected to emit single γ quanta. Then, a sample (from other work) that contained a modest activity of ^{178m2}Hf was measured at the same locations. The effect of sum signals was significant only when the ^{178m2}Hf source was present in close geometry while this effect did not appear in γ spectra taken at larger distances or with single-gamma sources. Finally, the deviation of the detector efficiency from the standard values was determined individually for the most important γ lines in the decay of ^{178m2}Hf. These results were used to measure the number of ^{178m2}Hf nuclei within the activated tantalum target based on the detected γ-ray intensity.

With the above-described conditions, a γ-ray spectrum of the Ta sample which was exposed to 4.5-GeV bremsstrahlung was accumulated during two weeks in order to collect sufficient statistics in the important lines. Fragments of the spectrum are given in Fig. 2 and well-manifested lines of ^{178m2}Hf are seen therein. The spectrum was analyzed using the "DEIMOS" code [11] and accurate numerical values were obtained for the line energy and area, as shown in Fig. 2. The number of counts at the peak channel are also indicated in Fig. 2 to characterize the collected statistics.

The statistical errors of the line areas were typically about 10%, but using the results for six intense γ lines it was possible to obtain much better accuracy for the number of ^{178m2}Hf nuclei in the sample. Fortunately, no deviations were found in the relative intensity of the γ lines as compared to the tabular values for ^{178m2}Hf. Also, the γ-line widths were in agreement with those expected for the detector as a function of E_γ. These meant that no overlap occurred between the lines of interest and those from background contributions. Natural background γ lines were definitely present in the spectrum, but did not disturb the detection of ^{178m2}Hf. In addition, lines of ^{172}Hf, ^{150}Eu and ^{133}Ba were found in the spectrum, being long-lived enough to have survived while other radionuclides decayed completely after such a long cooling time. The area of corresponding γ line allowed a determination of the production yield for each

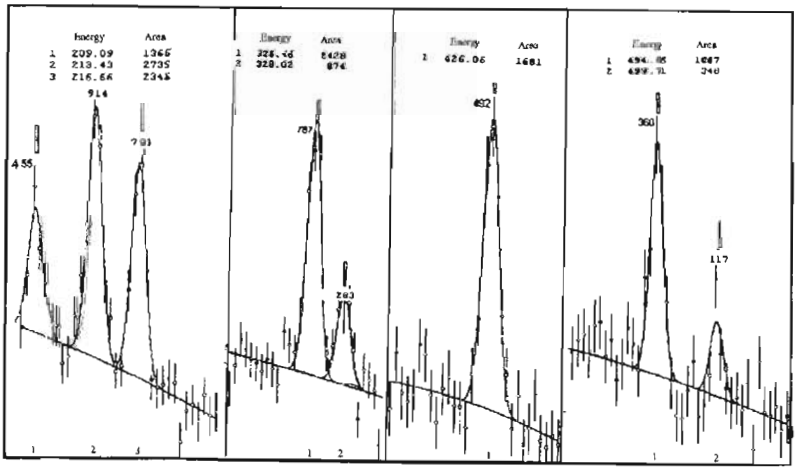

Fig. 2. Fragments of the γ spectrum obtained from the activated Ta sample. For each fragment, the observed lines are identified and their energies and areas are given as evaluated using the spectra-processing code. Six lines have energies that are in close agreement with the tabular values for ^{178m2}Hf: 213.4, 216.7, 325.6, 426.4, 495.0 and 574.2 keV (not shown).

Table 1
Measured production parameters for long-lived radioactive nuclides formed after activation of a Ta target with 4.5-GeV bremsstrahlung.

Nuclide	Type of yield	N_{at}	ICS (MeV barn)	$\bar{\sigma}$ (cm^2)
^{178m2}Hf	Indep.	$(1.57\pm0.08)\times10^{8}$	0.0255	2.55×10^{-29}
^{172}Hf	EC cum.	$(2.3\pm0.2)\times10^{10}$	3.74	3.74×10^{-27}
^{150}Eu	Indep.	$(8\pm2)\times10^{7}$	0.013	1.3×10^{-29}
^{133}Ba	EC cum.	$(8.7\pm0.9)\times10^{8}$	0.141	1.41×10^{-28}

given isotope after taking into account the decay factors, detector efficiency and quantum yield of the line. The latter parameters were taken from the tabular data [12]. The three above-described correction factors for the detector efficiency were utilized and it was found that the numbers of ^{178m2}Hf nuclei determined from different γ lines were practically identical. The six independent measurements were averaged and the standard deviation from the mean value was found to be 5%, being in agreement with the statistical errors deduced from the areas of the γ lines. In Table 1, the numbers of atoms produced by the bremsstrahlung irradiation of the Ta target are given for ^{178m2}Hf, ^{172}Hf, ^{150}Eu and ^{133}Ba.

3. Cross-sections

Having determined the number of product atoms, it was possible to evaluate the production cross-section based on a known number of projectiles reaching the target. The latter quantity was determined from the so-called "quantometer" unit, an optimized ionization chamber, that was installed in the bremsstrahlung beam for integration of the number of "equivalent" photons, N_{ph}. This number is defined by

$$N_{ph} = E_{max}^{-1}\int_0^{E_{max}} E_\gamma \frac{dN}{dE_\gamma}(E_\gamma)\,dE_\gamma \qquad (3)$$

for a continuous spectrum of photons with a spectral intensity dN/dE_γ and endpoint E_{max}.

The spectrum of bremsstrahlung photons emitted by electrons in matter was understood more than fifty years ago [13] and the Boethe–Heitler equation, corresponding to the ultra-relativistic case with an account of atomic screening, was used in this work. The use of this approximation is completely justified in the present experiment and gives the spectral density of photons per unit electron incident on a converter

$$\frac{d\sigma}{dE_\gamma} = \frac{4Z^2e^4}{137(mc^2)^2E_\gamma}\left\{\left[1+\left(\frac{E_e-E_\gamma}{E_e}\right)^2 - \frac{2(E_e-E_\gamma)}{3E_e}\right]\ln\left(183\times Z^{-1/3}\right) + \frac{(E_e-E_\gamma)}{9E_e}\right\}. \qquad (4)$$

In the present experiment, all photons generated by the converter reached the target and quantometer due to the narrow angular width of the high-energy bremsstrahlung, having a half-angle of $\theta_0 = mc^2/E_e \approx 0.1$ mrad. For a thick converter, the electron energy will vary considerably, so Eq. (4) must generally be integrated over E_e as it varies from the initial incident electron energy E_0 to some E_{min}. In the case of this experiment, the converter was thin and so it was possible to evaluate Eq. (4) without integration by using the mean value of electron energy, $\langle E_e\rangle < E_0$. Here the mean energy of electrons within the 0.3-mm tungsten converter was determined by considering radiative losses. The spectrum of the bremsstrahlung radiation was thereby determined quantitatively for the real experimental conditions and is shown in Fig. 3. The measured number of equivalent photons supplies an absolute calibration of the spectrum. The electron beam current can also be calculated using Eqs. (3) and (4).

As is mentioned above, the cross-section of photonuclear interactions demonstrates a generally decreasing trend with E_γ. It is quite large at $E_\gamma < 100$ MeV due to nuclear photoabsorption and

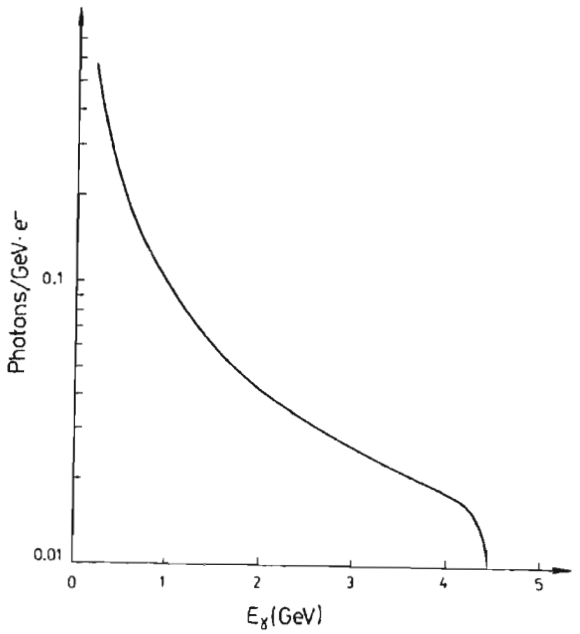

Fig. 3. Calculated and normalized spectral yield of the bremsstrahlung radiation emitted from the 0.3-mm W converter struck by the 4.5-GeV electron beam.

the quasi-deuteron mechanism. Then in the range of 200–800 MeV it is enhanced again because of resonant meson generation in interactions with individual nucleons. Above 1500 MeV the cross-section reaches an asymptotic value that is almost independent of energy, about 0.12 mb/nucleon. In combination with the photon spectrum shown in Fig. 3, which decreases in intensity rapidly approaching higher energies, this resulted in a drastically decreased yield, $Y_{nr}(E_\gamma)$, of photonuclear reactions as a function of E_γ. The yield detected from such a reaction must occur mainly in that part of the spectrum at $E_\gamma \leqslant 1000$ MeV, including the production of the ^{178m2}Hf isomer. Considering the lower-energy contributions, clearly ^{178m2}Hf was formed in the ^{181}Ta(γ, $p2n$) reaction at an excitation energy above 40–50 MeV. Thus, it was assumed here that the measured ^{178m2}Hf yield was primarily due to photons in the range of $50\,\text{MeV} \leqslant E_\gamma \leqslant 1050$ MeV range. The estimated inaccuracy due to this assumption, about 10%, is comparable with the statistical error of these measurements.

Thus, all necessary quantities were available from which to evaluate the integral cross-section, or ICS: the number of produced nuclei, the number of photons within the appropriate energy range and the thickness of the tantalum target. The attenuation of the bremsstrahlung flux within 2-mm target was also taken into account. The values obtained for the ICS and the mean cross-section, $\bar{\sigma}$, are given in Table 1. The mean cross-section corresponds to a 1000-MeV range of photon energy so that $\bar{\sigma} = \text{ICS}/(1000\,\text{MeV})$. The products ^{172}Hf, ^{150}Eu and ^{133}Ba are also characterized in Table 1. The errors in ICS and $\bar{\sigma}$ values were defined by the statistical errors in the measurements of N_{at} given in Table 1 and systematic errors may have arisen from subsequent numerical calculations based on N_{at}. These systematic errors were likely to be insignificant in comparison with the statistical errors. The ^{172}Hf and ^{133}Ba nuclides accumulated the total yield of the appropriate isobaric chains, while ^{178m2}Hf and ^{150}Eu were only produced independently in the reactions. As expected, the mean cross-section for ^{178m2}Hf is lower than that known for the $p+$Ta reaction at 660 MeV [5,6]. Roughly speaking, the order-of-magnitude scale difference between these processes can be explained by the nature of the electromagnetic interaction as compared to nucleon-induced reactions.

For a physical understanding of the nuclear reaction mechanism, the isomer-to-ground state ratio, σ_m/σ_g, is even more important, because it is sensitive to the angular momentum transferred to the reaction residue. Comparisons between the σ_m/σ_g obtained from different reactions also exclude scale differences between cross-sections. Unfortunately, the yield of stable ^{178}Hf ground-state nuclei could not be measured with activation techniques. The yield of ^{172}Hf, however, was detected successfully and by assuming a similar ^{178}Hf/^{172}Hf ratio as found in the $p+$Ta reaction [5,6] it was possible to deduce σ_g and therefore σ_m/σ_g values for the bremsstrahlung-induced reaction. The latter assumption is reasonable, but there is no guaranty of its quantitative accuracy. Therefore, only an estimate of the σ_m/σ_g value for ^{178m2}Hf in the $\gamma+$Ta reaction was possible. The inaccuracy in this value may approach 30–50%. The ratio

deduced in this way was

$$\frac{\sigma_m}{\sigma_g} \approx 0.032 \quad (5)$$

a little higher than the results of Refs. [5,6] for ^{178m2}Hf formation by the $p+$Ta interaction. This is not very surprising, recalling that the σ_m/σ_g ratio therefrom changes rather slowly with the proton energy [5,6], as confirmed later in Ref. [14]. On the other hand, the similarity of isomer population in $\gamma+$Ta and $p+$Ta interactions may mean that in meson generation by photons, a significant excitation energy and momentum are transferred to the nucleus. The subsequent stages of the reaction include the emission of nucleons, the same as in the case of a nucleon interaction with a heavy target. In the end, the residual nucleus has acquired a reasonably high angular momentum. Such a conclusion is essentially reliable and is now experimentally supported.

4. Optimization of productivity

In the present experiment, the converter and target were separated and the thickness of each was relatively small. But in a view of achieving the highest possible productivity, both thicknesses should be enlarged. In this way more quanta can be created by the converter, although obviously absorption will also be increased. A reasonable compromise would be to unify both converter and target which would then need to be a rather thick sample of Ta. The problem of optimization of such a unified assembly was solved analytically and is described below. Fig. 4 illustrates schematically the exposure of this sample configuration with an electron beam. The electron energy is reduced with thickness t due to the radiation stopping power, while ionization energy loss can be neglected in the GeV range. The upstream part of the sample serves mostly for bremsstrahlung generation and then those photons are absorbed in the downstream part mostly due to pair production—a small fraction of the photons are absorbed due to nuclear reactions. The tracks of photons from creation to absorption are also depicted in Fig. 4. Some small fraction of them can be transmitted

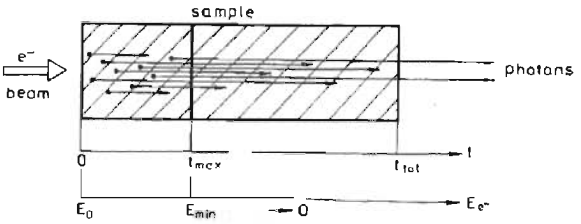

Fig. 4. Illustration of the generation and absorption of photons in a thick sample that unifies the functions of converter and target.

and leave the sample. The effective photon flux is dependent on the converter/sample thickness due to the competition between production and absorption and so the corresponding nuclear reaction yield also varies with t. It is necessary to calculate the optimum total thickness of the sample for the most effective production and use of bremsstrahlung, and thus to maximize the accumulation of radioactive products.

At any depth, t, within the sample the conversion efficiency to bremsstrahlung is proportional to the local energy of electrons, $E_e(t)$, because of the radiation-stopping function [13]

$$\left(\frac{dE_e}{dx}\right)_{rad} = c\,E_e. \quad (6)$$

At the same time, the total range of energies covered by the bremsstrahlung continuum, $0 \leqslant E_\gamma \leqslant E_e$, is also compressed. For $E_\gamma < 1050$ MeV, therefore, the spectral density of radiation is almost independent of changes in E_e in the range of 1050–4500 MeV and thus different parts of the electron paths in the sample provide equal contributions to dN_γ/dE_γ. It was explained above that the majority of the radionuclide production was created by the part of spectrum from $E_\gamma = 50$–1050 MeV. The spectral density, dN_γ/dE_γ, and total number of photons, N_γ, within this range of E_γ at $t = \ell$ can be expressed as an integral over the sample layer from $t = 0$ to ℓ

$$N_\gamma \sim \int_0^\ell \frac{dE_e}{dx}(t)\,E_e^{-1}\,e^{-\mu(\ell-t)}\,dt. \quad (7)$$

With the substitution of Eq. (6) into Eq. (7), one obtains

$$N_\gamma(\ell) \sim \frac{c}{\mu}\left(1 - e^{-\mu\ell}\right). \quad (8)$$

Photon absorption is taken into account by a linear attenuation coefficient μ that is weakly dependent on E_γ for energies greater than 100 MeV. The coefficients c and μ are expressed in cm^2 when the thickness values t and ℓ are expressed in atoms/cm^2. Using Eq. (8), one deduces the total nuclear reaction yield in the sample of total thickness d as

$$Y_{nr} \sim \int_0^d N_\gamma(\ell)\,\bar{\sigma}\,d\ell = \frac{\bar{\sigma}c}{\mu^2}(\mu d + e^{-\mu d} - 1) \qquad (9)$$

where $\bar{\sigma}$ is the mean cross-section of the reaction for E_γ within the range of interest.

Now, it is necessary to discuss some limiting factors on the sample thickness. After electrons penetrate through a thickness t_{max}, their energy is reduced to $E_{min} = 1050$ MeV and at greater depths only softer photons can be created. The selected range of E_γ is therefore not applicable and requiring more complicated calculations. For simplicity, here it is assumed that for depths within the sample of $t > t_{max}$ no photons are generated, but the full thickness of the sample can produce absorption of photons and nuclear reaction events as illustrated in Fig. 4. Under such conditions the nuclear reaction yield at the total thickness of the sample is expressed as follows:

$$Y_{nr}(t_{tot}) \sim \frac{\bar{\sigma}c}{\mu^2}\left[\mu t_{max} + e^{-\mu t_{tot}} - e^{-\mu(t_{tot}-t_{max})}\right]. \qquad (10)$$

The expression of Eq. (10) can be used to estimate the optimum thickness, t_{tot}, and the numerical value of the optimum yield, Y_{nr}.

In addition to the simplifying assumptions above, the straggling of electron energy and angle was completely neglected. However, this approach may lead to an underestimation of the yield, Y_{nr}, so Eq. (10) is still valuable for its predictive power. The equations above do not contain any numerical constants by which to provide an absolute calibration of the yield. Still in this experiment and under well-defined geometry the yield was measured and this is sufficient for the calibration. It is necessary to derive an equation corresponding to separated converter and target samples as was arranged in the experiment. Using the same theory as above, the case of separated samples is described by

$$Y_{nr} \sim \frac{\bar{\sigma}c}{\mu^2}(1 - e^{-\mu\ell})(1 - e^{-\mu d}) \qquad (11)$$

where ℓ and d are the converter and the target thicknesses, respectively. Finally, the ratio of the optimized yield for the unified target-converter sample to the yield in the experimental geometry, Y_{opt}/Y_{exp}, was calculated as a function of the t_{tot}/t_{max} ratio and is presented in Fig. 5. This function exhibits a growth, reaching saturation, as shown in the figure.

The value t_{max} was obtained to be of about 6.3 mm for a Ta sample with electron energies of $E_0 = 4.5$ GeV and $E_{min} = 1.05$ GeV. As is clear from Fig. 5, there is no reason to use $t_{tot} \geqslant 3t_{max}$. Thus, the optimum sample thickness should be about 19 mm of tantalum. The absolute productivity was also estimated by linking it to the experimentally observed production yield corresponded to the known numbers of equivalent photons and electrons incident on the converter. Finally, with a 19-mm thick tantalum sample in unified geometry, as many as 2.5×10^9 atoms/s of the ^{178m2}Hf isomer may be obtained with an electron beam current of

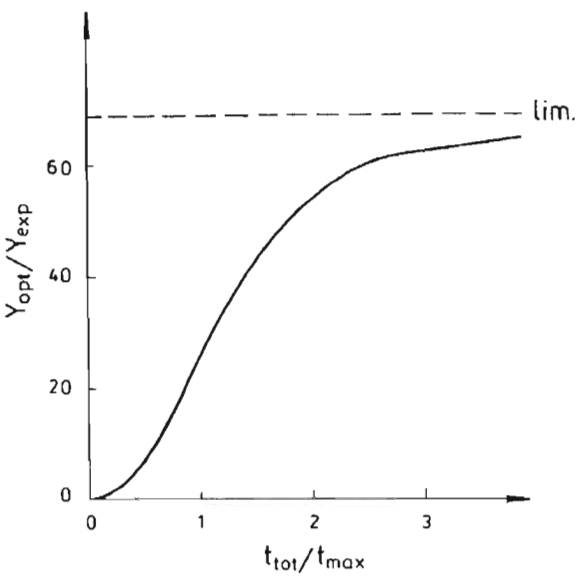

Fig. 5. Yield of nuclear reactions for production of ^{178m2}Hf in the unified sample, Y_{opt}, as a function of the sample thickness. The Y_{opt} value was normalized to the yield Y_{exp} taken from the experiment having separate converter and target.

100 μA. Such an intensity is achieved in modern linear electron accelerators and even higher currents may be reached in new systems that are under development.

Some of the simplifying assumptions described above do not influence the final productivity estimate due to the ability to calibrate the result with the present experimentally measured yield. Therefore, these assumptions do not serve as a source of inaccuracies in the calculated optimum value. However, two processes will be manifested within a thick unified sample which were not exhibited in the experimental conditions. First, the productivity value was evaluated in a linear approximation and so does not account for any second-order interactions, i.e. secondary radiation created by electrons and positrons after bremsstrahlung absorption with pair production. It is estimated that a correction to include secondary processes should not be higher than 15%. Second, nuclear reactions induced directly by beam electrons themselves, without first their conversion to bremsstrahlung, must contribute some additional yield of the isomer within a unified converter-target assembly (recall that in the present experiment, no electrons reached the target). The yield of electronuclear reactions, Y_{enr} was calculated as follows:

$$Y_{enr} = \int_{E_1}^{E_2} \frac{\bar{\sigma}\ k(E_e)}{dE_e/dx}\, dE_e \qquad (12)$$

where an integration is applied over the stopping range of electrons from energies of E_1 to E_2. The cross-section for electronuclear reactions is given by the function $\sigma_{enr} = \bar{\sigma}\ k(E_e)$ where $\bar{\sigma}$ is the photon-induced cross-section as used before. The ratio of electronuclear to photonuclear cross-sections, $k(E_e)$, is known for $E1$ multipolarity to be [15]

$$k(E_e) = \frac{2\ \ln(E_e/mc^2)}{137\pi}. \qquad (13)$$

In reality, however, the $k(E_e)$ value is higher by a factor of 2.5 for $E_\gamma > 100$ MeV [15], due to such processes as $E2$ absorption, the quasi-deuteron mechanism [16] and meson-production reactions. So, a factor of 2.5 was inserted into Eq. (13) and the result substituted into Eq. (12) prior to integration over the range of electron energies between 1050 and 50 MeV as was done for the photon-induced reaction. The stopping range in which electron energies change from 4500-1050 MeV is of less importance due to lower cross-sections and higher dE_e/dx, but this was nevertheless taken into account. Finally, the contribution of the electronuclear interaction was found to be about 0.13 Y_{phr}, where Y_{phr} was the yield determined before for the photonuclear reaction. The calculated productivity under optimum conditions was then corrected to include both secondary and electron-induced processes, giving a total yield

$$\sum Y_{opt} = 3.2 \times 10^9 \text{ atoms/(s 100 } \mu\text{A)} \qquad (14)$$

for the ^{178m2}Hf isomer. This is about 8 times lower than the yield achieved at Los Alamos with a proton beam of the same current. A lower productivity by electrons compared with protons could be entirely expected. But, it is perhaps surprising that the ratio is only 1/8, not by several orders-of-magnitude, and this is an important result of the experiment. One additional practical consideration should also be discussed. The volume density of power is higher in the case of electrons compared with protons due to the correspondingly larger stopping power. But this does not present a severe restriction because a multilayer tantalum sample in a water flow can effectively remove the heat released by the electron beam. It should be recalled that both radiation energy losses of electrons and photon absorption in water are negligible, as compared to Ta. In practice, it may be possible that electron beams can be more convenient and less expensive in operation than the meson-factory proton beam due to technical reasons.

5. Summary

The yield of the ^{178m2}Hf isomer was measured after irradiation of a tantalum target with 4.5-GeV bremsstrahlung. The integral and mean cross-section values and the isomer-to-ground-state ratio were newly obtained. An optimized scheme for the production of this isomer using electron

accelerators was proposed and evaluated. The maximum production yield was obtained and a comparison with the productivity of proton-induced reactions was discussed.

Acknowledgements

The authors gratefully acknowledge support by the US Air Force Office of Scientific Research under contract F49620-02-01-0187.

References

[1] P.M. Walker, G. Dracoulis, Nature 399 (1999) 35.
[2] J.J. Carroll, S.A. Karamian, L.A. Rivlin, et al., Hyperfine Int. 135 (2001) 3.
[3] H. Roberts, Hyperfine Int. 107 (1997) 91.
[4] H.A. O'Brien, Nucl. Instr. and Meth. B40/41 (1989) 1126.
[5] S.A. Karamian, J. Adam, D.V. Filossofov, et al., Nucl. Instr. and Meth. A 489 (2002) 448.
[6] S.A. Karamian, J. Adam, Czech. J. Phys. 53 (2003) B381.
[7] S.A. Karamian, J. Adam, P. Chaloun, et al., preprint JINR E6-2004-7, Dubna.
[8] Y.T. Oganessian, S.A. Karamian, Y.P. Gangrski, et al., J. Phys. G 18 (1992) 393.
[9] Y. Weixiang, L. Hanlin, Z. Wenrong, Chinese J. Nucl. Phys. 14 (1992) 326.
[10] S.A. Karamian, J.J. Carroll, J. Adam, et al., Laser Phys. 14 (2004) 438.
[11] J. Adam, J. Mrazek, J. Frana, et al., Meas. Tech. 44 (2001) 93.
[12] R.B. Firestone, V.S. Shirley, C.M. Baglin, et al., Table of Isotopes, 8th Edition, Wiley, New York, 1996.
[13] W. Heitler, The Quantum Theory of Radiation, Clarendon Press, Oxford, 1954.
[14] B.L. Zhuikov, M.V. Mebel, V.M. Kokhaniuk, et al., Phys. Rev. C 68 (2003) 054611
[15] V.G. Nedorezov, Y.N. Raniuk, Part. Nuclei 15 (1984) 379 (in Russian).
[16] J.S. Levinger, Phys. Lett. B 82 (1979) 181.

Available online at www.sciencedirect.com
SCIENCE DIRECT®
ELSEVIER
Nuclear Physics A 746 (2004) 617c–620c
NUCLEAR PHYSICS A

Studies of high-K isomers at TRIUMF-ISAC

M.B. Smith[a], P.M. Walker[a,b], R.S. Chakrawarthy[a], R.A.E. Austin[c], G.C. Ball[a], J.J. Carroll[d], E. Cunningham[a,b], P. Finlay[e], P.E. Garrett[f], G.F. Grinyer[e], G. Hackman[a], B. Hyland[e], K. Koopmans[a,c], W.D. Kulp[g], J.R. Leslie[h], A.A. Phillips[e], R. Propri[d], P.H. Regan[b], F. Sarazin[a], M.A. Schumaker[e], H.C. Scraggs[a], T. Shizuma[i], C.E. Svensson[e], J. von Schwarzenberg[j], J.C. Waddington[c], D. Ward[k], J.L. Wood[g], B. Washbrook[c] and E.F. Zganjar[l]

[a]TRIUMF, 4004 Wesbrook Mall, Vancouver, BC, Canada
[b]Department of Physics, University of Surrey, Guildford, Surrey, UK
[c]Department of Physics and Astronomy, McMaster University, Hamilton, ON, Canada
[d]Department of Physics and Astronomy, Youngstown State University, Ohio, USA
[e]Department of Physics, University of Guelph, Guelph, ON, Canada
[f]Lawrence Livermore National Laboratory, Livermore, California, USA
[g]School of Physics, Georgia Institute of Technology, Atlanta, Georgia, USA
[h]Physics Department, Queen's University, Kingston, ON, Canada
[i]Japan Atomic Energy Research Institute, Tokai, Ibaraki, Japan
[j]Institut für Isotopenforschung und Kernphysik, Universität Wien, Wien, Austria
[k]Nuclear Science Division, Lawrence Berkeley National Laboratory, California, USA
[l]Department of Physics and Astronomy, Louisiana State University, Louisiana, USA

The properties of high-K isomers have been investigated by measuring γ rays from a source of the 31-year $^{178}Hf^{m2}$ isomer and from the decay of implanted $^{178,179}Lu$ beams. Low-intensity transitions have been identified in the decay of $^{178}Hf^{m2}$, demonstrating a consistent extension of K-hindrance systematics to higher multipolarities, and elucidating the spin-dependence of the mixing between the two $K^\pi = 8^-$ bands. A search is underway for new isomers in $^{178,179}Lu$ and the preliminary results of the analysis are reported.

1. INTRODUCTION

Isomers are excited, metastable states of atomic nuclei, having long half-lives (a few nanoseconds to many years) compared to other nuclear states [1]. They arise principally from angular-momentum selection rules. In particular, the quantum number K (the angular-momentum projection on the body-fixed symmetry axis) is approximately conserved, which leads to the existence of high-K isomers. The study of such isomers provides information on a variety of nuclear structure effects, especially the interplay between single-particle and collective modes of excitation.

Although many high-K isomers are now known, theoretical calculations suggest that some of the most striking examples may be observed in the neutron-rich $A = 170 - 190$

0375-9474/$ – see front matter
doi:10.1016/j.nuclphysa.2004.09.101

region of the nuclear chart, where nuclei are characterised by prolate deformation. In this region the Fermi levels for both neutrons and protons are simultaneously in the upper parts of their respective shells, where the individual nucleon orbits have large K projections and excitations based on broken pairs can generate large K values. These neutron-rich nuclei are very difficult to access experimentally, largely because they cannot be reached using fusion-evaporation reactions with stable beams and targets. Recent work using inelastic excitation and transfer reactions (e.g. [2]) and relativistic projectile fragmentation (e.g. [3]) has made some progress into this unexplored terrain, and several new isomers have been discovered. With the recent developments in radioactive beam science, for example at TRIUMF's ISAC facility [4], further advances in the study of high-K isomers in neutron-rich species should be rapidly achievable. This paper reports on a recent radioactive-beam experiment aimed at the study of new high-K isomers in neutron-rich ^{178,179}Lu, as well as an earlier experiment to investigate the ^{178}Hf^{m2} isomer by detecting radiation from a chemically-separated sample.

2. DECAY OF THE ^{178}Hf^{m2} ISOMER

The second metastable state of ^{178}Hf, commonly referred to as ^{178}Hf^{m2}, lies 2.4 MeV above the ground state of ^{178}Hf. This remarkable isomer has angular momentum and parity $I^\pi = K^\pi = 16^+$ and a half-life of 31 years [5]. Its exceptionally long lifetime arises not only because of its high K value, but also because it lies lower in excitation energy than any other states of spin 14 or higher. Although the high-spin level structure of ^{178}Hf has been studied extensively, basic knowledge gaps remain and radiations emitted directly from the isomer itself have not, until now, been well established.

The decay of ^{178}Hf^{m2} has been investigated by studying the γ rays emitted by a radioactive sample containing approximately equal decay rates of ^{178}Hf^{m2} and ^{172}Hf. The source material was extracted from a Ta target, that had been irradiated with an intense beam of protons in 1980, and a 15 kBq source was prepared after chemical separation of the Hf isotopes. This source was placed at the centre of the 8π spectrometer [6], an array of 20 closely-packed, Compton-suppressed HPGe detectors situated at TRIUMF-ISAC, operating in standalone mode. Data were acquired over a 42-day period. High-multipolarity $M4$ and $E5$ transitions, definitive evidence for γ-ray emission from the isomer, have been identified using $\gamma - \gamma$ coincidence techniques. These are the first strongly K-forbidden examples with such high multipolarities, and demonstrate a consistent extension of K-hindrance systematics, with a reduced hindrance of approximately 100. Three other low-intensity transitions, between the two known $K^\pi = 8^-$ bands, have been identified in the decay of the ^{178}Hf^{m2} isomer, and the deduced branching ratios elucidate the decreasing mixing between the two bands with increasing angular momentum. Further details of the analysis and results can be found in Ref. [7].

3. SEARCH FOR NEW ISOMERS IN NEUTRON-RICH ^{178,179}Lu

In order to search for high-K isomers in neutron-rich species, the decay of radioactive ^{178,179}Lu beams has been studied. For both of these isotopes, multi-quasiparticle calculations based on the blocked-BCS method [8] suggest several potential high-spin isomers, i.e. states that have high-K values and relatively low excitation energies. The calcula-

tions suggest that the most likely candidate in ^{178}Lu is a four-quasiparticle state with $I^\pi = K^\pi = 16^+$ and an excitation energy below 2 MeV. For ^{179}Lu a five-quasiparticle isomer with $K^\pi = 43/2^+$ and excitation energy of approximately 4 MeV is predicted. Recent measurements [9] of projectile fragmentation reactions identify isomers with angular momenta exceeding these values, and suggest that these isomers are typically populated with cross-sections of $5-20\%$ of the ground-state production. If these isomers have favourable half-lives (several ms or more) they can thus be produced using the ISOL technique and transported to a low-background environment, such as the ISAC experimental hall, for spectroscopic studies.

The 8π spectrometer and its data acquisition system have recently been redesigned and upgraded for $\beta-\gamma$ coincidence experiments. SCEPTAR (SCintillating Electron-Positron Tagging ARray), an array of 20 plastic scintillators arranged in four rings of five detectors, is now housed inside a Delrin target chamber at the centre of the 8π spectrometer. A moving tape transport has also been installed, in order to move a backcoated polyester "Black Watch" tape to the centre of the target chamber, where beams are implanted on to the tape, and to transport long-lived activity to a storage box which is shielded from the HPGe detectors. Half of SCEPTAR, and the tape inside the target chamber, is shown in Fig. 1, with the lead shielding wall in the background.

The ^{178,179}Lu beams were produced following the bombardment of a Ta target with a 30 μA beam of 500 MeV protons from the TRIUMF cyclotron. The surface ion source was used to extract the ^{178,179}Lu beams, which were then mass separated and transported to the experimental area with an energy of 40 keV and intensities of approximately 10^7 ions/s. The Lu beams were implanted on to the tape at the mutual centre of the 8π spectrometer and SCEPTAR, and the tape was moved periodically to reduce the γ-ray background from the ground-state and long-lived isobar decays. Data were acquired with different trigger conditions for the plastic and Ge detectors and with various tape-cycle periods, in order to distinguish those γ rays associated with long- and short-lived decays. A LeCroy universal logic module and a Jorway sequencer were used to give an event tag and clock time (within a cycle) on an event-by-event basis. The data were sorted into two-dimensional $\gamma-\gamma$ and $\gamma-$ clock matrices for the portions of the data corresponding to the same trigger and cycling conditions, and a search has been performed for (relatively) short-lived decays of new isomeric states.

No new isomers have so far been assigned to the neutron-rich Lu isotopes in the preliminary analysis of the data. However, the technique of correlating γ rays with short decay half-lives is demonstrated in Fig. 2 for transitions fed by known long- and short-lived activities. Fig. 2(a) shows the total γ singles projection from the $A = 179$ data with an 80 s cycle period between tape motion, with data acquired as follows: 10 s with beam off, 60 s with beam on, and 10 s with beam off. Fig. 2(b) shows the corresponding spectrum collected with a shorter 3 s cycle period (0.5 s beam off, 2 s beam on, 0.5 s beam off). The ^{179}Lu peaks of interest are labelled with their energy in keV and contaminants from the decay of ^{163}Lu, which is ionised as an oxide before passing through the ISAC mass separator, are labelled with their energy and a #. The 592-keV γ ray, which de-excites the known $1/2^+$, 3.1 ms isomer in ^{179}Lu, is enhanced, relative to the other peaks in the spectrum of Fig. 2(a), in the data taken with the shorter tape cycle. The 612-keV ^{179}Lu gamma ray, which is fed by the long-lived ($T_{1/2} = 8.0$ min) β decay of ^{179}Yb and not by

Figure 1. Close-up view of ten of the SCEPTAR detectors and the tape inside the target chamber.

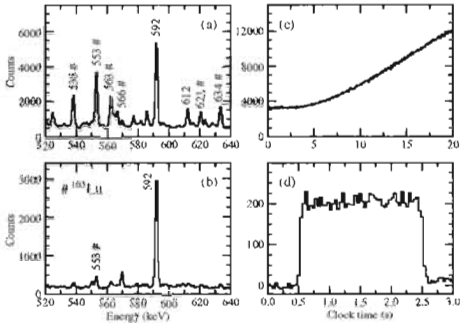

Figure 2. ^{179}Lu γ spectra for (a) an 80 s cycle and (b) a 3 s cycle. Clock spectra for the decay of (c) ^{178}Lu and (d) ^{179}Lu. See text for more details.

the $1/2^+$ isomer, is also labelled, and only appears in the spectrum of Fig. 2(a). This suggests that the 3.1 ms isomer is produced directly from the ISAC ion source, and is not only fed by the transitions following ^{179}Yb β decay. Fig. 2 also shows the activity as a function of clock time over one cycle, correlated with (c) the 213-keV ($4^+ \rightarrow 2^+$) transition in ^{178}Hf and (d) the 592-keV γ ray in ^{179}Lu. The ^{178}Hf spectrum was collected with a 20 s cycle (2.5 s beam off, 15 s beam on, 2.5 s beam off) and demonstrates the long grow-in curve associated with feeding from the known ($T_{1/2}$ = 23.1 min) 9^- isomer in ^{178}Lu. The grow-in curve for the 592-keV ^{179}Lu γ ray (Fig. 2(d)), from the same portion of the data as the spectrum shown in Fig. 2(b), exhibits almost immediate saturation of the transition rate when the beam is switched on, and equally fast decay of the transition when the beam is switched off. The spectrum is consistent with a 3 ms half-life for the transition, and confirms that the $1/2^+$ isomer in ^{179}Lu is produced directly from the ion source. This result demonstrates the feasibility of the technique described here, and has positive implications for the production of short-lived isotopes at ISAC.

REFERENCES

1. P.M. Walker and G.D. Dracoulis, Nature 399 (1999) 35.
2. R. D'Alarcao, et al., Phys. Rev. C 59 (1999) R1227.
3. Zs. Podolyak, et al., Phys. Lett. B 491 (2000) 225.
4. P. Bricault, et al., Nucl. Phys. A 701 (2002) 49c.
5. R.G. Helmer and C.W. Reich, Nucl. Phys. A 114 (1968) 649; 211 (1973) 1.
6. C.E. Svensson, et al., Nucl. Instrum. Methods Phys. Res. B 204 (2003) 660.
7. M.B. Smith, et al., Phys. Rev. C 68 (2003) 031302(R).
8. K. Jain, et al., Nucl. Phys. A 591 (1995) 61.
9. M. Pfützner, et al., Phys. Rev. C 65 (2002) 064604.

PHYSICAL REVIEW C 68, 031302(R) (2003)

γ rays emitted in the decay of 31-yr $^{178}Hf^{m2}$

M. B. Smith,[1,*] P. M. Walker,[1,2] G. C. Ball,[1] J. J. Carroll,[3] P. E. Garrett,[4] G. Hackman,[1] R. Propri,[3] F. Sarazin,[1] and H. C. Scraggs[1]

[1]*TRIUMF, 4004 Wesbrook Mall, Vancouver, British Columbia, Canada V6T 2A3*

[2]*Department of Physics, University of Surrey, Guildford, Surrey GU2 7XH, United Kingdom*

[3]*Department of Physics and Astronomy, Center for Photon-Induced Processes, Youngstown State University, Youngstown, Ohio 44555, USA*

[4]*Lawrence Livermore National Laboratory, Livermore, California 94551, USA*

(Received 25 June 2003; published 17 September 2003)

The spontaneous decay of the $K^\pi = 16^+$, 31-yr $^{178}Hf^{m2}$ isomer has been investigated with a 15-kBq source placed at the center of a 20-element γ-ray spectrometer. High-multipolarity $M4$ and $E5$ transitions, which represent the first definitive observation of direct γ-ray emission from the isomer, have been identified, together with other low-intensity transitions. Branching ratios for these other transitions have elucidated the spin dependence of the mixing between the two known $K^\pi = 8^-$ bands. The $M4$ and $E5$ γ-ray decays are the first strongly K-forbidden transitions to be identified with such high multipolarities, and demonstrate a consistent extension of K-hindrance systematics, with an inhibition factor of approximately 100 per degree of K forbiddenness. Some unplaced transitions are also reported.

DOI: 10.1103/PhysRevC.68.031302 PACS number(s): 23.20.Lv, 27.70.+q

One of the most remarkable isomers known in the $A \approx 180$ region of deformed atomic nuclei [1] is the second metastable state of ^{178}Hf, commonly referred to as $^{178}Hf^{m2}$. This state, which lies 2.4 MeV above the ground state of ^{178}Hf, has angular momentum and parity $I^\pi = K^\pi = 16^+$ (K is the angular-momentum projection on the body-fixed symmetry axis) and a half-life of 31 yr [2–5]. Its four-quasiparticle structure is based on a broken neutron (ν) pair and a broken proton (π) pair, each contributing $I^\pi = K^\pi = 8^-$. The exceptionally long lifetime of the isomer arises not only because of its high K value and the associated hindrance caused by the K-selection rule, but also because it lies lower in excitation energy than any other states of spin 14 or higher. This yrast trap is forced, therefore, to decay by transitions with both high multipolarity and a large change in K.

On account of its long half-life and high excitation energy, the $^{178}Hf^{m2}$ isomer has attracted considerable interest and experimental investigation. For example, enriched samples have been studied by laser hyperfine spectroscopy [6], and there is evidence that the isomer can be Coulomb excited in a multistep process from the $I^\pi = K^\pi = 0^+$ ground state [7]. A more controversial observation is the stimulated decay of the isomer, induced by x rays and synchrotron radiation, which has been reported by Collins *et al.* [8–11], but refuted by Ahmad *et al.* [12,13].

The high-spin level structure of ^{178}Hf has been studied extensively [3–5,14], but basic knowledge gaps remain. Surprisingly, radiations emitted directly from the isomer itself are not yet well established. The problem arises, in essence, because 99.9% of the isomer decay proceeds through a highly converted, 13-keV $E3$ transition ($16^+ \rightarrow 13^-$) which has not so far been directly detected. The suggestion by Khoo and Lövhöiden [4] that the isomer is at 2447.4 keV, deduced from its population from higher-energy states, is in conflict with the singles conversion-electron data of van Klinken *et al.* [5] for a 0.1%, $M4$ decay branch ($16^+ \rightarrow 12^-$) which implies an excitation energy of 2446.0 keV. Although the 1.4-keV difference in proposed isomer energies is small, it is well outside statistical uncertainties, and represents a basic difficulty with the current understanding of the isomer and its decay modes.

In the present γ-γ-coincidence study, the $M4$ γ-ray transition has been clearly identified, confirming the interpretation of van Klinken *et al.* [5]. We also establish the competing $E5$ γ-ray transition ($16^+ \rightarrow 11^-$) and additional low-intensity transitions that had not previously been placed in the $^{178}Hf^{m2}$ decay sequence. The results extend the general understanding of high-multipolarity, K-forbidden decays, and shed new light on the nature of the band mixing between members of the two $K^\pi = 8^-$ bands, which are populated in the isomer decay. Although the latter states are well known from in-beam γ-ray spectroscopic studies [4,14], significant additional band mixing information is now obtained.

The radioactive source material was extracted from a tantalum target, irradiated in 1980 with an intense proton beam at Los Alamos National Laboratory. Hafnium isotopes were chemically separated [15] and shipped to SRS Technologies, Alabama, where a 15-kBq source of $^{178}Hf^{m2}$ ($T_{1/2} = 31$ yr) was prepared. On delivery for the present measurement, the source also contained ^{172}Hf ($T_{1/2} = 1.9$ yr, in secular equilibrium with its daughter ^{172}Lu, $T_{1/2} = 6.7$ days) with a decay rate approximately equal to that of $^{178}Hf^{m2}$. The source was placed at the center of the 8π spectrometer [16], an array of 20 Compton-suppressed n-type HPGe detectors situated at TRIUMF-ISAC. The absolute full-energy-peak efficiency was 4% at 426 keV, and at that energy the final full width at half maximum energy resolution was 1.6 keV, after gain

*Email address: mbsmith@triumf.ca

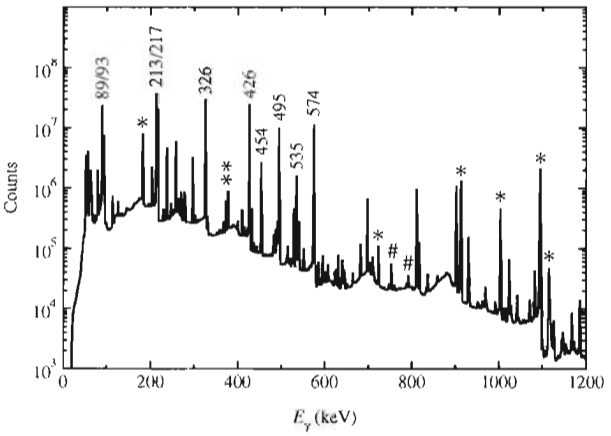

FIG. 1. Total γ-γ projection, from the data acquired with copper absorbers. The energy dispersion is 0.33 keV/channel. The most intense transitions in ^{178}Hf are labeled with their energy in keV. Sum peaks (#) and some of the most intense transitions from the ϵ decay of ^{172}Lu (*) are also indicated.

matching all the germanium detectors. The icosahedral geometry of the 8π spectrometer leads to minimal angular correlation effects [17].

When searching for extremely weak decay branches, many instrumental effects have to be taken into account, such as germanium x-ray escape events, peak summing, and scattering between detectors on opposites sides of the detector array. As part of this investigation, copper and lead absorbers, of thickness 0.5 mm and 1.0 mm, respectively, were placed (separately) in front of the germanium detectors for portions of the data taking. Data were acquired over a total period of 42 days as follows: 8 days with no absorbers, five days with the lead absorbers, and 29 days with the copper absorbers. Event pairs were sorted into γ-γ coincidence matrices, with a $\leqslant$20-ns time-difference requirement. Other timing conditions were also investigated. Using the RADWARE [18] software package, most of the analysis was performed with the data from the 29-day measurement. The corresponding total coincidence spectrum is shown in Fig. 1. The data taken with the lead absorbers, and without absorbers, were used independently to verify some of the results, and to obtain optimum data where low-energy peak summing otherwise limited the sensitivity. A major part of the data analysis was concerned with the identification of previously unreported γ-ray transitions in the complex decay scheme following the electron-capture (ϵ) decay of ^{172}Lu to ^{172}Yb [19]. More than 100 transitions have been newly placed in this decay (most being completely new to ^{172}Yb) and the details of these will be the subject of a separate report.

The emphasis of the present work was on the identification and characterization (in terms of energy and intensity) of low-intensity γ-ray transitions. Given the associated inherent limitations in counting statistics, the energy and efficiency calibrations were not themselves needed to very high accuracy. These calibrations were obtained internally from the well-known, intense decay transitions of ^{178}Hf^{m2} [5,20] and ^{172}Lu [19] giving, in the present work, energies and relative efficiencies to accuracies of $\pm$0.1 keV and 1.7%, respectively.

The sensitivity limit of the present measurement is at about the 0.001% level, i.e., 1 in 10^5 parent decays of ^{178}Hf^{m2} or ^{172}Lu. This is not only a matter of counting statistics. Of the various instrumental effects, the scattering between germanium γ-ray detectors, across the 8π spectrometer, is perhaps the most serious limitation. The use of a mass-separated sample of ^{178}Hf^{m2} could further improve the sensitivity. Within the obtained sensitivity limit, exotic α and β decays of ^{178}Hf^{m2}, whose possibility was discussed by van Klinken *et al.* [5], could not be detected, nor could any direct γ-ray decay into the ground-state band be identified.

After exhaustive investigation of the γ-ray coincidence relationships, only one additional source of activity was positively identified, close to the limit of sensitivity of the measurement. This is a product of the natural ^{232}Th decay series, namely the decay of ^{208}Tl to ^{208}Pb, with (583–2615)-keV coincidences [21]. In addition to this, also close to the limit of sensitivity, the following γ-ray energies were found to be in mutual coincidence: 154.4, 212.6, and 958.6 keV; further, 90.7- and 868.0-keV transitions were in coincidence with each other and with the 154.4- and 212.6-keV transitions, i.e., they appear to be in parallel with the 958.6-keV transition. While a 90.6-keV transition is well known in the ϵ decay of ^{172}Lu [19], the other four energies are clearly distinct from transition energies that can reasonably be associated with the decay of ^{178}Hf^{m2} and ^{172}Hf in the present source, though the 212.6-keV transition is close in energy to the intense 213.4-keV transition in ^{178}Hf. The origin of these five transitions is, at present, undetermined. However, their apparently long-lived ($\gg$1 year) parentage, and association with hafnium chemical extraction, makes their origin of great potential interest.

The partial level scheme of ^{178}Hf deduced from the present work, showing only those states involved in the decay of the $K^\pi = 16^+$ isomer (together with the $K^\pi = 8_2^-$ bandhead), is shown in Fig. 2. Transition energies and relative intensities, normalized to the 326-keV transition, are summarized in Table I. The ^{178}Hf^{m2} isomer was previously known to decay predominantly by an $E3$ conversion-electron transition of energy close to 13 keV [3–5], and evidence for a $M4$, 309.5-keV transition, from detection of conversion electrons in singles mode, was also reported [5]. In the present work, the clear observation of γ rays from the direct deexcitation of the isomer is reported for the first time, confirming the 309.5-keV, $M4$, $16^+ \rightarrow 12^-$ transition and adding the 587.0-keV, $E5$, $16^+ \rightarrow 11^-$ transition. These are illustrated in Fig. 3. In addition, the low-intensity 231-, 343- and 601-keV γ-ray transitions, which link members of the two $K^\pi = 8^-$ bands, have been observed in the decay path of ^{178}Hf^{m2}. These are illustrated in Fig. 4. The latter two transitions are known from in-beam studies [4,14], whereas the 231-keV $E2$ transition was previously reported [22] based on singles counting with a ^{178}Hf^{m2} source. These transitions have now been definitively established in the decay of the 31-yr isomer, from γ-γ coincidences.

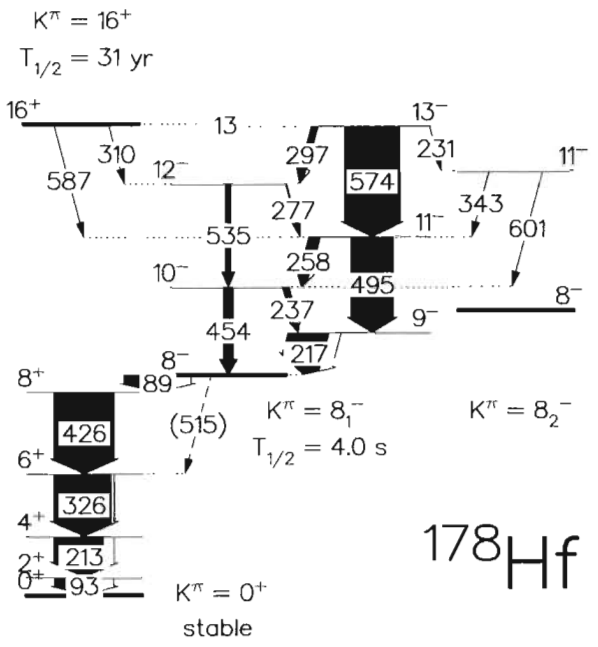

FIG. 2. Decay scheme of $^{178}Hf^{m2}$ deduced from the present work. The arrow widths represent the relative transition intensities, the unfilled parts corresponding to internal conversion. The dashed 515-keV, $8^- \rightarrow 6^+$ transition has not been established. The highly converted 13-keV transition is inferred from γ-ray coincidence relationships. Only the 11^- member of the 8_2 band is identified in the present work, though other band members are known from previous studies [4,14].

The expected 515-keV, $8^- \rightarrow 6^+$ transition from the 4-s isomer could not be established in this work. However, with the lead absorbers in front of the germanium detectors, the sum peak from 89- and 426-keV coincidences was highly attenuated, enabling a stringent limit to be placed on the 515-keV γ-ray intensity (see Table I).

Part of the analysis involved searching for the 129.4-, 210.3-, and 546.2-keV transitions, which Collins *et al.* [9,10] reported as being associated with the stimulated decay of $^{178}Hf^{m2}$, in the presence of a similar proportion of ^{172}Hf. In the present work, these transitions could not be found in the corresponding spontaneous decay. However, transitions at the nearby energies of 130.4 and 544.8 keV have been newly identified as being part of the ϵ decay of ^{172}Lu. It is not apparent how these might have influenced the earlier interpretation [9,10].

It is well known in ^{178}Hf that two $K^\pi = 8^-$ configurations, $\pi\{7/2[404], 9/2[514]\}$, and $\nu\{7/2[514], 9/2[624]\}$, mix together. (These are also the four quasiparticles that account for the structure of the $K^\pi = 16^+$ isomer.) Earlier work [3] established that the 8_1^-, 4-s isomer consists of 37(2)% π configuration and 63(2)% ν configuration. Also [3,5] there is evidence that the mixing matrix element V decreases with spin. Emery *et al.* [23] have shown that the conversion coefficients and branching ratios within the 8_1^- band can be understood with the specific spin dependence $V_I = V_{I=8}\exp\{-b[I(I+1)-K(K+1)]\}$, with $V_{I=8} = 159.2$ keV, $b = 0.00179$, and $K = 8$.

TABLE I. γ-ray energy, relative γ-ray intensity, initial and final spin and parity, multipole order λ, and reduced hindrance f_ν, for transitions in the decay path of $^{178}Hf^{m2}$. Uncertainties are given in parentheses.

E_γ (keV)	I_γ (%)	$I_i^\pi \rightarrow I_f^\pi$	λ	f_ν
12.7		$16^+ \rightarrow 13^-$	$E3$	66(1)
88.8(1)	68.7(12)	$8^- \rightarrow 8^+$	$E1$	79(1)
93.2(1)	19.0(3)	$2^+ \rightarrow 0^+$		
213.4(1)	85.7(15)	$4^+ \rightarrow 2^+$		
216.7(1)	69.5(14)	$9^- \rightarrow 8$		
230.8(1)	0.0060(10)	$13^- \rightarrow 11$		
237.4(1)	9.6(2)	$10^- \rightarrow 9$		
257.6(1)	17.5(4)	$11^- \rightarrow 10$		
277.4(1)	1.8(1)	$12^- \rightarrow 11$		
296.8(1)	10.9(2)	$13^- \rightarrow 12$		
309.5(1)	0.015(1)	$16^+ \rightarrow 12$	$M4$	72(2)
325.5(1)	100.0(17)	$6^+ \rightarrow 4^+$		
343.3(1)	0.0018(3)	$11^- \rightarrow 11$		
426.3(1)	102.2(18)	$8^+ \rightarrow 6^+$		
454.0(1)	17.4(4)	$10^- \rightarrow 8$		
495.0(1)	73.6(14)	$11^- \rightarrow 9$		
515.1	<0.0008	$8^- \rightarrow 6^+$	$M2$	>160
535.1(1)	9.5(2)	$12^- \rightarrow 10$		
574.3(1)	94.9(18)	$13^- \rightarrow 11$		
587.0(1)	0.0062(5)	$16^+ \rightarrow 11$	$E5$	165(5)
601.1(1)	0.0026(3)	$11 \rightarrow 10$		

It is now possible from the observed intensity of the 231-keV, $13^- \rightarrow 11^-$, $E2$ transition, relative to the 574-keV, $E2$ transition, to obtain an independent estimate of the mixing strength between the two 8^- structures. The determination of the relevant γ-ray intensities from the present coincidence data requires knowledge of other decay branches from members of the 8_2^- band, and for this purpose the intensities of Mullins *et al.* [14,24] have been used. (The intraband transitions account for about 10% of the decay intensity from the $I = 11$ member of the 8_2^- band.) It is notable that the 231-keV transition is the only stretched $E2$ transition established here between the two 8^- bands. While, in principle, the known $I \rightarrow I-1$ and $I \rightarrow I$ interband transitions can also be used to quantify the band mixing, the additional complication of $M1/E2$ admixtures, and the consequent need to quantify the magnetic and electric moments, limits the utility of that approach. Therefore, the identification of an interband $I \rightarrow I-2$, $E2$ transition can be considered to be especially valuable.

Applying standard two-band-mixing formulas (see, for example, Ref. [25]) together with the specified [23] spin-dependent mixing matrix element, the predicted $13^- \rightarrow 11^-$, $B(E2)$ ratio is 0.0054 compared with the present experimental value of 0.0057(9). The excellent agreement provides strong support for the interpretation of Emery *et al.* [23]. The other predicted $B(E2)$ ratios and the corresponding experimental limits are given in Table II. Also in the table are the $B(E2)$ ratios obtained by Karamian *et al.* [22] from singles γ-ray intensities, with evident disagreement for the $B(E2)$

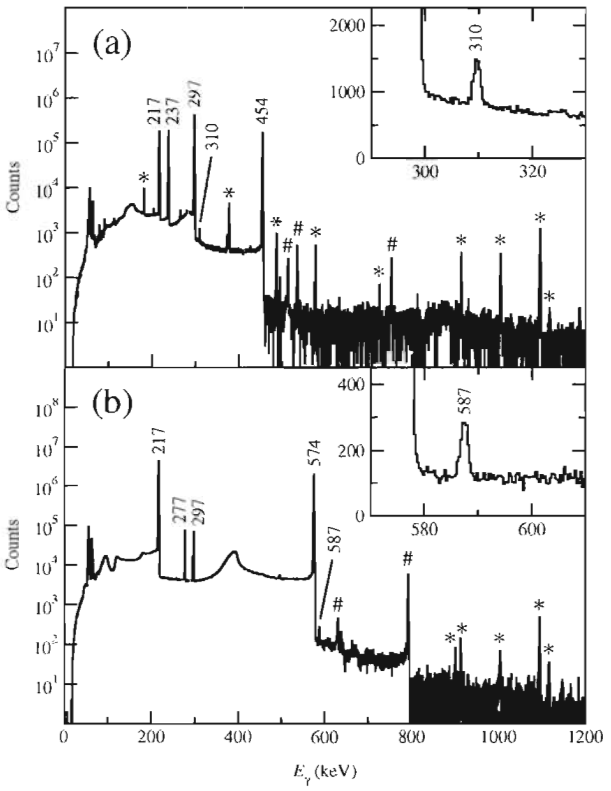

FIG. 3. Background-subtracted γ-ray coincidence spectra produced by gating on (a) the 535-keV transition and (b) the 495-keV transition. Transitions in ^{178}Hf are labeled with their energy in keV. Sum peaks (#) and contaminants from the ϵ decay of ^{172}Lu (*) are also indicated. The insets show the direct decays from ^{178}Hf^{m2}, on a linear scale.

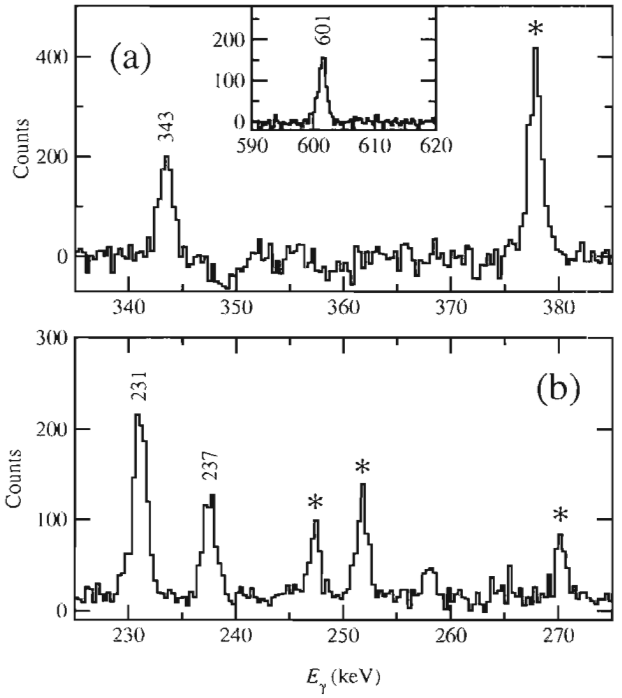

FIG. 4. Background-subtracted γ-ray coincidence spectra produced by gating on (a) the 231-keV transition and (b) the 601-keV transition. The inset shows a higher-energy portion of the spectrum gated on the 231-keV transition. Peaks associated with ^{178}Hf are labeled with their energy in keV, and impurities from the ϵ decay of ^{172}Lu (*) are indicated.

ratios from the $I=10$ and 11 levels. This disagreement presumably results from the poor peak-to-background ratio in singles counting.

The $M4$ and $E5$ transitions identified in the decay of ^{178}Hf^{m2} are the only known examples of such high-multipolarity transitions that are strongly K forbidden. The transitions go from the $K=16$ isomer to members of a $K=8$ band ($\Delta K=8$) and the degree of forbiddenness $\Delta K-\lambda$ is $\nu=4$ and 3, for the $M4$ and $E5$ transitions, respectively, where λ is the multipole order. If K were a strictly conserved quantity, then the transitions would be forbidden by angular-momentum vector coupling rules. However, K mixing leads to transitions that are hindered, rather than forbidden. A measure of the goodness of the K quantum number is the hindrance per degree of K forbiddenness (or reduced hindrance). This can be defined as $f_\nu=(F_W)^{1/\nu}$, where $F_W=T^\gamma_{1/2}/T^W_{1/2}$ is the hindrance factor, $T^\gamma_{1/2}$ is the partial γ-ray half-life, and $T^W_{1/2}$ is the corresponding Weisskopf single-particle estimate [21].

In a general analysis of K-forbidden transitions, Löbner [26] concluded that for each degree of K forbiddenness, transitions are typically retarded by a factor of 100, i.e., $f_\nu \approx 100$. In the present work, these systematics can now be extended to $\lambda=5$, with consistent results. The numerical values for ^{178}Hf, including the decay of the $K^\pi=8^-$ isomer, are given in Table I. For the 12.7-keV $E3$ transition, $f_\nu=66$ was evaluated using a conversion coefficient $\alpha=1.4\times10^7$ [27]. The $M2$, $8^-\rightarrow6^+$ decay from the $K^\pi=8^-$ isomer has $f_\nu>160$. The partial half-life of $>5\times10^5$ s for this 515-keV, γ-ray transition is greater than for either of the corresponding transitions in ^{180}Hf (501 keV, 1.4×10^5 s) or ^{182}Hf (507 keV, 1.7×10^4 s). Although the $M2/E3$ admixture is unknown for the ^{178}Hf case, the high reduced-hindrance limit is remarkable.

It is also striking that the Weisskopf hindrance factors F_W themselves vary over more than six orders of magnitude for the ^{178}Hf isomeric decays (discounting the $M2$ limit), while the reduced-hindrance values span the relatively narrow

TABLE II. Initial angular momentum, spin-dependent mixing matrix element, and ratio of out-of-band to in-band $E2$ strengths for $I\rightarrow I-2$ decays from $K^\pi=8_1^-$ band members in ^{178}Hf.

I	V (keV)	$R[B(E2)]$ Calc.	$R[B(E2)]$ Expt.	Ref. [22]
10	148.73	0.0111	<0.02	0.24(9)
11	142.99	0.0096	<0.02	0.21(2)
12	136.98	0.0076	<0.02	<0.034
13	130.75	0.0054	0.0057(9)	0.0049(8)

range of $f_\nu = 115 \pm 50$. These high reduced-hindrance values for the $^{178}Hf^{m2}$ decay transitions contrast with transitions from some other four-quasiparticle isomers in the same mass region [28], such as the $f_\nu = 2$ value for the $E2$ decay of a $K^\pi = 16^+$, 6-ns isomer in ^{182}Os [29]. For the purpose of building an understanding of K-mixing processes, it is important to be able to establish any hindrance-factor consistency, such as for given isomer decays with competing branches. The five $E2$ branches having $f_\nu \approx 5$, identified in the decay of the $K^\pi = 14^-$, 4-μs isomer in ^{174}Hf [30], provide another example. Thus, the picture emerges that isomers in a given nuclide may have reasonably well-defined decay patterns, but apparently similar isomers in different nuclides can have widely different reduced hindrances. This needs to be the focus of models to describe K-forbidden transition rates.

To summarize, the decay of $^{178}Hf^{m2}$ has been studied by coincidence γ-ray spectroscopy, with a transition sensitivity limit of about ten parts per million. New information on the structure of two interacting $K^\pi = 8^-$ rotational bands has been interpreted using a spin-dependent matrix element. The reduced-hindrance values for decays directly from $^{178}Hf^{m2}$ show good consistency, with $f_\nu \approx 100$.

Thanks are due to H. Roberts and M. Helba of SRS Technologies, for the loan of the hafnium source. G. D. Dracoulis, R.V.F. Janssens, S.A. Karamian, W.D. Kulp, and J.L. Wood are thanked for their valued contributions. Help with running the experiment is also acknowledged from D.M. Cullen, E. Cunningham, L.K. Pattison, S.V. Rigby, P. Schmelzenbach, D.T. Scholes, and C. Wheldon. J.J.C. and R.P. acknowledge support from US AFOSR Contract Nos. F496200210187.

[1] P.M. Walker and G.D. Dracoulis, Nature (London) **399**, 35 (1999).
[2] R.G. Helmer and C.W. Reich, Nucl. Phys. **A211**, 1 (1973).
[3] F.W.N. de Boer, P.F.A. Goudsmit, B.J. Meijer, J.C. Kapteyn, J. Konijn, and R. Kamermans, Nucl. Phys. **A263**, 397 (1976).
[4] T.L. Khoo and G. Løvhøiden, Phys. Lett. **67B**, 271 (1977).
[5] J. van Klinken, W.Z. Venema, R.V.F. Janssens, and G.T. Emery, Nucl. Phys. **A339**, 189 (1980).
[6] N. Boos *et al.*, Phys. Rev. Lett. **72**, 2689 (1994).
[7] A.B. Hayes *et al.*, Phys. Rev. Lett. **89**, 242501 (2002).
[8] C.B. Collins *et al.*, Phys. Rev. Lett. **82**, 695 (1999).
[9] C.B. Collins *et al.*, Phys. Rev. C **61**, 054305 (2000).
[10] C.B. Collins *et al.*, Hyperfine Interact. **135**, 51 (2001).
[11] C.B. Collins *et al.*, Europhys. Lett. **57**, 677 (2002).
[12] I. Ahmad *et al.*, Phys. Rev. Lett. **87**, 072503 (2001).
[13] I. Ahmad *et al.*, Phys. Rev. C **67**, 041305(R) (2003).
[14] S.M. Mullins, G.D. Dracoulis, A.P. Byrne, T.R. McGoram, S. Bayer, W.A. Seale, and F.G. Kondev, Phys. Lett. B **393**, 279 (1997); **400**, 401(E) (1997).
[15] K.E. Thomas, Radiochimica Acta **34**, 135 (1983).
[16] C.E. Svensson *et al.*, Nucl. Instrum. Methods Phys. Res. B **204**, 660 (2003).
[17] G.F. Grinyer *et al.*, Phys. Rev. C **67**, 014302 (2003).
[18] D.C. Radford, Nucl. Instrum. Methods Phys. Res. A **361**, 297 (1995).
[19] B. Singh, Nucl. Data Sheets **75**, 199 (1995).
[20] J.B. Kim *et al.*, J. Radioanalytical and Nuc. Chem. **215**, 229 (1997).
[21] R. B. Firestone, *Table of Isotopes*, 8th ed. (Wiley, New York, 1996).
[22] S. A. Karamian *et al.*, in *Proceedings of International Conference on Heavy Ion Physics, Dubna, 1997* (World Scientific, Singapore, 1998), p. 565.
[23] G. T. Emery, R. V. F. Janssens, J. van Klinken, and W. Z. Venema, KVI Annual report, 1979 (unpublished).
[24] G. D. Dracoulis (private communication).
[25] P.M. Walker, G.D. Dracoulis, A.P. Byrne, B. Fabricius, T. Kibedi, A.E. Stuchbery, and N. Rowley, Nucl. Phys. **A568**, 397 (1994).
[26] K.E.G. Löbner, Phys. Lett. **26B**, 369 (1968).
[27] F. Rösel, H.M. Fries, K. Alder, and H.C. Pauli, At. Data Nucl. Data Tables **21**, 91 (1978).
[28] P.M. Walker *et al.*, Phys. Lett. B **408**, 42 (1997).
[29] P. Chowdhury *et al.*, Nucl. Phys. **A485**, 136 (1988).
[30] P.M. Walker *et al.*, Phys. Rev. Lett. **65**, 416 (1990).

Photon scattering experiments off ^{176}Hf and the systematics of low-lying dipole modes in the stable even-even Hf isotopes ^{176,178,180}Hf

M. Scheck,[1] D. Belic,[1,*] P. von Brentano,[2] J. J. Carroll,[3] C. Fransen,[2] A. Gade,[2] H. von Garrel,[1] U. Kneissl,[1] C. Kohstall,[1] A. Linnemann,[2] N. Pietralla,[2] H. H. Pitz,[1] F. Stedile,[1] R. Toman,[3] and V. Werner[2]

[1]*Institut für Strahlenphysik, Universität Stuttgart, D-70569 Stuttgart, Germany*

[2]*Institut für Kernphysik, Universität zu Köln, D-50937 Köln, Germany*

[3]*Department of Physics and Astronomy, Youngstown State University, Youngstown, Ohio 44555, USA*

(Received 15 April 2003; published 25 June 2003)

The low-lying dipole strength distribution in the rare isotope ^{176}Hf was studied in nuclear resonance fluorescence experiments performed at the Stuttgart Dynamitron facility using bremsstrahlung beams with endpoint energies of 4.1 and 2.4 MeV. In total, about 55 excited spin-1 states, unknown so far, were observed in the excitation energy range up to 4 MeV. Detailed spectroscopic information has been obtained on excitation energies, spins, decay widths, decay branchings, and transition probabilities. Ascribing a positive parity to all observed $K=1$ states, the detected total $B(M1)\uparrow$ strength in the energy range of the *scissors mode* amounts to 2.56(6) μ_N^2, nearly as much as for well-deformed midshell rare-earth nuclei. The total strength is higher than in the heavier Hf isotopes ^{178,180}Hf, but fits well into the systematics. The observed low-lying $\Delta K=0$ transitions (with probable $E1$ character) lie in the energy range around 2 MeV, as expected from the systematics. The excitation probabilities correspond to values which are characteristic for nuclei in the transitional region from deformed rotors to more γ-soft nuclei.

DOI: 10.1103/PhysRevC.67.064313 PACS number(s): 25.20.Dc, 21.10.Re, 23.20.Lv, 27.70.+q

I. INTRODUCTION AND MOTIVATION

Low-lying dipole excitations in heavy nuclei are of considerable interest in modern nuclear structure physics. Both $M1$ and $E1$ excitations were studied systematically to test nuclear models. An outstanding example is the so-called $M1$ *scissors mode* [1] to which most attention was paid in the past. This mode was first observed in high-resolution electron scattering experiments in Darmstadt [2]. A series of subsequent nuclear resonance fluorescence (NRF) experiments (see, e.g., Refs. [3,4]) established the systematics of this common mode in deformed even-even nuclei at excitation energies around 3 MeV. Starting from nearly spherical nuclei to well-deformed rare-earth isotopes, the observed total $B(M1)\uparrow$ strength increases proportional to the square of the deformation parameter δ. It reaches a saturation value of about 3 μ_N^2 for midshell rare-earth nuclei and decreases towards more γ-soft nuclei [5,6] of the platinum region. Whereas the shape transition from nearly spherical nuclei around $N=82$ to axially symmetric rotors is well studied, there are less data for isotopes within the transitional region to γ-soft nuclei. The stable even-even Hf isotopes ^{176,178,180}Hf lie at the edge of this shape transition. They still exhibit pronounced rotational bands with excitation energy ratios E_{4+}/E_{2+} of 3.28, 3.29, 3.31, respectively, near the value 10/3, as expected for ideal rotor nuclei. In addition, the quadrupole deformation parameters[1] β_2 of 0.295, 0.280, and 0.273 clearly substantiate the well-deformed shapes of the even-even Hf isotopes. However, in our previous study of ^{178,180}Hf [9] already less $M1$ strength than in midshell nuclei was detected. Therefore, one aim of the present study was to investigate the rare, lighter Hf isotope ^{176}Hf (relative natural abundance 5.206%) to pin down the impact of the onset of this shape transition on the dipole strength distribution. Furthermore, it was of interest to search for the lowest $E1$ transitions, which can be ascribed to octupole bandheads [10], whereas in spherical nuclei the strongest low-lying $E1$ excitations are two-phonon excitations [11] of the type $2^+ \otimes 3^-$.

II. NUCLEAR RESONANCE FLUORESCENCE

Photon scattering, often referred to as nuclear resonance fluorescence (NRF), has proven to be the most sensitive tool to study low-lying dipole excitations in heavy nuclei. Besides precise excitation energies E_x, width ratios Γ_0^2/Γ (with Γ_0 and Γ being the ground-state transition width and total width, respectively) can be deduced from the measured integrated scattering cross sections $I_{S,0}$. Angular distribution measurements provide information on the spins J of the photoexcited states. Parities can be determined by polarization measurements. All these quantities can be extracted in a model-independent way. For deformed nuclei, K quantum numbers can be assigned to the photoexcited states within the validity of the Alaga rules [12] from the measured branching ratios $R_{expt.}$,

*Present address: Agilent Technologies, D-71034 Böblingen, Germany.

[1]For the definitions of the slightly different deformation parameter δ and β_2 mainly used in the literature, see Refs. [3,7,8].

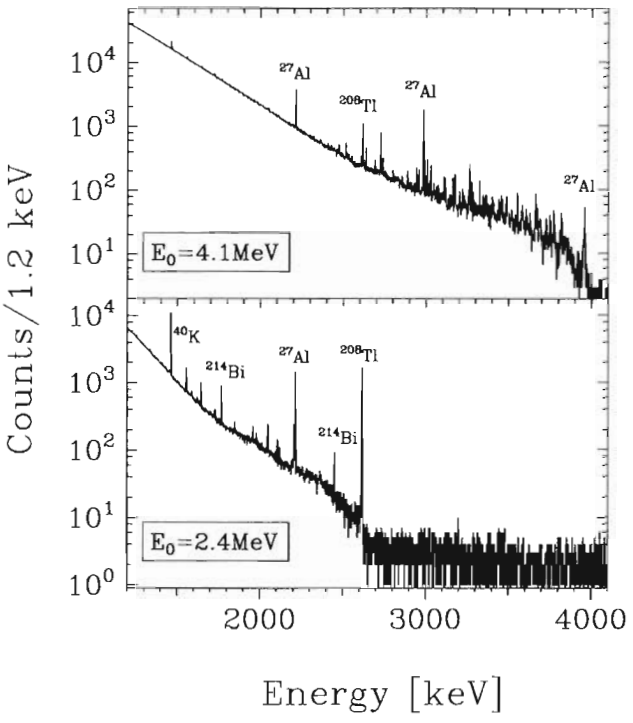

FIG. 1. Spectra of photons scattered off ^{176}Hf, measured at a scattering angle of 127° using bremsstrahlung beams of endpoint energies of 4.1 MeV (upper part) and 2.4 MeV (lower part), respectively. Calibration lines (^{27}Al), and background lines (mother activities: ^{40}K, ^{214}Bi, and ^{208}Tl) are marked (see text). Please note the logarithmic ordinate scale.

$$R_{expt.} = \frac{B(\Pi L; J \rightarrow J_f)}{B(\Pi L; J \rightarrow J_0)} = \frac{\Gamma_f}{\Gamma_0} \cdot \frac{E_{\gamma J_0}^3}{E_{\gamma J_f}^3}. \quad (1)$$

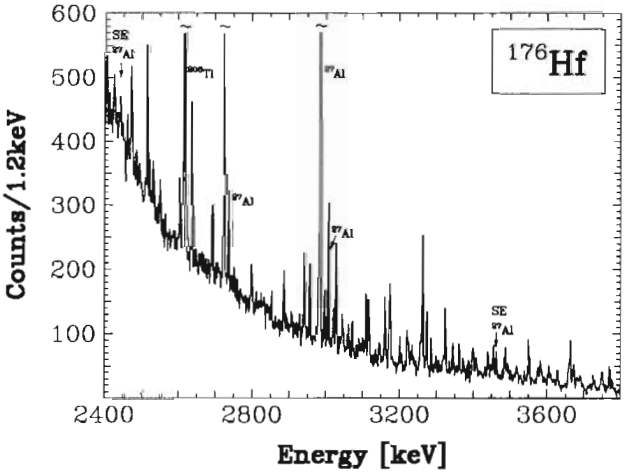

FIG. 2. Part of the ^{176}Hf(γ,γ') spectrum, measured at a scattering angle of 127° using a bremsstrahlung beam of an end point energy of 4.1 MeV (linear ordinate scale). The selected extended section covers the energy range where the scissors mode strength is expected. Calibration lines (^{27}Al) and background lines (^{208}Tl) are marked (see text).

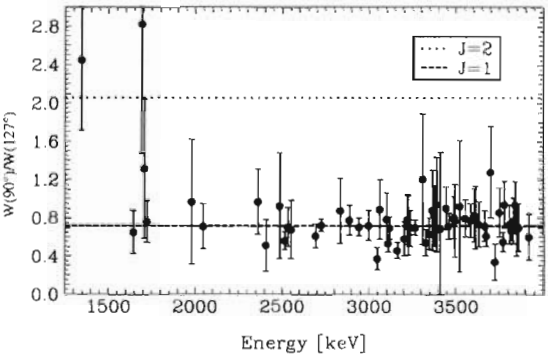

FIG. 3. Results of the angular distribution measurements. Plotted are the intensity ratios $W(\Theta=90°)/W(\Theta=127°)$ for the observed ground-state transitions. The dashed and dotted lines correspond to the values expected for pure dipole or quadrupole transitions, respectively (spin sequences 0-1-0 or 0-2-0).

The branching ratio for the decay of $J=1$ states to the first excited $J_f=2^+$ state and to the ground state ($J_0=0$) in deformed nuclei amounts to 2 or 1/2 for $\Delta K=0$ and $\Delta K=1$ transitions, respectively. The ground-state transition widths Γ_0 are directly related to the corresponding excitation probabilities $B(\Pi\,1)\uparrow$ and lifetimes $\tau=\hbar/\Gamma$. The formalism describing photon scattering experiments is summarized in more detail in Ref. [3].

III. EXPERIMENTAL DETAILS

The NRF experiments on ^{176}Hf were performed at the well-established Stuttgart bremsstrahlung facility [3]. Two measurements at bremsstrahlung endpoint energies of 4.1 and 2.4 MeV were carried out to achieve an optimal sensitivity over a broad range of excitation energies, and to enable the detection of weaker decay branchings. The dc electron currents used in the present experiments had to be limited, due to the thermal capacity of the radiator target, to about

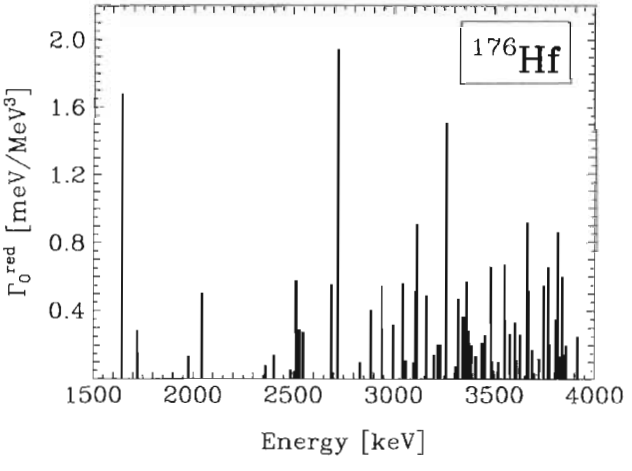

FIG. 4. Observed dipole strength distribution in ^{176}Hf. Plotted are the reduced dipole ground-state transition widths $\Gamma_0^{red} = \Gamma_0/E_\gamma^3$, which are proportional to the corresponding excitation probabilities $B(\Pi\,1)\uparrow$ (see text).

TABLE I. Numerical results for dipole excitations observed in the reaction ^{176}Hf (γ,γ'). Given are the excitation energies E_x, the integrated cross sections $I_{S,0}$, the ground-state transition widths Γ_0, the branching ratios $R_{expt.}$, the spins J and K quantum numbers of the photoexcited states, and the reduced ground-state transition widths Γ_0^{red}. In cases where parities could be assigned, the reduced excitation probabilities $B(M1)\uparrow$ or $B(E1)\uparrow$ are given, otherwise the reduced excitation probabilities are quoted for both parities ($E1$ and $M1$ multipolarities), see text.

E_x (keV)	$I_{S,0}$ (eV b)	Γ_0 (meV)	R_{expt}	J^π ($\hbar$)	K	Γ_0^{red} (meV/MeV^3)	$B(M1)\uparrow$ (μ_N^2)	$B(E1)\uparrow$ (10^{-3} e^2 fm^2)
1643	13.0(9)	7.5(4)	1.72(16)	1	0	1.68(8)		4.82(23)
1721	3.0(4)	1.5(2)	1.04(21)	1	(0)	0.29(3)		0.82(8)
1978	3.1(3)	1.1(1)		(1)		0.14(2)	0.036(4)	0.39(4)
2044	7.5(6)	4.3(3)	0.66(8)	1$^{(+)}$	1	0.50(3)	0.130(8)	
2361	3.8(7)	1.1(2)		(1)		0.08(2)	0.036(7)	0.40(7)
2405	4.0(6)	2.0(3)		1		0.14(2)	0.037(5)	0.41(6)
2484	2.6(6)	0.8(2)		(1)		0.05(1)	0.023(6)	0.26(6)
2514	12.6(12)	9.2(8)	0.37(9)	1$^{(+)}$	1	0.58(5)	0.150(13)	
2530	4.6(6)	4.7(5)	0.94(21)	1	(1)	0.29(3)	0.076(8)	
2548	3.8(7)	4.6(6)	1.27(31)	1	(0)	0.28(3)		0.80(10)
2690	8.9(9)	10.8(8)	1.04(15)	1	(0)	0.56(4)		1.59(12)
2722	43.3(33)	39.2(23)	0.45(5)	1$^{(+)}$	1	1.95(12)	0.504(30)	
2831	3.3(6)	2.3(4)		1		0.10(2)	0.026(5)	0.29(5)
2885	7.8(8)	9.7(8)	0.79(14)	1$^{(+)}$	1	0.40(4)	0.104(9)	
2940	13.7(12)	14.0(10)	0.40(7)	1$^{(+)}$	1	0.55(4)	0.143(10)	
2994	6.8(7)	8.5(7)	0.68(12)	1$^{(+)}$	1	0.32(3)	0.082(7)	
3044	6.2(8)	15.9(12)	2.40(37)	1$^{(-)}$	0	0.56(4)		1.61(12)
3059	3.9(6)	3.2(5)		1		0.11(2)	0.029(4)	0.32(5)
3098	3.5(6)	2.9(5)		(1)		0.10(2)	0.026(4)	0.28(5)
3107	12.4(11)	15.5(12)	0.53(9)	1$^{(+)}$	1	0.52(4)	0.134(10)	
3115	11.8(11)	27.6(17)	1.93(24)	1$^{(-)}$	0	0.91(6)		2.61(16)
3159	11.8(11)	15.4(12)	0.55(9)	1$^{(+)}$	1	0.49(4)	0.127(10)	
3200	5.3(7)	4.7(6)		1		0.14(2)	0.037(5)	0.41(6)
3218	7.6(9)	6.8(8)		1		0.21(2)	0.053(6)	0.59(7)
3222	4.1(7)	6.0(8)	0.66(18)	1$^{(+)}$	1	0.18(2)	0.046(6)	
3232	4.8(6)	7.0(8)	0.64(17)	1$^{(+)}$	1	0.21(3)	0.053(6)	
3261	33.1(26)	52.2(29)	0.77(9)	1$^{(+)}$	1	1.51(9)	0.390(22)	
3306	2.9(7)	2.8(7)		(1)		0.08(2)	0.020(5)	0.22(5)
3322	18.0(17)	17.3(17)		1		0.47(5)	0.122(12)	1.35(13)
3343	7.0(9)	13.7(14)	1.11(22)	1	(0)	0.37(4)		1.05(11)
3361	7.8(10)	21.7(16)	2.01(32)	1$^{(-)}$	0	0.57(4)		1.64(12)
3372	4.2(7)	10.9(11)	1.78(38)	1$^{(-)}$	0	0.29(3)		0.82(8)
3385	4.5(8)	7.8(10)	0.80(20)	1	(1)	0.20(3)	0.052(7)	
3406	5.3(9)	5.4(9)		(1)		0.14(2)	0.035(6)	0.39(6)
3438	8.5(10)	8.7(11)		1		0.22(3)	0.056(7)	0.62(8)
3454	10.4(12)	10.8(12)		1		0.26(3)	0.068(8)	0.75(8)
3485	11.5(16)	27.9(31)	1.40(31)	1	(0)	0.66(7)		1.89(21)
3490	4.3(11)	4.5(11)		1		0.11(3)	0.028(7)	0.30(8)
3519	4.2(13)	4.5(14)		(1)		0.10(3)	0.027(8)	0.30(9)
3550	19.0(23)	30.1(28)	0.48(8)	1$^{(+)}$	1	0.67(6)	0.174(16)	
3580	11.0(15)	12.2(17)		(1)		0.27(4)	0.069(10)	0.77(11)
3602	8.1(12)	15.6(18)	0.77(19)	1	(1)	0.33(4)	0.086(10)	
3608	4.9(11)	5.5(12)		1		0.12(3)	0.030(7)	0.34(7)
3627	7.0(10)	12.6(14)	0.61(15)	1$^{(+)}$	1	0.26(3)	0.068(8)	
3662	30.0(34)	45.3(42)	0.32(6)	1$^{(+)}$	1	0.92(9)	0.239(22)	
3671	15.6(15)	25.8(24)	0.44(10)	1$^{(+)}$	1	0.52(5)	0.135(12)	
3689	7.3(13)	8.6(15)		(1)		0.17(3)	0.045(8)	0.49(8)

TABLE I. (*Continued.*)

E_x (keV)	$I_{S,0}$ (eV b)	Γ_0 (meV)	R_{expt}	J^π ($\hbar$)	K	Γ_0^{red} (meV/MeV^3)	$B(M1)\uparrow$ (μ_N^2)	$B(E1)\uparrow$ (10^{-3} e^2 fm^2)
3722	5.2(10)	6.3(12)		(1)		0.12(2)	0.032(6)	0.35(7)
3746	13.4(18)	28.9(38)	0.84(23)	1	(1)	0.55(7)	0.143(19)	
3767	18.3(19)	35.0(29)	0.59(10)	1$^{(-)}$	1	0.66(5)	0.170(14)	
3774	9.2(12)	11.4(15)		1		0.21(3)	0.055(7)	0.61(8)
3805	10.3(13)	19.2(21)	0.52(12)	1$^{(-)}$	1	0.35(4)	0.090(10)	
3816	27.9(26)	47.9(39)	0.39(7)	1$^{(-)}$	1	0.86(7)	0.224(18)	
3824	5.9(11)	7.5(14)		(1)		0.14(3)	0.035(6)	0.39(7)
3838	10.6(15)	33.9(35)	1.61(33)	1$^{(-)}$	0	0.60(6)		1.72(18)
3844	6.3(12)	8.1(16)		(1)		0.14(3)	0.037(7)	0.41(8)
3856	8.8(16)	11.4(21)		(1)		0.20(4)	0.051(9)	0.57(10)
3916	11.5(19)	15.2(26)		(1)		0.25(4)	0.066(11)	0.73(12)

250 μA. The scattered photons were detected by three high-resolution Ge γ-ray detectors installed at angles of about 90°, 127°, and 150° with respect to the incoming bremsstrahlung beam. Each of the detectors had an efficiency of about 100% relative to a standard 7.6×7.6 cm^2 NaI(Tl) detector. The energy resolutions were typically about 2 keV at a photon energy of 1.3 MeV, and about 3 keV at 3 MeV. The detector at 127° was surrounded additionally by a BGO anti-Compton shield to improve its response function. With this arrangement the peak-to-background ratio could be improved by a factor of about 2.

The scattering target was sandwiched by ^{27}Al disks to provide the photon flux calibration [13]. A valuable metallic sample (total mass 1.764 g) was available, enriched to 77% in ^{176}Hf (relative natural abundance 5.206%) for the present experiments. The main impurity consisted of ^{177}Hf (11.5%). The residual impurities were ^{178}Hf (6.0%), ^{179}Hf (2.1%), and ^{180}Hf (3.5%). The excitations in the even-even isotopes ^{178,180}Hf were known from our previous NRF studies [9]. Excitations in ^{179}Hf can be neglected due to the very low abundance in the enriched target sample and the expected strength fragmentation in this odd-mass isotope. Excitations in ^{177}Hf, the main target impurity, can be distinguished, at least in principle, from those in ^{176}Hf due to the different angular distributions of the scattered photons and the different decay branchings in odd-mass and even-even nuclei (see Ref. [3]).

IV. RESULTS

Figure 1 shows the spectra of photons scattered off ^{176}Hf detected under a scattering angle of 127°. The spectrum depicted in the upper part was measured using a bremsstrahlung beam of an end point energy of 4.1 MeV. In the lower part the corresponding spectrum for an end point energy of 2.4 MeV is plotted. The photon flux calibration lines (^{27}Al) and the background lines stemming from natural environmental activities (mother activities: ^{40}K, ^{214}Bi, and ^{208}Tl) are marked in both spectra. All other peaks are ascribed to transitions in ^{176}Hf. The comparison between both spectra clearly documents the considerably enhanced peak-to-background ratio in the lower spectrum taken with a reduced end point energy of 2.4 MeV. This allows the detection and the identification of inelastic transitions, and hence the measurement of weaker decay branchings to lower-lying excited states with improved sensitivity.

In Fig. 2 an extended portion of the spectrum of scattered photons is depicted in the energy range where the scissors mode strength is expected from the systematics. A large number of peaks was well resolved and observed above the smooth continuous background. These peaks originate from the decay of the photoexcited states back to the ground state or to the first 2$^+$ state.

The spins of the observed photoexcited states can easily be assigned from the measured ratios of the intensities of scattered photons detected at scattering angles of 90° and 127°. In Fig. 3 the intensity ratios $W(\Theta=90°)/W(\Theta=127°)$ are plotted for the observed ground-state transitions. The dashed and dotted lines show the values expected for pure dipole or quadrupole cascades with spin sequences 0-1-0 and 0-2-0, respectively. Obviously, apart from some weaker excitations (with large uncertainties), all but two observed transitions are of dipole character, corresponding to spins $J=1$ of the excited states.

The dipole strength distribution detected in ^{176}Hf up to an excitation energy of 4 MeV is shown in Fig. 4. Plotted are the reduced ground-state transition widths $\Gamma_0^{red}=\Gamma_0/E_\gamma^3$ in the case of dipole transitions (excited states with $J=1$). These values are directly proportional to the reduced transition probabilities of interest, $B(E1)\uparrow$ or $B(M1)\uparrow$. For even-even nuclei a value of $\Gamma_0^{red}=1$ meV/MeV^3 corresponds to a $B(M1)\uparrow$ strength of 0.259 μ_N^2 or a $B(E1)\uparrow$ value of 2.866 $\times 10^{-3}$ e^2 fm^2. For $J=2$ states we define $\Gamma_0^{red}=\Gamma_0/E_\gamma^5$. For these quadrupole transitions a value of 1 meV/MeV^5 corresponds to a reduced excitation probability of $B(E2)\uparrow$ = 6225 e^2 fm^4.

The results obtained in the present experiment for dipole excitations are summarized in numerical form in Table I. The quoted quantities are the excitation energies E_x (with an estimated total uncertainty of $\leq$1 keV), the integrated scattering intensities $I_{S,0}$, the ground-state transition widths Γ_0, the

TABLE II. Numerical results for $E2$ excitations observed in the reaction ^{176}Hf (γ,γ'). Given are the excitation energies E_x, the integrated cross sections $I_{S,0}$, the ground-state transition widths Γ_0, the branching ratios $R_{expt.}$, the spins J and K quantum numbers of the photoexcited states, the reduced ground-state transition widths Γ_0^{red}, and the reduced excitation probabilities $B(E2)\uparrow$, see text.

E_x (keV)	$I_{S,0}$ (eV b)	Γ_0 (meV)	R_{expt}	J^π ($\hbar$)	K	Γ_0^{red} (meV/MeV^5)	$B(E2)\uparrow$ (e^2 fm^4)
1341	7.5(9)	1.4(1)	1.14(19)	2$^+$	2[a]	0.31(3)	1952(166)
1692	1.6(3)	0.2(1)		2$^+$		0.017(3)	106(21)
1704	1.7(3)	0.5(1)	1.1(1)[a]	2$^+$		0.035(4)	218(42)
2280	2.1(5)	1.0(2)	0.78(28)	(2)		0.016(3)	98(18)
3695	5.8(9)	4.1(6)		(2)		0.006(1)	37(6)

[a]Taken from literature [14].

branching ratios $R_{expt.}$, the reduced ground-state transition widths Γ_0^{red}, the assigned spins J and K quantum numbers. In the last two columns the reduced excitation widths $B(E1)\uparrow$ and $B(M1)\uparrow$ are given. In cases where no parity assignment was possible, the reduced excitation probabilities are quoted for both multipolarities ($E1$ and $M1$), as deduced from the measured reduced ground-state transition probabilities Γ_0^{red}. In Table II the same quantities are given for states where a spin $J=2$ state was assigned from the angular distribution measurements (quadrupole excitations).

V. DISCUSSION

Detailed spectroscopic information on about 55 spin-1 states in ^{176}Hf up to an excitation energy of 4 MeV has been obtained in the present experiments. Most of the levels were previously unknown. For the interpretation of these dipole excitations parity assignments are crucial, since in this low-energy range both magnetic and electric dipole excitations are expected. Besides the $M1$ scissors mode excitations, enhanced $E1$ transitions to the octupole bandheads should occur [10]. Unfortunately, explicit parity determinations using the Stuttgart Compton polarimeter could not be performed in reasonable running times due to the low scattering cross sections and the small available amount of enriched target material. Therefore, for the interpretation we apply an empirical rule of thumb to tentatively assign parities to the observed spin-1 levels. As verified in our numerous NRF experiments [3,9] on deformed nuclei, all stronger $\Delta K=1$ excitations were of magnetic character, whereas $\Delta K=0$ excitations were $E1$ transitions. The K quantum numbers of the photoexcited states can be determined from the measured decay branching ratios $R_{expt.}$ within the validity of the Alaga rules. Several spin-1 states exhibit $R_{expt.}$ values which, however, disagree with the Alaga rules indicating some K mixing. Tentative parity assignments are made if the decay branching ratios match reasonably close to the Alaga rules, and are indicated in Table I by parity assignments given in parentheses. For the following discussion we assume that states which exhibit a decay branching $R_{expt.}\leq 1$, corresponding to $K=1$ levels, should have spin and parity $J^\pi=1^+$, and levels with $R_{expt.}\geq 1$ have quantum numbers $J^\pi=1^-$ and $K=0$.

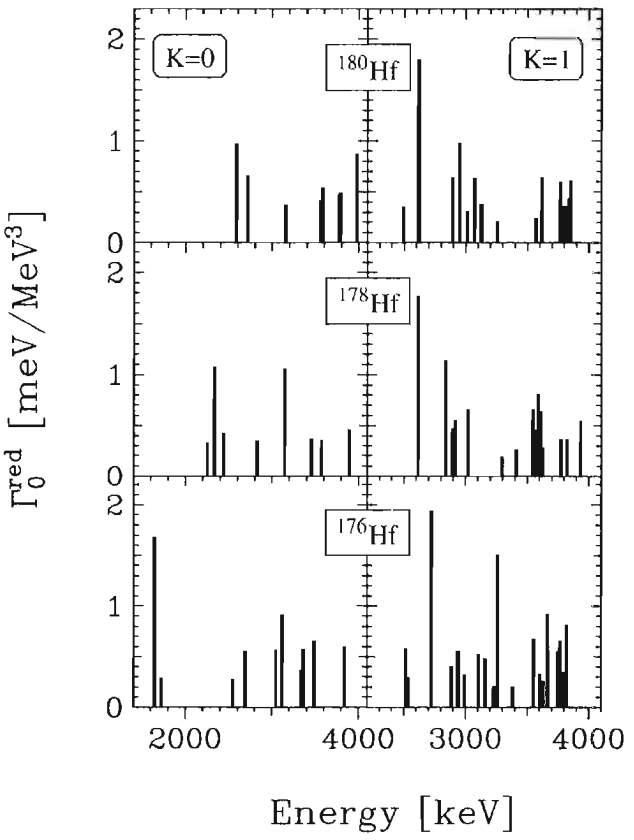

FIG. 5. Systematics of observed dipole strength distributions in ^{180,178,176}Hf. Plotted are the reduced dipole ground-state transition widths $\Gamma_0^{red}=\Gamma_0/E_\gamma^3$, which are proportional to the corresponding excitation probabilities $B(\Pi 1)\uparrow$. Left part: $K=0$ states. Right part: $K=1$ states.

In Fig. 5 the dipole strength distribution in ^{176}Hf observed in the present experiments is compared to the results of our previous studies on the heavier isotopes ^{178,180}Hf [9]. Plotted in each case are the reduced transition widths Γ_0^{red} as a function of the excitation energy, separately for $K=0$ levels (left part) and $K=1$ states (right part). According to the empirical rule discussed above, negative parities were ascribed to $K=0$ states and vice versa, positive parities to $K=1$ levels.

The $M1$ strength observed in ^{176}Hf is somewhat more fragmented than in ^{178,180}Hf. However, the distribution patterns look quite similar in all even-even Hf isotopes, with a strong excitation near 2.7 MeV and two strength concentrations at 3.0 and 3.7 MeV, respectively. Ascribing to all observed $K=1$ states a positive parity, the detected total $B(M1)\uparrow$ strength in the energy range of the scissors mode (here 2.4–3.7 MeV) amounts to 2.56(6) μ_N^2, nearly the same as for midshell rare-earth nuclei [3,4] but higher than that observed in ^{178,180}Hf [9]. The total $M1$ strength in ^{176}Hf fits well into the systematics. This can be seen in Fig. 6. Here the total $B(M1)\uparrow$ values measured in even-even nuclei are plotted as a function of the neutron number in the region of the neutron shell $N=82$–126. The data for the Hf isotopes are shown by filled triangles. The total $M1$ strengths ob-

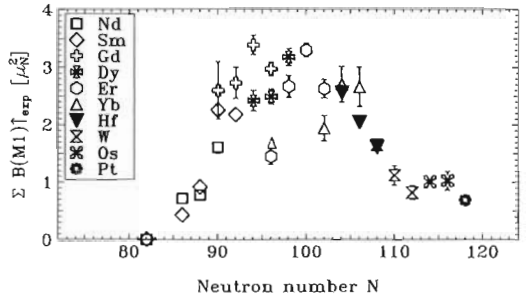

FIG. 6. Systematics of the total $B(M1)\uparrow$ strengths observed in even-even nuclei as a function of the neutron number (see Refs. [3,4]). The results for the Hf isotopes ^{176,178,180}Hf are shown by filled symbols.

served for the Hf isotopes, furthermore, are in good agreement with sum rule predictions [15]. The drop of the $M1$ strength at mass number $A \approx 180$ indicates the start of the shape transition region towards γ-soft nuclei at $A \approx 196$.

Also, the strength pattern for the excitation of $K=0$ states ($E1$ transitions) exhibits a smooth systematics. The excitation energies shift to higher energies with increasing mass number A (see left part of Fig. 5). In Fig. 7 the excitation energies of the lowest 1^- states in even-even nuclei in the mass range $A=130$–200 are plotted. For rotational nuclei, we consider the lowest 1^- states with $K=0$. Near the $N=82$ shell closure ($A \approx 140$), the $E1$ excitations in these spherical nuclei are known to be two-phonon excitations of the type $2^+ \otimes 3^-$ [11]. These excitations have rather high excitation energies of 3.5–4 MeV, which decrease going away from the shell closure [11]. In most deformed nuclei

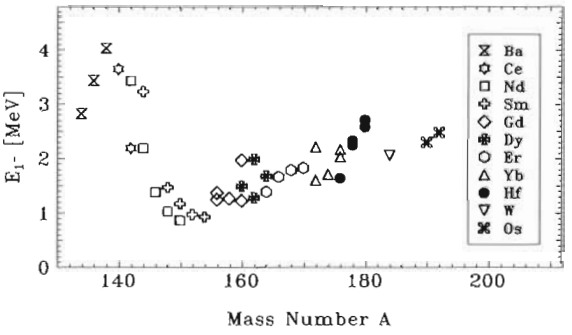

FIG. 7. Systematics of the excitation energies of the lowest observed $J^\pi = 1^-$ states in even-even nuclei of the $N=82$–126 shell as a function of the mass number A. The data for ^{176,178,180}Hf are emphasized by filled symbols, according to Ref. [10].

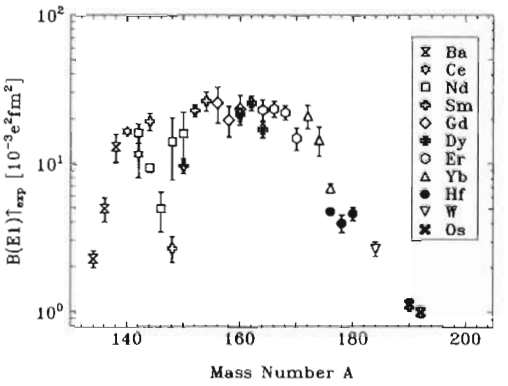

FIG. 8. Systematics of the reduced electric dipole excitation strengths $B(E1)\uparrow$ of the lowest (or lowest two) observed $J^\pi = 1^-$ states in even-even nuclei of the $N=82$–126 shell as a function of the mass number A. The data for ^{176,178,180}Hf are emphasized by filled symbols, according to Ref. [10].

the lowest $E1$ excitations correspond to transitions to the 1^- bandhead of the lowest $K=0$ octupole band [10]. The Hf data shown by filled symbols fit nicely into this systematics.

The $E1$ strengths of the lowest 1^- states are summarized in Fig. 8. High $B(E1)\uparrow$ values of about $20\times10^{-3}\ e^2\ \mathrm{fm}^2$ were observed for the $2^+ \otimes 3^-$ two-phonon excitations in spherical semimagic nuclei around $A=140$ and for transitions to the octupole bandheads in deformed midshell rotor nuclei. In between, around $A=146$, a remarkable reduction of the strengths is observed (for a detailed discussion, see Ref. [10]). An even more pronounced reduction is evident for nuclei in the mass region of a shape transition from well-deformed rotors to more γ-soft nuclei. Already for the isotopes ^{190,192}Os only very weak, nearly negligible low-lying $E1$ strength could be detected [16]. The data obtained for the Hf isotopes, shown in Fig. 8 by filled symbols, confirm this nearly linear $E1$ strength reduction with increasing mass number A. It is not yet understood how the apparent reduction of $E1$ strengths is linked to the shape transition. Comparison of Fig. 8 (logarithmic scale) and Fig. 6 yields an obviously different behavior of the $E1$ and $M1$ strength distributions as a function of the shape transition path.

ACKNOWLEDGMENTS

The financial support of the Stuttgart projects by the Deutsche Forschungsgemeinschaft (DFG) under Contract Nos. Kn154/30,31, Br799/11-1, Pi393/1-2, and by the U.S. AFOSR under Contract Nos. F49020-99-1-0262 and F49020-99-1-0263 is gratefully acknowledged.

[1] N. Lo Iudice and F. Palumbo, Phys. Rev. Lett. **41**, 1532 (1978).
[2] D. Bohle, A. Richter, W. Steffen, A.E.L. Dieperink, N. Lo Iudice, F. Palumbo, and O. Scholten, Phys. Lett. **137B**, 27 (1984).
[3] U. Kneissl, H.H. Pitz, and A. Zilges, Prog. Part. Nucl. Phys. **37**, 349 (1996).
[4] N. Pietralla, P. von Brentano, R.-D. Herzberg, U. Kneissl, J. Margraf, H. Maser, H.H. Pitz, and A. Zilges, Phys. Rev. C **52**, R2317 (1995).
[5] P. von Brentano, J. Eberth, J. Enders, L. Esser, R.-D. Herzberg, N. Huxel, H. Meise, P. von Neumann-Cosel, N. Nicolay, N. Pietralla, H. Prade, J. Reif, A. Richter, C. Schlegel, R. Schwengner, S. Skoda, H.G. Thomas, I. Wiedenhöver, G. Winter, and A. Zilges, Phys. Rev. Lett. **76**, 2029 (1996).

[6] A. Linnemann, P. von Brentano, J. Eberth, J. Enders, A. Fitzler, C. Fransen, E. Guliyev, R.-D. Herzberg, L. Käubler, A.A. Kuliev, P. von Neumann-Cosel, N. Pietralla, H. Prade, A. Richter, R. Schwengner, H.G. Thomas, P. Weisshaar, and I. Wiedenhöver, Phys. Lett. B **554**, 15 (2003).

[7] K.E.G. Löbner, M. Vetter, and V. Hönig, Nucl. Data, Sect. A **7**, 495 (1970).

[8] S. Raman, C.H. Malarkey, W.T. Milner, C.W. Nestor, Jr., and P.H. Stelson, At. Data Nucl. Data Tables **36**, 1 (1987).

[9] N. Pietralla, O. Beck, J. Besserer, P. von Brentano, T. Eckert, R. Fischer, C. Fransen, R.-D. Herzberg, D. Jäger, R.V. Jolos, U. Kneissl, B. Krischok, J. Margraf, H. Maser, A. Nord, H.H. Pitz, M. Rittner, A. Schiller, and A. Zilges, Nucl. Phys. **A618**, 141 (1997).

[10] C. Fransen, O. Beck, P. von Brentano, T. Eckert, R.-D. Herzberg, U. Kneissl, H. Maser, A. Nord, N. Pietralla, H.H. Pitz, and A. Zilges, Phys. Rev. C **57**, 129 (1998).

[11] W. Andrejtscheff, C. Kohstall, P. von Brentano, C. Fransen, U. Kneissl, N. Pietralla, and H.H. Pitz, Phys. Lett. B **506**, 239 (2001).

[12] G. Alaga, K. Alder, A. Bohr, and B.R. Mottelson, K. Dan. Vidensk. Selsk. Mat. Fys. Medd. **29**, 1 (1955).

[13] N. Pietralla, I. Bauske, O. Beck, P. von Brentano, W. Geiger, R.-D. Herzberg, U. Kneissl, J. Margraf, H. Maser, H.H. Pitz, and A. Zilges, Phys. Rev. C **51**, 1021 (1995).

[14] E. Browne and Huo Junde, Nucl. Data Sheets **84**, 337 (1998).

[15] N. Lo Iudice and A. Richter, Phys. Lett. B **304**, 193 (1993).

[16] C. Fransen, B. Krischok, O. Beck, J. Besserer, P. von Brentano, T. Eckert, R.-D. Herzberg, U. Kneissl, J. Margraf, H. Maser, A. Nord, N. Pietralla, H.H. Pitz, and A. Zilges, Phys. Rev. C **59**, 2264 (1999).

Hyperfine Interactions **143:** 37–54, 2002.

Initial Search for Triggered Gamma Emission from $^{178}Hf^{m2}$ Using the YSU Miniball Array

J. J. CARROLL[1], J. BURNETT[1], T. DRUMMOND[1], J. LEPAK[1], R. PROPRI[1], D. SMITH[1], S. A. KARAMIAN[2], J. ADAM[2], F. STEDILE[3] and F. J. AGEE[4]

[1] *Department of Physics and Astronomy, Center for Photon-Induced Processes, Youngstown State University, Youngstown, Ohio 44555, USA*

[2] *Joint Institute for Nuclear Research, Dubna, Moscow Region 141980, Russia*

[3] *Institut für Strahlenphysik, Universität Stuttgart, D-70569 Stuttgart, Germany*

[4] *Air Force Office of Scientific Research, AFOSR/NE, 4015 Wilson Blvd., Arlington, VA 22203, USA*

Abstract. Experiments with the long-lived, high-K isomer $^{178}Hf^{m2}$ have been recognized as intriguing tests of multi-quasiparticle state structures and their interactions with external radiation. A triggered release of the energy stored by this isomer, 2.5 MeV per nucleus or 1.2 GJ/gram, in the form of a gamma-ray burst might prove valuable for numerous applications. The observation of "accelerated" decay of $^{178}Hf^{m2}$ during irradiation by 90-keV bremsstrahlung has already been reported, but with poor statistical accuracy due to the experimental approach. That approach employed single Ge detectors to seek increases in the areas of peaks at energies corresponding to transitions in the spontaneous decay of the isomer. The need for better quality data to confirm those results has motivated the development of improved detection concepts. One such concept was utilized here to perform an initial search for low-energy (<20 keV) triggered gamma emission from $^{178}Hf^{m2}$ using the YSU miniball detector array.

Key words: triggered gamma emission, $^{178}Hf^{m2}$, nuclear batteries, multidetector systems.

1. Introduction

Even without coherence or directionality, a controlled release of nuclear energy in the form of gamma-ray bursts would be interesting from a physical perspective and perhaps useful in numerous applications [1, 2]. The amounts of energy that may be stored within nuclei, and are capable of being released as pure electromagnetic emission, can reach tremendous levels. When concentrated into a macroscopic sample, some long-lived nuclear excited states (*isomers*) can store orders-of-magnitude more energy per gram than that available from chemical compounds and may release that energy "cleanly", without the direct production of radioactive by-products. The 31-year isomer of ^{178}Hf lies at an excitation energy of 2.445 MeV, corresponding to an energy density of 1.2 gigaJoules per gram. If an X-ray pulse triggered all of these Hf isomers within a 1-g sample and all the stored energy was released during 1 ns, this would produce a 1-exaWatt (10^{18} Watts) gamma-ray flash. Perhaps even more impressive, the radiation flash would provide in excess of

40 krad/s through 4 inches of Pb (a brick) and at a distance of 100 m. Such isomeric nuclei are equivalent to nuclear batteries and one can speculate on their value, such as in producing a gamma-ray flash to cleanse an environment of biohazards. With such pure and applied physics motivations, there has been considerable research over the past few decades into how such control might be effected and which nuclides would provide the optimal materials [3].

The most obvious form of control is simply to be able to turn on, or at least enhance, the emission of gamma rays [4], effectively providing the ability to modify the lifetime of nuclear excited states [5–8]. One of the most promising approaches has been to employ externally-produced X-rays as a means of triggering the emission of gamma radiation [4] and many experiments over the past decade on control of gamma emission have focused on this idea. The use of X-rays was first proposed in 1974 [9] as a possible way to circumvent technological challenges to the creation of a gamma-ray laser. Some attractive features of X-rays are that they may be produced in significant fluxes by modest-sized devices, they may be shielded relatively easily, and unused incident photons and some emitted gamma rays might be "recycled" by Compton scattering and X-ray fluorescence to produce additional triggering. The present focus is therefore on X-ray driven gamma emission, sometimes called triggered gamma emission, to release upon demand the energy stored in nuclear isomers.

Isomers are commonly found to exist in many different nuclides, with a wide range of stored energies and halflives. Several physical mechanisms may provide isomerism [10, 11] and, in principle, several isomers may arise at different excitation energies within the same nucleus due to different mechanisms. For triggered gamma emission, the major focus has been on isomers that are sufficiently long-lived to permit their accumulation in appreciable amounts (that is, have a reasonable shelf-life): two examples are $^{178}Hf^{m2}$ and $^{180}Ta^{m}$, with halflives of 31 years and greater than 10^{15} years, respectively. In the most important cases, isomerism is due to angular momentum considerations. As one would expect for atomic electromagnetic transitions, the rate of nuclear gamma decay of an excited state is related to the energy and change of the angular momentum vector for the de-excitation transition. In nuclei, magnetic dipole transitions are the most common and higher-multipolarity electric and magnetic transitions occur, giving some excited states significant lifetimes. Such a *spin isomer* is $^{180}Ta^{m}$, where the long-lived state ($T_{1/2} > 10^{15}$ years) at 75 keV requires an M8 transition for its gamma decay. Additionally, many nuclei have axially symmetric deformed shapes and so it becomes possible to define the relative orientation of the angular momentum vector, designated by a new quantum number K. Electromagnetic transitions that require a change of K greater than the change of total angular momentum are further hindered, leading to enhanced isomerism. For $^{178}Hf^{m2}$, the 31-year isomer occurs mainly through an E3 transition that requires an excess of $\Delta K - \Delta L = 5$ – this is an archetype K isomer.

The identification of prime isomers for study and potential applications relies on a complex weighting of factors. At present thirty-two isomers are known possessing halflives greater than 3 days [3] and other long-lived metastables may eventually be found in searches for "extreme K isomers" [11]. Three parameters are especially important in considering the overall potential value of an isomer: the excitation energy of the state, its halflife, and the cross section for potential mass production by neutron capture (thus allowing reactor use). Clearly ^{178}Hf is one of the most interesting isomers from the perspective of energy storage with its 31-year, 2.445-MeV (m2) isomer, although the ability to mass produce it remains a question at this moment. Also, $^{178}Hf^{m2}$ may be useful in a pure gamma-burst application (having a stable ground state). The greatest emphasis of current research is on testing triggered emission of gamma radiation from this isomer.

2. Trigger model and $^{178}Hf^{m2}$

Studies of X-ray triggered gamma emission bear a striking similarity to decades-old research into the excitation of nuclear states, including isomers, by absorption of photons [12, 13]. Both occur through the two-step process depicted schematically in Figure 1. A nucleus is in a specific initial state that could be an isomer (to be triggered) or a ground state (as in traditional experiments), and is excited to reach an intermediate state by absorption of an incident photon. The intermediate state is necessitated by the angular momentum considerations – direct electromagnetic transitions between initial and final states are unlikely, or the upper of the two states would not be isomeric. The mediating level must therefore possess values of J (and perhaps K) intermediate between those of initial and final states. In the second step, the intermediate state decays with some branch leading, usually by a multiple-step gamma cascade, to the final state. The measurable parameters of the reaction are the excitation energy of the intermediate state from the initial level and the integral cross section, or ICS, for the overall initial-to-intermediate-to-final-state transfer.

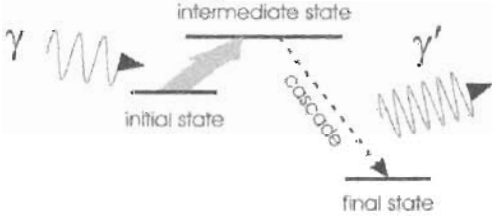

Figure 1. Schematic diagram showing the general process of X-ray driven (triggered) gamma emission if the initial state is an isomer and final state is the ground state. Equivalently, the diagram also represents photoexcitation if the roles (and energy positions) of the initial and final states are reversed. The γ corresponds to the incident photon that initiates the process while the γ' represents all the photons emitted during the cascade from intermediate state to final state.

Typical experiments for photoexcitation require intense irradiations using photon energies up to several MeV, so electron accelerators for bremsstrahlung production have been the most utilized. For triggering at low energies (less than about 200 keV), synchrotron radiation is becoming more valuable. In either case, if the irradiating spectrum is significantly broader than the absorption resonance that begins the process of Figure 1, the ICS is measured instead of the peak value of the Lorentzian cross section. The ICS gives the efficiency of the process and may be deduced from the final-state yield, N_f, according to

$$\mathrm{ICS}_{\mathrm{abs-meas}} = \frac{N_f}{N_T(\mathrm{d}\Phi/\mathrm{d}E)}, \tag{1}$$

where N_T is the number of target nuclei in the initial state being irradiated by photons having the spectral flux density (flux per energy interval) $\mathrm{d}\Phi/\mathrm{d}E$ at the absorption energy. It is then possible to relate the ICS (often expressed in cm^2 MeV or eV b) to the reduced transition probability, $B(EL; ML)$, according to standard formulations [14].

Triggered gamma emission has only been conclusively demonstrated for the isomer of ^{180}Ta. This metastable is of considerable interest for basic studies related to nuclear structure and astrophysical creation/destruction, but not particularly from the view of potential applications: the lowest-lying trigger level requires excitation by incident photons of about 1 MeV [15] while the isomer only stores 75 keV. The main reason that triggering of this isomer has been investigated for more than a decade is that experiments can be done in a relatively straightforward manner.

Experimentally, the main issue is how to tell if triggered gamma emission has occurred in detectable amounts. There are a limited number of general methods that can be utilized for the detection of triggered events and determination of the final-state yield:

1. Detection out-of-beam of short-lived products following triggering of a "stable" (extremely long-lived) isomer – so-called activation method,
2. Detection in-beam of an intensity enhancement of spontaneous decay radiation driven by the external irradiation,
3. Detection in-beam of a new gamma line corresponding to the triggering process that does not appear in the spontaneous decay of the isomer,
4. Detection in-beam of a unique gamma-ray cascade due to triggering that is significantly different from the spontaneous-decay cascade,
5. Detection out-of-beam of a loss in isomer activity as a result of "burn-up" of part of the metastable population during an intense irradiation, and
6. Detection in- or out-of-beam of an intensity enhancement in the equilibrium daughter radiation after "burning" an isomer to a radioactive state.

Early on, it was realized that the first (activation) method could be applied to study of $^{180}\mathrm{Ta}^{\mathrm{m}}$ since it is so long-lived ($T_{1/2} > 10^{15}$ years) and since its unstable ground state has a halflife of merely 8.2 hours. Any evidence of ground-state daughter radiation after exposure of a sample would clearly signal triggering (since

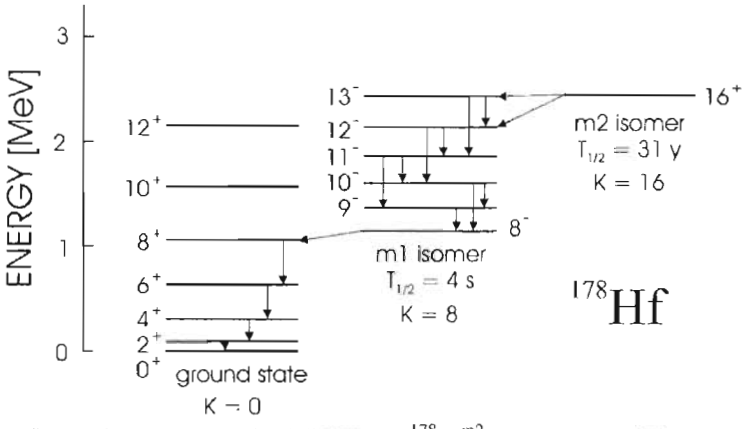

Figure 2. Schematic partial energy-level diagram for $^{178}Hf^{m2}$. The downward arrows show transitions that are part of the spontaneous decay cascade of the 31-year isomer, which is delayed upon reaching the 4-s isomer.

no daughter radiation is present otherwise). Also, macroscopic samples with gram sizes were available, meaning that even with a natural abundance of 0.012% significant numbers of target isomers were irradiated. With the possibility for off-line (post-irradiation) detection, depletion of $^{180}Ta^{m}$ due to triggered gamma emission was first demonstrated in 1987 [16]. Later, in-depth studies identified and characterized a number of trigger (intermediate) levels [17–20]. Although the large magnitudes of measured ICS were initially of concern, the later studies showed that they were indeed in general agreement with nuclear systematics [21]. The experimental situation with $^{178}Hf^{m2}$ is, unfortunately, more difficult.

The isomer $^{178}Hf^{m2}$ is not naturally occurring and at present is not available in amounts larger than about 10^{16} atoms in the metastable state. The ground state of ^{178}Hf is stable, as shown in the partial energy-level diagram of Figure 2 and additionally the 31-year halflife leads to a significant specific gamma-ray activity. Finally, the available samples contain ^{172}Hf as a production by-product (contaminant) at an activity that is presently nearly equivalent to that from $^{178}Hf^{m2}$. Taken together, these factors pose a much greater experimental challenge than that for studies of $^{180}Ta^{m}$.

It was first recognized in 1995 [22, 23] that experimental systematics for the photoexcitation of neighboring isomeric nuclei indicated that it might be possible to trigger gamma emission from $^{178}Hf^{m2}$ using incident X-rays having energies on the order of 300 keV or less. The first test of this idea was conducted in 1998 [5, 24] using a dental X-ray device to irradiate a sample containing 6×10^{14} $^{178}Hf^{m2}$ atoms and an HPGe detector was employed to acquire pulse-height gamma spectra during irradiations. A comparison of the gamma spectra obtained during irradiation with that obtained for an equivalent live time without irradiation suggested that some gamma rays corresponding to the spontaneous decay cascade were emitted more

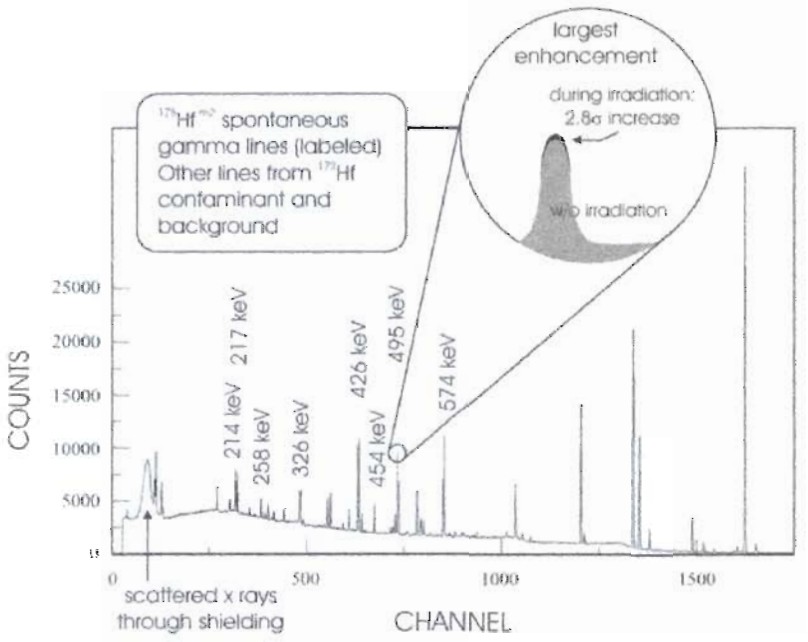

Figure 3. Pulse-height spectrum from an isomeric ^{178}Hf target obtained during irradiation with a dental X-ray device. The "zoom" depicts the largest enhancement observed in the experiment of [5], about 2.8σ for the 495-keV line.

frequently during the irradiations. That is, the corresponding peaks in the gamma spectrum increased in size (area) by small amounts that nevertheless suggested a rather large effect. The ICS was estimated to be about 10^6 eV b, considerably larger than that which would be expected based on established nuclear systematics [25–28]. The trigger energy was estimated to be about 40 keV in [5] and later revised to approximately 10 keV [29–33].

Figure 3 shows a pulse-height gamma spectrum observed in the experiment of [5]. The experiment was conducted applying the second approach mentioned above and clearly the results, despite being quite intriguing, suffer from poor statistics. The same degree of statistical uncertainty plagued other work conducted with bremsstrahlung sources [29–33] and even an upcoming publication [34] that employed monochromatized synchrotron radiation to test triggering. The difficulty lies in the possible presence of a small excess of gamma emission at energies corresponding to some of the spontaneous decay transitions. It can be expected that at least some of the spontaneous decay transitions will be part of a triggered cascade since all paths must eventually lead to the ground state through the lower part of the ground-state band. Therefore, an excess of counts may appear superimposed upon peaks of considerable size from the spontaneous decay activity, leading to

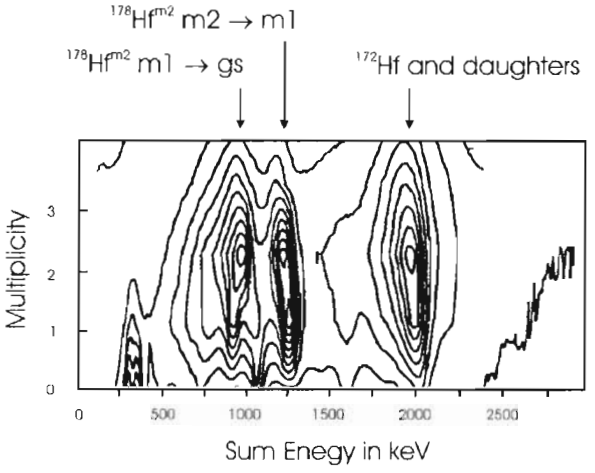

Figure 4. Sum-energy versus multiplicity in a bi-dimensional spectrum of gamma rays from a $^{178}Hf^{m2}$ sample (with contaminating ^{172}Hf) measured with the Darmstadt–Heidelberg crystal ball. The figure is reproduced in part from [36] by permission.

a large absolute uncertainty in the magnitude of any excess. If some of the same electromagnetic transitions participate from both triggering and natural decays, it is not possible to separate the two types of events using a single detector which only records the numbers of incident gamma rays and their individual energies.

A method that differentiates between triggered and spontaneous events, and gammas from the contaminating ^{172}Hf, was proposed in [35]. The concept hinges on a "natural gift" in ^{178}Hf of the 4-s m1 isomer, which delays the spontaneous decay cascade from the 31-year m2 isomer at an energy of 1.147 MeV. As seen in Figure 2, all electromagnetic decays are collective M1 or E2 transitions within bands except for those that depart from the two isomers. The lifetimes of the collective transitions are very short and so a natural decay from $^{178}Hf^{m2}$ leads to two bursts of closely coincident gamma rays. The upper part of the cascade, leading from m2 to m1, provides a total energy of 1.271 MeV and an average multiplicity (number of emitted gammas) of about 5 as seen from Figure 2. Likewise, the lower part of the cascade, leading from m1 to the ground state, releases a total energy of 1.147 MeV and has a multiplicity of exactly 5. It was proposed [35] that at least some branch of triggered decay will by-pass the m1 level, emitting a total of 2.445 MeV + trigger energy in a burst that is at most retarded by passing through the short-lived isomer at 1.554 MeV ($T_{1/2}$ = 77.5 ns, not shown in the figure). Thus, these triggered events will be distinguishable through the high sum energy of their gamma bursts and through their much higher multiplicity (perhaps more than 8, as needed to rid the nucleus of its total angular momentum of $\sim$ 16 in steps of 1 or 2). Decays of ^{172}Hf and its daughters lead to a sum energy of about 2 MeV and should be distinguishable from triggered decay of $^{178}Hf^{m2}$.

Since no naturally-occurring events produce such high (2.445 MeV +) energy events in coincident gamma rays, any triggered events detected with this value will appear superimposed on a zero background, leading to greatly improved statistical accuracy. A multi-detector array has already been used [36] to examine $^{178}Hf^{m2}$ in unrelated experiments and it was indeed possible to find the loci of data corresponding to the broken spontaneous decay cascade as shown in Figure 4.

3. Detection system

The experiment of Ref. [36] employed a multi-detector array of high intrinsic and geometric efficiency, the Darmstadt–Heidelberg crystal ball. For triggering experiments, that approach was modeled here on a smaller scale by the YSU miniball array. The miniball consisted of six 3″ × 3″ right-circular NaI detectors arranged to cover approximately 80% of 4π solid angle in the housing shown in Figure 5. Samples were suspended in the center and incident photons injected along one of the diagonals of the cubic housing. Unused flux exited that housing diagonal toward a beam dump. One 10% HPGe detector was used in the system and observed the samples through a gap between NaI scintillators along a different diagonal of the housing. To minimize the amount of Compton-scattered photons reaching the detectors, 1 mm Pb filters were placed over their end faces and their cylindrical surfaces were wrapped in several mm of lead to reduce environmental scattering from the beam dump.

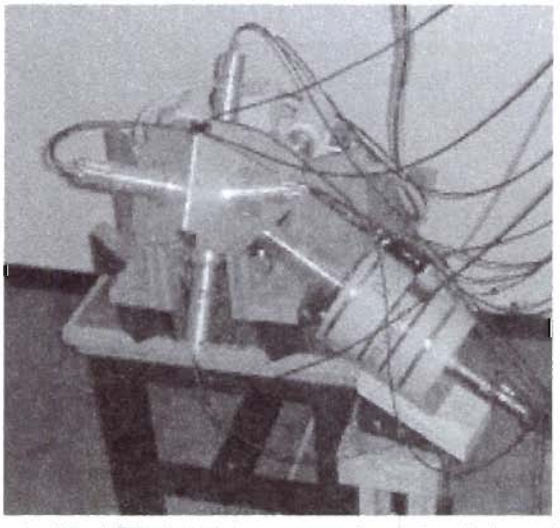

Figure 5. Photograph of the YSU miniball detector array for studies of triggered gamma emission from $^{178}Hf^{m2}$. The cubical housing holds the NaI and the Ge views the sample through a diagonal. Behind the miniball is the bremsstrahlung source used in this experiment.

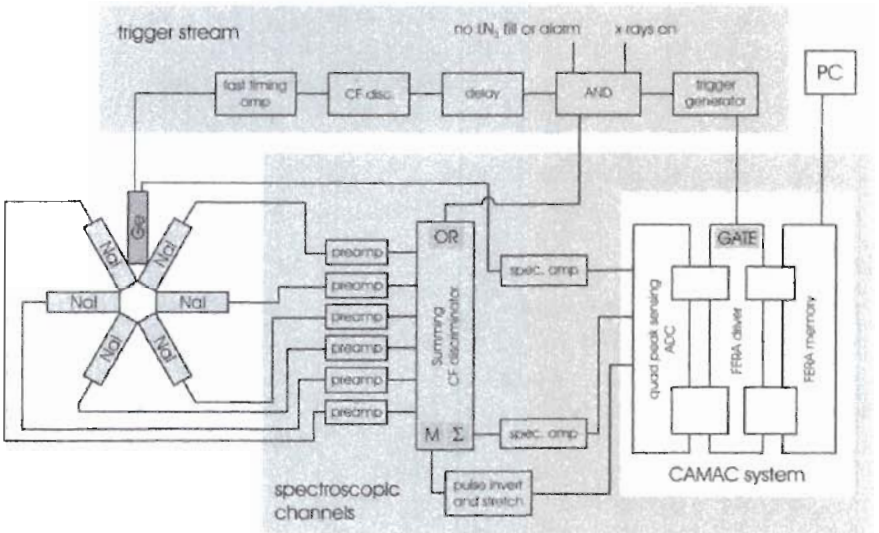

Figure 6. Schematic diagram of the data-acquisition electronics.

A branch of triggered events should produce high sum-energy cascades that include transitions in the lower part of the ground-state band (such as 93, 213 and 325 keV). For this reason, the Ge detector was used to measure the energy of one gamma ray in each burst with high precision (due to its excellent resolution) and to initiate the DAQ trigger stream. The data-acquisition system is shown schematically in Figure 6. A number of logical conditions were satisfied to generate an electronic trigger (gate) that caused a gamma burst to be recorded. In this system, using a pulsed bremsstrahlung source, these conditions were:

1. A gamma ray must be detected by the Ge and its energy must be greater than a chosen threshold.
2. X-rays must be incident on the sample (for beam-on measurements).
3. No error conditions are present (like a warm detector or a LN_2 autofill cycle in operation).
4. At least one of the miniball NaI must receive a gamma ray in coincidence with the Ge signal and the NaI gamma ray must have an energy greater than a chosen threshold.

The first condition was implemented using NIM logic from a constant-fraction (CF) discriminator, after processing the Ge signal with a fast (timing) filter amplifier. NaI signals were preamplified for impedence matching, then fed into separate channels of an Ortec CF8000 octal CF discriminator. NIM logic from the six active CF8000 channels were combined as an AND with the Ge logic signal. The logical output of the AND was of fixed width, initiated whenever the Ge and one or more NaI signals overlapped by at least 3 ns. This provided the fourth condition but

without imposition of good coincidence since the input logic signals were quite long compared to the overlap requirement. The second and third conditions were represented by logic pulses with durations of 100 ms and hundreds of s, respectively, and were implemented through gating the various units. All discriminator thresholds were set to correspond to 100 keV, the endpoint of the bremsstrahlung to be used in irradiations for this work.

The trigger stream produced a 3-μs gate for a CAMAC ADC system suitable for high data rates via FERA instruments. Individual signals to be recorded were digitized by a quad peak-sensing ADC, assembled into an event by a FERA driver and buffered into a FERA memory. Generation of new gates was inhibited for 20 μs after production of a trigger to allow the ADC to complete conversion of three active inputs. The maximum system throughput was 50 kHz from this restriction on the occurrence of gates. Upload of recorded events occurred only upon a buffer full condition. System control was accomplished using Sparrow KMaxNT® software customized for this application.

The three analog signals to be digitized in each event were the Ge signal pulse height, the summed NaI pulse height, and the detected multiplicity from the six NaI. The Ge spectroscopic signal was taken from its second preamplifier output and sent to a linear amplifier. The summed signal and multiplicity were both obtained from the CF8000 which provided a direct analog sum signal, a logic signal from each input channel, and an updating multiplicity signal that is proportional to the number of active channels. The analog sum was amplified by a second linear amplifier, while the short-duration multiplicity signal was stretched and inverted prior to digitizing. Delays were used where necessary to match the gate and three spectroscopic signals as shown in Figure 7.

Coincidence was defined in the most restrictive way from the updating multiplicity signal of Figure 8 after digitization. Digitizing the stretched pulse served to record an average pulse height for the signal and when histogrammed, this height was spread over many channels. Choosing only a small range of channels to represent a detected multiplicity of one, for example, a coincidence curve was obtained. The resolving time indicated there was about 150 ns – pulses from separate NaI arriving within this time appeared within the chosen histogram range. This time could in principle be reduced, but with a corresponding reduction in the total number of events accepted. Pile-up rejection was employed for the amplifier-ADC combinations, but did not affect sum energy signals due to individual pulses less than 500 ns apart.

General response of the system, including efficiency, was verified by using standard calibration sources. Of particular value was ^{60}Co whose decay produces two coincident gamma transitions with energies of 1173 and 1332 keV – the time delay between these photons is unmeasured and certainly less than 1 ns. Figure 9a shows a surface plot of the data obtained from this source while Figure 9b shows the same data as a gray-scale contour plot. In both cases, counts are located by the Ge pulse-height (y axis) and the NaI sum energy (x axis). The expected correlation

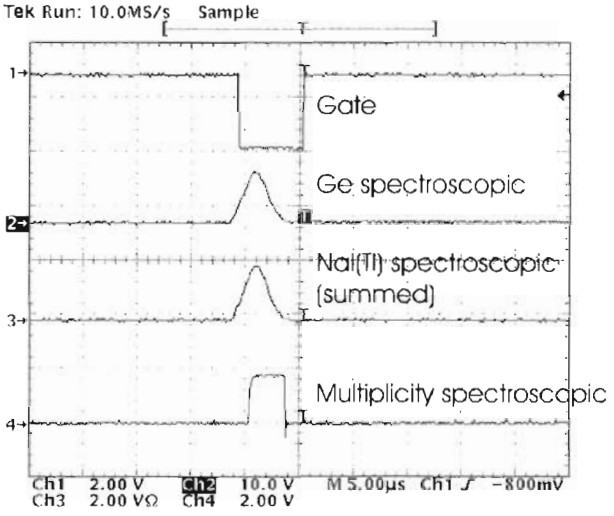

Figure 7. Temporal relationship between gate and spectroscopic signals to be digitized. For timing adjustment, a pulser was used to inject test pulses into the preamplifiers.

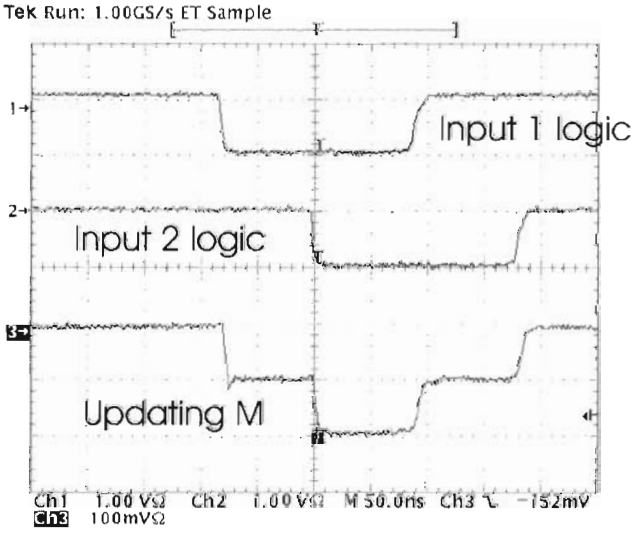

Figure 8. Updating multiplicity output from the CF8000 discriminator for the case of partial overlap between NIM logic signals from two separate NaI channels.

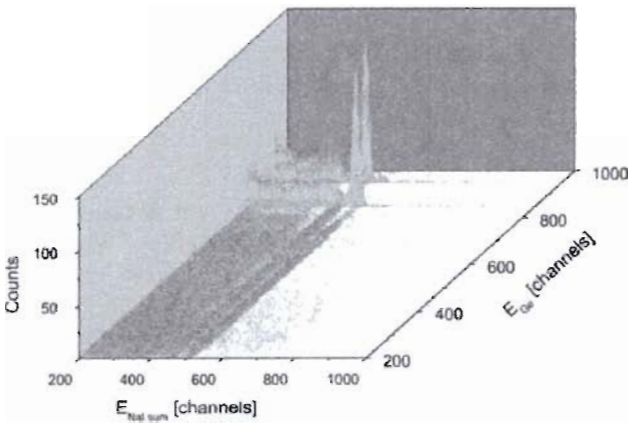

(a)

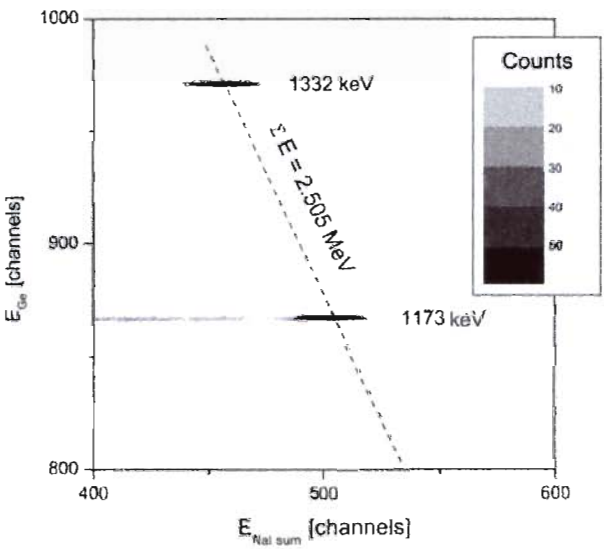

(b)

Figure 9. (a) Surface and (b) contour plots of data taken with the miniball for 1173 keV and 1332 keV gamma rays emitted from a ^{60}Co calibration source and acquired over about 15 hours. A line drawn through the loci of peak counts corresponds to a sum energy at 2.505 MeV.

is clearly seen: events in which the Ge detects the higher (1332 keV) transition and the miniball detects the lower (1173 keV) transition appear as one locus of counts while the reversed situation appears as a second locus. Both loci correspond to a total summed energy for the cascade of (1332 + 1173) keV = 2.505 MeV and this sum energy is depicted by a line drawn through both loci. The much greater

resolution of the Ge coordinate is evident. When applied to $^{178}Hf^{m2}$ samples, the larger number of peaks makes impractical a continued use of surface plots so in the following section, only contour plots will be used.

4. Experiment and results

Irradiations of samples were performed using a radiographic X-ray tube with a rotating anode operated in a pulse mode. Bremsstrahlung was produced for this experiment using an accelerating voltage of 100 kV (photon endpoint of 100 keV), anode current of 100 mA and a pulse duration of 100 ms. A repetition rate of 1/3 Hz was employed to maintain a safe rate of heat deposition to the anode, but it was necessary to allow the tube housing to cool for several hours after about each hour of pulsed irradiation. Overall, a total of 9 minutes of beam-on target time was accumulated during 4.5 hours of operational time, spread over a significantly longer period. The photon spectral intensity incident on the sample was determined by a custom EGSnrc simulation [37] and compared with an semi-empirical calculation [38] as shown in Figure 10. At lower accelerating voltages it was possible to acquire pulse-height spectra of the bremsstrahlung from a 10% HPGe detector operated in a pin-hole configuration and these spectra showed general agreement with the calculated results.

The isomeric sample was provided by SRS Technologies, Inc. and contained 3×10^{13} $^{178}Hf^{m2}$ atoms. The material was deposited into a 5-mm radius spot in the

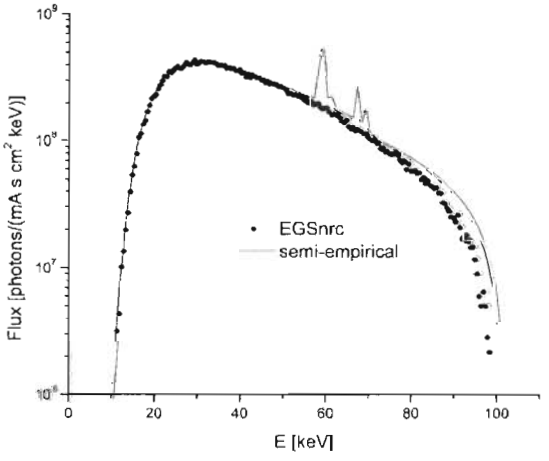

Figure 10. Plot of bremsstrahlung spectral intensity for the endpoint of 100 keV used in this experiment, calculated by a custom EGSnrc simulation [37] and the semi-empirical form of [38]. The X-ray tube used a standard 90/10 W/Re anode beveled at 12° and bremsstrahlung exited the tube through an inherent filtration equivalent to 1 mm Al. The EGSnrc code ran for 64.6 million histories (electrons incident on the anode) and production of characteristic X-rays was turned off to increase efficiency of the simulation (thus the lack of such X-rays in the EGSnrc spectrum).

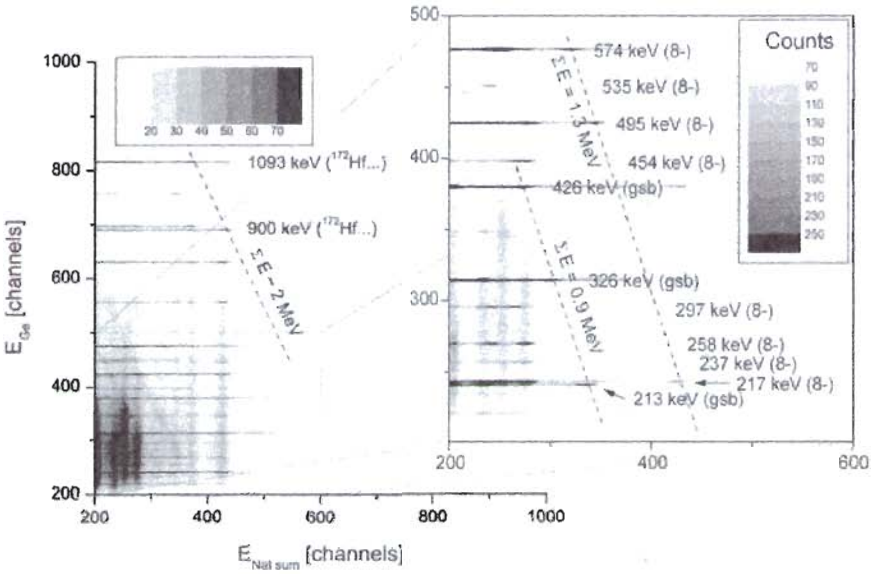

Figure 11. Contour plot of data taken with the miniball showing background radiation from the $^{178}Hf^{m2}/^{172}Hf$ sample. The zoom concentrates on gamma rays detected from $^{178}Hf^{m2}$ spontaneous decay. No bremsstrahlung was incident on the sample during acquisition of this data which was recorded for 11.5 h.

center cylindrical cavity of a plastic capsule. A dummy sample was also available, containing only ground state hafnium isotopes in natural abundances, deposited in the same manner and in the same total size and concentration as the isomeric sample.

Figure 11 shows data acquired from the isomeric sample without irradiation over a period of 11.5 hours. The full plot shows peaks from $^{178}Hf^{m2}$ and ^{172}Hf natural decays – the zoomed section concentrates on spontaneously-emitted gamma rays from $^{178}Hf^{m2}$. At Ge (y axis) channels near 250, the doublet at 213.4 keV (from the ground state band) and 216.6 keV (from the 4-s, m1 8-band) is resolved. Belonging to different parts of the broken spontaneous cascade, the members of the doublet correlate to the separate bursts in the broken decay of the 31-year isomer and their peak loci correspond to different sum-energy lines. The detected sum energy from the 4-s isomer decay was less than 1.147 MeV since the pulse discrimination and the Pb filters precluded the detection of the 88 and 93 keV transitions (both of which are also strongly converted) with significant efficiency. A sum energy line drawn near 2.0 MeV corresponds to gamma rays emitted in decays of ^{172}Hf and its daughters. Loci from these lines appear as expected in the spectrum of Figure 11, such as at 1093 keV (Ge) + 900 keV (NaI) and the reverse, but occur with generally lower probability due to the higher energy of these gamma rays. It is apparent that no experimental background of any kind occurs in a region

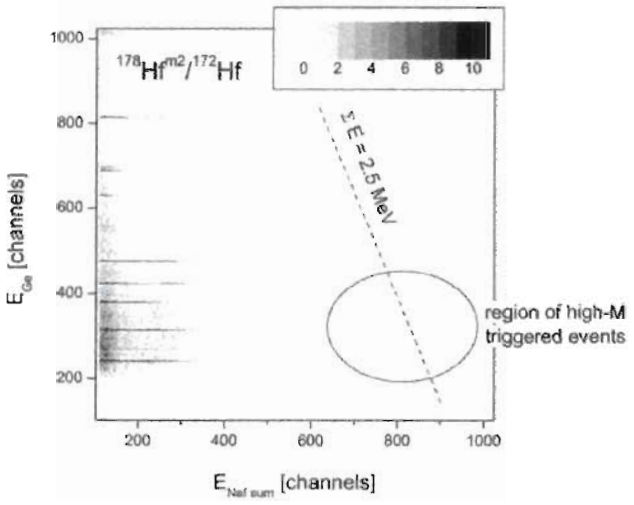

Figure 12. Contour plot of data taken with the miniball showing radiation from the $^{178}Hf^{m2}/^{172}Hf$ sample during 9 min of bremsstrahlung irradiation at 100 keV endpoint. The bremsstrahlung source was operated at 100 mA with 100 ms pulses at 0.33 Hz. The total real time was about 4.5 hours, but the actual experiment duration was much longer due to the need to allow the X-ray tube housing to cool periodically.

corresponding to detectable (>100 keV) members of the ground-state band and sum energy near 2.5 MeV, where triggered events would be expected to appear. All values of detected multiplicity are included in this plot.

Figure 12 shows similar data taken from the isomeric sample obtained during irradiation for a total of 9 minutes at 100 keV and 100 mA. In actuality, the experiment took a considerably longer time due to heating issues for both tube anode and housing. Despite the much shorter acquisition time, the features seen in Figure 11 appear corresponding to spontaneous decays from the sample. The region in which triggered events should appear is completely empty of counts. Again, all detected multiplicities are included in the plot.

5. Discussion

Reference [29] reported evidence of triggered gamma emission, as enhancements to spontaneous decay lines, and estimated the ICS to be greater than 2.2×10^{-22} cm^2 keV for incident photons less than 20 keV. The spectral intensity near 10 keV in the present experiment was about 10^8 photons/(s cm^2 keV) as determined by the EGSnrc simulation shown in Figure 10. Taking this intensity and the reported ICS, Equation (1) indicates that about 360 events should have occurred during the period of the irradiation used in this experiment.

The detection efficiency for the miniball system depends on the specific characteristics of a triggered event – for the following example, it is assumed that:

1. The energy of gamma rays emitted in a triggered event is 300 keV, similar to the average energy for spontaneous-decay transitions.
2. The triggered cascade has a high real multiplicity (number of transitions) of eight.

It is then possible to estimate the efficiency for observing an event in which the Ge and three of the NaI detect coincident photons from a triggered event (also leading to a high sum energy). The absolute full-energy peak efficiencies at 300 keV for the Ge and NaI are about 2% and 6%, respectively, considering the different distances to the sample. A simple Monte Carlo code may be employed to model efficiency for three NaI scintillators to detect gamma rays from the high-multiplicity cascade – the value is about 25%. Thus the overall detection efficiency for such a hypothetical event is 0.05%, or one out of every 2,000 events. This amount of triggering would require at least an increase to 50 minutes of irradiation time using the pulsed bremsstrahlung source. Of course, this represents a considerably longer real time due to the heat deposition considerations mentioned above. The present experiment provides an upper limit on the ICS for triggering on the order of 10^{-20} cm^2 keV for incident photons near 10 keV.

The experimental approach can be improved in several ways to provide higher event rates (based on reported ICS) and with even lower background. One approach is to use larger volume Ge and NaI detectors. This will not only increase the absolute detection efficiency, but also reduce the Compton background in relation to the corresponding full-energy peaks. It is clear from Figure 11 that random correlations between full energy peaks and Compton backgrounds in the different detectors make analysis of such bi-dimensional spectra more difficult and these correlations can be reduced by higher-efficiency detectors. In addition, a decrease in the resolving time between NaI signals will reduce such accidental coincidences. This is best accomplished by replacing the analog sum and multiplicity role of the CF8000 by a scheme that includes separate charge and arrival-time digitization for all the NaI signals. It will then be possible to employ software sorting on the data matrix for a range of coincidence windows from 10 ns to several μs. This has the added benefit of revealing any transitions due to cascades through the 78-ns isomer. Finally, the use of more intense irradiation sources, perhaps from synchrotrons, will increase the event rate in a straightforward manner. Upgrades will be conducted in all these directions prior to further experiments.

Acknowledgements

Support for this work was provided by the US Air Force Office of Scientific Research through contract F49620-99-1-0263. The authors are grateful to Pete Harvey, Sandia National Laboratories, and Noel Guardala of the Naval Surface Warfare Center, Carderock Division, for the loan of Ortec 113 preamplifiers during the

development of the DAQ system. Thanks also to Jim Corey, Sandia National Laboratories, for his help in arranging the loan of equipment therefrom. We also wish to acknowledge Hill Roberts and Mike Helba of SRS Technologies, Inc. for providing the isomeric sample.

References

1. Roberts, H., *Hyp. Interact.* **107** (1997), 91.
2. Soloway, S. and Harbison, J., *Am. Nucl. Soc. Trans.* **75** (1996), 20.
3. Carroll, J. J., Karamian, S. A., Rivlin, L. A. and Zadernovsky, A. A., *Hyp. Interact.* **135** (2001), 3.
4. Collins, C. B. and Carroll, J. J., *Hyp. Interact.* **107** (1997), 3.
5. Collins, C. B., Davanloo, F., Iosif, M. C., Dussart, R., Hicks, J. M., Karamian, S. A., Ur, C. A., Kirischuk, V. I., Carroll, J. J., Roberts, H. E., McDaniel, P. and Crist, C. E., *Phys. Rev. Lett.* **82** (1999), 695.
6. Godovikov, S. K., *Laser Phys.* **10** (2000), 1293.
7. Vysotskii, V. I., *Phys. Rev. C* **58** (1998), 337.
8. Shvyd'ko, Y. V., Hertrich, T., van Bürck, U., Gerdau, E., Leupold, O., Metge, J., Ruter, H. D., Schwendy, S., Smirnov, G. V., Potzel, W. and Schindelmann, P., *Phys. Rev. Lett.* **77** (1996), 3232.
9. Letokhov, V. S., *Sov. J. Quant. Elec.* **3** (1974), 360.
10. Collins, C. B. and Carroll, J. J., *Laser Phys.* **9** (1999), 1.
11. Walker, P. M. and Dracoulis, G. D., *Hyp. Interact.*, this volume.
12. Metzger, F. R., *Prog. Nucl. Phys.* **7** (1959), 54.
13. Kneissl, U., Pitz, H. H. and Zilges, A., *Prog. Part. Nucl. Phys.* **37** (1996), 349.
14. Karamian, S. A. and Carroll, J. J., *Laser Phys.* **11** (2001), 23.
15. Belic, D., Arlandini, C., Besserer, J., de Boer, J., Carroll, J. J., Enders, J., Hartmann, T., Käppeler, F., Kaiser, H., Kneissl, U., Kolbe, E., Langanke, K., Loewe, M., Maier, H. J., Maser, H., Mohr, P., von Neumann-Cosel, P., Nord, A., Pitz, H. H., Richter, A., Schumann, M., Volz, S., Thielemann, F.-K. and Zilges, A., *Phys. Rev. C* **65** (2002), 035801.
16. Collins, C. B., Eberhard, C. D., Glesener, J. W. and Anderson, J. A., *Phys. Rev. C* **37** (1988), 2267.
17. Collins, C. B., Carroll, J. J., Sinor, T. W., Byrd, M. J., Richmond, D. G., Taylor, K. N., Huber, M., Huxel, N., von Neumann-Cosel, P., Richter, A., Spieler, C. and Ziegler, W., *Phys. Rev. C* **42** (1990), 1813.
18. Belov, A. G., Gangrsky, Yu. P., Tonchev, A. P. and Zuzaan, P., *Hyp. Interact.* **107** (1997), 167.
19. Bikit, I., Lakosi, L., Sáfár, J. and Conkic, Lj., *Phys. Rev. C* **59** (1999), 2272.
20. Belic, D., Arlandini, C., Besserer, J., de Boer, J., Carroll, J. J., Enders, J., Hartmann, T., Käppeler, F., Kaiser, H., Kneissl, U., Loewe, M., Maier, H. J., Maser, H., Mohr, P., von Neumann-Cosel, P., Nord, A., Pitz, H. H., Richter, A., Schumann, M., Volz, S. and Zilges, A., *Phys. Rev. Lett.* **83** (1999), 5242.
21. Karamian, S. A., Collins, C. B., Carroll, J. J. and Adam, J., *Phys. Rev. C* **57** (1998), 1812.
22. Collins, C. B., Carroll, J. J., Taylor, K. N., Sinor, T. W., Hong, C., Standiford, J. D. and Richmond, D. G., *Laser Inter. Related Plasma Phenom.* **10** (1995), 151.
23. Collins, C. B., Carroll, J. J., Oganessian, Yu. Ts. and Karamian, S. A., *Laser Phys.* **5** (1995), 280.
24. Collins, C. B., Davanloo, F., Iosif, M. C., Dussart, R., Hicks, J. M., Karamian, S. A., Ur, C. A., Popescu, I. I., Kirischuk, V. I., Carroll, J. J., Roberts, H. E., McDaniel, P. and Crist, C. E., *Laser Phys.* **9** (1999), 8.
25. McNabb, D. P., Anderson, J. D. and Becker, J. A., *Phys. Rev. Lett.* **84** (2000), 2542.

26. von Neumann-Cosel, P. and Richter, A., *Phys. Rev. Lett.* **84** (2000), 2543.
27. Olariu S. and Olariu, A., *Phys. Rev. Lett.* **84** (2000), 2541.
28. Collins, C. B., Davanloo, F., Iosif, M. C., Dussart, R., Hicks, J. M., Karamian, S. A., Ur, C. A., Popescu, I. I., Kirischuk, V. I., Roberts, H. E., McDaniel, P. and Crist, C. E., *Phys. Rev. Lett.* **84** (2000), 2545.
29. Collins, C. B., Davanloo, F., Rusu, A. C., Iosif, M. C., Camese, D. T. Zoita, N. C., Hicks, J. M., Karamian, S. A., Ur, C. A., Popescu, I. I., Dussart, R., Pouvesle, J. M., Kirischuk, V. I., Strilchuk, N. V., McDaniel, P. and Crist, C. E., *Phys. Rev. C* **61** (2000), 054305.
30. Collins, C. B., Davanloo, F., Iosif, M. C., Dussart, R., Hicks, J. M., Karamian, S. A., Ur, C. A., Popescu, I. I., Kirischuk, V. I., Pouvesle, J. M., McDaniel, P. and Crist, C. E., *Phys. Atomic Nucl.* **63** (2000), 2067.
31. Collins, C. B., Zoita, N. C., Rusu, A. C., Iosif, M. C., Camese, D. T., Davanloo, F., Pouvesle, J. M., Dussart, R., Kirischuk, V. I., Strilchuk, N. V., Ur, C. A., Popescu, I. I. and Agee, F. J., *Laser Phys.* **11** (2001), 1.
32. Collins, C. B., Zoita, N. C., Rusu, A. C., Iosif, M. C., Camese, D. T., Davanloo, F., Pouvesle, J. M., Dussart, R., Kirischuk, V. I., Strilchuk, N. V., Ur, C. A., Popescu, I. I. and Agee, F. J., *J. de Phys. IV* **11** (2001), 437.
33. McDaniel, P., Personal communication, 2001.
34. Collins, C. B., Zoita, N. C., Rusu, A. C., Iosif, M. C., Camese, D. T., Davanloo, F., Emura, S., Uruga, T., Dussart, R., Pouvesle, J. M., Ur, C. A., Popescu, I. I., Kirischuk, V. I., Strilchuk, N. V. and Agee, F. J., *Europhys. Lett.* **57** (2002), 677.
35. Carroll, J. J. and Karamian, S. A., *Laser Phys.* **11** (2001), 23.
36. Kulessa, R., Gerl, J., Wollersheim, H.-J., Xie, H., Karamian, S. A., Oganessian, Yu. Ts., Briancon, Ch., Hussonnois, M. and Ender, Ch., GSI Scientific Report, Darmstadt, 1992, p. 86.
37. EGSnrc, National Research Council of Canada, 2000, http://www.irs.inms.nrc.ca/inms/irs/EGSnrc/EGSnrc.html.
38. Tucker, D. M., Barnes, G. T. and Wu, X., *Med. Phys.* **18** (1991), 402.

Hyperfine Interactions **143:** 7–11, 2002.

Proposal for Observation of a Hidden Nuclear Population Inversion

F. J. AGEE[1], J. J. CARROLL[2], L. A. RIVLIN[3] and V. VULETIC[4]
[1] *Air Force Office of Scientific Research, NE, 801 North Randolph Street, Arlington, Virginia 22203, USA*
[2] *Center for Photon-Induced Processes, Youngstown State University, Youngstown, Ohio 44555, USA*
[3] *MIREA Technical University, 78 Vernadsky Ave., Moscow 117454, Russia; Moscow State Institute for Radioengineering, Electronics and Automation (Technical University)*
[4] *Stanford University, Varian Building, 382 Via Pueblo Mall, Stanford, California 94305, USA*

Abstract. Observation of a hidden nuclear population inversion, as a precursive experimental proof of the concept of recoil-assisted gamma-ray lasing, can be accomplished by pure optical methods due to spectral shift of atomic transitions. This paper presents numerical estimates and a proposal for such a proof-of-principle experiment.

Key words: recoil-assisted nuclear gamma-lasing, laser cooling of atoms.

The eventual experimental demonstration of gamma-ray lasing (GRL) resting on the concept of recoil-assisted stimulated process in deeply cooled nuclear ensembles [1] is very promising. It is also very complex and challenging. The feasibility of such an experiment rests on the creation of a so-called hidden population inversion, one of the main points of a full-scale GRL experiment. An important precursive step would be to observe the principal existence of a hidden nuclear population inversion in an independent sub-threshold experiment without the requirements of a "hot" lab. Such an initial experiment looks much simpler than a full-scale above-threshold one and may be accomplished with mostly optical measurement methods and a rather modestly-powered non-coherent X-ray pump source. It is grounded on the fact that a hidden nuclear inversion occurring as a shift in velocity distribution between atom groups with excited and unexcited nuclei may be readily seen in a corresponding shift in the atom optical spectrum due to the Doppler effect. The need to utilize such a recoil-assisted approach to achieve a gamma-ray laser is reviewed in [2] in the context of difficult solid-state (non-recoil assisted) approaches as summarized in [3].

The general experimental scheme consists of a medium of nuclei bearing atoms cooled down to the temperature T and confined in a trap. Known methods of optical laser cooling may be employed to accomplish this. The atom velocity distribution

in this medium has a single narrow peak centered on the common translation velocity v_0 and with an average chaotic thermal velocity

$$\bar{v} \approx 1.5 \times 10^4 \sqrt{\frac{T}{A}} \text{ cm s}^{-1} \tag{1}$$

that depends on the temperature T (in K) and isotope number A (clearly the translation velocity can even be $v_0 = 0$). The nuclear medium is irradiated by a well-collimated non-coherent X-ray beam directed along the z axis of the experimental setup. As a result, due to absorption of an X-ray photon with energy $\hbar\omega \approx E_0$ an excited nucleus originally at rest acquires the kinetic recoil energy

$$E_{\text{rec}} = 0.53 \frac{E_0^2}{A} \text{ meV} \tag{2}$$

and a corresponding velocity increase in the z direction

$$\Delta v_z \approx 3 \times 10^4 \frac{E_0}{A} \text{ cm s}^{-1}, \tag{3}$$

where E_0 is the nuclear transition energy in keV. The typical figures are $E_{\text{rec}} = 10$ meV and $\Delta v_z = 100 \text{ m s}^{-1}$.

So after irradiation the atom velocity distribution in the z-direction changes and possesses two narrow peaks corresponding to the atoms having excited and unexcited nuclei. These peaks can be reliably resolved if

$$\Delta v_z \gg \bar{v} \tag{4}$$

and if the concentration ratio of excited nuclei n_2 over the unexcited ones n_1 exceeds a quantity

$$\frac{n_2}{n_1} > \exp\left(-6.15 \frac{E_0^2}{AT}\right). \tag{5}$$

This inequality expresses the requirement that the wing of the Maxwellian velocity distribution of atoms with unexcited nuclei does not overlap the maximum of the new peak in the distribution that originates from atoms with excited nuclei. It should be emphasized that this inequality definitely gives too weak of a limitation on the temperature because even in the sub-threshold case under consideration the ratio n_2/n_1 may be relatively small, but cannot be so small as to preclude the needed number of luminescent atoms for detection. A more realistic inequality follows from (4):

$$\sqrt{T} \ll 2 \frac{E_0}{\sqrt{A}} \text{ K}^{1/2}. \tag{6}$$

According to the concept of a recoil-assisted GRL, the appearance of two-atomic groups separated in the z-velocity domain manifests the production of a hidden nuclear inversion that could support a gamma-photon flux counter propagating relative to the direction of the pump X-ray beam.

If a pulsed X-ray irradiation is used, the pronounced hidden inversion exists only for limited time interval

$$\Delta t \ll \tau_{1/2} \tag{7}$$

that is shorter than the half-life time $\tau_{1/2}$ of the excited nuclear state. This is because a second recoil process accompanying the spontaneous gamma decay of excited nuclei smoothes the corresponding narrow atomic velocity peak. In the alternative case of continuous X-ray irradiation, the hidden inversion must be observed on the broad background of nuclei undergoing spontaneous decay. The same reason requires that the duration of the X-ray pump pulse, Δt_x, should be limited to

$$\Delta t_x \ll \tau_{1/2}. \tag{8}$$

This leads to the following estimate for the obtainable ratio of concentrations of excited to unexcited nuclei:

$$\frac{n_2}{n_1} \approx \frac{\lambda^2}{\tau_{1/2}} \frac{2J_2 + 1}{2J_1 + 1} j_x \Delta t_x, \tag{9}$$

where λ is the gamma wavelength, j_x is the brilliance (spectral density) of the X-ray source, and J_2 and J_1 are the angular momenta of upper and ground states of the gamma transition, respectively. One can see that the brilliance j_x must be relatively large to obtain a tangible amount of excited nuclei, say at least $j_x \sim 10^8$ photons per (cm^2 s Hz). For instance, $n_2/n_1 \sim 10^{-9}$ if $\lambda = 10^{-8}$ cm and $\Delta t_x/\tau_{1/2} = 0.2$. Then the inequality (5) can be much more than satisfied, if, for instance, $A = 50$ and $T = 10$ mK.

The appearance of a new group of atoms with velocity difference Δv_z (Equation (3)) simultaneously results in a Doppler shift $\Delta \nu_{\text{opt}}$ of the *optical* spectral line (observed in the $\pm z$ direction) of the atom group bearing nuclei in the excited state relative to the atom group bearing unexcited nuclei:

$$\Delta \nu_{\text{opt}} = \pm \frac{\Delta v_z}{c} \nu_{\text{opt}}. \tag{10}$$

The two split *optical* lines corresponding to atoms with excited and unexcited nuclei are, in principle, resolvable by optical spectroscopic methods only if

$$\Delta \nu_{\text{opt}} \gg \Delta \nu_T, \tag{11}$$

where

$$\Delta \nu_T = 7 \times 10^{-7} \nu_{\text{opt}} \sqrt{\frac{T}{A}} \tag{12}$$

is the Doppler broadening of the *optical* lines and ν_{opt} is the frequency of the optical transition.

So it follows from Equations (3) and (10)–(12) that

$$\sqrt{T} \ll 1.4 \frac{E_0}{\sqrt{A}} \text{ K}^{1/2} \tag{13}$$

which, of course, practically coincides with the inequality (6).

Optical spectral measurements should be accomplished during the time interval Δt shown in (7). Taking into account the typical characteristic time of optical luminescence $\Delta t_{\text{lum}} \approx 10$ ns, one must require that $\Delta t \gg \Delta t_{\text{lum}}$. So this leads to an estimate for the desired nuclear half-life (Equation (7)) to support this experiment

$$\tau_{1/2} \gg \Delta t \gg \Delta t_{\text{lum}} \approx 10 \text{ ns} \tag{14}$$

or perhaps slightly longer. Such a long lifetime would be unsuitable for a real above-threshold GRL experiment because of the extremely low temperature T of the nuclear medium that would be needed to provide a sufficiently high line-width ratio so that $\beta \to 1$. But in this sub-threshold experiment a ratio $\beta \ll 1$ is quite allowed. So for certain in this proof-of-principle experiment nuclides may not be used that are adequate for an above-threshold GRL experiment. Possibly it is more preferable now to choose an atom that is known to be suitable for laser cooling.

The reliable observation of two different atom groups separated by a velocity displacement Δv_z would be ***a convincing proof of the existence of the hidden nuclear population inversion*** arising as result of a non-coherent X-ray pump.

It seems that this observation can be made by purely optical methods. Crude estimates according to Equations (3) and (10)–(12) show that the necessary optical spectral resolution lies in the hundred MHz range. This figure does not exceed that achieved with precision optical spectroscopy. But it should be taken into account that for the spectral measurements only the atom luminescence radiation can be accepted that lies within a small solid angle around the $\pm z$ axis; because the task is to detect the Doppler shift in just these directions. So the useful optical photon flux to be detected shall be presumably very weak.

For this reason an alternative approach may possibly be more efficient: after pulsed X-ray pumping the beam of a tunable optical laser is directed along the z axis and excites an intense atomic luminescence into 4π. This luminescence is detected by photo-multipliers surrounding the atom medium. A tuned laser with a radiation line-width smaller than $\Delta \nu_T$ (Equation (12)) scans the Doppler-shifted atom lines and serves as a spectrum-analyzing device. The atom transition excited by the laser must not coincide with any transition used for the laser cooling process. This can be useful to filter the cooling radiation background. It is possible to use the cooling transition only if one turns off the cooling laser during detection.

As a by no means optimal example, let us consider the nuclide $^{179}\text{Ta}_{73}$. This isotope has an exited state with $E_0 = 30.7$ keV, $\tau_{1/2} = 1.42$ μs, transition multipolarity $E1$ and internal electron conversion coefficient $\alpha = 4.6$. So for this transition $E_{\text{rec}} = 2.8$ meV and $\Delta v_z = 50$ m s^{-1}. If one takes $T = 10$ mK, then $\bar{v} = 1.1$ m s^{-1} and the condition $\Delta v_z \gg \bar{v}$ is satisfied as well as the inequality (6): $0.1 \ll 4.7$.

Then one can take $\Delta t = \Delta t_x = 150$ ns $<< \tau_{1/2} = 1420$ ns. The concentration ratio $n_2/n_1 = 10^{-11}$ may be achievable if one uses an X-ray source with a brilliance of $j_x = 10^7$ photon per (cm^2 s Hz). And finally one has $|\Delta\nu_{\rm opt}| \approx 50$ MHz and the optical spectral resolution is acceptable because $\Delta\nu_{\rm opt}/\Delta\nu_T = 32 \gg 1$.

If one would like to use nuclides of atoms that are the standard objects of laser cooling experiments, the following ones can be recommended:

$$^{129}Cs_{55}\ (E_0 = 6.545\ \text{keV},\ \tau_{1/2} = 72\ \text{ns},\ E2),$$
$$^{134}Cs_{55}\ (E_0 = 11.24\ \text{keV},\ \tau_{1/2} = 46.6\ \text{ns},\ M1),$$
$$^{83}Rb_{37}\ (E_0 = 5.24\ \text{keV},\ \tau_{1/2} = 46.6\ \text{ns},\ M1,\ \alpha = 105!!),$$

and also some earth alkali metals. The possibility of using new methods [4] of laser cooling would greatly free the search for suitable atoms for the present experiment. With a suitable optical transition one can probably detect about 100 atoms or maybe fewer in a volume of 1 cm^3. A ratio of $n_2/n_1 = (10^{-9}–10^{-11})$ then corresponds to a required initial concentration of $n_1 = (10^{11}–10^{13})$ cm^{-3} which is certainly possible for enriched isotopes or for isotopes with high natural abundance.

Possibly it is interesting to investigate an alternative experimental version that completely eliminates the need for laser cooling. This consists of spectroscopic detection of the velocity of the recoiling nucleus, e.g., by transverse X-ray illumination of a collimated atomic beam. Collimation can easily produce an effective "transverse temperatures" of 1 K or less.

The bottom line: the analysis carried out here shows that the proposed proof-of-principle experiment on observation of a hidden nuclear inversion is not a simple one, but looks quite realizable. Such a precursive experiment is extremely important and clearly is much simpler than the full-scale above-threshold GRL experiment that it would serve to motivate.

References

1. Rivlin, L. A., *Quantum Electronics (Moscow)* **29** (1999), 467.
2. Carroll, J. J., Karamian, S. A., Rivlin, L. A. and Zadernovsky, A. A., *Hyp. Interact.* **135** (2001), 3.
3. Baldwin, G. C. and Solem, J. C., *Rev. Mod. Phys.* **69** (1997), 1085.
4. Vuletic, V. and Chu, S., *Phys. Rev. Lett.* **84** (2000), 3787.

Hyperfine Interactions **143:** 55–61, 2002.

Beam-Based Production of ^{178m2}Hf

J. PAUL FARRELL[1], V. DUDNIKOV[1], J. J. CARROLL[2] and G. MERKEL[3]
[1] *Brookhaven Technology Group, Inc., Setauket, NY, USA*
[2] *Youngstown State University, Youngstown, OH, USA*
[3] *Army Research Lab, Adelphi, MD, USA*

Abstract. In this study, the production yield for the reaction ^{176}Yb(^{9}Be, α3n)^{178}Hf was explored using the FN tandem injected superconducting LINAC at SUNY at Stony Brook at a ^{9}Be energy of 65 MeV. By comparing the experimental yield of ^{178}Hf ground state γ rays with those of ^{180}W as a function of energy, the cross section for production of the incomplete fusion γ rays in ^{178}Hf was evaluated. Coincidence measurements were made to get information about the population strength of the high spin states in ^{178}Hf. From these measurements, the maximum cross section for the reaction ^{176}Yb(^{9}Be, α3n)^{178m2}Hf is estimated to be no larger than 5 mb.

Key words: nuclear isomer, cross-sections, fusion reaction.

1. Introduction

This report concerns production of the nuclear isomer, ^{178m2}Hf (Hfm2), for experimental targets and as an energy-storage/energy-delivery system for defense and civilian applications. Nuclear isomers are long lived (> 1 ns) excited states of nuclei that release their excess energy by electromagnetic decay. The nuclear state energy densities stored in some isomers are 10^3 to 10^4 times higher per unit mass ($\approx 10^9$ J/g) than for chemical systems. This leads directly to the possible application of isomers as batteries to provide useful energy in space or battlefield operations or as flash discharge devices to provide an intense pulse of penetrating electromagnetic radiation.

The majority of nuclides, both stable and radioactive, have isomeric states, many with lifetimes ranging up to hundreds or even thousands of years. Transition energies range from a few electron volts to several MeV. High spin isomers in the mass region $A \approx 180$ are important candidates for compact energy storage systems because they have long lifetime and reasonably high energy storage per nucleus. Isomers in this region are deformed nuclei trapped in high spin states that are metastable due to the large multipole transition required for their electromagnetic decay to levels at lower energy. This high spin state of the isomer also inhibits the reverse process, so isomers are not created in significant quantity by direct absorption transitions from the ground state. The use of isomers for high density energy storage is enhanced by the theoretical consideration of K-mixing in excited nuclei and by the possibility of an efficient pumping process for γ ray lasers [1–3].

The 31-year metastable state in ^{178}Hf, which is designated ^{178m2}Hf, is one of the most promising isomers in terms of half-life and energy storage per nucleus (~2.446 MeV = 1.3 gigajoules/gram) [4]. This isomer has been the subject of much study over the past 10 years due to its possible use in gamma-ray lasers and other applications. Although some samples of this isomer have been produced and used in experiments on triggering, enormous difficulties exist in the methods of ^{178m2}Hf production.

The three methods that have been employed to produce ^{178m2}Hf isomer are:

1. Reactor-based (n, n′) and (n, xn) reactions in the MTR at ORNL [5, 6],
2. Beam-based ^{176}Yb(α, 2n) and ^{176}Yb(^{9}Be, α3n) particle beam based reactions [7],
3. 800 MeV proton spallation on thick Ta targets [8].

Reactor-based production of this isomer using (n, n′) and (n, xn) reactions has the potential to produce useful quantities of isomer and isotope but the isomer to ground state ratio is very low (~10^{-6}). This means that after production, extraordinary effort is needed to concentrate the isomer. Beam-based production has higher isomer-to-ground-state ratio (~10^{-2}), but the yield is low. While it is a disadvantage that beam-based methods have low production rates, *it is an advantage* that the parent material can be removed by chemical methods leaving the isomer, the ground state and whatever other isotopes are produced present in proportion to the reaction branching ratio. *Thus, beam-based production has the potential to yield much higher concentration of isomer as a starting point.*

2. Method

Two key issues must be addressed in producing the 31-year isomer of ^{178}Hf. The first one is to find stable heavy ion (HI) beams and targets that have a substantial probability of populating the ^{178}Hf channel; the second is to ensure the reaction brings in sufficient angular momentum to populate the high-spin 16^{+} isomer. Although HI fusion evaporation reactions have large cross sections, they are not easily employed to produce ^{178m2}Hf. ^{178}Hf is in the valley of stability, so only the (HI, xn) channels are strongly populated because of the difficulty of evaporating charged particles over the Coulomb barrier. Furthermore, ^{176}Yb(α, 2n), the only stable HI-target combination available for producing ^{178}Hf via neutron evaporation, yields a low cross-section to the 16^{+} isomer due to the angular momentum limitations of the alpha, when optimizing for 2n evaporation.

One way of circumventing this difficulty is to use an incomplete fusion reaction [9] where a massive transfer takes place. A ^{176}Yb(^{9}Be, α3n) reaction can be viewed as ^{9}Be breaking up into an alpha + ^{5}He with the subsequent fusion evaporation reaction ^{176}Yb(^{5}He, 3n) going to ^{178}Hf. By detecting the forward-going breakup α, the subsequent 3n evaporation was shown to bring in sufficient angular momentum to populate up to a 22^{+} member of a band that feeds into the 16^{+} isomer. Most of this work was performed at a ^{9}Be energy of 55 MeV; the energy limitation of the accelerator in this earlier study did not allow an optimization of

the isomer production, namely to maximize the (^{5}He, 3n) reaction cross section at the periphery of the nucleus where the breakup takes place [9].

3. Results

In this study, the production yield for the reaction ^{176}Yb(^{9}Be, α3n)^{178}Hf was explored at SUNY at Stony Brook using the FN tandem injected superconducting LINAC accelerator. The negative-ion sputtering source was optimized to produce 10 particle nano-amperes (pna) beam of ^{9}Be. An excitation function from 50 to 75 MeV for ^{9}Be on a 4 mg/cm^2 (2 MeV thick) ^{176}Yb target was measured with suppressed Ge detectors and pulsed beam-γ timing to reduce background from induced radioactivity. The excitation function results for expected fusion-evaporation reactions were consistent with CASCADE calculations, the strongest being ^{176}Yb(^{9}Be, 5n) producing γ rays in ^{180}W and with the ^{181}W(4n) and ^{179}W(6n) increasing at the low- and high-energy range, respectively. The CASCADE calculations as a function of energy are shown in Figure 1. The CASCADE calculation for the ^{176}Yb(^{9}Be, α3n) fusion evaporation to ^{178}Hf is expected to be small (see Figure 1). Note that the yield of ^{178}Hf from the incomplete fusion reaction discussed above is not included in Figure 1 because it cannot be calculated with the CASCADE codes.

By comparing the experimental yield of ^{178}Hf ground state γ rays with those of ^{180}W as a function of energy, the cross section for production of the incomplete fusion γ rays in ^{178}Hf can be evaluated because the cross section for ^{180}W is known with reasonable accuracy from the CASCADE calculations. The excitation results

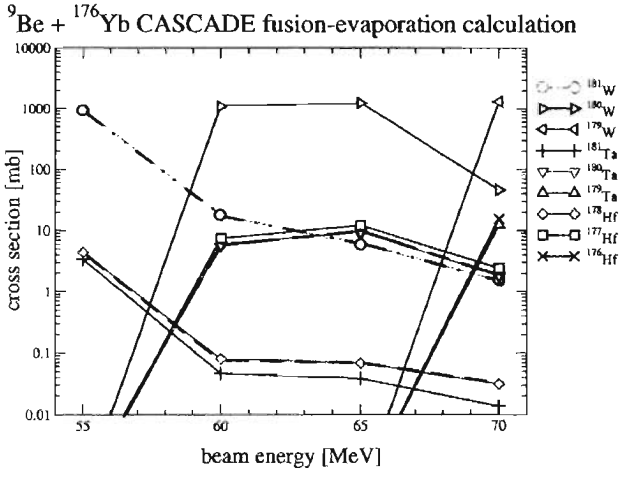

Figure 1. CASCADE calculation of cross section.

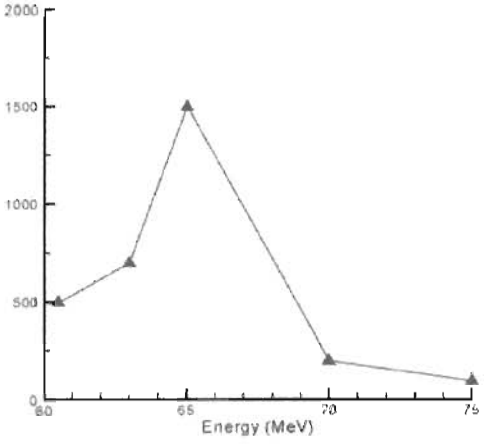

Figure 2. Excitation function shows the ^{178}Hf $6^+ \rightarrow 4^+$ measured cross section in millibarns.

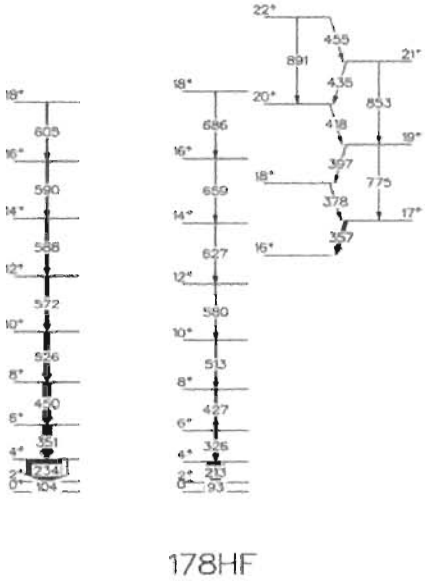

Figure 3. Partial energy levels in ^{178}Hf.

for the 326 keV (isolated in singles) $6^+ \rightarrow 4^+$ ^{178}Hf-γ ray are shown in Figure 2, where it can be seen that the incomplete fusion reaction to ^{178}Hf peaks at 65 MeV.

In order to get information on the population strength at high spins, and in particular to the 16^+ Hfm2 isomer, it was necessary to make coincidence measurements to isolate these weaker γ-ray transitions between the high spin band members, which are not isolated in singles. Partial energy levels of ^{178}Hf are shown

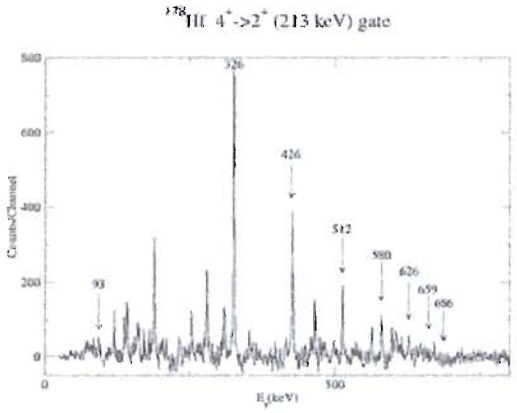

Figure 4. Coincidence spectra extracted from a sorted 2-dimensional coincidence matrix for both ^{178}Hf using a $4^+ \rightarrow 2^+$ gate on the ground-state transitions.

in Figure 3. The coincidence measurements were carried out at the 65 MeV cross section peak using the Stony Brook array of suppressed Ge detectors together with a fourteen-element BGO multiplicity filter.

The coincidence results allow a comparison of the population at higher spin in the ground-state bands and in the prompt coincidences for the 357, 377, 397, 417 keV in-band gamma rays, that feed the 31y 16^+ isomer in ^{178}Hf. Figure 4 shows the coincidence spectra extracted from a sorted 2-dimensional coincidence matrix for ^{178}Hf using a 4^+–2^+ gate on the ground-state transitions. This spectrum illustrates how the population yield drops off as the spin increases. The relative yield results are presented in Table I. From the efficiency calibrated coincidence matrix, the cross sections for population at higher spins in ^{178}Hf and, in particular to the band feeding the 16^+ isomer, can be evaluated from the knowledge of the CASCADE cross sections for ^{180}W.

Since the CASCADE calculation for the ^{176}Yb(^{9}Be, 5n) fusion evaporation reaction into ^{180}W at 65 MeV is 1000 mb, representing the population at the bottom of the ground-state band, the yield of the 18^+–16^+ ground-band transition feeding the 16^+ level is approximately 20 times less or 50 mb. However, for the incomplete fusion reaction to ^{178}Hf, the yield corresponds to approximately 400 mb at the bottom of the ground band but only 2 mb for the 18^+–16^+ ground-band transition. This shows that the incomplete fusion reaction drops off in yield considerably faster for increased angular momentum than for the fusion evaporation reaction. The fact that the α breakup occurs at the periphery where the ^{5}He achieves fusion for the incomplete fusion reaction has not improved the angular momentum population dependence compared to ^{9}Be where the fusion takes place at all impact parameters for the fusion evaporation reaction. With summing gate techniques, the γ-rays feeding the 16^+ isomer could be identified with the fitted

Table I. Relative yield

Band	Transition	Intensity	Error	Band	Transition	Intensity	Error
^{180}W	$18^+ \rightarrow 16^+$	4.75	0.29	^{178}Hf	$18^+ \rightarrow 16^+$	0.19	0.12
	$16^+ \rightarrow 14^+$	6.51	0.34		$16^+ \rightarrow 14^+$	0.32	0.15
	$14^+ \rightarrow 12^+$	8.61	0.42		$14^+ \rightarrow 12^+$	0.77	0.18
	$12^+ \rightarrow 10^+$	12.15	0.55		$12^+ \rightarrow 10^+$	2	0.23
	$10^+ \rightarrow 8^+$	17.16	0.72		$10^+ \rightarrow 8^+$	3.52	0.37
	$8^+ \rightarrow 6^+$	22.08	0.95		$8^+ \rightarrow 6^+$	5.18	0.39
	$6^+ \rightarrow 4^+$	27.47	1.24		$6^+ \rightarrow 4^+$	7.47	
	$4^+ \rightarrow 2^+$	107.38	12.08		$4^+ \rightarrow 2^+$	42.34	

Band	Transition	Intensity	Error
^{178m2}Hf	$22^+ \rightarrow 20^+$	0.08	0.21
	$21^+ \rightarrow 19^+$	0.16	0.42
	$19^+ \rightarrow 17^+$	0.27	0.28
	$22^+ \rightarrow 21^+$	0.05	0.25
	$21^+ \rightarrow 20^+$	0.27	0.26
	$20^+ \rightarrow 19^+$	0.2	0.51
	$19^+ \rightarrow 18^+$	0.36	0.25
	$18^+ \rightarrow 17^+$	0.91	0.72

intensities from the coincidence matrix. This analysis reveals large uncertainties for the coincidence yields for these γ-rays due to weak strengths, significant coincidence background and the fact that the coincidence cascade is cut off at the isomer. Estimated cross sections, extracted from these uncertain yields to the 31-year isomer, appear to be about the same (a few mb) as that for feeding the 16^+ ground state member. These data show an upper limit of 5 mb, at best. Since both bands in ^{178}Hf involve the same angular momentum requirements, similar yields are expected.

4. Conclusion

In conclusion, the yields as a function of angular momentum for the incomplete fusion reaction to ^{178}Hf drop off in such a way that that the high spin states above 16^+ are weakly populated, even though the low-spin ground-state transitions have reasonable cross sections. The cross section for the production of the 31-year 16^+ isomer in ^{178}Hf, even at the 65 MeV peak of the cross section discovered in these studies, is only a few mb and an upper limit of 5 mb.

Acknowledgements

The authors thank D. B. Fossan, C. Vaman, C. J. Chiara, T. Koike and K. Starosta of the State University of New York at Stony Brook for their help in this work. The target was prepared by Richard Lefferts. This work was supported by a Phase I SBIR through the Army Research Laboratory DAAD-17-01-C0018.

References

1. Collins, C. B. and Carroll, J. J., *Hyp. Interact.* **107** (1997), 3.
2. Baldwin, G. C. and Solem, J. C., *Reviews of Modern Physics* **69** (1997), 1085.
3. Olariu, S. and Olariu, A., *Phys. Rev. C* **58** (1998), 2560.
4. Collins, C. B. *et al.*, *Phys. Rev. Lett.* **82** (1999), 695.
5. Chadwick, M. B. and Young, P. G., *Nucl. Sci. Eng.* **108** (1991), 117.
6. McDaniel, P., private communication.
7. Oganessian, Y. T., Karamian, S. A. *et. al.*, *J. Phys. C Nucl. Part. Phys.* **18** (1992), 393.
8. Ahmad, I. *et al.*, *Phys. Rev. Lett.* **87** (2001), 072503.
9. Mullins, S. M. *et al.*, *Phys. Lett. B* **393** (1997), 279.

Hyperfine Interactions **143:** 69–78, 2002.

Possibility of Combining Nuclear Level Pumping in a Plasma with Lasing in a Solid

S. A. KARAMIAN[1] and J. J. CARROLL[2]
[1] *Joint Institute for Nuclear Research, 141980 Dubna, Russia*
[2] *Department of Physics and Astronomy, Center for Photon-Induced Processes, Youngstown State University, Youngstown, 44555, Ohio, USA*

Abstract. Nuclear isomers can be used for the storage and release of "clean" nuclear energy and several triggering schemes have been discussed. Here the possibility to utilize resonance between atomic and nuclear transitions in the form of a hybridization of atomic-nuclear excitation is considered. Several isotopes and specific nuclear levels are identified as candidates for triggering via atomic transitions. A variety of ionization states and atomic-shell configurations arises in a hot plasma generated by short high-power pulses of laser light. The non-radiative conversion of the ionization energy within an atom can be suppressed in the hot plasma surroundings. The time scales of different processes in nuclear, atomic and condensed-matter subsystems are compared and the fast ionization in a solid, X-ray radiance in a plasma, and sample melting and recrystallization may precede nuclear fluorescence. A time scale shorter than 0.1 ns makes this sequence promising for the collective excitation of short-lived modes in a nuclear subsystem.

Key words: laser pulse, solid, ionization, characteristic transition, nuclear excitation, ablation, recrystallization, fluorescence, time scale.

1. Introduction

A triggered release of isomer energy would be very attractive for the production of a source capable of emitting powerful pulses of radiation in the gamma-ray range. For example, self-stimulation of an isomeric transition could create a gamma-ray laser and such a device might also be possible using a triggered energy release as a precursive step to the lasing transition. There are, however, many problems to be solved since significant barriers are already well-known in the variants proposed for realizing a gamma-ray laser. The current status and issues related to the problem of nuclear isomer triggering by X-ray radiation has recently been reviewed in [1]. Also, a list of long-lived nuclear isomeric states has been given in [2] and new candidates for a triggered energy release have been discussed.

In the literature, many mechanisms of nuclear excitation by changes in electron configuration were proposed in addition to the straightforward process of resonance photon absorption. Among them are:

- nuclear excitation by electron transition (NEET),
- nuclear excitation by electron capture (NEEC), and

- laser-assisted NEET and electron bridge mechanisms.

Some valuable experiments and theoretical analyses performed in this field can be cited [3–14], but to this point the overall progress has been limited. Thus, continued efforts to find the best physical mechanism for nuclear level excitation (triggering) and suggestions of new experimental schemes are still relevant. The nuclides ^{181}Ta, ^{193}Pt, ^{201}Hg, ^{205}Pb, ^{229}Th and ^{235}U were proposed in [5, 9, 13] to be the best candidates for nuclear excitation by X-ray photons with $E_x < 7$ keV in a plasma. Here we will discuss other nuclei, in particular the ^{242}Am^{m} long-lived isomer ($T_{1/2} = 141$ y). These isotopes were selected based on their parameters of long lifetime (or stability), high production cross-section (if radioactive) and low multipolarity of the excited transition, such as M1, E1 or E2.

The efficiency of energy transfer from atomic to a nuclear subsystem is defined not only by the microscopic properties of atomic and nuclear levels, but also by the state of the host substance containing the atoms and their nuclei. Recently, new experimental results have been obtained on the time scale of the desorption of atoms from a solid surface to the ablation-cloud after a powerful femtosecond pulse of laser light [15] and on the subsequent relaxation of the solid sample (crystal) [16].

2. Processes in laser plasma

It is known that the interaction of a TeraWatt laser pulse with solid matter immediately generates an induced oscillation of electrons at the frequency of the laser light. This collective excitation of the electronic subsystem then decays via an energy transfer to highly-excited atomic states and/or deep ionization of the atomic shells. The nuclear subsystem can also be perturbed because of the interaction with fast electrons, characteristic X-rays, bremsstrahlung or black-body radiation. K and L electrons can be ejected from heavy atoms with the created vacancies serving as a source of characteristic photons with an energy useful for excitation of some specific nuclear states.

The excitation of nuclear levels in ^{201}Hg and ^{181}Ta isotopes by exposure to plasma radiation created by short laser pulses was tested in [3–5] and the utility of this concept was supported experimentally. A device for laser pumping of nuclear levels using this approach can, in principle, be small and simple in configuration. One possible scheme is shown in Figure 1 in which a focused laser beam creates a high-power density spot on the sample surface. The cross-sectional size of the spot can be as small as 100 μm. Excited electrons leave their atoms immediately and the solid matter is quickly transformed into a dense plasma of ionized atoms. Other radiation processes also develop rapidly and desorption of atoms to the vacuum and thermal ablation follow. Finally, the hot spot is recrystallized and at the end the ablation cloud is deposited onto the sample and surrounding surfaces.

The time scales of different processes are given in Table I. The relaxation of solid matter after the pulsed release of energy has been studied recently in [15, 16] for the case of femtosecond pulses of laser-light incident on metal and semicon-

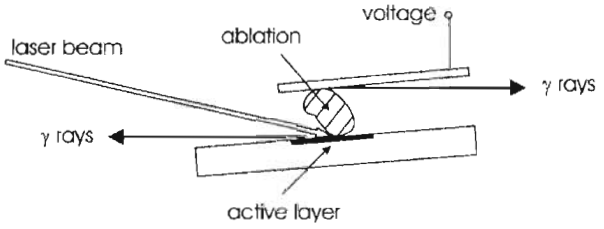

Figure 1. Schematic illustration of the nuclear level pumping by laser pulse.

Table I. Time scales of different processes induced by a powerful laser pulse in a solid

Process	Time scale [sec]
1. Electron-gas excitation	$\sim 10^{-15}$
2. X-ray emission past ionization	$\sim 10^{-16}$–10^{-15}
3. Ablation due to superthreshold power:	
(a) Fast desorption;	$\sim 2 \cdot 10^{-14}$
(a) Temperature mechanism	10^{-12}–10^{-11}
4. Recrystallization of melted layer	10^{-11}–10^{-10}
5. Nuclear fluorescence:	(including conversion)
(a) Collective E2 at $E_\gamma > 50$ keV;	$< 10^{-10}$
(b) Single-particle E1 at $E_\gamma > 50$ keV	$< 2 \cdot 10^{-10}$
6. Condensation of the ablation cloud	$\sim 10^{-8}$

ductor samples. It was found that all processes develop very rapidly and the solid is recrystallized within 100 ps. It is important to stress here a similar time scale characterizes pulsed energy release in solids due to an entirely different process [17, 18]. High-energy heavy ions may deposit a large amount of energy within the limited volume of a nuclear track in a solid. The electronic medium is immediately excited, the same as in the case of the laser pulse, and then a relaxation process follows. It was shown experimentally [17, 18] that in perfect crystals recrystallization is probably one of the final stages, yet it occurs within a time scale of 100 ps. This strong similarity in time scales is definitely not a coincidence, but confirms the general properties of processes in a solid after a pulsed energy release.

The time scale of nuclear fluorescence is defined by the lifetime of an excited level and can be estimated using standard systematics for the strength of nuclear electromagnetic transitions. As is clear in Table I, the decay time of the nuclear level is typically longer than the time scales of all other processes in the atomic and solid subsystems. Even recrystallization of a solid may happen before nuclear fluorescence events happen. Thus, nuclear radiance takes place from within solid surroundings and this is favorable for lasing.

Such a situation permits the occurrence of other attractive properties (discussed in [3–5]) for the scheme that employs laser pulses to pump a hypothetical γ-ray laser on nuclear levels. However, it is necessary to also discuss some disadvantages of the scheme depicted in Figure 1:

1. Some number of excited nuclei might be released into the gas phase due to ablation of atoms from the exposed surface. As long a time as about 10 ns is required for condensation of the ablation cloud back to the surrounding solid surfaces. Nuclear levels may be longer-lived, but for them the probability of excitation is decreased by their narrow widths. For levels with an optimum lifetime of about 100 ps, the efficiency of radiance in a solid will be reduced because of the losses of excited nuclei to the gas phase. A compromise can be found by the choice of the optimum surface power density for the laser. The rate of ablation can be reduced while the total number of excited nuclei is conserved. The full energy of the laser pulse can be distributed over larger area at the surface.
2. The resonance tuning between nuclear and atomic resonators cannot be perfect even when both frequencies coincide. The width of an atomic resonance is typically much larger than the nuclear one because of the orders-of-magnitude different lifetimes of the atomic and nuclear states.

These factors lead to a low value of the "Q-factor" corresponding to the resonance between nuclear and atomic modes. Such a situation has been confirmed recently in direct measurements of the probability of the NEET process obtained in the synchrotron-radiation experiment of [14]. The nuclear transition $3/2^+ \rightarrow 1/2^+$ with $E = 77.351$ keV in ^{197}Au was excited by nuclear conversion of the atomic MI $\rightarrow$ K transition after K-vacancy ionization. The difference in energy was only 51 eV, and this was comparable with the total width of the K-vacancy state. The probability of NEET was found to be $5 \cdot 10^{-8}$, being similar to the width ratio for nuclear and atomic states, Γ_n/Γ_a. The nuclear transition lifetime is known experimentally to be 2.76 ns and the atomic level width can be taken from the systematics of [19].

The mismatch of widths suppresses not only the NEET probability but also the integrated cross-section for the resonance photon absorption. This fundamental effect reduces the nuclear excitation probability and cannot be completely cancelled. It is only possible to discuss some modestly palliative options. The lifetime of an atomic transition is normally increased for lower-energy characteristic photons, the same as for nuclear transitions. One may suppose that vacancies in the M shell should be much longer-lived than K and L vacancies, and this would seem promising to reach comparable magnitudes for the atomic and nuclear widths. In fact, this is not the case. For characteristic energies below 15 keV, the radiative width decreases until it is lower than the width of the intrinsic conversion of the transition energy within atomic shell through the Auger and Coster–Kronig processes. The total width then primarily due to the latter two processes, and the fluorescence yield of X-ray photons will be much less than 1. Thus, the resonance photon excitation

process is suppressed not only due to the widths mismatch, but also directly due to the low yield of characteristic photons.

In a plasma, atoms are strongly ionized and the maximum of the charge-state distribution corresponds to values of $q = 10$–30, dependent on the plasma temperature [9]. This wide charge-state distribution creates a series of characteristic X-ray energies that deviate from the standard ones known for a single vacancy, and this is helpful for exact tuning of the atomic and nuclear transition energies. On the other hand, the high stage of ionization should be effective in suppressing the probability of the Auger and Coster–Kronig processes for soft characteristic transitions with $E_x \leqslant 10$ keV in strongly ionized heavy atoms. The total width of the atomic resonance is correspondingly decreased and the relative probability of radiative processes is thereby increased. Both effects are useful for the nuclear conversion of atomic excitation. Thus, one can anticipate that in plasma surroundings, even M vacancies might be active for the production of characteristic lines and for the resonance excitation of a nuclear transition via photon absorption and NEET processes.

The possibility of suppressing electron conversion of nuclear γ rays in a hot plasma was discussed in [4]. This effect increases the contribution of the radiative width to the total width of a nuclear level (decreasing the conversion coefficient), and it can be useful in some schemes of nuclear level pumping and radiance. In addition, the possibility to use the electron conversion of nuclear radiation for the separation of some specific nuclear states in a multilevel scheme has also been proposed in [4].

At present, however, we will stress that the hot plasma may serve as a tool for the suppression of the nonradiative conversion of the ionization energy within atom. This way the efficiency of energy transfer from an atomic to a nuclear mode can be significantly increased.

When nuclear and atomic transitions have the same energy and multipolarity, the hybridization of atomic-nuclear components is possible. The special wave function of the hybrid state includes such peculiarities as: beating in amplitude of the two modes with repumping of the energy, retardation in the decay time of both modes, nonexponential decay low, etc. As a result, the conversion of energy within the atom may be additionally suppressed, and the nuclear conversion of an electron transition may be enhanced. Such a hybridization was discussed in [20]. Finally, one can conclude that some processes exist that allow resonance energy transfer from atom ionization to nuclear excitation, despite the fact the atomic-nuclear resonance is not originally a very sharp resonance.

3. Candidates for the atomic–nuclear resonance

A fortunate similarity in energies of atomic and nuclear transitions can be found for some isotopes as listed in Table II. Resonance photon excitation of a nuclear level requires only the appropriate value of photon energy while multipolarity matching

Table II. Resonance between nuclear and atomic transitions and possible mechanism of excitation: PE – photoexcitation, NEET – nuclear excitation by electron transition

Nuclide	$T_{1/2}$	Nuclear transition	E^* (keV)	Electron transition	E_x (keV)	Discussed in Ref.	Mechanism
^{98}Tc	$4.2 \cdot 10^6$ y	$6^+ \rightarrow 5^+$ M1 and E2	21.8	$N_I \rightarrow K$ M1	20.98	[20]	PE and NEET
				$N_{IV} \rightarrow K$ E2	21.04		NEET and PE
^{103}Ru	39.3 d	$3/2^+ \rightarrow 5/2^+$ M1 and E2	2.81	$M_{IV} \rightarrow L_I$ E2	2.94	[20]	PE and NEET
				$M_{II} \rightarrow L_I$ E1	2.74		PE
				$M_I \rightarrow L_I$ M1	2.64		NEET and PE
^{161}Dy	Stable	$5/2^+ \rightarrow 5/2^-$ E1	25.652	Sn $L_{III} \rightarrow K$ E1	25.28	[21]	PE
^{181}Ta	Stable	$7/2^+ \rightarrow 9/2^-$ E1	6.238	$M_I \rightarrow L_{III}$ E1	7.17	[4]	PE and NEET
^{189}Os	Stable	$3/2^- \rightarrow 5/2^-$ M1 and E2	69.537	$M_I \rightarrow K$ M1	70.82	[22]	PE and NEET
^{197}Au	Stable	$3/2^+ \rightarrow 1/2^+$ M1 and E2	77.351	$M_I \rightarrow K$ M1	77.300	[14]	NEET and PE
^{235}U	$7 \cdot 10^8$ y	$7/2^- \rightarrow 1/2^+$ E3	0.0768	Plasma radiation	Continuous spectrum	[9]	PE
^{242}Am^m	141 y	$5^- \rightarrow 3^-$ E2	4.30	$L_{III} \rightarrow L_{II}$ M1 and E2	4.44	[20]	PE and NEET
				$N_{II} \rightarrow M_{II}$ M1	4.30		PE
				$N_{VII} \rightarrow M_{III}$ E2	4.24		NEET and PE

has no significance. Photons to be absorbed can even be emitted by an atom of another element present in the sample to form a catalyzing admixture. This kind example was proposed in [21] for the transition in the ^{161}Dy nucleus excited by the Sn K X ray with appropriate energy. A higher efficiency, however, must be reached when the characteristic X-ray energy is absorbed by the nucleus within the same atom.

The NEET process appears when both the energy and multipolarity of atomic and nuclear transitions are identical. In definition, NEET happens only within an individual atom–nucleus system. The examples of probable NEET manifestation are reduced in Table II, and among them is the case of ^{197}Au realized recently in the experiment of [14].

In Table II the difference in the energy of atomic and nuclear transitions appears to be not very small, in some cases being about 1 keV. But one must remember that atomic transition energies E_x are given for the single vacancy atom and this value will be different for each individual ionization state of the ion. In a hot plasma, a wide distribution of charge states arises and a series of atomic terms corresponds to them. Thus better conditions for an atomic–nuclear resonance may be created in a plasma and tuned by a variation of plasma temperature.

The long-lived ^{242}Am^{m} isomeric state with $I^{\pi} = 5^{-}$ seems to be a nucleus of special interest. Triggering via the E2 transition to 3^{-} state at 52.9 keV releases the energy stored in the form of isomeric excitation. The specific energy stored in a ^{242}Am^{m} sample may be as high as 20 MJ/g. Resonance triggering of ^{242}Am^{m} requires a transition energy of (4.30 ± 0.05) keV that can be supplied by an atomic transition in the Am atom – as many as three transitions have the appropriate energy. Photon absorption and NEET mechanisms both are possible, because the multipolarities can be also identical. The quantitative parameters are given in Table II.

In addition to the unknown strength of the nuclear transition in ^{242}Am, another problem has been visible that is connected with the rather low energy of the atomic transition, of about 4.3 keV. As is known, Auger and Coster–Kronig conversion dominates at such energies and the efficiency of energy transfer to the nuclear subsystem should be reduced. Fortunately, as we discussed above, the hot plasma condition suppresses the rate of Auger and Coster–Kronig processes. Thus, even an M vacancy in a heavy atom may have a noticeable fluorescence yield and the nuclear conversion of the atomic transition is not suppressed. Thus, the triggering of the ^{242}Am isomer remains one the best possibilities for pulsed release of "clean" nuclear energy and the observation of ^{242}Am^{m} triggering is one of the challenges of modern experimental physics.

In [2], we proposed the ^{242}Am^{m} and ^{177}Lu^{m} isomers as new candidates for triggered release of energy, in addition to the earlier discussed Hf isomers. Both nuclides are radioactive and can be produced with high yield in the reactors. The ^{242}Am^{m} isomer is normally accumulated in used reactor fuel as one of the radioactive products due to multiple neutron capture process. For ^{177}Lu^{m} production, one has to expose in a neutron flux a special target made of the enriched ^{176}Lu isotope. The lifetime of ^{177}Lu^{m} ($T_{1/2} = 161$ d) does not allow this material to remain ready for years after production for experiments. Thus, experiments with ^{177}Lu^{m} can be performed only if some standard or high-flux reactor, as well as the laboratories for chemical isolation and mass-separation of radioactive prod-

ucts, are available. Such requirements restrict the choice of institutions capable of developing an experimental program with $^{177}Lu^{m}$.

On the other hand, $^{177}Lu^{m}$ stores 20 times larger specific energy per nucleus than $^{242}Am^{m}$, and once triggered it will emit this energy in the form of short-wave γ radiation in the range of 100–200 keV. Because of the advantageous properties of $^{177}Lu^{m}$, we try to determine whether triggering is promising by X-ray and synchrotron radiation.

The level scheme of ^{177}Lu is not yet well-developed. Two rotational yrast bands with $K^{\pi} = 7/2^{+}$ and $9/2^{-}$ are known, and the $19/2^{+}$ and $19/2^{-}$ members of these bands lie at an excitation energy of 1093 and 1073 keV, respectively. The isomeric state $^{177}Lu^{m}$ with $K^{\pi} = 23/2^{-}$ has the excitation energy of 970 keV. One may assume possible triggering via an E2 transition with an energy of 103 keV from the $23/2^{-}$ to $19/2^{-}$ levels. Unfortunately, this transition would be strongly hindered by the K quantum number, because of a degree of K forbiddenness $= (\Delta K - \lambda) = 5$. Despite this, one may discuss that the K-mixed component of the wavefunction has a noticeable amplitude for the 6th level of the $K^{\pi} = 9/2^{-}$ band with $I = 19/2$. A comparison with the neighboring ^{176}Lu is reasonable and can be productive since it has been much better studied than ^{177}Lu as far as level spectroscopy.

A fragment of the ^{176}Lu level scheme is shown in Figure 2. The nearly stable ground state has $K^{\pi} = 7^{-}$ and the short-lived ($T_{1/2} = 3.7$ h) isomer with $K^{\pi} = 1^{-}$ lies at 123 keV. So, there are two systems of levels with high and low K values. They can be coupled only via some mediating levels possessing a special K-mixed wavefunction. Such levels do exist, as was shown in the experiments of [23–25]. In [23], the 1^{-} isomer was excited in irradiations of the ^{176}Lu target by intense radioisotope γ radiation of ^{60}Co and ^{137}Cs sources. The monoenergetic γ-radiation of ^{137}Cs consists of 662 keV photons, and successful population of the 1^{-} isomer shows the presence of some K-mixed level at an energy below 662 keV. The spectroscopic identification of this level has not yet been successful. However, in [25] a level with I, $K^{\pi} = 5, 4^{-}$ at 838 keV was definitely recognized as a mediating level between $K = 7$ and $K = 1$ levels.

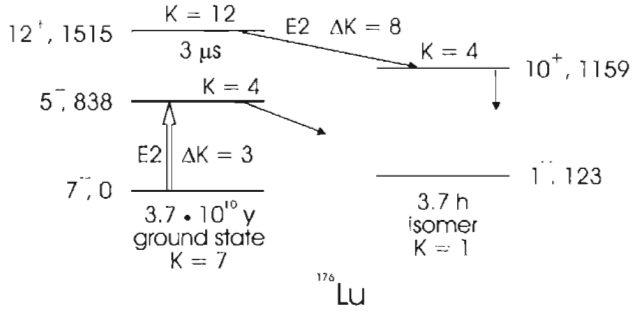

Figure 2. Mediating levels in ^{176}Lu, as can be deduced from [24, 25]. Energies of levels are given in keV.

Even more exotic properties have been found in [24] for the transition from the $I, K^{\pi} = 12, 12^{+}$ isomeric state at 1515 keV to the $I, K^{\pi} = 10, 4^{+}$ rotational state at 1159 keV. This transition should be strongly K-hindered, with $(\Delta K - \lambda) = 6$, but in experiments a rather low reduced hindrance factor has been found, meaning that the wavefunctions of the high-K isomeric state and the low-K rotational level are mixed. This is important for proposed triggering of the ^{177}Lu isomer. If the properties of ^{176}Lu and ^{177}Lu nuclei are similar, one may expect a successful ^{177}Lu^{m} triggering by synchrotron radiation. An experimental test would be intriguing and feasible.

To summarize, the time scale of different processes after pulsed release of energy are compared, and the typical time of nuclear fluorescence appears to be longer the atomic and solid relaxation processes. The possibility of nuclear radiance in solid surroundings after sample recrystallization is promising for lasing of nuclear γ rays. Nuclear excitation in a hot dense plasma via the resonance between atomic and nuclear transitions also possesses some attractive properties. Among them are the suppression of Auger and Coster–Kronig conversion of the ionization energy, the shift of the characteristic energies of the atomic levels, dependent on a charge state, and possible hybridization of the atomic–nuclear wave functions. The discussed processes may be useful for increasing the efficiency of nuclear excitation by a laser pulse. The nuclear state candidates for the pumping by atomic transitions are characterized. Among these are also promising candidates for triggered release of stored nuclear energy.

Acknowledgements

The authors gratefully acknowledge support from: (SAK) the US Air Force European Office of Aerospace Research and Development for the visit to the LASERS'01 Conference to participate in the 3rd AFOSR Isomer Workshop, and (JJC) AFOSR contract F49620-99-1-0263.

References

1. Carroll, J. J., Karamian, S. A., Rivlin, L. A. and Zadernovsky, A. A., *Hyp. Interact.* **135** (2001), 3.
2. Karamian, S. A. and Carroll, J. J., In: V. J. Corcoran and T. A. Corcoran (eds), *Proc. Int. Conf. on LASERS 2000*, STS Press, McLean, VA, 2001, p. 545.
3. Andreev, A. V., Gordienko, V. M., Dykhne, A. M. *et al.*, *JETP Pis'ma* **66** (1997), 312.
4. Andreev, A. V., Volkov, R. V., Gordienko, V. M. *et al.*, *JETP* **118** (2000), 1343.
5. Andreev, A. V., Gordienko, V. M. and Savel'ev, A. B., In: I. I. Popescu and C. A. Ur (eds), *Proc. Int. Workshop on Induced Gamma Emission, Predeal 1997*, Bucharest, 1999, p. 291.
6. Karpeshin, F. F., Harston, M. R., Attallah, F. *et al.*, *Phys. Rev. C* **53** (1996), 1640.
7. Karpeshin, F. F., Band, I. M. and Trzhaskovskaya, M. B., *Nucl. Phys. A* **654** (1999), 579.
8. Tkalya, E. V., *Nucl. Phys. A* **539** (1992), 209.
9. Harston, M. R. and Chemin, J. F., *Phys. Rev. C* **59** (1999), 2462.
10. Attallah, F., Aiche, M., Chemin, J. F. *et al.*, *Phys. Rev. C* **55** (1997), 1665.

11. Goldanski, V. I. and Namiot, V. A., *Yad. Fyz.* **33** (1981), 319.
12. Kalman, P. and Keszthelyi, T., *Phys. Rev. A* **47** (1993), 1320.
13. Irwin, G. M. and Kim, K. H., *Phys. Rev. Lett.* **79** (1997), 990.
14. Kishimoto, S., Yodo, Y., Seto, M. *et al.*, *Phys. Rev. Lett.* **85** (2000), 1831.
15. Schmidt, V., Husinsky, W. and Betz, G., *Phys. Rev. Lett.* **85** (2000), 3516.
16. Cavalleri, A., Siders, C. W., Brown, F. L. H. *et al.*, *Phys. Rev. Lett.* **85** (2000), 586.
17. Karamian, S. A., *Nucl. Instr. Meth. B* **51** (1990), 357.
18. Karamian, S. A., *Radiation Meas.* **25** (1995), 243.
19. Keski-Rahkonen, O. and Krause, M. O., *At. Data Nucl. Data Tables* **14** (1974), 139.
20. Karamian, S. A. and Carroll, J. J., *Laser Phys.* **12** (2002), 310.
21. Oganessian, Yu. Ts. and Karamian, S. A., *Laser Phys.* **5** (1995), 336.
22. Ahmad, I., Dunford, R. W., Esbensen, H. *et al.*, *Phys. Rev. C* **61** (2000), 051304.
23. Lakosi, L., Veres, A., Tam, N. C. and Pavliczek, I., *Nucl. Instr. Meth. A* **312** (1992), 17.
24. McGoram, T. R., Dracoulis, G. D. and Kibedi, T., *Phys. Rev. C* **62** (2000), 031303R.
25. Doll, C., Börner, H. G., Jaag, S., Käppeller, F. and Andrejtscheff, W., *Phys. Rev. C* **59** (1999), 492.

Hyperfine Interactions **143:** 111–119, 2002.

Gamma Spectroscopy of Hf-178m2 Using Synchrotron X-Rays

H. E. ROBERTS[1], M. HELBA[1], J. J. CARROLL[2], J. BURNETT[2], T. DRUMMOND[2], J. LEPAK[2], R. PROPRI[2], Z. ZHONG[3] and F. J. AGEE[4]
[1] *System Technology Group, SRS Technologies, Huntsville, Alabama 35806, USA*
[2] *Center for Photon Induced Processes, Youngstown State University, Youngstown, Ohio 44555, USA*
[3] *National Synchrotron Light Source, Brookhaven National Laboratory, NY, USA*
[4] *Office of Scientific Research, United States Air Force, Arlington, VA 22203-1977, USA*

Abstract. Preliminary survey experiments have been performed to examine the triggering of gamma emission from the 31-year Hf-178m2 isomer using intense monochromatic synchrotron radiation from the X15A beamline at the National Synchrotron Light Source at Brookhaven National Laboratory. Initial studies were performed to probe incident photon energies over the L_1, L_2, and L_3 X-ray edges of Hf and the 12–13 keV range. Resonances larger than the experimental minimum detectable level of 10^{-25} cm^2 keV were not observed.

Key words: Hf-178m2, nuclear isomer, isomer triggering, synchrotron radiation, gamma spectroscopy.

In 1999 Roberts and Carroll with Collins *et al.* [1] reported an accelerated emission from the 31-year isomer of Hf-178m2 when pumped by a low intensity bremstrahlung X-ray source with an end point energy of 90 keV. An effect on the order of 4% was reported. This resulted in a rather large estimate of the integrated cross section on the order of 10^{-21} cm^2 keV. In a follow-up experiment, Collins *et al.* [2] reported similar results but with the estimated integrated cross section somewhat reduced. In 2001 Ahmad *et al.* [3] reported observing no acceleration of emission using the same isomer, albeit more robustly packaged, when pumping with an intense synchrotron white beam. Additional synchrotron experiments by Roberts *et al.* are reported herein in which a monochromatic synchrotron radiation beam is used as the pumping source for Hf-178m2. The pumping energy was varied to cover several regions of interest in the range of 9.5–13.5 keV. All these various experiments [1–3] and the experiments reported herein used source material for the Hf-178m2 isomer obtained from a common Ta target used in 1980 as a target for a long duration proton irradiation at the Los Alamos Meson Production Facility, LAMPF.

The target used, Figure 1, contained approximately 1.8×10^{13} nuclei of the Hf-178m2 isomer along with ground state Hf-178 and the shorter-lived Hf-172 and its Lu-172 daughter in secular equilibrium. The source was prepared by deposition as the oxide evaporated from a solution of the hafnium in hydrochloric acid. The ratio of Hf-178 to Hf-178m2 and Hf-172 was approximately 2000 : 1. The Hf-178m2

Figure 1. Hf-178m2 target.

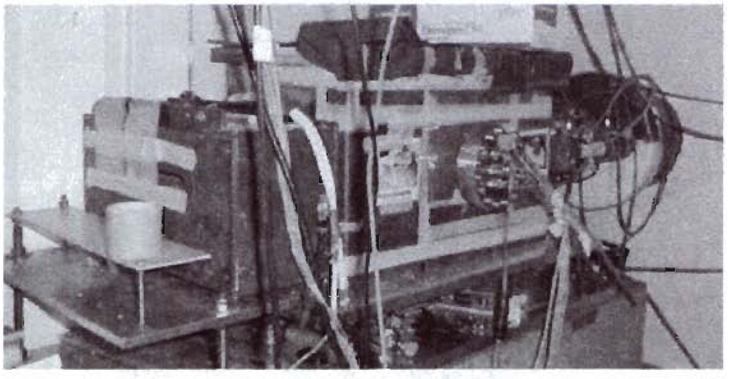

Figure 2. The X15A monochromator housing.

and the Hf-172 were in a ratio of approximately 10 : 1. The thin planar source was dry encapsulated in polycarbonate plastic. The total planar source deposition region was approximately 3 mm diameter, and essentially circular in form. The polycarbonate substrate and cover lid were each 0.48 mm in thickness.

This sample was irradiated in the X15A beamline of the National Synchrotron Light Source in a series of ten experiments conducted during a one week time-frame. The X15A output was passed through a silicon perfect crystal monochromator using [111] reflection and lead aperture [4], as shown in Figure 2. The beam at the target was a 2×5 mm rectangle well centered on the 3 mm isomer deposition. The target was placed at a 45 degree angle to the beam axis to facilitate monitoring of target emission by a nearby HPGe detector. Figure 3 shows the experimental arrangement of the target and its drive stage with respect to the beam, ion chambers, and HPGe detector. Initial beam centering on the target was confirmed visually using photo paper placed over the target. The target was then centered in the beam both vertically and horizontally by detecting the L_α edge absorption for Hf with

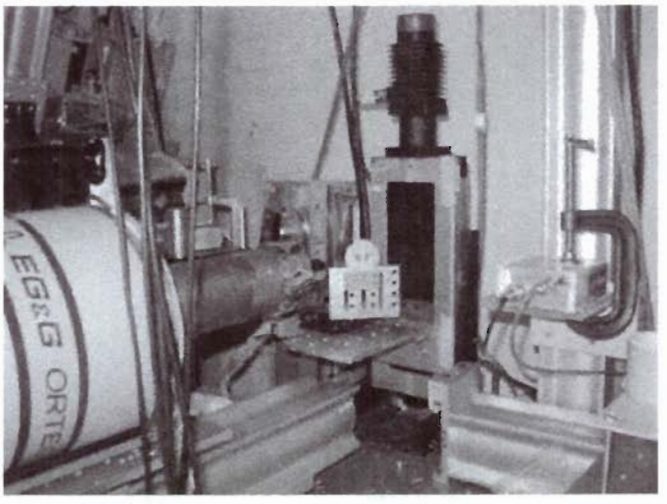

Figure 3. Hf target on stepper motor stage, HPGe detector, and ionization chambers.

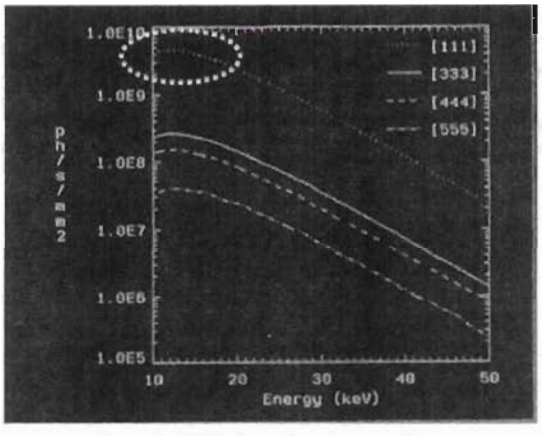

Figure 4. X15A beamline characteristics.

a post-target ionization chamber through which the beam was passed before the final beam stop in the radiation hutch. The absorption edge was maximized by fine positioning using stepper motor actuators on the target mount to center the target for maximum absorption. The beam was also monitored by a pre-target ionization chamber placed between the monochromator outlet aperture and the target. The flux of the beam over the range of energies used (9.5–13.5 keV) was 4.5×10^9 photons/s/mm^2 at the target, with a spectral width of approximately 2 eV. Figure 4 shows the X15A beam characteristics for various monochromator crystal orientations. The [111] reflection was used for these experiments. The beam was

swept in energy steps of about 0.67 eV per step. These are the first synchrotron experiments for pumping of this isomer that achieve 100% coverage in pump energy, rather than sampling a narrow energy slice at broad periodic intervals. At each energy data were typically collected for 20 seconds. A 0.2 keV survey region was covered in 300 steps of the monochromator angle, hence typically requiring 6000 seconds per 0.2 keV survey.

A 10% HPGe detector was placed at two different target distances of 16 and 4 cm orthogonal to the beam axis. The closer distance was found to be more suitable, but required careful placement of 1/16th inch lead sheeting over the detector to shield it from scattered X-rays in order to keep counting rates within the detector limits. The output of the detector was collected by an Ortec 973 fast amplifier. The counts were collected using an 8k ADC and by four single channel analyzers. Three were set to monitor specific principle lines in the target emission: the 213.4 keV, 325.6 keV and 426.4 keV lines. The fourth SCA monitored an injected pulser line at 1256 keV, well above any target lines of interest. The germanium detector was able to detect all the relevant γ lines of interest over the energy range from 46–2316 keV.

During a sweep of beam energy, the total counts per channel of the ADC were recorded as a function of channel and monochromator angle. Data at a given monochromator angle was collected for 20 seconds. The ADC spectrum and the SCA readouts were recorded after 20 seconds of irradiation at a fixed energy. The ADC and SCA data were cleared for the next data collection step. The monochromator angle was increased one step which decremented the beam energy by 0.67 eV. This process was under full automated computer control of the monochromator and data collection. A diagram of the entire experimental arrangement is shown in Figure 5.

The regions that have been surveyed in this first sequence of experiments are shown in Table I. No apparent enhancements were observed in the surveyed regions. Notice however, that the region surveyed is quite small compared to the earlier reported enhancements [1, 2] from a broadband X-ray pump source: a total of less than 2 keV out of a potential 40 keV region.

The experimental data were analyzed using the IDL software package for data visualization. A plot of an entire 6000 second (typical) data collection was developed for each run, as shown in Figure 6. This shows only data covering the energy region from 46–613 keV in the gamma-ray spectrum, which includes all the relevant Hf-178m2 lines. It is a quarter of the total data for an experiment. A full data set consists of a total of four such panels extending from 46–2316 keV, as shown in Figure 7. The data is presented as digitized gray scale. The total counts per ADC channel are converted to gray scale where the highest count is set to black. One pixel of the display screen represented the γ emission value for one discrete emission–excitation energy pair. By adjusting the conversion threshold and gain setting for the conversion, it was possible to quickly scan the large volume of data obtained from an experiment for any significant changes in γ emission. There had been reported at an Isomer Working Group workshop held in Telluride

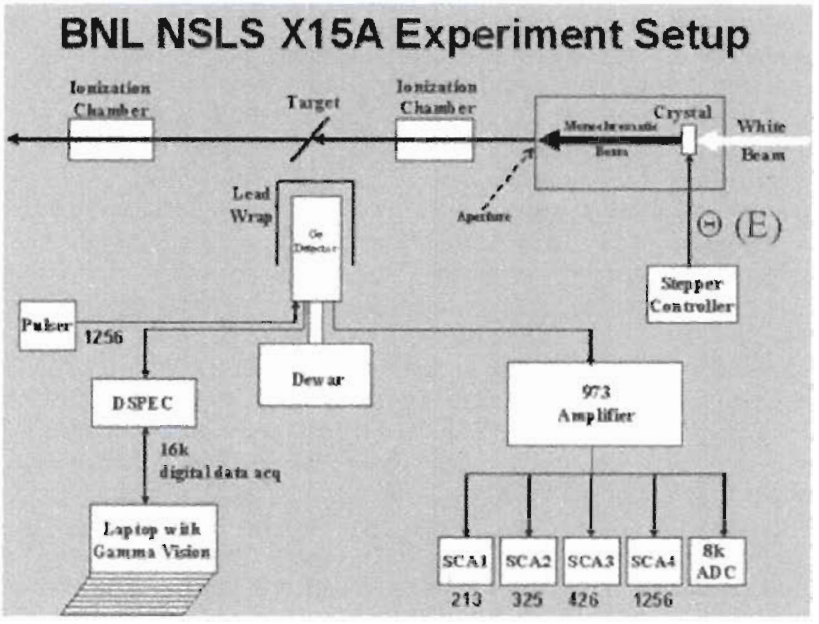

Figure 5. X15A experimental setup.

Table I. Energy ranges of survey regions

Experiment number	Lower energy bound	Upper energy bound
2	12.000 keV	13.000 keV
3	13.000 keV	13.500 keV
6	12.399 keV	12.599 keV
8	11.070 keV	11.470 keV
9	9.361 keV	9.761 keV
10	10.570 keV	11.070 keV
11	9.509 keV	9.667 keV
12	10.570 keV	10.850 keV
13a	12.600 keV	13.000 keV
13b	10.707 keV	10.849 keV

CO during May of 2001 some observations of enhancements using monochromatic synchrotron radiation beams fortuitously adjusted to an excitation energy so that apparently rather large changes in emission rate occurred when pumped with 12.5 keV monochromatic synchrotron radiation; enhancements interpreted by us to exceed the few percent reported in [1, 2]. A similar data analysis scheme was

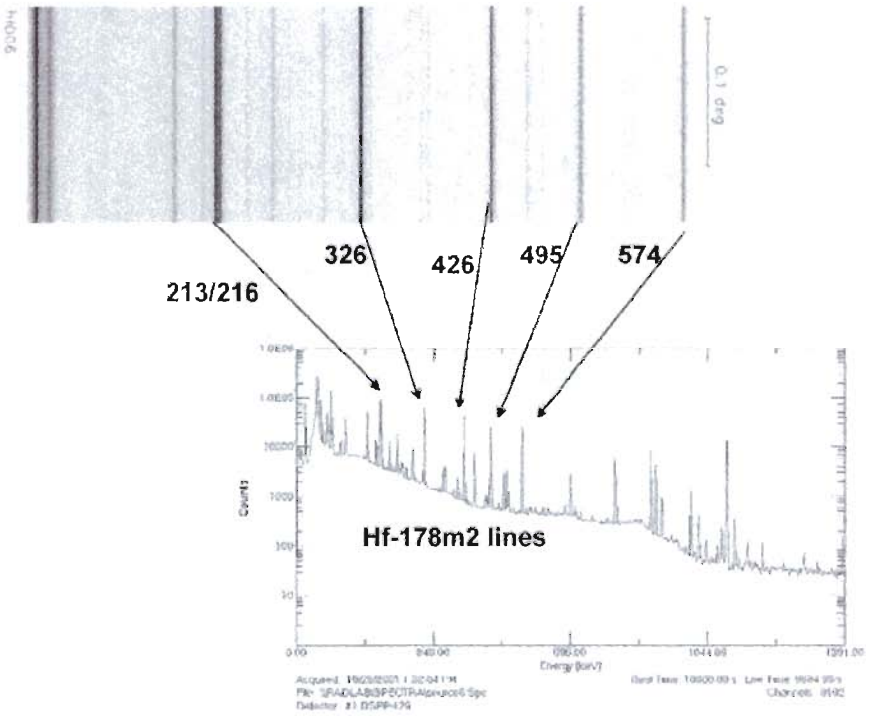

Figure 6. A 46–613 keV section of spectrum irradiated by 12.4–12.6 keV synchrotron radiation.

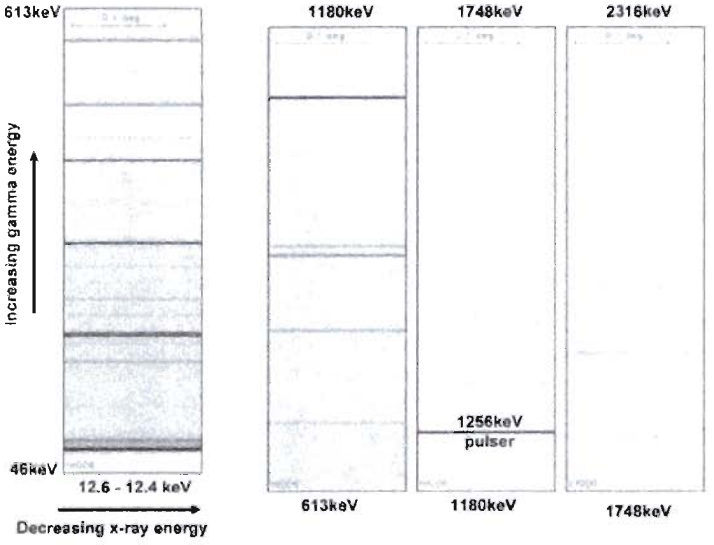

Figure 7. Full spectrum from 46–2316 keV irradiated by 12.4–12.6 keV synchrotron radiation.

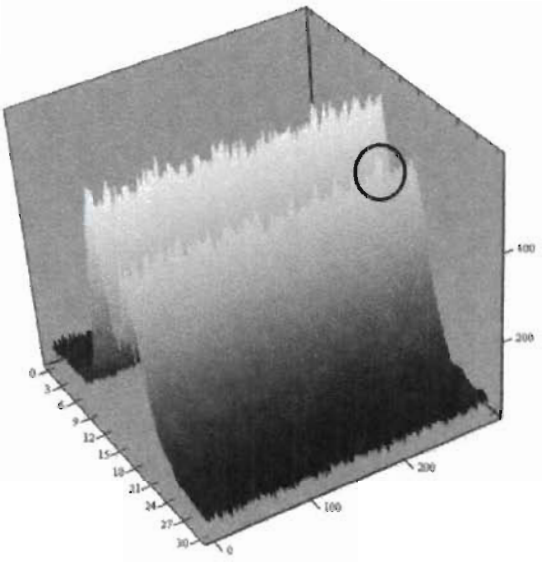

Figure 8. 213 and 217 keV lines irradiated by 12.6–12.4 keV synchrotron radiation. Feature at 12.4 keV highlighted.

used to scan for any such large signal events. Such an event could appear in at least two forms: (1) an enhancement of an existing line at a discrete excitation energy or range of excitation energies; or (2) as the appearance of a new emission line at a discrete energy or range of excitation energies. The first type of event would be observed in the data as a step change in the magnitude of a line, i.e., a "dark spot" on a line. The second type would be observed as the appearance of a "dark spot" unassociated with any existing line due to spontaneous decay. The data was rigorously searched for such irregularities by the entire experimental team. First a visual scan of all the Hf-178m2 lines was performed for any apparent irregularity. Threshold and gain settings were adjusted to maximize the relative differences in signal to noise levels present in the data. Then, the background was scanned for irregularities greater than the average local noise background. This process was successful in identifying several such events that were detectable by this means, but were found not to be statistically significant upon subsequent evaluation. This provided confidence that had any such significant irregularities existed in the data, such a process would have successfully screened for them.

When candidate events were identified a more rigorous data analysis was performed. One such event was identified for the 217 keV line during the energy sweep covering 12.6–12.4 keV at approximately 12.42 keV. Figure 8 shows a detail data analysis of this region. The "peak" just exceeds a 3σ significance. However, the variation of the entire line frequently approaches this level of significance, and there is no correlation between this event on the 217 keV line and any other lower-

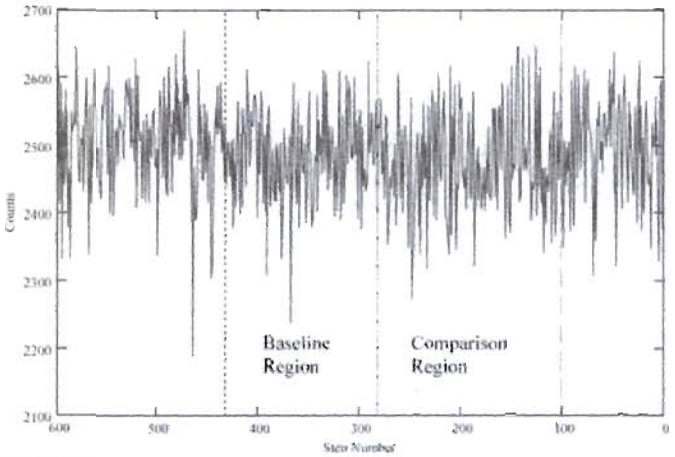

Figure 9. 215.3–220.3 keV region integrated counts irradiated with synchrotron radiation scanning from 11.07 keV (step 599) to 11.47 keV (step 0).

lying transitions in the ground state band which the 217 keV transition feeds. Other similar 3σ peaks were found on the 326 keV line, but at a beam energy of about 12.5 keV with no correlation to the peak seen on the 217 keV line. Taken together these events were judged unlikely to be anything other than uncorrelated random noise events. This is not unexpected given the large volume of data collected. Albeit, such events should be resampled to verify this conclusion. As of this time, no such resampling has been possible. No statistically significant peaks were identified in the background regions of the data. (i.e., in regions where no relevant Hf-178m2 lines are found.)

Given the minimum detectable counts above background, source activity, X-ray flux, and energy allows the calculation of a minimum detectable integrated cross section for these experiments. This is on the order of 10^{-25} cm^2 keV. Any events exhibiting cross-sections larger than this should have been readily apparent in the data. No such events were observed.

A third means of data analysis was performed looking at potential enhancements in the 217 keV line for pumping energies near the L1 edge. Figure 9 shows the integrated counts in a region of interest from 215.3–220.3 keV for synchrotron radiation pumping energies that range from 11.07 to 11.47 keV. (For comparison, the L_1 edge is at 11.27 keV.) A baseline region was arbitrarily set to cover energies from 11.18 to 11.28 keV, as indicated in Figure 9. A second comparison region is shown spanning energies from 11.28 to 11.4 keV. No statistical difference was observed between the baseline and comparison regions. The baseline region mean count is 2485 (66), while the comparison region mean count is 2478 (76). No enhancement was observed in this region near the L_1 edge.

While several such marginally significant events were detected, no experiments were possible to determine if the results were reproducible, due to limitations of beam time. Future experiments are planned to reexamine these energy regions identified as having potential candidate events. Also, future experiments are planned to complete the survey for excitation pump energies from 7 to 15 keV with 100% energy coverage as proven to be a workable protocol by these first such full coverage surveys.

Acknowledgements

The authors gratefully acknowledge support of this experiment by the US Army Research Laboratory through contract DAAD17-01-C-057, and by the US AFOSR through contract F40620-00-1-0263. This work was supported in part by US DOE contract DE-AC02-CH10886. The experimental source was provided by SRS Technologies through the US Air Force Research Laboratory Contract F29601-99-C-0011.

References

1. Collins, C. B., Davanloo, F., Dussart, R., Iosif, M. C., Hicks, J. M., Karamian, S. A., Ur, C. A., Popescu, I. I., Kirischuk, V. I., Carroll, J. J., Roberts, H. E., McDaniel, P. and Crist, C. E., *Phys. Rev. Lett.* **82** (1999), 695.
2. Collins, C. B., Davanloo, F., Rusu, A. C., Iosif, M. C., Zoita, N. C., Camase, D. T., Hicks, J. M., Karamian, S. A., Ur, C. A., Popescu, I. I., Dussart, R., Pouvesle, J. M., Kirischuk, V. I., Strilchuk, N. V., McDaniel, P. and Crist, C. E., *Phys. Rev. C* **61** (2000), 054305.
3. Ahmad, I., Banar, J. C., Becker, J. A., Gemmell, D. S., Kraemer, A., Mashayekhi, A., McNabb, D. P., Miller, G. G., Moore, E. F., Pangault, L. N., Rundberg, R. S., Schiffer, J. P., Shastri, S. D., Wang, T. F. and Wilhemy, J. B., *Phys. Rev. Lett.* **87** (2001), 072503.
4. Zhong, Z. Thomlinson, W., Chapman, D. and Sayers, D., *Nucl. Instr. Meth. Phys. Res. A* **450** (2000), 556.

Hyperfine Interactions **143:** 153–174, 2002.

Non-Radiative Triggering of Long-Lived Nuclear Isomers

A. A. ZADERNOVSKY[1] and J. J. CARROLL[2]
[1] *Applied Physics Laboratory, Quantum Nucleonics Section, R&D Department, Moscow Institute of Radioengineering, Electronics and Automation, Moscow 119454, Russia*
[2] *Center for Photon-Induced Processes, Department of Physics and Astronomy, Youngstown State University, Youngstown, Ohio 44555, USA*

Abstract. The triggering of long-lived isomeric nuclei by non-radiative excitation to a relatively short-lived mediating state is considered. Coulomb triggering in inelastic scattering of heavy ions, a transfer of triggering energy from resonant electron transitions of atomic shell (NEET) and triggering by capture of a free electron into a bound atomic state (NEEC) are discussed. Cross sections for the above processes of non-radiative triggering are presented and the relative efficiencies of these different triggering mechanisms are discussed. Numerical estimates are presented for the selected isomers.

Key words: triggered gamma emission, non-radiative nuclear excitation, nuclear isomers.

1. Introduction

Triggering of an isomeric nucleus implies a release of the energy stored in a long-lived nuclear state by exciting to some higher mediating level with subsequent prompt decay to lower states by emission of gamma radiation or by internal electron conversion. Such a scheme requires the existence of a higher state S (Figure 1) at an energy near that of the isomer state I which could be reached by either absorption of externally-produced X-ray radiation or by non-radiative excitation.

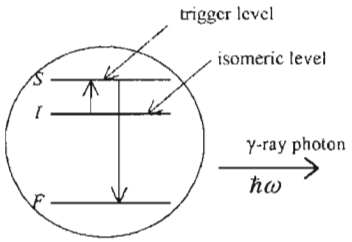

Figure 1. Schematic diagram showing the general process of triggered gamma emission if the initial state I is an isomer. Trigger level S could be reached by either absorption of externally-produced X-ray radiation or by non-radiative excitation.

The cross section for triggering of an isomer by the overall I-to-S-to-F transition can be expressed as

$$\sigma = \sigma_1 \frac{\Gamma_{SF}^{(\Gamma)}(1 + \alpha_{SF})}{\Gamma_S}, \tag{1}$$

where σ_1 is the cross section for the first-step nuclear excitation from the isomeric level I to a trigger level S with the total width Γ_S; and $\Gamma_{SF}^{(\Gamma)}$, α_{SF} are the partial radiation width and the internal conversion coefficient, respectively, of the second-step transition from S to a final nuclear state F.

Photon-triggered gamma emission from long-lived metastable nuclear excited states has been established since 1987 [1, 2]. Over the next decade the majority of experiments have been focused on the idea to employ externally-produced X-rays as a means of driving, or triggering, the emission of gamma radiation [3]. With these experimental results have come proposals for the creation of collective and avalanche-like incoherent gamma-ray bursts [4, 5] and even for the ultimate light source, a gamma-ray laser [6, 7]. The state-of-the-art in experimental results and concepts for more advanced production of gamma rays, driven by externally-produced X-rays, has been surveyed in the review of [8].

The purpose of this paper is to discuss some triggering processes that may release energy stored in a long-lived isomeric nuclear state by means of radiationless excitation to a relatively short-lived mediating state. Among these processes are: Coulomb triggering in inelastic scattering of nuclear particles or heavy ions, a transfer of triggering energy from resonant electron transitions of the atomic shell (the process is referred to as NEET – nuclear excitation by electron transition), and triggering of isomeric nuclei by capture of a free electron into a bound atomic orbital (the process is referred to as NEEC – nuclear excitation by electron capture). Cross sections for the above processes of non-radiative triggering are presented, with the relative efficiencies of different triggering mechanisms and some numerical estimates for the selected isomers.

2. Triggering of nuclear isomers by charged particle beams

When a moving charged particle in a beam comes close to a nuclear isomer it is deflected by the long-range Coulomb field arising from the nuclear electric charge. The relative motion of charged particles and a target nucleus produces a time-varying electromagnetic field that may cause a transition from an isomeric nuclear level to a lower nuclear state via some higher-lying intermediate level. Thus some of the beam particles may undergo an inelastic scattering accompanying by triggered emission of gamma quanta or by internal electron conversion.

There is a significant difference between excitation of a nuclear isomer by a beam of charged projectiles that are themselves nuclei (for instance, protons, alpha particles, etc.) and by a beam of electrons. Due to the relatively slow motion of projectiles with large mass, a beam of nuclear particles with energies up to 10 MeV can

only excite electric nuclear transitions with tangible cross sections. On the contrary, a beam of electrons with the same bombarding energies can excite both magnetic and electric nuclear transitions with comparable cross sections. Additionally, due to the attractive between a beam electron and a target nucleus, much higher-lying nuclear mediating excited states can be reached in electron excitation. At the same time, there is a strong competition between the process of nuclear excitation by inelastic electron scattering and that of bremsstrahlung creation, which is far more probable for electrons than for heavy nuclear projectiles. The large mass of the projectiles used in Coulomb excitation with nuclear particles does allow for a relatively simple analysis of that process in terms of a semi-classical approximation that is quite inappropriate for electron scattering. For these reasons, Coulomb excitation with nuclear particles and electrons are considered to be quite different fields both in theory and experiments. We discuss below the Coulomb excitation with nuclear particles only.

2.1. COULOMB TRIGGERING OF NUCLEAR ISOMERS

The cross section for the triggering process can be expressed by Equation (1) with the Coulomb excitation cross section σ_1 being used for the first-step nuclear transition from the isomeric level I to a mediating level S. Coulomb excitation of nuclei by beams of nuclear particles is a well-elaborated field of nuclear physics which is extensively used for the exploration of nuclear structure. We outline the theory of Coulomb excitation by nuclear projectiles following the famous books of [9, 10] and the classical review of Alder *et al.* [11].

It is usually assumed that the repulsion between the target nucleus and incident projectiles is strong enough to prevent the projectiles from entering the nucleus. In this case, we are sure that there is no direct nuclear interaction between the target nucleus and projectile. If the projectile moved in a classical orbit, this condition occurs when the distance of closest approach $2a$ in a head-on collision,

$$a = \frac{Z_1 Z_2 e^2}{m_0 v^2}, \tag{2}$$

is greater than the sum of the radii of target and projectile. This is equivalent to saying that the projectile energy must be less than that of the Coulomb barrier, E_B. Here, m_0 denotes the reduced mass of projectile and target nucleus, v is the projectile velocity at large distance, Z is the charge number, with subscripts 1 and 2 referring to projectile and target nuclei, respectively. The motion of the projectile, however, is not described correctly by a classical orbit but rather by a wave packet. It can be shown [10, 11] that a criterion required to exclude a direct nuclear interaction is that the dimensionless Sommerfeld parameter, η, is significantly greater than unity, i.e.

$$1 \ll \eta = \frac{a}{\lambda\!\!\!^{-}} = \frac{Z_1 Z_2 e^2}{\hbar v}, \tag{3}$$

where $\lambda\!\!\!^{-} = \hbar/m_0 v$ is the reduced De Broglie wavelength of the target nucleus at the distance of closest approach.

When the projectile passes the target nucleus it produces a pulse in the interaction energy and the temporal width of this pulse is on the order of a/v. Hence, the maximum frequency component in the pulse is on the order of v/a. This means that the probability for a nuclear transition with excitation energy ΔE will be negligibly small unless $\hbar v/a \geqslant \Delta E$. It is convenient to define the dimensionless parameter ξ as

$$\xi = \frac{a\Delta E}{\hbar v} = \eta \frac{\Delta E}{2E}, \tag{4}$$

where $E = m_0 v^2/2$. The excitation will be strong when $\xi < 1$. By applying the condition $\xi = 1$ and $E = E_B$ (the energy of Coulomb barrier can be approximately estimated by $E_B \approx Z_1 Z_2 A_2^{-1/3}$ MeV, where A_2 is the mass number of target nucleus and we neglect the radius of the projectile), one can estimate [9] the highest transition energy likely to be observed in Coulomb excitation to be about 4 MeV.

The quantum-mechanical treatment of Coulomb excitation of a nucleus, considering the interaction as arising from the exchange of a virtual photon between projectile and nucleus, gives rise to the following expression for the total excitation cross section by nuclear beams:

$$\sigma_C^{(n)} = A_{E(M)} \left(\frac{Z_1 e}{\hbar v_i} \right)^2 a^{-2L+2} B\big(E(M)L\uparrow\big) f_{E(M)L}(\eta_i, \xi), \tag{5}$$

where $B(E(M)L\uparrow)$ is the reduced transition probability associated with the nuclear excitation by the electric (EL) or magnetic (ML) 2^L-pole transition (measured in units of e^2 (length)^{2L} for EL or in μ_N^2 (length)$^{2L-2}$ for ML transitions and $\mu_N = e\hbar/2m_p c$ is the nuclear magneton), $A_E = 1$ and $A_M = (v_i/c)^2(v_f/v_i)$, and v_i and v_f are the initial and final velocity of projectile, respectively. The a and ξ values given by the so called symmetrized expressions

$$a = \frac{Z_1 Z_2 e^2}{m_0 v_i v_f} \tag{6}$$

and

$$\xi = \eta_f - \eta_i = \frac{Z_1 Z_2 e^2}{\hbar v_f} - \frac{Z_1 Z_2 e^2}{\hbar v_i} \tag{7}$$

which replace Equations (2) and (4), respectively. It is readily seen that the expressions of Equations (6) and (7) for a and ξ are equal to Equations (2) and (4), respectively, to lowest order in $\Delta E/E$. One can see from Equation (5) that the magnetic transitions are reduced by a factor of order $(v_i/c)^2$.

The difference between classical and quantal description of Coulomb excitation is mainly contained in the functions $f_{E(M)L}(\eta_i, \xi)$, which in the classical

case depend only on ξ and correspond to the limiting values of the quantum-mechanical functions $f_{E(M)L}(\eta_i, \xi)$ for $\eta_i \rightarrow \infty$. In the most practical cases, when $\eta_i > 10$ (see the requirement of Equation (3)), the quantal f functions differ only slightly from the classical limit and it is convenient to write $f_{E(M)L}(\eta_i, \xi) = f_{E(M)L}(\xi) \times R_{E(M)L}(\eta_i, \xi)$, where $f_{E(M)L}(\xi)$ is the classical f function and where the quantum effects are contained in the correction factor $R_{E(M)L}(\eta_i, \xi)$. Both the classical and the quantal correction functions are tabulated and plotted in [11] for nuclear transitions of different types and multipolarities.

We finish this section by compilation from the review of Alder *et al.* [11] convenient expressions for numerical computation of the Coulomb excitation cross section and by discussion the requirements to the range of projectile energies in nuclear beams. For application of the above formulas, it is convenient to write all parameters involved as functions of the initial energy of the incident projectile

$$E = \frac{m_1 v_i^2}{2}, \tag{8}$$

so that the final energy is obtained from the equation

$$\frac{m_1 v_f^2}{2} = E - \Delta E', \tag{9}$$

where the projectile energy loss $\Delta E'$ is related to the nuclear excitation energy ΔE by the expression

$$\Delta E' = \left(1 + \frac{A_1}{A_2}\right)\Delta E. \tag{10}$$

The nuclear mass numbers A_1 and A_2 correspond to the projectile and the target nucleus, respectively. Introducing

$$\varepsilon = \frac{\Delta E'}{E}, \tag{11}$$

into the symmetrized parameter a of Equation (6), we obtain

$$\begin{aligned} a &= \frac{1}{2}\left(1 + \frac{A_1}{A_2}\right)\frac{Z_1 Z_2 e^2}{E}(1-\varepsilon)^{-1/2} \\ &= 0.07199\left(1 + \frac{A_1}{A_2}\right) Z_1 Z_2 (1-\varepsilon)^{-1/2} E^{-1} 10^{-12}\ (\text{cm}), \end{aligned} \tag{12}$$

where E is the initial energy (Equation (8)) expressed in MeV. The parameter η (Equation (3)) for the initial and final states may be written, with E in MeV, as

$$\eta_i = 0.5 Z_1 Z_2 A_1^{1/2} (10.008 E)^{-1/2} \tag{13}$$

and

$$\eta_f = \eta_i (1-\varepsilon)^{-1/2}. \tag{14}$$

A convenient expansion of ξ (Equation (7)) in powers of the energy loss is given by the following, with E and $\Delta E'$ being expressed in MeV:

$$\xi = \frac{Z_1 Z_2 A_1^{1/2} \Delta E'}{12.65(E - \Delta E'/2)^{3/2}} \times \left(1 + \frac{5}{32}\left(\frac{\Delta E'}{E}\right)^2 + \cdots\right). \tag{15}$$

For electric excitations, the cross section is given by the expression

$$\sigma_C^{(n)} = c_{EL} E^{L-2}\left(E - \Delta E'\right)^{L-1} B(EL\uparrow) f_{EL}(\eta_i, \xi) \text{ (barns)}, \tag{16}$$

with

$$c_{EL} = \frac{Z_1^2 A_1}{40.03}\left[0.07199\left(1 + \frac{A_1}{A_2}\right) Z_1 Z_2\right]^{-2L+2}, \tag{17}$$

where E and $\Delta E'$ are expressed in MeV and the reduced nuclear transition probability $B(EL\uparrow)$ is measured in units of $e^2(10^{-24}\ \text{cm}^2)^L = e^2 \text{b}^L$.

Similarly, for the magnetic excitations the cross section is given by

$$\sigma_C^{(n)} = c_{ML} E^{L-3/2}\left(E - \Delta E'\right)^{L-1/2} B(ML\uparrow) f_{ML}(\eta_i, \xi) \text{ (barns)} \tag{18}$$

with

$$c_{ML} = 5.888 \times 10^{-9} Z_1^2\left[0.07199\left(1 + \frac{A_1}{A_2}\right) Z_1 Z_2\right]^{-2L+2}, \tag{19}$$

where E and $\Delta E'$ are expressed in MeV and the reduced nuclear transition probability $B(ML\uparrow)$ is measured in units of $\mu_N^2(10^{-24}\ \text{cm}^2)^{L-1} = \mu_N^2 \text{b}^{L-1}$.

The range of projectile energies that can be employed in the excitation of a given nuclear level is limited on the low-energy side by the condition $\xi \leqslant 1$, since otherwise the collision becomes adiabatic and the excitation cross section becomes small. According to Equation (15), this condition may also be written

$$E \geqslant 0.2 Z_1 \left(\frac{A_1}{Z_1}\right)^{1/3} \left(\frac{Z_2}{\Delta E}\right)^{2/3}, \tag{20}$$

where E and ΔE are the bombarding energy and the excitation energy in MeV and the center-of-mass corrections and the relative energy loss $\Delta E/E$ are neglected.

On the other hand, for too high bombarding energies, the projectiles may penetrate into the nucleus and the interpretation of the observed excitations then becomes more difficult due to the onset of direct nuclear reactions. Assuming the energy of projectile is less than that of the Coulomb barrier E_B, we obtain

$$E \leqslant E_B = Z_1 Z_2 A_2^{-1/3}, \tag{21}$$

where E is measured in MeV.

2.2. NUMERICAL ESTIMATES

Numerical estimates of the triggering cross sections for several isomers by a beam of protons with energies of 1 MeV and 10 MeV are collected in Table I. One can see that for trigger transitions with relatively high multipole orders (E9 for $^{179}_{72}\mathrm{Hf}^{m2}$, $M4$ for $^{178}_{72}\mathrm{Hf}^{m2}$ and $E5$ for $^{177}_{71}\mathrm{Lu}^{m}$), the increase in the cross section with growing proton energy proves to be much greater than for transitions of low multipolarity($E2$ for $^{242}_{95}\mathrm{Am}^{m}$ and $^{174}_{71}\mathrm{Lu}^{m}$). We consider below numerical estimates for two of the selected isomers in more detail.

$^{242}_{95}\mathrm{Am}^{m}$:

For numerical estimation of the cross sections for triggering of $^{242}_{95}\mathrm{Am}^{m}$ isomer by a beam of protons with energy 1 MeV, we can use expression (1) with $\sigma_1 = \sigma_C^{(n)}$ (16). Since the first-step transition is electric quadrupole, we obtain a Weisskopf estimate for the reduced transition probability of $B(E2\uparrow) = 5.70 \times 10^{-3} e^2\mathrm{b}^2$ and with $c_{L2} = 5.30 \times 10^{-4}$, $\xi = 32.2 \times 10^{-3}$, $\eta_i = 15.02$, $f(\xi, \eta_i) \approx 0.895$ we obtain $\sigma_C^{(n)} = 2.7 \times 10^{-6}$ barns. Taking into account that $\Gamma_{SF}^{(r)}(1 + \alpha_{SF})/\Gamma_S \approx 1$, we come to the estimate $\sigma = 2.7 \times 10^{-6}$ barns for the triggering cross section of $^{242}_{95}\mathrm{Am}^{m}$.

A similar estimate for a beam of 10-MeV protons gives rise to an order-of-magnitude greater cross section, $\sigma = 2.7 \times 10^{-5}$ barns. Note that the energy of the Coulomb barrier (Equation (21)) is estimated to be $E_B = 15.2$ MeV, so the requirement of Equation (21) holds. For a proton energy of 0.1 MeV, the triggering cross section is estimated to be three orders-of-magnitude less, or $\sigma = 8.6 \times 10^{-9}$ barns.

$^{179}_{72}\mathrm{Hf}^{m2}$:

Since the first-step transition of $^{179}_{72}\mathrm{Hf}^{m2}$ is electric with $L = 9$, we obtain a Weisskopf estimate for the reduced transition probability of $B(E9\uparrow) = 1.32 \times 10^{-6} e^2\mathrm{b}^9$, and $c_{E9} = 8.47 \times 10^{-14}$, $\xi = 3.98 \times 10^{-4}$, $\eta_i = 11.38$, $f(\xi, \eta_i) \approx 10^{-10}$. This gives the Coulomb excitation cross section $\sigma_1 = \sigma_C^{(n)} = 1.1 \times 10^{-29}$ barns for a beam of 1-MeV protons. Taking into account the relative intensities (Table I) for the gamma emission lines accompanying decay of the intermediate state S, we come to a set of cross sections of $\sigma = 7.8 \times 10^{-30}, 2.6 \times 10^{-30}, 0.6 \times 10^{-30}$ barns for the process of triggered de-excitation of $^{179}_{72}\mathrm{Hf}^{m2}$ with emission of 1105.91, 983.17, 891.5 keV gamma quanta, respectively.

Increasing the energy of the incident protons leads to an appreciable rise in the triggering cross sections. For instance, 10-MeV protons (which is less than the Coulomb barrier E_B = 12.8 MeV) give $\sigma_C^{(n)} = 1.1 \times 10^{-14}$ barns and hence $\sigma = 7.8 \times 10^{-15}, 2.6 \times 10^{-15}, 0.6 \times 10^{-15}$ barns for emission of 1105.91, 983.17, 891.5 keV gamma quanta, respectively.

Table I. Numerical estimates of the cross sections for triggering of selected isomers by a beam of protons. The data for nuclear isomers are taken from [34]

Isomer	Energy (keV) and half-life of isomeric state		First-step (trigger) transition energy (keV), type and multipole order		Second-step transition energy (keV), type and multipole order		Relative intensities of emission lines	Coulomb barrier (MeV)	Coulomb triggering cross section (barns) by a beam of protons with energy E	
	E_I	$T_{1/2_I}$	E_{SI}	$I \to S$	E_{SF}	$S \to F$	I_γ	E_B	$E = 1$ MeV	$E = 10$ MeV
$^{242}Am^m$	48.63	141 y	4.27	$E2$	52.9	E2	100	15.2	2.7×10^{-6}	2.7×10^{-5}
$^{178}Hf^{m2}$	2446.05	31 y	39.15	$M4$	626.2	M1	100	12.8	8.8×10^{-20}	8.8×10^{-14}
					348.5	M1	37		3.2×10^{-20}	3.2×10^{-14}
$^{179}Hf^{m2}$	1105.84	25.05 d	0.07	$E9$	1105.91	M1	100	12.8	7.8×10^{-30}	7.8×10^{-15}
					983.17	E2	33		2.6×10^{-30}	2.6×10^{-15}
					891.5	E1	8		0.6×10^{-30}	0.6×10^{-15}
$^{174}Lu^m$	170.83	142 d	29.47	$E2$	155.59	E2	7.8	12.7	2.2×10^{-7}	2.4×10^{-6}
					88.54	M1	100		2.8×10^{-6}	3.1×10^{-5}
$^{177}Lu^m$	970.17	160.4 d	15.10	$E5$	716.69	M1	16.7	12.6	1.6×10^{-16}	1.9×10^{-9}
					544.35	M1	17.4		1.7×10^{-16}	2.0×10^{-9}
					313.33	E2	37		3.5×10^{-16}	4.2×10^{-9}
					168.61	M1	100		9.4×10^{-16}	1.1×10^{-8}

3. Triggering of nuclear isomers via coupling to atomic electron shell

Transferring energy from atomic shells to the nucleus could induce triggering of an isomer. The energy released during recombination of a vacancy in an atomic electron shell may lead to the first step of isomer excitation via absorption of a virtual photon. The most widely known candidates for such processes are second-order non-radiative processes of nuclear excitation via resonance electron transition (NEET) [12–18] with the same multipolarity, via electron capture from the continuum by a vacancy in an electron shell (NEEC) [19–23] and nuclear excitation via a third-order mechanism which is referred to as the inverse electron bridge (IEB) [24–27].

In the NEET triggering process, an electron from a higher electron shell makes a transition to fill a hole in an inner electron shell while at the same time the nucleus makes a resonant transition from a long-lived isomeric state to a higher excited state with subsequent prompt decay to lower nuclear states. The first-step nuclear excitation via the resonance electron transition is thus the inverse of the bound internal conversion process [28] in which a nucleus de-excites by excitation of a bound electron to a higher-lying bound orbital. Experimental evidence for the bound internal conversion process has been found [29] in the internal conversion decay of highly ionized ions of ^{125}Te in charge states ranging between 44^+ and 48^+. Direct observation of the NEET process has been reported recently [30] in the excitation of ^{197}Au from the ground state to the first excited state with irradiation by synchrotron radiation. It was concluded that K-shell photoionization was responsible for NEET excitation of ^{197}Au with a branching probability of $(5.0 \pm 0.6) \times 10^{-8}$.

In the NEEC process the first-step excitation of isomer is produced via free-to-bound electron transitions rather than via transitions between two bound states. This process is just the inverse of the well-known process of nuclear de-excitation by internal electron conversion.

Instead of capturing an electron from a beam of incident particles, a variant of NEEC by target electron capture was suggested in [21, 22]. In this case, bare nuclei or highly stripped ions from a beam are channeled through a single crystal and the target electrons in the channel are captured into inner-shell atomic orbital of an incident nucleus. To conserve energy, the nucleus is simultaneously excited. The NEEC cross section is especially large when the speed of ions satisfies a resonant condition. At present, there are no reliable experimental NEEC results. Theoretical estimates for the NEEC cross section are very diverse and its real magnitude is in need of experimental verification.

In the IEB process of nuclear excitation, tuned frequency laser radiation produces a two-quantum electron transition between atomic shells with emission of a virtual photon and nuclear excitation occurs as a consequence of resonance absorption of this virtual photon.

We restrict our further discussion to NEET and NEEC triggering of isomeric nuclei.

3.1. NEET TRIGGERING OF NUCLEAR ISOMERS

The cross section for the NEET triggering process is determined by Equation (1) with the NEET cross section, $\sigma_1 = \sigma_1^{(\mathrm{NEET})}$, for the first-step isomer excitation. Nuclear triggering by NEET implies an in-advance creation of a hole (vacancy) in an inner atomic shell by some incident ionizing electron beam or by externally-produced X-ray radiation. If we denote the cross sections for hole production by an electron beam as $\sigma_i^{(e)}$ and by X-ray radiation as $\sigma_i^{(r)}$, then the cross section for the NEET process can be expressed by

$$\sigma_1^{(\mathrm{NEET})} = \sigma_i^{(e,r)} P_{\mathrm{NEET}}, \tag{22}$$

where P_{NEET} is the probability for energy transfer from an electron transition to a resonant nuclear transition. There are a number of theoretical studies on the NEET process [12–18], which were reviewed in detail in [17, 18]. We use a formula for calculating the NEET probability presented in [17] and confirmed in later discussions on this problem [18, 23], namely

$$P_{\mathrm{NEET}} = \left(1 + \frac{\Gamma_f + \Gamma_S}{\Gamma_i}\right) \frac{E_{\mathrm{int}}^2(i \to f, I \to S)}{(E_{\mathrm{N}} - E_{\mathrm{A}})^2 + (\Gamma_i + \Gamma_f + \Gamma_S)^2/4}, \tag{23}$$

where $E_{\mathrm{N}} - E_{\mathrm{A}}$ is the energy difference between the corresponding nuclear and atomic transitions. The initial atomic state i (we use small letters to denote atomic states) in Equation (23) is the state having a hole in an inner electron shell, whereas the final state f corresponds to the atom having a hole in a higher electron shell. Thus we consider the process of atomic de-excitation not as an electron transition but rather as a hole transition from lower atomic levels to higher ones. The energy widths of the initial and final hole atomic states are Γ_i and Γ_f, respectively, and Γ_S is the energy width of a mediating (trigger) nuclear level S.

The key value in Equation (23) is the interaction energy between nucleus and atomic electron shell. It contains the matrix element of the interaction and can be expressed for 2^L-pole transitions as follows:

$$E_{\mathrm{int}}^2(i \to f, I \to S) = 4\pi e^2 \frac{(2L+1)}{[(2L+1)!!]^2} \left(\frac{E_{\mathrm{N}}}{\hbar c}\right)^{2L+2} \times \left(j_i \tfrac{1}{2} L 0 \middle| j_f \tfrac{1}{2}\right)^2 \left|\mathrm{M}_L^{E(M)}\right|^2 B\big(E(M)L \uparrow\big), \tag{24}$$

where j_i, j_f denote the total angular momentum of the initial and final atomic states, respectively, $\left(j_i \frac{1}{2} L 0 \middle| j_f \frac{1}{2}\right)$ designates the Clebsch–Gordan coefficient, $\mathrm{M}_L^{E(M)}$ is the matrix element of the i-to-f 2^L-pole atomic transition (EL or ML), and $B(E(M)L \uparrow)$ is the reduced transition probability associated with the nuclear excitation by the multipole transition (EL or ML) from I to S state.

There is a simple relation between the probability of NEET and the energy widths of the radiative nuclear and atomic transitions involved. Indeed, the partial radiation width of the S-to-I nuclear transition is given by [10]

$$\Gamma_{SI}^{(\mathrm{r})} = 8\pi \frac{(L+1)}{L[(2L+1)!!]^2}\left(\frac{E_{\mathrm{N}}}{\hbar c}\right)^{2L+1} B\big(E(M)L\downarrow\big), \tag{25}$$

where the reduced transition probability $B(E(M)L\downarrow)$ for the decay is related by

$$GB\big(E(M)L\downarrow\big) = B\big(E(M)L\uparrow\big) \tag{26}$$

to the reduced transition probability $B(E(M)L\uparrow)$ entering into Equation (24), where the statistical 'spin factor' $G = (2J_S + 1)/(2J_I + 1)$. The partial radiation width of the i-to-f atomic transition is determined by the expression [31]

$$\Gamma_{if}^{(\mathrm{r})} = e^2 \frac{E_{\mathrm{N}}}{\hbar c}\frac{2L(2L+1)}{L+1}\left(j_i \frac{1}{2} L0 \middle| j_f \frac{1}{2}\right)^2 \big[\mathrm{Re}\big(M_L^{E(M)}\big)\big]^2. \tag{27}$$

Combining Equations (25), (27) with Equation (24) we can rewrite Equation (23) in a more suitable form:

$$P_{\mathrm{NEET}} = G\frac{\Gamma_{SI}^{(\mathrm{r})}}{\Gamma_S}\frac{\Gamma_{if}^{(\mathrm{r})}}{\Gamma_i}\frac{(1+\delta^{-2})}{1+(\Gamma_i+\Gamma_f)/\Gamma_S}\frac{(\Gamma_i+\Gamma_f+\Gamma_S)^2/4}{(E_{\mathrm{N}}-E_{\mathrm{A}})^2+(\Gamma_i+\Gamma_f+\Gamma_S)^2/4}, \tag{28}$$

where the parameter δ is defined by

$$\delta = \frac{\mathrm{Re}(M_L^{E(M)})}{\mathrm{Im}(M_L^{E(M)})}. \tag{29}$$

3.2. ATOM IONIZATION CROSS SECTION

We consider hole production in an inner atomic shell with electron ionizing energy E_{i} by X-ray radiation with a photon energy E close to the threshold of ionization, $(E - E_{\mathrm{i}})/E_{\mathrm{i}} \ll 1$. The cross section can be represented as [32]

$$\sigma_{\mathrm{i}}^{(\mathrm{r})} = \frac{2\pi^2}{3}\left(\frac{4}{2.72}\right)^4 \frac{\alpha}{(Z-\beta)^2}\left(\frac{E_{\mathrm{i}}}{E}\right)^{8/3} a_{\mathrm{B}}^2, \tag{30}$$

where $\alpha = e^2/\hbar c = 1/137.03$ is the fine structure constant, $a_{\mathrm{B}} = \hbar^2/me^2 = 0.529 \times 10^{-8}$ cm the Bohr radius, and β is the number of electrons screening the motion of the considered electron.

Unlike atomic ionization by electron impact, ionization by photon absorption is a selective process, so that photoionization of inner electron shells practically does not influence electrons in upper shells. The photoionization cross section has

a maximum near the threshold energy of ionization E_i and then it diminishes with an increase in the photon energy.

The cross section for ionization of an inner atomic shell with angular momentum l and total number of electrons n_l by bombardment with electrons of energy E can be represented in the form [32, 33]

$$\sigma_i^{(e)} = \pi a_B^2 \left(\frac{R}{E_i}\right)^2 \frac{n_l}{2l+1} \Phi(u), \tag{31}$$

where E_i is the electron ionizing energy, $R = me^4/2\hbar^2 = 13.6$ eV is the Rydberg constant and the function $\Phi(u)$ with argument $u = (E - E_i)/E_i$ was tabulated in [32]. For a crude numerical estimate, it can be represented as

$$\Phi(u) = \left(\frac{u}{u+1}\right)^{3/2} \frac{C}{u+\varphi} \tag{32}$$

with $C = 5$–10, $\varphi = 1$–2 for s-atomic shells, $C = 20$–40, $\varphi = 2$–5 for p-atomic shells and $C = 40$–60, $\varphi = 5$–10 for d-atomic shells. The cross section $\sigma_i^{(e)}$ is equal to zero at $E = E_i$, grows with an increase of E up to a maximum value at $E \approx (2$–$5)E_i$, and then decreases with continued growth in the energy of electrons in the beam.

3.3. NUMERICAL ESTIMATES

For a crude estimate of the NEET probability from Equation (28) for $M1$ or $E1$ transitions, we assume $\Gamma_{sI}^{(r)}/\Gamma_S \sim \Gamma_{if}^{(r)}/\Gamma_i \sim 10^{-1}$–$10^{-2}$, $(\Gamma_i + \Gamma_f)/\Gamma_S \sim 10^7$–$10^9$, $\delta^{-2} \sim 10^3$, $G = (2J_S + 1)/(2J_I + 1) \sim 0.1$ and $|E_N - E_A| \sim 5(\Gamma_i + \Gamma_f + \Gamma_S)$. Under these assumptions, the probability for NEET is estimated to be $P_{NEET} \sim 10^{-9}$–10^{-13}. The NEET probabilities for transitions of consecutive multipole orders decreases by 5–6 orders of magnitude.

A screening of isomers has been made in order to pick out the candidates with the appropriate arrangement of the nuclear and atomic states. The relevant fragments of the atomic and nuclear level diagrams for the selected isomeric nuclides suitable for triggering by the NEET process are shown in Figure 2. The energies of atomic levels (E_b is the binding electron energy) and nuclear levels are taken from [34]. Numerical estimates of the NEET triggering cross sections for the selected isomers are collected in Table II. The last two columns contain estimates for in-advance hole creation by X radiation with photon energy close to the ionization energy and by a beam of electrons with the energy nearly 4–5 times the ionization energy. Estimates for widths of the atomic hole states are taken from [31, 32]. We consider below the numerical estimates for three of the selected isomers in more detail.

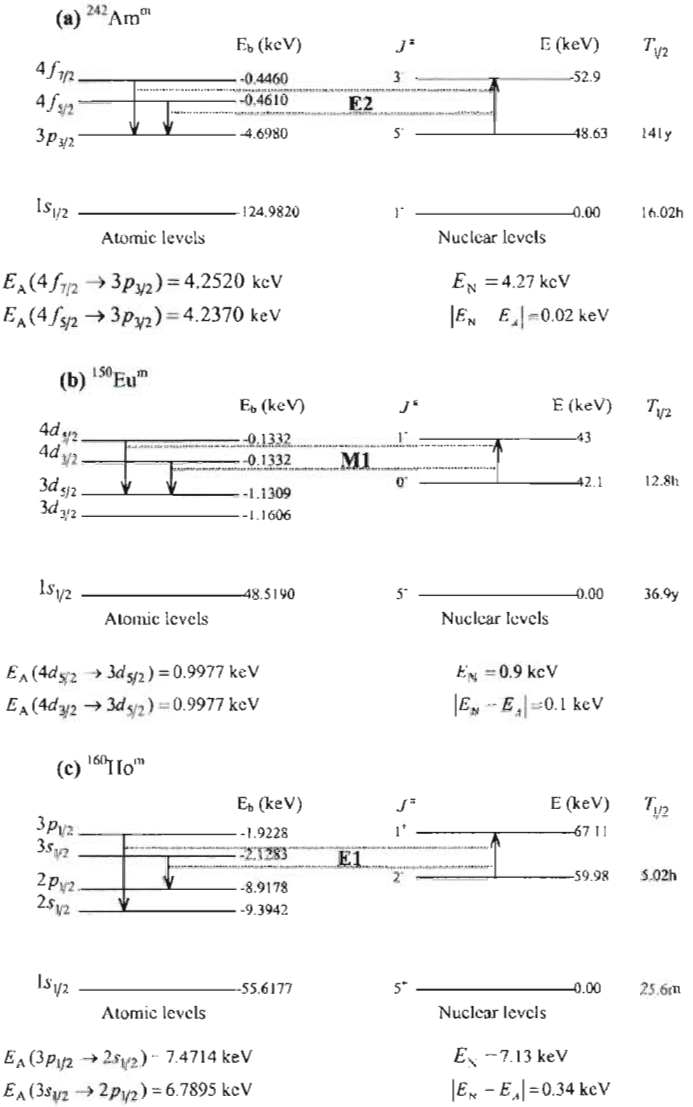

Figure 2. Atomic and nuclear level diagrams for several isomeric nuclei suitable for triggering by the NEET process.

$^{242}_{95}Am^{m}$:

To estimate the probability of NEET excitation to the trigger level of $^{242}_{95}Am^{m}$ (Figure 2a), we use Equation (28) with $\Gamma_{SI}^{(r)}/\Gamma_S = 3.43 \times 10^{-6}$ and $\Gamma_S \approx \Gamma_{SF}^{(r)} =$

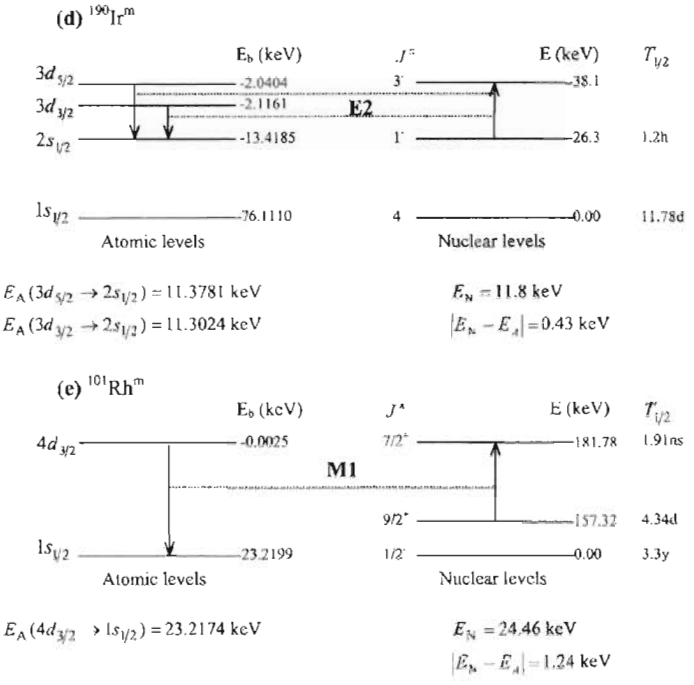

Figure 2. (Continued.)

3.0×10^{-11} eV (Weisskopf estimate), $\Gamma_{if}^{(r)}/\Gamma_i = 10^{-4}$, $(\Gamma_i + \Gamma_f)/\Gamma_S = 1.3 \times 10^{12}$ (taking into account that $\Gamma_i \sim 10$ eV for the N-electron shell and $\Gamma_f \sim 30$ eV for the M-shell), $\delta^{-2} \sim 10^3$, $E_N - E_A = 20$ eV, $G = (2J_S + 1)/(2J_I + 1) = 7/11$. As a result, we obtain $P_{NEET} = 0.82 \times 10^{-19}$.

The cross section for hole production by X-ray radiation (Equation (30)) with photon energy $E \sim 5$ keV is $\sigma_1^{(r)} = 8.7 \times 10^{-22}$ cm^2, so that the cross section for the first-step excitation is estimated to be $\sigma_1^{(NEET)} = \sigma_1^{(r)} P_{NEET} = 7.1 \times 10^{-41}$ cm^2. Since for $^{242}_{95}Am^{m}$ $\Gamma_{SF}^{(r)}(1 + \alpha_{SF})/\Gamma_S \sim 1$, we obtain the following estimate of the cross section for the NEET triggering of $^{242}_{95}Am^{m}$: $\sigma = 7.1 \times 10^{-17}$ barns.

The cross section for hole production by a beam of 20-keV electrons can be estimated to be $\sigma_i^{(e)} = 3.6 \times 10^{-21}$ cm^2 (31) and the cross section for the triggering by NEET is estimated to be $\sigma = 2.9 \times 10^{-16}$ barns.

$^{190}_{77}Ir^{m}$:

We perform a similar estimate of the NEET excitation probability (28) for the isomer $^{190}_{77}Ir^{m}$ with $\Gamma_{SI}^{(r)}/\Gamma_S = 1.05 \times 10^{-8}$ and $\Gamma_S \approx \Gamma_{SF}^{(r)} = 1.12 \times 10^{-6}$ eV (Weisskopf estimate), $\Gamma_{if}^{(r)}/\Gamma_i = 10^{-4}$, $(\Gamma_i + \Gamma_f)/\Gamma_S = 4.5 \times 10^7$ (taking into account that $\Gamma_i \sim 20$ eV for the M-electron shell and $\Gamma_f \sim 30$ eV for the L-shell),

Table II. Numerical estimates of the cross sections for NEET triggering of selected isomers

Isomer	Energy (keV) and half-life of isomeric state		Trigger transition energy (keV) and mulipole order		Atomic transition energy (keV)	Energy mismatch (keV)	Probability of NEET	NEET triggering cross section (barns)	
	E_I	$T_{1/2_I}$	E_N	$I \to S$	E_A	$\lvert E_N - E_A \rvert$	P_{NEET}	ionization by X-ray radiation	ionization by beam of electrons
$^{242}_{95}Am^m$	48.63	141 y	4.27	E2	4.25	0.02	8.2×10^{-20}	7.1×10^{-17}	2.9×10^{-16}
$^{150}_{63}Eu^m$	42.1	12.8 h	0.9	M1	1.0	0.1	1.3×10^{-9}	1.3×10^{-26}	4.1×10^{-25}
$^{160}_{67}Ho^m$	59.98	5.02 h	7.13	E1	7.47	0.34	1.02×10^{-9}	1.5×10^{-26}	1.3×10^{-26}
$^{190}_{77}Ir^m$	26.3	1.2 h	11.8	E2	11.38	0.42	1.9×10^{-19}	2.2×10^{-16}	1.2×10^{-16}
$^{101}_{45}Rh^m$	157.3	4.34 d	24.46	M1	23.22	1.24	2.8×10^{-12}	7.4×10^{-19}	2.2×10^{-20}

$\delta^{-2} \sim 10^3$, $E_N - E_A = 420$ eV, $G = (2J_S + 1)/(2J_I + 1) = 7/3$. We find the value $P_{NEET} = 1.9 \times 10^{-19}$.

The cross section for hole production by X-ray radiation (Equation (30)) with 15-keV photons is given by $\sigma_i^{(r)} = 1.12 \times 10^{-21}$ cm^2, whereas the cross section for hole production by a beam of 50-keV electrons can be estimated at $\sigma_i^{(e)} = 5.9 \times 10^{-22}$ cm^2. Bearing in mind that for $^{190}_{77}$Ir^m the ratio $\Gamma_{SF}^{(r)}(1 + \alpha_{SF})/\Gamma_S \sim 1$, we can estimate the cross section for triggering by NEET as $\sigma = 2.2 \times 10^{-16}$ barns for hole production by X-ray radiation and as $\sigma = 1.2 \times 10^{-16}$ barns for hole production by an electron beam.

$^{101}_{45}$Rh^m:

For the $^{101}_{45}$Rh^m isomer, we use $\Gamma_S = 2.39 \times 10^{-7}$ eV and $\alpha_{SI} = 20.8$ (experimental data taken from [34]), $\Gamma_S \approx \Gamma_{SI}^{(r)}(1 + \alpha_{SI})$, $\Gamma_{SI}^{(r)}/\Gamma_S = 1/(1 + \alpha_{SI}) = 0.046$ and $\Gamma_{if}^{(r)}/\Gamma_i = 10^{-1}$, $(\Gamma_i + \Gamma_f)/\Gamma_S = 8.41 \times 10^7$ (with $\Gamma_i \sim 20$ eV for the K-electron shell and $\Gamma_f \sim 0.1$ eV for the N-shell), $\delta^{-2} \sim 10^3$, $E_N - E_A = 1240$ eV and $G = (2J_S + 1)/(2J_I + 1) = 4/5$. This leads to an estimate of $P_{NEET} = 2.8 \times 10^{-12}$.

The cross section for hole production by X-ray radiation with the 25-keV photons is given by $\sigma_i^{(r)} = 3.0 \times 10^{-21}$ cm^2, whereas the cross section for hole production by a beam of 100-keV electrons can be estimated to be $\sigma_i^{(e)} = 5.9 \times 10^{-22}$ cm^2.

For $^{101}_{45}$Rh^m, the ratio $\Gamma_{SF}^{(r)}(1 + \alpha_{SF})/\Gamma_S$ is estimated to be 8.8×10^{-11} (Weisskopf estimate for $\Gamma_{SF}^{(r)}$ and $\alpha_{SF} = 0$) and this provides $\sigma = 7.4 \times 10^{-19}$ barns for the NEET triggering cross section with hole production by the X-ray radiation and $\sigma = 2.2 \times 10^{-20}$ barns with hole production by an electron beam.

3.4. NEEC TRIGGERING OF NUCLEAR ISOMERS

The cross section for the NEEC triggering process is determined by Equation (1) with the NEEC cross section $\sigma_1 = \sigma_1^{(NEEC)}$ for the first-step isomer excitation. Nuclear excitation by electron capture (NEEC) is the process by which energy is transferred from a free-to-bound electron transition to the nucleus and, thus, is resonant in character. If we denote the energy of the captured free electron by E_e and the ionization energy of the bound electron after capture by E_i, then energy conservation specifies the resonance energy needed for beam electrons to cause triggering by NEEC, $E_e = E_{SI} - E_i$, where E_{SI} is the nuclear triggering energy.

A crude estimate of the NEEC cross section was first presented in [19, 20]. However this estimate was based on a number of approximations of dubious validity, leading to a nuclear excitation cross section that was independent of nuclear parameters. More recently, the NEEC cross section has been considered [21] by a scaling procedure, so in this case the cross section was given in terms of product of an Auger decay cross section and a ratio of quantities pertaining to the Auger decay rate and internal conversion decay rate. The degree of approximation introduced in

this scaling procedure is not clear. In the following we use the NEEC cross section presented in [22, 23], where the NEEC process was reconsidered with an explicit treatment of the electron nuclear interaction. Treating NEEC as one of the channel of the process of electron scattering on an atom with resonance state being the nuclear trigger level S, the NEEC cross section can be expressed in the form [23]

$$\sigma_1^{(\mathrm{NEEC})}(E) = S_0 \frac{\pi}{2k^2} \frac{\alpha_{SI}^{(\mathrm{p})} \Gamma_{SI}^{(\mathrm{r})} (\Gamma_i + \Gamma_f + \Gamma_S)}{(E - E_\mathrm{e})^2 + (\Gamma_i + \Gamma_f + \Gamma_S)^2/4}, \tag{33}$$

where k is the wave number of the incident electron of energy E, $\Gamma_{SI}^{(\mathrm{r})}$ is the radiation width of the S-to-I nuclear transition, $\alpha_{SI}^{(\mathrm{p})}$ is the partial coefficient of internal electron conversion via the shell into which electron capture occurs, Γ_i is the energy width of initial atomic state with a vacancy in an electron atomic shell and Γ_f is the energy width of final atomic state after capture of electron. The factor S_0 is a function of the nuclear spins, J_I and J_S in isomeric and trigger states, respectively, the total angular momentum, j of the captured electron and the total angular momentum, j_0 of the continuum orbit from which capture occurs.

The rate of triggering by electron capture is expressed by

$$W_{\mathrm{NEEC}} = \frac{\Gamma_{SF}^{(\mathrm{r})}(1 + \alpha_{SF})}{\Gamma_S} \int_{E=0}^{\infty} \sigma_1^{(\mathrm{NEEC})}(E) F_\mathrm{e}(E)\, \mathrm{d}E, \tag{34}$$

where $F_\mathrm{e}(E)$ is the electron flux density at an energy E. Under the assumption that $F_\mathrm{e}(E)$ has a broad energy distribution around the resonance energy E_e with the energy width that is much greater then the width of resonance, the expression for this rate reduces

$$W_{\mathrm{NEEC}} = F_\mathrm{e}(E_\mathrm{e}) S_0 \frac{\lambda_\mathrm{e}^2}{4} \alpha_{SI}^{(\mathrm{p})} \Gamma_{SI}^{(\mathrm{r})} \frac{(1 + \alpha_{SF}) \Gamma_{SF}^{(\mathrm{r})}}{\Gamma_S}, \tag{35}$$

where $F_\mathrm{e}(E_\mathrm{e})$ is the electron flux density at the resonance energy E_e and λ_e is the wavelength of the incident electrons with the resonance energy E_e, so that $\lambda_\mathrm{e} = 2\pi\hbar/\sqrt{2mE_\mathrm{e}}$.

In Equation (33) we assume that the width of resonance is dominated by a homogeneous natural broadening inherent to a single atom rather than inhomogeneous broadening. Otherwise, the width $\Gamma_i + \Gamma_f + \Gamma_S$ should be replaced either by the Doppler width for an ensemble of atoms or by the Stark width in a plasma. It should be noted, however, that the NEEC triggering integral cross section, $\mathrm{ICS}_{\mathrm{NEEC}}$, which can be found from Equation (35) by

$$\mathrm{ICS}_{\mathrm{NEEC}} = S_0 \frac{\lambda_\mathrm{e}^2}{4} \alpha_{SI}^{(\mathrm{p})} \Gamma_{SI}^{(\mathrm{r})} \frac{(1 + \alpha_{SF}) \Gamma_{SF}^{(\mathrm{r})}}{\Gamma_S}, \tag{36}$$

is insensitive to reductions in the cross section itself due to broadening of any kind, since the integral remains the same as the resonance width increases accordingly.

In the opposite limiting case when the energies of all electrons in the flux are falling into resonance, the cross section for triggering of nuclear isomers by NEEC takes the form

$$\sigma = S_0 \frac{\lambda_e^2}{2\pi} \frac{\alpha_{SI}^{(p)} \Gamma_{SI}^{(r)}}{\Gamma} \frac{(1 + \alpha_{SF}) \Gamma_{SF}^{(r)}}{\Gamma_S}, \tag{37}$$

where Γ is the energy width of the resonance (Doppler or Stark).

For a specific nuclear triggering energy, the resonance requirement, $E_e = E_{SI} - E_i$, can be satisfied exactly for some values of the energies of incident electrons and the ionization energies of the bound electrons after capture. Thus, in general a large number of atomic orbitals with $E_i < E_{SI}$ could participate in the NEEC process. In addition, since electron capture could in principle occur into a shell without a hole (for instance, in the case of a partly filled electron shell), the NEEC process does not require the initial bound electron state to be excited. Naturally, the NEEC probability via higher-lying orbitals tends to be less than those for lower-lying ones due to the decrease in coupling between electrons and atomic nucleus. This means that the partial internal conversion coefficient drops and one might expect a reduction in the NEEC cross section (Equation (37)) and in the integral cross section (Equation (36)) in spite of an increase for the resonance wavelength λ_e of free electrons involved into the NEEC process.

The key value in expressions (36) and (37) is the partial internal conversion coefficient $\alpha_{SI}^{(p)}$ that is unknown. This makes estimates of the NEEC probability extremely uncertain.

3.5. NUMERICAL ESTIMATES

For numerical estimates it is convenient to use the relations $\lambda_e^2 = 1.50 \times 10^{-17}/E_e$ where E_e and λ_e are measured in keV and in cm, respectively. The Doppler width in an ensemble of nuclei with mass number A can be easily estimated from $\Gamma_D = 7.11 \times 10^{-7} E_{SI} \sqrt{T/A}$, where the triggering energy E_{SI} and Γ_D are measured in keV and the temperature T of the nuclear ensemble is in K.

$^{242}_{95}Am^m$:

In order to obtain a crude numerical estimate of the NEEC cross section (Equation (37)) and the integral cross section (Equation (36)) for $^{242}_{95}Am^m$, we assume that the NEEC process occurs via a partly filled O-shell with $E_i \sim 0.1$ keV. Then the resonance electron energy in a beam is $E_e \approx E_{SI} = 4.27$ keV and $\lambda_e^2 = 3.52 \times 10^{-18}$ cm^2. Since $\Gamma_{SI}^{(r)} = 1.03 \times 10^{-16}$ eV, $\Gamma_S \approx \Gamma_{SF}^{(r)} = 3.0 \times 10^{-11}$ eV (Weisskopf estimate) and $\Gamma = \Gamma_D = 3.4 \times 10^{-3}$ eV at temperature $T = 300$ K, we obtain $\Gamma_{SI}^{(r)}/\Gamma = 1.03 \times 10^{-13}$. Unfortunately, the coefficient of internal electron conversion via O-shell of $^{242}_{95}Am^m$ is unknown. Taking into account that the O-shell electrons are weakly bound up with the nucleus, we assume somewhat arbitrarily

a value $\alpha_{SI}^{(p)} = 10^{-5}$. Under these assumptions and using the estimates $S_0 \sim 0.01$ and $\Gamma_{SF}^{(r)}(1 + \alpha_{SF})/\Gamma_S \sim 1$, we obtain for the NEEC triggering cross section by a resonant electron beam the value of $\sigma = 1.7 \times 10^{-15}$ barns. The integral cross section (36) for $^{242}_{95}\mathrm{Am}^{m}$ can be estimated to be $\mathrm{ICS}_{\mathrm{NEEC}} = 0.9 \times 10^{-20}$ b keV.

4. Discussion of cross sections and conclusion

The cross sections of all the above considered non-radiative triggering processes contain the reduced transition probability for the first-step nuclear excitation, $B(E(M)L\uparrow)$, from an isomeric state to a higher-lying intermediate state, a quantity that also appears in expressions for radiative nuclear transitions. However, the electromagnetic field acting on an isomeric nucleus during non-radiative triggering differs in various respects from that involved in triggering by externally-produced photons radiation. This implies certain essential differences between the two types of triggering mechanisms. It concerns, first of all, the Coulomb triggering by bombarding isomers with charged nuclear particles. While in the radiation field the magnetic and electric field strengths are of equal magnitude, the magnetic field of the bombarding particle is only of order v/c as compared with the electric field. Therefore, as we can see from Equation (5), magnetic excitation cross sections are reduced with respect to electric ones by a factor $(v/c)^2$, apart from differences in the nuclear matrix element.

A further difference is connected with the relative contributions of the various multipole components. While in radiative processes the relative intensities of consecutive multipole orders involve a factor $|(\omega/c)R_0|^2$, where $\omega = \Delta E/\hbar$ is the frequency of the trigger transition and R_0 is the nuclear radius, Equation (5) shows that the corresponding factor in Coulomb excitation is $(R_0/a)^2$. The latter factor is much larger than the former one since, according to Equation (4), we have $(\omega/c)a = (v/c)\xi \ll 1$. Therefore, the cross section for Coulomb excitation does not decrease as rapidly with increasing multipole order as does the cross section for radiative nuclear transitions. This is of great importance for isomers with a trigger transition of high multipole order. For instance, the isomer $^{179}_{72}\mathrm{Hf}^{m2}$ with as large multipole order of the trigger transition as $E9$ has the Coulomb cross section $\sigma \sim 10^{-15}$ barns for triggering by a beam of 10-MeV protons. In contrast, the cross section for triggering by externally-produced resonance X-ray radiation, given by the expression

$$\sigma = G\frac{\lambda_{SI}^2}{2\pi}\frac{\Gamma_{SI}^{(r)}}{\Gamma}\frac{(1+\alpha_{SF})\Gamma_{SF}^{(r)}}{\Gamma_S} \tag{38}$$

is estimated to be the extremely small value of $\sigma \sim 10^{-105}$ barns for the X-ray wavelength $\lambda_{SI} = 1.8 \times 10^{-6}$ cm that corresponds to the triggering energy of 0.07 keV and for the total width of the resonance Γ corresponding to the Doppler width $\Gamma_D = 6.5 \times 10^{-8}$ keV at temperature $T = 300$ K. For the isomer $^{242}_{95}\mathrm{Am}^{m}$, with a trigger transition of $E2$ multipole order, $\lambda_{SI} = 2.9 \times 10^{-8}$ cm and $\Gamma_D =$

Table III. Numerical estimates of the cross sections for triggering of $^{242}_{95}Am^{m}$ isomer

Coulomb triggering cross section (barns)		NEET triggering cross section (barns)		NEEC triggering cross section (barns)	X-ray radiation triggering cross section (barns)
10 MeV proton beam	1 MeV proton beam	ionization with X-ray radiation	ionization with electron beam	resonance electron beam	resonance X-ray radiation
2.7×10^{-5}	2.7×10^{-6}	7.1×10^{-17}	2.9×10^{-16}	1.7×10^{-15}	2.6×10^{-6}

3.4×10^{-6} keV at temperature $T = 300$ K, the difference between the cross sections is not so impressive: the cross section for triggering by a beam of 10-MeV protons is $\sigma = 2.7 \times 10^{-5}$ barns, whereas the cross section for triggering by resonance X-ray radiation is estimated to be $\sigma = 2.6 \times 10^{-6}$ barns.

The relative efficiencies of the discussed triggering mechanisms can be compared explicitly by collecting together (Table III) the cross sections for the isomer $^{242}_{95}Am^{m}$, since among the above considered nuclides only $^{242}_{95}Am^{m}$ seems triggerable by any of these mechanisms. One can see that the most efficient triggering occurs with beams of nuclear particles and with externally-produced resonance X-ray radiation.

It should be noted, however, that in typical experiments on X-ray radiation triggering, devices producing bremsstrahlung have been the most utilized. It is not possible with continuous spectra to measure the triggering cross section to determine the absolute and relative probabilities of the reaction. Instead, the nearly constant spectral intensity over the absorption resonance leads to a measurement of the integral of the triggering cross section, $ICS_{X\text{-ray}}$, and its expected value can be estimated from the expression

$$ICS_{X\text{-ray}} = G\frac{\lambda_{SI}^2}{4}\Gamma_{SI}^{(r)}\frac{(1+\alpha_{SI})\Gamma_{SI}^{t}}{\Gamma_S}. \tag{39}$$

In particular, for $^{242}_{95}Am^{m}$ Equation (39) with the single-particle Weisskopf estimate for the partial radiation widths gives the value $ICS_{X\text{-ray}} = 1.4 \times 10^{-11}$ b keV which is 9 orders-of-magnitude greater then ICS_{NEEC}.

Naturally, for correct comparison of the efficiencies of different triggering mechanisms in a specific conditions (for instance, in laser-produced plasmas) not only should the cross sections be taken in to account, but also the corresponding fluxes in likely trigger environments (flux of charged nuclear particles, fluxes of ionizing electrons and X-ray radiation, bremsstrahlung produced by charged particle motion, etc.).

It should be noted that for the overwhelming majority of isomers the reduced transition probabilities of trigger transitions are unknown. The empirical values of

the nuclear transition probabilities obtained from lifetime determinations of gamma transitions and, thus, the actual values of triggering cross sections may show significant departures from the above estimates based on the single-particle Weisskopf approximation. For instance, electric dipole transitions, which have been observed in low-energy nuclear spectra, have in most cases transition probabilities many orders-of-magnitude smaller than those obtained from Weisskopf estimates. In contrast, low-energy electric quadrupole transitions are often enhanced as compared with single-particle estimates. So $E2$ transitions with a strength of 10–100 single particle units occur systematically in most regions of elements. While from this point of view the $^{242}_{95}Am^{m}$ isomer with $E2$ trigger transition seems immediately attractive, it may have a significantly decreased trigger transition probability due to the 3-fold excess orientation change (i.e., due to the effect of the K quantum number). This may produce a reduction of the transition rate and, thus, of the triggering cross sections by a factor of as much as $10^3 - 10^4$. Thus for a real evaluation of the possibility to use an isomer for obtaining the triggered gamma emission, it is extremely important to determine experimentally the reduced transition probabilities of the nuclear transitions involved. However, since the cross sections for triggering a particular isomer with any of the discussed processes involve the same reduced transition probability for its trigger transition, one can be certain that the above estimates give a correct view of the relative efficiencies of the considered triggering mechanisms.

Acknowledgements

The authors wish to acknowledge partial support of this research by U.S. CRDF-R.F. Ministry of Education Award VZ-010-0 (AAZ) and by US Air Force Office of Scientific Research grant F49620-99-1-0263 (JJC).

References

1. Collins, C. B., Eberhard, C. D., Glesener, J. W. and Anderson, J. A., *Phys. Rev. C* **37** (1988), 2267.
2. Collins, C. B., Carroll, J. J., Sinor, T. W., Byrd, M. J., Richmond, D. G., Taylor, K. N., Huber, M., Huxel, N., von Neumann-Cosel, P., Richter, A., Spieler, C. and Ziegler, W., *Phys. Rev. C* **42** (1990), 1813.
3. Collins, C. B. and Carroll, J. J., *Hyp. Interact.* **107** (1997), 3.
4. Rivlin, L. A. and Zadernovsky, A. A., *Laser Phys.* **6** (1996), 956.
5. Zadernovsky, A. A., *Laser Phys.* **10** (2000), 71.
6. Baldwin, G. C. and Solem, J. C., *Rev. Mod. Phys.* **69** (1997), 1085.
7. Rivlin, L. A., Quantum Electronics (invited paper) **29** (1999), 467.
8. Carroll, J. J., Karamian, S. A., Rivlin, L. A. and Zadernovsky, A. A., *Hyp. Interact.* **135** (2001), 3.
9. Newton, J. O., In: W. D. Hamilton (ed.), *The Electromagnetic Interaction in Nuclear Spectroscopy*, North-Holland, Amsterdam, 1975.
10. Eisenberg, I. M. and Greiner, W., *Excitation Mechanisms of the Nucleus*, North-Holland, Amsterdam, 1988.

11 Alder, K., Bohr, A., Huus, T., Mottleson, B. and Winther, A., *Rev. Mod. Phys.* **28** (1956), 432.
12. Morita, M., *Prog. Theor. Phys.* **49** (1973), 1574.
13. Otozai, K., Arakawa, R. and Morita, M., *Prog. Theor. Phys.* **50** (1973), 1771.
14. Ljubicic, A., Kekez, D. and Logan, B. A., *Phys. Lett. B* **272** (1991), 1.
15. Ho, Y.-K., Zhang, B.-H. and Yuan, Z.-S., *Phys. Rev. C* **44** (1991), 1910.
16. Tkalya, E. V., *Nucl. Phys. A* **539** (1992), 209.
17. Tkalya, E. V., *Sov. Phys. JETP* **75** (1992), 200.
18. Ho, Y.-K., Yuan, Z.-S., Zhang, B.-H. and Pan, Z.-Y., *Phys. Rev. C* **48** (1993), 2277.
19. Goldanskii, V. I. and Namiot, V. A., *Sov. J. Nucl. Phys.* **33** (1981), 169.
20. Goldanskii, V. I. and Namiot, V. A., *Phys. Lett. B* **62** (1976), 393.
21. Cue, N., Poizat, J.-C. and Remillieux, J., *Europhys. Lett.* **8** (1989), 19.
22. Yuan, Z. S. and Kimball, J. C., *Phys. Rev. C* **47** (1993), 323.
23. Harston, M. R. and Chemin, J. F., *Phys. Rev. C* **59** (1999), 2462.
24. Batkin, I. S., *Sov. J. Nucl. Phys.* **29** (1979), 903.
25. Pisk, K., Kremar, M., Ljubicic, A. and Logan, B. A., *Phys. Rev. A* **47** (1993), 1320.
26. Karpeshin, F. F., Band, I. M., Trzhaskovskaya, M. B. and Zon, B. A., *Phys. Lett. B* **282** (1992), 267.
27. Kalman, P. and Keszthelyi, T., *Phys. Rev. C* **49** (1994), 324.
28. Karpeshin, F. F., Harston, M. R., Attallah, F., Chemin, J. F. and Scheurer, J. N., *Phys. Rev. C* **53** (1996), 1640.
29. Carreyre, T., Harston, M. R. *et al.*, *Phys. Rev. C* **62** (2000), 024311.
30. Kishimoto, S., Yoda, Y. *et al.*, *Phys. Rev. Lett.* **85** (2000), 1838.
31. Chen, M. H., In: B. Grasemann (ed.), *Atomic Inner-Shell Physics*, Plenum Press, New York, 1985.
32. Sobelman, I. I., Vainshtein, L. A. and Yukov, E. A., *Excitation of Atoms and Broadening of Spectral Lines*, Springer, Berlin, 1981.
33. Massey, H. S. W. and Gilbody, H. B., *Electronic and Ionic Impact Phenomena*, Vol. 4, Oxford, 1974.
34. Firestone, R. B., *Table of Isotopes*, Lawrence Berkeley National Laboratory, University of California, 1998.

Photo-induced depopulation of the $^{180}Ta^m$ isomer via low-lying intermediate states: Structure and astrophysical implications

D. Belic,[1,*] C. Arlandini,[2] J. Besserer,[3] J. de Boer,[3] J. J. Carroll,[4] J. Enders,[5,†] T. Hartmann,[5] F. Käppeler,[2] H. Kaiser,[5,‡] U. Kneissl,[1] E. Kolbe,[6] K. Langanke,[7] M. Loewe,[3] H. J. Maier,[3] H. Maser,[1] P. Mohr,[5] P. von Neumann-Cosel,[5] A. Nord,[1,*] H. H. Pitz,[1] A. Richter,[5] M. Schumann,[2] F.-K. Thielemann,[6] S. Volz,[5] and A. Zilges[5]

[1]*Institut für Strahlenphysik, Universität Stuttgart, D-70569 Stuttgart, Germany*

[2]*Institut für Kernphysik, Forschungszentrum Karlsruhe, D-76021 Karlsruhe, Germany*

[3]*Sektion Physik, Ludwig-Maximilians Universität München, D-85748 Garching, Germany*

[4]*Department of Physics and Astronomy, Youngstown State University, Youngstown, Ohio 44555*

[5]*Institut für Kernphysik, Technische Universität Darmstadt, D-64289 Darmstadt, Germany*

[6]*Institut für Physik, Universität Basel, CH-4056 Basel, Switzerland*

[7]*Institute of Physics and Astronomy, University of Aarhus, DK-8000 Aarhus C, Denmark*

(Received 6 September 2001; published 14 February 2002)

The photo-induced depopulation of the quasistable isomer ($t_{1/2} \geq 1.2 \times 10^{15}$ yr) in ^{180}Ta with angular momentum and parity $J^\pi = 9^-$ at an excitation energy $E_x = 75$ keV was studied at the new bremsstrahlung irradiation facility installed at the Stuttgart 4.3 MV DYNAMITRON accelerator in the energy range of bremsstrahlung end point energies between $E_0 = 0.8$–3.1 MeV. The onset of the isomer depopulation could be observed starting at an end point energy of $E_0 \approx 1$ MeV, i.e., at an intermediate state of ^{180}Ta at or below that energy. Higher-lying intermediate states were found at 1.22, 1.43, 1.55, 1.85, 2.16, 2.40, 2.64, and 2.80 MeV. The extracted integrated cross sections show a remarkably strong depopulation of the $^{180}Ta^m$ isomer by photoexcitation. The results are compared with previous experiments and recent quasiparticle-phonon model calculations. Implications of the results for a possible nucleosynthesis of ^{180}Ta in the *s* process and the neutrino process are discussed.

DOI: 10.1103/PhysRevC.65.035801 PACS number(s): 25.20.Dc, 23.20.Lv, 97.10.Cv, 27.70.+q

I. INTRODUCTION AND MOTIVATION

Amongst about 300 naturally occurring isotopes there are only nine with odd proton and odd neutron numbers. The heaviest of them, ^{180}Ta, owes its existence to a low-lying isomer at an excitation energy of 75 keV while the ground state is unstable ($t_{1/2} = 8.1$ h), see Fig. 1. The extremely long half-life ($t_{1/2} \geq 1.2 \times 10^{15}$ yr) results from the large spin difference of the aligned coupling of $\pi 9/2[514] + \nu 9/2[624]$ states to a total spin $J^\pi = 9^-$ compared to the antialigned $\pi 7/2[404]$ and $\nu 9/2[624]$ ground-state (g.s.) configuration leading to $J^\pi = 1^+$. The stretched two-quasiparticle nature makes it an interesting candidate in the search for possible structure effects of excitations built on isomers as was done, for example, in studies using targets of the famous 31 yr, $J^\pi = 16^+$ isomer in ^{178}Hf [1–3] or radioactive ^{174m}Hf beams [4]. The natural abundance of ^{180}Ta presents another interesting puzzle. With tantalum being the rarest element and having a relative abundance of 0.012% only, ^{180}Ta is nature's rarest (quasi)stable isotope. Despite its rarity, its nucleosynthesis has been a mystery for a long time because it is bypassed by the main production processes of heavy nuclei [5]. However, two weak paths within the *s* process have been suggested. One possibility would be β decay of the $J^\pi = 8^-$ isomer in ^{180}Hf [6]. However, present experimental limits exclude significant contributions to the ^{180}Ta abundance by this process [7]. Alternatively, low-lying states in ^{179}Hf may β decay to ^{179}Ta under *s*-process conditions, and subsequent neutron capture also leads to ^{180}Ta [8]. The latter scenario requires a temperature of about 3×10^8 K. In order to quantify this path, the neutron capture cross section of the radioactive ^{179}Ta ($t_{1/2} = 665$ d) needs to be measured [9]. The neutron capture cross section of $^{180}Ta^m$ recently was

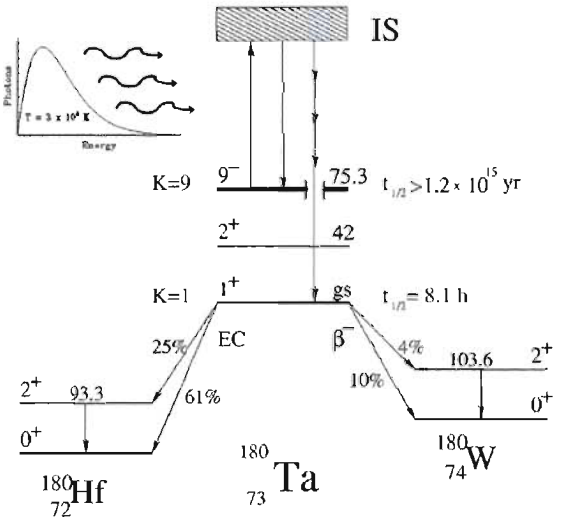

FIG. 1. Low-energy level and decay scheme of ^{180}Ta.

*Present address: Agilent Technologies Deutschland, D-71034 Böblingen, Germany.

†Present address: NSCL, MSU, East Lansing, MI 48824.

‡Present address: Büro Fritz GmbH, D-64683 Einhausen, Germany.

measured in the keV energy range for a detailed *s*-process analysis of the nucleosynthesis of $^{180}Ta^{m}$ [10].

The decay properties of ^{180}Ta may be considerably modified in the stellar environment because of its isomeric nature. The photon bath accompanying the *s* process can depopulate the isomer by resonant photoabsorption into higher-lying intermediate states (IS's) with a branching to the g.s. (typically by a cascade because of the large angular momentum difference). Such an electromagnetic coupling of the isomer and g.s. may destroy all or parts of the synthesized ^{180}Ta. Thus, considerable experimental efforts have been made in recent years to search for IS's of astrophysical relevance.

It may be noted that the resonant depopulation of long-lived isomers is also discussed as a possible driving mechanism for a γ-ray laser [11]. Recently, it has been demonstrated for the nucleus ^{103}Rh that population inversion can be achieved in resonant photoabsorption from bremsstrahlung fields [12]. The nucleus ^{180}Ta is one of the rare cases where typical cross sections can be determined experimentally. This provides a benchmark for the critical discussion (see Refs. [13–15]) of recent work claiming to have observed resonant depopulation of the 31 yr, $J^{\pi}=16^{+}$ isomer in ^{178}Hf by x rays [16]. However, recent experiments by Ahmad *et al.* [17] seem to rule out the results of Ref. [16].

Activation measurements have been performed with real photons from bremsstrahlung [18–20] or strong radioactive sources [20–22] and with Coulomb excitation [23–25]. The principle of detection in the activation experiments is sketched in Fig. 1. After irradiation one searches for population of the g.s. by its specific decay features. The strongest decay branch is by electron capture to the g.s. of ^{180}Hf with the signature of characteristic Hf x rays. There are also weaker branches populating the 2_1^+ states in ^{180}Hf and ^{180}W. Direct information on the energies and cross sections of IS's can only be extracted from measurements of excitation functions with photon beams of variable energy.

Alternatively, ^{180}Ta has been studied recently in great detail by γ spectroscopy [26–32]. Contrary to high-spin studies after fusion-evaporation reactions, these investigations used light-ion and light heavy-ion incomplete fusion reactions to enhance the sensitivity in the spin window around $J=9$ of interest here. A wealth of spectroscopic data has been obtained, but only recently has there been a concrete suggestion [33] of a connection between levels and transitions seen in the spectroscopic data and the intermediate states observed in photoactivation experiments. Additionally, in-beam Coulomb excitation experiments were performed [34,35]. A recent study demonstrates population of the g.s. following Coulomb excitation, but the IS could not be identified so far [35].

All scattering experiments off ^{180}Ta are limited by the extremely low natural abundance of ^{180}Ta. Here, we report a new photo-induced depopulation experiment using the world's resources of enriched (to 5.45%) ^{180}Ta material. Data were taken at the high-current Dynamitron accelerator at Stuttgart with a setup optimized for the off-line activation detection [36]. This allowed for the first time to extract IS's down to $E_x \approx 1$ MeV. The astrophysical consequences for a possible *s*-process production have been discussed elsewhere [38]. Additionally, nuclear resonance fluorescence (NRF) measurements have been performed with the enriched target to search for decay branches of IS's back to the $J^{\pi}=9^{-}$ isomer. The present work provides a full account of the experimental results and discusses their nuclear structure and astrophysical implications.

II. PHOTOACTIVATION AND PHOTON SCATTERING TECHNIQUES USING BREMSSTRAHLUNG

Photoactivation (depopulation or population of long-lived isomers in photo-induced reactions) and photon scattering off bound nuclear states (nuclear resonance fluorescence) share the principal advantage of a well-known reaction mechanism. Model-independent information can be extracted from both kinds of experiments since both the excitation (photoabsorption) and deexcitation processes (electromagnetic decays) proceed via the well-known electromagnetic interaction.

A. Photoactivation of isomers

Isomeric states which differ substantially in spin from the ground state cannot be depopulated or populated directly in photo-induced reactions due to the low transfer of angular momentum by photons. Therefore, the photoactivation process has to proceed indirectly via the resonant excitation of a higher-lying excited state, a so-called intermediate state (IS). Its decay subsequently can feed the isomeric or ground state, respectively, via electromagnetic transitions (γ transitions or internal conversion processes).

Unfortunately, there is a lack of monochromatic, tunable photon sources of high spectral intensity at MeV energies. However, the availability of high-current, low-energy electron accelerators can provide intense bremsstrahlung photon sources which can be used for improved photoactivation experiments [36].

The excitation energies and strengths of the IS can be extracted from bremsstrahlung-induced activation experiments by measuring the activation yields Y_{BS} as a function of the bremsstrahlung end point energy E_0. Since bremsstrahlung has a continuous energy distribution, the yields are given by the following integral:

$$Y_{BS}(E_0) \sim \int_0^{E_0} \sigma(E_\gamma) \cdot N_{BS}(E_0, E_\gamma) \cdot dE_\gamma, \qquad (1)$$

where $\sigma(E_\gamma)$ is the total photoreaction cross section as a function of the photon energy E_γ, corresponding to the energy E_{IS} of the intermediate state above the 75 keV isomer. The excitation energy E_x relative to the ground state of ^{180}Ta is given by $E_x = E_{IS} + 75$ keV. The quantity $N_{BS}(E_0, E_\gamma)$ represents the continuous bremsstrahlung spectral density with an end point energy E_0. The unquoted constant of proportionality is determined by the usual quantities such as target thickness, detector efficiencies, and the functions for the irradiation and counting times, respectively.

Low-energy, thick target bremsstrahlung spectra [39] show a nearly linear shape in the neighborhood of the end-point energy. This gives rise to an approximately linear yield

curve for one IS [40]. The onset of the yield curve is given by the excitation energy E_{IS} of the first IS. Each kink in the yield curve corresponds to the excitation energy of a further IS. The change of slope is proportional to the excitation strength of the respective IS (see, e.g., Ref. [41], and references therein).

In the following we summarize the relations needed for the description of the depopulation of a long-lived isomer by photoexcitation (the corresponding expressions for the population of isomers can be found elsewhere [36,40–42]). From the yield curve analysis the total detected activity I_D can be extracted, corresponding to the integrated cross section of the IS leading to a depopulation of the isomeric state,

$$I_D = g_{IS}\left(\frac{\pi\hbar c}{E_{IS}}\right)^2 \cdot \Gamma_{ISO} \cdot \frac{\Gamma_{g.s.}}{\Gamma}. \tag{2}$$

Here, Γ_{ISO} denotes the partial decay width of the IS back to the isomeric state, $\Gamma_{g.s.}$ stands for the total decay width of the IS to the short-lived ground state bypassing the isomeric state, and Γ is the total decay width of the IS. The spin factor g_{IS} takes into account the statistical weights of intermediate and isomeric states, respectively:

$$g_{IS} = \frac{2J_{IS}+1}{2J_{ISO}+1}. \tag{3}$$

Recent complementary investigations of both photoactivation with bremsstrahlung of variable end point energies *and* on-line nuclear resonance fluorescence experiments have demonstrated the reliability of modern photoactivation experiments and their analysis [36,43]. However, it should be emphasized that for a correct analysis of the yield curve all low-lying IS's have to be detected or known. Otherwise, the extracted cross sections are overestimated.

B. Photon scattering

Photon scattering nowadays represents an established technique in nuclear structure physics. In NRF experiments using continuous bremsstrahlung as a photon source and stable isotopes as targets all excited states with a sufficiently large ground-state decay width Γ_0 are excited simultaneously. Such experiments provide data concerning the following spectroscopic quantities: Precise excitation energies E_x can be extracted from the spectra of the scattered photons and the integrated scattering cross sections $I_{S,0}$ in the case of ground-state transitions are proportional to Γ_0^2/Γ. Therefore, the ground-state transition widths Γ_0 and the total widths Γ of the excited states can be extracted from the scattering intensities if all decay branchings are observed or known from other experiments. These quantities can be converted into reduced transition probabilities $B(E1)\uparrow, B(M1)\uparrow, B(E2)\uparrow$, or lifetimes $\tau = \hbar/\Gamma$. The formalism describing photon scattering experiments is summarized in previous reviews [44,45]. In the present case of photon scattering off a target nucleus in an isomeric state the integrated scattering cross section $I_{S,0}$ has to be replaced by the corresponding cross section $I_{S,ISO}$ and the widths Γ_0 by Γ_{ISO}, respectively.

C. Combined analysis of photoactivation and photon scattering experiments

Photoactivation and NRF experiments complement each other in an ideal way. The excitation energies and strengths of the IS can be determined directly and rather precisely, in on-line NRF experiments. However, the photoactivation technique offers some unique advantages for investigations of the depopulation or population of the isomers. The possible low-level, off-line detection of the activation yields and the higher available photon fluxes at irradiation facilities, as compared to the well-collimated narrow photon beams needed in photon scattering experiments, enables a considerably higher detection sensitivity.

Whereas in NRF experiments on nuclei existing in a long-lived isomer mainly excited states with a predominant decay to the isomeric state ($\Gamma_{ISO}/\Gamma \approx 1$) are observed, in photoactivation experiments IS's can be detected with decay branchings $\Gamma_{ISO}/\Gamma \ll 1$ which populate in a decay cascade the ground state bypassing the isomeric state. The new information obtained in this case is the effective branching ratio $\Gamma_{g.s.}/\Gamma$. This branching ratio $\Gamma_{g.s.}/\Gamma$ normally cannot be determined in NRF experiments. Therefore, photoactivation and photon scattering experiments are complementary spectroscopic methods. In the most favorable case where the intermediate state can be observed in both the photon scattering and photoactivation experiments, the ratio of the integrated cross sections directly provides the branching ratio $\Gamma_{g.s.}/\Gamma_{ISO}$ without knowledge of the angular momentum J_{IS} and the total width Γ,

$$\frac{I_D}{I_{S,ISO}} = \frac{\Gamma_{g.s.}}{\Gamma_{ISO}}. \tag{4}$$

D. Yield curve analysis

The yield curves measured in bremsstrahlung-induced reactions have to be transformed into the photonuclear cross sections or strength distributions of interest (in the case of bound states). These unfolding procedures have a long tradition in photonuclear physics (see, e.g., Ref. [46]). Nevertheless, since the unfolding in principle corresponds to a differentiation of the yield curve it is very difficult to avoid the generation and amplification of spurious structures and oscillations in the deduced cross sections even when applying sophisticated techniques such as variable energy binnings and smoothing procedures (see, e.g., Ref. [47]). A reliable unfolding represents a tough task already in the case of a rather smooth cross section curve, like giant resonances, but is even more difficult in the present case of discrete excitation strengths to bound states. The yield curves in the present experiments were taken in rather wide energy steps. In view of this limited number of data points and their scattering due to non-negligible systematic uncertainties the application of complete unfolding procedures seems to be inappropriate.

Therefore, a simple and more pragmatic analysis was applied to extract the integrated cross sections I_D.

The peak areas observed in the photon spectra of the off-line activation measurements were normalized for the corresponding irradiation and counting times. Low residual activities eventually existing from repeated irradiations of the sole enriched sample were properly corrected. The photon flux and the photon energy distribution were calculated for each end point energy by Monte Carlo simulations using the code GEANT 3.21. These calculations were experimentally checked by on-line NRF experiments and by simultaneous photoactivation measurements on ^{115}In [36]. From the onset of the activation the first IS was assumed at about 1.01 MeV above the isomer. In the following analysis the excitation energy of 1.01 MeV was used as a starting value for the analysis of the first part of the yield curve. In the first step of the analysis the data points up to the first kink in the yield curve were included. The energetic position of the lowest IS and its integrated depopulation cross section were then varied to deduce a best value for the cross section of the first IS from all yield points up to the first kink (see Fig. 5 below). By this, the integrated depopulation cross section I_D of the lowest IS could be determined. These values then are used for the next step in the data analysis where the yield points up to the second kink are taken into account. As a starting value the energetic position of the first kink is taken. Then the integrated cross section I_D is calculated for all yield data points up to the second kink subtracting the contribution of the lower-lying IS. Both the energetic position E_{IS} *and* the integrated cross section I_D are varied until the deduced cross sections are constant for all yield points considered. This analysis procedure was continued step by step from kink to kink of the yield curve over the whole energy range investigated in the present experiments (see Sec. IV C). It is clear from the analysis procedure that the values for the lower-lying IS's have a strong effect on the results for the higher-lying ones, leading to larger errors for both the energies E_{IS} and the cross sections I_D.

This analysis is very sensitive to the energetic position of the IS. For pronounced kinks a variation of only 20 keV leads to a much worse description of the measured yield points (reflected by an increase or decrease of the deduced integrated cross section). From this, the errors of the energies E_{IS} can be estimated and are quoted in Table I. These errors, depending on the changes of the slope of the yield curve, are comparable (20–60 keV) to the uncertainties for the absolute calibration of the bremsstrahlung endpoint energy of about 30 keV [36]. This type of analysis has been checked by applying it to measurements of the photoactivation of the ^{115}In^m isomer [36], where the energies and integrated cross sections of the IS's are known. The good agreement of the deduced results and those calculated from literature data [37] demonstrates the reliability of the applied analysis.

TABLE I. Intermediate states (IS's) observed in the photo-induced depopulation of ^{180}Ta^m. Given are the energies E_{IS} of the observed intermediate states (with respect to the isomer at 75 keV) with their uncertainties from the yield curve analysis (see text), the total integrated depopulation cross sections I_D, and the branching ratios $\Gamma_{ISO}\cdot\Gamma_{g.s.}/\Gamma$ [see Eq. (2)]. For the cross sections and branching ratios, statistical and systematical errors are quoted separately (in this order).

E_{IS} (MeV)	I_D (eV b)			$g_{IS}\cdot\Gamma_{ISO}\cdot\Gamma_{g.s.}/\Gamma$ (meV)		
1.01 [a]	0.057	±0.003	±0.015	0.015	±0.001	±0.004
1.22(2)	0.27	±0.02	±0.07	0.103	±0.008	±0.027
1.43(2)	0.24	±0.04	±0.06	0.126	±0.022	±0.033
1.55(3)	0.70	±0.09	±0.18	0.44	±0.06	±0.11
1.85(5)	1.11	±0.14	±0.29	1.0	±0.1	±0.3
2.16(2)	2.8	±0.3	±0.7	3.3	±0.3	±0.9
2.40(6)	3.5	±0.6	±0.9	5.2	±0.8	±1.4
2.64(3)	13	±1	±3	23	±2	±6
2.80(4)	36	±2	±9	73	±3	±19

[a]Fixed by the onset of the activation.

III. EXPERIMENTAL DETAILS

A. Irradiation facility

At the bremsstrahlung irradiation facility [36] installed recently at the Stuttgart DYNAMITRON accelerator, typical dc electron currents of 400–450 μA could be used on the water cooled bremsstrahlung production target in the whole energy range of interest (0.8 – 4 MeV). To achieve the highest possible photon flux the distance between the radiator target and the Ta samples to be activated was only about 9 cm. The samples could be transported to the activation location by a remotely controlled worm driven support. Details of the setup and the performed calibrations can be found in Ref. [36].

B. Ta targets

The availability of a highly precious Ta sample, representing the world's stock of enriched ^{180}Ta^m material, together with the new irradiation facility dramatically improved the sensitivity of the present study compared to older ones. In total about 150 mg of Ta_2O_5 material, enriched to 5.45% in ^{180}Ta^m, were available, corresponding to about 6.7 mg of ^{180}Ta^m. In view of the high price of the material, conventional target preparation methods like tablet pressing could not be applied since this technique is affected with appreciable material loss. Therefore, the Ta_2O_5 powder was packed into a graphite container consisting of a base and a cover. The target area was 1 cm^2, and the areal density amounted to 123 mg/cm^2 of Ta. The graphite container was fairly transparent for photons with energies of more than 50 keV. Therefore, the absorption of the Hf characteristic x rays by the graphite cover of the target was negligible. The target setup is described in more detail in Ref. [48].

Alternating with this sole enriched target assembly, foils of natural Ta metal (diameter 20 mm and total mass of Ta $\approx$1.5 g, corresponding to 0.18 mg of ^{180}Ta) were activated at bombarding energies above 1.7 MeV. In addition, a sample consisting of 150 mg natural Ta_2O_5, prepared in exactly the same way as the enriched target, was activated at higher bombarding energies around 3 MeV to verify the enrichment

factor. Typical irradiation and activation counting times were about two half-lives (12–20 h).

C. Photon detection system

After the irradiations characteristic x rays and nuclear γ rays from the activated samples were measured offline in a separate counting room using two well-shielded, high-resolution, low-energy photon (LEP) detectors facing each other [36]. The planar LEP crystals had a diameter of 52 mm and a sensitive volume of 42 cm^3. Background radiation was efficiently reduced by a sophisticated shield made of high-purity copper and lead. The excellent energy resolution of about 470 eV at 55 keV enabled the separation of the $K_{\alpha 1}$ (55.79 keV) and $K_{\alpha 2}$ (54.61 keV) characteristic x-ray lines of ^{180}Hf following the electron-capture decay of the ^{180}Ta ground state (see Fig. 1). The relative efficiencies of the detectors were determined using a ^{133}Ba γ source. At 59.5 keV the absolute efficiencies were measured by means of a calibrated ^{241}Am source. Total absolute efficiencies of about 20% and 28% at 55 keV could be achieved for both detectors, respectively. The estimated relative systematic uncertainties of these values are below 11%.

D. Photon scattering experiments

Supplementary photon scattering experiments were performed likewise at the bremsstrahlung facility of the Stuttgart accelerator [44]. The measurements were carried out at a bremsstrahlung end point energy of 1.5 MeV to achieve an optimal sensitivity at low excitation energies around 1 MeV where the lowest IS is assumed to lie. The dc electron currents used in the present experiments had to be limited, due to the thermal capacity of the radiator target, to values ≤ 420 μA. The scattered photons were detected by three high-resolution Ge γ-ray spectrometers installed at angles of about 90°, 127°, and 150° with respect to the incoming bremsstrahlung beam. The efficiencies of all three detectors amounted to about 100% each, relative to a standard 7.6 cm×7.6 cm NaI(Tl) detector. The energy resolution of all detectors was typically about 2 keV at a photon energy of 1.3 MeV. The Ge detector at 127° in addition was surrounded by a BGO anti-Compton shield [49] to improve its response function and hence to increase detection sensitivity.

In a first measurement, sheets of natural Ta metal were used as targets with a total mass of 1.797 g. A target of 1.011 g of LiF served as photon flux monitor. The total effective time of data collection in this measurement was 2 days. In a second run the enriched target sample of 150 mg Ta_2O_5 (enriched to 5.45% in $^{180}Ta^{m}$) together with the LiF material was bombarded for about 10 days at the same end-point energy of 1.5 MeV.

IV. RESULTS

A. Photon spectra of activated Ta samples

Figure 2 shows examples of the low-energy γ-ray and x-ray spectra of the enriched Ta sample from photoactivation

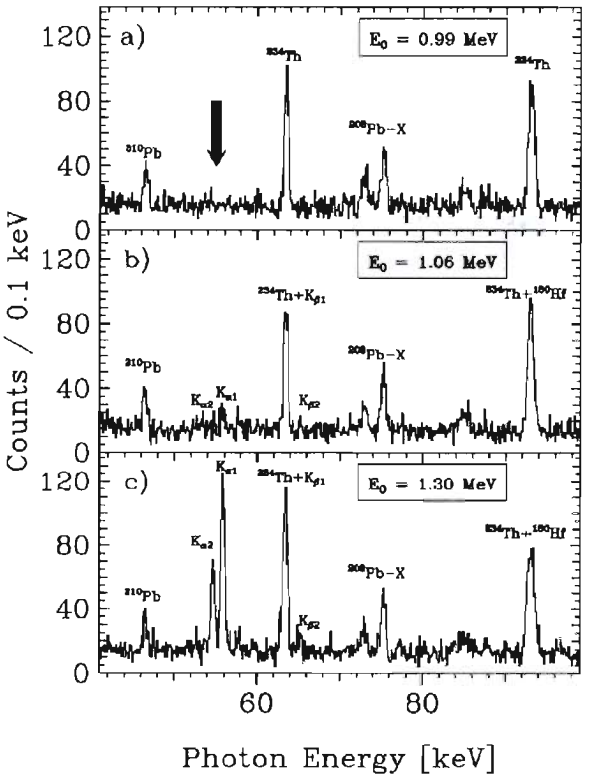

FIG. 2. Low-energy γ-ray and x-ray spectra of the enriched Ta sample from photoactivation at E_0=0.99, 1.06, and 1.30 MeV (a), (b), and (c). The Hf characteristic x rays are labeled by $K_{\alpha_{1,2}}$ and $K_{\beta_{1,2}}$. Background lines stemming from nuclear γ transitions in isotopes of natural decay chains or characteristic x rays are marked by the corresponding isotope symbols. In the top panel the energetic position of the Hf K_{α} lines is indicated by a bold arrow.

at the low bremsstrahlung end point energies of 0.99, 1.06, and 1.30 MeV. The Hf characteristic x rays of interest are labeled $K_{\alpha_{1,2}}$ and $K_{\beta_{1,2}}$. The origin of background lines is explained in the caption of Fig. 2.

The top panel shows the photon spectrum of the enriched target bombarded with bremsstrahlung of an end point energy E_0=0.99 MeV. Only background lines are visible. At the energetic position of the Hf K_{α} lines of interest, marked by an arrow, no peaks could be detected. The onset of the depopulation of the $^{180}Ta^{m}$ isomer has been observed starting at about $E_0 \geq 1.02$ MeV. In the middle panel, showing the spectra after an activation with E_0=1.06 MeV, the Hf characteric x rays could already be identified unambiguously. The spectrum taken after an activation at E_0=1.30 MeV is shown in the lowest panel and exhibits clearly the characteric x rays and nuclear γ transitions specific for the decay of the ground state of ^{180}Ta. The spectrum is dominated by the well-resolved K_{α_1} and K_{α_2} lines of Hf at 55.79 and 54.61 keV, respectively. The corresponding K_{β_1} and K_{β_2} peaks are also visible. Unfortunately, there are accidental overlaps of background lines (nuclear γ transitions following the β decay of ^{234}Th) with the K_{β_1} line and the $2^+ \rightarrow 0^+$ γ transi-

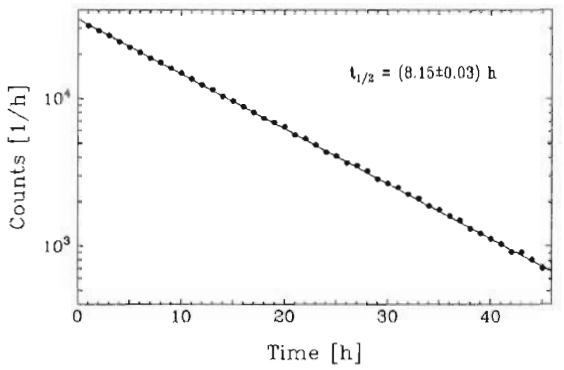

FIG. 3. Measured decay curve of the Hf K_α lines after photoactivation of the enriched Ta sample using bremsstrahlung with an end point energy of 3.1 MeV. The irradiation time was about 10 h. The statistical uncertainties of the data points are smaller than the symbol sizes.

tion in the residual nucleus ^{180}Hf, respectively. Therefore, the analysis was restricted to the K_α lines.

B. Half-life of the ^{180}Ta ground state

Additional proof for observing the ^{180}Ta ground-state decay is a confirmation of the lifetime in a time differential measurement. The results are depicted in Fig. 3. The enriched Ta sample was irradiated for about 10 h with bremsstrahlung of 3.1 MeV end point energy. The measurement of the activity covered about eight half-lives. The straight line represents a least squares fit to the data. The half-life could be determined from the slope rather precisely to $t_{1/2}^{exp} = (8.15 \pm 0.03)$ h, in good agreement with literature data [50].

To search for further possible short-lived isomers in ^{180}Ta two evaluation techniques were applied. First, a decay curve was generated from the list mode data with time binnings of 10 min. Covering the time range of the first 3.5 h no additional time component could be detected. As an alternative evaluation, the technique of using a compressed ^{2}log time scale [52] was applied. This method is known to be very sensitive to disentangle different time components in decay curves [52]. Also this analysis of the total data resulted in an excellent fit to the data [53] assuming only one half-life. The obtained value $t_{1/2} = 8.18(2)$ h was in perfect agreement with both the above-mentioned result of the traditional analysis and the best value given in the literature [50]. Therefore, the existence of further isomers with half-lives larger than a few minutes and essential contributions to the decay of the intermediate states can be excluded on the basis of the present experiments.

C. Activation yields and integrated depopulation cross sections

The relative yields, extracted from the peak areas of the ^{180}Hf K_α lines normalized to the number of incident electrons and to the irradiation and counting times, are plotted in Fig. 4 as a function of the bremsstrahlung end point energy.

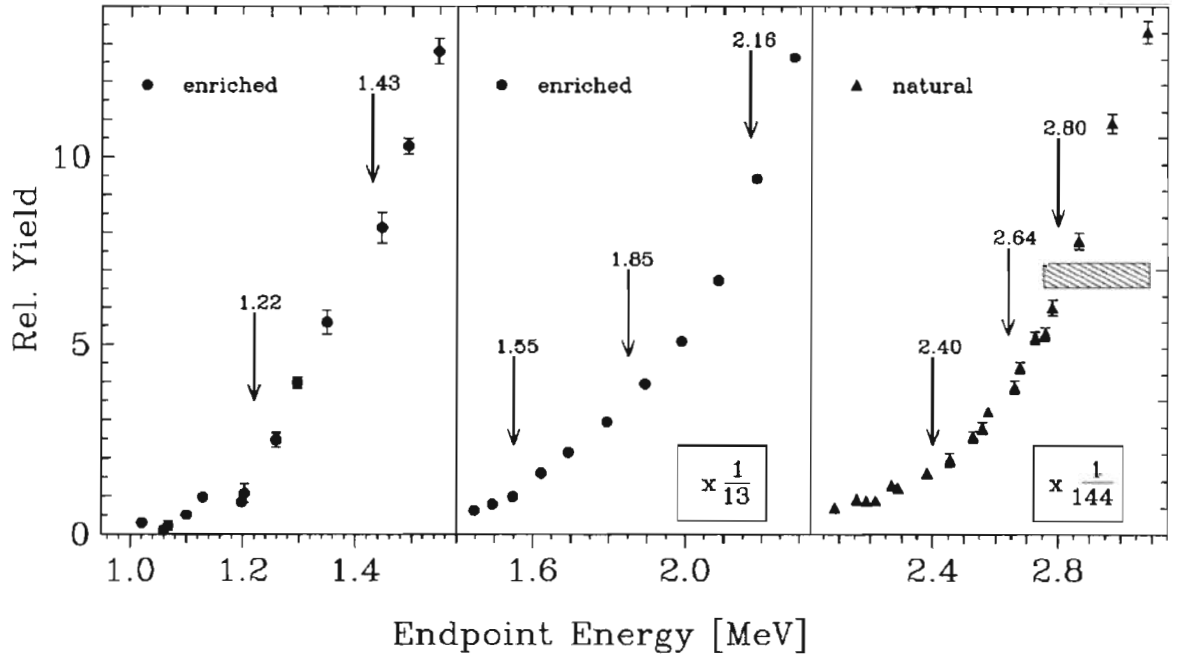

FIG. 4. Measured yields in a linear scale as a function of the end point energy. Shown are the peak areas of the Hf K_α lines, normalized to the number of incident electrons and the irradiation and measuring times (see text). Up to end point energies of 2.3 MeV (left and middle parts of the figure) the enriched sample was activated; for higher bombarding energies metallic natural Ta targets could be used (right part of the figure). The ordinate scales are properly changed to allow a clearly arranged linear presentation. The arrows mark the kinks in the yield curve caused by the different intermediate states. The hatched area in the right part of the figure represents the sensitivity limit reached in the experiments of Collins *et al.* (Ref. [19]).

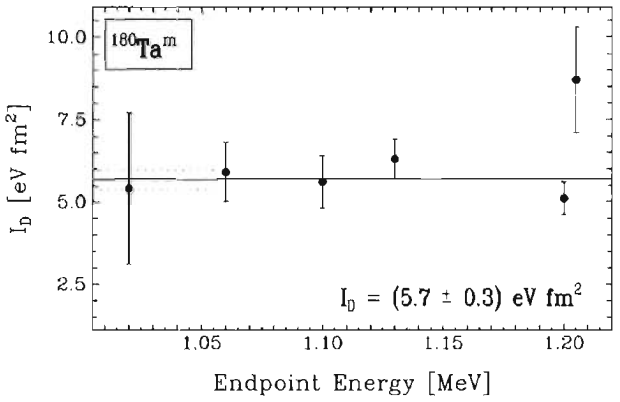

FIG. 5. Integrated depopulation cross section I_D of the first intermediate state (IS) according to the analysis of the lowest six yield data points, and assuming the energetic position of the first IS at $E_{IS}=1.01$ MeV above the isomer at 75 keV.

A linear scale for the ordinate was chosen for better visibility of the various kinks. Due to the large range of measured yields the figure is divided into three parts. The corresponding reduction factors for the scales in the middle and right part are given as insets. In the reduction factor of the right part the lower ^{180}Ta amount of a factor of 48 as compared to the enriched sample is taken into account. The low-energy activations were performed using the enriched target sample, while for end point energies above 2.3 MeV (right part) metallic sheets of natural Ta could be used. The arrows mark the kinks in the yield curve caused by the various IS's and the corresponding excitation energies E_{IS} are given in MeV.

The availability of the enriched target material, together with the new bremsstrahlung irradiation setup, has improved the sensitivity of the present study by a factor of about 4000 compared to previous experiments (Ref. [19], and references therein). For comparison, the sensitivity limit of the experiment by Collins *et al.* [19] is shown as a hatched area in the right part of Fig. 4.

The quantitative analysis of the yield curve, explained in Sec. II D, provided the numerical results summarized in Table I. Given are the excitation energies E_{IS} of the IS and the integrated depopulation cross sections I_D which can be expressed in terms of width ratios $g_{IS}\cdot\Gamma_{ISO}\cdot\Gamma_{g.s.}/\Gamma$. The values for the energies E_{IS} and the integrated cross sections I_D were obtained from fits to the various linear sections of the yield curve. By way of example, the resulting best fit is shown in Fig. 5 for the data available to determine the lowest IS at 1.01 MeV photon energy.

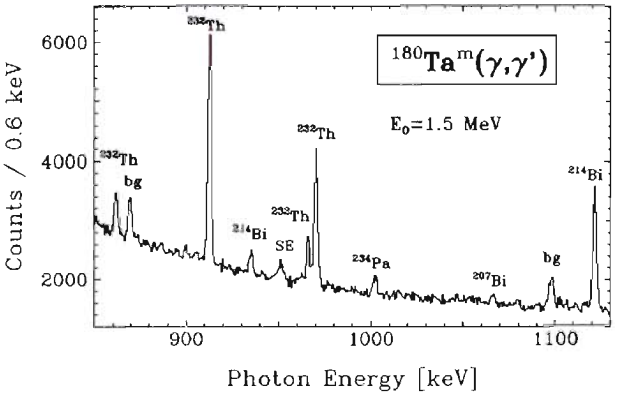

FIG. 6. Spectrum of photons scattered off the enriched $^{180}Ta^{m}$ sample using a bremsstrahlung beam of an end point energy of 1.5 MeV. Background transitions are marked. No peak which may be ascribed to transitions in ^{180}Ta or ^{181}Ta could be observed.

The given uncertainties of the excitation energies E_{IS} are estimated from the analysis of the yield curve (see Sec. II D). In addition, an overall uncertainty of the order of 30 keV exists due to systematic errors in the absolute calibration of the bremsstrahlung end point energies. The errors of the integrated cross sections are dominated by the systematical ones due to the necessary absolute calibrations. The relative error of the photon flux calibration amounts to about 10%, the uncertainties of the absolute efficiency determinations of the low-energy photon detectors to 11%. Furthermore, the relative intensities of the ^{180}Hf K_α lines (per g.s. decay of ^{180}Ta) are known with a relative precision of 5% only. It is obvious that the systematical errors of the integrated depopulation cross sections increase considerably for the higher-lying IS's due to unavoidable error propagation in the yield curve analysis. For these reasons statistical and systematical errors are quoted separately in Table I.

D. Results from photon scattering experiments

The first photon scattering experiments using natural Ta metallic targets, performed with bremsstrahlung of an end point energy of 1.5 MeV, failed to detect any excitation in ^{180}Ta. Obviously, the total amount of $^{180}Ta^{m}$ ($\approx$0.2 mg) contained in the natural sample was much too small. An estimate of the integrated scattering cross section of a hypothetical excitation at an excitation energy around 1 MeV provided a rather high detection limit of about $I_S \leqslant 80000$ eV b only. Therefore, in a subsequent photon scattering experiment the enriched sample, containing in total 6.7 mg of $^{180}Ta^{m}$, was used as a scattering target. Furthermore, the period of data collection was extended to 10 days.

Figure 6 shows the observed spectrum of scattered photons. The marked peaks correspond to known background γ rays. Unfortunately, none of the peaks observed could be ascribed to transitions in ^{180}Ta. Surprisingly, also no low-energy transitions in ^{181}Ta, which made up 95% of the Ta sample, could be detected. Obviously, there is a lack of dipole strength at low energies and the stronger dipole excitations in ^{181}Ta are concentrated at higher excitation energies of about 2.3 and 3.0 MeV, as observed in previous photon scattering experiments off ^{181}Ta [51]. The sensitivity limit in the present photon scattering experiments was estimated from the statistics of the continuous background distribution. Requiring a peak area larger than a 2σ deviation of the corresponding background counts, no excitation in the most interesting energy range around 1 MeV could be detected with an integrated scattering cross section of $I_S \geqslant 200$ eV b. This limit is about a factor of 400 lower than that derived from the experiment using the metallic natural Ta sheets. Nevertheless, it is still four orders of magnitude larger than the g.s.

decay branch observed in the photoactivation experiment.

V. DISCUSSION

A. Comparison with previous investigations

Previous measurements of ^{180}Ta excitation functions by photoactivation with bremsstrahlung have been reported in Refs. [19,54]. In Ref. [19] an onset of ^{180}Ta g.s. decay was observed at an end point energy of about 2.8 MeV and IS's at 2.8(1) and 3.6(1) MeV were deduced. Because of the coarse energy steps of the excitation function the lower IS might correspond to the intermediate levels at E_{IS}=2.64 and 2.80 MeV from the present work. For comparison of the integrated cross sections with the value given in Ref. [19] the contributions of lower-lying IS's, observed for the first time in the present experiment, must be subtracted. After the correction an integrated cross section of 58(17) eV b is found, about 50% higher than in the present work but still within statistical and systematical uncertainties of both the present data and that of Ref. [19]. Karamian *et al.* [54] extended the measurements of the ^{180}Ta$^m(\gamma,\gamma')$ reaction up to E_0 =7.6 MeV and deduced the g.s. population branching ratio as a function of E_0.

Isomer depopulation by strong radioactive ^{60}Co sources has also been searched for [20–22]. Only in Ref. [22] was a weak positive signal observed. However, subsequent measurements with an improved detection setup confirmed the result with much better statistics [55]. Because the photon flux was determined using ^{115}In as a reference (see Ref. [36]), the measured yield can be converted to an integrated cross section for an excitation energy close to the dominant IS in ^{115}In at E_x=1.078 MeV resulting in I_D =0.13(4) eV b. The larger I_D value with respect to the lowest IS found in the present work (cf. Table I) can be understood from the additional contribution of the next-higher IS at E_{IS}=1.22 MeV. With reasonable assumptions about the photon flux at the higher energy the findings of Refs. [22,55] are in agreement with the results presented in Table I.

A comparison of the photoexcitation results to those of Coulomb excitation experiments is less straightforward. In general, Coulomb excitation functions are less sensitive to the excitation energy of the IS and contributions of several IS's cannot be decomposed. However, because of the strong excitation energy dependence of the Coulomb excitation cross section it is reasonable to assume that only a single IS (lowest in energy) is responsible for the observed yield. The ^{32,36}S induced experiments of Schlegel *et al.* [23] indicated $E_{IS}\leq 1$ MeV, but the Hf K x-ray signal was hampered by a strong Ta x-ray signal resulting from β decay produced in background reactions. Depopulation of the isomer was also observed in light-ion induced Coulomb excitation, but the data suggested a significantly higher energy at E_{IS} $\approx$2.2 MeV [24]. Recent experiments using ^{36}S and ^{64}Ni beams and enriched targets find a clear signal compatible with an IS at E_{IS}=1.08(4) MeV [25,56]. One should note the different selectivity of Coulomb excitation where $E2$ and $E3$ transitions are favored. This might explain the nonobservation of the lowest IS. For example, assuming an $M1$ transition Coulomb excitation would be negligible.

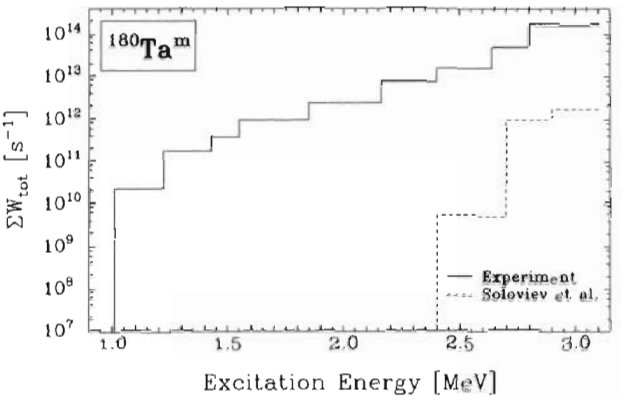

FIG. 7. Summed experimentally determined transition rates ΣW_{tot} (full line) in comparison with the results of the calculations by Soloviev *et al.* (Refs. [57,58]), see the hatched line.

B. Comparison with theoretical calculations

The theoretical description of heavy odd-odd nuclei is particularly difficult due to the complicated interplay of single-particle and collective degrees of freedom. Nevertheless, Soloviev [57] has studied the excitation spectrum of collective vibrations built on the $J^\pi=9^-$ and $J^\pi=16^+$ high-spin isomers in ^{180}Ta and ^{178}Hf, respectively, in the framework of the quasiparticle-phonon model (QPM) in a deformed single-particle basis. Recently, also the photodeexcitation process of ^{180}Ta^m was treated by extending the model space to include collective excitations built on the g.s. and a calculation of all possible transitions between these groups of states [58].

The transition rate W for one excited state is given by

$$W=\frac{8\pi}{\hbar}\sum_{\pi L}\frac{L+1}{L[(2L+1)!!]^2}\cdot\left(\frac{E_\gamma}{\hbar c}\right)^{2L+1}\cdot B(\pi L). \quad (5)$$

For the multipolarities relevant for photon scattering this leads to

$$W(E1)=1.59\times10^{15}E_\gamma^3\cdot B(E1)\uparrow, \quad (6)$$

$$W(E2)=1.22\times10^{9}E_\gamma^5\cdot B(E2)\uparrow,$$

$$W(M1)=1.76\times10^{13}E_\gamma^3\cdot B(M1)\uparrow,$$

where W is in units of 1/s, E_γ is in MeV, and the reduced transition probabilities are in e^2 fm^{2L} for electric and in μ_N^2 for magnetic transitions.

The total transition rate W_{tot} for the two-step process of the excitation of an IS and its decay to the vibrational states built on the ground state can be calculated from the experimentally measured integrated cross section I_D using Eq. (2),

$$W_{tot}=1.52\times10^{15}\cdot I_D\cdot\left(\frac{E_\gamma}{\pi\hbar c}\right)^2, \quad (7)$$

where I_D is in units of eV fm^2.

For comparison of the experimental data with the QPM calculations [58], the hatched line in Fig. 7, the total transi-

tion rate ΣW_{tot} summed over the contributions of all IS's up to a certain excitation energy was calculated. The results are plotted in Fig. 7 as a solid line.

Below E_x=2.7 MeV the QPM calculations find very little coupling between isomer and ground state. A sudden onset is observed around 2.7 MeV related to the decisive role of two-phonon excitations. These strong contributions are theoretically explained as a three-step process: In the first step, IS's are excited by fast dipole transitions through one-phonon components of the wave functions of the vibrational states built on the isomer, while the second step is dominated by collective $E2$ transitions from two-phonon components of these states to the one-phonon vibrational states built on the ground state. The third step is a complicated γ cascade from the vibrational states to the ^{180}Ta ground state.

However, even at higher energies, where significant transition rates are calculated in Ref. [58], the data are underpredicted by about two orders of magnitude. One possible explanation for this shortcoming could be the assumption of K symmetry. This may approximately hold for energies below $E_x \approx 1$ MeV, but at higher excitation energies K mixing might be expected to increase the transition rates considerably. A dramatic reduction of K hindrance factors has been observed for multi-quasi-particle isomers in the $A=180$ mass region (see, e.g., Ref. [59]) and complete K mixing near the neutron binding energy has been observed [54]. The systematics reveal a striking dependence on the energy relative to the yrast level indicating statistical mixing as the most important source [60]. For excitation energies of more than 2.5 MeV above the yrast line (note that the isomer in ^{180}Ta is the 9^- yrast state) these results suggest that K hindrance plays a limited role only.

Another QPM calculation for ^{180}Ta has been performed by Alexa *et al.* [61] limited to lower excitation energies but including Coriolis mixing. Because of the latter, some IS candidates appear below 1.5 MeV, but the transition rates are again much smaller than found experimentally.

C. Astrophysical implications: the nucleosynthesis of $^{180}Ta^m$

As pointed out in the introduction, the nucleosynthesis of $^{180}Ta^m$ is a yet unsolved problem. The production mechanism is not clear but possible paths have been predicted for the s process [8], the ν process [62], and the p process [63]. The relevance of the present work lies in the experimental information on an electromagnetic coupling between the long-lived isomer and the short-lived ground state. Depending on the temperature of the stellar environment, the photon bath present during the different processes may effectively depopulate the isomer and destroy parts or all of synthesized $^{180}Ta^m$.

1. s-process considerations

The role of the isomer depopulation in s-process scenarios has been discussed in detail in Ref. [38]. Therefore, we restrict ourselves here to one particular aspect. The present results largely exclude s-process production of $^{180}Ta^m$ with typical temperatures deduced from branching points in the canonical model [5]. However, within the most advanced dynamical models [64] freshly synthesized ^{180}Ta can survive because of strong convection with a time scale still shorter than the effective lifetime at maximum s-process temperatures of about 3×10^8 K. At these temperatures the effective lifetime is almost exclusively determined by the energy of the lowest IS. It must be noted that the available data do not permit to distinguish whether the onset of isomer depopulation at $E_{IS} \approx 1$ MeV is due to the lowest IS or due to reaching the sensitivity limit of the experiment. The yield data (Fig. 4) could alternatively be interpreted as arising from an IS at even lower energy with correspondingly smaller integrated cross sections.

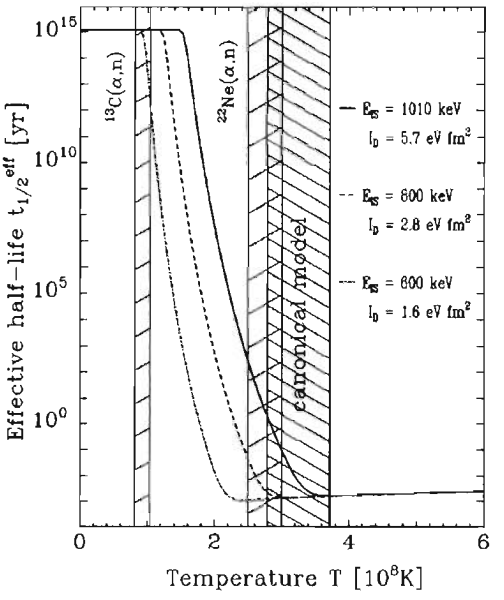

FIG. 8. Reduction of the $^{180}Ta^m$ effective half-life in the presence of a stellar photon bath deduced from the photoactivation cross sections measured in the present experiments assuming the lowest IS at excitation energies of 1.01, 0.8, and 0.6 MeV above the isomer, respectively. Thermal energy ranges expected under s-process conditions are indicated (\\\\) for the canonical model (Ref. [5]) and for a more realistic model (Ref. [64]) which distinguishes burning phases (///) where different (α,n) reactions serve as neutron sources, see text.

The impact of such an assumption is demonstrated in Fig. 8. The effective half-life is shown as a function of the photon bath temperature for the properties of the lowest IS (at E_{IS} = 1.01 MeV) deduced from the data and assuming lower energies E_{IS}= 800 and 600 keV with I_D corrected to account for the measured yields. The typical temperature regimes of the canonical and dynamical s-process models are shown as hatched areas. Even at the lower temperatures assumed in the dynamical model, for ^{22}Ne(α,n) induced synthesis the effective half-life of ^{180}Ta would be reduced to the g.s. half-life for $E_{IS}\approx$700 keV precluding any production. Note that the burning phases with neutron production by the ^{13}C(α,n) reaction do not contribute to the ^{180}Ta synthesis because the temperature is too low to induce β decay from excited states in ^{179}Hf [8].

Due to the strong energy dependence new experimental efforts to lower the sensitivity threshold would be of considerable importance.

2. Neutrino nucleosynthesis

As an alternative astrophysical site for the production of ^{180}Ta Woosley *et al.* proposed the neutrino nucleosynthesis in a type II supernova [62]. As the newly born neutron star remnant cools mainly by neutrino-pair production with approximately equal luminosities for all three neutrino flavors, the outer shells of the star are subjected to immensely high fluxes of neutrinos. For the neutrino nucleosynthesis neutral-current reactions by ν_x neutrinos (customarily used for supernova ν_μ and ν_τ neutrinos and their antiparticles which all have quite similar distributions) are of special interest as they have noticeably larger average energies ($\langle E_{\nu_x}\rangle \sim 25$ MeV) than supernova ν_e and $\bar{\nu}_e$ neutrinos ($\langle E_{\nu_e}\rangle \sim 12$ MeV, $\langle E_{\bar{\nu}_e}\rangle \sim 16$ MeV, see Ref. [65]). Inelastic scattering by ν_x neutrinos dominantly excites nuclei to levels above particle thresholds. The subsequent nuclear decays, mainly by proton or neutron emission, contribute to the element synthesis of the daughter nuclides. It has been observed that supernova neutrino nucleosynthesis can become a significant production process for the daughter nuclide if one wants to explain abundance ratios of parent to daughter which exceed about 10^3 [66]. In that case a ppm (or less) neutrino spallation of the parent is sufficient to explain the abundance of the daughter. Obviously the process does not affect the parent abundance.

One such pair of nuclides is ^{181}Ta and ^{180}Ta with an observed abundance ratio of $R = {}^{180}\mathrm{Ta}/{}^{181}\mathrm{Ta} = 1.2\times 10^{-4}$. Woosley *et al.* proposed that ^{180}Ta can be made by $(\nu_x, \nu_x' n)$ reactions on preexisting ^{181}Ta [62]. As the actual site for the ^{180}Ta production, these authors identified the neon burning shell, which is also the site of the p (or gamma) process, where explosive burning leads to photodisintegration of nuclei existing in these mass zones from prior burning during stellar evolution. At larger stellar radii, the inelastic scattering rate, which, due to its dependence on the neutrino flux, scales inversely with the square of the radius, is too small while at smaller radii, the produced ^{180}Ta is destroyed by photodissociation when the shock wave passes subsequently through the neon shell and heats the matter to a few 10^9 K. In their nucleosynthesis calculations Woosley *et al.* find an overproduction rate of the ^{180}Ta/^{181}Ta abundance ratio in massive stars which would be sufficient to explain the observed abundance of ^{180}Ta. This study, however, has been based on a rather crude estimate of the total inelastic neutrino scattering cross section on ^{181}Ta which was obtained from the estimate of the ^{56}Fe cross section by scaling with the ratio of mass numbers [62]. This estimate is likely too large for at least two reasons: (i) While calculations reveal that the total inelastic neutrino scattering cross section for supernova ν_x neutrinos indeed scales approximately with the mass number, it is the partial $^{181}\mathrm{Ta}(\nu_x, \nu_x' n)$ cross section which matters for the neutrino nucleosynthesis of ^{180}Ta. This partial cross section is noticeably smaller than the total cross section as most of the Gamow-Teller excitations are below the neutron threshold in ^{181}Ta ($E_n \sim 7.6$ MeV), while part of the forbidden strength is expected to be located above the two-nucleon threshold $E_{2n} \sim 17.9$ MeV. (ii) After neutrino nucleosynthesis and passage of the shock wave only a fraction of the ^{180}Ta will be in the isomeric state and will thus survive.

Recalling the strong sensitivity of the ^{180}Ta s-process abundance on details of the astrophysical s process and hence its potential importance as a constraint for the site and dynamics of the process, it is obviously quite relevant to determine how much ^{180}Ta can be produced by alternative astrophysical sites, e.g., by neutrino nucleosynthesis. For that reason we have performed a detailed calculation of the $^{181}\mathrm{Ta}(\nu_x, \nu_x' n)$ cross section. We assume a two-step process. In the first step the $^{181}\mathrm{Ta}(\nu_x, \nu_x')^{181}\mathrm{Ta}^*$ cross section is calculated as a function of excitation energy in ^{181}Ta within the random phase approximation. The ^{181}Ta ground state is described in the spherical approximation assuming equal fillings of all m states in the valence shell. This approximation is reasonable as the ν_x neutrinos mainly excite collective modes which are not too sensitive to detailed nuclear structure [67]. Details of the model and the adopted formalism can be found in Refs. [68,69]. As residual interaction a zero-range Landau-Migdal interaction is chosen. For the supernova ν_λ neutrinos a Fermi-Dirac spectrum with temperature $T = 8$ MeV and zero chemical potential is adopted. These neutrinos are already energetic enough that the dependence of the multipole operators on the momentum transfer has to be taken into account. Here, we follow the formalism derived in Ref. [70] and consider multipole excitations with spin up to $J = 4$ and both parities.

In the second step for each final state with well-defined energy the branching ratios into the various decay channels are calculated using the statistical model code smoker [71]. Possible final states in the residual nucleus considered by the smoker code are experimentally known levels supplemented at higher energies by an appropriate level density formula [71]. As decay channels the code considers proton, neutron, and α and γ emissions. If the decay leads to an excited level of the residual nucleus (e.g., to $n + {}^{180}\mathrm{Ta}^*$), we calculate the branching ratios for the decay of this state in an analogous fashion. Keeping track of the energies of the ejected particles and photons during the cascade, and weighting them with appropriate branching ratios and the corresponding $^{181}\mathrm{Ta}(\nu, \nu')^{181}\mathrm{Ta}^*$ cross section, the various partial particle and photon spectra are determined. The branching ratios are found to be quite insensitive to the spin assignments of the decaying states. This allows us to sum over the different multipole contributions before multiplying with the branching ratios.

A total inelastic cross section for supernova ν_x scattering off ^{181}Ta of 144×10^{-42} cm^2 is deduced. Note that this cross section per nucleon is very close to the ^{56}Fe cross section per nucleon, given in Ref. [72]. About 37% of the cross section lies below the neutron threshold, corresponding mainly to Gamow-Teller excitations. The excited states decay by gamma emission back to the ^{181}Ta ground state and thus do not contribute to the ^{180}Ta production. The excited states

above the neutron threshold decay by neutron emission, as the large Coulomb barriers severely suppress decay into the proton and α channels. However, in about one third of the cases the neutron emission populates the daughter nucleus ^{180}Ta in an excited state above its respective neutron threshold. Thus, these states decay again by neutron emission, leading to states in ^{179}Ta and hence also do not contribute to the ^{180}Ta production. We thus find a partial ^{181}Ta$(\nu_x,\nu_x' n)$ cross section of 57×10^{-42} cm^2 for reactions which lead to particle-bound states in ^{180}Ta and will end up either in the ground state or in the long-lived isomer. Our cross section is smaller than the one used by Woosley *et al.* by a factor of 4.2. The lifetimes of both states are long compared to the time which proceeds between neutrino nucleosynthesis in the neon shell and arrival of the supernova shock wave. The shock wave will heat the matter to temperatures in excess of 10^9 K which is hot enough to bring the ground state and the isomeric state into thermal equilibrium. Neglecting freeze-out effects and assuming a temperature of $T\sim10^9$ K leads to about 73% population of the produced ^{180}Ta nuclei in the isomeric state.

Inserting these cross sections into the model of Ref. [62], the net production rate of ^{180}Ta by neutrino nucleosynthesis is about a factor of 6 smaller. The resulting overproduction rate for the ^{180}Ta/^{181}Ta abundance ratio makes neutrino nucleosynthesis still a potential ^{180}Ta production site. It would be quite welcome if this crude estimate is followed up by detailed nucleosynthesis calculations using the improved neutrino cross sections. Finally we remark that production of ^{180}Ta by charged-current reactions on ^{180}W or ^{180}Hf is rather unimportant since for the $\bar{\nu}_e$-induced reaction on ^{180}Hf the cross section is strongly reduced due to the appreciable neutron excess, while the (ν_e,e^-) reaction on ^{180}W does not contribute since the ^{180}W abundance is two orders of magnitude smaller than the ^{181}Ta abundance.

3. *p-process nucleosynthesis*

As yet another alternative to the *s* process, a *p*-process origin of ^{180}Ta has been proposed [63]. Because of a delicate balance between ^{180}Ta production and destruction by (γ,n) reactions it works only in a constrained temperature window around $T=2\times10^9$ K [73] and is therefore strongly dependent on the underlying model. Because of the higher temperatures with respect to the *s* process, higher-lying IS's may be important for the effective half-life. This has to be implemented in further analyses of the *p*-process nucleosynthesis of ^{180}Ta.

VI. SUMMARY AND OUTLOOK

The present work provides a comprehensive study of the depopulation of the long-lived isomer $^{180}Ta^m$ by resonant photoabsorption for bremsstrahlung end point energies below 3 MeV. With the improved experimental setup and the use of the world's stock of isotopically enriched ^{180}Ta material an unprecedented sensitivity could be reached. This allowed the identification of IS's with sizable integrated cross sections down to excitation energies of about 1 MeV.

With reasonable assumptions on the branching ratio of IS's between decay to the g.s. and back decay to the isomer one finds rather large electromagnetic transition probabilities typical of unhindered transitions. This implies considerable *K* mixing already at low energies. Theoretical interpretations of this phenomenon are presently missing. Microscopic QPM calculations, while providing a satisfactory description of collective excitations built on the isomer, underpredict the g.s. decay by about 2 to 3 orders of magnitude.

The astrophysical implications of the present results for explosive production scenarios need further exploration. Experimentally, new measurements with improved experimental limits would be of high importance to provide a final answer to the still open possibility of an *s*-process synthesis of $^{180}Ta^m$.

Finally, the combination of NRF and photoactivation techniques at the new facility at Stuttgart certainly represents an important step for further studies on nuclear structure as well as astrophysical problems. An interesting application for the latter could be ^{176}Lu which has been shown to be a thermometer of the *s* process due to the occurrence of a low-lying IS [74,75].

ACKNOWLEDGMENTS

The authors wish to thank G. Sletten and C. Günther for lending the LEP detectors used in the experiments. We are grateful to N. Auerbach, G.D. Dracoulis, E.B. Norman, T. Rauscher, G. Sletten, the late V.G. Soloviev, S.E. Woosley, and L. Zamick for enlightening discussions. The support by the Deutsche Forschungsgemeinschaft under Contract Nos. Kn 154/30 and FOR 272/2-1, the BMBF under Contract No. 06DA915I, the Munich Tandem Accelerator Laboratory, the FZ Karlsruhe, and by the U.S. AFOSR under Contract No. F49020-99-1-0263 is gratefully acknowledged.

[1] N. Boos, F. Le Blanc, M. Krieg, J. Pinard, G. Huber, M. D. Lunney, D. Le Du, R. Meunier, M. Hussonnois, O. Constantinescu, J. B. Kim, Ch. Briançon, J. E. Crawford, H. T. Duong, Y. P. Gangrski, T. Kuhl, B. N. Markov, Yu. Ts. Oganessian, P. Quentin, B. Roussiere, and J. Sauvage, Phys. Rev. Lett. **72**, 2689 (1994).

[2] S. Deylitz, B. D. Valnion, K. El Abiary, J. de Boer, N. Gollwitzer, R. Hertenberger, G. Graw, R. Kulessa, Ch. Briançon, D. Le Du, R. Meunier, M. Hussonnois, O. Constantinescu, S. Fortier, J. B. Kim, L. H. Rosier, G. Rotbard, Yu. Ts. Oganessian, S. A. Karamian, H. J. Wollersheim, H. Folger, J. Gerl, Th. Happ, and C. Hategan, Phys. Rev. C **53**, 1266 (1996).

[3] E. Lubkiewicz, H. J. Wollersheim, R. Kulessa, Ch. Briançon, W. Brüchle, O. Constantinescu, M. Debowski, E. Ditzel, H. Folger, J. Gerl, F. Hannachi, T. Happ, M. Hussonnois, E. Jäger, S. Karamian, M. Kaspar, Th. Kröll, Yu. Ts. Oganessian, I. Pe-

ter, H. Schaffner, S. Schremmer, R. Schubert, N. Trautmann, K. Vetter, and G. Zauner, Z. Phys. A **355**, 377 (1996).
[4] T. Morikawa, Y. Gono, K. Morita, T. Kishida, T. Murakami, E. Ideguchi, H. Kumagai, G. H. Liu, A. Ferragut, A. Yoshida, Y. H. Zhang, M. Oshima, M. Sugawara, H. Kusakari, M. Ogawa, M. Nakajima, H. Tsuchida, S. Mitarai, A. Odahara, M. Kidera, M. Shibata, J. C. Kim, S. J. Chae, Y. Hatsukawa, and M. Ishihara, Phys. Lett. B **350**, 169 (1995).
[5] F. Käppeler, Prog. Part. Nucl. Phys. **43**, 419 (1999).
[6] H. Beer and R. A. Ward, Nature (London) **291**, 308 (1981).
[7] S. E. Kellogg and E. B. Norman, Phys. Rev. C **46**, 1115 (1992).
[8] K. Yokoi and K. Takahashi, Nature (London) **305**, 198 (1983).
[9] M. Schumann and F. Käppeler, Phys. Rev. C **60**, 025802 (1999).
[10] K. Wisshak, F. Voss, C. Arlandini, F. Bečvář, O. Straniero, R. Gallino, M. Heil, F. Käppeler, M. Krtička, S. Masera, R. Reifarth, and C. Travaglio, Phys. Rev. Lett. **87**, 251102 (2001).
[11] C. B. Collins and J. J. Carroll, Hyperfine Interact. **107**, 3 (1997).
[12] F. Stedile, E. Fill, D. Belic, P. von Brentano, C. Fransen, A. Gade, U. Kneissl, C. Kohstall, A. Linnemann, P. Matschinsky, A. Nord, N. Pietralla, H. H. Pitz, M. Scheck, and V. Werner, Phys. Rev. C **63**, 024320 (2001).
[13] S. Olariu and A. Olariu, Phys. Rev. Lett. **84**, 2541 (2000).
[14] D. P. McNabb, J. D. Anderson, J. A. Becker, and M. S. Weiss, Phys. Rev. Lett. **84**, 2542 (2000).
[15] P. von Neumann-Cosel and A. Richter, Phys. Rev. Lett. **84**, 2543 (2000).
[16] C. B. Collins, F. Davanloo, M. C. Iosif, R. Dussart, J. M. Hicks, S. A. Karamian, C. A. Ur, I. I. Popescu, V. I. Kirischuk, J. J. Carroll, H. E. Roberts, P. McDaniel, and C. E. Crist, Phys. Rev. Lett. **82**, 695 (1999).
[17] I. Ahmad, J. C. Banar, J. A. Becker, D. S. Gemmell, A. Kraemer, A. Mashayeki, D. P. McNabb, G. G. Miller, E. F. Moore, L. N. Pangault, R. S. Rundberg, J. P. Schiffer, S. D. Shastri, T. F. Wang, and J. B. Wilhelmy, Phys. Rev. Lett. **87**, 072503 (2001).
[18] J. J. Carroll, J. A. Anderson, J. W. Glesener, C. D. Eberhard, and C. B. Collins, Astrophys. J. **344**, 454 (1989).
[19] C. B. Collins, J. J. Carroll, T. W. Sinor, M. J. Byrd, D. G. Richmond, K. N. Taylor, M. Huber, N. Huxel, P. von Neumann-Cosel, A. Richter, C. Spieler, and W. Ziegler, Phys. Rev. C **42**, R1813 (1990).
[20] Zs. Németh, F. Käppeler, and G. Reffo, Astrophys. J. **392**, 277 (1992).
[21] E. B. Norman, S. E. Kellogg, T. Bertram, S. Gil, and P. Wong, Astrophys. J. **281**, 381 (1984).
[22] I. Bikit, L. Lakosi, J. Sáfár, and Lj. Čonkić, Astrophys. J. **522**, 419 (1999).
[23] C. Schlegel, P. von Neumann-Cosel, F. Neumeyer, A. Richter, S. Strauch, J. de Boer, C. H. Dasso, and R. J. Peterson, Phys. Rev. C **50**, 2198 (1994).
[24] M. Schumann, F. Käppeler, R. Böttger, and H. Schölermann, Phys. Rev. C **58**, 1790 (1998).
[25] M. Loewe, J. Besserer, J. de Boer, H. J. Maier, M. Würkner, J. Srebrny, T. Czosnyka, J. Iwanicki, P. J. Napiorkowski, P. von Neumann-Cosel, A. Richter, C. Schlegel, H. J. Wollersheim, P. Alexa, A. I. Levon, S. A. Karamian, and G. Sletten, Acta Phys. Pol. B **30**, 1319 (1999); (private communication).
[26] G. D. Dracoulis, F. G. Kondev, A. P. Byrne, T. Kibedi, S. Bayer, P. M. Davidson, P. M. Walker, C. Purry, and C. J. Pearson, Phys. Rev. C **53**, 1205 (1996).
[27] G. D. Dracoulis, S. M. Mullins, A. P. Byrne, F. G. Kondev, T. Kibedi, S. Bayer, G. J. Lane, T. R. McGoran, and P. M. Davidson, Phys. Rev. C **58**, 1444 (1998).
[28] T. R. Saitoh, N. Hashimoto, G. Sletten, R. A. Bark, S. Tormanen, M. Bergstrom, K. Furuno, K. Furutaka, G. B. Hagemann, T. Hayakawa, T. Komatsubara, A. Maj, S. Mitarai, M. Oshima, J. Sampson, T. Shizuma, and P. G. Varmette, Nucl. Phys. **A660**, 121 (1999).
[29] G. D. Dracoulis, T. Kibedi, A. P. Byrne, R. A. Bark, and A. M. Baxter, Phys. Rev. C **62**, 037301 (2000).
[30] C. Wheldon, P. M. Walker, P. Chowdhury, I. Shestakova, R. D'Alarcao, I. Ahmad, M. P. Carpenter, D. M. Cullen, R. V. F. Janssens, T. L. Khoo, F. G. Kondev, C. J. Lister, C. J. Pearson, Zs. Podolyak, D. Seweryniak, and I. Wiedenhoever, Phys. Rev. C **62**, 057301 (2000).
[31] E. B. Norman (private communication).
[32] C. Günther (private communication).
[33] P. M. Walker, G. D. Dracoulis, and J. J. Carroll, Phys. Rev. C **64**, 061302(R) (2001).
[34] M. Loewe, J. de Boer, H. J. Maier, M. Würkner, P. Olbratowski, J. Srebrny, J. Choinski, T. Czosnyka, J. Iwanicki, P. J. Napiorkowski, G. Hagemann, G. Sletten, S. A. Karamnian, P. von Neumann-Cosel, A. Richter, C. Schlegel, and H. J. Wollersheim, Z. Phys. A **356**, 9 (1996).
[35] C. Schlegel, P. von Neumann-Cosel, J. de Boer, J. Gerl, M. Kaspar, I. Kozhoukharov, M. Loewe, H. J. Maier, P. J. Napiorkowsky, I. Peter, M. Rejmund, A. Richter, H. Schaffner, J. Srebrny, M. Würkner, and H. J. Wollersheim, Eur. Phys. J. A **10**, 135 (2001).
[36] D. Belic, J. Besserer, C. Arlandini, J. de Boer, J. J. Carroll, J. Enders, T. Hartmann, F. Käppeler, H. Kaiser, U. Kneissl, M. Loewe, H. Maser, P. Mohr, P. von Neumann-Cosel, A. Nord, H. H. Pitz, A. Richter, M. Schumann, S. Volz, and A. Zilges, Nucl. Instrum. Methods Phys. Res. A **463**, 26 (2001).
[37] J. Blachot, Nucl. Data Sheets **86**, 151 (1999).
[38] D. Belic, C. Arlandini, J. Besserer, J. de Boer, J. J. Carroll, J. Enders, T. Hartmann, F. Käppeler, H. Kaiser, U. Kneissl, M. Loewe, H. J. Maier, H. Maser, P. Mohr, P. von Neumann-Cosel, A. Nord, H. H. Pitz, A. Richter, M. Schumann, S. Volz, and A. Zilges, Phys. Rev. Lett. **83**, 5242 (1999).
[39] S. Lindenstruth, A. Degener, R. D. Heil, A. Jung, U. Kneissl, J. Margraf, H. H. Pitz, H. Schacht, U. Seemann, R. Stock, and C. Wesselborg, Nucl. Instrum. Methods Phys. Res. A **300**, 293 (1991).
[40] P. von Neumann-Cosel, N. Huxel, A. Richter, C. Spieler, J. J. Carroll, and C. B. Collins, Nucl. Instrum. Methods Phys. Res. A **338**, 425 (1994).
[41] C. B. Collins, J. J. Carroll, K. N. Taylor, D. G. Richmond, T. W. Sinor, M. Huber, P. von Neumann-Cosel, A. Richter, and W. Ziegler, Phys. Rev. C **46**, 952 (1992).
[42] E. C. Booth and J. Brownson, Nucl. Phys. **A98**, 529 (1967).
[43] P. von Neumann-Cosel, A. Richter, C. Spieler, W. Ziegler, J. J. Carroll, T. W. Sinor, D. G. Richmond, K. N. Taylor, and C. B. Collins, Phys. Lett. B **266**, 9 (1991).

[44] U. Kneissl, H. H. Pitz, and A. Zilges, Prog. Part. Nucl. Phys. **37**, 349 (1996).
[45] U. E. P. Berg and U. Kneissl, Annu. Rev. Nucl. Part. Sci. **37**, 33 (1987).
[46] O. Bogdankevich and F. Nikolaev, *Methods in Bremsstrahlung Research* (Academic, New York, 1966).
[47] E. Bramanis, T. Deague, R. Hicks, R. Hughes, E. Muirhead, R. Sambell, and R. Stewart, Nucl. Instrum. Methods **100**, 59 (1972).
[48] H. J. Maier, R. Grossmann, H. U. Friebel, and D. Frischke, Nucl. Instrum. Methods Phys. Res. A **438**, 163 (1999).
[49] H. Maser, S. Lindenstruth, I. Bauske, O. Beck, P. von Brentano, T. Eckert, H. Friedrichs, R. D. Heil, R.-D. Herzberg, A. Jung, U. Kneissl, J. Margraf, N. Pietralla, H. H. Pitz, C. Wesselborg, and A. Zilges, Phys. Rev. C **53**, 2749 (1996).
[50] *Table of Isotopes*, 8th ed., edited by R. B. Firestone and V. S. Shirley (Wiley, New York, 1996).
[51] A. Wolpert, O. Beck, D. Belic, J. Besserer, P. von Brentano, T. Eckert, C. Fransen, R.-D. Herzberg, U. Kneissl, J. Margraf, H. Maser, A. Nord, N. Pietralla, and H. H. Pitz, Phys. Rev. C **58**, 765 (1998).
[52] H. Bartsch, K. Huber, U. Kneissl, and H. Sattler, Nucl. Instrum. Methods **121**, 185 (1974).
[53] D. Belic, Doctoral thesis, Universität Stuttgart, 2001.
[54] S. A. Karamian, C. B. Collins, J. J. Carroll, and J. Adam, Phys. Rev. C **57**, 1812 (1998).
[55] L. Lakosi and T. C. Nguyen, Nucl. Phys. **A697**, 44 (2002).
[56] M. Loewe, Doctoral thesis, Ludwig-Maximilians Universität München, 2002.
[57] V. G. Soloviev, Nucl. Phys. **A633**, 247 (1998).
[58] V. G. Soloviev, A. V. Sushkov, and N. Yu. Shirikova, Phys. At. Nucl. **64**, 1199 (2001); (private communication).
[59] P. M. Walker, G. Sletten, N. L. Gjørup, M. A. Bentley, J. Borggreen, B. Fabricius, A. Holm, D. Howe, J. Pedersen, J. W. Roberts, and J. F. Sharpey-Schafer, Phys. Rev. Lett. **65**, 416 (1990).
[60] P. M. Walker, D. M. Cullen, C. S. Purry, D. E. Appelbe, A. P. Byrne, G. D. Dracoulis, T. Kibedi, F. G. Kondev, I. Y. Lee, A. O. Macchiavelli, A. T. Reed, P. H. Regan, and F. Xu, Phys. Lett. B **408**, 42 (1997).
[61] P. Alexa, I. Hřivnáčová, and J. Kvasil, Acta Phys. Pol. B **30**, 1323 (1999).
[62] S. E. Woosley, D. H. Hartmann, R. D. Hofmann, and W. C. Haxton, Astrophys. J. **356**, 272 (1990).
[63] N. Prantzos, M. Hashimoto, M. Rayet, and M. Arnould, Astron. Astrophys. **238**, 455 (1990).
[64] R. Gallino, C. Arlandini, M. Busso, M. Lugaro, C. Travaglio, O. Straniero, A. Chieffi, and M. Limongi, Astrophys. J. **497**, 388 (1998).
[65] H.-T. Janka and W. Hillebrandt, Astron. Astrophys. **224**, 49 (1989); Astron. Astrophys., Suppl. Ser. **78**, 375 (1989).
[66] S. E. Woosley (private communication).
[67] A. Hektor, E. Kolbe, K. Langanke, and J. Toivanen, Phys. Rev. C **61**, 055803 (2000).
[68] E. Kolbe, K. Langanke, and P. Vogel, Phys. Rev. C **50**, 2576 (1994).
[69] E. Kolbe, K. Langanke, and P. Vogel, Nucl. Phys. **A652**, 91 (1999).
[70] J. D. Walecka, in *Semi-Leptonic Weak Interactions in Nuclei in Muon Physics*, edited by V. W. Hughes and C. S. Wu (Academic, New York, 1975).
[71] J. J. Cowan, F.-K. Thielemann, and J. W. Truran, Phys. Rep. **208**, 208 (1991); T. Rauscher and F.-K. Thielemann, At. Data Nucl. Data Tables **74**, 1 (2000).
[72] J. Toivanen, E. Kolbe, K. Langanke, G. Martinez-Pinedo, and P. Vogel, Nucl. Phys. A (to be published).
[73] M. Rayet, M. Arnould, M. Hashimoto, N. Prantzos, and K. Nomoto, Astron. Astrophys. **298**, 517 (1995).
[74] N. Klay, F. Käppeler, H. Beer, and G. Schatz, Phys. Rev. C **44**, 2839 (1991).
[75] K. T. Lesko, E. B. Norman, R.-M. Larimer, B. Sur, and C. B. Beausang, Phys. Rev. C **44**, 2850 (1991).

"Forced-Gamma Emission" Studies Involving Nuclear Isomers Using Fast Neutrons and Bremsstrahlung X Rays

N. A. Guardala[+], J. L. Price[+], J. H. Barkyoumb[+], R. J. Abbundi[+], G. Merkel[*] and J.J. Carroll[#]

[+] *NSWC/Carderock Division, 9500 MacArthur Blvd, W. Bethesda, MD 20817-5700*
[*] *Army Reserch Lab/Adelphi, 2800 Powder Mill Road, Adelphi MD*
[#] *Dept. Of Physics and Astronomy, Youngstown State Univ., Youngstow, Ohio*

Abstract. We propose to perform a series of experiments involving nuclear isomers which will investigate the probabilities and mechanisms for de-exciting the isomeric level down to the ground state upon exposure to external radiation in the form of fast neutrons and bremsstrhalung x rays. The isomers have half-lives on the order of 1 hr to 10 days which is a convenient time scale to measure statistically meaningful changes in the specific activities of the isomeric state. Furthermore, the selected isomers are relatively easy to produce in our laboratory in sufficient quantities so that they can be made in a reasonable time frame and without recourse to any exotic means of production, handling or preparation and without the need for high-purity separated isotopes as the *feedstock*. We believe that studies undertaken in this fashion will produce fundamentally valuable information on the factors which govern and influence *"forced-gamma emission"* in nuclear isomers This type of information will potentially be very useful in similar studies involving longer-lived isomers such as: ^{178m2}Hf, ^{242m}Am and ^{108m}Ag which have the potential to be used in various emerging new technologies in the later part of the 21st Century.

INTRODUCTION

Recently, there has developed serious interest in the nuclear physics community to study nuclear isomers from not only the point of view of nuclear structure phenomena but also as a means of producing technologically valuable devices mostly for use as compact power sources that require a minimum amount of auxiliary and supporting machinery and equipment. The isomers which would be used in these type of power devices would all have half-lives in the tens to hundreds of years regime and therefore would allow them to be stored *"on-the-shelf"* for long periods of time. When it was desired to release the stored energy of the isomeric levels in brief time interval it has proposed that exposing the specific isomer to an external radiation of the right energy will result in transitions from the isomeric state to nuclear levels that are no longer forbidden to cascade via γ-ray emission to the ground state.

This process of applying suitable external radiation to an isomer and then observing the *"normal"* γ-ray decay to the ground state has been termed *triggering*, and that is the term by which this process has become known widely. While there are many known isomers which have the potential to serve as excellent candidates to observe this phenomena of triggering , in only case, ^{180m}Ta (1) has this been observed unequivocally. Another isomer in this mass region, ^{178m2}Hf (2) has drawn a significant amount of attention in terms of experimental efforts to determine the probability to trigger forced-gamma emission in it. In particular, the efforts have been directed to determine the probability for its triggering using x rays in the 20-130 kev region, with reports that the decay of ^{178m2}Hf can be produced by using x rays as low as 20 keV in energy. Studies using synchrotron radiation have attempted to measure the cross section for triggering using radiation in this energy range.

ISOMERS SELECTED FOR *"TRIGGERING"* STUDIES

We have selected eight isomers to be used in thish study of triggering probabilities and mechanisms. They are in increasing mass order: ^{87m}Sr, ^{103m}Rh, ^{111m}Cd, ^{115m}In, ^{189m}Os, ^{193m}Ir and ^{199m}Hg. The values of $t_{1/2}$ for these isomers ranges from 42.6 min for ^{199m}Hg up to 57.4 d for ^{125m}Te. All of these isomers can be produced via fast neutron inelastic scattering, n,n'γ from the ground state directly to isomeric level or from the ground state to excited states which are strongly coupled to the isomeric level. In certain instances we hope to be able to determine the probabilities for the these two processes as a function of neutron energy to proceed in most of these selected isomers. In all cases, we have prepared samples of these isomers previously in our laboratory by exposing suitable amounts of nuclei to our fast neutron beam and counting the normal decay of the particular isomer. The cross sections for producing these isomers (regardless of which mechanism is responsible) is varies from 0.2 – 2 barns in the energy range of 0.3 -- 3 MeV. This is an energy range easily accessible with our accelerator-based fast neutron source.

In addition to fast neutron triggering studies which will be applied to all of the selected isomers, there exists the possibility that some of these isomers may be triggered using bremsstrahlung x rays. These isomers must possess energy levels that are separated by less than 200 keV in energy so that the bremsstrahlung x-ray source available at NSWC/Carderock can be used to study triggering.

Experimental MethodsTo Determine Triggering Probabilities and Mechansims

The experiments to be performed at NSWC/Carderock to determine if forced-gamma emission i.e."*triggering*" is either occurring or has occurred can be divided into two types: a) the method of determining *'burnup"* which is a measurement of the specific activity of the isomer before and after exposure to the triggering radiation source. If triggering has occurred (and minimal or zero production of the isomer has occurred simultaneously) then the specific isomer activity should be less then what would be expected from the normal γ decay . b) In-beam measurements of γ-ray transitions taking place while the external radiation is applied to the isomer.

This method is applicable only in the case of photon triggering and not for triggering brought about through the n,n'γ process. The reason is that the amount of background γ-rays produced from inelastic scattering from other levels which are not related to the isomer is much too large and thereby overwhelms the probabilities of observing γ-ray cascades which would be indicative of triggering events taking place. The photon method is much more "gentle" in terms of the number of states which can be populated both in the isomer and from ground state levels. Therefore coincident measurements of γ-rays will be attempted at NSWC using the suitable isomers which seem to have the possibilities for x-ray triggering based on the knowledge of the appropriate values ΔE, the energy difference between the isomeric level and a level which is strongly connected to a cascade to the ground state and on angular momentum considerations such that the transition form the isomeric level to the intermediate level is favored and then of course that the transition from this intermediate level to the ground state is favored. This set of processes if of course the definition of triggering. The final transition from the intermediate level can either proceed directly to the ground state or to the ground state by a series of γ-ray transitions, i.e. a cascade.

Properties Of The Selected Isomers

The isomers listed above fall into two kinds of groupings based on a generalized assessment of their nuclear properties. These properties are a function of the mass of the nuclide, A and where it appears in the periodic table, as a function of Z. The first group contains nuclei with $A < 116$ and $Z < 50$. The second group has $A > 125$ and $Z > 51$. In fact, besides ^{125m}Te the majority in this group has $188 > A < 200$. It is this particular region of the periodic table where isomeric structures and their relationship to the overall trend in nuclear shape and level structure becomes increasingly complex and hence deserving of study.

The first group consisting of the lighter–mass isomers are so-called spin isomers (3). These nuclei have single unpaired nucleon spins which are couple to specific values of the orbital angular momentum based on the properties of the orbitals that they occupy. These orbitals are generally "out-of-place" in terms of their relative positions regarding the energy and angular momentum schemes taking place inside their respective nuclei. An inversion can be thought to be taking place where these "intruder" states become lower in energy that the normal situation that would be predicted. This inversion places the isomeric level in a

position where it is isolated energetically from states with similar values of angular momentum, i.e. states to which γ-ray transitions would be most favored given the typical selection rules. These selection rules generally place severe restrictions on electromagnetic transitions which require changes in angular momentum with values greater than 3 (4).

As an example consider the 43 min ^{111m}Cd isomer whch has the isomeric state at 396 keV above the ground state. The isomeric level has a spin of 11/2- while the ground state is at spin ½+. A transition between the two states requires the emission of a γ ray with 3 units of angular momentum and this is the primary reason for the 43 min value of $t_{1/2}$. However a level at only 20.5 keV exists above the isomeric level with spin of 7/2+. This level at 416.7 keV is strongly connected to the first excited state at 245 keV with spin of 5/2+, the downward γ-ray transition between them is 100%. This means that of all the so-called spin isomers selected only this particular 20.5 keV transition has the potential to bring about triggering using the bremsstrahlung x-ray source at our disposal due to the reasonably small change in angular momentum between the isomeric state and the triggering level and the small value of ΔE.

The other spin isomers mentioned have energy spacing between the isomeric level and possible triggering levels that is not possible to use the x-ray source at NSWC to bring about triggering. For these other spin-isomers the only alternative is to use the n,n'γ mechanism. Fortunately, fast neutrons with significantly larger energy are available using the NSWC tandem Pelletron and fast neutrons are capable of providing larger inputs of angular momentum via inelastic collisions than photo-absorption can. As much as 8 units of angular momentum can be transferred using neutrons in the 1 MeV energy range while with photons the limit is 3 units.

In the case of the second grouping of isomers the angular momentum considerations based on isomer formation, stability and potential de-excitation are more complicated. This is due to the more complex interaction and arrangement of nuclear levels based on angular momentum coupling which goes beyond the simpler considerations of single particle-orbital angular momentum coupling. Collective angular momentum of the entire nucleus becomes significant and introduces new quantum numbers which in turn place new restrictions on the possible electromagnetic transitions that are possible. This phenomena of collective motion results in typical band structures based on collective excitations (typically rotational excitations) as was the case with the spin isomers inversion of the normal patterns can occur in terms of angular momentum (now collective or rotational angular momentum values) and energy sequencing.

Collective states nearby to each other may then interact in such a way as to produce *mixing*, i.e. lose their distinctive angular momentum qualities so that electromagnetic transitions have a greater probability of occurring then what we have been predicted at lower energies. These effects may be further enhanced as the interactions between single particle motion become more strongly coupled to the collective motions at the highest observable energies. The possible γ-ray transitions would become less hindered due to considerations and restrictions based on changes in angular momentum. This mixing would then allow for rapid γ-ray transitions down to the ground state.

These kind of phenomena would be expected in nuclei in which shape coexistence is possible as well as transitions between nuclear shapes. Especially attractive is the situation where quasi-continua are either known or would be expected to exist. It is these kind of states brought about by the nuclear dynamics of shape changes at high spin and high excitation energies that may provide important and stimulating information about the mechanisms and probabilities of triggering. Additionally, this kind of information may be very valuable in designing triggering schemes for the potentially technologically attractive isomers such as: ^{178m2}Hf, ^{242m}Am, and ^{177m}Lu. All of these isomers have collective and rotational angular momentum considerations attached them in terms of their isomer levels and for potential triggering modes.

All of the isomers of this second grouping, the collective/rotational isomers have nuclear excited states with sufficiently small values of ΔE that they can be reached using the NSWC bremsstrahlung source so that they can not only be studied via the n,n'γ process (in burnup mode) but they can also be studied with triggering photon excitation in both the burnup and coincident in-beam mode.

Finally these isomers would be ideal to study at high excitation energies, ca. 2-3 MeV, with the most energetic neutrons available from our accelerator-based source. As previously mentioned in these types of nuclei the possibilities exist that these high-energy states based on band structures have the desired properties of *mixing levels* and would lead to an enhancement in the forced-gamma emission process.

Experimental Approach

The two major experimental facilities available at NSWC for these studies are 1) the 3 MV tandem Pelletron accelerator which produces fast neutrons by either the $^{7}Li(p,n)^{7}Be$ reaction and the $^{9}Be(p,pn)2^{4}He$ reaction. These reactions have both been used extensively in the past for a variety of neutrons experiments and exposures over a period of nearly ten years of continuous operation. These two fast neutron-producing reactions will be used first to prepare quantities of the particular isomer via the n,n'γ process.

After suitable times of irradiation depending on the production cross sections and the value of $t_{1/2}$ for the particular isomer, the samples will have their specific isomer activity measured at NSWC with a Ge(Li) γ-ray detector for an appropriate time depending on $t_{1/2}$. Then the sample will be reintroduced into the fast neutron beam produced by either of the proton-induced reactions mentioned previously.

Again depending on the amount of isomer material produced and its characteristic $t_{1/2}$ it will re-irradiated with fast neutrons. This may be done with different samples at a variety of different neutron energies. Then the samples will have their isomer activity remeasured to determine if burnup has taken place and if it has to what extent. In this fashion a traditional excitation function (or for this kind of study a *"de-excitation function")* will be generated. We reiterate that although doing in-beam measurements of the γ-ray spectra in particular doing γ-γ coincidence measurements would be the ideal method of providing definitive information concerning triggering mechanisms it is not possible in this instance primarily due to the relative small concentration of isomer (ppm-ppb's) in the total mass of sample.

This means that only indirect evidence for the states participating in triggering will be obtained. Furthermore, studies of the behaviour of the isomer production cross section using the n,n'γ process will have to be undertaken first as a function of energy to ascertain what the *"build-up"* factor for each isomer is as a function of neutron energy before determining the burnup factor as a function of neutron energy. All of the selected isomers will be produced using the n,n'γ method and all will be measured for burnip by exposure to neutrons suitable to cause de-excitation. We have discussed previously how fast neutrons are far less selective in causing excitation then photons so that a much larger array of potential triggering states and mechanisms would be available through their use then with x rays.

The available fluxes of fast neutrons from the two reactions are ca. 10^{9}-10^{10} n/cm^{2}/s at a position right behind either the Li or Be target (a distance of about 1 cm). For instances where it may be worthwhile to investigate isomer production or burnup with neutron energies lower than 300 keV , suitable moderators such as: high-purity graphite or D_2O are available.

In the case of photo-absorption type measurements of triggering the isomers to be studied are: ^{111m}Cd, ^{125m}Te, ^{189m}Os, ^{191m}Ir, ^{195m}Pt and ^{199m}Hg. The other isomers have values of ΔE too large to be useful with the x-ray source available at NSWC (7). In all of these cases both burnup first and then in-beam coincidence measurements will be performed.

The NSWC bremsstrahlung source is capable of delievering 7 x 10^{10} photons/cm^{2}/sec at a distance of 10 cm from the W target. It is a Phillips MG 225 x-rat source which has and endpoint energy of 225 keV and a maximum intensity of photons at 160 keV.

Conclusions

An attempt will be made using the facilities of NSWC/Carderock to study systematically some of the fundamental issues and parameters involved in the triggering of nuclear isomers. A variety of isomers each with slightly different nuclear properties will be used. All of these isomers can be produced in sufficient quantity at the NSWC tandem accelerator facility without resort to extraordinary means or expense. After producing them using the n,n'γ method the isomers will be studied systematically by exposing them to a range of fast neutron energies for de-excitation function measurement and a selected number having the right energy spacings will be studied for x-ray triggering probabilities.

References

1. Belic, D., et al, *Phys. Rev. Lett.* **83**, 5242-5245(2000).

2. Ahmad, I., et al, *Phys. Rev. Lett.* **87**, 07253-072255(2001).

3. Evans, R. D., *Chapter 6, Effects of Nuclear Moments and Parity on Nuclear Transitions.* in The Atomic Nucleus, New York, McGraw-Hill Pub., pp. 229-236(1955).

4. Marmier, P. and Sheldon, E., *Chapter 9, Radiative Transitions in Nuclei* in Physics of Nuclei and Particles, Volume 1, New York, Academic Press, pp. 414-460,(1969).

Driven energy release of nuclear isomers

L.A. Rivlin,* J.J. Carroll, and F. J. Agee*****

***MIREA Technical University, Moscow, RUSSIA,** rivlin140322@mccinet.ru
****Youngstown State University, OH, US,** jjcarroll@cc.ysu.edu
*****US Air Force Office of Scientific Research, VA, US,** jack.agee@afosr.af.mil

The prospects for using nuclear isomers as a new type of nuclear fuel are based on the existence of nuclei with long-lived metastable states and specific energy content of many tens of megajoules per gram [1,2].

The lifetimes of isomeric metastable states are long and sometimes come to hundreds and even thousands of years. This is because the corresponding decau transitions are very strongly forbidden, in particular due to large spin differences between levels. So the main task that must be solved if one wishes to release the stored isomer energy is to bypass this hindrance.

One of the possible ways to do this is to carry out a so-called "anti-Stokes" radiative transition that includes two transitions occurring in series. The first one excites the isomer nucleus from a metastable state up to a higher-situated auxiliary level, often called an intermediate state. The second one is a downward transition from the auxiliary level to the ground state, or at least to a level which will begin a cascade toward the ground state. So the strongly forbidden transition is bypassed. The anti-Stokes radiative transition having a stimulated second step was often investigated with application to nuclear gamma-ray lasing ([3-8] and a lot of another papers). There are many well-known experimental efforts to observe the driven decay of metastable isomer states [1, 9-16].

An alternative way to release the isomeric energy is connected with a two-quanta radiative transition ignited by two external counter-propagating gamma-photon beams with a quantum energy equal to one half the metastable state energy. This approach leads, in fact, to replacing the small probability transition with large spin difference by two joined transitions with twice lower spin differences [17-22]. It is important that the counter-propagating stimulating photon beams make possible a two-quanta emission process for all the nuclei, independent of their chaotic velocities. This is evident from the laws of energy and momentum conservation applied to the mentioned two-quanta emission process:

$$\hbar\omega_1 + \hbar\omega_2 = E_0 + \hbar\delta\omega\frac{u}{c} - \frac{(\hbar\delta\omega)^2}{2Mc^2} \qquad (1)$$

Here E_0 is the transition energy, M is the nucleus mass, $\omega_{1,2}$ are the frequencies of the two counter-propagating photons with difference $\delta\omega = \omega_1 - \omega_2$, u is the individual nucleus velocity component along the first photon wave vector, and c is the speed of light. One can see that all the nuclei with different chaotic individual velocities u are involved in the emission process only if $\delta\omega = 0$.

In a single-quantum process, this chaotic behaviour of nuclei would cause undesirable Doppler line broadening that leads to a drastic decrease of the gain and the efficiency of the total energy release process. The two-quanta approach is free from this negative feature. This is quite similar to the well-known method of sub-Doppler spectroscopy.

Recent progress in the development of high-reflectivity x-ray mirrors [23] renews interest in this two-quanta radiative driving of isomer decay because a Fabry-Perot resonator makes it possible to intensify the process due to the combined stimulating action of external gamma beams and the intra-resonator photon fields. We present here the main results of the theoretical analysis of such a combined driving process including data on emission dynamics, CW and pulsed mode of operation, stability criteria, etc.

To investigate the emission dynamics we consider a very simple model setup consisting of an active medium of length L, with concentrations n_2 and n_1 of metastable and ground-state nuclei, respectively, and with two mirrors having reflection coefficients R_0 and R_L, placed at the points $z = 0$ and $z = L$. An external ignition beam with the photon flux density J_{ign} ($cm^{-2}\,s^{-1}$ per natural line width) penetrates into the medium through the semitransparent mirror at the point $z = 0$.

The time behaviour of the output photon flux density $J_{out}(L)$ through the mirror with $R = R_L$ and total difference in nucleus concentration

$$N = \int_0^L (n_2 - n_1)dz \qquad \left(cm^{-2}\right) \qquad (2)$$

is governed by two equations:

$$\frac{dJ_{out}(L)}{dt} =$$

$$= \frac{c}{L}\left[\frac{1+R_L}{1-R_L}\frac{\beta N}{2}J_{out}^2(L) - \chi nL J_{out}(L) - 2\frac{1-R_L R_0}{(1+R_L)(1+R_0)}J_{out}(L) + 2\frac{1-R_0}{1+R_0}\frac{1-R_L}{1+R_L}J_{ign}\right] \tag{3}$$

and

$$\frac{dN}{dt} = -\frac{J_{out}^2(L)}{2}\left(\frac{1+R_L}{1-R_L}\right)^2 \beta N + PL \tag{4}$$

where β $(cm^4 s)$ is the cross-section of the two-quanta stimulated transition, χ is the total cross-section of internal photon losses of all kinds, the total concentration of nuclei is $n = n_2 + n_1$, and P $(cm^{-3} s^{-1})$ is the flux at which new isomer nuclei are fed into the cavity.

These approximate equations are valid under the assumptions

$$\beta J_{out}^2(L)\frac{L}{2c} << \left(\frac{1-R_L}{1+R_L}\right)^2 << 1 \tag{5}$$

that can be satisfied in many simple cases.

The two main modes of operations are the CW and pulsed emission. The CW mode can be analyzed by setting derivatives to zero in Eqs. (3) and (4). This gives stationary solutions for the total nucleus difference concentration

$$N_0 = 2\frac{PL}{\beta}\left[\frac{\chi nL + 2(1-R_L R_0)(1+R_L)^{-1}(1+R_0)^{-1}}{PL + 2(1-R_0)(1+R_0)^{-1}J_{ign}}\right]^2 \tag{6}$$

and for the output photon flux density

$$J_{out}(L) = \frac{1-R_L}{1+R_L}\frac{PL + 2J_{ign}(1-R_0)(1+R_0)^{-1}}{\chi nL + 2(1-R_L R_0)(1+R_L)^{-1}(1+R_0)^{-1}} \tag{7}$$

The $N_0(P)$ curve (6) has an arch-like form with a maximum

$$N_0(\max) = \frac{\left[\chi nL + 2(1-R_L R_0)(1+R_L)^{-1}(1+R_0)^{-1}\right]^2}{4\beta J_{ign}(1-R_0)(1+R_0)^{-1}} \tag{8}$$

at the feeding nucleus flux value

$$PL = 2J_{ign}(1-R_0)(1+R_0)^{-1} \tag{9}$$

The signs of the time derivatives dN/dt at the points declining from both ascending and descending branches of the stationary $N_0(P)$ curve (6) show that only the ascending branch is stable. So the maximum stable CW output photon flux is equal to

$$J_{out}(L) = \frac{1-R_L}{1+R_L}\frac{2PL}{\chi nL + 2(1-R_L R_0)(1+R_L)^{-1}(1+R_0)^{-1}} =$$

$$= \frac{1-R_L}{1+R_L}\frac{4J_{ign}(1-R_0)(1+R_0)^{-1}}{\chi nL + 2(1-R_L R_0)(1+R_L)^{-1}(1+R_0)^{-1}} \qquad (10)$$

and can be reached at the $N_0(\max)$ of Eq. (8) and the PL of Eq. (9).

It must be emphasized that despite of expectations, the stable CW emission can be sustained only at the non-zero ignition ($J_{ign} > 0$).

If the feeding isomer flow is absent ($P=0$), only a pulsed mode of operation is possible due to gradual expenditure of the initial isomer store, N_0, according to

$$N = N_0 \exp\left[-\frac{\beta}{2}\left(\frac{1+R_L}{1-R_L}\right)^2 W\right] \qquad (11)$$

where

$$W = \int_0^t J_{out}^2(L)dt \quad . \qquad (12)$$

The emission time behaviour is governed by the nonlinear equation

$$\frac{L}{2c}\left(\frac{dW}{dt}\right)^{-1/2}\frac{d^2W}{dt^2} = N_0\frac{dW}{dt}\exp\left[-\frac{\beta}{2}\left(\frac{1+R_L}{1-R_l}\right)^2 W\right] -$$

$$-\left[\chi nL + 2\frac{1-R_L R_0}{(1+R_L)(1+R_0)}\right]\sqrt{\frac{dW}{dt}} + 2\frac{1-R_L}{1+R_L}\frac{1-R_0}{1+R_0}J_{ign} \qquad (13)$$

for the new variable W defined by Eq. (12). Unfortunately, this equation can't be solved analytically, only using computer simulation. Nevertheless, it is possible to obtain some information on the turning off of ignition, bypassing this procedure.

The emission process starts at $t = 0$ and $J_{out}(L) = 0$ only if the derivative in Eq. (3) is positive, i.e. in the presence of ignition ($J_{ign} > 0$). Then at $t = t^*$ and $W = W^*$, $N(W^*) = N^*$ (Eq. (11)) and $J_{ign} > 0$, the emission pulse can reach a maximum value of $J_{out}{}^*(L)$ which is determined by the condition

$$\left[J_{out}*((L))\right]^2 - \frac{2}{\beta N*}\frac{1-R_L}{1+R_L}\left[\chi nL + 2\frac{1-R_L R_0}{(1+R_l)(1+R_0)}\right]J_{out}*(L) + \\ + \frac{4}{\beta N*}\left(\frac{1-R_L}{1+R_L}\right)^2 \frac{1-R_0}{1+R_0} J_{ign} = 0 \qquad (14)$$

But if at $0 < t = t** < t*$, $0 < W = W** < W*$, and $N* < N = N** < N_0$, the output photon flux is sufficiently large

$$J_{out}**(L) \geq \frac{2}{\beta N**}\frac{1-R_L}{1+R_L}\left[\chi nL + 2\frac{1-R_L R_0}{(1+R_L)(1+R_0)}\right] , \qquad (15)$$

then the pulse will proceed to increase even when the ignition is switched off ($J_{ign} = 0$). However, in this case the maximum output photon flux will be lower than in the presence of ignition with $J_{out}**(L) < J_{out}*(L)$.

And finally it is useful to give some example (certainly, not the optimal one!): the isomeric nucleus $^{242}_{95}Am$ with $E_0 = 48{,}6\ keV$, lifetime 141 yr, transition multipolarity $E4$, $\chi \approx 10^{-20}\ cm^2$ and specific energy content 20 MJ/g. A medium with $L = 100\ cm$ and cross-section 0.01 cm^2 stores an energy about 80 J if the initial isomer concentration is $n_2 = 10^{16}\ cm^{-3}$. One half of this energy can be emitted into a directed gamma-photon pulse. The values estimated for the needed ignition photon flux density $J_{ign} > 10^{20}\ cm^{-2}\ s^{-1}$ and the total ignition flux $10^{18}\ s^{-1}$ are not sufficiently trustworthy because they are based on a very crude theoretical estimation of the coefficient $\beta \approx 10^{-40}\ cm^4\ s$ [20]. Future work will investigate the feasibility of such two-photon initiated energy release from nuclear isomers in more detail.

*)This work (LAR) was partly supported by the ISTC (Grant # 2651p).

References

1. Collins C.B. and Carroll J.J. – Hyperfine Interactions, **107**, 3, (1997)
2. Walker P h. and Drakoulis G. – Nature, **399**, 35, (May 6, 1999)
3. Baklanov E.V and Chebotaev V.P. – Sov. J. Quant. Electronics, **3**, 634, (1976)
4. Rivlin L.A. - Sov. J. Quant. E lectronics, **3**, 676, (1977
5. Arad B., Eliezer S., Paiss Y. – Phys. Lett. A, **74**, 395, (1979)
6. Becker W., Schlicher R.R., Scully M.O. - Phys. Lett. A, **106**, 441, (1984)
7. Eliezer S. et al. – Laser Physics, **5**, 323, (1995)
8. Rivlin L.A. – Quant. Electronics (Moscow), **29**, 467, (1999)

9. Collins C.B. et al. – Phys. Rev. C, **37**, 2267, (1988)
10. Collins C,B, et al. - Phys. Rev. C, **42**, R1813, (1990)
11. Carroll J.J. et al. - Phys. Rev. C, **43**, 1238, (1991)
12. Collins C.B. et al. - Laser and Particle Beams, **11**, 43, (1993)
13. Collins C,B, et al. - Phys. Rev. Lett., **82**, 695, (1999)
14. Collins C,B, et al. – Laser Physics, **9**, 8, (1999)
15. Carroll J.J. et al. – Hyperfine Interactions **135**, 3, (2001)
16. Ahmad I. et al. - Phys. Rev. Lett., **87**(7), (Aug. 13, 2001)
17. Rivlin L.A. – 12th LIRPP Conf., Osaka, 1995. AIP Conf. Proc. **369**(2), 766, (1996)
18. Rivlin L.A. — Laser Physics, **5**, 297, (1995)
19. Rivlin L.A. - Laser and Particle Beams, **14**, 93, (1996)
20. Rivlin L.A. and Zadernovsky A.A.— Laser Physics, **6**, 956, (1996)
21. Rivlin L.A. - Hyperfine Interactions **107**, 57, (1997)
22. Rivlin L.A. — Laser Physics, **9**, 12, (1999)
23. Shvyd'ko Yu.V. et al.– Phys. Rev. Lett., **90**(1), Jan. 10, (2003)

Laser Physics, Vol. 13, No. 8, 2003, pp. 1–6.

Hybridization of Atomic–Nuclear Excitations and Pumping of Nuclear Levels

S. A. Karamian[1], Carroll[2]

[1] *Joint Institute for Nuclear Research, Dubna, Moscow region, 141980 Russia*

[2] *Department of Physics and Astronomy, Center for Photon-Induced Processes, Youngstown State University, Youngstown, Ohio, 44555 USA*

e-mail: karamian@jinr.ru

Received September 3, 2002

Abstract—Gamma emission driven by external electromagnetic radiation describes processes that may release isomeric nuclear energy in a "clean" way, as bursts of incoherent or coherent gamma rays without the production of radioactive byproducts. Different schemes and best candidates for the isomer de-excitation via pumping of a triggering level are considered. Short, high-power pulses of laser light must be the most economic source for nuclear isomer triggering either directly by a strong electromagnetic field or by dense radiation. The processes of deep ionization of the atomic shells with subsequent radiative and nonradiative decay of the vacancies are of special interest. The time scales of different processes in nuclear, atomic, and condensed-matter subsystems are compared.

1. INTRODUCTION

The creation of collective and avalanche-like γ-ray bursts and ultimately a coherent gamma-ray laser was explicitly proposed in the 1960s, and since that time many publications have followed along this research direction. Major interest was given to the gamma analog of an optical ruby laser based on the idea of inverted population of some excited level. However, tough restrictions became clearly visible for the realization of this idea. During the latter years, a new concept has been formulated, namely, to use nuclear isomers as an active medium. Some possibilities for the creation of a γ-ray pulsed source have been proposed and studied. The historical and modern status were reviewed recently in [1].

Another principle was developed after significant progress was made in the technique of high-current electron accelerators. Compton backscattering of optical-range photons in interaction with a relativistic electron beam serves as a source of polarized, directed, and quasi-monochromatic γ rays. The frequency of photons in the laboratory system is increased after scattering due to the Doppler effect, and photons are shifted to the gamma range because of the high relativistic factor of the electrons. This way, using a 1-GeV electron storage ring, a high-intensity polarized γ beam with tunable energy up to 50 MeV was obtained in [2]. The ultraviolet photons generated in the free-electron laser have been scattered in a cavity by the initial electron beam. However, such a γ-ray source in practical realization turns out to be a big, stationary system, interesting in principle and useful for research programs, but not transportable and restricted in the flexibility necessary for applications. A free-electron laser alone with 4 wigglers has a length of 20 m, in addition to the heavy and expensive electron accelerator and storage ring.

In the simpler version of [3], the external optical laser photons interact with a lower energy electron beam. It would also be important that the same powerful laser pulse be used in the laser electron gun of the accelerator [4]. Such a version is more flexible, but high quantitative parameters—the spectral density of γ rays and their energy—have not yet been attained in current experiments. It was proposed recently [5] to arrange a scheme where laser photons are backscattered by an ultrarelativistic, crystallized heavy-ion beam. Again, a very big accelerator and storage-ring cooler are necessary. Thus, despite the impressive progress made in accelerators, schemes for the creation of compact pulsed γ-ray sources are still lacking and much is still needed for future research programs. We are going to discuss the possibilities provided by the high-power pulses of laser light and by x-ray sources for isomer triggering, taking into account that such techniques are by orders of magnitude more economical than synchrotrons and other relativistic accelerators.

2. ACCELERATION OF NUCLEAR LEVEL DECAY

Most attractive would be the direct stimulation of a nuclear-state decay by a strong electromagnetic field, as was proposed 20 years ago in [6] for acceleration of β decay. In a strong field of the laser wave, the nuclear level should be split with the formation of sidebands: 2 virtual sublevels with practically the same energy, but with higher or lower angular momentum values. Decay of nuclear levels is typically retarded due to the strong changes of spin quantum numbers. The appearance of these sidebands allows lower multipolarity transitions, 2

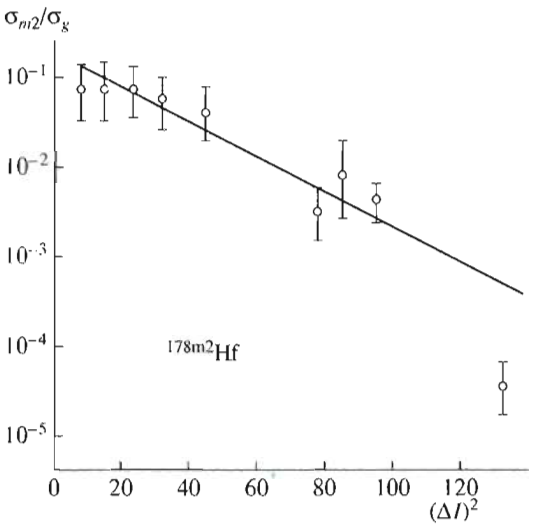

Fig. 1. Isomer to ground state ratios for production of the ^{178m2}Hf 16^+ isomer in reactions with photons, fast neutrons, and ^{4}He ions systematized versus the square of the spin deficit. Experimental points are from [11].

and, as a result, the rate of transition can be increased by orders of magnitude. This idea should be applicable not only for β decay but also for γ- and electron conversion decays of an isomeric level. An attempt to observe the acceleration of ^{125}I electron capture decay by synchrotron radiation was described in [7]. Also in [1], we proposed to explain by this process the results of experiments [8] on ^{178m2}Hf isomer accelerated decay under x-ray irradiation of an isomeric sample. However, more experiments are still necessary to prove the presence of the effect of external field and to estimate its strength.

In the same group of direct effects of laser radiation on nuclear decay should be included the laser-assisted TEEN proposed in [9] for isomers of the type of ^{229}Th and ^{235}U. These levels are characterized by low excitation energy comparable to atomic electron transitions in the valence zone. The nuclear and atomic transitions are normally out of resonance, but the defect of resonance can be covered with the absorption of a laser photon. Thus, the laser-assisted transfer of energy from the nuclear excited state to the atomic shell serves as a mechanism effective for accelerated nuclear decay. Experiments in this direction are of interest, as for another mechanism also discussed in [9], namely, radiation-accompanied NEET. In this case, the atomic transition energy exceeds the excitation energy of a nuclear level, but the latter is still available for excitation by an electron transition if the "extra resonance" energy is radiated in the form of an additional photon. Such a radiative mechanism can be effective provided the appropriate level schemes exist and could be useful for triggering a nuclear isomer via the excitation of an intermediate level.

The latter example corresponds already not to the direct effect of external radiation but to the "up-conversion" scheme of the triggered decay. The vacancy in an atomic shell is created in the first stage, and then the ionization energy is converted into nuclear excitation plus an emitted photon. Below, we discuss in more detail the possibilities for isomer triggering in the up-conversion scheme through the mechanisms of resonance photon absorption and resonant nonradiative NEET.

The triggered decay of the isomer in this scheme is similar to the population of isomeric states in nuclear reactions. Indeed, in both cases, the population or depopulation of definite levels occurs in cascades of transitions from upper lying levels. In [10], we analyzed the theoretical prediction for photon-induced nuclear reactions and found that the integrated cross section of nuclear photoabsorption can be predicted in absolute value if the spectroscopic factor of each individual transition is known. Such theoretical support allows the analysis of branching ratios both for isomer population and depletion. The isomer to ground state ratios σ_m/σ_g were systematically measured for population of isomers in nuclei near $A = 180$ in [11–13], while the depopulation was studied in detail only for the ^{180m}Ta isomer [14–16].

In Fig. 1, the systematics of the cross section for the ^{178m2}Hf isomer production are given following the experimental results of [11, 13]. One can see that the σ_{m2}/σ_g ratio is an exponentially decreasing function of the $(\Delta I)^2$ parameter, where ΔI is the difference between the isomeric spin and the mean angular momentum of the reaction residue. The exponential dependence is explained in the statistical theory of nuclear reactions by the spin dependence of the level density. The results in Fig. 1 were taken in (γ, n), $(n, 2n)$, and $(^4\text{He}, 2n)$ reactions. To populate the high-spin, 16^+, isomeric state of ^{178}Hf, the deficit of spin has to be accumulated in a cascade of γ transitions in the excited reaction residue. The mean value is not the only significant parameter of the residual spin distribution; the width is also important and it is not the same for different reactions. The deviation of some points from the straight line in Fig. 1 is just a manifestation of the spin-distribution widths. It is clear from systematics like Fig. 1 that the population of isomers is regulated by the angular momentum released in the reaction, in comparison with the final-state (isomer) spin.

For the isomer depopulation, a different mechanism has been established from the systematics after analysis of the results taken in [10, 13–16], despite the schematical similarity between the population and depopulation processes in the γ cascades occurring through higher lying levels. In the case of an exposed isomeric target, the photon absorption leads to the high-spin excited level and a cascade leading to the ground state is still possible despite the large spin difference. This is because of the existence of rotational bands built on the

ground state and other low-spin levels. The level populated in the first step from the isomer is surrounded by other levels of comparable spin, and the transitions to these rotational states are not forbidden by angular momentum. Thus, one could expect a very high probability of depopulation. Experiment shows, however, that this is not the case at excitation energies $E^* < 3$ MeV. The comparable-spin rotational levels are available at such energies, and even at lower excitations the transitions to them are still forbidden due to the mismatch in the K quantum numbers. Such a situation is clearly evident from the experiments performed in [14–16]. At low E^*, there exist two independent systems of levels with low and high K, the transitions between them being severely hindered. With growth in E^*, some K-mixing strength appears, and at E^*, near the neutron binding energy $B_n \sim 7$–8 MeV, complete K mixing takes place. At this energy, K is no longer a good quantum number, but below 2–3 MeV it strongly influences the electromagnetic transition rates. So, the isomer depopulation at low energy depends on the existence of some special intermediate level characterized by the admixture of K-violating strength. Such levels may randomly appear even at rather low E^*, and it is a challenge to find them experimentally.

For the ^{180m}Ta depopulation, mediating levels have been observed down to $E^* \approx 1.07$ MeV [14], and their strength regularly increases to higher E^*. The nuclear structure interpretation of them has been discussed in [17], together with other examples of K-mixing states in neighboring nuclei. The experimental data available
3 for other nuclides is typically on the lifetimes and branching ratios in the decay of relatively short-lived isomeric states [17]. The photon-induced transformation from high to low K values has been experimentally studied only for ^{180}Ta and in some experiments with ^{176}Lu as well. The conclusion obtained in the ^{180}Ta case (see above) should be verified; the ^{176}Lu experiments provide such a comparison.

A fragment of the ^{176}Lu level scheme is shown in Fig. 2. The nearly stable ground state has $K^\pi = 7^-$, and the short-lived ($T_{1/2} = 3.7$ h) isomer with $K^\pi = 1^-$ lies at 123 keV. So, at low E^*, there are two systems of levels with high and low K values. They can be coupled only via some mediating levels possessing special K-mixing wave functions. Such levels do exist, as was shown in the experiments in [18–21]. In [19], the 1^- isomer was excited in irradiations of the ^{176}Lu target by intense radioisotope γ radiation of ^{60}Co and ^{137}Cs sources. The monoenergetic γ radiation of ^{137}Cs consists of 662-keV photons, and successful population of the 1^- isomer shows the presence of some K-mixed level at an energy below 662 keV, accessible to Compton scattered photons if not to the direct source radiation. Sspectroscopic identification of this level has not yet been successful. However, in [20], the level with I, $K^\pi = 5$, and 4^- at 838 keV was definitely recognized as a mediating level between the $K = 7$ and $K = 1$ levels. Even more exotic properties were found in [21] for the transition from the

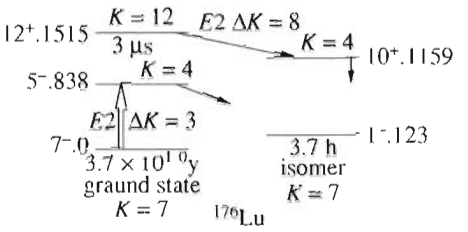

Fig. 2. Mediating levels in ^{176}Lu, as deduced from [20, 21]. Energies of levels are given in keV.

I, $K^\pi = 12$, 12^+ isomeric state at 1515 keV to the I, $K^\pi = 10$, 4^+ rotational state at 1159 keV. This transition should be strongly K-hindered, with $(\Delta K - \lambda) = 6$, but in experiment a rather low reduced hindrance factor has been found. Clearly, the wave functions of the high-K isomeric state and the low-K rotational level are mixed.

This is important for the proposed [13, 22] triggering of the ^{177}Lu isomer. The ^{177m}Lu 161-d-lived isomer can be produced in reactor irradiations in a quantity of milligrams. It stores a specific energy of about 1 MeV per nucleus and once triggered will emit this energy in the form of short-wave γ radiation in the range of 100–200 keV. If the properties of ^{177}Lu and ^{176}Lu are similar, one may expect a successful ^{177m}Lu triggering by x-ray radiation via a rotational level as a mediating state. Two rotational yrast bands with $K^\pi = 7/2^+$ and $9/2^-$ are known, and the $19/2^+$ and $19/2^-$ members of these bands lie at an excitation energy of 1093 and 1073 keV, respectively. The isomeric ^{177m}Lu level with $K^\pi = 23/2^-$ has an excitation energy of 970 keV. One may assume possible triggering via an $E2$ transition with an energy of 103 keV from the $23/2^-$ to $19/2^-$ levels. This transition would be strongly hindered by the K quantum number because of the degree of K forbiddenness of $(\Delta K - \lambda) = 5$. Despite this, one may consider that the K-mixed component of the wave function has a noticeable amplitude for the sixth level of the $K^\pi = 9/2^-$ band with $I = 19/2$.

The ^{242m}Am long-lived ($T_{1/2} = 141$ years) isomer is another promising candidate for triggering (see the discussion in [13, 22]). It is normally accumulated in spent reactor fuel as a radioactive product due to the multiple neutron capture process. The specific energy stored by ^{242m}Am is much lower than in the case of ^{177m}Lu, but this is compensated by a higher total weight of the available material and by its very long lifetime. This 5^- level lies at an excitation energy of 48.6 keV, and triggering via the $E2$ transition to the 3^- state at 52.9 keV releases the isomeric excitation energy. Resonance triggering of ^{242m}Am requires a transition energy of (4.30 ± 0.05) keV, which can be supplied by an atomic transition in the Am atom; as many as three transitions, $L_{III} \longrightarrow L_{II}$, $N_{VII} \longrightarrow M_{III}$, and $N_{II} \longrightarrow M_{II}$, may have the appropriate energy. Both photon absorption and NEET mechanisms are possible because the multipolarities

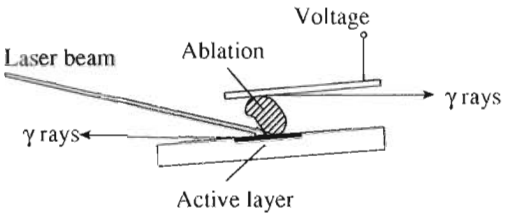

Fig. 3. Schematic illustration of nuclear level pumping by a laser pulse.

can also be identical. Despite the promising properties of ^{242m}Am, it would be difficult at the moment to predict quantitatively the efficiency of energy release in irradiations of this active material. This remains one the challenges of modern experiments.

In addition to the unknown strength of the nuclear transition in ^{242}Am, another problem has been known that is connected with the rather low energy of the atomic transition, of about 4.3 keV. It is known that Auger and Coster–Kronig conversion dominates at such energies and the efficiency of energy transfer to a nuclear subsystem should be reduced. Fortunately, as we discuss below, the plasma conditions suppress the rate of nonradiative conversion within atomic shells. Thus, even an M vacancy in a heavy atom may have a noticeable fluorescence yield and the nuclear conversion of the atomic transition is also not suppressed.

3. PROCESSES IN LASER PLASMA

It is known that the interaction of a terawatt laser pulse with solid matter immediately generates an induced oscillation of electrons at the frequency of the laser light. This collective excitation of the electronic subsystem then decays via an energy transfer to highly excited atomic states and/or to deep ionization of the atomic shells. The nuclear subsystem can also be perturbed because of the interaction with fast electrons, characteristic x-ray photons, or bremsstrahlung or black-body radiation. K and L electrons can be ejected from heavy atoms with the created vacancies serving as a source of characteristic photons with an energy useful for excitation of some specific nuclear states.

Time scale of different processes induced by a powerful laser pulse in a solid

	Process	Time-scale, s
1	Electron-gas excitation	$\sim 10^{-15}$
2	X-ray emission past ionization	$\sim 10^{-16}$–10^{-15}
3	Ablation due to superthreshold power:	
	(a) fast desorption;	$\sim 2 \times 10^{-14}$
	(b) temperature mechanism	10^{-12}–10^{-11}
4	Recrystallization of melted layer	10^{-11}–10^{-10}
5	Nuclear fluorescence	Accounting for conversion
	(a) collective $E2$ at $E_\gamma > 50$ keV	$<10^{-10}$
	(b) single-particle $E1$ at $E_\gamma > 50$ keV	$<2 \times 10^{-10}$
6	Condensation of the ablation cloud	$\sim 10^{-8}$

The excitation of nuclear levels in ^{201}Hg and ^{181}Ta isotopes by exposure to plasma radiation created by short laser pulses was tested in [23] and the utility of this concept was supported experimentally. A device for laser pumping of nuclear levels using this approach can, in principle, be small and simple in configuration. One possible scheme is shown in Fig. 3, in which a focused laser beam creates a high-power density spot on the sample surface. The cross-sectional size of the spot can be as small as 100 μm. Excited electrons leave their atoms immediately, and the solid matter is quickly transformed into a dense plasma of ionized atoms. Other radiation processes develop rapidly, and desorption of atoms to vacuum and thermal ablation follow. Finally, the hot spot is recrystallized and at the end the ablation cloud is deposited onto the sample and surrounding surfaces.

The time scales of different processes are given in the table. The relaxation of solid matter after the pulsed release of energy was studied recently in [24, 25] for the case of femtosecond pulses of laser light incident on metal and semiconductor samples. It was found that all processes develop very rapidly and the solid is recrystallized within 100 ps. It is important to stress here that a similar time scale characterizes pulsed energy release in solids due to an entirely different process [26, 27]. High-energy heavy ions may deposit a large amount of energy within the limited volume of a nuclear track in a solid. The electronic medium is immediately excited, the same as in the case of the laser pulse, and then relaxation processes follow. It was shown experimentally in [26, 27] that, in perfect crystals, recrystallization is one of the final stages but occurs within a time scale of 100 ps. This strong similarity in time scale is definitely not a coincidence, but confirms the general properties of processes in a solid after pulsed energy release.

The time scale of nuclear fluorescence is defined by the lifetime of an excited level and can be estimated using standard systematics for the strength of nuclear electromagnetic transitions. As is clear in the table, the decay time of the nuclear level is typically longer than the time scales of all other processes in atomic and solid subsystems. Even recrystallization of a solid may happen before nuclear fluorescence events occur. Thus, nuclear radiance takes place from within solid surroundings, and this is favorable for lasing.

Such a situation permits the occurrence of other attractive properties (discussed in [23]) for the scheme that employs laser pulses to pump a hypothetical γ-ray laser on nuclear levels. However, it is necessary to also

discuss some disadvantages of the scheme depicted in Fig. 3.

(1) A certain number of excited nuclei will be released into the gas phase due to ablation of atoms from the exposed surface. As long a time as about 10 ns is required for condensation of the ablation cloud back to the surrounding solid surfaces. Nuclear levels may be longer lived, but for them the probability of excitation is decreased by their narrow width. For levels with an optimum lifetime of about 100 ps, the efficiency of radiance in a solid will be reduced because of the losses of excited nuclei to the gas phase. A compromise can be found by the choice of the optimum surface power density for the laser. The rate of ablation can be reduced while the total number of excited nuclei is conserved. The full energy of the laser pulse can be distributed over a larger area on the surface.

(2) The resonance tuning between nuclear and atomic resonators cannot be perfect even when both frequencies coincide. The width of an atomic resonance is typically much larger than the nuclear one because of the lifetimes of the atomic and nuclear states having different orders of magnitude.

This difference leads to a low value of the "Q factor" corresponding to the resonance between nuclear and atomic modes. Such a situation was confirmed recently in direct measurements of the probability of the NEET process obtained in a synchrotron-radiation experiment [28]. The nuclear transition $3/2^+ \longrightarrow 1/2^+$ with $E = 77.351$ keV in ^{197}Au was excited by nuclear conversion of the atomic $MI \longrightarrow K$ transition after K-vacancy ionization. The difference in energy was only 51 eV, and this was comparable with the total width of the K-vacancy state. The probability of NEET was found to be 5×10^{-8}, which is similar to the width ratio for nuclear and atomic states, Γ_n/Γ_a. The nuclear transition lifetime is known experimentally to be 2.76 ns, and the atomic level width can be taken from the systematics of [29].

The mismatch of widths suppresses not only the NEET probability but also the integrated cross section for the resonance photon absorption. This fundamental effect reduces the nuclear excitation probability and cannot be completely cancelled. It is only possible to discuss some modestly palliative options. The lifetime of an atomic transition is normally increased for lower energy characteristic photons, the same as for nuclear transitions. One may suppose that vacancies in an M shell should be much longer lived than K and L vacancies, and this would seem promising to reach comparable magnitudes for the atomic and nuclear widths. In fact, this is not the case. For characteristic energies below 15 keV, the radiative width decreases until it is lower than the width of the intrinsic conversion of the transition energy within the atomic shell through the Auger and Coster–Kronig processes. The total width is then primarily due to the latter processes, and the fluorescence yield of the x-ray photons will be much less than 1. Thus, the resonance photon excitation process is suppressed not only due to the mismatch of the widths but also directly due to the low yield of characteristic photons.

In plasma, atoms are strongly ionized and the maximum of the charge-state distribution corresponds to values of $q = 10$–30, depending on the plasma temperature [30]. This wide charge-state distribution creates a series of characteristic x-ray energies that deviate from the standard ones known for a single vacancy, and this is helpful for exact tuning of the atomic and nuclear transition energies. On the other hand, the high stage of ionization should be effective in suppressing the probability of the Auger and Coster–Kronig processes for soft characteristic transitions with $E_\lambda \leq 10$ keV in strongly ionized heavy atoms. The total width of the atomic resonance decreases correspondingly, and the relative probability of radiative processes thereby increases. Both effects are useful for the nuclear conversion of atomic excitation. Thus, one can anticipate that, in plasma surroundings, even M vacancies must be active for the production of characteristic lines and for the resonance excitation of a nuclear transition via photon absorption and NEET processes.

In [23], the possibility was discussed of suppressing the electron conversion of nuclear γ rays in a hot plasma. This effect increases the contribution of the radiative width to the total width of a nuclear level (decreasing the conversion coefficient), and it can be useful in some schemes of nuclear level pumping and radiance. In addition, the possibility of using the electron conversion of nuclear radiation for the separation of some specific nuclear states in a multilevel scheme has also been proposed [23].

At present, however, we will stress that the hot plasma may serve as a tool for suppressingthe nonradiative conversion of the ionization energy within an atom. In this way, the efficiency of energy transfer from the atomic to nuclear mode can be significantly increased.

When nuclear and atomic transitions have the same energy and multipolarity, the hybridization of atomic–nuclear components is possible. The special wave function of the hybrid state includes such peculiarities as a beating in amplitude of the two modes with repumping of the energy, retardation in the decay time of both modes, low nonexponential decay, etc. As a result, the conversion of energy within the atom may be additionally suppressed and the nuclear conversion of an electron transition may be enhanced. This kind of hybridization was discussed in [13]. Finally, one can conclude that some processes exist that allow resonance energy transfer from atom ionization to nuclear excitation, despite the fact that the atomic–nuclear resonance is not originally very sharp.

4. SUMMARY

Nuclear excitation in a hot dense plasma via the resonance between atomic and nuclear transitions possesses some attractive properties. Among them are the possible hybridization of the atomic–nuclear wave functions and the suppression of Auger and Coster–Kronig conversion of the ionization energy and the shift of the characteristic energies of the atomic levels, depending on the charge state. The discussed processes may be useful for increasing the efficiency of nuclear excitation by a laser pulse. The nuclear state candidates for the pumping by atomic transitions are characterized. Among these are also promising candidates for the triggered release of stored nuclear energy.

The time scale of different processes after the pulsed release of energy are compared, and the typical time of nuclear fluorescence appears to be longer than the atomic and solid relaxation processes. The possibility of nuclear radiance in solid surroundings after sample recrystallization is promising for lasing of nuclear γ rays.

The acceleration of nuclear decay through the direct influence of external electromagnetic radiation is also possible, and such a possibility still cannot be excluded for some complete experiment. As a result, not only complicated experiments with synchrotron radiation but also simple schemes are still relevant for observing the decay of nuclear isomers, for instance, in a cavity exposed to a powerful laser beam or in the chamber of a high-efficiency ion source.

ACKNOWLEDGMENTS

The authors wish to acknowledge general support (J.J.C.) and travel support (S.A.K.) to the International Workshop on Laser Physics 2002 (LPHYS'02) provided by AFOSR grant no. F496200210187.

REFERENCES

1. Carroll, J.J., Karamian, S.A., Rivlin, L.A., and Zadernovsky, A.A., 2001, *Hyperfine Interact.*, **135**, 3.
2. Park, S.H., Litvinenko, V.N., Tornow, W., and Montgomery, C., 2001, *Nucl. Instrum. Methods Phys. Res. A*, **475**, 425.
3. Ohgaki, H., Noguchi, T., Sugiyama, S., *et al.*, 1996, *Nucl. Instrum. Methods Phys. Res. A*, **375**, 602.
4. Farrell, P., private communication.
5. Habs, D., 2002, Presentation at *11th International Laser Physics Workshop* (Bratislava).
6. Reiss, H.R., 1983, *Phys. Rev. C*, **27**, 1199.
7. Soloway, S. and Harbison, J., 1996, *Trans. Am. Nucl. Soc.*, **75**, 20.
8. Collins, C.B., Davanloo, F., Iosif, M.C., *et al.*, 1999, *Phys. Rev. Lett.*, **82**, 695.
9. Karpeshin, F.F., Band, I.M., and Trzhaskovskaya, M.B., 1999, *Nucl. Phys. A*, **654**, 579.
10. Karamian, S.A. and Carroll, J.J., 2001, *Laser Phys.*, **11**, 23.
11. Oganessian, Yu.Ts., Karamian, S.A., Gangrski, Yu.P., *et al.*, 1992, *J. Phys. G*, **18**, 393.
12. Karamian, S.A., de Boer, J., Oganessian, Yu.Ts., *et al.*, 1996, *Z. Phys. A*, **356**, 23.
13. Karamian, S.A. and Carroll, J.J., 2002, *Laser Phys.*, **12**, 310.
14. Belic, D., Arlandini, C., Besserer, J., *et al.*, 1999, *Phys. Rev. C*, **65**, 035801.
15. Karamian, S.A., Collins, C.B., Carroll, J.J., and Adam, J., 1998, *Phys. Rev. C*, **57**, 1812.
16. Karamian, S.A., Collins, C.B., Carroll, J.J., *et al.*, 1999, *Phys. Rev. C*, **59**, 755.
17. Walker, P.H., Dracoulis, G.D., and Carroll, J.J., 2001, *Phys. Rev. C*, **64**, 061302(R).
18. Lakosi, L., 1996, *Z. Phys. A*, **356**, 155.
19. Lakosi, L., Veres, A., Tam, N.C., and Pavliczek, I., 1992, *Nucl. Instrum. Methods Phys. Res. A*, **312**, 17.
20. Klay, N., Kappeler, F., Beer, H., and Shatz, G., 1991, *Phys. Rev. C*, **44**, 2839.
21. McGoram, T.R., Dracoulis, G.D., and Kibedi, T., 2000, *Phys. Rev. C*, **62**, 031303(R).
22. Karamian, S.A. and Carroll, J.J., 2001, Talk at *International Conference LASERS'01* (Tucson); *Hyperfine Interact.* (in press).
23. Andreev, A.V., Gordienko, V.M., Dykhne, A.M., *et al.*, 2000, *JETP*, **118**, 1343.
24. Schmidt, V., Husinsky, W., and Betz, G., 2000, *Phys. Rev. Lett.*, **85**, 3516.
25. Cavalleri, A., Siders, C.W., Brown, F.L.H., *et al.*, 2000, *Phys. Rev. Lett.*, **85**, 586.
26. Karamian, S.A., 1990, *Nucl. Instrum. Methods Phys. Res. B*, **51**, 357.
27. Karamian, S.A., 1995, *Radiat. Meas.*, **25**, 243.
28. Kishimoto, S., Yodo, Y., Seto, M., *et al.*, 2000, *Phys. Rev. Lett.*, **85**, 1831.
29. Keski-Rahkonen, O. and Krause, M.O., 1974, *At. Data Nucl. Data Tables*, **14**, 139.
30. Harston, M.R. and Chemin, J.F., 1999, *Phys. Rev. C*, **59**, 2462.

SPELL: 1. wigglers, 2. sidebands, 3. nuclides, 4. suppressingthe

Laser Physics, Vol. 14, No. 2, 2004, pp. 1–4.

Formation of the High-Spin ^{179m2}Hf Isomer in Reactor Irradiations

S. A. Karamian[1], J. J. Carroll[2], J. Adam[1], E. N. Kulagin[1], and E. P. Shabalin[1]

[1] *Joint Institute for Nuclear Research, Dubna, 141980 Russia*

[2] *Department of Physics and Astronomy, Youngstown State University, Youngstown, Ohio, 44555 USA*

e-mail: karamian@sungraph.jinr.ru

Received September, 2003

Abstract—The second isomer ($T_{1/2}$ = 25.1 d) in ^{179}Hf is one of a number of nuclear states that is interesting from the point of view of triggering a release of "clean" nuclear energy because it stores a specific energy of about 0.5 MJ/mg. The yield of this isomer in nuclear reactions is restricted due to its high spin, $I^{\pi} = 25/2^{-}$. The productivity of previously known methods was enough for the creation of experimental amounts but not for potential applications. In this paper, we show that irradiations in a reactor by the fast neutron flux within the fission spectrum are useful for the accumulation of ^{179m2}Hf in an amount of 10^{16} nuclei. In an experiment performed in the Dubna IBR-2 reactor, the yield, cross-section σ_m, and isomer-to-ground state ratio σ_m/σ_g were measured for the ^{179}Hf$(n, n'\gamma)^{179m2}$Hf reaction. The systematics of the σ_m/σ_g values deduced from the experimental data available for this isomer are discussed.

Production cross-sections in neutron capture reactions with thermal neutrons are typically low for high-spin isomers with $I \geq 10$. The isomer ^{177m}Lu ($I^{\pi} = 23/2^{-}$) is an exception that confirms the general tendency, because the high spin of the target ^{176g}Lu ($I^{\pi} = 7^{-}$) nucleus provides a rather modest spin deficit $\Delta I = 4\hbar$ in the ^{176}Lu$(n, \gamma)^{177m}$Lu reaction. In contrast with neutron capture, fast neutron reactions supply additional possibilities. The production of high-spin isomers in micro- and milligram amounts would be important for using them in experiments on triggering and controlled release of energy, as is discussed in [1]. The properties of the ^{179m2}Hf isomer ($T_{1/2}$ = 25.1 d, $I^{\pi} = 25/2^{-}$, E^* = 1.106 MeV) make it one of the best candidates for triggering experiments, even in comparison with the ^{178m2}Hf isomer, which has been widely used in recent years in many studies.

The yields of high-spin ^{178m2}Hf and ^{179m2}Hf isomers were measured in reactions with neutrons [2–4], with bremsstrahlung photons [5, 6], with a ^{4}He-ion beam [7, 8], and with protons at intermediate energy [9, 10]. The spallation reaction with protons shows [9, 10] the best absolute productivity, ~3×10^{11}/s, because a massive target can be irradiated with a high-current proton beam. However, many undesired radioactive nuclides are produced at intermediate energies and radiation-safety restrictions require a long "cooling" time of the target before chemical processing. This delayed processing is possible for the 31-years-lived ^{178m2}Hf but not for the 25-days-lived ^{179m2}Hf. The spallation reaction is therefore not the best for ^{179m2}Hf production. The ^{176}Yb(α, n) reaction was used for the population of the ^{179m2}Hf state when it was originally discovered in [11]. The yield of the reaction was not discussed in [11] but later, when ^{179m2}Hf was detected from the same projectile-target combination (^{4}He + ^{176}Yb) in the accumulation of the ^{178m2}Hf isomer. It was shown that a rather low production yield, of about 10^7/s, can be reached for ^{179m2}Hf at an optimum energy and with the ^{4}He-ion beam current as high as 100 μA. This means that a method of ^{179m2}Hf production with high yield and efficiency has not been known until now. Obviously, neutron irradiation is potentially the method of highest productivity and the yield of ^{179m2}Hf in reactor irradiations should be examined.

Metal ^{nat}Hf foils 1 mm in thickness were activated in an external channel of the IBR-2 reactor at FLNP, JINR, Dubna, and were then studied using a 20% efficiency Ge gamma detector. This was accomplished by spectrometric electronics, which allowed a count rate up to 20 kCs/s with a reasonable dead time and conservation of spectral resolution on the level of 1.8 keV for ^{60}Co lines. Standard test sources were used for energy and efficiency calibrations. The neutron spectrum at the location of the target was known from previous experiments. But in addition, NiCr-alloy samples were used as spectators for the calibration of the thermal and fast neutron fluences in each irradiation by the resulting ^{51}Cr and ^{58}Co activities. The Hf samples were irradiated with and without Cd shields, and the method of Cd difference allowed isolation of the effect of thermal neutrons and deduction of the thermal cross section.

In measured spectra of activated Hf, the γ lines were observed and quantitatively determined for the following radionuclides: ^{175}Hf, ^{179m2}Hf, ^{180m}Hf, and ^{181}Hf. The bulk of the activity was defined by ^{175}Hf and ^{181}Hf formed in (n, γ) reactions. The contribution due to the activation of admixtures of other elements in the Hf

Production of the ^{179m2}Hf isomer in reactions with neutrons

Reaction	^{178}Hf(n, g) ^{179m2}Hf		^{179}Hf $(n, n'\gamma)$ ^{179m2}Hf	^{180}Hf $(n, 2n)$ ^{179m2}Hf
Energy	thermal	resonance	$E_n \geq 1.5$ MeV	$E_n \geq 14.8$ MeV
ΔI [$\hbar$]	12	12	15/2	12
σ; I_γ [mb]	≤0.2	≤13	4.5 ± 0.5	25*
σ_m/σ_g	$\leq 2.4 \times 10^{-6}$	$\leq 7 \times 10^{-6}$	1.6×10^{-3}	7×10^{-3}

* Ref. [3]. The value may include some contribution from the $(n, n'\gamma)$ reaction.

material was negligible. Only Zr is present in a quantity of about 3%, while the concentration of other elements can be estimated on a level $\leq 10^{-5}$ g/g. As was expected, the self-absorption in the 1-mm Hf sample attenuated fluxes of both thermal and resonance neutrons and the reduction factor was estimated by the detected yield of ^{175}Hf and ^{181}Hf. With such internal calibration of the fluxes, the deduced values of the thermal cross section and the resonance integral for ^{180m}Hf isomer production in the ^{179}Hf(n, γ) reaction appear to be in good agreement with the tabular data [12]. Low intensity γ lines of ^{178m2}Hf could not be found in the spectra because of the much higher count rate of other nuclides listed above.

The yield of the high-spin ^{179m2}Hf isomer was not high and obviously originated from reactions with fast neutrons. Such a conclusion is definite, because the effect of thermal neutrons was found to be insignificant in that bare and Cd-shielded samples showed the same activation within the standard error. The possible reactions leading to ^{179m2}Hf are listed in Table 1. The upper limit on σ_{th} is the result of the present measurement. Formally, one may assume that the detected yield of ^{179m2}Hf reflects the resonance integral and then the value of 13 mb is deduced. But we suppose that the (n, γ) reaction with slow neutrons makes a completely negligible contribution and thus 13 mb is again the upper limit. Most favorable is the $(n, n'\gamma)$ reaction, because the spin deficit ΔI is not so high in this case as compared to the other reactions listed in Table 1. The ^{179m2}Hf isomer has an excitation energy of 1.106 MeV; thus one should assume an effective threshold value of about 1.5 MeV for its population in $(n, n'\gamma)$ reactions. The number of neutrons with $E_n \geq 1.5$ MeV was determined using the above-mentioned calibration with the NiCr spectator and the known fast-neutron spectrum at the location of the target.

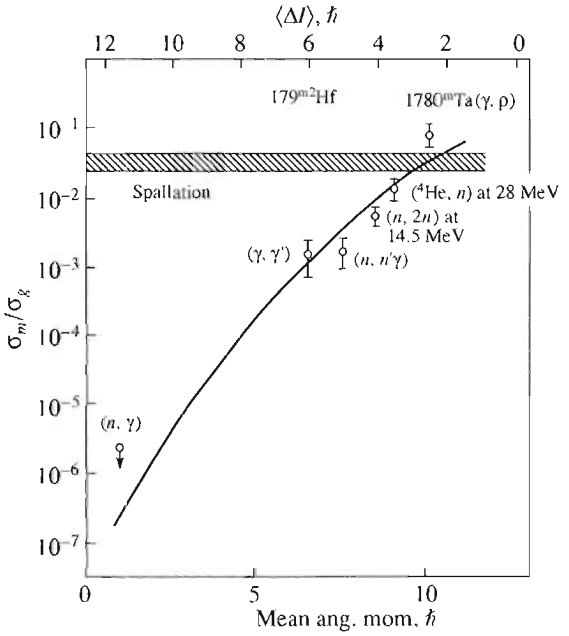

Fig. 1. Systematics of the isomer-to-ground state ratios for the production of the ^{179m2}Hf isomer in different reactions. The solid curve is used to guide the eye.

After all, the cross section and isomer-to-ground state ratio σ_m/σ_g were determined for production of the ^{179m2}Hf isomer in the ^{179m2}Hf$(n, n'\gamma)$ reaction. The latter values were found to be promising for the accumulation of ^{179m2}Hf in reactor irradiations. The relatively good ratio of σ_m/σ_g is understood because the modest spin deficit in the reaction is partially covered by the angular momenta of the bombarding and emitted neutrons. The effect of particle angular momenta should be stronger for the $(n, 2n)$ reaction at 14.8 MeV, and indeed an even higher isomer-to-ground state ratio is deduced for the ^{180}Hf$(n, 2n)^{179m2}$Hf reaction, which is in accordance with the experimental results from[3].

In [4], it was proposed that the $(n, n'\gamma)$ reaction could make a comparable contribution at 14.8 MeV as compared with the $(n, 2n)$ yield. But in the case of reactor irradiations, the production of ^{179m2}Hf due to the $(n, 2n)$ reaction should be neglected, because the reactor spectrum falls exponentially and the effective threshold of the ^{180}Hf$(n, 2n)^{179m2}$Hf reaction is as high as about 10 MeV.

In Fig. 1, the systematics are shown for the ^{179m2}Hf isomer-to-ground state ratio versus mean angular momentum of the reaction product. The latter parameter is determined from the standard recommendations

of nuclear reaction physics. The spin difference, ΔI, of the entrance and exit channels of the reaction is also included. Figure 1 is plotted using the results of Dubna experiments [6–8, 10] plus the measurement [3] for the $(n, 2n)$ reaction. One can see a strong growth of the σ_m/σ_g values with the angular momentum, and this is explained by the decrease in the ΔI value. The spin deficit ΔI should be covered by the cascade of statistical γ rays during the later stages of the reaction. Naturally, a low ΔI value can be reached easier than high values and the probability is correspondingly changed as shown in Fig. 1. The mean angular momentum of the spallation product has not been known, and the measured σ_m/σ_g value is shown as a strip in Fig. 1. The strip width reflects the standard errors of the measurements. The intersection of the strip with the regular curve of the systematics may serve to estimate the angular momentum of the spallation product. The discussed regularities are more or less typical for the production of high-spin isomers in nuclear reactions. In particular, similar manifestations were observed and discussed for ^{178m2}Hf in [7, 13].

Using the production cross section measured for the ^{179}Hf$(n, n'\gamma)^{179m2}$Hf reaction (see Table 1), one can estimate the rate of production and the absolute quantity that can be accumulated. Assuming that 1 g of enriched ^{179}Hf is exposed at the reactor core to a flux of about 5×10^{14} n/cm^2 s during 1 month, more than 10^{16} isomeric ^{179m2}Hf nuclei should be produced. This quantity is definitely enough for the preparation of a ^{179m2}Hf target for use in triggering experiments.

Fortunately, the neutron irradiation of ^{179}Hf in a reactor leads only to the production of ^{179m2}Hf and ^{180m}Hf activities, and the latter one is short-lived, with $T_{1/2} = 5.5$ h. No significant background activities are created if the ^{179}Hf material is chemically purified and highly enriched. The admixtures of ^{174}Hf and ^{180}Hf should besuppressed, otherwise long-lived backgrounds from ^{175}Hf and ^{181}Hf will arise. Anyway, the use of pure isotopic ^{179}Hf target allows one to suppress the backgrounds and to avoid a strong activation.

However, this method of isomer production has some disadvantages. The feedstock ^{179}Hf material cannot be separated from the produced isomeric ^{179m2}Hf either by chemical processing or by isotope separation. For many experiments with isomeric targets, the presence of a large amount of stable ground-state nuclei would create backgrounds much more intense than the useful signal. The separation of isomer from the ground state is a technically difficult problem, but laser separation methods may be capable of solving it. In the literature [14], experiments are described along this direction and they are promising specifically for Hf isomer isolation from the ground state of the same nuclide.

Finally, let us discuss the problem of the "burnup" of the produced isomeric nuclei in reactor irradiations. Thermal neutron capture is the most destructive process, because the cross section σ_{th} can be as high as thousands of barns for isomers. Unfortunately, they have not yet been measured and this is a challenge for modern neutron experiments. Nevertheless, if the fluence of neutrons in reactor irradiation reaches a value near 10^{21} n/cm^2, then the accumulation process can be disturbed by destruction due to the thermal neutron capture reaction on the produced isomer. The same is also true for resonance neutrons, but their flux is typically lower than that of thermal neutrons. The feedstock isotopes are also in danger of useless depletion under high-fluence neutron irradiations because of their possible transmutation to the neighboring (A + 1) isotope of the same element instead of $(n, n'\gamma)$ production of the desired isomer.

The restrictions due to the transmutation and burnup processes are insignificant for the present experiment because the fluence values used are low, being of about 10^{16} n/cm^2. Even a 30-day irradiation at a flux of 5×10^{14} n/cm^2 s discussed above should not be extremely dangerous. But strictly speaking, this is dependent on the unknown σ_{th} and resonance integral I_γ values for the ^{179m2}Hf nuclei.

Attempts to produce ^{178m2}Hf in massive neutron irradiations, like the experiment in [2], should be definitely influenced by burnup of the isomeric nuclei. The destruction of ^{178m2}Hf was tested in experiments in [15] when its transmutation to ^{179m2}Hf was observed in the ^{178m2}Hf$(n, \gamma)^{179m2}$Hf reaction. The σ_{th} cross section and I_γ value had been determined by the method of activation for this partial branch of the neutron capture reaction. And the yield of the stable ground state of ^{179}Hf could not be measured. However, for the burnup, the total capture cross section is important, including both isomeric and ground state population. According to [16], the isomer and ground state can be populated with comparable cross section after neutron capture to highly excited compound states. Consequently, we may assume now that the total σ_{th} and I_γ values are just two times higher those measured for the final ^{179m2}Hf state.

With such an assumption, the fluence dependence of ^{178m2}Hf isomer accumulation is calculated and shown in Fig. 2.

The transmutation functions are also given for stable feedstock isotopes. The cross sections of neutron capture and I_γ values are accounted for following [12]. The ^{178m2}Hf production cross section was taken from [2], and the destruction process is estimated as described above based on the results from [15]. One can see that, at fluences above 10^{21}/cm^2, the accumulation curve deviates strongly from a linear function and even decreases. This is due to both the transmutation of the feedstock ^{177}Hf target nuclei and to the burnup of the accumulated ^{178m2}Hf. The conclusion can be drawn that the role of destruction is underestimated in [2] for ^{178m2}Hf. One note more: the stable ^{179}Hf isotope is long-

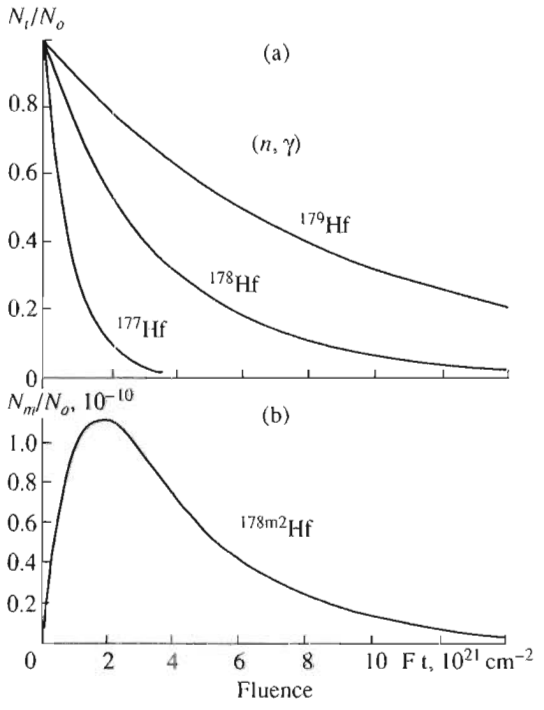

Fig. 2.

lasting in the neutron flux, so it can be effectively used for the accumulation of the ^{179m2}Hf isomer within the irradiation time restricted by the isomer lifetime.

In summary, the ^{179}Hf$(n, n'\gamma)^{179m2}$Hf production reaction is shown to be a method of accumulation of the ^{179m2}Hf high-spin isomer. It can be stored in an amount of 10^{16} atoms for a reasonably lost cost, observing the radiation safety conditions in standard reactor irradiations. Other neutron-induced reactions with Hf nuclides are also discussed regarding aspects of production and transmutation of their isomers.

ACKNOWLEDGMENTS

The authors gratefully acknowledge support through Youngstown State University from US Air Force Office of Scientific Research contract F49620-02-01-0187.

REFERENCES

1. J. J. Carroll, S. A. Karamian, L. A. Rivlin, and A. A. Zadernovsky, Hyperfine Interact. **135**, 3 (2001).
2. R. G. Helmer and C. W. Reich, Nucl. Phys. A **211**, 1 (1973).
3. Yu. Weixiang *et al.*, Chin. J. Nucl. Phys. **14** (4), 326 (1992).
4. M. B. Chadwick and P. G. Young, Nucl. Sci. Eng. **108**, 117 (1991).
5. Yu. Ts. Oganessian and S. A. Karamian, Hyperfine Interact. **107**, 43 (1997).
6. S. A. Karamian and J. J. Carroll, Laser Phys. **12**, 310 (2002).
7. Yu. Ts. Oganessian, S. A. Karamian, Yu. P. Gangrski, *et al.*, J. Phys. G **18**, 393 (1992).
8. Yu. Ts. Oganessian, Yu. P. Gangrsky, B. Gorsky, *et al.*, in *Proceedings of International Conference on Exotic Nuclei* (World Sci., Singapore, 1991), p. 311.
9. H. A. O'Brien, Nucl. Instrum. Methods Phys. Res. B **40/41**, 1126 (1989).
10. S. A. Karamian, J. Adam, D. V. Filossofov, *et al.*, Nucl. Instrum. Methods Phys. Res. A **448**, 489 (2002).
11. H. Hübel, R. A. Naumann, M. L. Andersen, *et al.*, Phys. Rev. C **1**, 1845 (1970).
12. S. F. Mughabghab, *Neutron Cross Sections* (Academic, New York, 1984), Vol. 1, Part B.
13. S. A. Karamian and J. Adam, Czech. J. Phys. **53** (Suppl. A) (2003); Preprint No. E6-2002-206, JINR (Joint Inst. for Nuclear Research, Dubna, 2002).
14. J. Billowes, Nucl. Phys. A **682**, 206c (2001).
15. S. A. Karamian, Yu. Ts. Oganessian, J. Adam, *et al.*, in *Proceedings of International School–Seminar on Heavy-Ion Physics* (World Sci., Singapore, 1998), p. 565.
16. S. A. Karamian, C. B. Collins, J. J. Carroll, *et al.*, Phys. Rev. C **59**, 755 (1999).

SPELL: 1. besuppressed

Laser Physics, Vol. 14, No. 2, 2004, pp. 1–8.

Possible Ways for Triggering the ^{179m2}Hf isomer\

S. A. Karamian[1], J. J. Carroll[2], L. A. Rivlin[3], A. A. Zadernovsky[3], and F. J. Agee[4]

[1] *Joint Institute for Nuclear Research, Dubna, 141980 Russia*
[2] *Department of Physics and Astronomy, Youngstown State University, Ohio, 44555 USA*
[3] *MIREA Technical University, 78 Vernadsky Prospekt, Moscow, 117454 Russia*
[4] *Air Force Office of Scientific Research, NE, 4015 Wilson Blvd., Arlington, VA, 22203 USA*
e-mail: karamian@sungraph.jinr.ru
Received September 19, 2003

Abstract—Realistic approaches to triggering of the ^{179m2}Hf isomer are discussed. The nuclear level scheme of ^{179}Hf suggests three promising ways for triggering, but two of them are seemingly closed by the high multipolarities of the required electromagnetic transitions. New possibilities are deduced by utilizing a model of atomic–nuclear compound states to overcome such restrictions. A new and productive method of observing triggering would be based on the use of an electron cyclotron resonance ion trap (ECRIT). Some quantitative details of the behavior of ^{179m2}Hf and ^{242m}Am atomic–nuclear systems in an ECRIT environment are examined. Many important parameters are as yet unknown, and they can be estimated only after the new type of experiments proposed here, in which high rates of triggering are possible.

1. INTRODUCTION

The idea to observe the induced decay of a nuclear level has been known in the literature for more than 50 years, and the application of such a process to the creation of the gamma-ray laser has also been proposed. In photon-induced nuclear reactions using bremsstrahlung sources, the population and induced depopulation of nuclear isomeric states were conclusively observed. Astrophysical science employed this knowledge for the evaluation of the production and burnup of some special nuclear states in stellar conditions. This effect strongly influences the cycles of isotope production in stars and, finally, their observed abundances. Papers [1–3] provide a good orientation on this topic.

Another branch of applications relies on the creation of pulsed γ ray sources and, in an extreme case, of a γ ray laser. Most experiments along this line have been performed on the long-lived ^{180m}Ta and ^{178m2}Hf isomers and remain of considerable importance. The bremsstrahlung from medical units and, recently, synchrotron radiation have been used for these experiments. The general problem of X-ray driven gamma emission is reviewed in [4].

The probability of inducing depopulation of an isomeric level strongly depends on the intrinsic microscopic structure of the participating nuclear states. In deformed nuclei are found the well-known K isomers that are formed due to the partial conservation of the K quantum number. The importance of K conservation and the possibilities for K mixing have been discussed, for instance, in [5, 6]. The ^{178m2}Hf isomer is considered to be the most promising K-isomer because of its high excitation energy, about 2.45 MeV. The specific energy stored in the form of nuclear excitation is highest for ^{178m2}Hf in comparison with other isomers. In addition, one may expect the presence of some level with a K-mixed wavefunction not far above the isomeric state because the K-mixing amplitude generally grows strongly with the excitation energy [7, 8]. Based on this expectation, experiments on triggering of ^{178m2}Hf have been developed extensively over the past few years. In principle, however, it was clear even earlier that other isomers can also be attractive for a triggered release of "clean" nuclear energy. Previously, we and other authors listed long-lived isomers that may be potentially useful for investigation, but detailed analysis only began in 2000.

In [9], the properties of the ^{177m}Lu and ^{242m}Am isomers were discussed based on nuclear spectroscopic and nuclear reaction data. Their advantages for triggering experiments were concluded because of the favorable position of a triggering level, appropriate decay properties, and effective production possibilities. Recently, the description a technical project for the creation of ^{177m}Lu isomeric targets has been appeared in the literature [10], meaning that some steps for isomer applications are in progress.

An additional proposal on a way to use individual excited sates of definite nuclides for pumping or triggering was presented in [11–13] and concrete properties of some states were analyzed. New ideas on the hybridization of the atomic–nuclear excitation of possible suppression of the Auger conversion in highly ionized plasma and of possible nuclear fluorescence past restoration of a solid lattice were also given in [11–13]. Another group of nuclear states was described in [14], in which numerical estimations for triggering cross sections via photon absorption, NEET, and Coulomb excitation mechanisms were obtained in a classical manner. Unfortunately, the resulting values were extremely low, thus eliminating optimistic expectations for real exper-

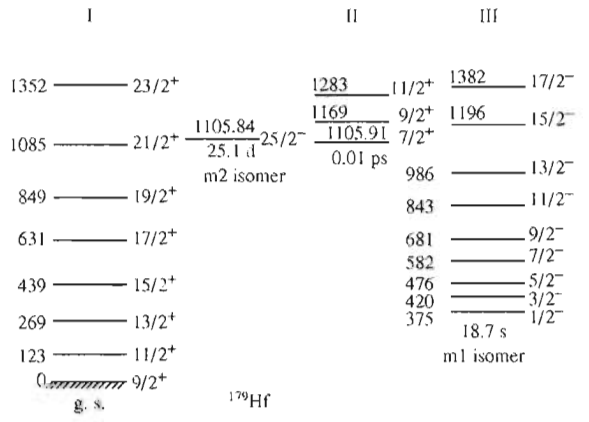

Fig. 1. Level bands in ^{179}Hf – candidates for three ways of triggering the ^{179m2}Hf isomer.

iments. The Coulomb excitation approach to pumping was introduced in [15], and at that time it was already clear that a reasonably high rate of nuclear level pumping can be achieved only for the electromagnetic transitions of collective nature when the reduced probability is enhanced by a factor of 100 above the standard Weisskopf strength. Therefore, it was not unexpected that the calculations in [14] predicted very low probabilities for strongly hindered transitions. New mechanisms should be sought to enhance the possibilities of triggering.

In the present article, we will stress the properties of the ^{179m2}Hf isomer as a candidate for triggering experiments. This high-spin (25/2$^-$) K isomer has a reasonably long half-life ($T_{1/2}$ = 25.1 d) and a rather high excitation energy of 1.106 keV, corresponding to the accumulation of about 0.5 MJ/mg in specific energy. After being triggered, this nuclide would emit a series of photons in the ultrashort wave band of γ rays of 200 to 300 keV.

New possibilities for triggering experiments will be described. In particular, triggering may be strongly realized in plasma surroundings within an electron cyclotron resonance ion trap.

2. PRODUCTION OF ^{179m2}Hf

The high-spin and high-K isomer in ^{179}Hf was discovered 30 years ago [16] using the producing reaction of ^{176}Yb(^{4}He, n)^{179m2}Hf. The quantity of isomer produced was sufficient for its identification, spectroscopic studies, and decay scheme construction. However, the absolute yield of isomeric nuclei was not reported. Later, within a program of irradiations for the accumulation of ^{178m2}Hf in a similar reaction, ^{176}Yb(^{4}He, 2n), the ^{179m2}Hf isomer was also detected and its absolute yield and excitation function were measured [17]. It was clear that ^{179m2}Hf was produced with a cross section that was much lower (by a factor of about 20) as compared to ^{178m2}Hf. This means a possible accumulation of only about 10^{13} atoms of ^{179m2}Hf after a one-month irradiation with a high-current cyclotron using a 30-MeV ^{4}He-ion beam. Such a quantity restricts the possibilities for practical applications, as well as the majority of experiments using ^{179m2}Hf as a target.

Recently, production of the ^{179m2}Hf isomer has been successfully observed [18] in the spallation of Ta to Re targets with intermediate energy protons in the range of 200–660 MeV. Its yield is even a little higher than the yield of ^{178m2}Hf. As is known, many current trigger experiments with ^{178m2}Hf targets use material produced in the spallation reaction at the Los Alamos 800-MeV high-current proton-beam facility. But this production method cannot be used for ^{179m2}Hf because of its 25.1-day half-life. The massive irradiated targets at Los Alamos were kept for cooling over a period of (10–20) years before processing because of their extremely high activities. The ^{179m2}Hf nuclide would be decayed completely after such long cooling, while such a period has little impact on the quantity of ^{178m2}Hf ($T_{1/2}$ = 31 years). Thus, until 2003, no effective method for ^{179m2}Hf target preparation was known.

Irradiation of a hafnium metal target of natural isotopic composition was arranged [19] at the Dubna IBR-2 reactor. The yield of ^{179m2}Hf was reliably detected by γ-spectrum measurements after activation of the target. It was shown that ^{179m2}Hf can be stored in an amount of above 10^{16} atoms after irradiation in standard reactors as the result of the ^{179}Hf(n, $n'\gamma$)^{179m2}Hf reaction with fast neutrons of the fission spectrum. If a purified highly enriched ^{179}Hf target is used in reactor irradiations, one may expect the production of a rather clean activity of ^{179m2}Hf. The number of atoms produced should be enough for many experiments with this isomeric material, but for some types of studies the presence of stable ^{179g}Hf nuclei in much larger amounts may create a significant background. Prior to such experiments, methods for separation of the isomeric and ground states of the same nuclide would be needed. Technical possibilities for this separation exist today [20], being in preparation especially for hafnium.

The potential for production of significant amounts of ^{179m2}Hf opens some new options for trigger experiments and requires a careful analysis of possible triggering experiments with this special isomer.

3. POSSIBLE SCHEMES FOR TRIGGERING OF ^{179m2}Hf

The partial level scheme of ^{179}Hf is shown in Fig. 1, in accordance with [21, 22]. In this figure, three bands are shown in addition to the m2 isomeric state and were selected according to some advantageous properties

that make these bands interesting for triggering. Three different ways for triggering can be considered, one for each of the bands shown. The different properties of each band, when used to provide an intermediate state for triggering, lead to a great variation among the technical methods likely to be most effective for the observation of triggering.

I. One possible means of triggering may exploit an assumed K-mixed component of the wavefunction for states in the ground-state band (g.s.b.), in particular, for the $21/2^+$ and $23/2^+$ levels. The up-conversion scheme of triggering was discussed earlier for ^{178m2}Hf and ^{177m}Lu isomers. A favorable, low-multipolarity E1 transition is possible for triggering by resonance absorption of photons in the excitation of the $23/2^+$ g.s.b. level in ^{179}Hf from the $25/2^-$ m2 state. Unfortunately, the energy of this transition is rather high, 246 keV, meaning that, for the release of γ radiation by triggering of the isomer, one has to use incident radiation of comparable wavelength. This is not economic from the perspective of quantum efficiency. The transition to the lower lying member of the g.s.b. having $21/2^+$ is accompanied by the release of 21 keV in each event. The transition has a multipolarity of M2 and occurs in the spontaneous decay of the ^{179m2}Hf isomer. A triggered transition to the lower lying level should also be possible, similar to the excitation of the higher level. The mechanism is quite different, however, as it is not resonance photon absorption but stimulated resonance emission. The rate of isomer decay can be increased due to such stimulated emission and also as a result of stimulated electron conversion under not resonance photon irradiation. Quantitative estimations of the possible decay acceleration are difficult because there are several unknown probabilities of the processes. Experiments on resonance stimulation of ^{179m2}Hf isomer decay under 21-keV photon irradiation look promising and can be realized with bright synchrotron (wiggler) radiation sources.

II. This approach may be discussed because a $7/2^+$ level is known in ^{179}Hf and is located very close above the m2 isomer. One can see in Fig. 1 that the transition energy corresponds to the far UV band being 70 eV; however, a large spin difference makes this transition seemingly impossible. Still, in a very dense radiation bath, like that produced by a high-intensity free electron laser or high-power optical laser beam, the transition may have a detectable probability via multiphoton absorption or other mechanisms that include the coupling of nuclear and atomic excitations. The latter topics are discussed below after a description of the technical possibilities for operating with highly ionized atomic states in plasma created by modern ion sources or by the interaction of short, powerful laser bursts with a solid.

III. Another way of triggering via the band built on the 19-s lived ^{179m1}Hf isomer looks attractive. The m1 state is not populated in the m2 spontaneous decay, and if m1 appears following irradiation of an m2 sample, then triggering will be strongly confirmed. High experimental sensitivity is the advantage of this method of observation. However, a problem arises due to the large difference of spin and K quantum numbers between the initial and final levels in triggering. According to [23], there exists the possibility to ameliorate this restriction using the capture of an additional photon.

A sample should be exposed simultaneously to gamma photons for the resonance nuclear transition and to a high-density optical laser beam. The transition to the $15/2^-$ state of this band requires a resonance photon energy near 90 keV (see Fig. 1), i.e., within the frequency band covered by the bremsstrahlung and synchrotron radiation sources. The multipolarity is $L = 5$, instead of $L = 9$ as in case II. And even additional photon capture in the scheme of [23] might not be enough to successfully reduce the hindrance factors. The same is definitely also true for case II, and in fact new mechanisms should be proposed to realize these high-multipolarity electromagnetic transitions. As mentioned above, the Coulomb excitation reaction does not improve the situation decisively, but some processes, including the hyperfine interaction of nucleus and atomic shells, can be valuable.

4. TECHNICAL SCHEMES OF TRIGGERING

Historically, the triggering of isomers was suggested to be a photon-induced process, either through self-triggering in stimulated emission or through the up-conversion scheme via photon absorption from an isomer to a short-lived level. The experiments with ^{180m}Ta and ^{178m2}Hf isomers follow the up-conversion scheme and use incident bremsstrahlung or synchrotron radiation as the triggering agent. The highest sensitivity could be reached with the beams from undulators or wigglers installed in electron synchrotrons. Experiments are in progress [25–27] using the brightest synchrotron light sources at SPring-8 and Argonne and Brookhaven National Laboratories. The experimental details are described in the cited references. The photon absorption scheme remains attractive for the triggering of isomers and for the ^{179m2}Hf isomer in particular. The first and third approaches described above for ^{179m2}Hf can be experimentally tested using intense X-ray sources.

Another technical possibility arises when one uses the radiation environment in the dense plasma created by a short pulse of laser light interacting with a solid. The excitation of the isomeric state in ^{181}Ta has been reported [28] and explained as a photon absorption process from the continuous spectrum of plasma radiation, which is quite intense near the energy needed for the isomeric state excitation, i.e., near 6.24 keV.

In our works [11, 12], the idea to use atomic–nuclear resonance in a highly ionized plasma, in addition to photon absorption, was stressed. It was realized that a

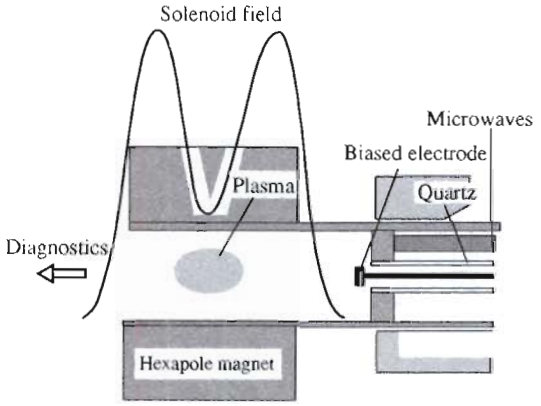

Fig. 2. Schematic layout of a typical ECR array.

large-amplitude resonance between nuclear and atomic transitions requires matching not only the frequencies (transition energies) but also the widths of the resonances. The atomic transition is normally shorter lived than the nuclear one, and the width of the latter is much smaller. The narrow nuclear transition should be coupled with the wider atomic one and the overall resonance amplitude is reduced. In this way, a low probability near 10^{-7} for nuclear excitation by electron transition (NEET) can be understood in agreement with the measurements [29] for ^{197}Au nuclei.

The situation for triggering of the ^{242m}Am isomer was analyzed in [12, 13]. It was clarified that the conversion of the ionization energy within atomic shells via Auger and Coster–Kronig nonradiative processes could be another important factor reducing the NEET probability. Fortunately, in hot plasma surroundings, auto-ionization processes are suppressed because of the high charge state of ions and the removal of a majority of the outer electrons. This serves as a feedback mechanism for the enhancement of radiative and NEET processes. The presence of many charge states is also valuable for exact matching of the nuclear and atomic energies, because the atomic transition energy depends on the charge state. An atomic–nuclear width mismatch exists in the case of triggering for the ^{242m}Am isomer. Indeed, the radiative lifetime of a vacancy in the M shell of the americium atom is estimated [30] to be about 10 fs, while the triggering level located 4.2 keV above the isomeric state in the ^{242}Am nucleus has a lifetime of about 100 ps. These different width values lead to a decrease in the NEET probability. However, the relatively long time of nuclear fluorescence can be very important in another advantageous aspect.

In [12], it was proposed that nuclear level pumping in a hot dense plasma can be combined with lasing in a solid. The time scale of the processes following the pulsed release of energy in a solid was considered, and it was concluded, based on known experiments, that the solid matter could be recovered and recrystallized within a time scale of about 100 ps. The characteristic time of nuclear fluorescence can be of such order of magnitude or longer; i.e., the radiance happens in almost cold crystalline matter. This is favorable for increasing the probability of collective radiance within the Mössbauer scheme of the γ-ray laser. In the literature, the understanding that a hot pumping contradicts the use of Mössbauer resonance processes dominates. Now, we suppose [12] that this may not be absolutely true in all cases.

In [13], the possible hybridization of the atomic and nuclear excitation is stressed and it is proposed that the plasma surrounding in modern ion sources or ion traps (the same as in laser plasma) can also be productive for the nuclear level pumping via atomic–nuclear resonance. The role of hybridization for ^{179m2}Hf triggering is discussed in the next section within the scheme of a nucleus–atomic compound system. Here, more details on the ion source are given.

Electron cyclotron resonance ion sources (ECRIS) and ion traps (ECRIT) have found wide application in accelerator techniques and in physical studies over the past 15 years. The typical layout of ECRIT elements is shown in Fig. 2. Ions are confined in the cylindrically symmetric cavity by a magnetic field in the axial direction created by two solenoids and in the radial direction, by the hexapole magnet. The ionization of the residual atoms in the vacuum is produced by electrons accelerated in the microwave electromagnetic field. The electrons circle around magnetic field lines under the condition of cyclotron resonance, and the high density of electrons creates a plasma in the central volume of the cavity. The microwaves and working gas are supplied from the right side along the axis, and the left side can be used for the extraction of ions in the ECRIS version of the array or for diagnostics by the X-ray radiation emitted from the plasma.

It is well known that the plasma density in an ECR array increases with the frequency applied and with the magnetic field strength. At the more or less standard frequency of about 15 GHz, a plasma density of above 10^{12} ions/cm^3 can be achieved. The typical time of confinement is about 1 ms before ions (atoms) are absorbed by the wall. However, if hot walls are used, one can expect multiple cycles of usage for each individual atom. The spectrum of ion charge states extracted from ECRIS is rather wide, and a high grade of ionization can be reached. The 20^+ and 30^+ ions of heavy element atoms are typically produced in ECRIS.

In singly ionized atoms of a heavy element, the lifetime of vacancy for inner shells such as L and M should be about 0.1–1.0 fs according to [30]. This is due to both Auger auto-ionization and radiative transitions of free or outer electrons to fill the vacancy. In ECR surroundings, when an ion is stripped to a high charge state, these processes are significantly retarded. Indeed,

Isomeric atom in ECRIT; estimated parameter values

Parameter	Value	Remark
Number of isomeric atoms in plasma	10^{13}	10% concentration
Time of confinement	$(10^{-3}–10^{0})$ s	Dependent on the array design
Electron excitation rate	$\sim 10^{5}$/ion s	Deduced from the measured current of ions
Detectable rate of triggering	$\geq 10^{4}$/s	For 10^{13} nuclei of ^{242m}Am
Detectable NEET probability, P_{NEET}	$\geq 10^{-14}$	Lower limit
Triggering rate with $P_{NEET} = 10^{-10}$	$\sim 10^{8}$/s	High productivity

free electrons are accelerated to the keV energy range and the probability of recombination is greatly reduced. When the outer shell electrons are removed, Auger conversion is stopped.

In a more quantitative approach, an ion can capture an electron, but it becomes stripped again. The yield of a specific charge state is defined by the cross-sectional ratio of the electron capture and loss. This means that the ion remains in its most likely charge state almost 50% of the time because of the balance between capture and loss processes.

This does not imply that all electrons are frozen into the inner orbitals of the ion. In reality, the cross section for bound electron excitation can be higher than the electron capture cross section and the electron shells of the ion are systematically perturbed with the excitation of electrons to higher shells. In a capture event, high angular momenta atomic levels are also populated. One can presume that in highly charged ions the outer electrons are removed, but vacant levels are systematically fed by the excitation of inner-shell electrons. This provides the unique possibility of confining strongly ionized atomic species for a long time and of observing their excitation and fluorescence.

In particular, the described processes may be very useful for the nuclear conversion of the atomic ionization energy. When Auger conversion is stopped, the electron excitation can decay only with the fluorescence photon emission or with the transfer of energy to the matching nuclear transition. To consider this case, let us discuss some numerical estimates for ^{242}Am. The hypothetical nuclear triggering level at 52.8 keV has a half-life of about 10^{-10} s according to standard nuclear spectroscopic calculations and taking into account the experimental conversion coefficient. The width of this state is 10^{-4} of the M-vacancy radiative width, and the nuclear/atomic width ratio seems relatively moderate. The NEET probability, however, is defined by the partial width of the triggering transition, not by the full width of the triggering level. The low-energy (4.2 keV) E2 radiative transition to the nuclear trigger level is characterized by a width as low as 10^{-8} of the total width of the upper level. As a result, the probability of NEET is estimated to be $\sim 10^{-12}$. Such an estimation contains the Weisskopf strength of a single-particle nuclear transition but considers there to be no hindrance by the K quantum number. Taking into account the likely K hindrance, even lower values are expected, although this effect may not be large because NEET includes an electron transition. It is well known that hindrance factors for electron conversion are reduced in comparison with those for the photon emission process. In any event, 10^{-12} can be taken for orientation as a more or less optimistic estimation of the NEET probability in ^{242}Am.

Absolute calculation of the triggering yield in ECRIT conditions is quite difficult because some parameters are still unknown. The estimated values are given in Table 1. As was discussed, an individual atom can be kept in the ECR volume as long as 0.1–1.0 s if it is multiply desorbed from the hot walls. During 1 s, the atom remains mostly in a high-charge state and its inner shells are multiply excited to unoccupied levels. Each time, there is a certain probability for nuclear excitation that should be multiplied by the number of attempts and the number of atoms.

The whole volume of the active ECR zone may contain 10^{13} isomeric atoms. Based on the total beam current extracted from an ECRIS, one may assume that the electron excitation rate for ions is as high as 10^{5}/s. Combining these numbers with the NEET probability (10^{-12}), one deduces the triggering event rate to be 10^{6}/s. This is definitely enough for the detection of triggering, and even a rate lower by 2 orders -of magnitude can be successfully detected for the case of ^{242m}Am according to [9]. It should be noted, however, that such a rate of triggering, being a lower limit, corresponds to an extremely low NEET probability of about 10^{-14}. Thus, one concludes that ECRIT can be very productive for nuclear excitation and triggering. With higher physical probability, the yield of radiation can achieve a level interesting for applications, not only for measurements of significant parameters. In the following section, we discuss transitions between atomic–nuclear hybrid states. Hopefully, the hindrance factors can be reduced and the probability of nuclear excitation thereby enhanced.

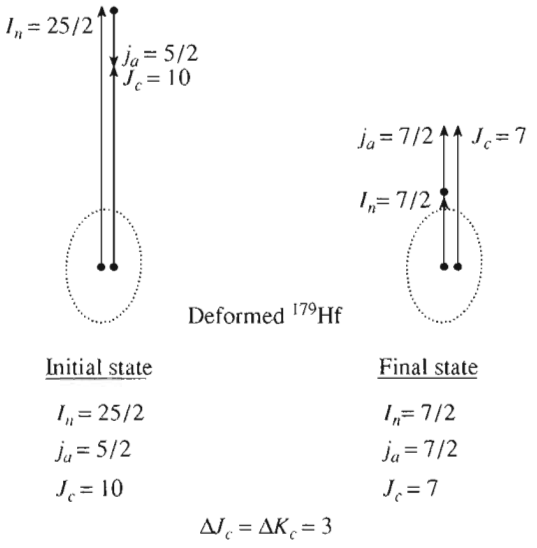

Fig. 3. Atomic–nuclear compound states that can be formed before and after ^{179m2}Hf triggering.

5. ROLE OF ATOMIC–NUCLEAR COMPOUND STATES

If one uses scheme II for ^{179m2}Hf triggering (see Fig. 1), the transition will have a rather low energy of only about 70 eV. A similar energy nuclear transition in ^{235}U can be excited in hot plasma conditions according to [31]. In the case of ^{179}Hf, a high multipolarity, $L = 9$, almost cancels the transition strength. But such restrictions would be significantly moderated in a model that considers the electromagnetic transition in the compound system including both nuclear and atomic subsystems. An approach to the compound states has been discussed in [32, 33].

The total angular momentum of the compound system[1] J_c is formed as a vector sum of nuclear and atomic spins. This is illustrated in Fig. 3 for the specific case of ^{179m2}Hf triggering via method II. The initial compound state contains an isomeric nucleus with $I_n = 25/2$ and a valence electron in the O V shell with $j_a = 5/2$. The final state corresponds to the nucleus in the triggering level with $I_n = 7/2$ and the electron at the N VII orbit with $j_a = 7/2$. The transition between initial and final states combines the nuclear triggering transitions plus the O V $\longrightarrow$ N VII electron transition. In total, the compound system changes the angular momentum by a value of $\Delta J_c = 3$, compared with $\Delta I_n = 9$.

The transition rate should be increased by many orders of magnitude, 10^{15}–10^{20}, when the multipolarity is changed from $L = 9$ to $L = 3$. For a reasonable probability of triggering to be expected within the compound mechanism, octupole transitions are among the most typical for the nuclear case. However, two additional problems should be discussed.

First, what happens to the K-hindrance factor within such a scheme? In Fig. 3, one can see that all vectors I_n, j_a, and J_c are aligned along the symmetry axis of the nucleus shown in the form of an ellipsoid. The quadrupole deformation is really a property of the ^{179}Hf nucleus, and the K quantum number is defined as the projection of angular momentum onto the symmetry axis. When alignment takes place as in Fig. 3, the compound state formally should have $K_c = J_c$. The additional hindrance by K does not exist because $\Delta K_c = \Delta J_c = L = 3$. The established rule defines the degree of K hindrance to be $(\Delta K - L)$ and there is no hindrance if $(\Delta K - L) = 0$. Thus, the scheme shown in Fig. 3 provides a rather low multipolarity of the electromagnetic transition and excludes the effect of K hindrance even when the pure nuclear transition is strongly forbidden by ΔI and ΔK.

A second question arises: What is the amplitude of the hybridization of atomic and nuclear states? They may be completely decoupled and still compound states may arise, in principle, but with very low contribution to the wavefunction. Even if only a little admixture is present in the wavefunction of the system, this can be important in the case of strongly forbidden transitions. When the transition is almost stopped due to high ΔI and ΔK values, the admixture of compound states may allow a small but reasonable probability. It would not be easy to calculate the amplitude of hybridization quantitatively, although some physical arguments can be proposed.

A 70 eV virtual photon responsible for the triggering of the ^{179m2}Hf isomer has a wavelength of $\lambda = 2.8 \times 10^{-7}$ cm, i.e., larger than the radius of the vacant N VII orbital. This is also true for other cases, when deeper orbit vacancies are used for NEET. One can think that the electromagnetic wave covers both a nucleus and the electron orbit within one wavelength and this provides a feedback for the coupling of nuclear–atomic states.

Let us characterize in more detail the ^{179m2}Hf triggering via scheme II using the compound states shown in Fig. 3. In the singly ionized atom, the atomic transition O V $\longrightarrow$ N VII has an energy of about 10 eV, which is not enough for nuclear excitation of the $7/2^+$ level located 70 eV above the $25/2^-$ isomer. But when more electrons are removed, the energy of the electron transition grows significantly and matching with the nuclear transition energy can be reached. Also, the Auger conversion is excluded when weakly bound electrons are stripped. Due to that, the N VII vacancy can decay only via a radiative process or nuclear conversion, when a valence electron appears in the O V orbital. The lifetime of the vacancy is increased to longer than 1 ps [30], while the nuclear lifetime of the $7/2^+$ triggering level at 1.105.91 keV should be about

[1] $J_c = F$, where the symbol F is used in some publications.

0.01 ps according to standard nuclear estimations. In this case, the nuclear-to-atomic widths ratio is reversed, $\Gamma_n \gg \Gamma_a$, unlike the more typical situation when $\Gamma_n \ll \Gamma_a$. Consequently, under the conditions of atomic–nuclear resonance, the nuclear conversion should dominate beyond the radiative decay of the N VII vacancy.

Finally, energy matching in this scheme can be reached and the width mismatch works in favor of nuclear conversion of the atomic transition. Thus, the probability of ^{179m2}Hf triggering is restricted only because the nuclear transition is deeply suppressed by high ΔI and ΔK values. But, as we discussed above, in the scheme of compound atomic–nuclear states, the ΔI and ΔK restrictions are moderated or even nearly cancelled. The probability of the process is defined by the amplitude of the atomic–nuclear hybridization with formation of the compound states. The latter amplitude has not yet been reliably calculated, but might be large enough to have a positive effect.

A similar scheme may also be useful for the third scheme of ^{179m2}Hf triggering, but with some modification. In this scheme, the excitation of a hypothetical triggering level requires 90 keV photon absorption, so bremsstrahlung or synchrotron radiation photons should be used. The multipolarity of the nuclear transition is high, $L = 5$, and nuclear excitation is normally stopped due to this. If the isomeric atom is ionized and excited, some atomic transition may accompany the 90 keV photon absorption. The spin deficit can be supplied by the simultaneous atomic transitions and then the nuclear-excitation gateway becomes open. Appropriate conditions can be created by exposing the isomeric sample simultaneously to hard X-ray radiation and to powerful pulses of optical laser photons. This would be nuclear excitation assisted by electron transitions.

The triggering of ^{242m}Am by the electron transition to the M or L vacancy [12] in the americium atom uses, in principle, a scheme similar to the discussed above in scheme II for ^{179m2}Hf triggering. Only the energy of transition is 60 times higher. But again the combination of nuclear and atomic spins might be helpful to exclude the retardation of the transition due to the ΔI and ΔK differences. Therefore, the NEET probability of 10^{12} for ^{242m}Am triggering estimated in the previous section should be increased rather than decreased. If in reality it is on the order of 10^{-10}, the triggering rate reaches 10^8/s, i.e., 200 times higher than the spontaneous decay rate. Thus, in ECRIT conditions, the rate of decay can be strongly accelerated, and this is important for applications.

6. SUMMARY

Within a mechanism of atomic–nuclear resonance, or NEET, the isomer triggering yield is restricted mostly by three different factors:

(1) A frequency detuning between nuclear and atomic transitions.

(2) A mismatch of widths of nuclear and atomic states.

(3) A strong retardation of nuclear transitions because of high multipolarity and K hindrance.

In an atom that is deeply ionized to high charge states, the appropriate transitions can be found for NEET in some nuclei and the detuning problem is solved because of the charge-dependent position of the atomic levels. The probability of nuclear conversion of the atomic transition is normally reduced by a few orders of magnitude due to the mismatch of the widths. However, in some cases, for instance in ^{179m2}Hf triggering, the nuclear conversion is not suppressed but dominates because of the reversed width ratio. The third reason is most fundamental, and there is a possibility to decrease the retardation factors or even cancel them in a model of the atomic–nuclear compound states. The strength of manifestation of such states depends on the amplitude of the atomic–nuclear coupling that results from the hybridization of the wavefunctions.

New experiments on isomer triggering in plasma surroundings using a modern electron cyclotron resonance ion trap, ECRIT, are proposed. They can be productive not only as a test of the technical parameters of the ECRIT array but also for the estimation of some fundamental physical values, such as the amplitude of atomic–nuclear hybridization.

The approaches to real triggering of the ^{179m2}Hf isomer are newly developed. The behavior of the ^{179m2}Hf and ^{242m}Am atomic–nuclear systems in ECRIT is treated in some quantitative details.

ACKNOWLEDGMENTS

The authors gratefully acknowledge general support from AFOSR contract F4962D-02-1-0187 (JJC), travel support from this contract to LPHYS'03 through Youngstown State University (SAK), and the support by ISTC Project #2651p and U.S. CRDF-R.F. Ministry of Education Award VZ-010-0 (LAR and AAZ). We also thank S.N. Bogomolov for his introductory remarks on the modern status of ECR techniques.

REFERENCES

1. D. Belić, C. Arlandini, J. Besserer, *et al.*, Phys. Rev. C **65**, 035801 (2002).
2. L. Lakośi and T. C. Nguyen, Nucl. Phys. A **697**, 44 (2002).
3. C. Doll, H. G. Börner, S. Jaag, *et al.*, Phys. Rev. C **59**, 492 (1999).
4. J. J. Carroll, S. A. Karamian, L. A. Rivlin, and A. A. Zadernovsky, Hyperfine Interact. **135**, 3 (2001).
5. Yu. Ts. Oganessian and S. A. Karamian, Hyperfine Interact. **107**, 43 (1997).

6. P. M. Walker and G. D. Dracoulis, Nature **399**, 35 (1999).
7. S. A. Karamian, C. B. Collins, J. J. Carroll, and J. Adam, Phys. Rev. C **57**, 1812 (1998).
8. P. M. Walker, Hyperfine Interact. **143**, 143 (2002).
9. S. A. Karamian, in *Proceedings of Internationl Workshop on Physics of Isomers, Pushkin* (2000), p. 164; Preprint No. E6-2000-233, JINR (Joint Inst. for Nuclear Research, Dubna, 2000).
10. L. Maunoury, P. Delbourgo-Salvador, P. Aubert, *et al.*, Nucl. Phys. A **701**, 286c (2002).
11. S. A. Karamian and J. J. Carroll, Laser Phys. **12**, 310 (2002).
12. S. A. Karamian and J. J. Carroll, Hyperfine Interact. **143**, 69 (2002).
13. S. A. Karamian and J. J. Carroll, Laser Phys. **13**, 1182 (2003).
14. A. A. Zadernovsky and J. J. Carroll, Hyperfine Interact. **143**, 153 (2002).
15. Yu. Ts. Oganessian and S. A. Karamian, Laser Phys. **5**, 336 (1995).
16. H. Hübel, R. A. Naumann, M. L. Andersen, *et al.*, Phys. Rev. C **1**, 1845 (1970).
17. Yu. Ts. Oganessian, Yu. P. Gangrsky, B. Gorski, *et al.*, in *Proceedings of International Conference on Exotic Nuclei* (World Sci., Singapore, 1992), p. 311.
18. S. A. Karamian, J. Adam, D. V. Filossofov, *et al.*, Nucl. Instrum. Methods Phys. Res. A **489**, 448 (2002).
19. S. A. Karamian, J. J. Carroll, J. Adam, *et al.*, in *Book of Abstracts: VIII International Conference on Nucleus–Nucleus Collisions* (Moscow, 2003), p. 119.
20. J. Billowes, Nucl. Phys. A **682**, 206c (2001).
21. S. M. Mullins, G. D. Dracoulis, A. P. Byrne, *et al.*, Phys. Rev. C **61**, 044 315 (2000).
22. E. Browne, Nucl. Data Sheets **55**, 483 (1998).
23. H. R. Reiss, Phys. Rev. C **27**, 1229 (1983).
24. C. B. Collins and J. J. Carroll, Hyperfine Interact. **107**, 3 (1997).
25. I. Ahmad, J. C. Banar, J. A. Becker, *et al.*, Phys. Rev. C **67**, 041 305 (2003).
26. C. B. Collins, N. C. Zoita, A. C. Rusu, *et al.*, Europhys. Lett. **57**, 677 (2002).
27. H. E. Roberts, M. Helba, J. J. Garroll, *et al.*, Hyperfine Interact. **143**, 111 (2002).
28. A. V. Andreev, R. V. Volkov, V. M. Gordienko, *et al.*, Pis'ma Zh. Eksp. Teor. Fiz. **69**, 343 (1999).
29. S. Kishimoto, Y. Yodo, M. Seto, *et al.*, Phys. Rev. Lett. **85**, 1831 (2000).
30. O. Keski-Rahkonen and M. O. Krause, At. Data Nucl. Data Tables **14**, 139 (1974).
31. M. R. Harston and J. F. Chemin, Phys. Rev. C **59**, 2462 (1999).
32. O. Kocharovskaya, R. Kolesov, and Yu. Rostovtsev, Phys. Rev. Lett. **82**, 3593 (1999).
33. Yu. Rostovtsev, R. Kolesov, and O. Kocharovskaya, Hyperfine Interact. **143**, 121 (2002).

SPELL: 1. wiggler, 2. wigglers

AN EXPERIMENTAL PERSPECTIVE ON TRIGGERED GAMMA EMISSION FROM NUCLEAR ISOMERS

J. J. Carroll
Department of Physics and Astronomy, Youngstown State University,
Youngstown, Ohio 44555 USA
jjcarroll@cc.ysu.edu

ABSTRACT

The study of triggered depopulation of nuclear isomers, with accompanying gamma emission, is a rapidly-changing field which is only now attaining some degree of maturity. Because isomer decays via electromagnetic transitions are strongly inhibited, the interaction of these levels with externally-produced photons provides an important probe of nuclear structure. Also, since some isomers may store large amounts of energy for long times, a number of applications have been proposed, including the creation of a gamma-ray laser. Early experiments conclusively demonstrated triggering of the 10^{15}-year isomer of ^{180}Ta, but even a partial correlation of the effect with known levels could only be obtained recently. Investigations of triggering for the 31-year isomer of ^{178}Hf were initially guided just by systematics and experiments are characterized by considerable controversy. Against this background, the field of triggered gamma emission is entering a new phase in which improved level data allow targeting of specific potentially-useful transitions. This paper summarizes the current state-of-the-art and discusses the changing nature of the field.

INTRODUCTION

Metastable excited nuclear states, isomers, have been a major subject of inquiry since their discovery in 1921, with studies motivated in different ways by their physical properties. Isomer halflives run the gamut from rather modest (like the $T_{1/2} \sim 14$ ms shape isomer of ^{242}Am) to extremely long (like the essentially stable spin isomer ^{180m}Ta, with $T_{1/2} > 10^{15}$ years). In all cases, the existence of an isomer reflects specific nuclear structure that creates some type of potential barrier against electromagnetic decay of the metastable level to lower-lying states. For so-called spin isomers, it is the angular momentum arising from a particular single-particle configuration that provides such a barrier, forcing electromagnetic decays to be restricted to high multipolarities. A further inhibition for K isomers of deformed nuclei comes from a need to significantly re-orient the angular momentum vector, whose projection on the body axis of nuclear symmetry is K. A full discussion of the underlying mechanisms of isomer formation is beyond this present paper, but an excellent review may be found in Ref. [1]. The population and decay of isomers can give considerable insight into nuclear structure.

Isomers have also been of great interest for potential applications, primarily due to the ability of some isomers to store tremendous amounts of energy, e. g. the K isomer ^{178m2}Hf stores 2.46 MeV per nucleus, or about 1.2 GigaJoules/gram, with a halflife of 31 years. Its natural decay follows a complex cascade of transitions that has recently been clarified [2], terminating at the stable ground state. Harnessing this stored energy could give a source of "clean" nuclear

energy for various applications [3]. Some other isomers do not have stable ground states, but might still be valuable in providing a sequence of energy-releasing beta or alpha decays. It is amusing to note that the potential for applications of nuclear isomers has been featured lately in the popular press, with somewhat negative views [4, 5].

Whatever the motivation, much effort has been expended to investigate the triggering of an energy release from long-lived isomers, mainly as a burst of gamma rays. A number of issues come to the fore when considering this topic: what isomers would be best to examine, what mechanism(s) would allow external control or bypass of the natural decay, and how would one experimentally measure a triggered release from small amounts of isomers. Of course, the experimental goal would be to measure the energy required for the triggering entity (photons, neutrons, etc.) and the cross section for the reaction.

In 2001, an extensive review [6] discussed the general topic with a focus on triggering initiated by photons and a view of the systematics of isomer triggering as deduced from the closely-related "activation" of isomers. Just one isomer exists in nature (^{180m}Ta) and its triggered energy release has been conclusively demonstrated (see Refs. [7, 8] and references therein). Up to now the main method of predicting possible trigger energies for other isomers was to consider their relationship to the systematics of isomer activation for neighboring isotopes and to trigger levels found to depopulate ^{180m}Ta. This approach was most notably used in the case of the 31-year isomer of ^{178}Hf. It was suggested in 1995 that on this basis a trigger level might be found "near 2.8 MeV" [9] from the "speculation that [trigger] levels are prevalent and lie between 2.5 – 2.8 MeV" [10]. First trigger experiments were attempted in 1996 by inelastic scattering of alpha particles at Orsay, with a repeat in 1997, but as yet no firm results are known. The first photon triggering experiments began in late 1998 and the positive indications reported therefrom [11, 12] began the present intense, and controversial, period of research.

The field of study of triggered gamma emission from isomers is now moving into a new era, defined by less reliance on systematics predictions and utilizing the greatly improved spectroscopic level data from more traditional experiments. With the ability to identify and target specific potential trigger transitions, one can anticipate a greatly increased pace of research. Thus, with this changing approach, and the new body of intriguing results for triggered emission from ^{178m2}Hf, it is useful to consider the state of the field and a perspective on recent experiments. This paper aims to provide a context in which interested scientists can make their own evaluations of the status of the field.

ESTABLISHED TRIGGERING OF ^{180m}Ta

The rarest isotope of the rarest element, and the only naturally-occurring isomer, is the 75-keV metastable state of ^{180}Ta. Its halflife of more than 10^{15} years reflects the fact that an M8 electromagnetic transition is required for spontaneous decay to the unstable ground state ($T_{1/2}$ = 8.1 h). The possible depletion of this isomer, with accompanying gamma emission, due to incident photons might severely impact models of the isotope's production in stars [13]. For this reason, and the general motivations mentioned before, triggered gamma emission of this isomer has been studied for more than a decade. The first demonstration [14] that the isomer could be depleted was accomplished by irradiating tantalum samples with 6-MeV

bremsstrahlung from a medical linac. There was essentially no guidance prior to that experiment as to what transition energies might cause triggering – fortunately, this did not stop the attempt at detecting an effect.

Though the isomer population was depleted, the single initial measurement with a fixed continuum of incident photons could not identify what energy caused the triggering. It was left for later, more detailed studies [8, 15, 16] to determine what the trigger energies were and to measure their integral cross sections, ICS. It is interesting to note that after a strong trigger level near 2.8 MeV was found [15], there was concern that the measured transition strength was far greater than that consistent with established nuclear systematics [17]. Subsequent experiments [8, 16] showed that strength to be an overestimation due to contributions from lower-lying trigger levels that were unresolved in the earlier study of Ref. [15]. In the end, the triggering of ^{180}Ta was found to be in reassuring agreement with established nuclear bounds [18]. The strong triggering level near 2.8 MeV forms one of the bases for expecting similar transitions in neighboring nuclei, perhaps for triggering other isomers.

An identification of triggering energies with known levels from detailed spectroscopic measurements waited until 2001 [7]. It is now possible to predict specific gamma rays that would be emitted in some triggered events, a critical guide to future experiments that aim to better characterize the process. This can be viewed as the first real bridge between experiments on triggering and traditional nuclear physics.

DEVELOPMENT OF SYSTEMATICS

In the early 1990's, a focused series of experiments (Refs. [19-21] and references therein) were performed to investigate the activation of various isomers, including many in the A~ 180 region of nuclides. The general process of photo-activation involves two distinct steps: First, a nucleus in its ground state absorbs an incident photon and becomes excited to a so-called intermediate state. Then, the intermediate state decays electromagnetically with some branch leading by a cascade to an isomeric level. Utilizing bremsstrahlung to reach excitation energies of a few MeV, numerous intermediate states were found and, interestingly, all tested isotopes near mass 180 showed the presence of an intermediate state near 2.8 $\pm$ 0.3 MeV [21]. Also, the integral cross sections for these particular intermediate states were deduced to be quite large and they were termed giant pumping resonances.

In parallel, different measurements were focusing on anomalous spontaneous decays of some shorter-lived isomers in the mass 180 region. One particular example, ^{174}Hf, deserves special mention. The 14^+ isomer of this isotope lies at 3.312 MeV and is characterized by K = 14, differing by 6 or more units from the levels to which it primarily decays. But anomalous decays from this isomer were detected in 1990 [22] that seemed to occur through a mediating level at 2.685 MeV into the K = 0 ground-state band. Only 0.7% of the isomer decays followed this path, but even this was a surprise since overall ΔK = 14 would be needed in just two steps. A later experiment studied this mediating state in more detail [23] and described a mechanism by which significant mixing in the wavefunction between high- and low-K components played the important role. Other K-mixed states at energies from 2 – 3 MeV were found in nearby isotopes (see the survey in Ref. [24]) to facilitate some isomer decays, leading to halflives that were much

shorter than expected. The key point is that these isomers lay above the mediating states and could therefore decay through them spontaneously. An isomer lying below a level possessing significant K-mixed character would be longer-lived, but the nucleus could, in principle, be excited to that state. If the K-mixed state had a measurable decay branch that cascaded to the ground state, this would provide a triggered release of the isomer energy [9].

The above systematics arguments suggested that intermediate states near 2.8 MeV might be readily available for triggered gamma emission in isotopes near A ~ 180. Recognizing [10, 25] that the 31-year isomer ^{178m2}Hf lies at 2.445 MeV, this nuclide became the primary candidate for testing. It was not possible to specifically identify what energy might be suitable for triggering with photons, but the limited information available[1] from the Orsay experiments only seemed consistent with triggering at less than 100 keV. Thus, this was the regime of initial interest.

PHOTON TRIGGERING EXPERIMENTS FOR ^{178m2}Hf

The first published experiment investigating triggered gamma emission from ^{178m2}Hf was conducted in late 1998 [11]. This paper reported evidence of triggered gamma emission which was seen to occur when a sample containing 6.3×10^{14} ^{178m2}Hf nuclei was irradiated with a modest x-ray tube. A positive indication of triggering was deduced by comparing the gamma rays emitted from the sample during irradiation with those emitted due to natural decay with no irradiation. The bremsstrahlung endpoints of the x-ray tube were 70 and 90 keV, thus the supposed trigger energy must lie at lower energies. Most surprising was the corresponding integral cross section calculated from the reported effect, about 10^{-21} cm^2 keV, or 10^6 eV b in more standard nuclear units. This magnitude was astounding, being much larger than expected nuclear transition strengths [26, 27] and, in fact, within a few orders-of-magnitude of atomic cross sections (when integrated over some reasonable energy width).

The natural decay of ^{178m2}Hf follows the scheme shown in Fig. 1(a). These transitions are well-established [28], although a recent work [2] found additional less intense transitions. A gamma-ray spectrum obtained by standard techniques would show peaks and Compton continua due to these transitions. The isomeric material was obtained from material produced at Los Alamos in 1980 [29] and contained a significant contamination of the radioisotope ^{172}Hf.

Differences in the areas of peaks seen in gamma spectra were observed after scaling the spectra for different effective count durations. In the main, a channel-by-channel subtraction was done to detect residual changes in peak sizes. The best evidence of triggering was a 2.8σ increase in the emission of the 495-keV transition located above the 4-s, 8- first isomer of ^{178}Hf. Figure 1(b) shows the transitions which were reported to show enhancements due to triggering. Concern over the analytical method was discussed in Ref. [30].

The statistically modest, yet very intriguing, evidence made it clear that improved techniques and studies were imperative. Thus, Refs. [11, 12] began a continuing period of fascinating, but controversial results. To gain a proper perspective of the published results, and

[1] The data were not distributed to participants (incl. this author) and only a few screen dumps are available for review.

therefore the status of investigation, it is necessary to consider the body of literature in totality. Table I presents a very brief summary of these results as a guide to the reader.

Following the experiment of Ref. [31], an ambitious series of measurements was performed[2] in early 2002 which have not yet been submitted for publication, although partial results have been presented at several meetings [32, 33]. Of the six general techniques [6] that may be used to detect triggering, three approaches were employed in these experiments. These included attempts to detect statistically-significant increases (enhancements) in emission of natural decay transitions, emission of new, prompt triggered cascades that by-passed the 4-s isomer, and depletion of the total activity of the ^{178m2}Hf isomer after an intense irradiation. The X15A (bending magnet) and X17B1 (wiggler) beamlines at BNL's National Synchrotron Light Source were utilized, with the wiggler being used for a long "burn-up" attempt without in-beam detection. Single and multi-detector systems recorded gamma spectra with monochromatic irradiation of an isomeric sample at X15A and counting durations were about 500 s at each incident monochromatic energy. The L_1, L_2 and L_3 edges were scanned. Be was used to encapsulate the Hf deposit. For irradiations performed using the "white" beam, spectra were acquired for about 11 hours each with the Hf deposit in the beam, out of the beam and with no beam. No evidence to support triggered gamma emission at energies $<$100 keV was seen in-beam and no significant depletion of isomer activity was detected after the wiggler irradiation.

It is difficult to reconcile the positive results with the null measurements above and in Table I. The null measurements were obtained by several groups (comprised by individuals from various national and international institutions) and using a variety of experimental techniques. The differences just among the positive reports themselves are also difficult to understand and this is only confused further by the new report [34] that triggered (enhanced) emission at 213 keV occurs within a few tens of nanoseconds after the short pulses of monochromatic synchrotron radiation coming from the electron bunches. This proposal might explain why null results were obtained from experiments that acquired data for essentially continuous periods of seconds or more. During such longer periods, increased emission in short bursts might well be lost among naturally emitted gammas from the spontaneous decay that accumulate steadily. Of course, this proposed burst emission would contradict the positive report of Ref. [35], obtained with tens of seconds acquisitions at the SPring-8 synchrotron.

Clearly, further studies are needed to resolve the current, and rapidly-changing landscape regarding triggering of ^{178m2}Hf at low energies (less than 100 keV). While that work continues, the possibility of so-called mid-energy triggering (100 keV to a few MeV) has yet to be explored. For these energies, specific potential trigger transitions can be targeted based on state-of-the-art level data.

---

2. Collaboration of Brookhaven National Lab (Z. Zhong), SRS Technologies, Inc. (M. Helba, H. Roberts) and Youngstown State University (J. Burnett, J. Carroll, T. Drummond, J. Lepak, R. Propri).

TARGETED TRANSITIONS FOR TRIGGERING STUDIES

Level schemes like that reported[3] in Ref. [36] provide important guidance to known electromagnetic transitions that might enable triggering. It was determined that the 14^-, 68-μs isomer (with K = 14) decayed with several branches, one of which led to the 4-s isomer band and another of which led to the 31-year, 16^+ isomer (K = 16) as shown in Fig. 2(a). The essential point is that the latter transition has an E2 character and with L= 2 and ΔK = 2, there is no K hindrance. Thus, the 126-keV transition from the 16^+ isomer to the 14^- isomer should produce triggered gamma emission in a cascade that closely resembles the natural decay of the 31-year state. It is important to note that no triggering experiment performed to-date utilized an irradiation with significant levels of photons above 100 keV. Depletion of ^{178m2}Hf using incident 126-keV photons would be, if demonstrated experimentally, an example of "mid-energy" triggering. Although perhaps of less value for potential applications, this would nevertheless be a valuable scientific step.

At even higher excitation energies, it is reasonable to expect a number of additional trigger transitions as K conservation plays a lesser role [37] (or, as for the 126-keV transition there is no excess ΔK at all). A first indication of such higher-lying trigger states may be inferred from a recent experiment [38]. Multiple Coulomb excitation was used to excite levels as high as 20^+ in the ground-state band of ^{178}Hf from a non-isomeric target and it was a surprise to discover that, as a result, the 31-year isomer was populated. It was interpreted to be caused by electromagnetic transitions from the J = 14 – 20 members of the ground-state band to levels in the band of the 31-year isomer. Most intriguing is that any decays from the ground-state band directly to this isomer can serve as triggering transitions when one begins with an isomeric target. Three potential transitions of this type may be proposed from the level scheme of Ref. [38], at 331, 990 and 1676 keV as shown in Fig. 2(b). It remains for experiments to test triggering at these energies, as well as at 126 keV.

The ability to target specific potential transitions in studies of triggered gamma emission is a major improvement. While many examples might be cited, this paper will conclude by brief discussions of ^{179m}Hf ($T_{1/2}$ = 25.1 d) and ^{242m}Am ($T_{1/2}$ = 141 y; different from the shape isomer of this isotope).

The long-lived isomer of ^{242}Am may be produced by neutron capture with a significant cross section [6] and is partnered with a ground state having a 16-h halflife. The level data shows that at just 4.3 keV above the 5^- isomer lies a 3^- level that can be reached by an E2 transition, as shown in Fig. 3. This transition has not been observed experimentally, which may be an indication of significant K hindrance since the isomer and potential trigger level lie in K = 5 and 1 bands, respectively. The possibility of using 4.3-keV photons to release not only the 49 keV stored by the isomer, but also that resulting from the chain beginning with the ground-state transmutation, makes ^{242m}Am of particular interest for experiments.

Production of ^{179m}Hf has recently been reported via the (n, n') reaction [39], and with a cross section sufficient for the preparation of experimental targets. Most intriguing is that for

---

[3] Special thanks to F. Kondev, G. Dracoulis and P. Regan for returning attention to this paper and its relevance to triggering of ^{178m2}Hf.

this $25/2^-$ isomer, lying at 1.106 MeV, three potential trigger schemes may be identified from the level data, each of which reflects different mechanisms and would require quite different experimental approaches. A full discussion of these schemes may be found in Ref. [40].

So far, published work only reflects studies of photon triggering of isomers. The approach of using incident electron beams is also attractive and deserves attention.

SUMMARY

The study of triggered gamma emission, with its insight into nuclear structure and possible impact on applications, has long relied on systematics as the primary (and sometimes only) guide to experiments. With the advent of more detailed spectroscopic level schemes, it is now possible to target specific transitions for investigation in the case of many isomers. The field is rapidly-changing and perhaps the controversial results for triggering of ^{178m2}Hf are merely signs of its growing maturity.

ACKNOWLEDGMENTS

The author gratefully recognizes S. Karamian and M. Harston for their many valuable discussions on this manuscript. This work was supported by the US Air Force Office of Scientific Research grant F49620-02-1-0187.

FIGURE CAPTIONS

Figure 1. Schematic showing (a) the transitions (grey) most responsible for the natural decay of ^{178m2}Hf. Newly discovered [2] weak natural transitions are not included. Solid arrows in the other panels show transitions reported to be enhanced under irradiation. The unfilled arrow is a transition reported to reduce its emission under irradiation. Widths of the arrows give the relative enhancements for the given experiment.

Figure 2. Partial level schemes for ^{178}Hf showing decay transitions that may allow triggering when beginning with isomeric nuclei: (a) The known transition [36] at 126 keV and branches that would initiate a triggered gamma cascade to the 4-s isomer band; (b) transitions inferred from the results of Ref. [38], with possible decays leading directly to the 31-year isomer in bold that might allow triggering if beginning with isomeric nuclei.

Figure 3. Partial level scheme for ^{242}Am showing a potential 4.3-keV trigger transition.

TABLE I (part 1): Published results on triggering of ^{178m2}Hf. Irradiations were from: bremsstrahlung (B), "white" synchrotron radiation (SR), and monochromatic SR (MSR). The ICS are in cm^2 keV and all energies are in keV. Gammas from the natural decay cascade in Fig. 1 used as evidence of triggering are identified, e. g. (b – ?1) indicates transition 1 in Fig. 1(b). "Disc." gives this author's comments on major points, while the other entries are from the publications. Refs. [41, 42] are essentially duplicate reports.

Ref.:	Collins 1999 [11]	Collins 1999 [12]	Collins 2000 [43]	Collins 2001 [44]*	Collins 2001 [45]
Trigg:	Yes	Yes	Yes	Yes	Yes
Irr:	B	B	B	B	B
E_{trigg}:	< 70	< 90	< 20	Not deduced	Not deduced
ICS:	10^{-21} if $E_{trigg} = 40$	2×10^{-21} if $E_{trigg} = 30$	$> 2.2 \times 10^{-22}$ if $E_{trigg} < 20$	Not deduced	Not deduced
Evidence:	495 peak ↑ 2.8σ (b - γ1)	426 peak ↑ 2% (c - γ1)	325 peak ↑ 1.5σ (d - γ1)	New small peak near 130 seen coincident with 213	213, 325 & 426 peaks ↑ 1%, 2% w/different x-ray tube currents, 50 mA, 80 mA
	426 peak ↑ 1.6σ (b - γ2)	325 peak ↑ 2% (c - γ2)	213/217 peak ↑ 3.3σ (d – both γ2)	No details, but similar result from SPring-8 MSR	
			New weak peaks at 210 and 546		
Concl:	Triggered cascade mainly same as natural	Triggered cascade different somewhat from natural	Triggered cascade not same as natural	Triggered cascade misses transitions above 4-s isomer	Triggered cascade misses all transitions above 4-s isomer
Disc:	574 peak ↓ 1.22σ (b - γ3)	No information about 495	213 below, 217 above 4-s isomer in natural cascade	130 peak has different width from nearby large peak	Statistics insufficient to prove linear scaling
	Extra normalization between irr. and non-irr. spectra		No mention of 495 or 426	γ near 130 from ^{172}Hf chain [2]	
			γ near 210 and 546 part of ^{172}Hf decay [2]	Ge detector cannot reach quoted 250 ps timing	

* This paper mainly reviews earlier results - only its new results are summarized here.

Table I (part 2): Continuation of published results on triggering of ^{178m2}Hf.

Ref.	Ahmad 2001 [46]	Collins 2002 [35]	Ahmad 2003 [47]	Roberts 2003 [31]	Carroll 2003 [48]
Trigg:	No	Yes	No	No	No
Irr:	SR	MSR	SR	MSR	B
E_{trigg}:	None	Near L_1, L_3 edges	None	None	None
ICS:	$< 10^{-26}$ for 8 – 60	$\sim 2 \times 10^{-23}$ for L_1*	$< 10^{-26}$ for 6 – 20	$< 10^{-25}$	$< 10^{-20}$ if $E_{trigg} = 10$
Evidence:	Null measure-ment	213/217 ↑ ~ 4.1σ by summing spectra (e γ1 & γ2)	Null measure-ment	Null measure-ment	Null measure-ment
Concl:	Upper limit for prompt or slow (via 4-s isomer) triggering over broad range of energies	Largest ↑ near L_1 – about 10^{-3} of atomic photo-ionizations cause trigg.	Upper limit for prompt or slow triggering, for broad range of energies > 6	Scanned L_1, L_2 and L_3 edges and 12.7 (E of 1st decay natural transition)	Initial test of multi-detector for high sensitivity of prompt triggering
		Triggering due to NEET		20-s data acquisition at each MSR energy	Need Upgrade to reduce time resolution < 150 ns
		States null measure-ment [46] was due to opaque sample near edges		No significant changes > 3σ seen in any peaks	Should use with SR source
Disc:	Authors of [43] argued that Al in sample for this expt. removed SR photons < 20 necessary for triggering	Beam-on data taken for continuous 60-s periods at each MSR energy	Be capsule used to eliminate suggested filtering of incident photons near L edges	Measure-ment done in fall 2001 at BNL	Measure-ment done in late 2001; also done at BNL MSR early 2002
		Gross counts used for peaks		Follow-up expts. done in early 2002	Upcoming experiment at SPring-8 MSR

* Paper gives cross section, not ICS. This value estimated from quoted cross section ~ 2×10^{-22} cm^2 and ~ 100 eV wide range over which enhancement was summed.

REFERENCES

1. P. M. Walker and G. Dracoulis, Nature **399**, 35 (1999).
2. M. B. Smith, P. M. Walker, G. C. Ball, et al., Phys Rev. C **68**, 031302(R) (2003).
3. H. Roberts, Hyperfine Int. **107**, 91 (1997).
4. "Gamma-ray weapons could trigger next arms race," D. Hambling, in *New Scientist*, August 13, 2003.
5. "Handliches Höllenfeuer," M. Becker, in *Der Spiegel*, August 14, 2003.
6. J. J. Carroll, S. A. Karamian, L. A. Rivlin, et al., Hyperfine Int. **135**, 3 (2001).
7. P. M. Walker, G. D. Dracoulis, and J. J. Carroll, Phys. Rev C **64**, 061302 (2001).
8. D. Belic, C. Arlandini, J. Besserer, et al., Phys. Rev. Lett. **83**, 5242 (1999).
9. C. B. Collins and J. J. Carroll, Laser Phys. **5**, 209 (1995).
10. C. B. Collins, J. J. Carroll, Y. T. Oganessian, et al., Laser Phys. **5**, 280 (1995).
11. C. B. Collins, F. Davanloo, M. C. Iosif, et al., Phys. Rev. Lett. **82**, 695 (1999).
12. C. B. Collins, F. Davanloo, M. C. Iosif, et al., Laser Phys. **9**, 8 (1999).
13. P. von Neumann-Cosel, Nucl. Phys. **A719**, 21C (2003).
14. C. B. Collins, C. D. Eberhard, J. W. Glesener, et al., Phys. Rev. C **37**, 2267 (1988).
15. C. B. Collins, J. J. Carroll, T. W. Sinor, et al., Phys. Rev. C **42**, 1813 (1990).
16. D. Belic, C. Arlandini, J. Besserer, et al., Phys. Rev. C **65**, 035801 (2002).
17. Z. Németh, Phys. Rev. C **45**, 467 (1992).
18. S. A. Karamian and J. J. Carroll, Laser Phys. **11**, 23 (2001).
19. J. J. Carroll, M. J. Byrd, D. G. Richmond, et al., Phys. Rev. C **43**, 1238 (1991).
20. J. J. Carroll, T. W. Sinor, D. G. Richmond, et al., Phys. Rev. C **43**, 879 (1991).
21. C. B. Collins, J. J. Carroll, K. N. Taylor, et al., Phys. Rev. C **46**, 952 (1992).
22. P. M. Walker, G. Sletten, N. L. Gjørup, et al., Phys Rev. Lett. **65**, 416 (1990).
23. N. L. Gjørup, P. M. Walker, G. Sletten, et al., Nuclear Physics **A582**, 369 (1995).
24. J. J. Carroll, Examination of critical issues in the use of ^{178}Hf for high energy density applications,in AFOSR Summer Faculty Research Program (1996) Report 6-1.
25. C. B. Collins, J. J. Carroll, K. N. Taylor, et al., Laser Inter. Related Plasma Phenom. **10**, 151 (1995).
26. D. P. McNabb, J. D. Anderson, and J. A. Becker, Phys. Rev. Lett. **84**, 2542 (2000).
27. P. v. Neumann-Cosel and A. Richter, Phys. Rev. Lett. **84**, 2543 (2000).
28. National Nuclear Data Center Online Evaluated Nuclear Structure Data File (ENSDF), Brookhaven National Laboratory, (2003)
29. H. A. O'Brien, Nuclear Instruments and Methods **B40/41**, 1126 (1989).
30. S. Olariu and A. Olariu, Phys. Rev. Lett. **84**, 2541 (2000).
31. H. Roberts, M. Helba, J. J. Carroll, et al., Hyperfine Int. **143**, 111 (2003).
32. J. Burnett, R. Propri, T. Drummond, et al., posters at the APS Division of Nuclear Physics Fall Meeting, Conference Experience for Undergraduates, East Lansing, MI, October 11, 2002.
33. J. J. Carroll, presentation at the 17th International Conference on the Application of Accelerators in Research and Industry (CAARI 2002), Denton, TX, November 12-16, 2002.
34. C. B. Collins, presentation at the 5th AFOSR Isomer Workshop (hosted by LPHYS'03), Hamburg, Germany, August 15, 2003.
35. C. B. Collins, N. C. Zoita, A. C. Rusu, et al., Europhys. Lett. **57**, 677 (2002).

36. T. L. Khoo and G. Løvhøiden, Physics Letters **67B**, 271 (1977).
37. S. A. Karamian, C. B. Collins, J. J. Carroll, et al., Phys. Rev. C **57**, 1812 (1998).
38. A. B. Hayes, D. Cline, C. Y. Wu, et al., Phys. Rev. Lett. **89**, 242501 (2002).
39. S. A. Karamian, J. J. Carroll, J. Adam, et al., Laser Phys. **this volume** (2004).
40. S. A. Karamian, J. J. Carroll, L. A. Rivlin, et al., Laser Phys. **this volume** (2004).
41. C. B. Collins, F. Davanloo, M. C. Iosif, et al., Phys. Atomic Nucl. **63**, 2067 (2000).
42. C. B. Collins, N. C. Zoita, A. C. Rusu, et al., J. de Phys. IV **11**, 437 (2001).
43. C. B. Collins, F. Davanloo, A. C. Rusu, et al., Phys. Rev. C **61**, 054305 (2000).
44. C. B. Collins, A. C. Rusu, N. C. Zoita, et al., Hyperfine Int. **135**, 51 (2001).
45. C. B. Collins, N. C. Zoita, A. C. Rusu, et al., Laser Phys. **11**, 1 (2001).
46. I. Ahmad, J. C. Banar, J. A. Becker, et al., Phys. Rev. Lett. **87**, 0725031 (2001).
47. I. Ahmad, J. C. Banar, J. A. Becker, et al., Phys Rev. C **67**, 041305(R) (2003).
48. J. J. Carroll, J. Burnett, T. Drummond, et al., Hyperfine Int. **143**, 37 (2003).

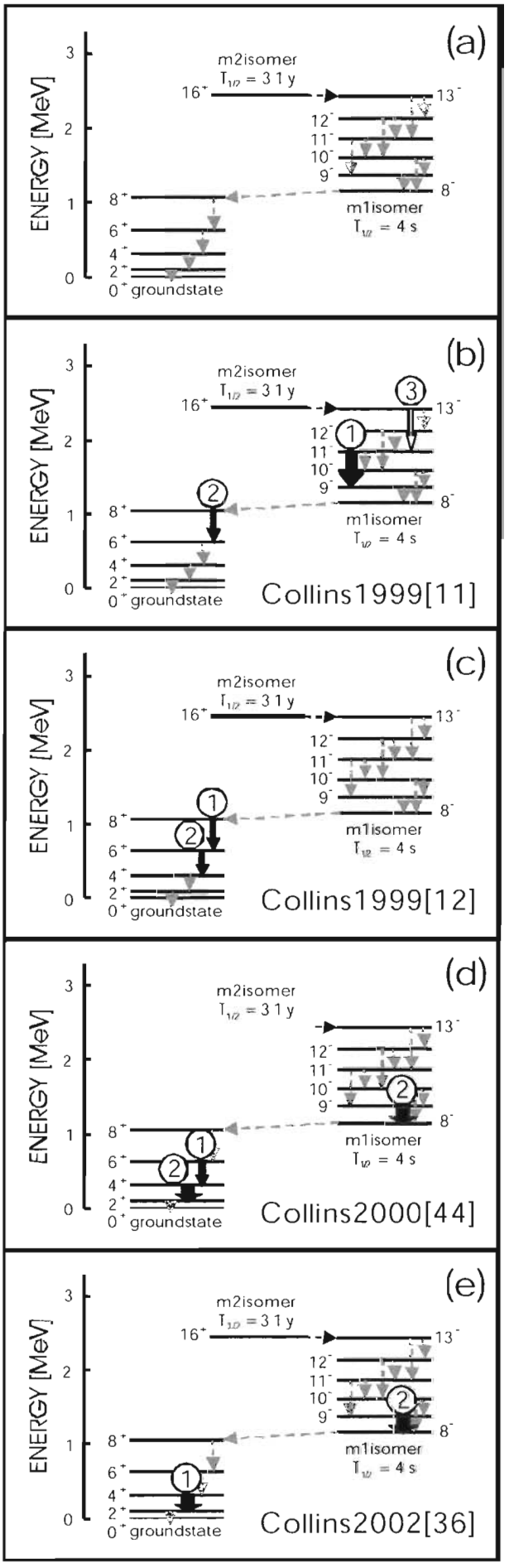
(a)
ENERGY [MeV]
m2isomer
$T_{1/2}$ = 3.1 y
16+
13-
12-
11-
10-
9-
8-
m1isomer
$T_{1/2}$ = 4 s
8+
6+
4+
2+
0+ groundstate
(b)
Collins1999[11]
(c)
Collins1999[12]
(d)
Collins2000[44]
(e)
Collins2002[36]

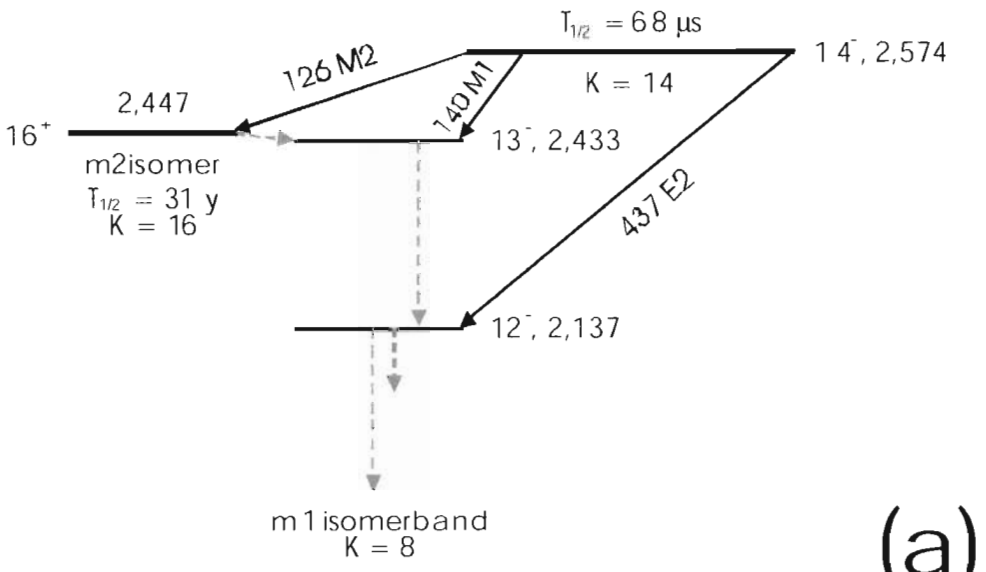
T1/2 = 68 µs
K = 14
14-, 2,574
126 M2
140 M1
2,447
16+
m2isomer
T1/2 = 31 y
K = 16
13-, 2,433
437 E2
12-, 2,137
m1 isomerband
K = 8

(a)

(b)

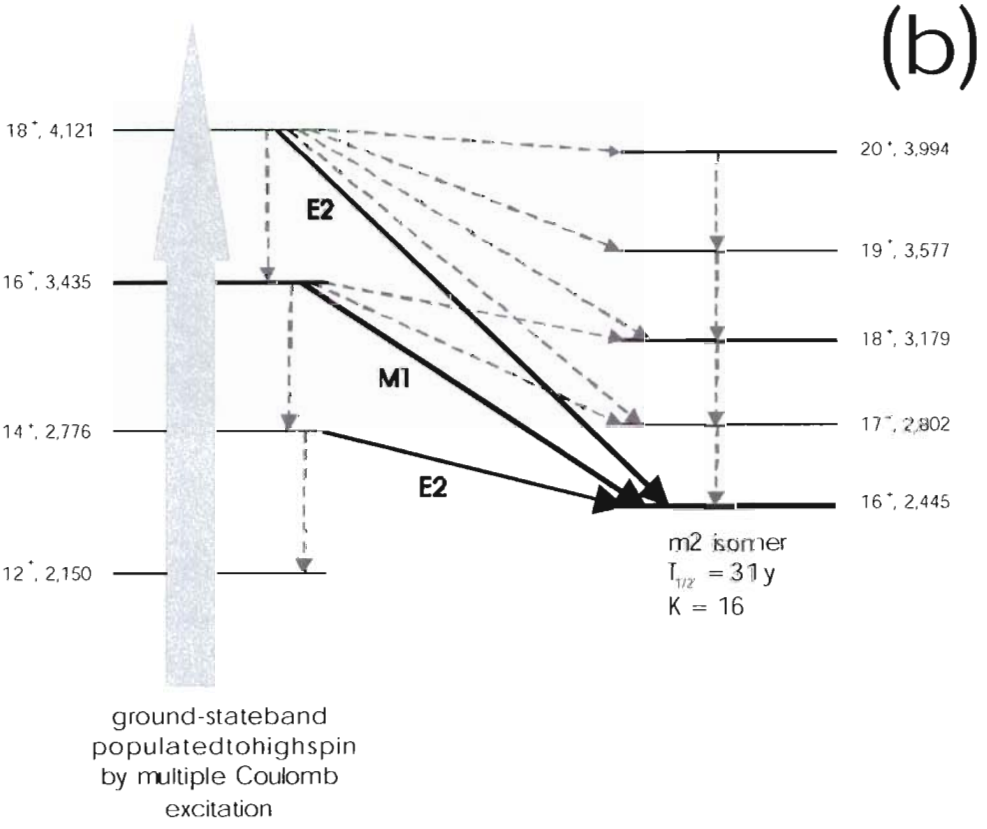
18+, 4,121
16+, 3,435
14+, 2,776
12+, 2,150
E2
M1
E2
20+, 3,994
19+, 3,577
18+, 3,179
17-, 2,802
16+, 2,445
m2 isomer
T1/2 = 31 y
K = 16
ground-stateband
populatedtohighspin
by multiple Coulomb
excitation

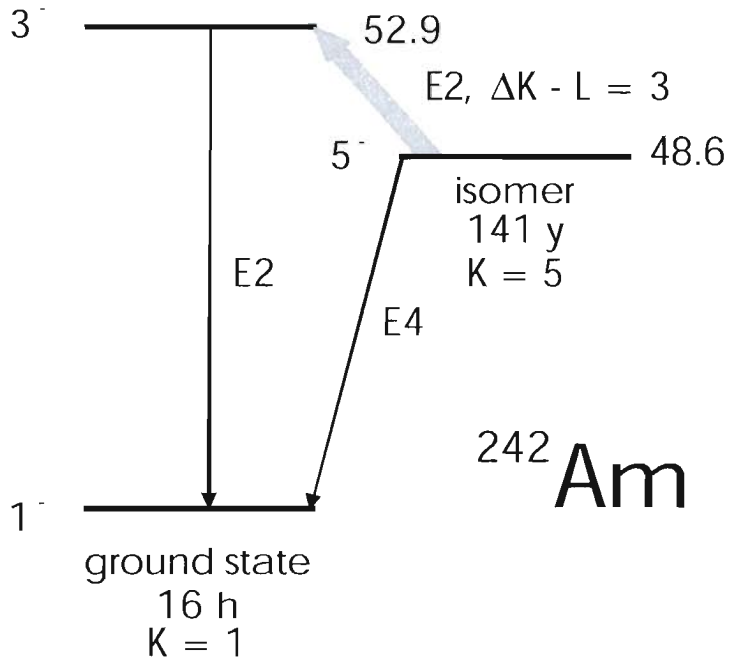
3⁻
52.9
E2, ΔK - L = 3
5⁻
48.6
isomer
141 y
K = 5
E2
E4
242Am
1⁻
ground state
16 h
K = 1

APPENDIX B

INVITED PRESENTATIONS DURING GRANT

"Foundations of isomer physics for energy applications," *7th AFOSR Workshop on Isomers and Quantum Nucleonics*, Dubna, Russia, June 26 – July 1, 2005.

"Isomers, or how I learned to stop worrying and love nuclear physics," Sigma Xi, Army Research Laboratory Chapter, 94th Aero Squadron Restaurant, College Park, Maryland, January 29, 2005.

"An experimental perspective on triggering energy release from nuclear isomers," Army Research Laboratory, Adelphi, Maryland, January 28, 2005.

"An experimental perspective on releasing energy from nuclear isomers," *35th Winter Colloquium on the Physics of Quantum Electronics*, Snowbird, Utah, January 2 – 6, 2005.

"Update on research into triggered energy release from nuclear isomers," *Contemporary Energetic Research Conference, Science and Technology Expert Partnership*, McLean, VA, July 20, 2004.

"Prospects for controlled energy release from nuclear isomers: Lessons from the past (and present) and a look to the future," *Frontiers of Non-linear Physics: Mini-Symposium on Gamma-Ray Optics and Quantum Nucleonics*, Georgy Zhukov Volga Cruise, Russia, July 5 – 12, 2004.

"Nuclear isomers, triggered gamma emission and the hafnium controversy," Triangle Universities Nuclear Laboratory, Duke University, April 22, 2004.

"An Experimental Perspective on Triggered Gamma Emission from Nuclear Isomers," *LPHYS'03*, Hamburg, Germany, August 25 - 29, 2003.

"Nuclear isomers and triggered gamma emission," *Energy storage and other opportunities with nuclear isomers*, Idaho State University-INEEL, Pocatello, Idaho, August 14, 15, 2003.

"YSU SIER project on triggered gamma emission," DARPA/MTO SIER HIPP Meeting, Arlington, VA, May 15, 16, 2003.

"Study of triggering of electromagnetic pulses from isomeric materials," AFOSR Atomic and Molecular Program Review, Charleston, SC, February 19 – 21, 2003.

"Release of energy from nuclear isomers: Issues and status," Institute for Defense Analyses, Alexandria, VA, January 13, 2003.

"YSU SIER project on triggered gamma emission," DARPA/MTO SIER Program Kick-Off, Arlington, VA, December 10, 2002.

"Search for low-energy triggering of gamma emission from $^{178}Hf^{m2}$ using synchrotron radiation," *Conference on Applications of Accelerators in Research and Industry (CAARI '02)*, Denton, TX, November 14, 2002.

"Status of the YSU project on triggered gamma emission," *4th AFOSR Isomer Workshop*, Air Force Research Laboratory, Albuquerque, NM, October 24, 2002.

"Triggered gamma emission for ultra-compact power sources," Synchrotron Radiation Research Center, Hsinchu, Taiwan, September 12, 2002.

"Triggering of long-lived isomers as a 'clean' release of nuclear energy," Institute of Applied Physics, Nizhny Novgorod, Russia, June 27, 2002.

"X-ray driven gamma emission," *International Quantum Electronics Conference*, Moscow, Russia, June 25, 2002.

"Nuclear isomers and x-ray driven gamma emission," *Jet Propulsion Laboratory Advanced Space Propulsion Workshop*, Pasadena, CA, June 5, 2002.

"Nuclear isomers and x-ray driven gamma emission," *Science and Technology Expert Partnership Symposium on New Materials III*, Washington, DC, April 4, 2002.

APPENDIX C

CONTRIBUTED PRESENTATIONS DURING GRANT

"Search for triggered gamma emission from ^{178m2}Hf at SPring-8," *American Physical Society, Division of Nuclear Physics Fall Meeting*, Chicago, Illinois, October 27 – 30, 2004.

"Experiments on triggered gamma emission from nuclear isomers," *American Physical Society April Meeting*, Philadelphia, Pennsylvania, April 5 – 8, 2003.

"X-ray driven gamma emission," *Ohio Section Meeting of the American Physical Society*, Youngstown, Ohio, April 12 – 13, 2002.